Gebhard Mathis
Editor

Chest Sonography

Fifth Edition

Springer

Chest Sonography

Gebhard Mathis
Editor

Chest Sonography

Fifth Edition

Springer

Editor
Gebhard Mathis
Rankweil, Austria

ISBN 978-3-031-09441-5 ISBN 978-3-031-09442-2 (eBook)
https://doi.org/10.1007/978-3-031-09442-2

This Springer imprint is published by the registered company Springer Nature Switzerland AG
The registered company address is: Gewerbestrasse 11, 6330 Cham, Switzerland

Contents

Indications, Technical Equipment and Investigation Procedure

S. Beckh

Contents

G. Mathis (ed.), *Chest Sonography*, https://doi.org/10.1007/978-3-031-09442-2_1

1

1.1 Indications

Ultrasonography of the lung has now become an established imaging procedure for chest diseases. Owing to comprehensive scientific investigations and studies (Beckh et al. 2002; Beaulieu and Marik 2005; Mathis et al. 2005; Niemann et al. 2009; Reuß 2010; Reissig et al. 2012; Volpicelli et al. 2012; Bartheld 2013; Squizzato et al. 2013) the "Point of Care Ultrasound" (POCUS) has been widely accepted as a basic tool with rapid diagnostic information in medical examination.

In emergency cases and in intensive care medicine the findings of ultrasound allow a conclusive and strategic course of action (Diacon et al. 2005; Soldati et al. 2006; Arbelot et al. 2008; Copetti and Cattarossi 2008; Copetti et al. 2008; Noble et al. 2009; Moore and Copel 2011; Blank and Heinzmann 2012; Volpicelli et al. 2012; Böer et al. 2014; Squizzato et al. 2015; Blank et al. 2019; Mayo et al. 2019; Kluge et al. 2020; Soldati et al. 2020). The acceptance of the method is reflected in a number of well-known international guidelines (Havelock et al. 2010; Hooper et al. 2010; Piscaglia et al. 2012; Bamber et al. 2013; Cosgrove et al. 2013; Detterbeck et al. 2013; AWMF Leitlinie 2015, 2018; Ewig et al. 2016; Dalhoff et al. 2018; Rose et al. 2017; Stoelben et al. 2018).

New developed handheld devices in the size of a mobile phone create an "ultrasound-stethoscope". In this dimension ultrasound may provide an imaging diagnosis even in most difficult situations (Bachmann Nielsen et al. 2019; Soldati et al. 2020). Thus bedside imaging information in isolated patients will be much easier (Kluge et al. 2020; Soldati et al. 2020).

The usefulness of chest sonography is proven in permanent enlargement of applications (Lesser 2017; Davidsen et al. 2020).

The ultrasound image does not provide a complete overview of the chest. However, it does show a certain portion of the chest and thus provides diagnostic information about a variety of problems (Fig. 1.1).

About 99% of the ultrasonic wave is reflected by the healthy lung. Intrapulmonary processes can be registered by ultrasound only when they extend to the visceral pleura or can be visualized through a sound-conducting medium such as fluid or consolidated lung tissue (Fig. 1.2).

Acoustic shadowing occurs due to nearly complete absorption of the ultrasonic wave on bone, especially behind the sternum, the scapula, and the spine. Impairment due to the rib shadow can be balanced, at least in part, by appropriate breathing techniques.

The immediate retrosternal and posterior portions of the mediastinum cannot be viewed from the percutaneous aspect. Transesophageal and transbronchial ultrasound may be used additionally, but it should be noted that these examination procedures are invasive in

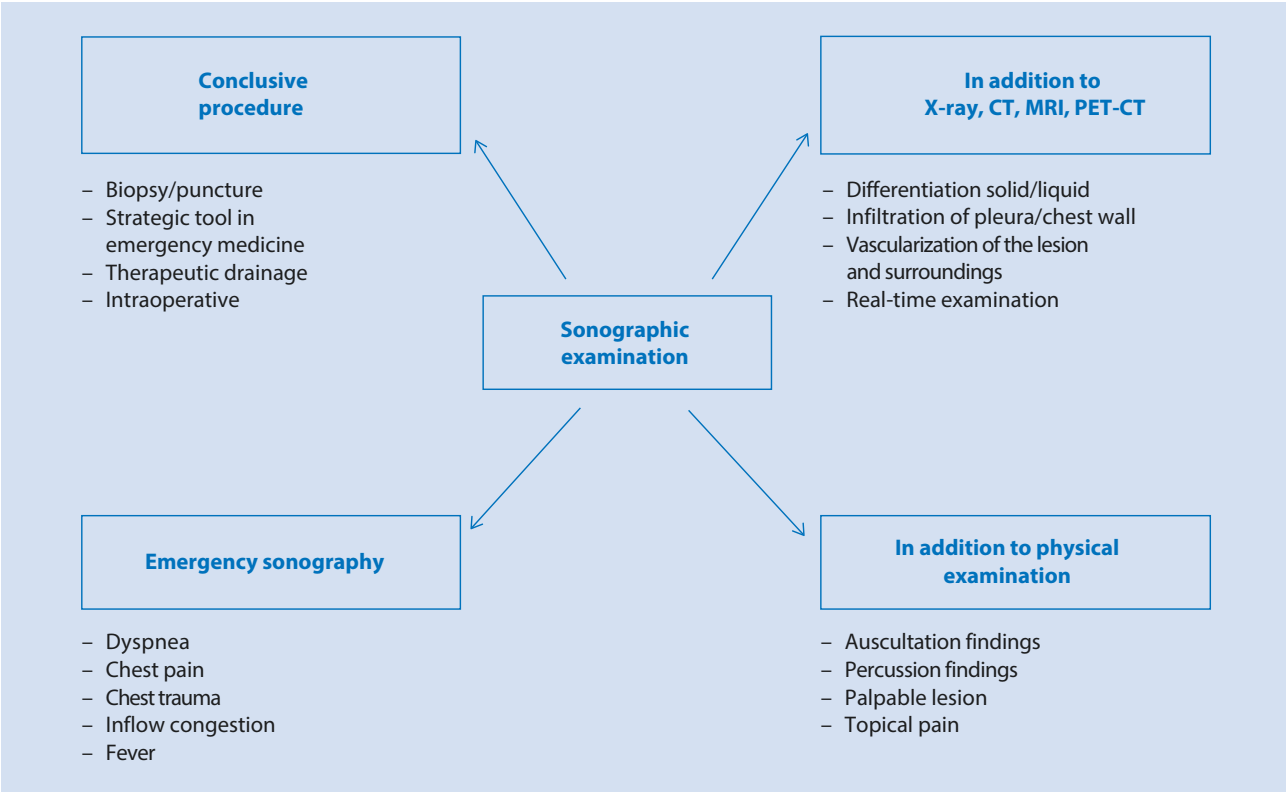

Fig. 1.1 Spectrum of applications of ultrasonography for pleural and pulmonary diseases

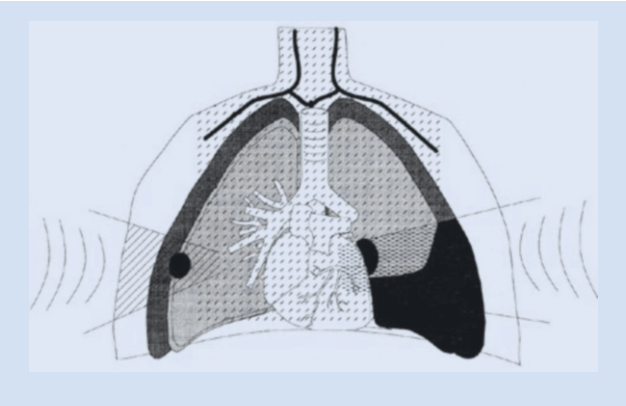

Fig. 1.2 Entities and pathological changes that can be accessed by ultrasound

terms of effort and handling (Lam and Becker 1996; Aabakken et al. 1999; Herth et al. 2004; Annema et al. 2010; Haas et al. 2010; Walker et al. 2012; Silvestri et al. 2013; ► Sect. 6.2, ► Chap. 7).

Ultrasonography provides diagnostic information during the investigation of individual entities in the chest (Overview).

Diagnostic Information During the Investigation of Individual Entities in the Chest

- Chest wall
  - Benign lesions:
    - Benign neoplasms (such as lipoma)
    - Hematoma
    - Abscess
    - Reactivated lymph nodes
    - Perichondritis, Tietze syndrome
    - Rib fracture
  - Malignant lesions:
    - Lymph node metastases (primary diagnosis and the course of disease under treatment)
    - Growing invasive carcinomas
    - Osteolyses
- Pleura
  - Solid structures:
    - Thickening of the pleura, callosity, calcification, asbestos-induced plaques
  - Space-occupying lesion:
    - *Benign:* fibrous tumor, lipoma
    - *Malignant*: clearly identifiable metastases, diffuse carcinosis, pleural mesothelioma
  - Fluid:
    - Effusion, hemothorax, pyothorax, chylothorax
  - Dynamic investigation:
    - Pneumothorax
    - Differentiating between an effusion and a callosity
    - Adherence of a space-occupying lesion
    - Invasion by a space-occupying lesion
    - Mobility of the diaphragm
- Lung
  - Interstitial syndrome
  - *Benign peripheral lesions*:
    - Inflammation, abscess, embolism, atelectasis
  - *Malignant peripheral lesions*:
    - Peripheral metastasis, peripheral carcinoma, tumor/atelectasis
  - Mediastinum, percutaneous:
    - Space-occupying lesions in the upper anterior mediastinum
    - Lymph nodes in the aortopulmonary window
    - Suspected thrombosis in the vena cava and its afferent vessels
    - Visualization of collateral circulation
    - Pericardial effusion

Additional pathologies of the heart that can be visualized by ultrasonography will not be addressed in this book; for further information the reader may consult appropriate echocardiography textbooks.

1.2 Required Technical Equipment

Devices used for ultrasound investigation of the abdomen and the thyroid may also be used for investigation of the chest. A high-resolution linear transducer of 5–10 MHz is suitable for imaging the **chest wall** and the **parietal pleura** (Mathis 2004). Additionally, the recently introduced probes of 7.5–18 MHz are very useful for evaluating **lymph nodes** (Prosch et al. 2014), nerves (Winter et al. 2019) the **pleura**, and the **surface of the lung**.

A convex or sector probe of 3–4 MHz ensures sufficient depth of penetration for investigation of the **lung** (Mathis 2004).

Vector, sector or narrow convex probes are recommended for the **mediastinum**. The smaller the footprint, the better the probe can be placed on the jugulum or the supraclavicular fossa. The frequency range should be 3.5–5 MHz. It should be noted that the device settings commonly used for examining the heart are not suitable for the rest of the mediastinum. Contrast, image rates and the grayscale balance must be aligned to the visualization of mediastinal structures.

A special probe with an appropriate connecting channel to the ultrasound device is needed to perform a transesophageal ultrasound investigation.

Endobronchial ultrasonography is performed with special thin high-frequency probes (12–20 MHz) which are introduced through the working channel of the flexible bronchoscope.

1

1.3 Investigation Procedure

1.3.1 Chest Wall, Pleura, Diaphragm, Lung

The investigation should be performed, as far as possible, with the patient seated, during inspiration and expiration, and if necessary in combination with respiratory maneuvers such as coughing or "sniffing". Raising the arms and crossing them behind the head expands the intercostal spaces and facilitates the access. The transducer is moved from ventral to dorsal along the longitudinal lines in the chest (Fig. 1.3):

- the anterior median line
- the sternal line
- the parasternal line,
- the middle and lateral clavicular line,
- the anterior, middle and posterior axillary line,
- the lateral and medial scapular line, and
- the paravertebral line.
- the posterior median line

The respective anatomic location of the findings should be mentioned in the report.

Subsequent transverse transducer movement parallel to the ribs in the intercostal spaces (Fig. 1.4) provides the additional information needed for accurate localization of the respective finding.

The investigation of lesions behind the scapula should be performed under maximum adduction of the arm with encirclement of the contralateral shoulder (Fig. 1.5).

The supraclavicular access enables the investigator to view the apex of the lung (▶ Sect. 1.3.2).

From the suprasternal aspect one is able to inspect the upper anterior mediastinum (▶ Chap. 6). From the abdominal aspect one can investigate the diaphragm from the subcostal approach through the transhepatic route on the right side (Fig. 1.6), and to a limited extent from the trans-splenic route on the left side.

Additionally, the longitudinal acoustic plane from the flank shows both costodiaphragmatic recesses (Fig. 1.7b).

The supine patient is examined in the same manner. The abdominal access is better in this setting, but the intercostal view might be more difficult because the mobility of the pectoral girdle is limited.

In emergency situations the chest should be divided in four quadrants on each side. The transducer will be positioned in turn on each quadrant (Fig. 1.7a)

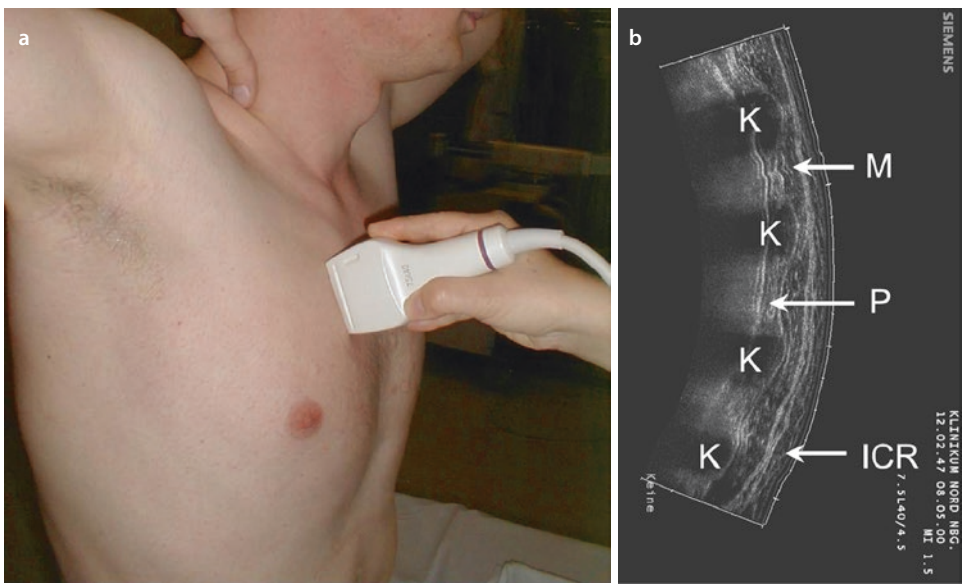

Fig. 1.3 **a, b** Investigation of the seated patient. **a** Linear probe placed longitudinally on the right parasternal line. **b** Corresponding longitudinal panoramic ultrasound image (SieScape). (*K* Cartilaginous insertion of a rib, *ICR* Intercostal space, *M* Muscle, *P* Pleural line)

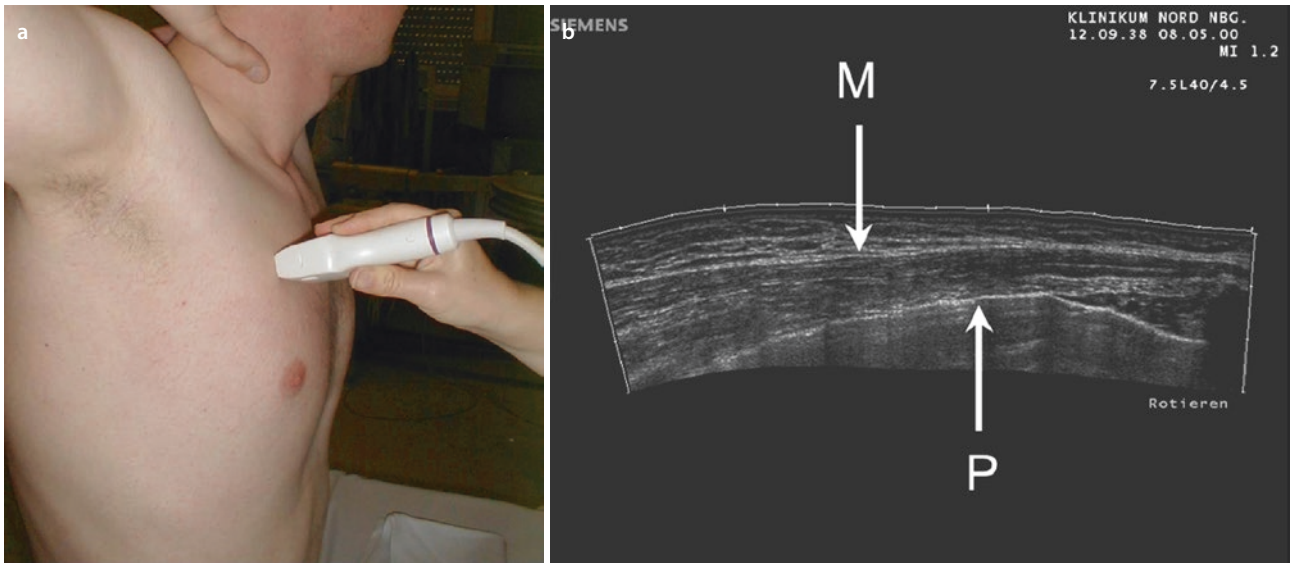

Fig. 1.4 **a, b** Investigation of the seated patient. **a** Linear probe placed parallel to the ribs in the 3rd intercostal space. **b** Corresponding transverse panoramic ultrasound image (SieScape). (*M* Muscle, *P* Pleural line)

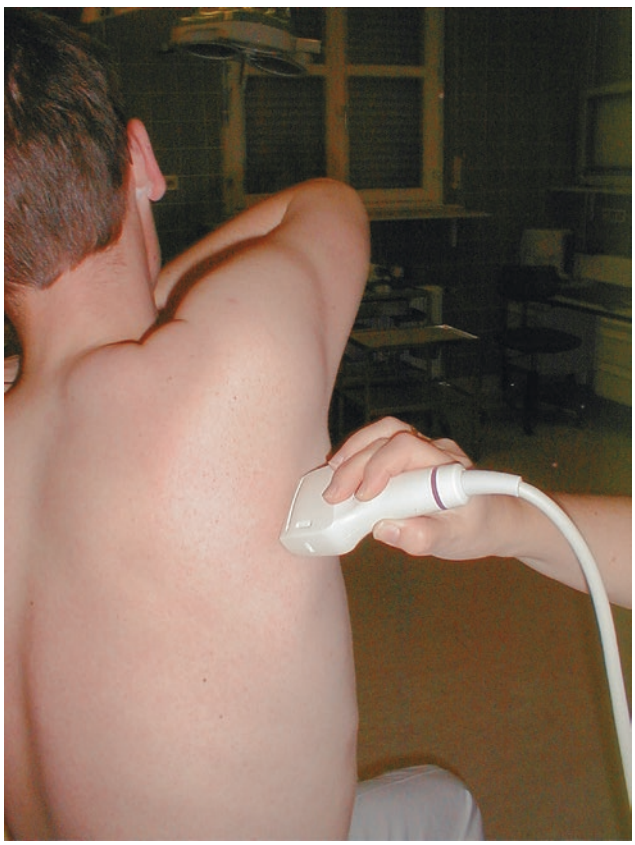

Fig. 1.5 Position of the patient for investigating retroscapular entities

1.3.2 Investigation of the Upper Thoracic Aperture

Special approaches are needed to investigate the upper thoracic aperture. The patient is required to lie flat for the investigation of cervical and supraclavicular lymph nodes, ideally with a hyperextended cervical spine (Prosch et al. 2014). The axillary region is investigated with the patient's arm in elevated position. High-resolution transducers of 5–18 MHz are used to view the structure of lymph nodes and the brachial plexus, including its branches. The thoracic aperture and the supraclavicular region should be investigated by ultrasound in cases of the following questions:

- Invasion of a Pancoast tumor
- Lymph node staging
- Trauma (parturition, accident)
- Puncture of the upper thoracic aperture
- Brachial plexus block (anesthesia)

The investigation is started at the base of the lateral cervical region (Fig. 1.8a, b).

The nerve branches pass through the gap between the anterior and middle scalene muscle, in lateral and downward direction. The branches reach the axilla by passing between the first rib and the clavicle. The course of the nerve branches along the axillary artery is registered by the infraclavicular approach (Fig. 1.9a–d).

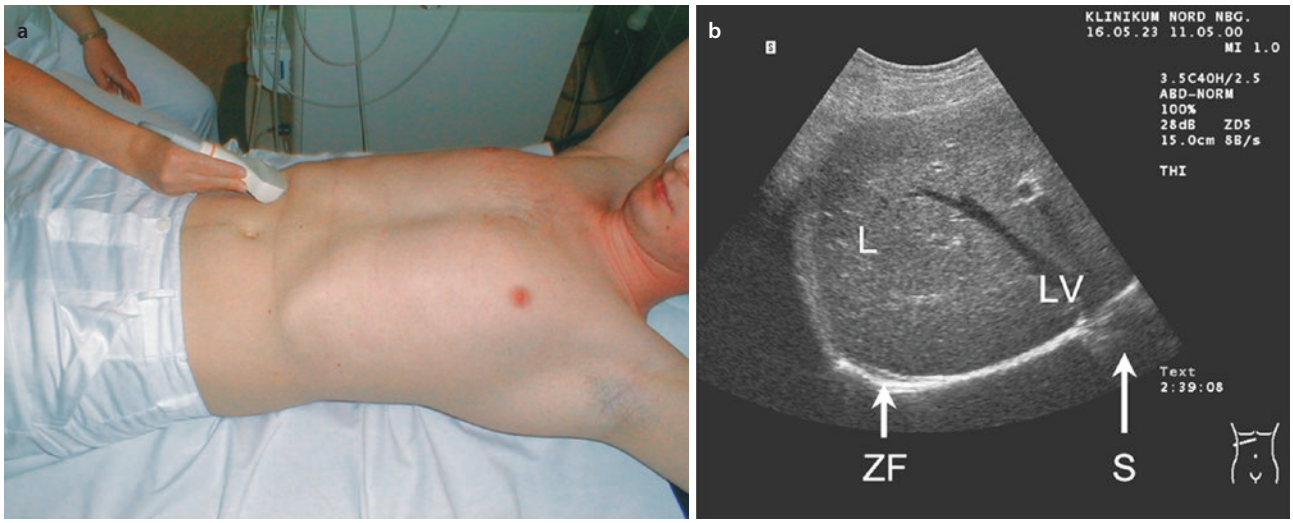

Fig. 1.6 **a, b** Transhepatic investigation. **a** Convex probe placed subcostally from the right side, tilted slightly in cranial direction. **b** Corresponding ultrasound image (*L* Liver, *LV* Hepatic vein, *S* Reflection of the liver above the diaphragm, *ZF* Diaphragm)

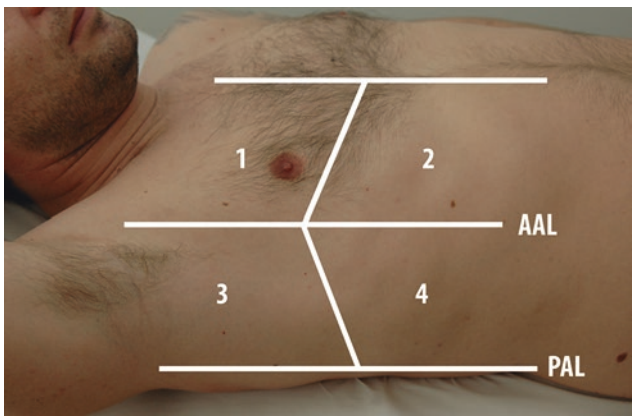

Fig. 1.7 **a** Investigation of the lying patient. a Division of chest in four quadrants in case of emergency examination. **b** Lateral aspect (*ZF* Diaphragm). A lung with normal mobility is shifted during inspiration into the costodiaphragmatic recess and obscures the upper margin of the liver

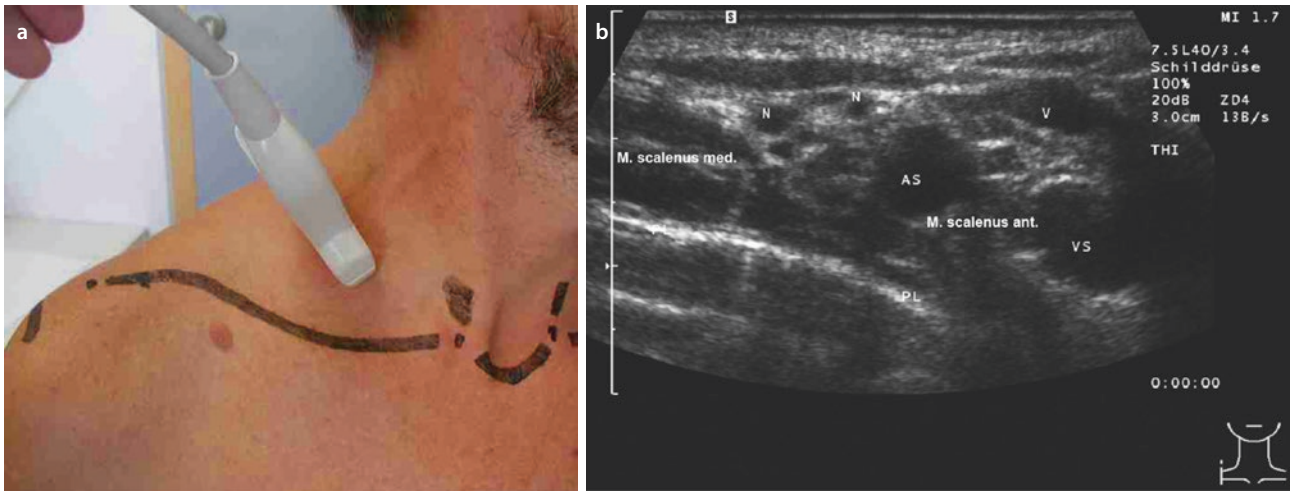

Fig. 1.8 **a, b** Investigation of the upper thoracic aperture. **a** Semisagittal longitudinal section at the base of the lateral cervical region. **b** Corresponding ultrasound image (*AS* Subclavian artery, *VS* Subclavian vein, *PL* Pleura, *N* Branches of the brachial plexus, *V* Innominate vein)

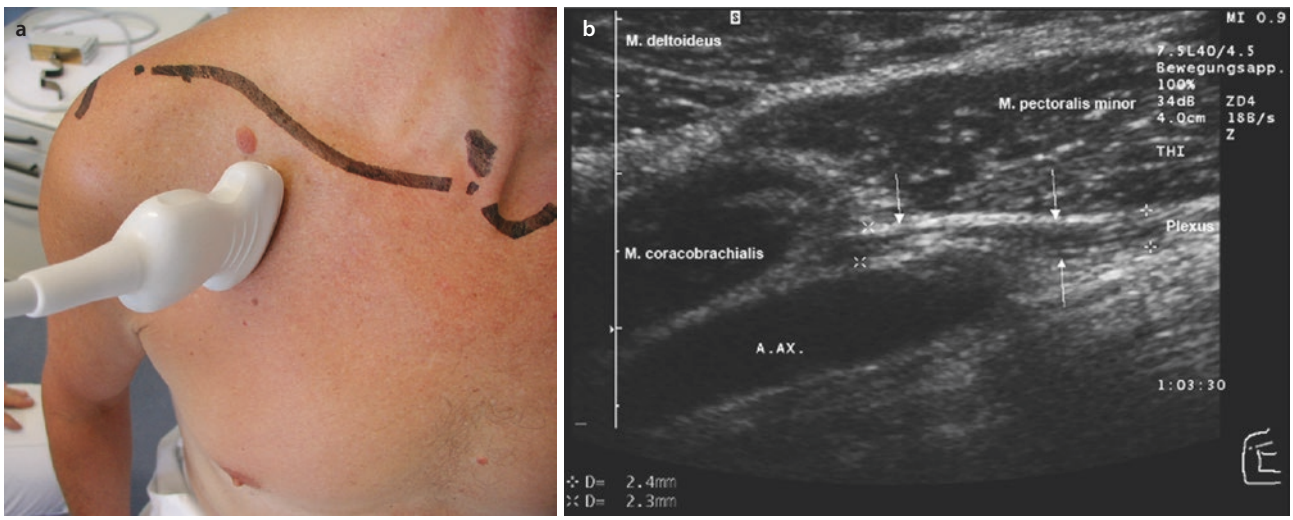

Fig. 1.9 **a–d**. **a** Oblique infraclavicular longitudinal section in the medioclavicular line. **b** Corresponding ultrasound image (*A.Ax.* Axillary artery). *Arrows* and *crosses* mark the course of the plexus nerve. **c** Infraclavicular cross-section parallel to the clavicle in the mid-clavicular line. **d** Corresponding ultrasound image. *Arrow* on the pleural line

1

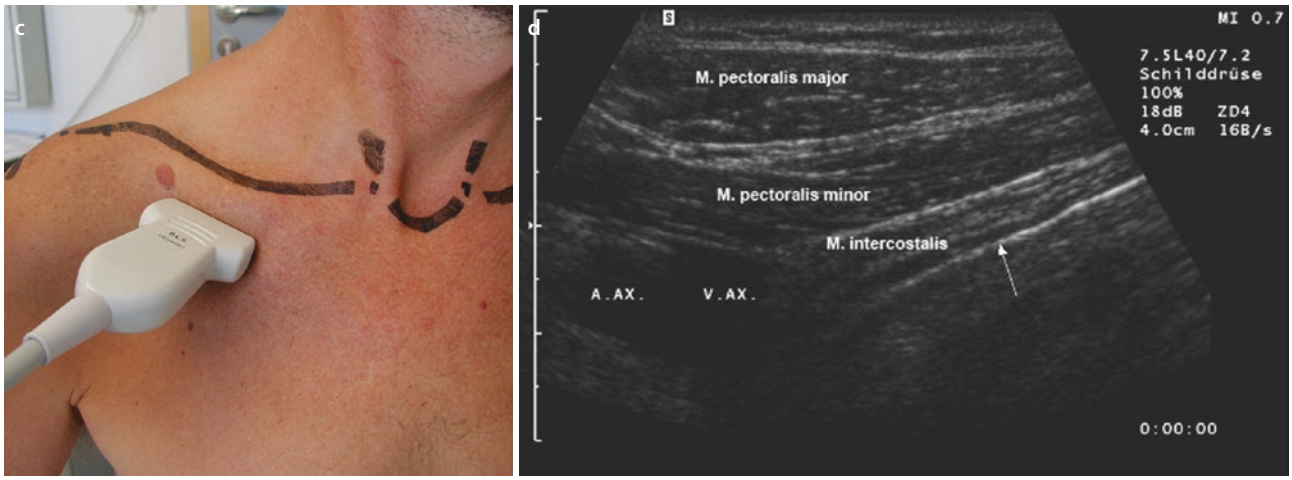

Fig. 1.9 (continued)

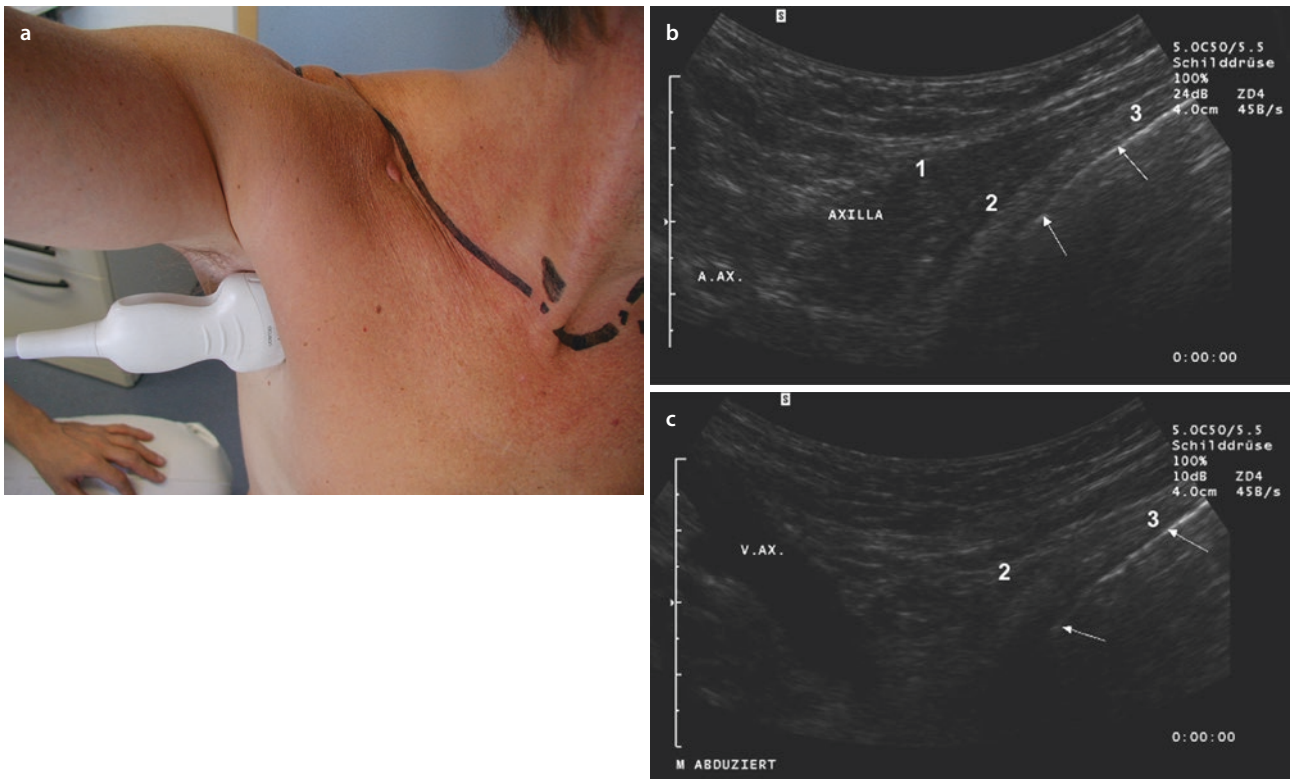

Fig. 1.10 **a** Transaxillary longitudinal section in the mid-axillary line. **b** Corresponding ultrasound image—dorsally tilted view. *1* Anterior serratus muscle, *2* Intercostal muscle, *3* Pleural line (*arrows*). **c** Corresponding ultrasound image—ventrally tilted view

The investigation is concluded by using the transaxillary approach (Fig. 1.10a–c).

With regard to transesophageal and transbronchial ultrasonography, please refer to the corresponding chapters.

Conclusion (See Abstract)

Thanks to excellent resolution and the possibility of dynamic investigation, ultrasonography provides crucial information in patients with chest disease. Entities of the chest wall and changes in pleura can

be visualized directly with ultrasound; pulmonary processes can be registered by ultrasound when they extend to the visceral pleura or when the ultrasonic wave is able to pass through a sound-conducting medium. The anterior portions of the mediastinum can be viewed percutaneously by the use of special sonic windows. To investigate the chest, one should use a combination of a linear transducer (5–7.5 MHz) for the near field and a convex or sector probe (3.5–5 MHz) for the deeper regions. High-resolution transducers of 5–18 MHz are needed to investigate the upper thoracic aperture and the supraclavicular region, in order to visualize the nerve branches of the brachial plexus and the structure of lymph nodes.

References

Aabakken L, Silvestri GA, Hawes R et al (1999) Cost-efficacy of endoscopic ultrasonography with fine-needle aspiration vs. mediastinotomy in patients with lung cancer and suspected mediastinal adenopathy. Endoscopy 31:707–711

Annema JT, van Meerbeck JP, Rintoul RC et al (2010) Mediastinoscopy versus endosonography for mediastinal nodal staging of lung cancer. A randomized trial. JAMA 304:2245–2252

Arbelot C, Ferrari F, Bouhemad B, Rouby JJ (2008) Lung ultrasound in acute respiratory distress syndrome and acute lung injury. Curr Opin Crit Care 14:70–74

AWMF Leitlinie (2015) Registernummer 065 – 002. S2-Leitlinie: Diagnostik und Therapie der Venenthrombose und der Lungenembolie.

AWMF Leitlinie (2018) Registernummer 020/007OL. S3-Leitlinie: Prävention, Diagnostik, Therapie und Nachsorge des Lungenkarzinoms

Bachmann Nielsen M, Cantisani V, Sidhu PS et al (2019) The use of handheld ultrasound devices—an EFSUMB position paper. Ultraschall Med 40:30–39. https://doi.org/10.1055/a-0783-2303

Bamber J, Cosgrove D, Dietrich CF (2013) EFSUMB guidelines and recommendations on the clinical use of ultrasound elastography. Part 1: Basic principles and technology. Ultraschall Med 34:169–184

Beaulieu Y, Marik PE (2005) Bedside ultrasonography in the ICU. Part 1, Part 2. Chest 128:1766–1781

Beckh S, Bölcskei PL, Lessnau KD (2002) Real-time chest ultrasonography. A comprehensive review for the pulmonologist. Chest 122:1759–1773

Blank W, Heinzmann A (2012) Thoraxsonographie im Notfall. Klinikarzt 41:28–32

Blank W, Mathis G, Osterwalder J (2019). Kursbuch Notfallsonografie. 2. Aufl. Stuttgart:Thieme 201

Böer J, Braun B, Heinzmann A (2014) Notfallsonographie an thorax und abdomen. In: Ultraschalldiagnostik- Lehrbuch und Atlas. EcomedMEDIZIN Heidelberg 65.ErgLfg, Kap. III-5, 1-8

Copetti R, Cattarossi L (2008) Ultrasound diagnosis of pneumonia in children. Radiol Med 113:190–198

Copetti R, Soldati G, Copetti P (2008) Chest sonography: a useful tool to differentiate acute cardiogenic pulmonary edema from acute respiratory distress syndrome. Cardiovasc Ultrasound 6:16

Cosgrove D, Piscaglia F, Bamber J et al (2013) EFSUMB guidelines and recommendations on the clinical use of ultrasound elastography. Part 2: clinical applications. Ultraschall Med 34:238–253

Dalhoff K, Abele-Horn M, Andreas S et al (2018) S 3 Leitlinie: Epidemiologie, Diagnostik und Therapie erwachsener Patienten mit nosokomialer Pneumonie—Update 2017. Pneumologie 72(01):15–63. https://doi.org/10.1055/s-0043-12173

Davidsen JR, Lawaetz Schultz HH, Henriksen DP et al (2020) Lung ultrasound in the assessment of pulmonary complications after lung transplantation. Ultraschall Med 41:148–156. https://doi.org/10.1055/a-0783-2466

Detterbeck FC, Zelman Lewis S, Diekemper R et al (2013) Executive summary. Diagnosis and management of lung cancer, 3rd ed: American College of Chest Physicians evidence-based clinical practice guidelines. Chest 143:7S–37S

Diacon AH, Theron J, Bolliger CT (2005) Transthoracic ultrasound for the pulmonologist. Curr Opin Pulm Med 11:307–312

Ewig S, Höffken G, Kern W et al (2016) S 3 Leitlinie: Behandlung von erwachsenen Patienten mit ambulant erworbener Pneumonie und Prävention—Update 2016. Pneumologie 70(03):151–200. https://doi.org/10.1055/s-0042-101873

Haas AR, Vachani A, Sterman DH (2010) Advanvces in diagnostic bronchoscopy. Am J Respir Crit Care Med 182:589–597

Havelock T, Teoh R, Laws D et al (2010) Pleural procedures and thoracic ultrasound: British Thoracic Society pleural disease guideline 2010. Thorax 65:ii61–ii76

Herth FJ, Becker HD, Eberhardt R (2004) Endobronchialer Ultraschall beim Bronchialkarzinom. Radiologe 44:457–464

Hooper C, Gary Lee YC, Maskell N (2010) Investigation of a unilateral pleural effusion in adults: British Thoracic Society pleural disease guideline 2010. Thorax 65:ii 4-ii 17

Kluge S, Janssens U, Welte T et al (2020) Empfehlungen zur intensivmedizinischen Therapie von Patienten mit COVID-19. Med Klin Intensivmed Notfmed 115:175–177. https://doi.org/10.1007/s00063-020-00674-3

Lam S, Becker HD (1996) Future diagnostic procedures. Chest Surg Clin N Am 6:363–380

Lesser TG (2017) Stellenwert der Thorax- und Lungensonografie in der Thoraxchirurgie. Ultraschall Med 38:592–610. https://doi.org/10.1055/s-0043-119873

Mathis G (2004) Thoraxsonography—Part I: chest wall and pleura. Praxis 93:615–621

Mathis G, Blank W, Reißig A et al (2005) Thoracic ultrasound for diagnosing pulmonary embolism. A prospective multicenter study of 352 patients. Chest 128:1531–1538

Mayo PH, Copetti R, Feller-Kopman D et al (2019) Thoracic ultrasonography: a narrative review. Intensive Care Med 45:1200–1211. https://doi.org/10.1007/s00134-019-05725-8

Moore CL, Copel JA (2011) Point-of-care ultrasonography. N Engl J Med 364:749–757

Niemann T, Egelhof T, Bongratz G (2009) Transthoracic sonography for the detection of pulmonary embolism—a meta- analysis. Ultraschall Med 30:150–156

Noble VE, Lamhaut L, Capp R et al (2009) Evaluation of a thoracic ultrasound training module for the detection of pneumothorax and pulmonary edema in the prehospital physician care providers. BMC Med Educ 9:3

Piscaglia F, NolsØe C, Dietrich CF et al (2012) The EFSUMB Guidelines and Recommendations on the Clinical Practice of Contrast Enhanced Ultrasound (CEUS): Update 2011 on non-hepatic applications. Ultraschall Med 32:33–59

Prosch H, Meng S, Bernathova M (2014) Supradiaphragmale Lymphknoten. In: Ultraschalldiagnostik—Lehrbuch und Atlas. EcomedMEDIZIN Heidelberg 63.Erg.Lfg. Kap III-1.6.2, 1–36

Reissig A, Copetti R, Mathis G et al (2012) Lung ultrasound in the diagnosis and follow-up of community- acquired pneumonia. A prospective multicenter diagnostic accuracy study. Chest 142:965–972

Reuß J (2010) Sonografie der Pleura. Ultraschall Med 31:8–25

Rose M, J. Liese, M. Barker et al. 2017. S2k—Leitlinie: Management der ambulant erworbenen Pneumonie bei Kindern und Jugendlichen. AWMF Registernummer 048-013

Silvestri GA, Gonzalez AV, Jantz MA et al (2013) Methods for staging non-small cell lung cancer. Diagnosis and management of lung cancer, 3rd ed: American College of Chest Physicians evidence-based clinical practice guidelines. Chest 143:e211S–e250S

Soldati G, Testa A, Silva F et al (2006) Chest ultrasonography in lung contusion. Chest 130:533–538

Soldati G, Smargiassi A, Inchingolo R et al (2020) Proposal for international standardization of the use of lung ultrasound for COVID-19 patients; a simple, quantitative, reproducible method. J Ultrasound Med 39:1413–1419

Squizzato A, Rancan E, Dentali F et al (2013) Diagnostic accuracy of lung ultrasound for pulmonary embolism: a systematic review and meta-analysis. J Thromb Haemost 11:1269–1278

Squizzato A, Galli L, Gerdes VEA (2015) Point-of-care Ultrasound in the diagnosis of pulmonary embolism. Crit Ultrasound J 7:7. https://doi.org/10.1186/s13089-015-0025-5

Stoelben E et al, 2018. S3-Leitlinie: Diagnostik und Therapie von Spontanpneumothorax und postinterventionellem pneumothorax. AWMF–Register Nr. 010–007

Volpicelli G, Elbarbary M, Blaivas M et al (2012) International evidence-based recommendations for point-of-care lung ultrasound. Intensive Care Med 38:577–591

von Bartheld MB, Dekkers OM, Szlubowski A et al (2013) Endosonography vs conventional bronchoscopy for the diagnosis of sarcoidosis: the GRANULOMA randomized clinical trial. JAMA 309:2457–2464

Walker CM, Chung JH, Abbott GF (2012) Mediastinal lymph node staging: from noninvasive to surgical. AJR 199:W54–W64

Winter N, Dammeier N, Schäffer E et al (2019) Nerve ultrasonography as an additive tool to clinical examination and electrodiagnostics in sporadic mononeuritis—imaging is the key. Ultraschall Med 40:465–472. https://doi.org/10.1055/a-0919-4768

Ultrasonography of the Chest Wall

Helmut Prosch

Contents

G. Mathis (ed.), *Chest Sonography*, https://doi.org/10.1007/978-3-031-09442-2_2

2

2.1 Introduction

Due to its rather superficial location, the chest wall is almost ideally suited for ultrasound investigation. The primary indications for performing an ultrasonography of the chest wall include the clarification of swelling or suspicious findings in the chest wall on palpation, and targeted investigation of painful sites in the chest wall (Abstract). Furthermore, ultrasonography of the chest wall plays an important role in performing biopsies and planning surgery for tumors of the chest wall or space-occupying lesions of the lung invading the chest wall . Last but not least, ultrasound plays an important role in the investigation of lymph nodes

Indications for an Ultrasound Investigation of the Chest Wall

- Swelling of the chest wall
- Pain
- Ambiguous findings on palpation
- Ambiguous findings on X-rays
- Chest trauma
- Tumor staging
- Intervention
- Follow-up, monitoring progress

2.2 Accumulation of Fluid

2.2.1 Hematomas

Depending on their red blood cell content and degree of organization, hematomas may cause a variety of echo patterns. Usually they are anechoic or hypoechoic (Fig. 2.1). Occasionally one finds subtle veil-like internal echoes. Intermediate forms may be seen in rare cases, which include more dense echoes in the internal spaces. Organized hematomas may be very inhomogeneous in terms of their echo pattern.

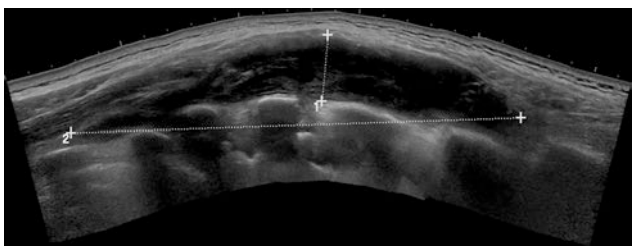

Fig. 2.1 Hematoma. Extensive hematoma of the dorsal portion of the chest wall after a fracture of the scapula and a serial rib fracture. Ultrasound investigation reveals an anechoic septated hematoma measuring 15 cm in length

2.2.2 Abscesses of the Chest Wall

Depending on their cell and protein content, a variety of internal structures may be found in an abscess cavity. Thus, the content of abscesses may be similar to that of hematomas. Quite often they cannot be delineated by ultrasound investigation alone, especially because there may be many intermediate stages such as infected hematomas. A major difference between abscesses and sterile hematomas is that abscesses tend to be accompanied by a capsule of differing shape, with floating internal structures (Fig. 2.2). In the majority of cases, clinical features such as reddening of the overlying skin clearly indicate the presence of an abscess.

2.2.3 Postoperative Seromas

Postoperative seromas are frequently observed after a muscle-sparing lateral thoracotomy. Postoperative seromas are largely anechoic, round or bizarre in shape, and do not have a capsule Lymphatic cysts have a similar structure and are mainly round or -oval. Occasionally the occluded lymphatic vessel can be visualized.

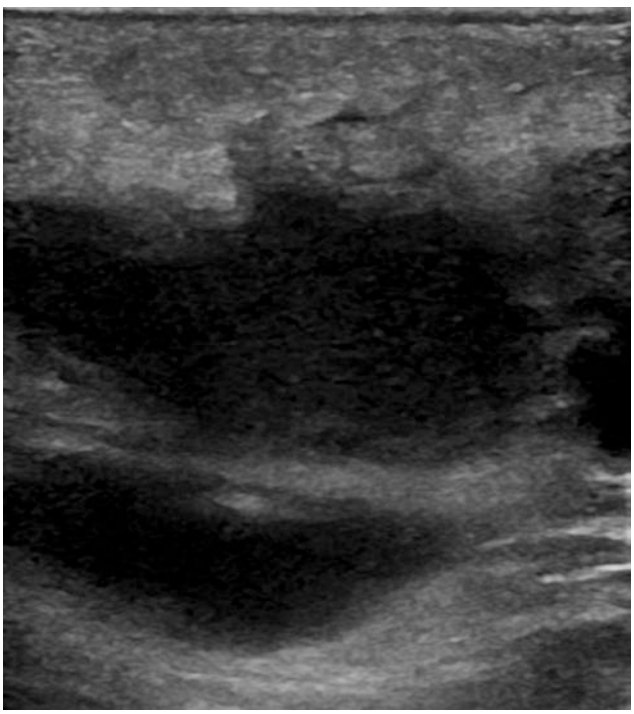

Fig. 2.2 A painful swelling in the right armpit raises suspicion of a sweat gland abscess. Ultrasonography reveals a largely anechoic space-occupying lesion measuring 3 x 1.5 cm in size. The moderately echogenic margin is indicative of an incipient capsule. The ultrasound-guided puncture reveals pus

2.3 Space-Occupying Lesions of the Chest Wall

Tumors of the chest wall are rather rare and usually benign. In most cases, the clinical symptoms alone permit conclusions about the benign or malignant nature of the lesion. Benign tumors are usually asymptomatic, grow slowly, and retain their tissue margins. In some tumors such as lipomas or fibromas, the combination of clinical symptoms and ultrasound features is so typical that a biopsy is not required. In contrast, malignant tumors grow rather rapidly, invasively, and are painful.

2.3.1 Lipoma and Fibroma

Lipomas are the most common tumors of the chest wall and are usually diagnosed by clinical investigation. 'The echogenicity of lipomas and fibromas depends on their cellular fat content, the quantity of connective tissue, and interstitial impedance differences. The texture may range from hypoechoic to relatively echodense (Fig. 2.3). Their demarcation from the environs may be blurred, and a capsule may develop.

2.3.2 Neurogenic Tumors

Neurogenic tumors such as schwannomas or neuromas are seen on ultrasound as oval hypoechoic lesions with sharp demarcations, and therefore do not differ significantly from space-occupying lesions of a different etiology. Evidence of the corresponding nerve is a diagnostic sign of a neurogenic tumor (Fig. 2.4).

2.3.3 Sarcoma and Soft Tissue Metastases

A major criterion of a malignant space-occupying lesion is the presence of invasive growth (Fig. 2.5). In terms of echotexture it is frequently hypoechoic, with inhomogeneous hyperechoic portions. The use of color-Doppler ultrasonography may be helpful in assessing hypoechoic structures suspected of being malignant. The suspicion of a malignant lesion may be confirmed by the type of vascularization and the course of vessels.

Knowledge of the pattern of vascularization is also very helpful in performing ultrasound-guided punctures. In this convenient location, which is usually very close to the transducer, an ultrasound-guided puncture is very useful because it provides material for histological investigation and subsequent confirmation of the diagnosis.

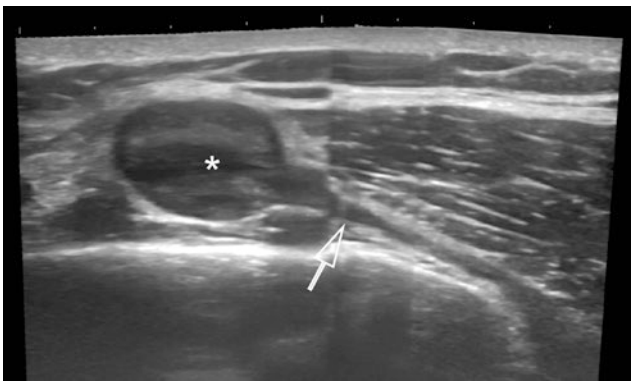

Fig. 2.4 Neurofibroma of the chest wall (*) in a patient with known neurofibromatosis. Evidence of the corresponding nerve is a diagnostic sign of a neurogenic tumor (*arrow*). Courtesy of Gerd Brodner, Medical University of Vienna

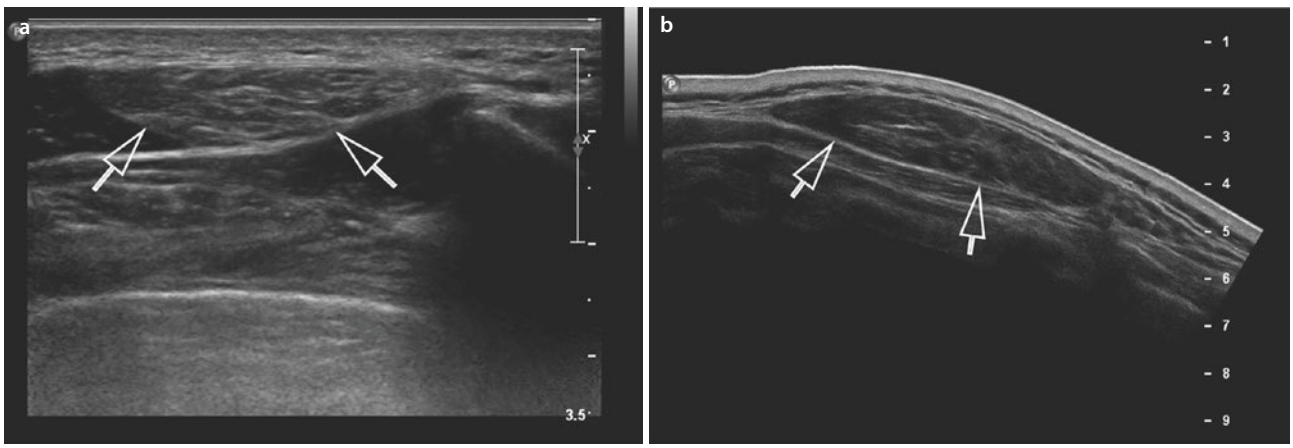

Fig. 2.3 **a**, **b** Lipomas of the chest wall: **a** Lipoma with a hyperechoic texture, **b** Lipoma with a hypoechoic texture

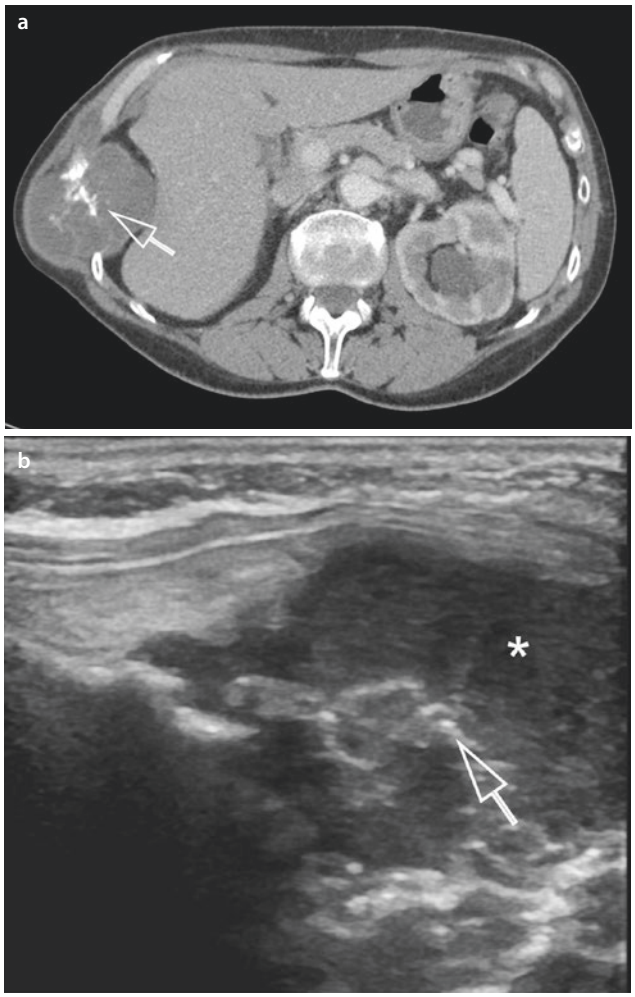

Fig. 2.5 **a**, **b** Chondrosarcoma of the chest wall **a** CT reveals an extensive space-occupying lesion with dense soft tissue and chondroid calcifications (*Arrow*). **b** Ultrasonography shows an inhomogeneous hypoechoic space-occupying lesion (*) with coarse cloddy calcifications (*Arrow*). An ultrasound-guided biopsy was able to confirm the suspected chondrosarcoma

The treatment of choice for a sarcoma is usually radical surgery. The resection margins and microscopic nodules can be determined better by performing a preoperative ultrasound investigation than by CT or MRT (Briccoli et al. 2007a, b). However, a preoperative CT and MRI are necessary to determine the intraosseous spread of the tumors, their depth, and exclude pulmonary metastases.

2.4 Lymph Nodes

Subcutaneous palpable swellings are usually caused by enlarged lymph nodes . The ultrasound morphology of lymph nodes is indicative of their etiology and permits a tentative assessment of the malignant or benign nature of the lesions in accordance with the patient's clinical condition (Table 2.1). High-frequency probes provide a highly differentiated B-mode image. The pattern of vascularization on color Doppler provide information about the type of lymph nodes. The possibility of assessing the malignant or benign nature of a lesion has certainly been improved by the better resolution of the B-mode image as well as the use of various Doppler procedures for the assessment of vascularization patterns (Ying et al. 2004).

However, the benign or malignant nature of a lesion can only be established tentatively by its ultrasound morphology. Confirmation of the diagnosis requires a histological investigation of tissue obtained by performing a puncture. Alternatively, the course of the disease will confirm the diagnosis. In clinical practice, changes in ultrasound morphology are especially significant. Thus, ultrasound follow-up investigations are useful to confirm the diagnosis of inflammatory disease and document the success of treatment in cases of malignant lymph nodes.

2.4.1 Inflammatory Lymph Nodes

Inflammatory lymph nodes are rarely larger than 20 mm in size. They usually have smooth margins, are oval, triangular, or longitudinal (Fig. 2.6). A typical feature of lymphadenitis is the presence of lymph nodes arranged like a pearl necklace along lymph node stations. In accordance with the anatomical structure, one frequently finds a more or less echogenic internal zone which is referred to as the hilar fat sign and corresponds to the fatty and connective tissue in the center of the lymph nodes. This sign is especially seen in healing inflammatory processes. The zone, with sharp edges as opposed to the surroundings, is hypoechoic. One commonly finds regular courses of vessels in this region on Doppler ultrasound. The lymph node hilum with the afferent and efferent vessels are also seen.

2.4.2 Tuberculosis

After the lung, lymph nodes are the second most common site of manifestation of tuberculosis (TB). Lymph node tuberculosis occurs in about 90%of patients without accompanying pulmonary tuberculosis.

On the B-mode ultrasonography image, lymph nodes are seen in various forms in the presence of tuberculosis. Some patients have rather sharply demarcated and sequentially arranged lymph nodes, whereas others have lymph nodes spreading into the environs diffusely or centrally fused hypoechoic lymph nodes with blurred margins, similar to metastases of solid tumors (Figs. 2.7 and 2.8). The pattern of vascularization of

Table 2.1 Ultrasound morphology of lymph nodes

	Inflammatory	Malignant lymphoma	Lymph node metastasis
Shape	Oval, longitudinal	Round, oval	Round
Edge	Smooth	Smooth	Irregular
Demarcation	Sharp	Sharp	Blurred
Growth	Pearl-necklace-like	Expansive, displacing	Invasive
Movability	Good	Good to moderate	Poor
Echogenicity	Hypoechoic margin, "hilar fat sign"	Hypoechoic, pseudocystic	Inhomogeneous, hypoechoic
Vascularization	Regular, central	Irregular	Corkscrew-like

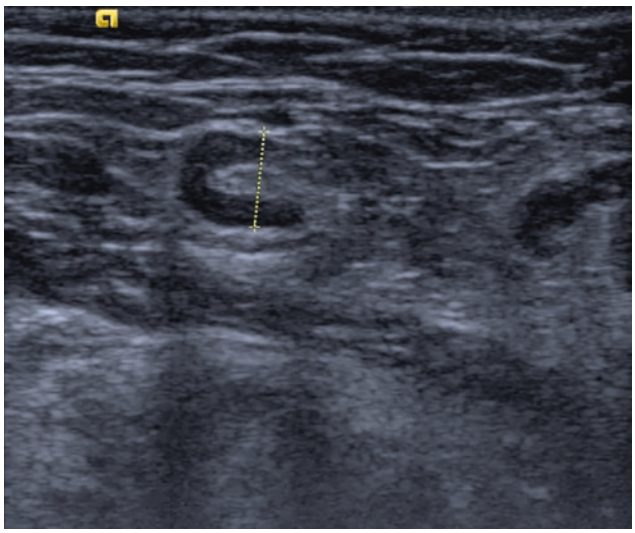

Fig. 2.6 Ultrasound image of a normal lymph node with a bean-shaped appearance, a hyperechoic hilum, and a hypoechoic cortex

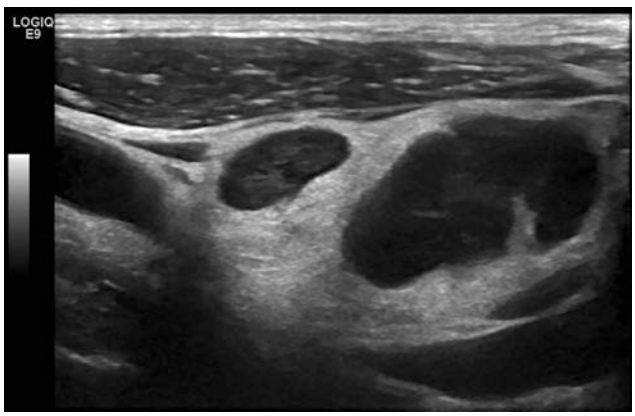

Fig. 2.7 Bean-shaped hypoechoic lymph nodes with sharp margins and a significant surrounding soft tissue edema

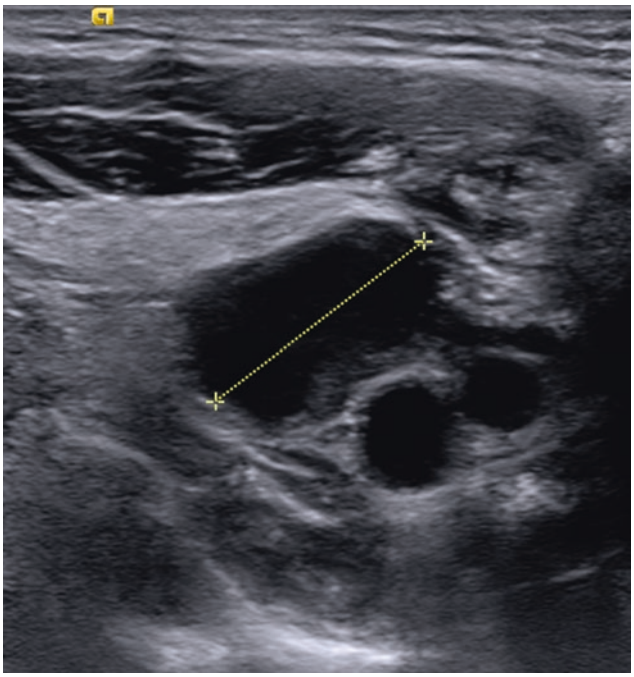

Fig. 2.8 Pseudocystic necrosis of a lymph node in the presence of lymph node tuberculosis

tuberculotic lymph nodes cannot be distinguished from that of lymph node metastases.

2.4.3 Malignant Lymphoma

On the B-mode ultrasound image, lymph nodes in the presence of lymphoma are usually round, hypoechoic, with sharp margins, without a hilum, and thus cannot be distinguished from lymph node metastases of solid tumors (Fig. 2.9). Markedly poor echogenicity of

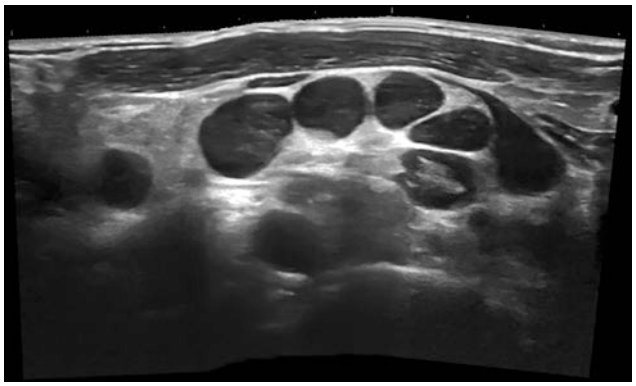

Fig. 2.9 Lymph nodes arranged sequentially in a cobblestone-like pattern, in a patient with a small-cell lymphocytic lymphoma. The lymph nodes are round, with sharp margins, hypoechoic, and without a hilum

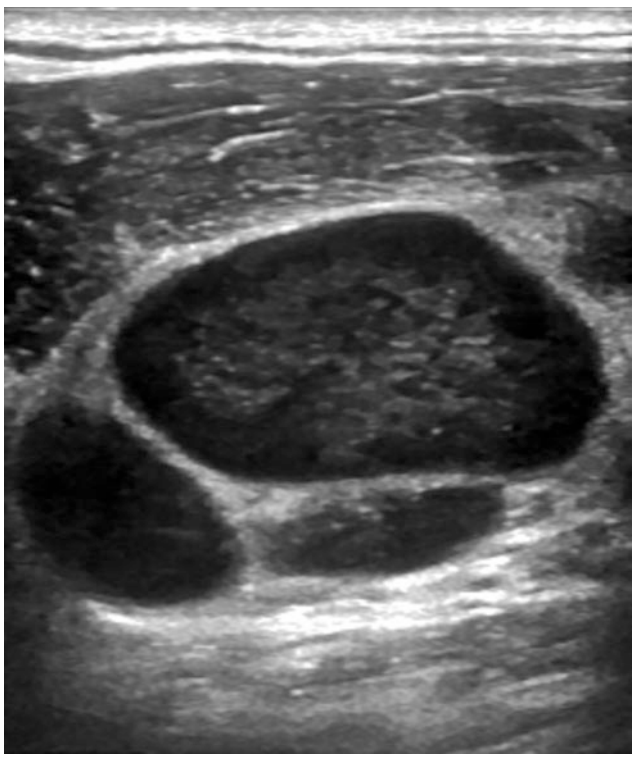

Fig. 2.10 Micronodular pattern of a lymph node in a patient with a small-cell lymphocytic lymphoma

the lymph node could be interpreted as sign of lymphoma. On older ultrasound devices the lymph nodes look almost like cysts. On modern ultrasound devices, high-resolution transducers usually show a micronodular reticular internal echo (Fig. 2.10) (Ahuja et al. 2001). Lymph nodes arranged bilaterally around a vessel ("sandwich-like") may be interpreted as a sign of a malignant lymphoma. The vascularization of malignant lymphomas may be regularly enhanced or even irregular at the edges.

2.4.4 Lymph Node Metastases

On the B-mode ultrasonography image, round lymph nodes and the loss of the hyperechoic hilum are signs of lymph node metastases (Fig. 2.11). The demarcation is frequently blurred. Aggressive growth in terms of the invasion of muscles and vessels may be observed. Lymph node metastases are usually irregularly hypoechoic. Lymph node metastases of papillary thyroid carcinomas may be hyperechoic due to thyroglobulin deposits (Esen 2006). Size is an unreliable criterion of malignancy. In supraclavicular lymph nodes, a transverse diameter of 5 mm or more is considered pathological. Occasionally one also finds reactive lymph nodes in the vicinity of metastatic lymph nodes. The pattern of vascularization of lymph node metastases is very characteristic: vessels tend to be located at the edges, are distributed unevenly, follow a chaotic route, flow in various directions, and show changes in color (Tschammler et al. 2002).

Non-palpable lymph node metastases can be seen on ultrasound. Therefore, in the presence of breast cancer an ultrasound investigation of the axilla is recommended in preoperative staging and when monitoring the progress of disease (Ciatto et al. 2007; Krishnamurthy et al. 2002; Johnson et al. 2011).

An ultrasound investigation of the supraclavicular region is especially important in staging bronchial carcinoma because enlarged and usually non-palpable supraclavicular lymph nodes are found in as many as 51% of patients with mediastinal N3 lymph nodes (Prosch et al. 2007a, b; van Overhagen et al. 2004). An inoperable tumor stage (III B) can be demonstrated with minimal

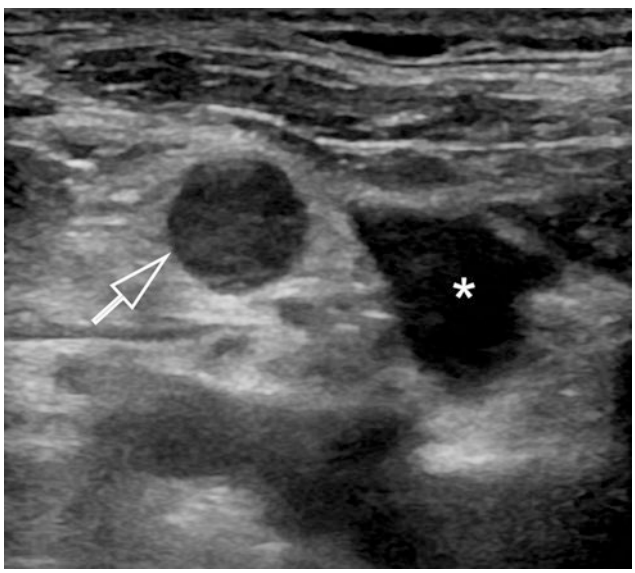

Fig. 2.11 Lymph node metastasis of a supraclavicular lymph node *(arrow)* immediately adjacent to the jugular vein *(*)*. On ultrasound the lymph node has rounded contours and no fatty hilum

risk, at a low cost, by performing an ultrasound-guided biopsy of the lymph nodes (Figs. 2.12, 2.13, and 2.14).

The change in the size of lymph node metastases is a useful parameter of its progress. Despite the fact that the patient responds to chemotherapy or radiotherapy, reactive lymph nodes may persist.

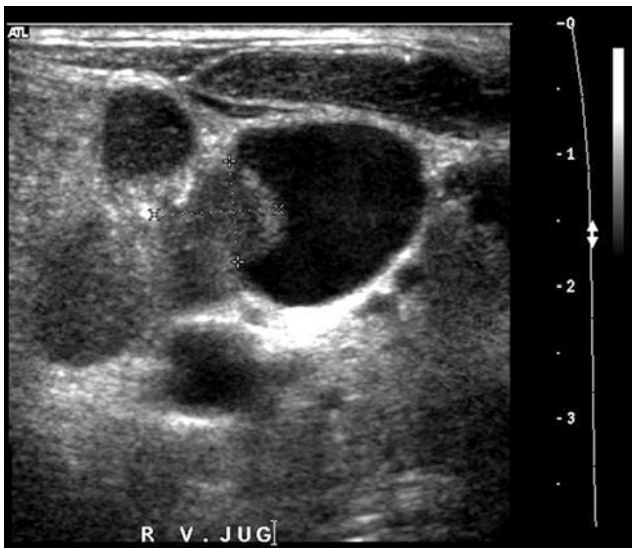

Fig. 2.12 Supraclavicular lymph node metastasis of a squamous cell carcinoma of the lung with disruption of the capsule and invasion into the adjacent jugular vein

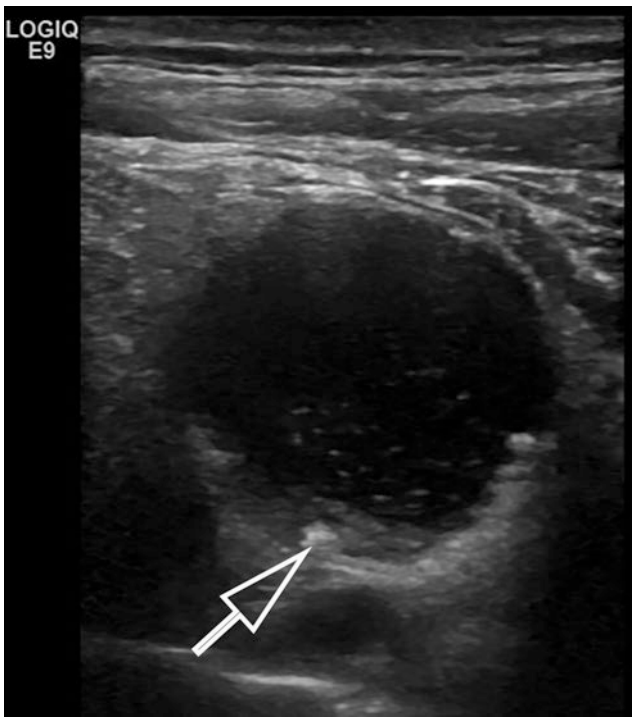

Fig. 2.13 Supraclavicular lymph node metastasis of an ovarian carcinoma. The lymph node is seen on ultrasound as a nearly anechoic (cystic) rounded lesion with sharp margins and calcified edges (*arrow*)

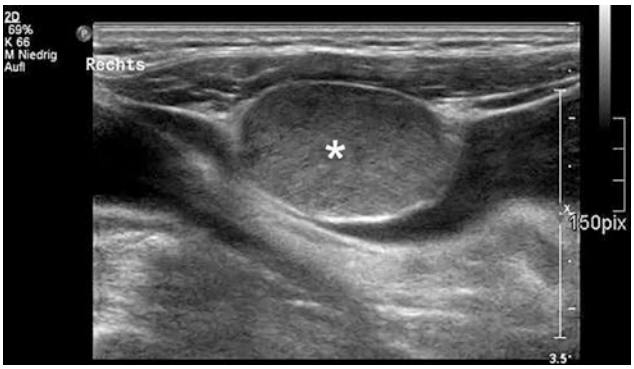

Fig. 2.14 Supraclavicular lymph node metastasis of an adenocarcinoma of the lung. On high-resolution ultrasound it is seen as a largely homogenous hyperechoic oval lymph node with sharp margins and without a hyperechoic hilum (*)

2.5 Bony Thorax

2.5.1 Fractures of the Ribs and the Sternum

Non-displaced rib fractures may be difficult to diagnose in clinical routine because rib fractures frequently escape detection even on targeted X-rays of the ribs. However, timely detection of a rib fracture is important for early initiation of appropriate pain treatment on the one hand, and for differential diagnosis on the other. A number of studies performed in the last few decades have shown that rib fractures are demonstrated with much greater sensitivity by a targeted ultrasound investigation than by an X-ray of the ribs (Bitschnau et al. 1997; Griffith et al. 1999a, b; Turk et al. 2010; Battle et al. 2019). In 19 of 20 patients with no rib fractures on conventional X-rays, Turk et al. found rib fractures in the ultrasound investigation (Turk et al. 2010.

By performing a targeted investigation at the site of pain, a rib fracture can be detected quite rapidly even by an inexperienced investigator. In contrast, the diagnostic reliability of ultrasonography in demonstrating fractures of the sternum is poor.

Criteria of a fracture on ultrasound investigation include direct evidence of a fracture gap or a cortical step (Fig. 2.15). In cases of a very narrow fracture gap (more marrow than the lateral resolution capacity of ultrasound), the fracture may be demonstrated indirectly by the evidence of reverberation echoes or the so-called chimney phenomenon “. These reverberation artefacts arise at the boundaries of fracture fragments and extend vertically into the deeper aspect. In non-displaced fractures, the chimney phenomenon can be triggered by gentle pressure on the point of pain. Some patients have a circumscribed hematoma , which is an indirect sign of a fracture.

Demonstration or exclusion of concomitant injuries like a pneumothorax, a hemothorax , a lung contusion, or injuries to the organs of the upper abdomen are clinically more important than the detection of rib fractures. In clinically stable patients, the rib fracture itself *and* the concomitant injuries can be clarified by performing an ultrasound investigation (Wüstner et al. 2005).

The narrow gap between the osseous cartilaginous portion of the rib and the primary bony rib, a regular phenomenon in elderly patients, may lead to the false-positive diagnosis of a rib fracture (Fig. 2.16).

Anatomical conditions and normal variants should be considered when assessing the sternum as well, in order to rule out the risk of false-positive diagnoses. The normal discrete cortical interruption in the synchondrosis between the corpus and the manubrium should not be mistaken for a fracture. Various forms of missing fusion or bone appositions that may occur in rare cases should also be taken into account (Chan 2009; Hyacinthe et al. 2012).

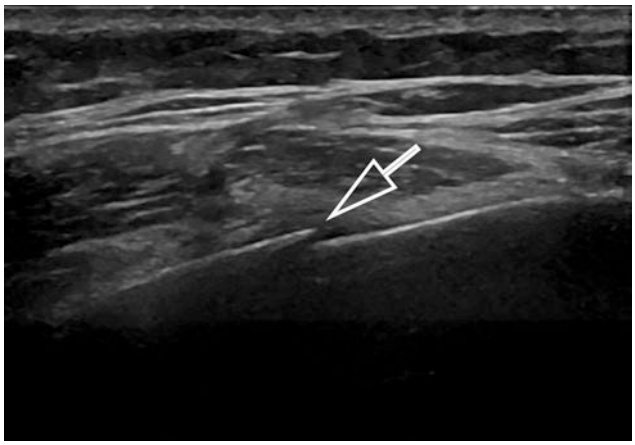

Fig. 2.15 Rib fracture with a cortical step directly at the site of pain

In clinical monitoring one first finds a local hematoma as a hypoechoic/anechoic edge in the region of the fracture gap. The subsequent formation of callus is marked by incipient organization and consolidation. The beginning calcification causes fine acoustic shadows or even complete ossification. Once this has been concluded, all that remains is a forward hump of the continuous and strong cortical reflex (Fig. 2.17). Disrupted healing can be easily established by the absence of continuous ossification. Consolidation starts from the 3rd to 4th week after an injury; in normal cases complete restitution is achieved after a few months (Friedrich and Volkenstein 1994).

2.5.2 Osteolytic Metastases

An osteolysis is usually a tumor metastasis. A notable aspect of an osteolysis is an interrupted and destroyed cortical reflex with pathological echo transmission. Osteolytic metastases are usually well demarcated, round or oval space-occupying lesions, partly hypoechoic, and of gross echostructure. Color-coded duplex ultrasonography demonstrates corkscrew-like newly formed vessels. In tumor staging, ultrasound is a reliable procedure to differentiate rib fractures from bone metastases (Paik et al. 2005). In cases of doubt, an ultrasound-guided biopsy can be used at minimal risk for histological investigation and confirmation.

During ongoing treatment, osteolysis in the bony portion of the chest serves as a progress parameter in the presence of multiple myeloma, small-cell bronchial carcinoma, prostate or breast carcinoma. An increase or decrease in size on the one hand, and a change in internal structures in terms of ultrasound morphology on the other, can be compared and documented. Recalcification under treatment is seen earlier on ultrasonography than on X-rays.

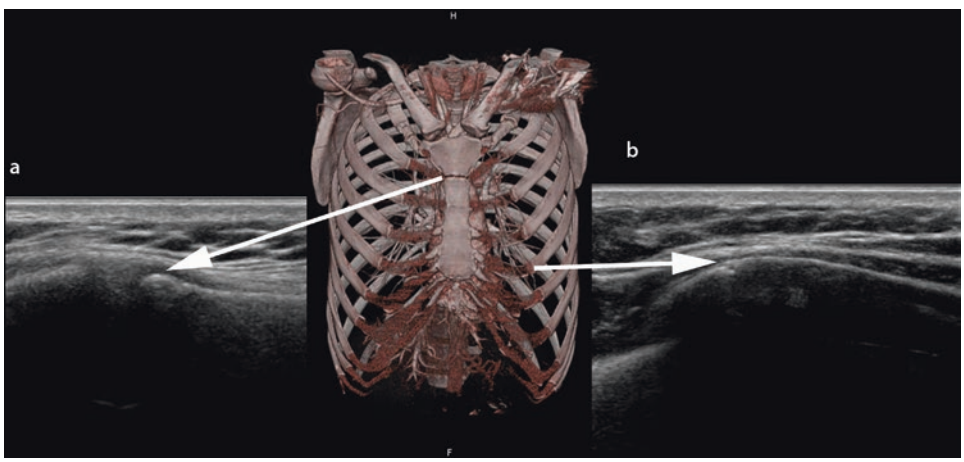

Fig. 2.16 Potential reasons for a false-positive diagnosis of a rib fracture on ultrasound investigation. **a** Cortical interruption in the region of the synchondrosis between the corpus and the manubrium. **b** Gap between the osseous cartilaginous portion of the rib and the primary osseous rib

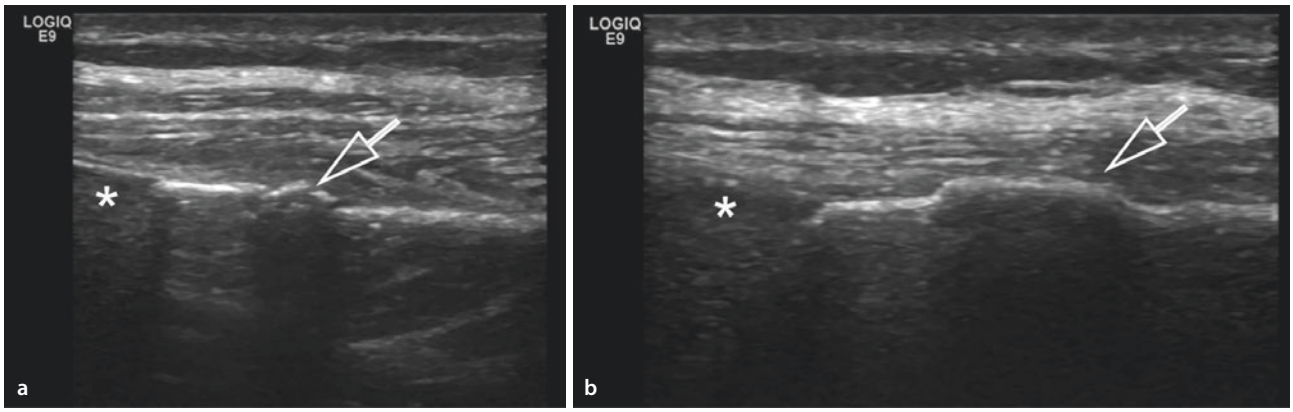

Fig. 2.17 **a**, **b** Fracture **a** A recent fracture (*arrow*) of a rib in the ventral portion of the costal arch, close to the cartilaginous part (*). **b** Complete healing and a minimal hump: a residual finding after 3 months (*arrow*)

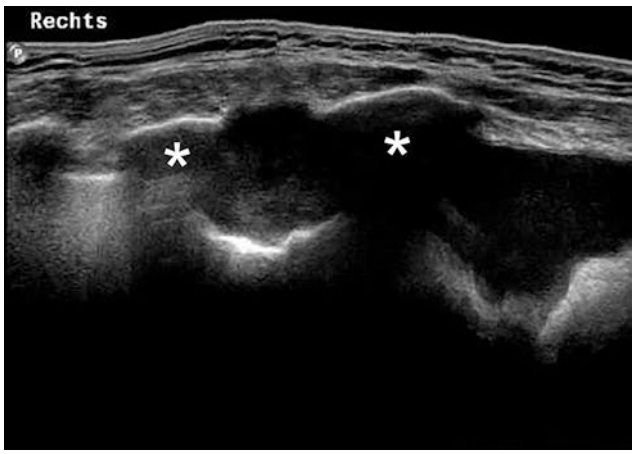

Fig. 2.18 Panoramic view of a lung carcinoma invading the chest wall (arrow) between two ribs (*)

Cave

The staging of bone metastases cannot be performed by ultrasonography. It would be meaningful to examine the sites of positive scintigraphy findings, palpable swellings, and painful sites.

2.5.3 Invasion of the Chest Wall by Bronchial Carcinoma

Percutaneous ultrasonography is especially informative for the assessment of an invasion of the chest wall by a lung carcinoma. According to the TNM staging system, an invasion of the chest wall is defined as a T3 tumor and is found in 6% of patients at the time of diagnosis (Mountain 1997; Facciolo et al. 2001). Invasion of the chest wall as such is no exclusion criterion for curative resection of the tumor but is of crucial importance for the surgical procedure because parts of the chest wall also must be resected in these cases (Fig. 2.18).

Owing to its high spatial resolution, ultrasonography is markedly superior to CT for evaluating an invasion of the chest wall (sensitivity 89–100 % versus 42–68 %) (Bandi et al. 2007; Suzuki et al. 1993). Reliable signs of invasion include direct evidence of tumor spread into the chest wall or rib destruction (cf. Overview, Fig. 2.19) (Bandi et al. 2007). Widening of the pleura and/or limited respiratory motion of the tumor are interpreted as indirect signs because an inflammatory reaction of tissue surrounding a tumor may also cause both of these changes.

Signs of Invasion of the Chest Wall

Reliable signs

- Direct evidence of chest wall invasion
- Rib destruction

Additional signs

- Pleural thickening
- Limited respiratory motion

Preoperative clarification of an invasion of the chest wall is especially significant in tumors that invade the chest wall at the apex of the lung; these are referred to as Pancoast tumors. ‘According to the TNM staging system, Pancoast tumors are T3 tumors as long as they do not invade the mediastinum, a vertebral body, the subclavian artery or vein, the C8 nerve root or higher (Detterbeck et al. 2013a, b). The imaging procedure of choice for the investigation of a Pancoast tumor is an MRI scan. In patients who cannot be investigated by MRI due to contraindications, invasion of the nerve roots or the plexus can be determined by a targeted ultrasound investigation (Fig. 2.20).

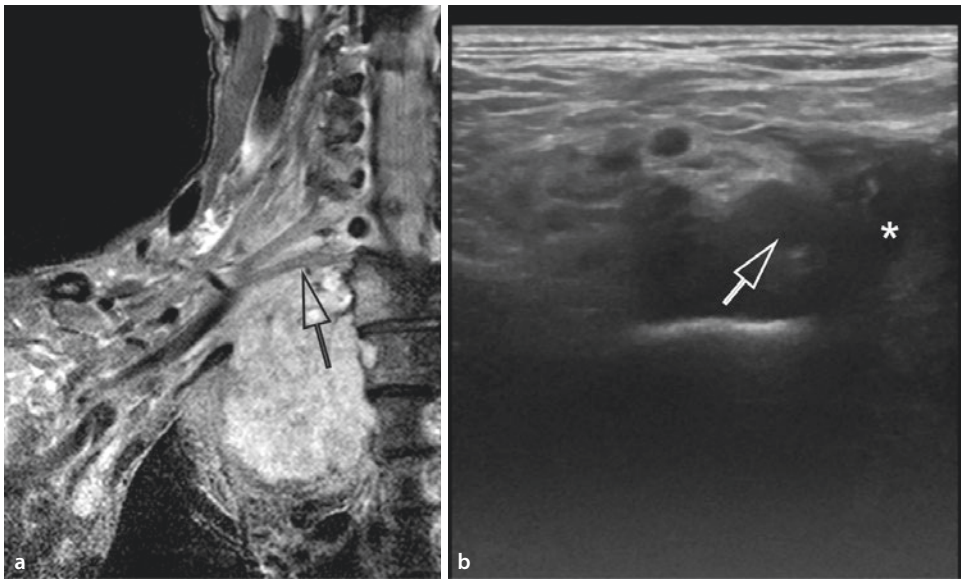

Fig. 2.19 **a**, **b** Pancoast tumor on the right side **a** MRI (coronal T2 STIR) shows an extensive tumor growing around the C8 nerve root and touching the C7 root. **b** High-resolution ultrasound. The C8 nerve root (*arrow*) in the efferent portion is entirely ensheathed by the tumor (*) and swollen

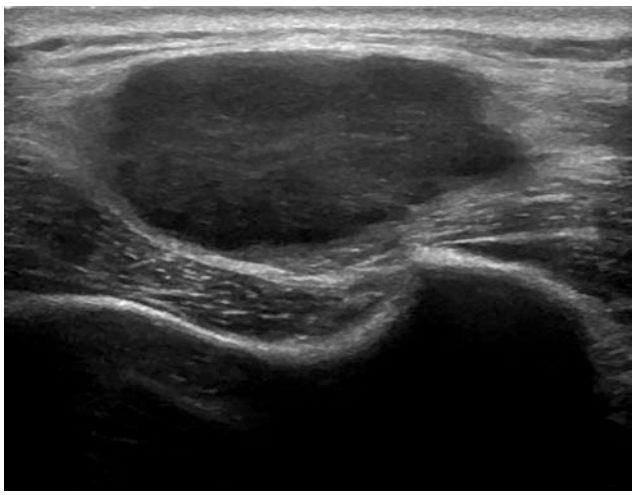

Fig. 2.20 Soft tissue metastasis of a squamous cell carcinoma. On ultrasound the metastasis is seen as a hypoechoic space-occupying lesion with partly sharp and partly blurred margins

Conclusion

Fractures of the ribs as well as the sternum are seen well on ultrasound. Fracture diagnosis based on ultrasound is not only more sensitive than conventional X-rays, but also provides reliable and rapid views of soft tissue lesions, hematomas and pleural effusions.

The visualization of lymph nodes and a tentative assessment of the malignant or benign nature of a lesion are important indications to perform an ultrasound investigation of the chest wall. In case a puncture needs to be performed for the purpose of treatment, all ambiguous lesions of the chest wall can be easily accessed for an ultrasound-guided puncture and subsequent histological confirmation of the diagnosis. The risk associated with puncture are very low because of the convenient location of the lesions. When the malignant nature of a chest wall lesion has been proven, its progress under treatment can be monitored by ultrasonography.

References

Ahuja AT, Ying M, Yuen HY, Metreweli C (2001) "Pseudocystic" appearance of non-Hodgkin's lymphomatous nodes: an infrequent finding with high-resolution transducers. Clin Radiol 56(2):111–115. https://doi.org/10.1053/crad.2000.0642

Bandi V, Lunn W, Ernst A, Eberhardt R, Hoffmann H, Herth FJ (2007) Ultrasound vs. computed tomography in detecting chest wall invasion by tumor: a prospective study. Chest. https://doi.org/10.1378/chest.07-1656

Battle C, Hayward S, Eggert S, Evans PA (2019) Comparison of the use of lung ultrasound and chest radiography in the diagnosis of rib fractures: a systematic review. Emerg Med J 36(3):185–190. https://doi.org/10.1136/emermed-2017-207416

Bitschnau R, Gehmacher O, Kopf A, Scheier A, Mathis G (1997) Ultraschalldiagnostik von Rippen- und Sternumfrakturen. Ultraschall Med 18(4):158–161

Briccoli A, Galletti S, Salone M, Morganti A, Pelotti P, Rocca M (2007a) Ultrasonography is superior to computed tomography and magnetic resonance imaging in determining superficial resection margins of malignant chest wall tumors. JUM J Ultrasound Med 26(2):157–162

Briccoli A, Galletti S, Salone M, Morganti A, Pelotti P, Rocca M (2007b) Ultrasonography is superior to computed tomography and magnetic resonance imaging in determining superficial resection margins of malignant chest wall tumors. J Ultrasound Med 26(2):157–162

Chan SS (2009) Emergency bedside ultrasound for the diagnosis of rib fractures. Am J Emerg Med 27(5):617–620. https://doi.org/10.1016/j.ajem.2008.04.013

Ciatto S, Brancato B, Risso G, Ambrogetti D, Bulgaresi P, Maddau C, Turco P, Houssami N (2007) Accuracy of fine needle aspiration cytology (FNAC) of axillary lymph nodes as a triage test in breast cancer staging. Breast Cancer Res Treat 103(1):85–91. https://doi.org/10.1007/s10549-006-9355-0

Detterbeck FC, Postmus PE, Tanoue LT (2013a) The stage classification of lung cancer: diagnosis and management of lung cancer, 3 Aufl. American college of chest physicians evidence-based clinical practice guidelines. Chest J 143(Suppl. 5):e191S–e210S. https://doi.org/10.1378/chest.12-2354

Detterbeck FC, Postmus PE, Tanoue LT (2013b) The stage classification of lung cancer: diagnosis and management of lung cancer, 3rd ed.: American College of chest physicians evidence-based clinical practice guidelines. Chest J 143(Suppl. 5):e191S–e210S. https://doi.org/10.1378/chest.12-2354

Esen G (2006) Ultrasound of superficial lymph nodes. Eur J Radiol 58(3):345–359. https://doi.org/10.1016/j.ejrad.2005.12.039

Facciolo F, Cardillo G, Lopergolo M, Pallone G, Sera F, Martelli M (2001) Chest wall invasion in non-small cell lung carcinoma: a rationale for en bloc resection. J Thorac Cardiovasc Surg 121(4):649–656. https://doi.org/10.1067/mtc.2001.112826

Friedrich RE, Volkenstein RJ (1994) Diagnose und Repositionskontrolle von Jochbogenfrakturen. Ultraschall Med 15(4):213–216. https://doi.org/10.1055/s-2007-1003967

Griffith JF, Rainer TH, Ching ASC, Law KC, Cocks RA, Metreweli C (1999a) Sonography compared with radiography in revealing acute rib fracture. AJR Am J Roentgenol 173(6):1603–1609

Griffith JF, Rainer TH, Ching ASC, Law KL, Cocks RA, Metreweli C (1999b) Sonography compared with radiography in revealing acute rib fracture. Am J Roentgenol 173(6):1603–1609

Hyacinthe AC, Broux C, Francony G, Genty C, Bouzat P, Jacquot C, Albaladejo P, Ferretti GR, Bosson JL, Payen JF (2012) Diagnostic accuracy of ultrasonography in the acute assessment of common thoracic lesions after trauma. Chest 141(5):1177–1183. https://doi.org/10.1378/chest.11-0208

Johnson S, Brown S, Porter G, Steel J, Paisley K, Watkins R, Holgate C (2011) Staging primary breast cancer. Are there tumour pathological features that correlate with a false-negative axillary ultrasound? Clin Radiol 66(6):497–499. https://doi.org/10.1016/j.crad.2010.11.015

Krishnamurthy S, Sneige N, Bedi DG, Edieken BS, Fornage BD, Kuerer HM, Singletary SE, Hunt KK (2002) Role of ultrasound-guided fine-needle aspiration of indeterminate and suspicious axillary lymph nodes in the initial staging of breast carcinoma. Cancer 95(5):982–988. https://doi.org/10.1002/cncr.10786

Mountain CF (1997) Revisions in the international system for staging lung cancer. Chest 111(6):1710–1717

Paik SH, Chung MJ, Park JS, Goo JM, Im JG (2005) High-resolution sonography of the rib: can fracture and metastasis be differentiated? AJR Am J Roentgenol 184(3):969–974. https://doi.org/10.2214/ajr.184.3.01840969

Prosch H, Strasser G, Sonka S, Oschatz E, Mashaal S, Mohn-Staudner A, Mostbeck GH (2007a) Cervical ultrasound (US) and US-guided lymph node biopsy as a routine procedure for a staging of lung cancer. Ultraschall Med 28(6):598–603. https://doi.org/10.1055/s-2007-963215

Prosch H, Strasser G, Sonka C, Oschatz E, Mashaal S, Mohn-Staudner A, Mostbeck GH (2007b) Cervical ultrasound (US) and US-guided lymph node biopsy as a routine procedure for a staging of lung cancer. Ultraschall in Der Medizin 28(6):598–603. https://doi.org/10.1055/s-2007-963215

Suzuki N, Saitoh T, Kitamura S (1993) Tumor invasion of the chest wall in lung cancer: diagnosis with US. Radiology 187(1):39–42

Tschammler A, Beer M, Hahn D (2002) Differential diagnosis of lymphadenopathy: power Doppler vs color Doppler sonography. Eur Radiol 12(7):1794–1799

Turk F, Kurt AB, Saglam S (2010) Evaluation by ultrasound of traumatic rib fractures missed by radiography. Emerg Radiol 17(6):473–477. https://doi.org/10.1007/s10140-010-0892-9

van Overhagen H, Brakel K, Heijenbrok MW, van Kasteren JH, van de Moosdijk CN, Roldaan AC, van Gils AP, Hansen BE (2004) Metastases in supraclavicular lymph nodes in lung cancer: assessment with palpation, US, and CT. Radiology 232(1):75–80

Wüstner A, Gehmacher O, Hammerle S, Schenkenbach C, Hafele H, Mathis G (2005) Ultraschalldiagnostik bei stumpfen Thoraxtrauma. Ultraschall Med 26(4):285–290. https://doi.org/10.1055/s-2005-858524

Ying M, Ahuja A, Brook F (2004) Accuracy of sonographic vascular features in differentiating different causes of cervical lymphadenopathy. Ultrasound Med Biol 30(4):441–447. https://doi.org/10.1016/j.ultrasmedbio.2003.12.009

Pleura

Joachim Reuß and Alexander Heinzmann

Contents

G. Mathis (ed.), *Chest Sonography*, https://doi.org/10.1007/978-3-031-09442-2_3

3

In the normal thorax the transthoracic sonographic view reaches to the pleura at the most. The healthy air containing lung is not depictable due to the total sound reflection at its surface. In the early years of ultrasound up to the nineteen eighties the presentation of pleural effusions was considered the only reasonable application for chest sonography apart from echocardiography.

The bony chest cage impedes the presentation of the pleura because of the shadows behind the ribs and the sternum. An appropriate examination technique allows an insight to the pleura through the intercostal spaces, when angulating the transducer also to the parietal pleura behind the ribs. By respiratory maneuvers the lungs move up and down. The visceral pleura slides through the intercostal field of view and thereby becomes sonographically visible. The diaphragmatic pleura is seen best in deep inspiration through the abdomen using liver and spleen as an acoustic window. The pleura of the apex of the lung is directly detectable through the supraclavicular fossa. The scapula as an osseous obstacle can be shifted or rotated by arm movements in medial or lateral direction. The mediastinal pleura and its continuation along the spine is largely invisible by transthoracic examination (see ► Chap. 1).

3.1 Technical Visualization of the Pleura

The pleural surface of the lung can be approximately estimated by means of CT sectional images. Supposing the invisibility of the mediastinal pleura about 70% of the pleural surface can be visualized by a transthoracical approach (Reuss 2010). Fortunately most of the pathologic changes of the pleura are in this region. Pathologic changes exclusively located at the mediastinal pleura are rare.

The normal pleura is approximately 0.2 mm thick. This is within the range of the axial resolution of 0.2 mm of a 10 MHz-transducer. Nevertheless the visualization of the pleura also succeeds with a transducer with lower frequency due to the differences in the impedance between the pleura and the neighbouring layers of fat and fluid (■ Fig. 3.1). The visceral pleura covers the aerated lung. At this interface arises a total reflection of the ultrasound, visible on the screen as a very bright line including the visceral pleura (Reuss et al. 2002). Actually the visceral pleura is not really visible when the healthy lung is filled with air. In case of an usually hypoechogenic subpleural consolidation of the lung the visceral pleura is demarcated with the same echogenicity and thickness as the parietal pleura (■ Fig. 3.2).

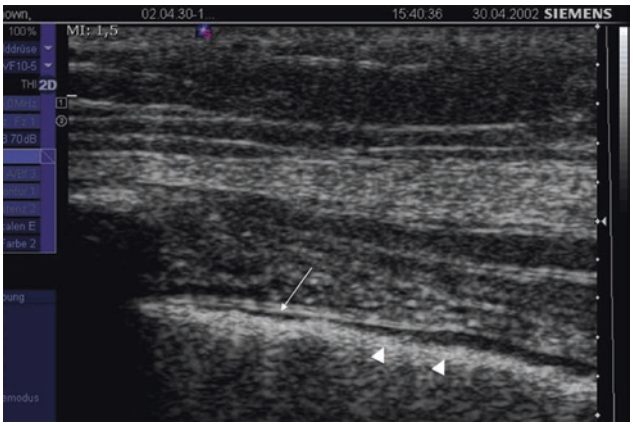

■ **Fig. 3.1** Clearly identifiable double contour in the region of the parietal pleura (arrow) corresponding to the actual parietal pleura and the endothoracic fascia. Disproportionately thick visceral pleura (arrow heads), due to an artifact

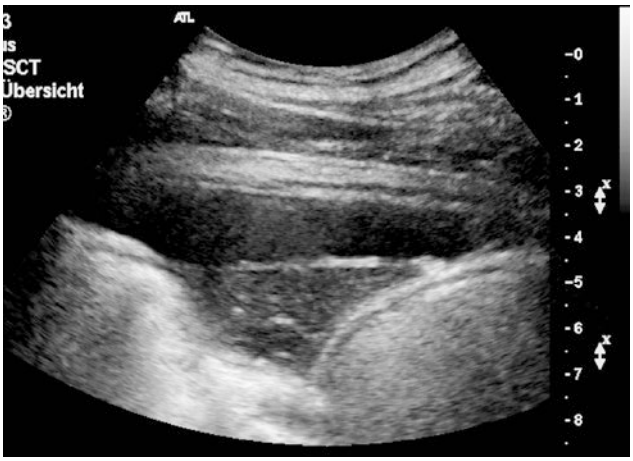

■ **Fig. 3.2** Subpleural consolidation in a patient with lung embolism and pleural effusion. Thus the pleura is delineated separately from the total reflection at the air in the lung. Visceral and parietal pleura are displayed equally thick and equally echogenic

3.2 Indications for Pleural Sonography

The clinical questions that indicate an ultrasound examination of the pleura are manifold (Reuss 2010) (■ Table 3.1). However wide overlap with indications for ultrasound of the chest wall, lung, diaphragm and abdomen is present. Only the symptom dyspnea may be triggered by sonographically visible changes such as pleural effusion, pleurisy, pleural tumor, pleural fibrosis or pneumothorax, but also by interstitial syndrome in cardiac failure, ARDS, pneumonia, lung atelectasis due to a central lung tumor and lung embolism, a diaphragmatic paresis or diaphragmatic eventration due to ascites. The broad use of thoracic ultrasound is worthwile (Mathis 1997). Almost always, the two main clinical

Table 3.1 Symptoms and situations indicating ultrasound of the pleura

Dyspnea ± attenuation of percussion sounds	Pleural effusion	Size/volume Suspected cause Parapneumonic Heart failure Malignant Concomitant effusion in – Pancreatitis – Polyserositis – Liver cirrhosis – Renal failure – Septicemia
Dyspnea + pain	Pneumothorax Pleurisy	
Respiratory dependent chest pain	Pleurisy	Concomitant pleurisy in – Pneumonia – Lung embolism Chest wall processes – Rib fracture – Abscess – Metastasis – Hematoma/seroma
Before intended thoracocentesis	Verification of effusion Free floating/loculated effusion	Diaphragmatic eventration Solid lesion/tumor Diagnostic/therapeutic thoracocentesis possible?
	catheter pleurodesis – Before – after	– Pleural space empty? – Pleurodesis successful?
Radiologically proven pleural based lung consolidation	Solid/liquid Pleural mass	Mass starting from – Chest wall – Lung – Diaphragm
Known underlying disease	Tumor – Diagnosis/staging	– Effusion – Pleural metastasis
	Pneumonia	Parapneumonic effusion – Size/volume – Septated? – Echogenic => empyema?
	Cardiac failure	Decompensated with effusion?
	Renal failure/liver cirrhosis	Concomitant effusion
	Lupus erythematodes/other systemic diseases	Polyserositis
Trauma	Pleural effusion Hematothorax Pneumothorax	
Artificial ventilation	conventionally-radiologically occult pneumothorax conventionally-radiologically occult effusion	Sulcus anterior syndrome

symptoms of the thorax, namely dyspnea and pain, are of great importance. After patients history and clinical examination, thoracic sonography should be carried out quickly as the diagnostic tool of first choice. Thoracic sonography performed promptly in the clinic, practice, and emergency medicine is rewarding (Mathis, 1997) and sets an early diagnostic course.

3.3 Normal Pleura

In transthoracic intercostal examinations the intercostal space is smoothly limited by the very thin, moderately echogenic parietal pleura. Provided good examination conditions there is occasionally a double line visible representing the parietal pleura and the endothoracic fascia (Reuss et al. 2002) (◘ Fig. 3.1). Between parietal pleura and intercostal muscles is an individually very different hypoechoic layer, the extrapleural fat layer. The visceral pleura is separated from the parietal layer by the thin anechoic pleural space. Inwards the pleural space follows the normally hyperechogenic line of the visceral pleura sliding up and down with respiration. Pleural sliding is diagnostically important to prove normal conditions. Missing pleural sliding may have different causes (◘ Table 3.2). Absence of pleural sliding can be found among different conditions, in pneumothorax, emphysema, pleural rind, but also physiologically in the area of the lung apex. Here, one must not misinterpret the sometimes barely perceptible sliding movements as pneumothorax.

Normally both pleural sheets are completely smooth. Occasionally comet-tail-artifacts with a ring-down-effect are originating from the visceral pleura, mostly in elder persons due to small scars in the pleura or subpleural lung. Particularly common are comet-tail-artifacts starting from the diaphragmatic pleura, depicted in a transhepatic or translienal view. Similar artifacts also originating from the visceral pleura must be differentiated. These artifacts are laser-like traversing to the bottom of the screen without ring-down-effect and move breath dependent with the visceral pleura. These artifacts are called B-lines and represent interstitial subpleural changes in the lung, mostly in cardiac lung edema, less often in lung fibrosis or in the border area of focal malignant or benign subpleural lung lesions (see ▶ Chap. 4). Hence B-lines are not of real pleural origin.

◘ **Table 3.2** Missing pleural sliding, differential diagnosis

Pneumothorax	Pleural space not visible Missing lung puls No B-lines Occasionally “lung point” (see below)
Emphysema	Minimal or missing pleural sliding, minimal respiratory excursions
Pleural fibrosis	Hypoechoic or mostly hyperechoic pleural thickening
Apex of lung	Also normally minimal sliding

3.4 Pleural Effusion

In erect position free floating effusion is located in the lowest parts of the costo-diaphragmatic pleural recessus. The effusion is surrounded by the chest wall, the diaphragm and the inferior parts of the lung (◘ Figs. 3.3 and 3.4). most pleural effusions are echofree, especially in cardiac failure, severe hypalbuminemia, overhydration in renal insufficiency and in decompensated liver cirrhosis. Even in small effusions an air-free sonolucent cuspidate compression atelectasis waving breath-dependently is visible (see ▶ Sect. 5.4). In the sitting position also minute effusions of 20 ml are detectable (Gryminski et al. 1976; Kocijancic et al. 2004) (◘ Fig. 3.5). In conventional X-ray of the chest the minimal detectable volume is about 100 ml (Colins et al. 1972).

Color Doppler demonstrates the breath-dependent and pulse-dependent internal movement in the effusion (◘ Fig. 3.6). Color Doppler can be used to visualize respiratory- and pulse-dependent internal fluid movement in the effusion and thus delineate echo-poor to echo-free solid structures from fluid (◘ Fig. 3.6). However, lung motion also triggers a color signal over the lung. This color Doppler signal is not always reliable, especially in very small effusions. This respiratory dependent color signal is not very reliable to distinguish

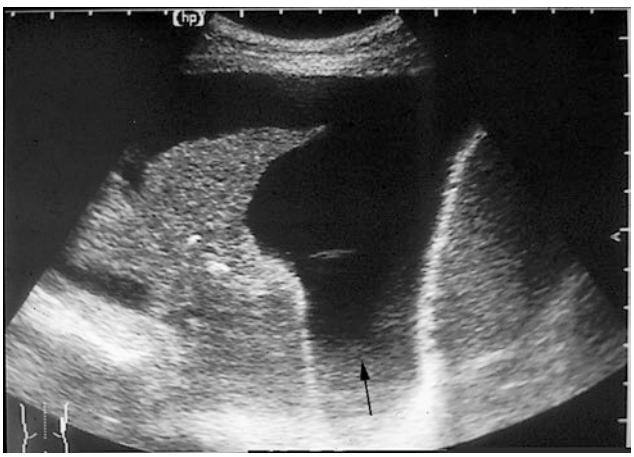

◘ **Fig. 3.3** Large nearly echofree pleural effusion. The echoes in the deep parts of the effusion are artifacts (arrow). Lung compressed with minimal residual air in central bronchi

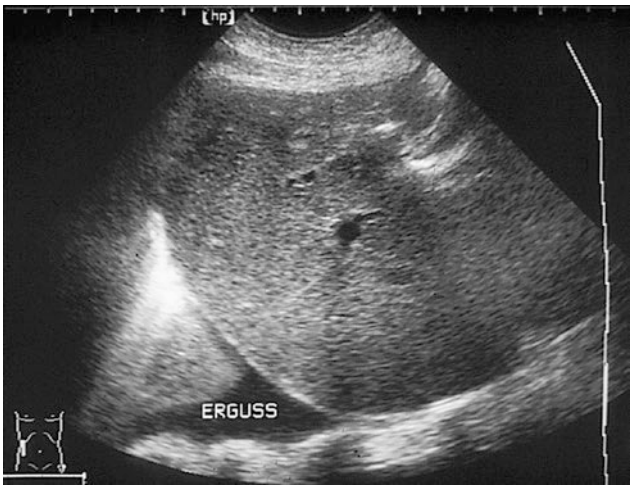

Fig. 3.4 Small posterior pleural effusion between spine and diaphragm in a transhepatic examination

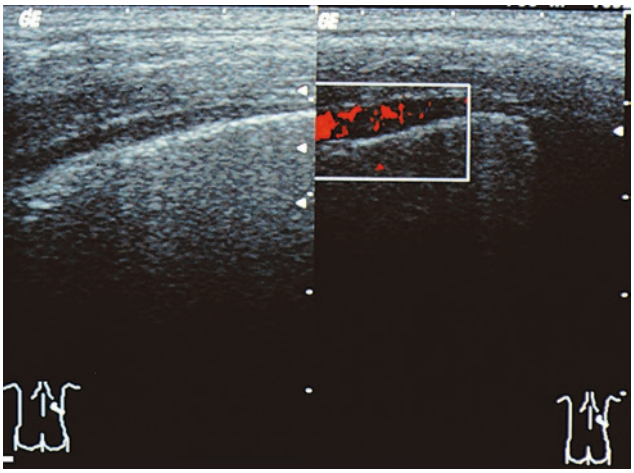

Fig. 3.6 Small pleural effusion. The flow signals in the effusion are produced by the pulse and breath synchronous inner shift and characterize the anechoic region as fluid

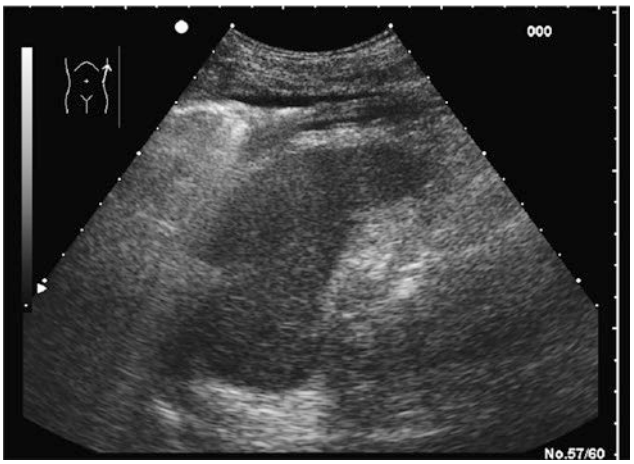

Fig. 3.5 Very small strip-like postoperative pleural effusion in the angle between ribs and diaphragm. The deformation during respiration in the dynamic examination excludes a circumscribed pleural thickening

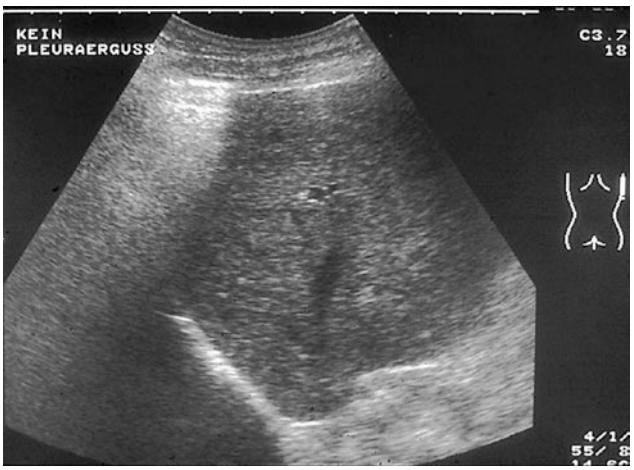

Fig. 3.7 No presentation of fluid between lung and liver, thus ruling out free floating pleural effusion. To rule out a captured effusion, the whole pleura must be examined

echopoor thickenings of the pleura from minute strip like effusions. However, a color signal is triggered also by the lung movement.

Large pleural effusions can fill the whole hemithorax forming a serothorax. Then the lung is completely collapsed and can only be seen as a small airfree lobed structure in the hilus, possibly a residual bronchoaerogram of the large bronchi in the hilus. In a serothorax after pneumonectomy the collapsed lung is lacking.

In the supine patient the pleural effusion is extending along the lateral chest wall. In a conventional chest-X-ray such an effusion is noticed only as a slight uniform unilateral opacification. Owing to a missing difference in lung transparency bilateral effusions are not detectable even under study conditions. The ultrasound examination of the supine patient must be performed from the posterior axillary line possibly after slight rotation of the patient.

In the erect patient a freefloating effusion can be ruled out by examining the whole inferior pleura (Fig. 3.7). Only aerated lung with its typical reflection is visible. For this purpose a supine patient has to be rotated completely on the left or right side.

3.4.1 Volume Assessment

Measuring of the volume of a pleural effusion by means of ultrasound is not possible. Several proposals have been made to estimate the volume reaching correlation coefficients up to 0.75. The difference to the actual volume may be substantially. But for clinical purposes the

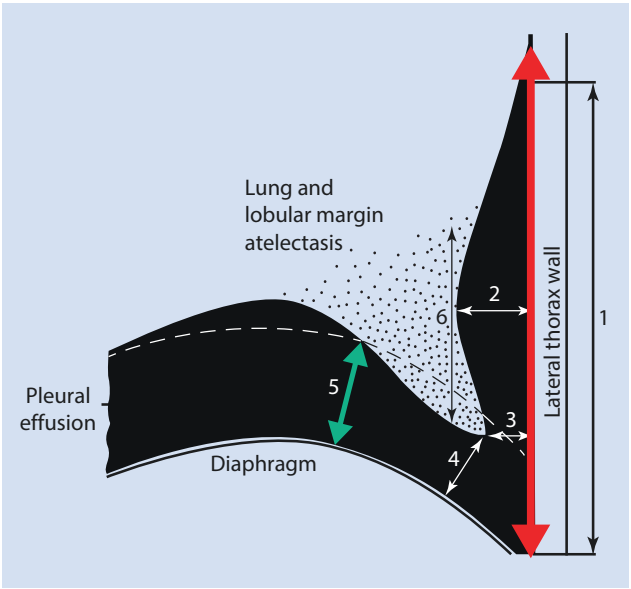

Fig. 3.8 Schematic presentation of volume estimation of pleural effusions. Valuable parameters are maximal extension of the effusion (1), inferior distance between lung and diaphragm (4), and the subpulmonary extension of the effusion (5). The thickness of the layer between lung and chest wall (2), the distance between an inferior atelectasis and the chest wall (3) and the extension of the atelectasis (6) are not suitable for the volume estimation (according to Goecke and Schwerk 1990)

Table 3.3 Estimation of the effusion volume in supine patients

Author	Result	Comment
Roch et al. (2005)	PLDbasal > 5 cm corresponding > 500 ml effusion volume PLDbasal = distance between basal lung and posterior chest wall end expiratorically	Sens. 83%, spec. 90% Low interobserver variance
Balik et al. (2006)	V (ml) = 20 × Sep (mm) V = effusion volume Sep = separation distance between basal lung and chest wall in posterior axillary line	Correlation coefficient $r = 0.72$
Eibenberger et al. (1994)	Effusion thickness dorsobasal 20 mm corresponding 380 ± 130 ml 40 mm corresponding 1000 ± 330 ml Measurement expiratorically	Correlation coefficient $r = 0.80$
Vignon et al. (2005)	Effusion thickness dorsobasal > 45 mm right/ > 50 mm left corresponding > 800 ml effusion volume	Sens. 94% right, 100% left Spec. 76% right, 67% left

estimation is mostly sufficient. Volume estimation may be important in the follow up of effusions under conservative treatment or to forecast a positive effect of a thoracocentesis in dyspnoeic patients. Thoracocentesis of an effusion volume less than 500 ml is successful only in exceptional cases concerning the respiratory function. For less experienced examinators it may be helpful to estimate the volume by a formula (Fig. 3.8).

Numerous formulas exist for calculating effusion volume (Kelbel et al. 1991; Roch et al. 2005; Balik et al. 2006; Eibenberger et al. 1994; Vignon et al. 2005; Goecke and Schwerk 1990; Hassan et al. 2017)

The following methods for estimating pleural effusion volume have been found to be practical:

1. With the patient seated, the maximum effusion height is measured along the laterodorsal thoracic wall (H). The height in centimeters multiplied by the empirical factor of 90 gives the effusion volume in milliliters (correlation coefficients 0.73) (Goecke and Schwerk 1990).

$$V = H(\text{in cm}) \times 90$$

2. With the patient lying on his back, possibly also ventilated (whose upper body is raised approximately 15° for sonographic examination), the measurement of the maximum distance (D) in millimeters between the parietal and visceral pleura is performed in end expiration. The volume in milliliters is calculated multiplied by the empirical factor of 20 (correlation coefficient 0.72).

$$V = D(\text{in mm}) \times 20$$

3. When calculating the effusion volume with the current highest correlation coefficient of 0.83, add the lateral effusion height (H) in centimeters with the distance of the diaphragm to the lung in centimeters (D) in a sitting patient and multiply by the empirical factor of 70 (Hassan et al. 2017) (Table 3.3).

$$V = H(\text{in cm}) + D(\text{in cm}) \times 70$$

3.4.1.1 Etiology of Pleural Effusion

Depending on the etiology of the effusion, the content may present differently. Transudates in cardiac failure, hypoproteinemia or liver cirrhosis are usually echofree (Yang et al. 1992). Due to considerable differences in the impedances in the effusion and in the aerated lung or the chest wall arise scatter artifacts in the effusion. These artifacts shift typically with the transducer movements (Fig. 3.3).

Blood, pus or chylus reflect the ultrasound differently, therefore these effusions are echogenic (Figs. 3.9 and 3.10). The internal echoes shift breath and pulse dependant in the effusion, sometimes nearly circular. Protein agglomerates in inflammatory and malignant effusions

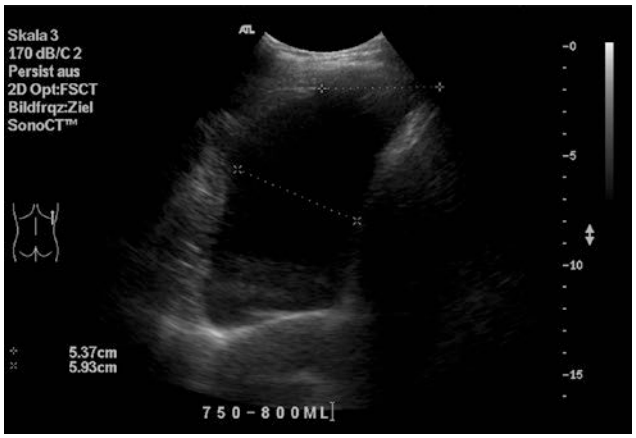

Fig. 3.9 Exclusively subpulmonary pleural effusion in severe right heart failure, latero-posterior longitudinal section. The infrapulmonary and lateral diameters of the effusion add up to an estimated volume 720 ml, according to the formula of Goecke and Schwerk. In exclusively subpulmonary effusions this formula underestimates the actual volume. Actually aspirated volume 850 ml

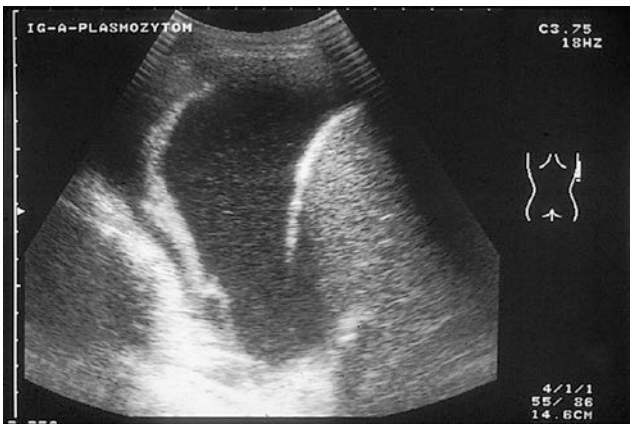

Fig. 3.10 Echogenic protein containing pleural effusion in a patient suffering from an IgA-myeloma. In contrast to artificial echoes these echoes move swinging or rotating synchronous with breath or pulse. Inflammatory, hemorrhagic or chylous effusions present in a similar manner. Transudates are usually echofree

also cause an echogenic appearance of the effusion (Chian et al. 2004). A reliable distinction between transudates and exudates by ultrasound is impossible. Also one third of exudates appear echofree (Yang et al. 1992). Modern ultrasound devices are highly sensitive and show occasionally internal echoes also in transudates (Fig. 3.11). If diagnostically necessary a thoracocentesis is acquired. The indication should be provided generous (Hooper et al. 2010). With the patient's consent this is possible immediately after sonographically establishing a puncture site. The aspirate is then further analyzed in the laboratory depending on the specific issue (Table 3.4).

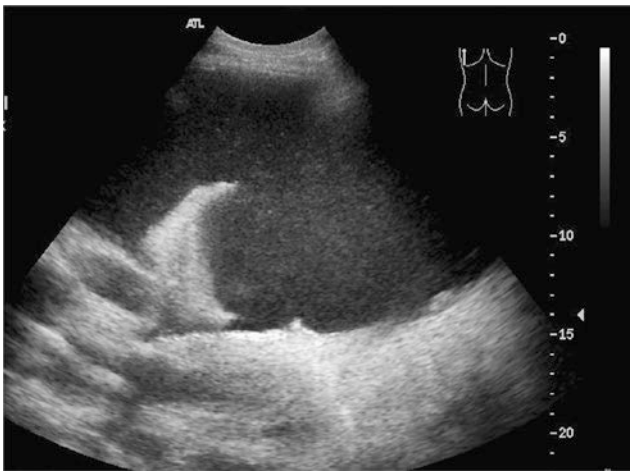

Fig. 3.11 Homogenous echogenic pleural effusion with atelectasis of the lower lobe of the lung. Lack of fever or clinical signs of inflammation and no trauma in the history is unlikely for an empyema or hematothorax. Aspiration reveals a chylous effusion due to metastases of a lung carcinoma in the mediastinum with destruction of the thoracic duct

Table 3.4 Analysis of aspirate from pleural effusions

Macroscopy	**Appearance**	**Clear, turbid, purulent, bloody**
	Consistency	**Runny, viscous, ropy, frothy**
Leucocytes	Transudate < 1000/µl Exudate > 1000/µl	
Hemoglobin	Hematocrit	Almost equal to blood => hematothorax
Clinical chemistry	pH	<7.2 => parapneumonic, empyema
	Total protein	Limit transudate/exudate 3 g/dl
	Glucose	< 60 mg/dl or quotient effusion/serum < 0.5 => parapneumonic, rheumatic, tbc
	LDH	Quotient effusion/serum >0.6 => parapneumonic
Bacteriology	Culture aerobic and anaerobic and	Gram staining
In case of clinical suspicion	Tbc-PCR and –culture, cytology, virology, tumor-marker, cholesterol, triglycerides, chylomicrones, lipase	

3.4.2 Complicated Parapneumonic Effusion

Infected, septated and captured pleural effusions are referred to as complicated (Light 2006). Rounded margins due to the adhesion of the pleural layers are characteristic for captured pleural effusions, a finding similar to that in CT and MRI. Captured and loculated effusions show less deformation as free floating effusions when holding the transducer fixed to the chest wall. Compared to CT and MRI ultrasound is the best method to detect septations. Septations often develop spontaneously in a parapneumonic effusion or in an empyema (Figs. 3.12 and 3.13). Inadaquately treated parapneumonic effusions have a high risk of prolonged hospitalization, prolonged systemic toxicity, increased mortality after late or inadequate tube drainage, a residual decline of respiratory function, a local spreading of the inflammation and an increased mortality (Light 2006). The prognostic risk of parapneumonic effusions is rising correlated to an increasing volume. Captured or septated effusions and a thickened pleura are typical signs of an increased risk. Ultrasound is best suitable to detect effusion volume, loculation and pleural thickening. A negative bacterial culture or Gram staining and a pH > 7.20 in the aspirate mark a low risk. Aspirates with positive culture or Gram staining, purulent aspirates or a pH < 7.20 are typical for an empyema (Colice et al. 2000; Heffner 2010) (Table 3.5).

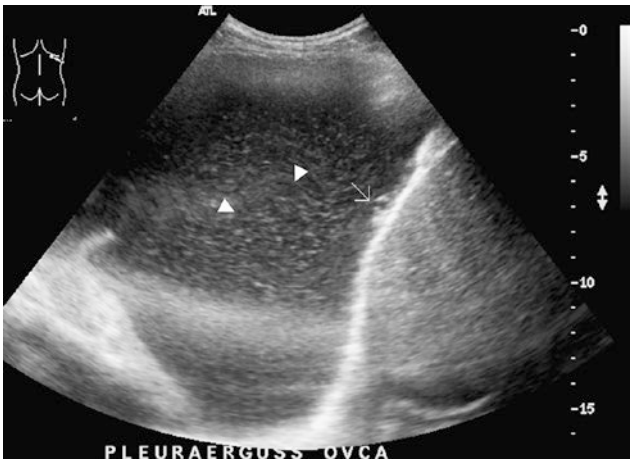

Fig. 3.12 Malignant pleural effusion in metastasized ovarian carcinoma. Even on the stationary image one suspects the dynamic circular movement of the echoes in the effusion (arrowheads). Deep in the effusion strip-like artifacts. Small pleural metastasis on the diaphragm (arrow)

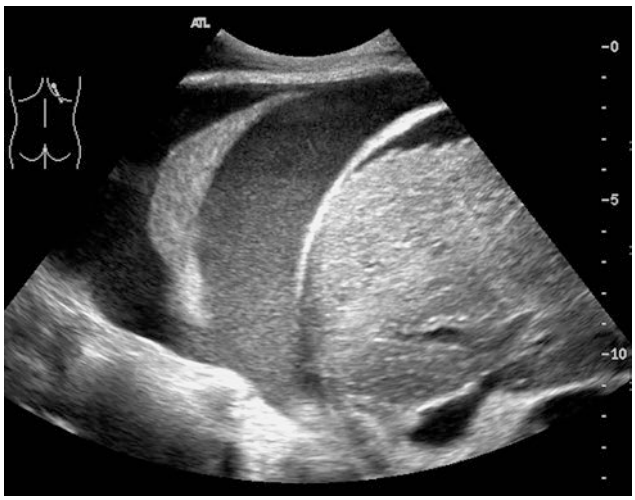

Fig. 3.13 Partly clear echogenic effusion, the subphrenic ascites and the humpy cirrhotic liver clearly depictable. The aspirate of the effusion clear, with a protein content of 29 g/L formally a transudate.

Hemorrhagic as well as malignant effusion can also appear septated or loculated. Also as a result of multiple thoracocenteses fibrinous strings and bands appear. Fibrinous strands, pleural thickenings and accompanying consolidations of the lung are nearly always indicating an exudate, except the typical compression atelectasis of the lower lobe of the lung.

To exclude septations prior to each diagnostic pleurocentesis and especially prior to a therapeutic thoracocentesis an ultrasound scan should be done. Punctering of single chambers, if necessary, may be carried out under ultrasound guidance. Different echogenic content of chambers may indicate a partial empyema or hemorrhage.

3.4.3 Pleural Empyema

Pleural empyemas usually present as capsulated, low to moderately echogenic and relatively homogenic effusions. Owing to the adhesions they are not free floating when changing the patients position. Usually the pleura is thickened. With the panoramic function of modern ultrasound scanners also large empyemas can be mapped in their whole extension.

In CT empyemas appear with moderately and uniformly thickend pleura with relatively smooth margins to the cavity (Light 2006). The separation of the pleural sheets, known as “split pleura sign”, may also be depicted by ultrasound. Usually the inflammatory infiltration into the surrounding lung is limited. Passive atelectases close to the empyema may occur. Complex septations and passive atelectases support with a sensitivity of only 40% the diagnosis of an empyema. A pleural puncture is needed to confirm the diagnosis.

A careful and differentiated transthoracic ultrasound examination can already clarify the therapeutic pathway with establishing the diagnosis (Figs. 3.14 and 3.15). Loculated empyema are not suitable for percutaneous

Table 3.5 Parapneumonic pleural effusion and empyema

	Uncomplicated PPE	Complicated PPE	Empyema
Pleural morphology	Thin	Fibrinous exudates, septations	Thickened, granulation tissue, septae and loculations
Pleural aspirate	Clear	Turbid	Purulent
pH	>7.30	7.1–7.2 (7.3)	<7.1
Lactatdehydrogenase	<500 U/L	>1000 U/L	>1000 U/L
Glucose	>60 mg/dl	<40 mg/dl	<40 mg/dl
Cytology	PMN +	PMN ++	PMN +++
Microbiology	Sterile aspirate	Occasionally positive (microscopically and in culture)	Often positive (microscopically and in culture)

Examination of pleural fluid; PMN polymorphonuclear cells; PPE parapneumonic effusion
According to Tasci et al. (2005)

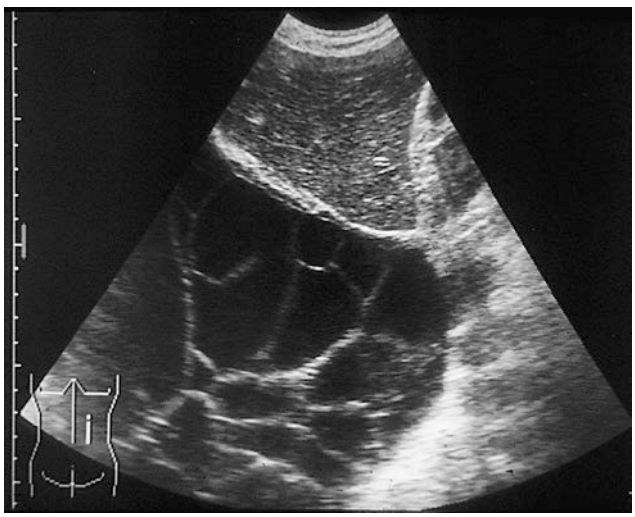

Fig. 3.14 Honeycomb-like loculated post-inflammatory pleural effusion. Ultrasound avoids frustraneous puncture attempts with a possible risk of injury

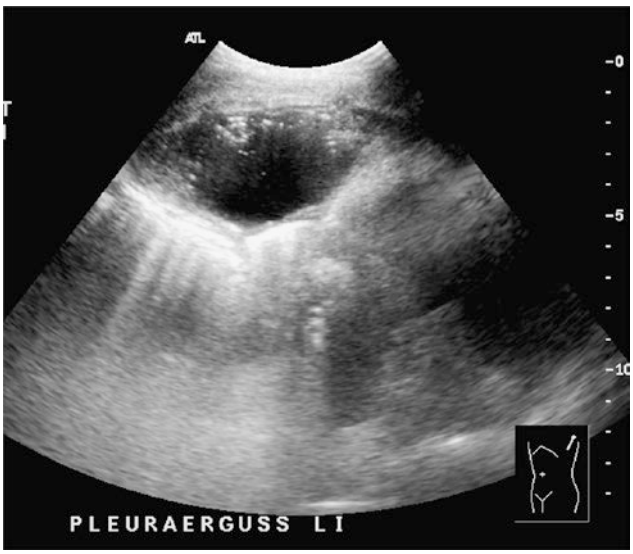

Fig. 3.15 Captured effusion after pancreatitis. Radiologically the effusion the formation impresses as a pleural based tumor. A reliable differentiation of a unilocular empyema is impossible, therefore a diagnostic puncture is needed

tube drainage. Such empyema need a surgically or video assisted thoracoscopically guided drainage with destruction of the septae (Fig. 3.16). Unilocular empyema nowadays are drained transthoracically with tubes of 10–30 Char. under ultrasound guidance. Highly viscous contents of an empyema need a greater diameter of the tube (Figs. 3.17, 3.18, and 3.19) (see ▶ Chap. 10).

A lung abscess may be difficult to differentiate from a pleural empyema. Lung abscesses often have an extended inflammatory infiltration and atelectatic parts of the surrounding lung, mimicking a very thick wall. Repositioning the patient air containing lung abscesses present with a change of the air-fluid level. Air content is a reliable sign for a connection of a lung abscess to a bronchus. After multiple previous punctures also pleural empyema may contain a few air. Gas-forming bacteria are rare in pleural empyema. The prove of vessels in the pericavitary consolidation occurs more frequently around an abscess and is not typical for an empyema. But using CEUS vessels may be found also around an empyema.

For the transthoracic therapy of a lung abscess it is crucial not to drain through aerated lung. The drainage should strictly be performed in an area where the pleural

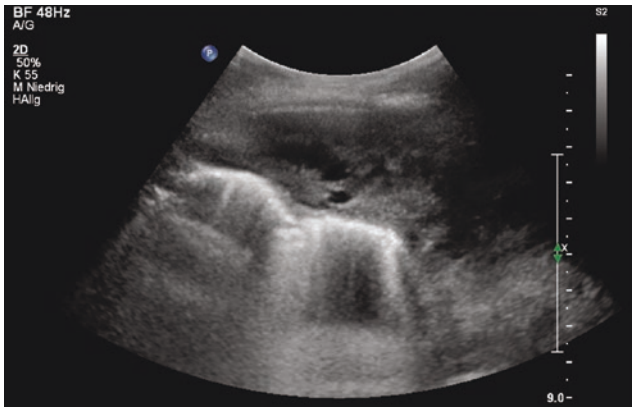

Fig. 3.16 30 year old patient suffering from pneumonia, only few residual air in the lung parenchyma. Around the consolidated lung a septated effusion with irregular thickened and not well demarcated pleural sheets. Sonographically the image of a complicated effusion. The aspirate showed 8500/µl leucocytes and pH 7.05 according to an empyema. Drainage by video-assisted thoracoscopy

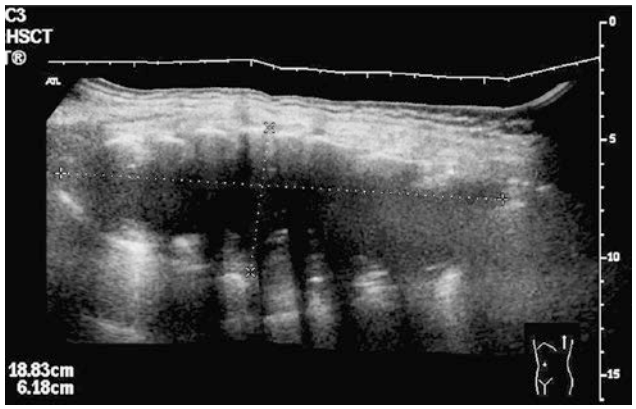

Fig. 3.17 Pleural empyema spreading over multiple intercostal spaces. The ribs with their shadows clearly visible. Volumetry and overall view is possible with the panoramic function

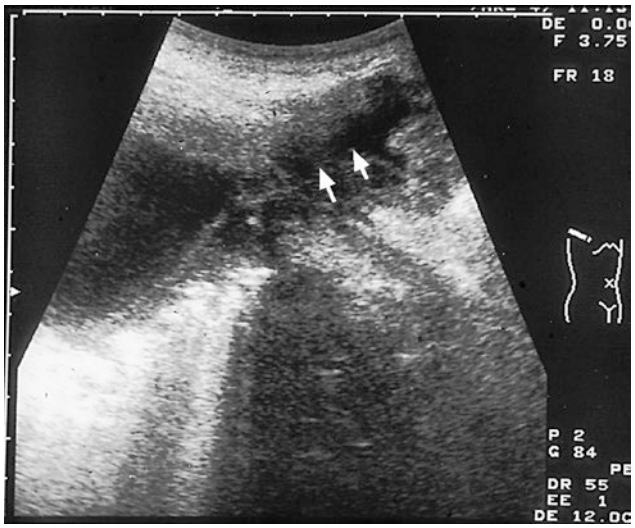

Fig. 3.18 Pleural empyema with thickened wall with relatively smooth margins and clearly visible split pleura. Partial evacuation of the empyema via a fistula through the chest wall, surrounded by inflammatory infiltrations (arrows)

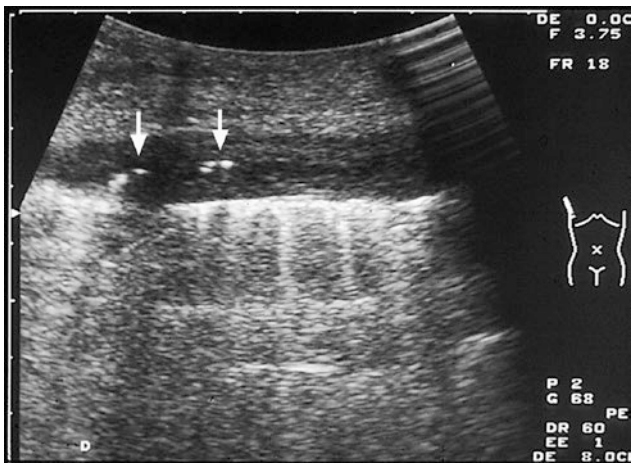

Fig. 3.19 Clearly visible thickening of the pleural sheets in an already drained empyema. Small air bubbles in the otherwise empty cavity

sheets are glued together, otherwise there is a high risk for the development of an additional pleural empyema.

3.4.4 Hematothorax, Chylothorax

A hematothorax develops posttraumatic, occasionally after interventions, e.g. after faulty puncture with injury of the lung or a vessel in the chest wall. Rarely a hematothorax occurs induced by a disease-related or anticoagulant-related coagulopathy. Not so rare is a hematothorax or hemorrhagic effusion in primary or secondary tumor diseases of the pleura, especially pleural mesothelioma.

Blood in the pleural cavity may present very differently. Fresh blood is mostly echofree similar to the flowing blood in the vessels. Newly coagulated blood may be considerably echogenic, clots are usually moderately echogenic and may appear like solid tissue, frequently with cystic inclusions. After secondary liquefaction of the clots the pleural content is again echofree. Frequently septae develop in hematothoraces. Septae are obstacles for a sufficient drainage, therefore hematothoraces should be drained very early, e.g. immediately after admission to a hospital in the emergency room. Thick drainage tubes should be preferred. Determining the puncture site by ultrasound reduces the risk of secondary intervention related injuries of diaphragm, liver or

spleen, especially in case of an unknown elevation of the diaphragm. Without a sufficient drainage of a hematothorax frequently develops a pleural peel with restriction of ventilation.

Injuries or tumor related destructions of the thoracic duct lead to a chylothrax. The effusion mostly appears moderately echogenic, sometimes highly echogenic. The aspirate looks milky, with a high concentration of triglycerides and chylomicrons. The cause for the leakage may be very small tumors or metastases e. g. due to breast cancer or lung cancer. These small tumors may be very difficult to localize.

3.4.5 Pleurodesis

In malignant pleural diseases with recurrent large effusions and consecutive dyspnea, mainly due to pleural carcinosis, pleurodesis is a beneficent palliative therapy. Spraying talc solution thoracoscopically over the pleura achieves the best results. But this procedure cannot be performed in every patient and everywhere. For catheter pleurodesis the pleura is emptied via a ultrasound guided drainage tube. Through this tube the talc solution is instillated into the pleural cavity. In successful pleurodesis pleural gliding is no more visible by ultrasound (Figs. 3.20, 3.21, and 3.23). In inadequate pleurodesis ultrasound differentiates much better between residual effusion, septation, lung consolidation or partial lung atelectasis than conventional chest-X-ray does. This success can be secured by ultrasound after thoracoscopical pleurodesis too. For clarification of this problem a computed tomography is nearly never necessary. Ultrasound nowadays has the advantage to be available nearly everywhere in hospitals and private practice.

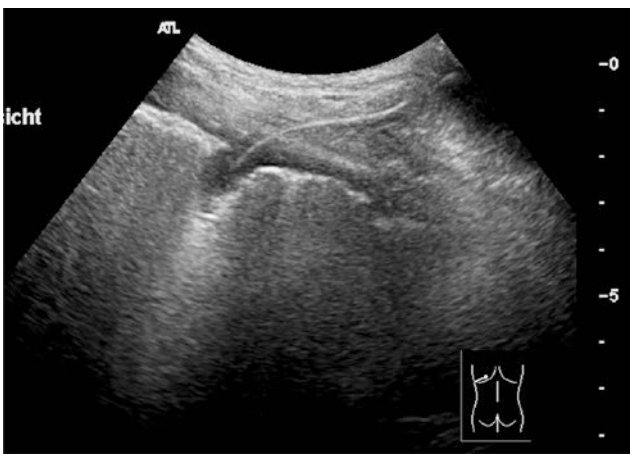

Fig. 3.20 After successful pleurodesis. The drainage tube used for application of the talc suspension still in situ. The surrounding pleura hypoechoic and thickened. In the dynamic examination no gliding sign

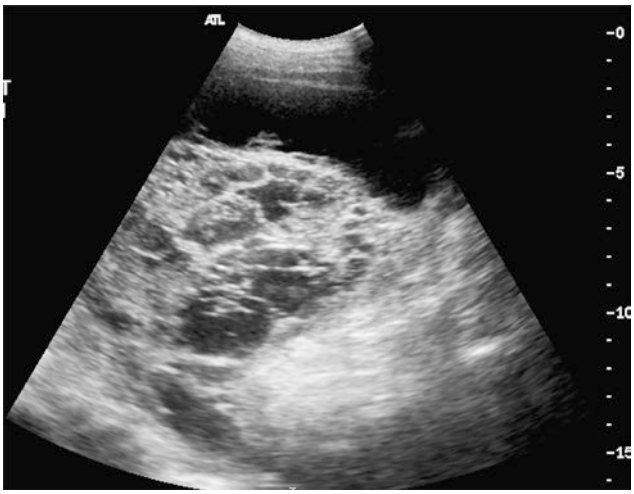

Fig. 3.21 Extended fibrinous clot after attempted pleurodesis. Inferior lung fixed to the diaphragm but not to the chest wall. Beneath the clot a significant effusion, included in the clot also liquid parts

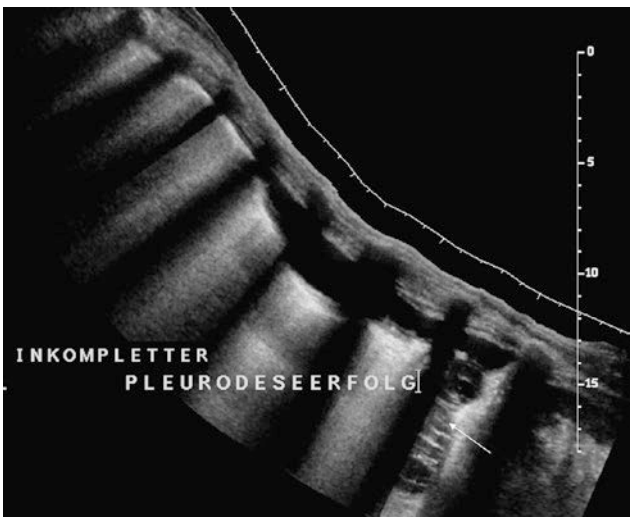

Fig. 3.22 Incomplete pleurodesis. In the left part of the image the visceral pleura fits tight to the parietal pleura, there no gliding sign. In the right part of the image the pleural sheets apart with effusion in between. The inferior lung fixed with multiple fibrinous strings (arrow). Panoramic view with eight ribs in cross section and their shadows

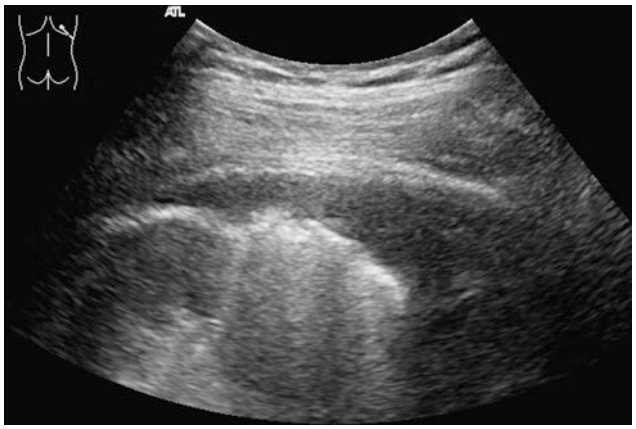

Fig. 3.23 Successful pleurodesis with formation of a broad hypoechoic pleural peel. Owing to the scarred distortions the lung surface irregular

3.5 Solid Pleural Changes

Pleural thickenings may occur diffuse, circumscribed, ribbon-shaped, nodular, regular, irregular, hypoechoic or complex structured. The changes may be limited to a single pleural sheet or affect both sheets. In an effusion or in case of a preserved gliding sign the thickening can be clearly assigned to the parietal or visceral pleura, depending on the movement with the lung. In case of interconnected pleural sheets the original pleural cavity can only be guessed by an echogenic partly interrupted line. Pleural thickenings can be observed in inflammatory diseases as well as in primary or secondary tumorous diseases. From the sonographic shape or structure of a pleural thickening cannot be deduced the etiology even though hypoechoic nodules are typical for metastases.

3.5.1 Pleuritis

Breath dependent chest pain and pleural rales are typical for pleuritis. To confirm the diagnosis multiple diseases like cardiac chest pain and myocardial infarction have to be ruled out. Conventional chest X-ray may present an opacification corresponding to a small effusion, but is often completely inconspicuous and therefore does not rule in nor rule out pleuritis. In most of these patients abnormalities of the pleura can be detected by ultrasound (overview).

Sonographical findings in pleuritis (acc. to Gehmacher et al. 1997)

- rough appearance and interruption of the normally smooth pleura (89.4%)
- small subpleural consolidations with a diameter between 0.2 and 2.0 cm (63.8%), which picks up increased contrast on CEUS

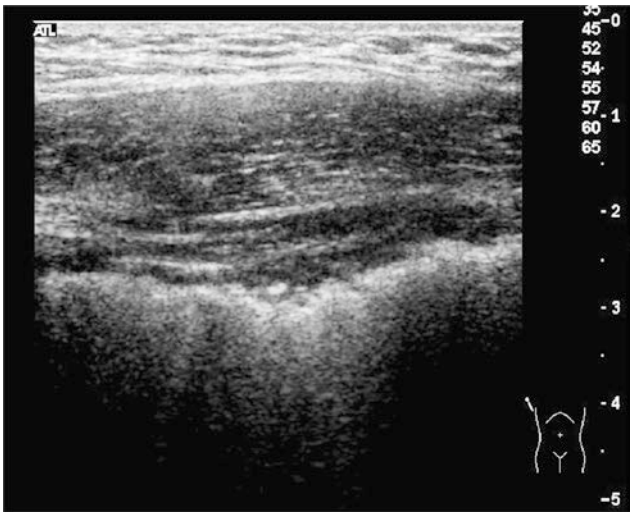

Fig. 3.24 Acute pleuritis with moderately thickened pleura, the line of the parietal pleura irregular edged. Examination in the painful area of the chest

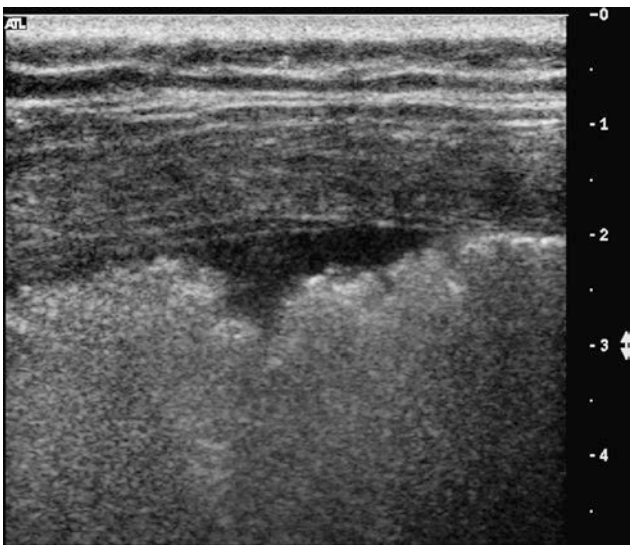

Fig. 3.25 35y old female patient in the 24. week of gestation with localized breath dependent pain. Small subpleural consolidation in pleuritis. This small consolidation could also be assigned to a lung embolism, but there was no other evidence for that

- localized parietal or basal pleural effusions (63.8%)
- CEUS: early marked contrast enhancement of the pleura

In most cases the parietal pleura is hypoechoic to moderately echogenic thickened. The lung gliding is restricted due to the pain (Fig. 3.24) (Gehmacher et al. 1997; Volpicelli et al. 2012). Small wedge-shaped echopoor subpleural consolidations occur as a sign of inflammatory co-reaction of the lung (Fig. 3.25).This is interpreted as a focal interstitial syndrome, especially when B-lines appear at the edges or comet tails behind the

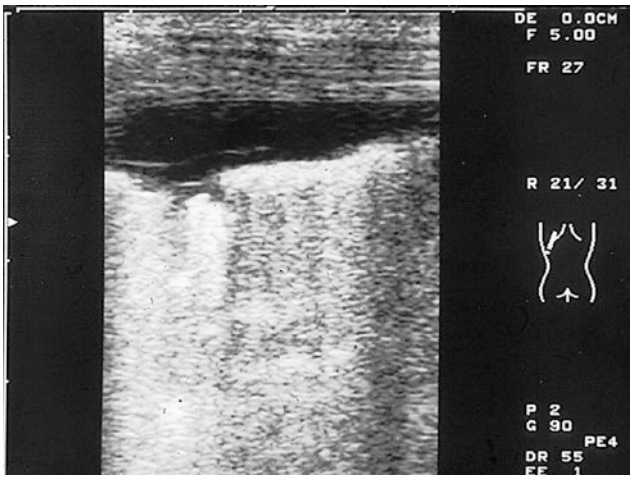

Fig. 3.26 Tuberculous pleuritis without thickening of the parietal pleura, irregular visceral pleura and tiny nodular subpleural consolidations. Thin fibrinous strands in the effusion. Diagnosis confirmed by detection of mycobacterium tuberculosis in the aspirate

small conciliations (see ▶ Chap. 4; Lichtenstein et al. 1997). More extended hypoechoic consolidations suggest the suspicion of subpleural infiltrations in a viral pneumonia. Typical consolidations of a bacterial pneumonia can be accompanied by a pleuritis (Fig. 3.26, see ▶ Sect 5.1). Apart from the real pleural thickening ribbon-shaped moderately echogenic fibrinous deposits are detectable continuing as strings and bands through the accompanying effusion. In the late phase they are responsible for the loculation (Fig. 3.14).

Perfusion in the thickened pleura is only detectable by color Doppler in 23.4% of patients (Gehmacher et al. 1997). In contrast enhanced ultrasound (CEUS) the hyperemia is visible. The inflammatory thickened pleura and particularly the accompanying pneumonic consolidations display after application of contrast medium (e.g. Sonovue®) a very short time to enhancement in contrary to peels, tumors or the muscles in the chest wall (Görg et al. 2005). Though contrast enhancing agents are rarely necessary to confirm the diagnosis.

3.5.2 Pleural Peels

A pleural peel is a fibrosis of the pleura and develops as a result of different diseases like pleuritis or empyema, but also postoperatively (Table 3.6). Initially the pleural sheets glue together. The subsequent fibrosis spreads from one sheet to the other and produces a thickening of the pleura of sometimes several centimeters. Lung sliding is no more possible. Calcified peels are easily detectable by X-ray. Non-calcified peels manifest radiologically as parietal opacification at the chest wall or in the angle between chest wall and diaphragm. Sonographically peels are moderately echogenic, in the individual case

Table 3.6 Causes of pleural fibrosis

Spontaneously arising inflammatory diseases	Pleuritis Pleural empyema
Induced inflammation	Pleurodesis
Trauma	Chest wall trauma with pleural injury Hematothorax Recurrent pneumothorax Postoperatively, especially after pleurectomy

Table 3.7 Differential diagnosis of pleural fibrosis

Pleural effusion
Acute fibrinous pleuritis
Pleural carcinosis
Pleural mesothelioma
After pleurodesis
Extended pleural plaques after asbestos exposition
Subpleural consolidations, e.g. – Lung contusion – Lymphomatous infiltrations
Subpleural lipomatosis

sometimes nearly echofree, mimicking a small shell-like effusion. The missing of lung gliding and deformation during breathing rules an effusion out (Table 3.7). The demarcation of the fibrosis against the chest wall or the lung may be smooth, but often bizarre irregular (Fig. 3.27). In the latter case the differentiation from an infiltration by a pleural carcinosis or mesothelioma is difficult (Fig. 3.28). Hyperechoic calcifications with shadows are typical for old fibroses. Residual air in adjacent lung consolidations must be excluded. Extended shell-like calcifications prevent any deeper sonographical insight into the chest. Cyst-like inclusions in peels as probable residuals of former effusions are not so rare. Atypical vessels can be ruled out by color Doppler.

3.5.3 Pleural tumors

Primary benign and malignant pleural tumors are rare in contrast to metastases. Sometimes pleural tumors are accidentally discovered during a chest ultrasound. In most cases parietal tumors are previously detected by other imaging procedures like conventional chest-X-ray, computed tomography or magnetic resonance imaging. For further clarification a "point-of-care"- ultrasound examination is performed.

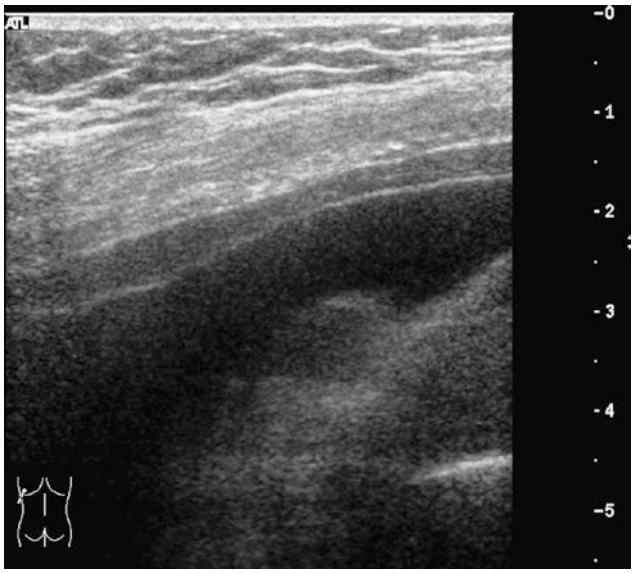

Fig. 3.27 Unusual pleural peel. The parietal pleura is thickened up to 6mm, but smooth demarcated. The visceral pleura is not involved. Large pleural effusion due to cardiac failure

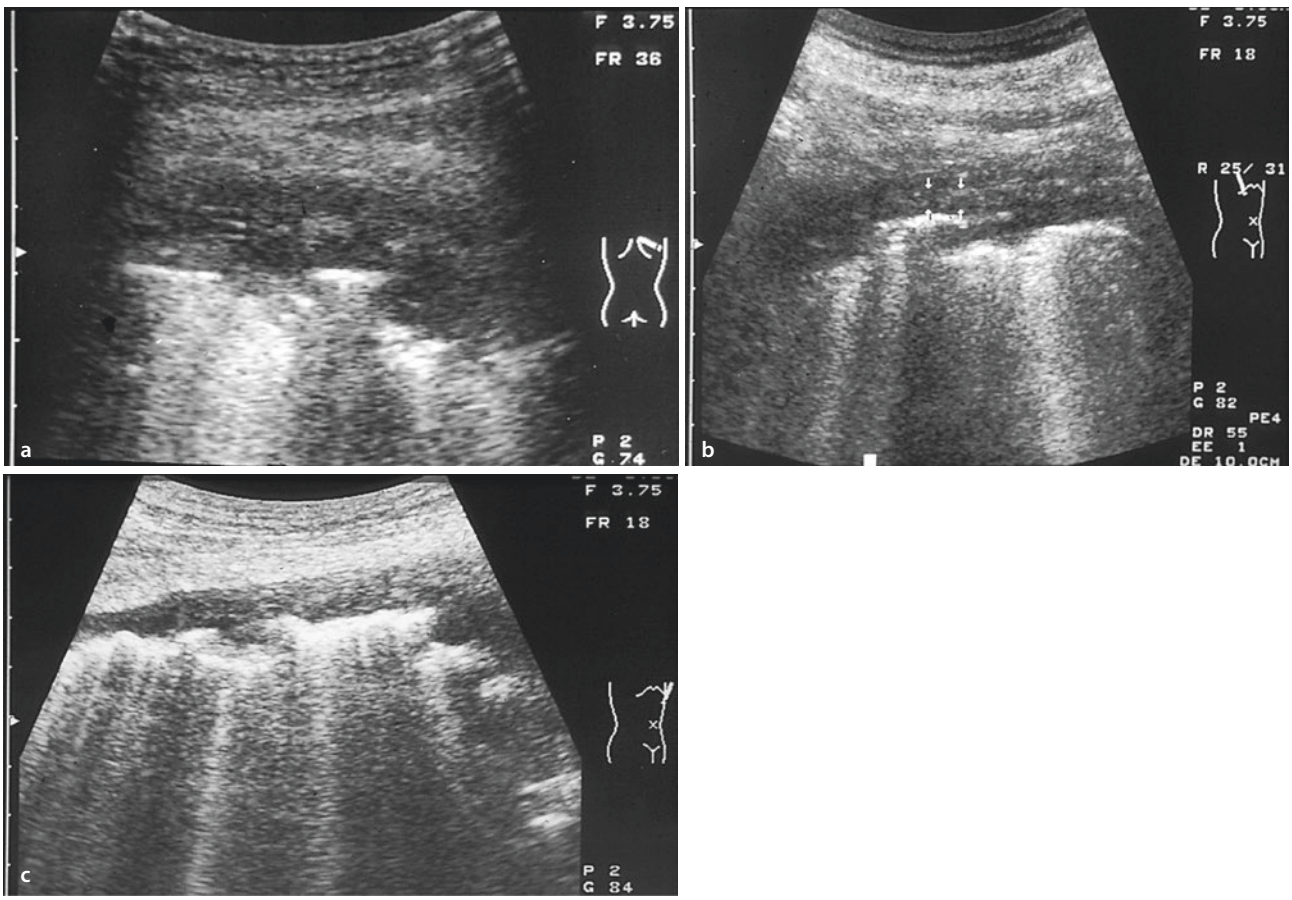

Fig. 3.28 **a**–**c** Extended moderately echogenic masses with irregular demarcation in the pleural area are ambiguous without otherwise reliable clinical data and therefore need to be proven histologically. A differentiation between fibrosis, pleural carcinosis and pleural mesotheliom solely by ultrasound is difficult or impossible. **a** Extended pleural fibrosis in a young woman after several operations in the chest. The cause for the first operation was a already existing peel of unknown origin suspected to be a tumor. **b** Slowly growing radiologically detectable non-calcified "pleural peel". Because of the clinical suspicion of a occult carcinoma repeated transthoracic biopsies which revealed at last the "peel" as pleural carcinosis in CUP-syndrome. Between the arrows one believes to recognize the former pleural cavity. **c** Nearly identical ultrasound image as in a and b, but histologically a pleural mesothelioma in a former asbestos worker

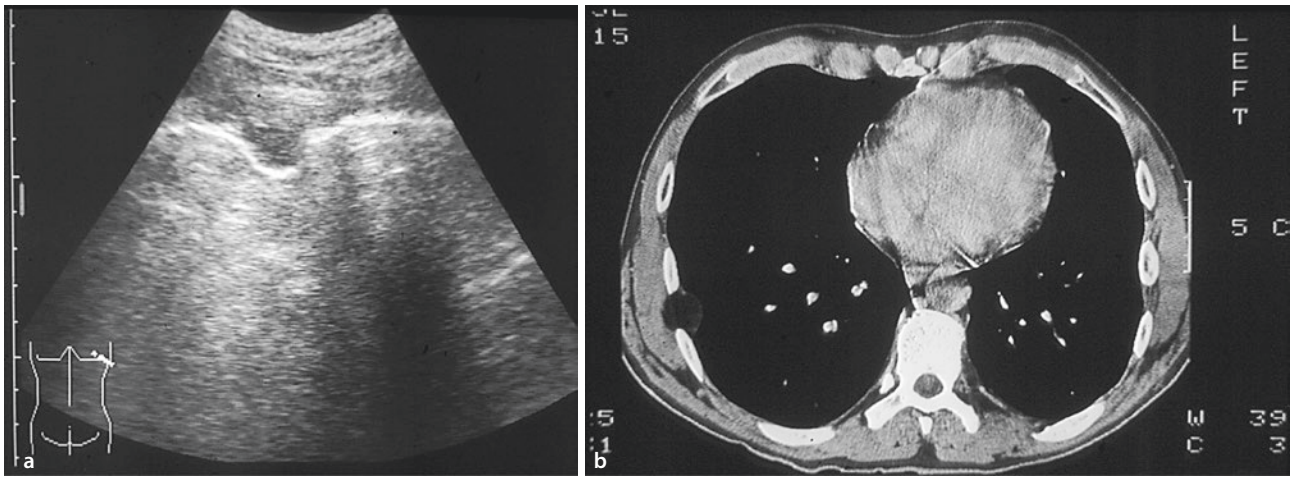

Fig. 3.29 **a**, **b** **a** Small round clearly demarcated tumor of the parietal pleura. The lung is gliding breath-dependently unimpeded over the tumor. The tumor is isoechogenic compared to the chest wall muscles. In chest-X-ray a small pleural based lesion was noticed. **b** Also in computed tomography a well demarcated tumor with fat density corresponding to a lipoma. No histological confirmation, but stable over many years in follow-up

3.5.3.1 Benign Pleural Tumors

Benign tumors like lipomas, neurinomas, chondromas, fibromas or benign mesotheliomas account for less than 5% of all pleural tumors. In chest-X-ray they are noticed as pleural based opacifications with smooth margins. Frequently they give rise to extended diagnostic examinations to rule out a pleural metastasis or a peripheral lung cancer. Sonographically most of the benign pleural tumors are moderately echogenic and clearly demarcated by a thin capsule. Depending on the size they displace neighboring structures, but are not growing invasively (Fig. 3.29). However, displacement and invasion are not always clearly to distinguish. Transpleural growth with missing lung gliding is compatible with malignant infiltration. Small accompanying pleural effusion can also occur with benign pleural tumors. A distinction of the different benign pleural tumors by means of ultrasound is impossible. The classification of the benign tumors by small needle biopsy specimens or only by cytology is often very difficult or impossible for the pathologist. Calcifications are more common in benign tumors. Density measurements as in CT, e.g. in lipomas, are not available in ultrasound.

Solitary fibrous tumors of the pleura, formerly known as hemangiopericytoma, are often asymptomatic and are discovered by chance in an advanced stage. Two third of all cases are originating from the visceral pleura. Occasionally this can be depicted by CEUS. However, the often existing peduncle often comes up during the operation. The tumor shows beside well perfused areas also necroses and cystic parts. Most of these tumors turn out as benign, also histologically, but may metastasize after decades. Even after malignant transformation the tumors have a good prognosis, also after operation of recurrent masses. The secretion of insulin-like- growth-factor in large tumors can cause recurrent and difficult to treat hypoglycemias (Abu Arab 2012; Cardillo et al. 2012).

3.5.3.2 Pleural Metastasis

Pleural metastases are frequently occurring in advanced breast and lung cancers, but in many other tumors as well. The development of pleural metastases is often combined with pleural effusions. This acoustic window facilitates the displaying of the metastases. If suspicious lesions are already located by other imaging procedures, also the rare metastases without effusion are easily to depict by ultrasound. Ultrasound is in these cases usually used for the assignment of the lesion either to the lung, pleura or chest wall, to distinguish whether they are solid or liquid and to guide the transthoracic biopsy.

In a newly discovered pleural effusion of unknown origin the pleura should be scanned for suspicious metastatic lesions. A regular search for a pleural effusion in oncologic patients can reveal the occurrence of pleural metastases the first time. But since ultrasound is only a conditionally appropriate procedure for intrapulmonary metastases, an additional CT is mandatory.

Most of the metastases are located on the pleura along the chest wall, the diaphragm and in the pleural recessus, that is in regions that are well accessible for ultrasound (Figs. 3.30, 3.31, 3.32, and 3.33). Pleural metastases are mainly hypoechoic to moderately echogenic. In rare cases they seem to be echofree, mimicking liquid formations. Metastases are nodular, round, hemispherical or broad-based polyp-like protruding into the effusion. Metastases are, of course, of varying size and are detectable from a size of 1–2 mm. Large metastases can invade deeply the underlying lung or chest wall. An interrupted or missing demarcation of the vicinity or

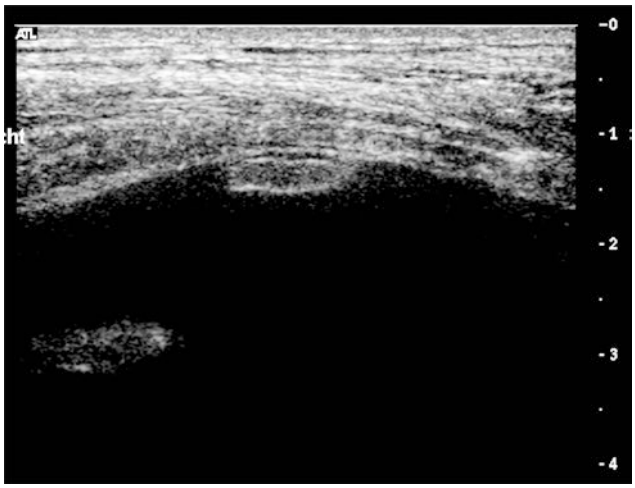

Fig. 3.30 Metastasis located on an otherwise normal parietal pleura. Metastasized breast carcinoma. Large pleural effusion

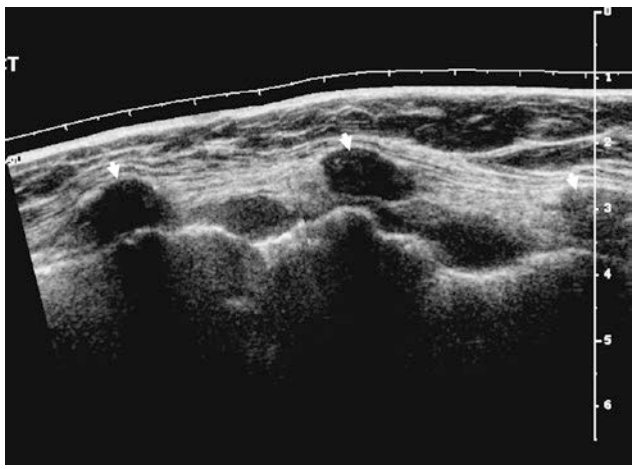

Fig. 3.31 Pleural metastases in a patient with breast carcinoma and ovarian carcinoma in her history. The origin of the metastasis can only be proven by biopsy and histology. The parietal metastases are invading the chest wall and the visceral pleura, discernable by the rough lung surface and the missing gliding sign. Parasternal longitudinal section on the right side in the region of the cartilaginous ribs (arrows)

pseudopodia-like branches indicate malignancy. Due to the lower echogenicity they are distinguishable from the chest wall or the diaphragm. Single, well demarcated metastases cannot be differentiated from benign pleural tumors by means of ultrasound alone. Multiple occurrence of identical possibly different sized formations is nearly proving metastases especially in a known underlying malignant disease. Therefore a biopsy is not required in every case. In first detected and suspected, but not proved primary tumor an ultrasound guided needle biopsy may clarify the tumor diagnosis (Adams & Gleeson 2001). Single metastases located in the visceral pleura may occur like a peripheral lung cancer. Both lesions can spread to the other parietal pleural in the same way leading to an adhesion of the pleural sheets.

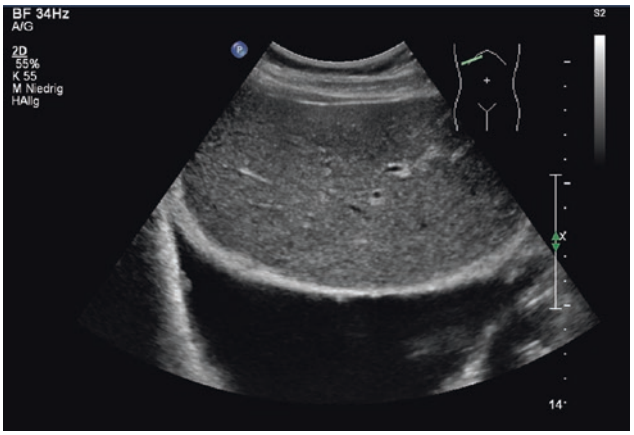

Fig. 3.32 Patient with breast carcinoma supposed to have a singular liver metastasis. Sonographically a pleural effusion with small metastasis in the pleural recesses

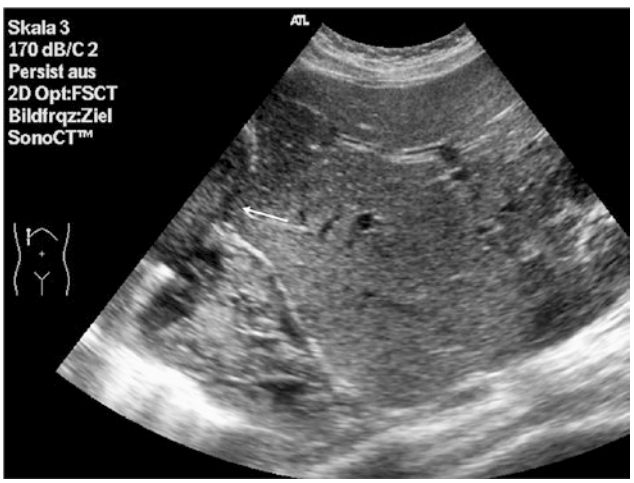

Fig. 3.33 Extended pleural carcinosis due to an endometrial cancer, known since 2 years. The diaphragm walled in, deformed and partially destructed by the carcinosis (arrow), furthermore invasion of the liver

Fibrinous clots adjacent to the pleura after trauma or interventions may appear like metastases. In the real time examination metastases are rigid whereas fibrin clots slosh forth and back. In CEUS fibrin clot do not enhance contrast medium.

An expanded plate-like carcinosis of the pleura with or without effusion is rare. The sonomorphological distinction from peels or a mesothelioma is difficult. Even the needle biopsy may fail, when malignant, inflammatory-reactive and fibrinous areas and small blood clots are close together.

In CEUS most metastases enhance only moderately, dependent also from the grade of vascularization of the primary tumor. In the early arterial phase the supply through parietal pleural vessels or peripheral bronchial vessels may be observed. Visceral pleural metastases are not supplied by pulmonary arterial vessels, therefore the

Table 3.8 Differential diagnosis of pleural metastasis

Single benign pleural tumor
Fibrinous clot after trauma or intervention
Chest wall tumor
Subpleural lung tumor/metastasis – Peripheral lung cancer – Subpleural metastasis – Lung embolism – Granuloma/rheumatic nodule – Atelectasis/obstructive atelectasis – Lung contusion
Capsuled pleural effusion
Localized pleural empyema
Irregular shaped and demarcated pleural peel
Uni- or oligolocalized pleural mesothelioma
Pancoast tumor with chest wall infiltration

beginning of the early arterial phase in the metastases is markedly later (>10 s) than in a surrounding atelectasis or pneumonia (3–10 s). See Table 3.8.

3.5.3.3 Malignant Pleural Mesothelioma

The malignant pleural mesothelioma with an incidence of about 20/1 Mio inhabitants is one of the less frequent tumors in Germany. Most affected patients had contact to asbestos in their history (Neumann et al. 2013). Asbestos as well-known trigger of this disease is banned in the whole European Union since 2005. In western Germany sprayed asbestos is prohibited already since 1979, a general prohibition followed in 1993 (no general asbestos ban up to now in the United States of America). Today a delay between exposition and disease outbreak up to 50 years is accepted, explaining the still rising incidence. In Germany a plateau is expected for the year 2030 (Lehnert et al. 2009).

Asbestos plaques in the pleura characterize people with previous exposure to asbestos. These patients bear a risk to develop a mesothelioma. Asbestos plaques occur as calcified or noncalcified pleural thickenings typically in the posterior-inferior parts of the parietal pleura. Their appearance in chest-X-ray and computed tomography is well known. Members of risk groups are surveyed radiologically. Plaques are not only shaped like a mesa-like, but also flat tapering plaques are common. Preferably with high resolution transducers the moderately echogenic plaques with their smooth boundaries are detected in the parietal pleura with breath dependent gliding of the lung. The internal structure of the plaques is according to previous observations homogenous.

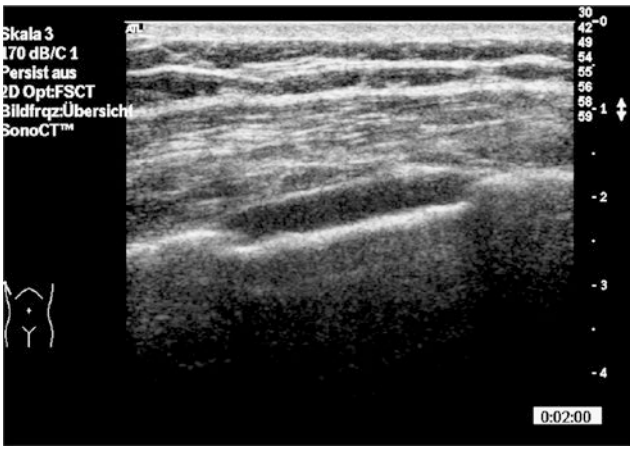

Fig. 3.34 Hypoechoic asbestos plaque with typical table-mountain-like appearance in the posterior-inferior pleura on the right side

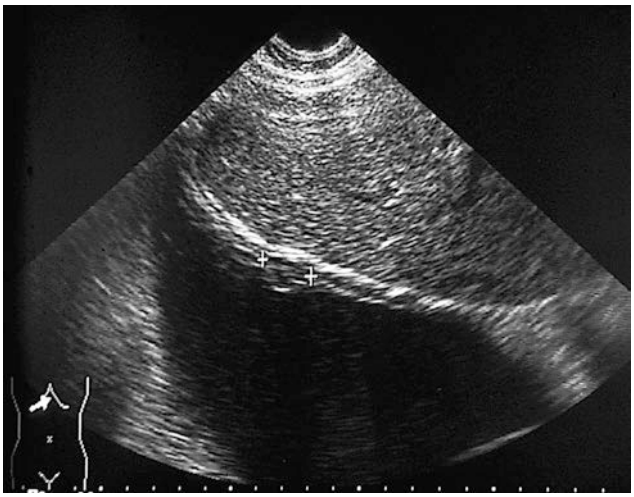

Fig. 3.35 Newly diagnosed mesothelioma spreading tapestry-like nearly over the whole pleura of the right hemithorax, single nodules (between the markers). The patient was admitted to the hospital because of dyspnea within 2 days. In the chest-X-ray a "white hemithorax". Decade-long asbestos exposition

About 10% of the plaques calcify and then present high echogenic and with shadows. Tiny effusions may occur.

Compared to the plaques mesotheliomas have an irregular edged and often unclear boundary. Beside tumorous mesotheliomas exist also tapestry-like spreaded mesotheliomas with embedded nodules in the pleura (Figs. 3.34 and 3.35).

The infiltration of the chest wall and the diaphragm is best depicted with high frequency transducers as hypoechoic streaky branches (Figs. 3.36 and 3.37). The tumor spreads early to the other pleural sheet. In an ultrasound study 28% of the patients both sheets of the pleura were affected at first diagnosis. Accompanying pleural effusions may be echogenic due to hemorrhage.

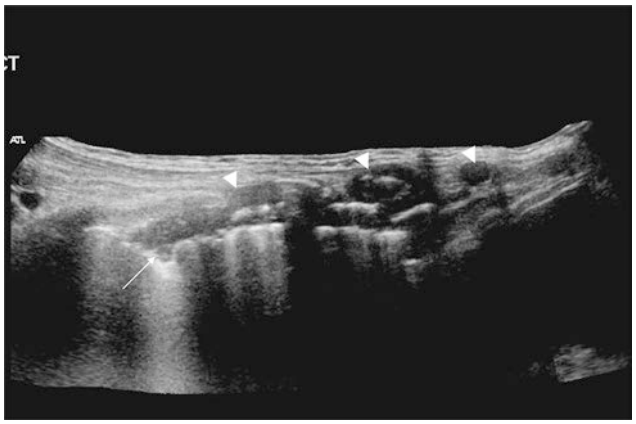

Fig. 3.36 Pleural mesothelioma. Already extended chest wall infiltration with inclusion of the ribs (arrow heads), and lung infiltration (arrow)

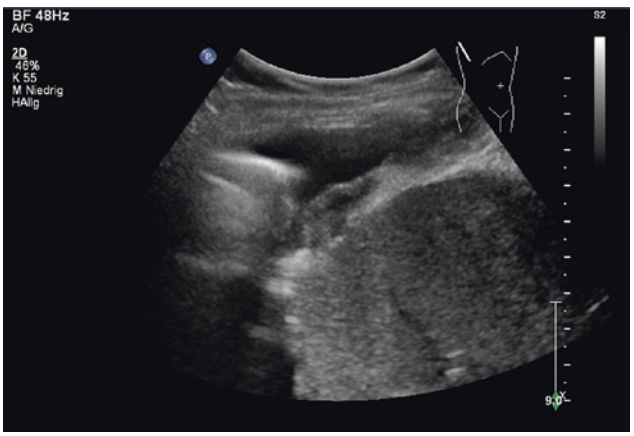

Fig. 3.37 Former asbestos workers with pleural mesothelioma. In the pleural recesses markedly thickened hypoechoic inhomogeneous pleura corresponding to the tumor. Deep infiltration into diaphragm and chest wall. The diaphragm at the dome destroyed. Small tumor dependent effusion

Making the diagnosis by cytology of the effusion or blind pleural biopsy (Abrams needle) is only in about 30% of patients successful. Thoracoscopically gathered biopsies achieve a positive diagnosis in over 90%. Percutaneous imaging guided biopsies have a comparable good success rate.

After biopsies by operation or thoracoscopy about 40% of patients develop metastases in the biopsy channel in the chest wall, but also 0-15% of patients after percutaneous biopsies, especially along the channels of the drainage tubes (Geiger et al. 2003). Therefore a short time radiation of the concerned area of the chest wall is recommended e.g. with 3 × 7 Gray. Curative operations in pleural mesothelioma are possible only in few patients.

Computed tomography is the standard procedure for the lymph node situation in mesotheliomas. For lack of detailed ultrasonographic studies the magnetic resonance imaging is the gold standard for treatment planning concerning infiltration of chest wall and diaphragm. In an older study ultrasonography was also very sensitive in detecting this infiltration. The presentation of the pericardial invasion by ultrasound is highly specific (Layer et al. 1999). Data from large studies are lacking.

3.6 Pneumothorax

A pneumothorax can occur spontaneously, but also after trauma or pleurodesis. Symptoms may be mild dyspnea to severe rapidly increasing shortness of breath in tension pneumothorax (Fig. 3.38). A spontaneous pneumothorax represents often predominantly with chest pain.

Sonomorphologic signs of pneumothorax are (Alrajab et al. 2013, Soldati et al. 2008, Wilkerson & Stone 2010, Yarmus & Feller-Kopman 2012) (Table 3.9):

- Absence of lung sliding (horizontal breathsynchronous movement of the lung in relation to the loco-constant reflex of the parietal pleura).
- Absence of vertical artifacts (vertical, breathsynchronous reflexes that begin at the visceral pleura and do not attenuate distally).
- Evidence of lung point (transition from breathsynchronously moving lung to standing air column of pneumothorax) (Lichtenstein et al. 2000).
- Absence of lung pulse on color or power Doppler (pulse-synchronous vertical movement of the pleura by transmission of the heartbeat through healthy lung tissue to the pleura).
- For documentation of an existing pneumothorax or normal findings, short video loops of the present or just absent pleural sliding are useful. It is also possible to obtain a side-differentiated image of pulmonary sliding or lung pulses with the aid of color or power Doppler (Figs. 3.39 and 3.40).
- To diagnose an incomplete pneumothorax, the examination should be extended dorsolaterally.

In patients with emphysema the extend of lung gliding is reduced and may be difficult to detect. B-lines in a healthy lung are often completely lacking.

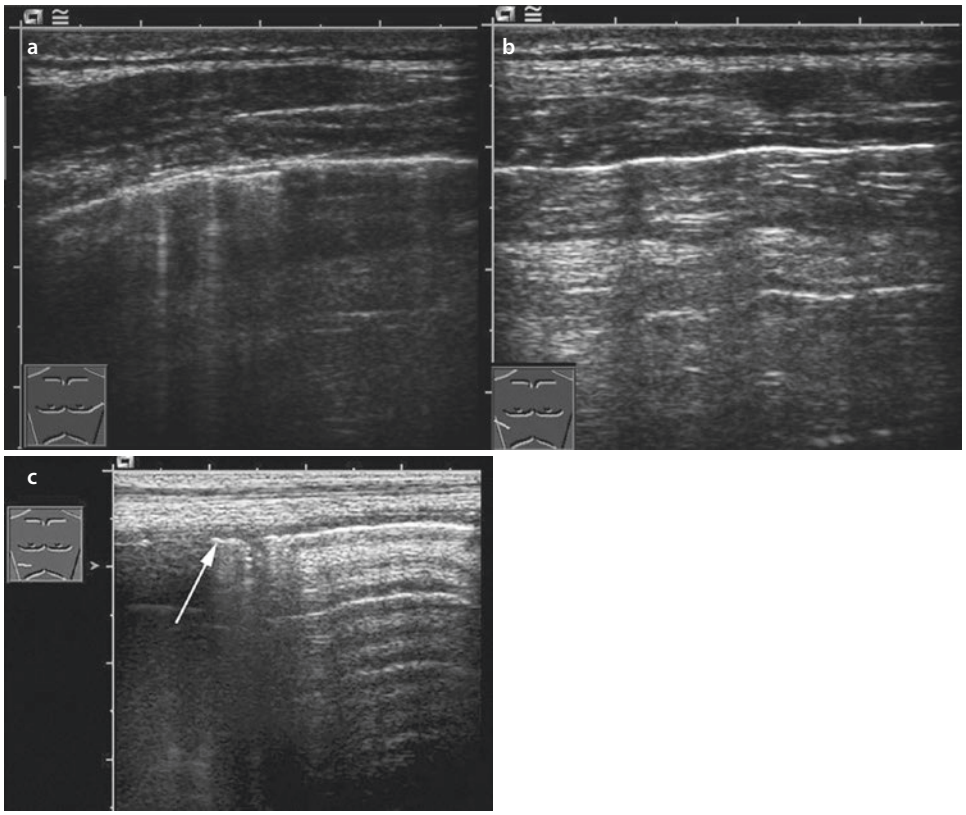

Fig. 3.38 **a**–**c** Pneumothorax. **a** Ventilated side with pleural reflex and few B-lines. The ventilated lung is gliding synchronous with breathing. **b** Inforced pleural reflex at the entering of the air-filled pleural cavity with multiple horizontal reverberation artifacts. **c** Lung point (arrow), normally aerated lung on the left, air in the pleural space on the right (partial pneumothorax)

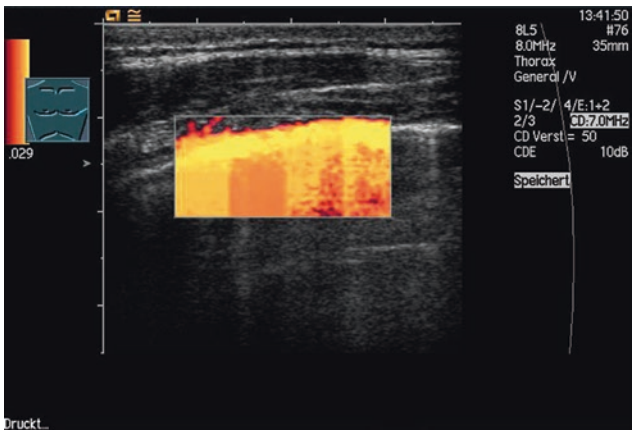

Fig. 3.39 Color sign to rule out a pneumothorax. The color signal can represent either the lung gliding (breathsynchronous) or the lung pulse (pulsesynchronous)

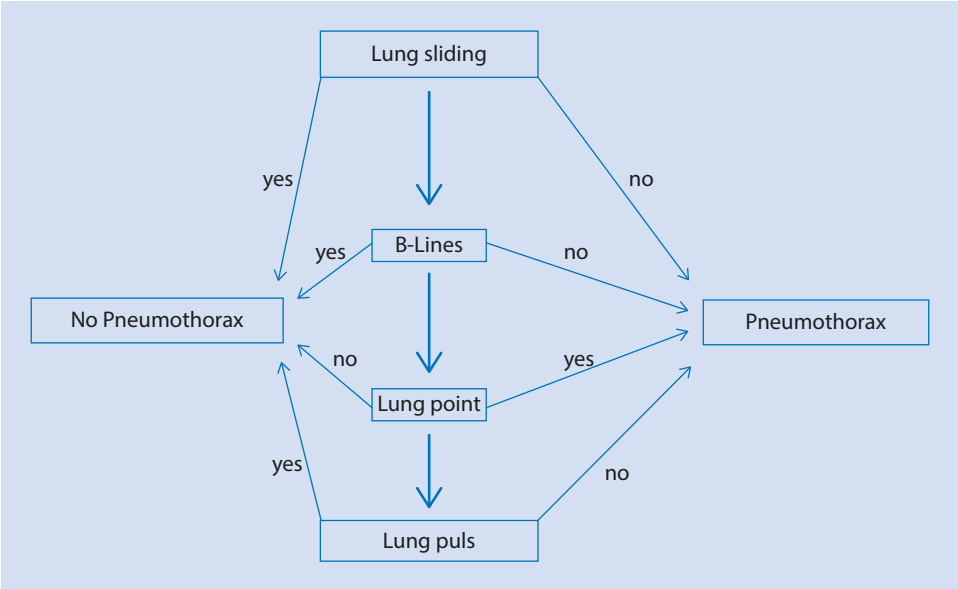

Fig. 3.40 Algorithm in suspected pneumothorax (acc. to Volpicelli et al. (2012))

Table 3.9 Diagnostic signs to detect or exclude a pneumothorax

Pneumothorax	No	Gliding sign	Yes	No pneumothorax
	No	B-lines	Yes	
	No	Lung puls	Yes	
	yes	Lung point	No	

3.7 Traumatic Changes in the Pleural Cavity

Small pleural effusions without compromising respiratory effects are common after mild to moderate chest trauma. E-fast (extended focused abdominal sonography in trauma) detects these usually non-hemorrhagic effusions. Merely only a sonographic follow up is needed.

The result of a primary or secondary bleeding into an effusion is a hemorrhagic effusion. Depending on the content of blood the effusion appears more or less echogenic. The internal echoes are moving breath dependent, often circular. The hemoglobin concentration is usually significantly lower than in a venous blood sample.

A hemothorax contains pure blood in the pleura, the hemoglobin concentration in a punctured and venous sample are almost equal. A hemothorax results usually due to a trauma, occasionally spontaneously in patients with not well-adjusted anticoagulation. Liquid blood is often completely anechoic (Fig. 3.41). Coagulation develops different grades of echogenicity. Then the echogenic pleural content is deformable, e.g. by respiration, but is obviously not liquid. Later the hemorrhage gets organized and a fibrosis develops. To prevent this process a hemothorax should be drained early with large-caliber tubes. Patients with a severe chest trauma should be examined soon by ultrasound already in the emergency room, if possible earlier at the scene or in the ambulance. If fluid is detected in the

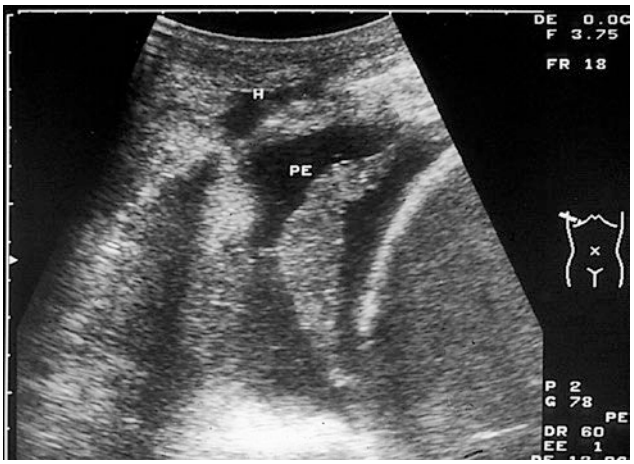

Fig. 3.41 Emergency examination in the surgical emergency room in a roofer, fallen from the roof. Dyspnea and severe chest pain on the right side. Echofree but still bloody effusion with lung atelectasis and partial rupture of the chest wall. Fluid mass included in the chest wall at the same location as a visible hematoma at the skin

pleura and a bloody effusion is confirmed by aspiration, immediately a tube drainage is administered after previous sonographical localization of a suitable puncture site. The following computed tomography then shows possible further injuries, especially at the spine and the big vessels.

As a result of stab injuries, rib fractures with pike-like broken ribs penetrating into the lung or due to an explosion trauma with lung rupture a pneumothorax can occur. Patients with a tension pneumothorax develop rapidly increasing dyspnea and a shock. By ultrasound the diagnosis of a pneumothorax is established within a few seconds (see ▶ Sect. 3.6) and the mandatory chest tube immediately can be administered. Supine chest-X-ray displays in only 50% a traumatic pneumothorax. Many emergency physicians nowadays know about the high potentials of ultrasound to prove a pleural effusion or a pneumothorax with high sensitivity and specificity.

A chest wall emphysema may prohibit the sonographic examination of the pleura (see ▶ Chap. 2). A posttraumatic chest wall emphysema is often combined with a pneumothorax.

3.8 Diaphragm

The diaphragm is routinely displayed by ultrasound during a transabdominal examination of spleen and liver, but attracts little attention. Many studies in the last few years dealt with the diaphragm.

3.8.1 Normal Diaphragm

The muscular part of the diaphragm inserts in the region of the lower aperture of the thorax at the ribs, the sternum and the spine. The diaphragmatic muscle presents in the ultrasound image as a narrow three-layered structure, the real muscle in the middle hypoechoic. During respiration, especially during forced respiration, the thickening in the contraction is visible (◘ Fig. 3.42). In particular in patients suffering from chronic obstructive lung disease the contraction-dependent thickening can be well recognized. The dome of the diaphragm consists of only a thin aponeurosis, sonographically often not to separate from the line of total reflection at the bottom of the lung. The diaphragmatic crura can be discovered on both sides of the upper abdominal aorta cranial of the origin of the celiac axis. In posterior longitudinal sections through liver or spleen the diaphragmatic crura can be found as strictly muscular organ along the spine. Normally the trigonum sternocostalis on both sides cannot be seen as well as the posterior hiatus pleuroperitonealis Bochdalek on both sides.

Normally the diaphragm bulges like a dome into the lower thorax. The flattening of the diaphragm in obstructive lung diseases can be detected in the individual case by ultrasound, not only radiologically. In severe emphysema the diaphragm may be bulged inversely.

In obese or COLD- patients often exist furrows of the diaphragm, impressing consecutively the liver. The diaphragmatic duplication is well detectable in the furrow at the liver surface. An "unsuccessful" flat transverse section through such a furrow can fake a focal liver

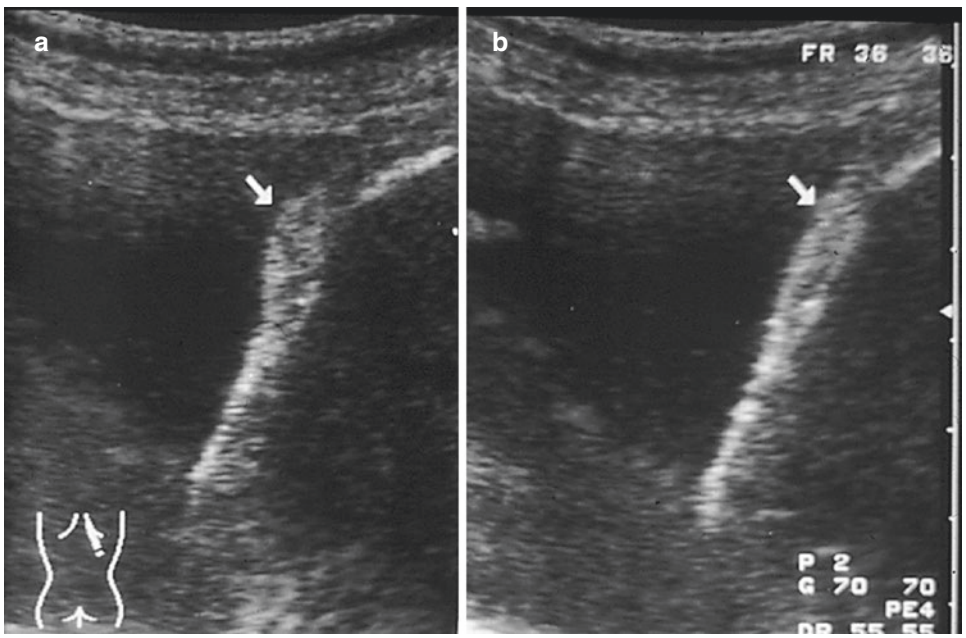

◘ **Fig. 3.42** **a**, **b** Diaphragm with pleural effusion, the transition of the thicker muscular part into the aponeurosis in the dome is well to differentiate. In inspiration the muscle shortens and becomes thicker (**a**, arrow) and slackens during expiration (**b**, arrow)

lesion. Furrows at the spleen are usually only detectable in splenomegaly.

3.8.2 Visualization

Because of the pleural recesses and the normal air-filled lung the diaphragm is only depictable through the abdomen, through the liver on the right side and through the spleen on the left side. A pleural effusion enables to demonstrate the complete diaphragm through the pleural cavity. Then the aponeurosis in the dome is also clearly to visualize. Under real time conditions the diaphragmatic motion can be observed and, if necessary, recorded in a short video clip.

3.8.3 Diaphragmatic Hernia

Congenital hernias are only exceptionally discovered in the adult. The most important findings are abdominal organs, located in the thorax, e.g. mostly gut, less common liver, spleen or kidneys. In newborns with severe respiratory insufficiency a congenital diaphragmatic hernia has to be considered. According to a S1-guideline (Leutner et al. 2016) the standard diagnostic procedure in infants is a chest-X-ray. But gut in the chest can also be proven by means of ultrasound. Skilled ultrasound specialists are able to find a diaphragmatic hernia also in fetuses beyond the 18. week of gestation (Fig. 3.43).

The esophagogastric transition zone can be nearly regularly demonstrated as round multilayered formation. Axial sliding hernias are occasionally visible by ultrasound, but its evidence is of limited value. In reflux complaints endoscopy is mandatory to find a possible Barrett's esophagus.

3.8.4 Diaphragmatic Rupture

Ruptures of the diaphragm after severe abdominal or chest traumas occur in 1–3%. Only in one quarter of the patients these ruptures are detected preoperatively (Rubikas 2001; Ozpolat et al. 2009). The displacement of abdominal organs into the chest is the main sonographical symptom. The patients often have a hemorrhagic effusion. This ultrasound window improves the visualization of the diaphragm.

The margins of the rupture and the gap in the diaphragm are only depictable in individual cases (Fig. 3.44). A seeming gap in the diaphragm caused by an edge shadow artifact should not be misleading. The changing localization of the gap with changing the position of the transducer excludes an actual gap. These severe ill patients need a computed tomography to visualize preoperatively additional findings in the chest, abdomen, retroperitoneum and skeleton which are not demonstrable by ultrasound. In many of these cases the sonographic proof of liquid in the abdomen by FAST leads to an emergency operation. Then intraoperatively the diaphragmatic rupture turns out (Hansen and Muhl 1997).

Occasionally diaphragmatic ruptures are diagnosed years after the trauma, e.g. due to small rupture without severe symptoms. With time, the traumatic hernia canal widens and larger parts of the abdominal organs are displaced into the chest and cause respiratory insufficiency or perfusion disturbances at the herniated organs.

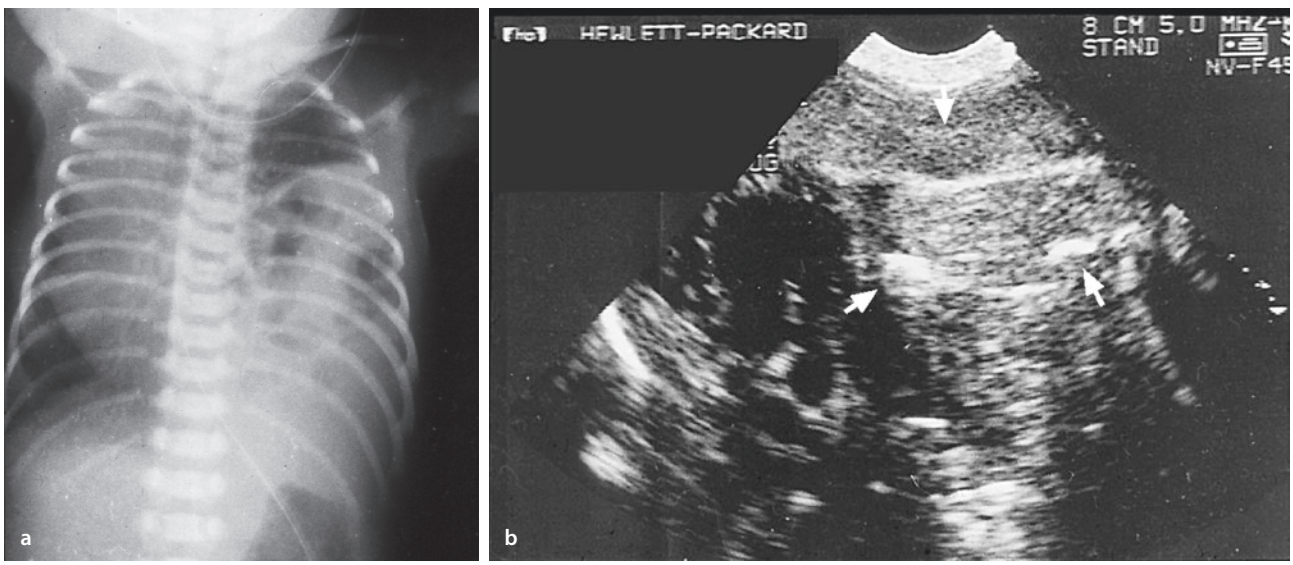

Fig. 3.43 **a**, **b** **a** Chest-X-ray of an infant with gas-containing intestinal organs in the left hemithorax indicating a large congenital diaphragmatic hernia. **b** Typical ultrasound image of a congenital diaphragmatic left-sided hernia with the stomach beneath the clearly identifiable heart. Subxiphoidal cross section. (Courtesy Prof. Manfred Teufel, Children's hospital, Klinikverbund Südwest, Bunsenstr.120, D 71032 Böblingen)

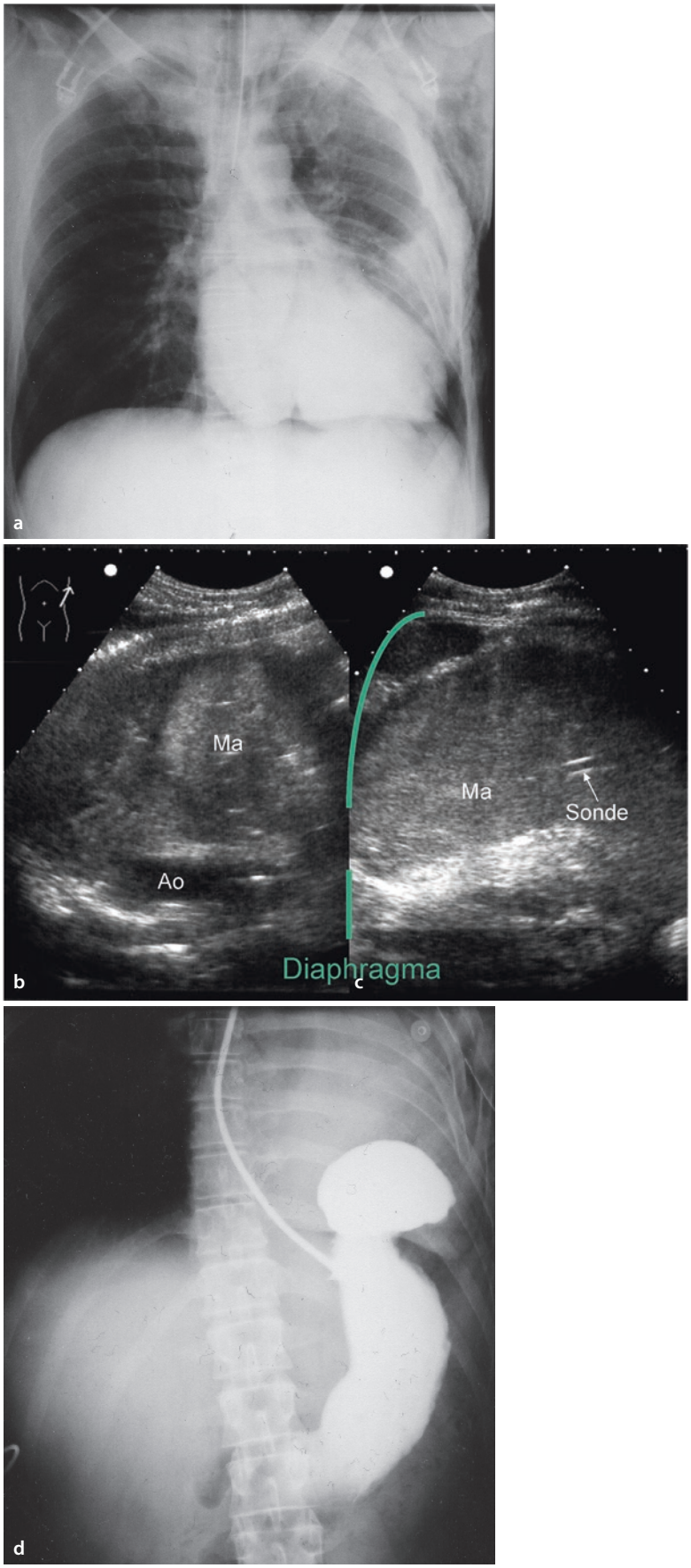

Fig. 3.44 **a**–**d** Male patient after fall from a balcony in the fourth floor. Despite tube drainage due to hematothorax worsening oxygen saturation in mechanical ventilation. **a In the chest-X-ray** opacification infero-lateral on the left, therefore immediate ultrasound examination because of suspected not drained part of the hematothorax. **b** Sonographically in the chest a round inderterminable structure filled with echogenic fluid. **c** Below the diaphragm parts of the stomach with tube. In the dynamic examination the stomach can be tracked through the diaphragm into the chest (composite image). **d** Confirmation of the diagnosis by filling the stomach with contrast via the tube. In CT the diaphragmatic rupture shown but misinterpreted

3.8.5 Diaphragmatic Tumors

Primary tumors of the diaphragm are rare and the diagnosis is usually not made in early stages, at most as an incidental finding (Belaabidia et al. 2006) (Figs. 3.45 and 3.46). Also metastases in the diaphragm are rare, but may cause pain by infiltrating adjacent nerve plexuses (Figs. 3.47 and 3.48). Diaphragmatic metastases are typically enclosed in the diaphragm in contrary to pleural or—less common—peritoneal metastases placed on the diaphragm. Large pleural metastases may infiltrate into or break through the diaphragm (Figs. 3.47, 3.48, and 3.49). Pleural mesotheliomas may present an infiltration of the diaphragm as well as into the liver or spleen. By ultrasound not only the tumor infiltration is visible but also the tumor related fixation and paresis of the diaphragm.

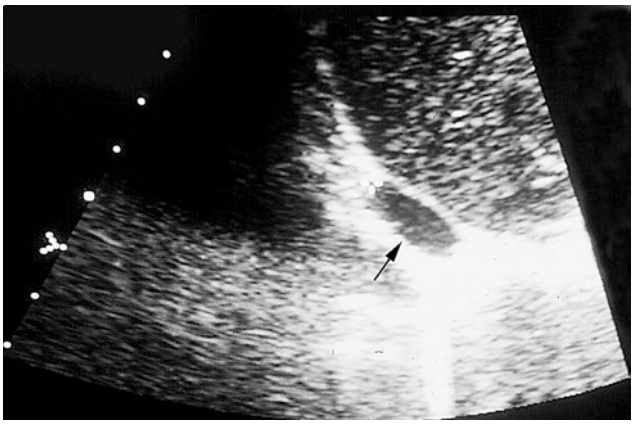

Fig. 3.45 Rare finding of a lipoma in the diaphragm. Smoothly demarcated tumor (arrow) presenting in similar fashion in CT showing fat density

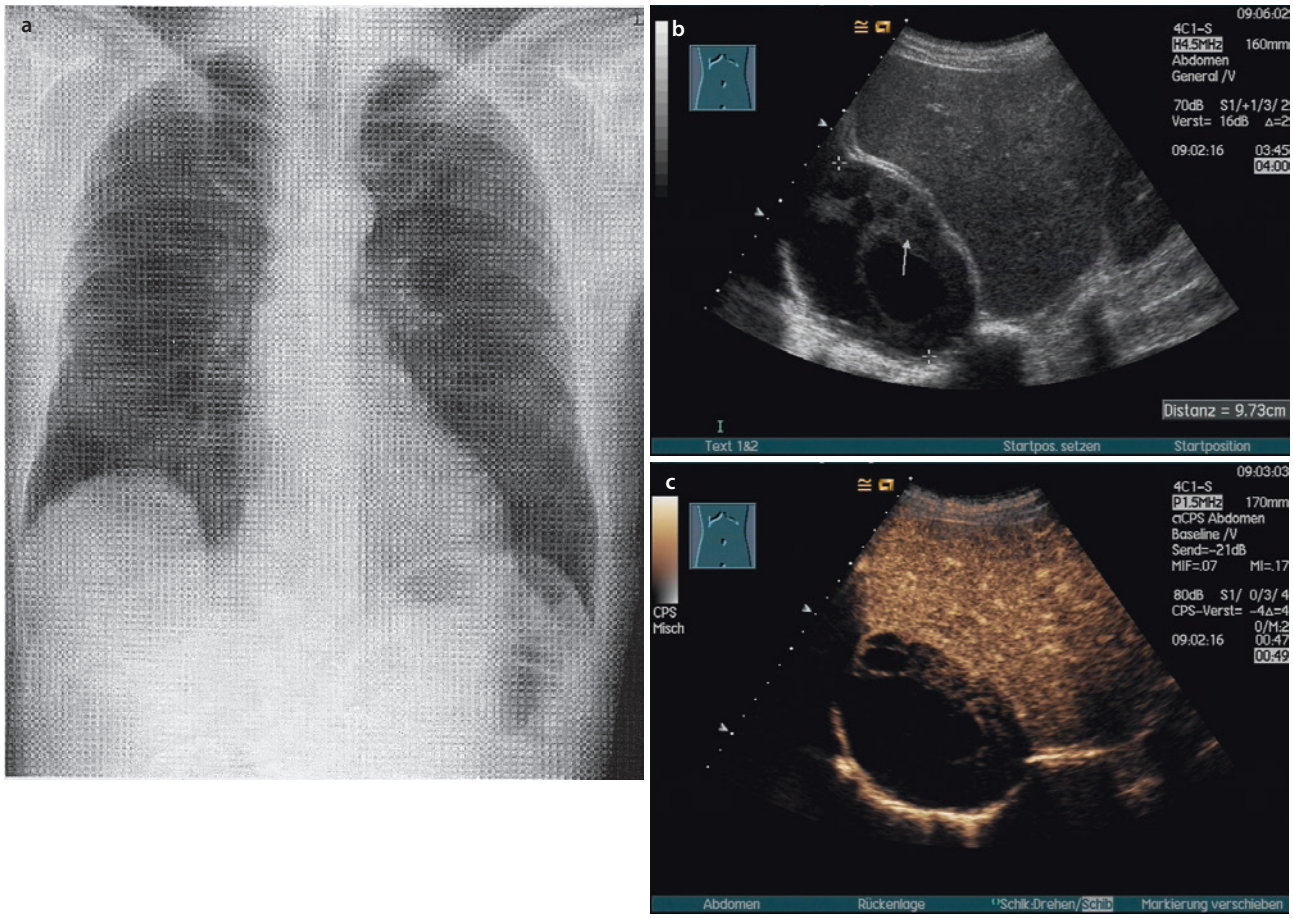

Fig. 3.46 **a**–**c** **a** Smoothly demarcated opacification at the diaphragm in chest-X-ray, incidental finding. In retrospect this lesion was already guessed on a previous chest-X-ray 7 years earlier. **b** By ultrasound a cyst-like lesion with solid parts and septae seeming to originate from the diaphragmatic pleura. No calcifications, with color-Doppler no vessels detectable. **c** By CEUS in the bronchial-arterial phase the solid parts and the septae contrast enhancing, the vessels originating from the diaphragm. Thus a hydatid disease ruled out, the echinococcus titer negative. The tumor was removed by operation, histologically a solitary fibrous tumor of the diaphragm with low malignant tendency (Prof. Katenkamp, Jena, Germany), formerly known as hemangiopericytoma

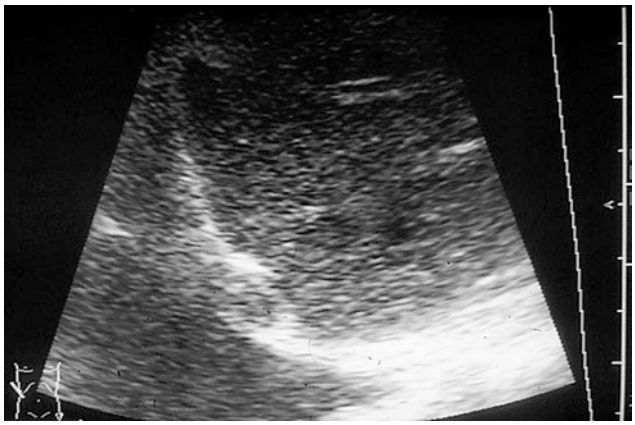

Fig. 3.47 In ultrasound a similar finding like in Fig. 3.45 in a patient with known lung cancer, so far no metastases. The lesion was found during a routine follow up examination. Computed tomography could not comprehend the lesion. By ultrasound guided puncture a metastasis of the known lung cancer confirmed

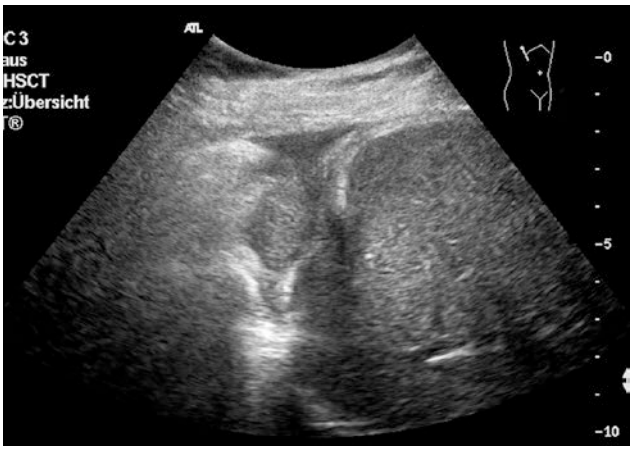

Fig 3.49 Pleural metastasis with deep infiltration, deformation and destruction of the diaphragm. Pleural carcinosis with effusion. 19 years ago diagnosis of a breast cancer, two years ago diagnosis of a ovarian cancer

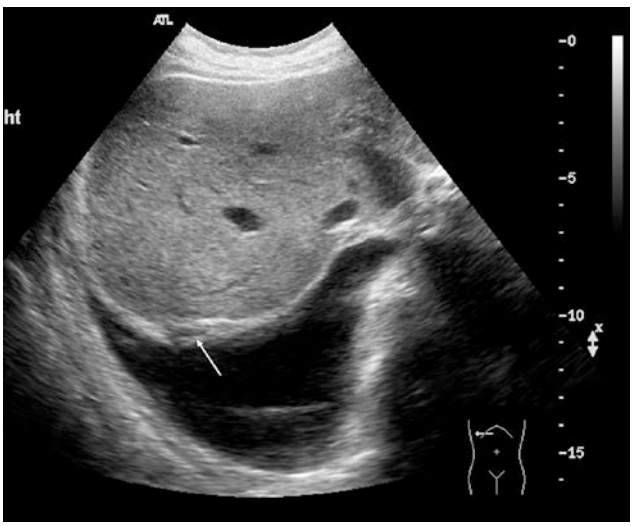

Fig. 3.48 Metastasis of a breast cancer in the diaphragm. Artificial echoes in a large pleural effusion

3.8.6 Diaphragmatic Eventration

Behind the radiological description of a diaphragmatic eventration can hide different situations. The diaphragm can in fact be dislocated due to paresis or due to displacement by giant organs or liquid collections. Unusual inferior lung consolidations or tumors or a subpulmonary effusion can pretend a diaphragmatic eventration. By ultrasound the situation can soon be clarified (Table 3.10).

3.8.7 Functional Examination

The real time ultrasound examination offers the best conditions for the functional examination of the diaphragm. A normal bilateral up-and-down-movement of the diaphragm with respiration, identical on both sides, is clearly visible. Pleural peels close to the chest wall cause a immobility of the parietal part of the diaphragm. A residual motion can be detected, ruling out a complete phrenical paresis. Old pleural lesions may be very discreet in the image, so that the dynamic examination with demonstration of the "sticking" is important. Short video clips are optimal for the documentation of the diaphragmatic motion. Using the time-motion-mode not only the movement of the diaphragm can be detained, but also the extent of the motion can approximately be measured. For this measurement the transducer, preferably a phased-array-transducer, is positioned on the abdomen in the medioclavicular or anterior axillary line, directed to the posterior part of the diaphragm, thus ensuring that the diaphragm in the B-mode is well detectable and during respiration is moving towards the transducer. From the time-motion-curve

Table 3.10 Sonographically discernable causes of a diaphragmatic eventration

Unilateral	Abdominal cause	Large liver or spleen Large liver tumors Subphrenical capsulated liquid formations (seroma, bilioma, abscess) Unilateral paresis of the diaphragm
	Cause in the chest = seemingly eventration	Atypical inferior lung consolidation (pneumonia, atelectasis) Subpulmonary effusion, capsulated or loculated Inferior pulmonary, pleural or diaphragmatic tumor, possibly in combination with lung atelectasis
Bilateral	Abdominal cause	Abdominal obesity Ascites
	Cause in the chest = seemingly eventration	Bilateral subpulmonary effusion Bilateral inferior atelectasis

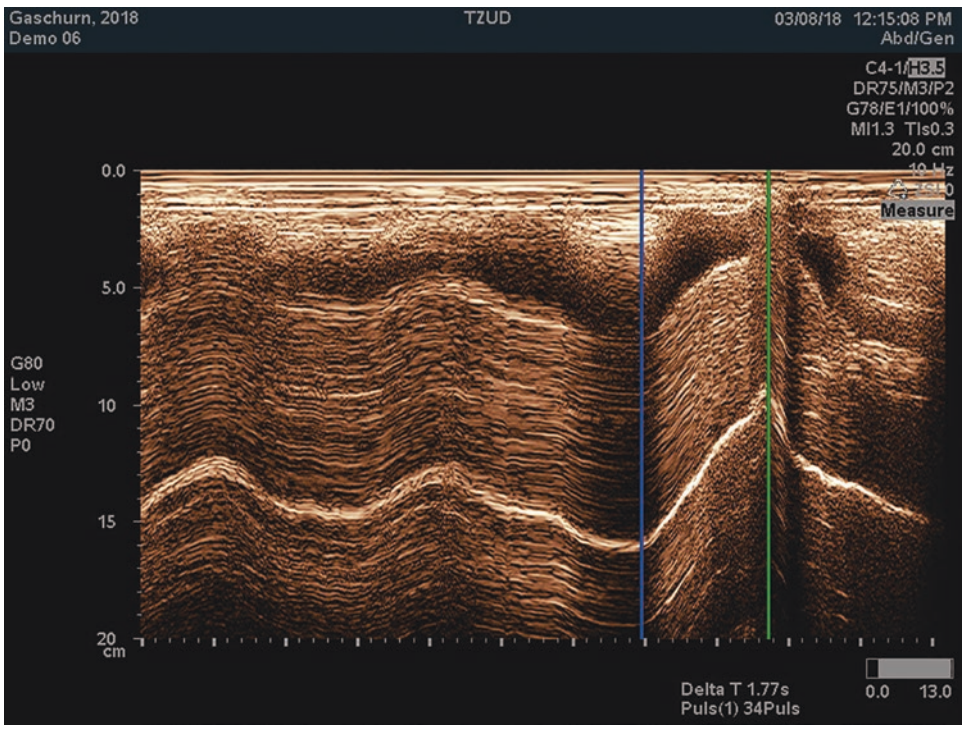

Fig. 3.50 Diaphragm mobility in M-mode. Left for calm breathing, right for deep inspiration

different parameters can be picked out. The most frequently used parameter is the shift of the diaphragm in centimeter during normal and forced breathing (Figs. 3.50, 3.51 and 3.52). Other values are the contraction velocity of the diaphragm as well as the inspiration and breath cyclus time (Lloyd et al. 2006; Matamis et al. 2013; Soilemezi et al. 2013). See Table 3.11

A phrenical paresis is immediately noticed by missing or paradoxical diaphragmatic movement (Lloyd et al. 2006). Tumors at the neck or in the mediastinum causing the paresis are detectable by ultrasound. Diaphragmatic pareses acquired during birth can be recorded sonographically by the pediatrician (Urvoas et al. 1994). Normal chest_X-rays do not allow a reliable conclusion concerning the diaphragmatic function, but ultrasound (Epelman et al. 2005). Patients after stroke and residual dysphagia show a markedly reduced diaphragmatic motility, in normal breathing as well as under forced breathing and when coughing. The reduced motility correlates with lung function. In studies these data are already included in the rehabilitation planning (Jung et al. 2014). A sonographical assessment after long-term mechanical ventilation in adults provides information about the function and the respiratory mechanical function can be estimated—sufficient experience and expertise provided (Dorffner et al. 1998,

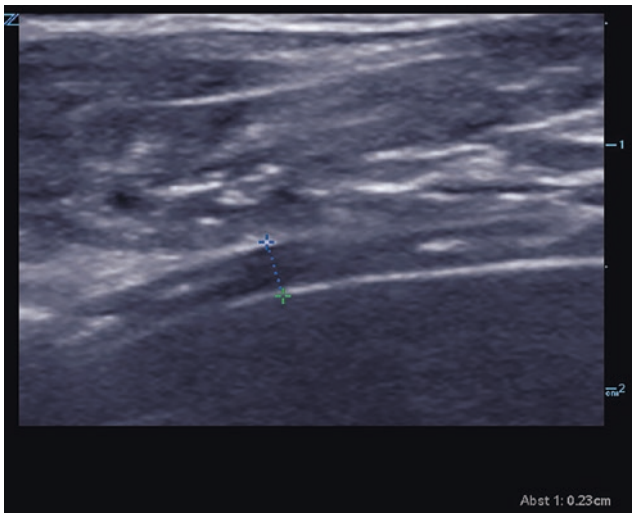

Fig. 3.51 Diaphragm thickness at expiration 23 mm

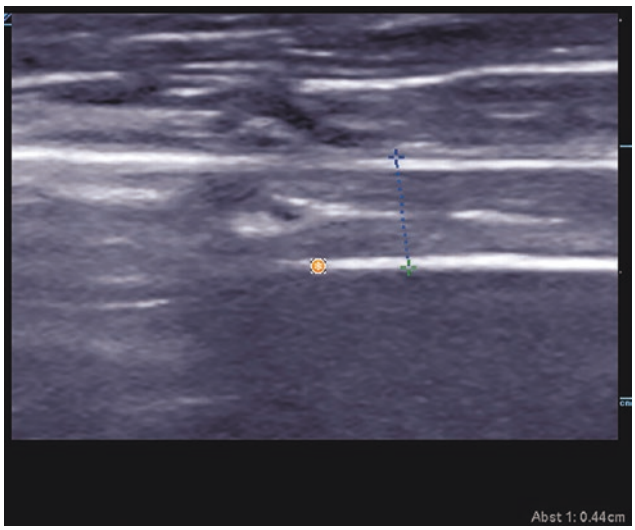

Fig. 3.52 Diaphragm thickness at deep inspiration 44 mm

Table 3.11 Benchmarks for diaphragmatic motion measured by ultrasound (according to Matamis et al. 2013)

		Normal values	
		m	f
Motion (cm)	Normal breathing	1.8	1.6
	Forced breathing	7.0	5.7
	Sniffing	2.9	2.6
	Mechanical ventilation	1.8	
Contraction velocity (cm/s)	Slope	1.3	

Goligher et al. 2015). This protects the patients against premature extubation and serves as basis for an additional forced training in the weaning phase (Gibis et al. 2019, Turton et al. 2019).

References

Abu Arab W (2012) Solitary fibrous tumours of the pleura. Eur J Cardiothorac Surg 41(3):587–597

Adams RF, Gleeson FV (2001) Percutaneous image-guided cutting-needle biopsy of the pleura in the presence of a suspected malignant effusion. Radiology 219(2):510–514

Alrajab S et al (2013) Pleural ultrasonography versus chest radiography for the diagnosis of pneumothorax: review of the literature and meta-analysis. Crit Care 17(5):R208

Balik M et al (2006) Ultrasound estimation of volume of pleural fluid in mechanically ventilated patients. Intensive Care Med 32(2):318

Belaabidia B et al (2006) Léiomyosarcoma of the diaphragm: a case report and review of the literature. Cancer Radiother 10(3):137–141

Cardillo G et al (2012) Solitary fibrous tumors of the pleura. Curr Opin Pulm Med 18(4):339–346

Chian CF et al (2004) Echogenic swirling pattern as a predictor of malignant pleural effusions in patients with malignancies. Chest 126(1):129–134

Colice GL et al (2000) Medical and surgical treatment of parapneumonic effusions: an evidence-based guideline. Chest 118(4):1158–1171

Colins JD et al (1972) Minimal detectable pleural effusions. A roentgen pathology model. Radiology 105(1):51–53

Dorffner R et al (1998) The value of sonography in the intensive care unit for the diagnosis of diaphragmatic paralysis. Rofo 169(3):274–277

Eibenberger KL et al (1994) Quantification of pleural effusions: sonography versus radiography. Radiology 191(3):681–684

Epelman M et al (2005) M-mode sonography of diaphragmatic motion: description of technique and experience in 278 pediatric patients. Pediatr Radiol 35(7):661–667

Geiger D et al (2003) Thoraxwandinfiltration und Stichkanalinvasion beim malignen Pleuramesotheliom. Ultraschall Med 24:34 abstract

Gehmacher O et al (1997) Can pleurisy be detected with ultrasound? Ultraschall Med 18(5):214–219

Gibis N et al (2019) Sonographically measured improvement in diaphragmatic mobility and outcomes among patients requiring prolonged weaning from the ventilator. Open Respir Med J 13:38–44

Goecke W, Schwerk WB (1990) Die Real-Time-Sonographie in der Diagnostik von Pleuraergüssen. In: Gebhard J, Hackelöer BJ, von Klinggräff G, Seitz K (eds) Ultraschalldiagnostik 89. Springer, Berlin

Goligher EC et al (2015) Measuring diaphragm thickness with ultrasound in mechanically ventilated patients: feasibility, reproducibility and validity. Intensive Care Med 41(4):642–649

Görg C, Bert T, Görg K (2005) Contrast-enhanced sonography for differential diagnosis of pleurisy and focal pleural lesions of unknown cause. Chest 128(6):3894–3899

Gryminski J, Krakówka P, Lypacewicz G (1976) The diagnosis of pleural effusion by ultrasonic and radiologic techniques. Chest 70(1):33–37

Hansen M, Muhl E (1997) Blunt thoracic trauma--therapeutic relevance of results of roentgen image, ultrasound and computerized tomography. Langenbecks Arch Chir Suppl Kongressbd 114:458–460

Hassan M et al (2017) Validation of equations for pleural effusion volume estimation by ultrasonography. J Ultrasound 20(4):267–271

Heffner JE (2010) Management of the patient with a malignant pleural effusion. Semin Respir Crit Care Med 31(6):723–733

Hooper C, Lee YCG, Maskell N (2010) Investigation of a unilateral pleural effusion in adults: british thoracic society pleural disease guideline. Thorax 65(Supl. 2):ii4–ii17

Jung KJ et al (2014) Ultrasonographic diaphragmatic motion analysis and its correlation with pulmonary function in hemiplegic stroke patients. Ann Rehabil Med 38(1):29–37

Kelbel C et al (1991) Diagnosis of pleural effusions and atelectases: sonography and radiology compared. Rofo 154(2):159–163

Kocijancic I, Kocijancic K, Cufer T (2004) Imaging of pleural fluid in healthy individuals. Clin Radiol 59(9):826–829

Layer G et al (1999) MRT, CT and sonography in the preoperative assessment of the primary tumor spread in malignant pleural mesothelioma. Rofo 170(4):365–370

Lehnert M et al. (2009) Incidence of malignant mesothelioma in Germany 2009–2013. Cancer Causes & Control 28:97–105

Leutner A et al (2016) Congenital diaphragmatic hernia (CDH), S1-guideline of the German Society for Pediatric Surgery. Arbeitsgemeinschaft Wissenschaftlich-Medizinischer Fachgesellschften AWMF

Lichtenstein D et al (1997) The comet-tail artifact. An ultrasound sign of alveolar-interstitial syndrome. Am J Respir Crit Care Med 156(5):1640–1646

Lichtenstein D et al (2000) The "lung point": an ultrasound sign specific to pneumothorax. Intensive Care Med 26(10):1434–1440

Light RW (2006) Parapneumonic effusions and empyema. Proc Am Thorac Soc 3(1):75–80

Lloyd T et al (2006) Diaphragmatic paralysis: the use of M mode ultrasound for diagnosis in adults. Spinal Cord 44(8):505–508

Matamis D et al (2013) Sonographic evaluation of the diaphragm in critically ill patients. Technique and clinical applications. Intensive Care Med 39(5):801–810

Mathis G (1997) Thoraxsonography—Part I: Chest wall and pleura. Ultrasound Med Biol 23(8):1131–1139

Neumann V et al. (2013) Malignant pleural mesothelioma. Dtsch Arztebl 110(18):319–326

Ozpolat B et al. (2009) Diaphragmatic injuries: a surgical challenge. A report of forty-one cases. Thorac Cardiovasc Surg 57(6):358–362

Reuss J (2010) Sonography of the pleura. Ultraschall Med 31(1):8–22. quiz 23-5

Reuss J, Blank W, Drews U et al (2002) Sonographisch-anatomischer Vergleich des Aufbaus der inneren Thoraxwand zwischen Interkostalmuskulatur und Pleuraspalt. Ultraschall Med 23(Suppl. 1):70

Roch A et al (2005) Usefulness of ultrasonography in predicting pleural effusions > 500 mL in patients receiving mechanical ventilation. Chest 127(1):224–232

Rubikas R (2001) Diaphragmatic injuries. Eur J Cardiothorac Surg 20(1):53–57

Soilemezi E et al (2013) Sonographic assessment of changes in diaphragmatic kinetics induced by inspiratory resistive loading. Respirology 18(3):468–473

Soldati G et al (2008) Occult traumatic pneumothorax: diagnostic accuracy of lung ultrasonography in the emergency department. Chest 133(1):204–211

Tasci S et al (2005) Long-term outcome of intrapleural fibrinolytic therapy via small-bore catheter drainage in the management of complicated parapneumonic effusion and empyema-a case series. Med Klin (Munich) 100(4):181–185

Turton P, ALAidarous S, Welters I (2019) A narrative review of diaphragm ultrasound to predict weaning from mechanical ventilation: where are we and where are we heading? Ultrasound J 11(1):2

Urvoas E et al (1994) Diaphragmatic paralysis in children: diagnosis by TM-mode ultrasound. Pediatr Radiol 24(8):564–568

Vignon P et al (2005) Quantitative assessment of pleural effusion in critically ill patients by means of ultrasonography. Crit Care Med 33(8):1757–1763

Volpicelli G et al (2012) International evidence-based recommendations for point-of-care lung ultrasound. Intensive Care Med 38(4):577–591

Wilkerson RG, Stone MB (2010) Sensitivity of bedside ultrasound and supine anteroposterior chest radiographs for the identification of pneumothorax after blunt trauma. Acad Emerg Med 17(1):11–17

Yang PC et al (1992) Value of sonography in determining the nature of pleural effusion: analysis of 320 cases. AJR Am J Roentgenol 159(1):29–33

Yarmus L, Feller-Kopman D (2012) Pneumothorax in the critically ill patient. Chest 141(4):1098–1105

Interstitial Syndrome

Giovanni Volpicelli and Luna Gargani

Contents

G. Mathis (ed.), *Chest Sonography*, https://doi.org/10.1007/978-3-031-09442-2_4

4

4.1 General Considerations

It is standard textbook knowledge that «because ultrasound energy is rapidly dissipated by air, ultrasound imaging is not useful for the evaluation of the pulmonary parenchyma» (Manaker and Weinberger 2008). The concept that ultrasound cannot be employed for evaluating the lung is linked to the presence of air, which determines a very high acoustic mismatch with the surrounding tissues, causing a complete reflection of the ultrasound beam, which prevents the creation of real imaging of the pulmonary parenchyma. In a normally aerated lung, the only detectable structure is the pleura, visualized as a hyperechoic horizontal line. Even this image is an artefact due to a reverberation phenomenon at the interface between alveolar air and the soft tissues of the thoracic wall. Below the pleural line, the artefact image of the lung moves synchronously with respiration against the chest wall. In addition, some hyperechoic, horizontal lines arising at regular intervals from the pleural line can be seen: the A-lines (Fig. 4.1). However, even if the corresponding lung area is imaged only as artifacts at ultrasound, these give many important clinical information (Volpicelli 2013).

When combined with a respiratory movement, the reverberation artefacts represent a sign of normal or excessive content of air in the alveolar spaces. When the air content decreases and lung density increases due to the presence in the lung of exudate, transudate, collagen, blood, hyper cellularity, the acoustic mismatch between the lung and the surrounding tissues is lowered, and the ultrasound beam will be partly reflected at deeper zones and repeatedly. This phenomenon creates on the screen some vertical reverberation hyperechic artefacts, known as B-lines, formed by multiple short horizontal lines that are repeated in a vertical tight sequence (Fig. 4.2). B-lines belong to the family of the comet-tail artefacts, very well known in abdominal ultrasound (Ziskin et al. 1982). In some studies, published before an experts agreement on nomenclature that was obtained in the recent consensus conference on lung ultrasound (LUS), B-lines have also been addressed as comet-tail artifacts or ultrasound lung comets (Volpicelli et al. 2012). B-lines are defined as discrete laser-like vertical hyperechoic reverberation artifacts that arise from the pleural line, extend to the bottom of the screen without fading, and move synchronously with lung sliding. Multiple B-lines are considered the sonographic sign of lung interstitial syndrome, and their number increases along with decreasing air content and increase in lung density (Volpicelli et al. 2012).

Therefore, although air limits the reconstruction of a real image of the normal lung, the alteration in the balance between air and fluids of the diseased lung significantly modifies the normal ultrasound pattern. This can happen both in case of deflation of the lung with maintenance of a constant weight, but also when the weight of the lung rises for the increase in fluids, cells, connective tissue or blood content. In other words, whether the cause is a simple deflation or an increase in fluids and cellularity of the lung parenchyma, ultrasound is highly sensible to variations of the organ density as deduced by studies on phantoms, animal models and humans (Volpicelli 2013).

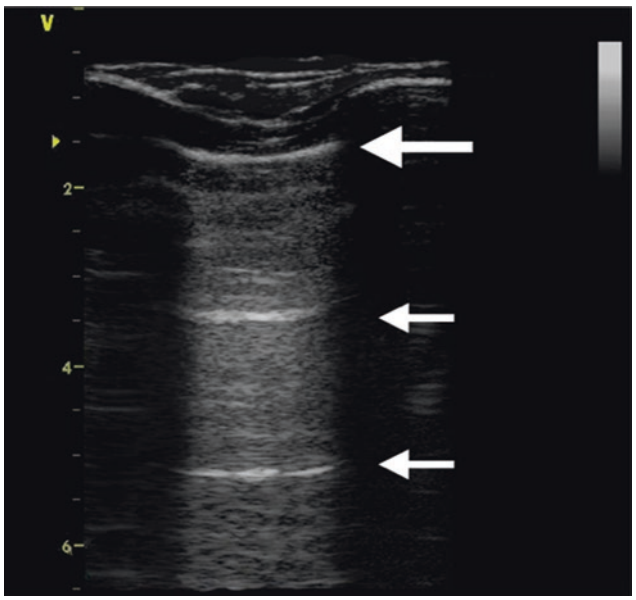

Fig. 4.1 The white arrows indicate the linear echoic images corresponding to the pleural line (large arrow) and the A-lines (small arrows)

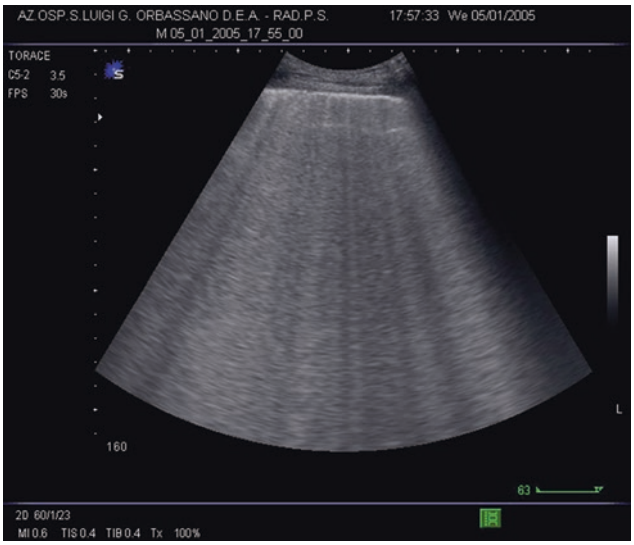

Fig. 4.2 An ultrasound lung scan showing multiple B-lines, in a case of acute pulmonary edema

Thus, the acoustic limitations of ultrasound in the assessment of an air-rich organ such as the lung can paradoxically become a diagnostic advantage. The artifacts created by the mismatch between air and tissues in the lung are easy to detect and correspond to their quantitative balance.

However, the diagnostic approach based on LUS can vary according to different settings and clinical situations, following the main principle of what is today known as "point-of-care ultrasound" (Moore and Copel 2011). On occasion, the best efficacy of the method is obtained by a clinically driven, focused assessment. If properly driven and correctly interpreted, even signs that have low significance in the general population become highly accurate for diagnosing specific pulmonary conditions (Gargani and Volpicelli 2014). The correlation with the specific setting and patient's symptoms of presentation, the clinical history, but also the evolution of the clinical situation and the corresponding change in the ultrasound pattern during the time course of our observation and treatment, may be crucial for a correct interpretation.

4.2 Interstitial Syndrome

The interstitial syndrome is a condition where alveolar air is impaired due to increase of fluids in the interstitium, but some lung aeration is still preserved as opposed to a condition of complete consolidation of the lung. The potential of LUS for the diagnosis of the interstitial syndrome has been mainly shown in studies on critically ill patients and in patients attending the emergency department (Lichtenstein and Meziere 2008; Pivetta et al. 2015). Also, some other studies showed the usefulness in chronic fibrosis and in chronic renal failure patients submitted to dyalisis (Reissig and Kroegel 2003; Mallamaci et al. 2010).

The main principle of the ultrasound diagnosis of interstitial syndrome is based on the recognition of B-lines, a rough and very basic count in the single scan and the count and distribution of positive scans. At least three B-lines visualized in a longitudinal view, define a positive scan. The bilateral distribution of multiple positive scans in at least two different chest areas per side, generally define the condition of diffuse interstitial syndrome. Isolated positive scans, or more than one but not bilateral, are diagnostic of a focal interstitial syndrome (Volpicelli et al. 2012).

Even if detection of the B-line pattern cannot differentiate between cardiogenic edema, ARDS and pulmonary fibrosis, this simple bedside technique has immediate effect in the in real-time diagnostic process of the critically ill and dyspneic patients. The use of a simplified LUS protocol was more accurate than the conventional tools in the first 2 h initial diagnoses in acute respiratory failure, showing a better immediate effect and yielding correct prompt diagnoses in 90.5% of patients (Lichtenstein and Meziere 2008).

In the evaluation of patients with acute respiratory failure, the B-line pattern allows for a differentiation between a cardiogenic and a respiratory origin of the disorder, because exacerbation of COPD, pulmonary embolism, pneumonia, pneumothorax yield a non-interstitial ultrasound pattern (Gargani et al. 2008; Zanobetti et al. 2011). In selected patients with acute decompensated heart failure or end stage renal failure, B-lines represent a sign of extravascular lung water, which allows monitoring of pulmonary congestion by simply observing its clearance at repeated LUS examinations (Volpicelli et al. 2008). In ARDS patients submitted to invasive ventilation with positive pressure, sonographic evaluation for B-lines allows monitoring of re-aeration and can be used to guide therapeutic maneuvers (Bouhemad et al. 2011).

4.3 Technique

In a patient with acute dyspnea, if cardiogenic pulmonary edema is in the differential diagnosis, LUS will be used to examine the anterior and lateral chest to detect the diffuse signs of interstitial and alveolar edema, which usually respect three highly specific features: they are correlated with the severity of the respiratory failure, follow a regular and symmetric spatial distribution, and usually progress from the lateral inferior (dependent zones) to the anterior upper chest areas. The scanning technique that should be employed in the emergency setting is the eight-zone examination, consisting of scanning four chest areas per side: areas 1 and 2 denote the upper anterior and lower anterior chest, while areas 3 and 4 denote the upper lateral and basal lateral chest, respectively (Fig. 4.3) (Volpicelli et al. 2006). In the critically ill patient with acute respiratory failure, a more rapid anterior two-region scan may be even sufficient to rule out the interstitial syndrome due to cardiogenic acute pulmonary edema (Lichtenstein and Meziere 2008). However, this focused anterior scanning, while still highly accurate in acute situations in the critically ill, may not be sufficient in patients who are not so severely dyspnoic, since presence of B-lines on the anterior chest usually denotes a more severe degree of pulmonary congestion in case of heart failure. This interpretation is an example of adaptation of the LUS technique and signs to the specific setting and clinical condition.

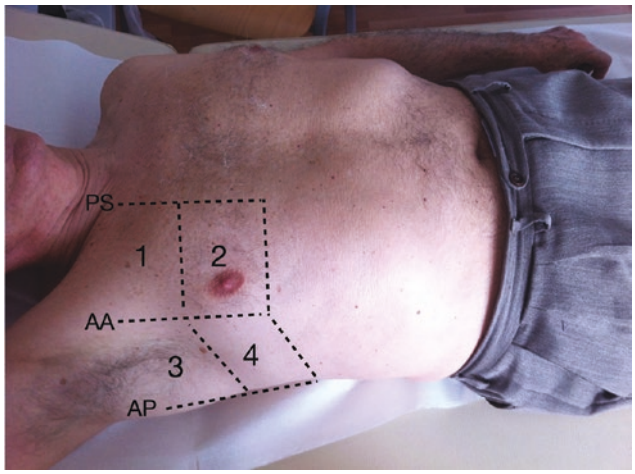

Fig. 4.3 The eight zones examination consisting of scanning four chest areas per side: the upper (1) and lower (2) anterior, the upper (3) and basal (4) lateral. PS parasternal line, AA anterior axillary line, AP posterior axillary line

In the setting of chronic patients, with less time pressure and more borderline cases, the scanning technique should always be more comprehensive. It can include the anterior, lateral, but also the dorsal chest. Different approaches have been proposed: a detailed scanning scheme has been used in many studies on patients with heart failure, on dialysis, and with pulmonary fibrosis, focused on the assessment of the consistency and distribution of B-lines. This comprehensive approach is particularly useful for quantifying the extent of the LUS abnormalities, and for assessing intra-patient variations after therapeutic interventions, including dialysis. Ultrasound scanning of the anterior and lateral chest is obtained on the right and left hemithorax, from the second to the fourth (on the right side to the fifth) intercostal spaces, and from the parasternal line to the axillary line. The posterior chest is scanned along the paravertebral line, scapularis line and posterior axillary line. The sum of the B-lines found on each scanning site yields a score denoting the extent of the pulmonary interstitial syndrome (see below for the techniques of quantifications).

In the case of limited time, even in a chronic setting the examination can be more focused and should be clinically driven. In patients with heart failure, it is important to scan also the dependent zones, i.e., lung posterior basis if we are evaluating an out-patient, or along the posterior and mid-axillary lines if we are scanning an in-patient who has been lying down for many hours. In patients with interstitial lung disease such as pulmonary fibrosis, it is mandatory to scan the posterior chest, because the disease generally starts in this region of the lung (Gargani and Volpicelli 2014).

The patient can be scanned in any decubitus, since lung abnormality distribution does not change so rapidly that significant information would be missed (apart from pleural effusion) just by changing the patient's position. Moreover, in the case of pulmonary congestion, even if the position of B-lines changes, the overall distribution tends to remain the same, without clinically relevant differences. The supine position is ideal for scanning the anterior chest, whereas the lateral chest may be examined in the semi-supine position (on the left decubitus to scan the right axillary lines, and on the right decubitus to scan the left axillary lines). The optimum position for scanning the posterior chest is with the patient sitting on the bed, his/her back turned to the operator. Indeed, it is possible also to scan patients while they are standing, sitting or lying flat, without significant differences in results. The only real limitation is when LUS needs to be extended to the dorsal chest of a patient lying down who is intubated in the intensive care unit, or a patient who is unconscious and cannot be moved. In these situations, using small probes that may be better placed between the bed and the patient may allow the best result (Fig. 4.4).

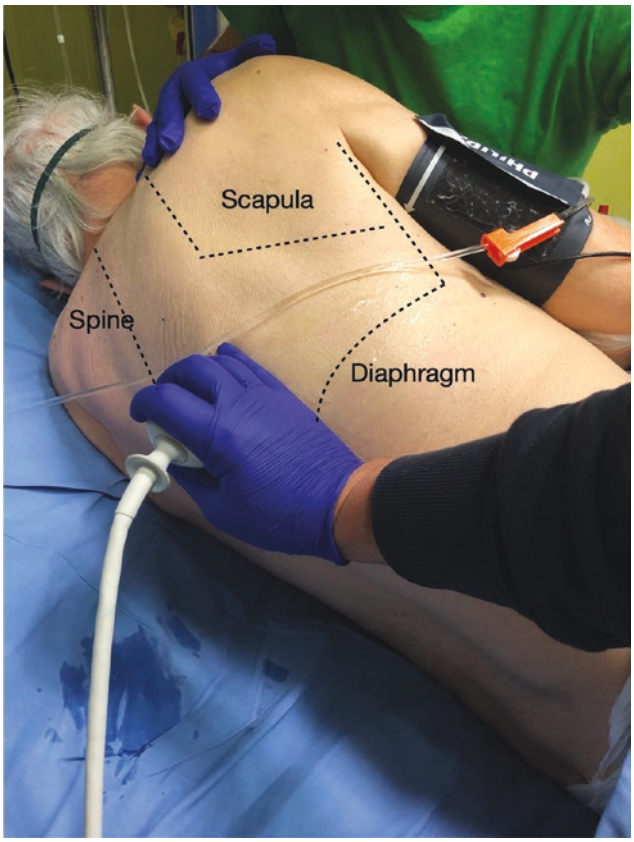

Fig. 4.4 The use of small probes may be helpful in examining the dorsal scans in bedridden patients

Although the number of B-lines may be slightly different when using different probes in a specific chest site,

the overall clinical picture does not change by changing the transducer. The possibility of easily assessing B-lines with any kind of transducer is one of the advantages of this technique, so no one should give up on scanning a patient just because the "ideal" probe is not available. Portable machines and pocket-sized devices have also been proposed for assessing B-lines. There is no need for a second harmonic or Doppler imaging mode, so even very old ultrasound machines can be employed. Normally the focus should be positioned at the pleural line level.

4.4 Interpretation of the Sonographic Interstitial Syndrome

Interpretation of LUS images is usually not very challenging. We must keep in mind that LUS is more affected by lack of specificity than lack of sensitivity. A LUS pattern showing multiple B-lines may be not enough to establish a specific diagnosis, since it can be linked to different pathologic conditions. Indeed, this limitation in specificity is a common feature of several diagnostic tools that we routinely interpret in daily clinical practice, from physical examination to EKG, from chest X-ray to more sophisticated instrumental findings. The power of these tools resides in the interpretation of signs when combined with each other at bedside, together with a consideration of the overall clinical picture. When all patient characteristics are taken into account, including history, symptoms, physical examination, setting, comorbidities, medications, etc., specificity can increase significantly. For example, in a patient with systemic sclerosis and without any known left heart conditions, presence of multiple B-lines is more probably related to pulmonary fibrosis than to extravascular lung water. On the other hand, presence of multiple diffuse bilateral B-lines in a patient with reduced cardiac function is more likely to be related to extravascular lung water than to fibrosis.

Distribution of B-lines and pleural line characteristics are also crucial to increasing the specificity of LUS. B-lines due to cardiogenic pulmonary edema are usually bilateral, start appearing in the dependent zones and usually diffusing or recovering symmetrically. B-lines due to pulmonary fibrosis generally start at the posterior lung basis, and are often associated with irregularity of the pleural line and subpleural small consolidations. In contrast to pulmonary edema due to congestion or overhydration, acute lung injury/ARDS shows a inhomogeneous and irregular pattern, featuring many subpleural consolidations, highly fragmented pleural line and intense hyperlucent multiple B-lines alternating with spared areas (Fig. 4.5). This irregular distribution of B-lines contrasts with that observed

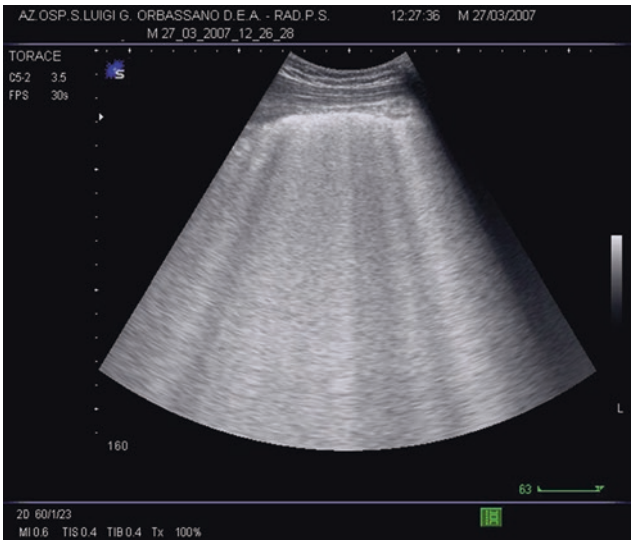

Fig. 4.5 This lung scan shows highly fragmented pleural line and intense hyperlucent multiple B-lines (alternating with spared areas when looking at the other zones). This pattern is typical of ARDS

in cardiogenic pulmonary edema, where B-lines are usually detected in more homogenous distribution, which is gravity-related, while it is quite rare when visualizing subpleural consolidations.

Dynamic response to therapy can also be useful for increasing the accuracy of LUS. In the case of multiple bilateral B-lines that are dissolved in days during ordinary treatment, or even in a few hours by an acute diuretic load, the cardiogenic or volume overload origin of B-lines is strongly suggested (Volpicelli et al. 2008). Similarly, in end-stage renal disease patients, B-lines decreasing or even disappearing after either a hemodialysis or peritoneal dialysis session, indicate pulmonary congestion due to overload (Mallamaci et al. 2010).

Additional information deriving from a bedside focused ultrasound evaluation of other organs may also be helpful. This approach has been described in patients with undifferentiated hypotension, where the integrated point-of-care multiorgan ultrasonography of the heart, inferior vena cava, lungs and abdomen significantly agreed with a final clinical diagnosis obtained by retrospective chart review (Volpicelli et al. 2013).

A controversial issue is quantification of B-lines. In critically ill patients the assessment can be qualitative, since the ultrasound finding of acute conditions is usually well defined and clear. For instance, in a critically ill patient with acute respiratory failure, if the underlying condition is cardiogenic pulmonary edema, the sonographic appearance of the lungs will be striking, with multiple diffuse bilateral B-lines that may even become very intense and numeorus to convey a picture of "white sonographic lung". In these patients, B-lines can also be found in the least dependent zones, i.e. the anterior chest.

On the contrary, finding a limited number of B-lines (even if bilateral) in a very symptomatic respiratory failure patient should lead to excluding the diagnosis of a cardiogenic origin of the actual condition, and orientate the diagnosis towards infection or other conditions.

In non-critical patients, a more careful assessment and quantification of B-lines may be useful, especially for the follow-up of a chronic condition. A semi-quantification of B-lines has been proposed and subsequently used in many papers from different research groups. This quantification is made possible by counting all B-lines in a specific scanning site. Zero is defined as a complete absence of B-lines in the investigated area, whereas when using a cardiac probe the full white screen in a single scanning site is considered as corresponding to ten B-lines (Gargani and Volpicelli 2014). However, B-lines cannot always be easily enumerated, especially if they are many, since they often tend to be confluent. A helpful rule is to consider the percentage of the scanning site occupied by B-lines (i.e. the percentage of white screen compared to black screen below the pleural line) and then divide it by ten. For clinical purposes, the final number of B-lines can then be categorized ranging from mild to severe degrees, similar to what is done for most echocardiographic parameters (Gargani and Volpicelli 2014). This counting approach can be imprecise when considering single scanning sites, but nevertheless provides a reliable overall LUS picture, allowing more accurate monitoring of patients, both in acute conditions—i.e., rapid changes after diuretic therapy or dialysis—but also in stable outpatients. Moreover, this approach has shown good intraobserver and interobserver variability, around 4–5% in many studies and never superior to 7%.

In the past two decades lung ultrasound has been proposed to assess interstitial lung diseases by detecting and quantifying sonographic B-lines. They have a good diagnostic accuracy, especially high sensitivity, and correlate well with HRCT findings (Wang et al. 2017). The number of B-lines evident on LUS imaging may be a valuable marker of disease severity in patients with interstitial pneumonia (Asano et al. 2018; Xie et al. 2019).

In ARDS, it has been shown that B-lines correlate with interstitial involvement of the lungs, and B-pattern-predominant lungs are suggestive of alveolar processes such as ARDS. Ultrasonography has a role in both the diagnosis and management of ARDS (Papazian et al. 2016).

In times of COVID-19, bedside real-time lung ultrasound could support and integrate lung imaging with several advantages for the detection of pulmonary involvement. Lung ultrasound is showing a growing value in everday clinical practice, especially in the emergency and intensive care units (Gargani et al. 2020).

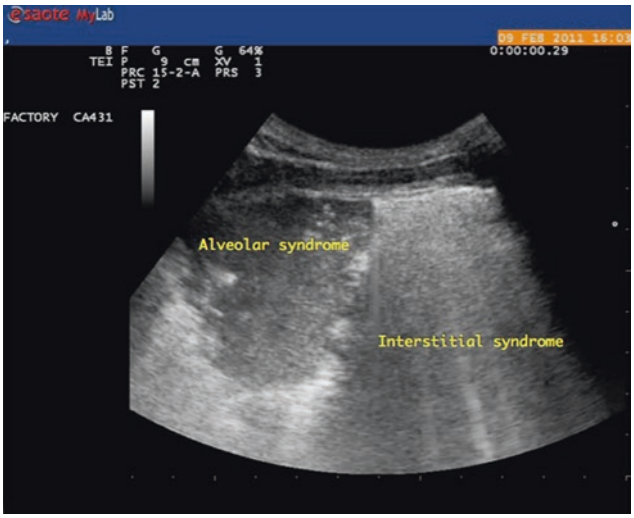

Fig. 4.6 This lung scan shows a focal interstitial syndrome around the pulmonary consolidation (alveolar syndrome), in a case of pneumonia

A focal interstitial syndrome can sometimes be the "peripheral alarm" of a more medial pathological condition, for example in the case of peri-lesional interstitial edema, due to either inflammation or other causes of localized consolidations (Fig. 4.6).

4.5 Limitations

It must be emphasized that LUS does not rule out pulmonary abnormalities that do not reach the pleura. The pulmonary interstitial syndrome from some specific etiologies sometimes may save the subpleural space, which will prevent visualization by sonography. However, these are only rare conditions particularly in emergency situations. Indeed, most of the lung conditions observed in the critically ill and emergency situations are characterized by lesions that reach the lung surface. The analysis of the lung anatomy may help to understand the reason. The secondary pulmonary lobule is the fundamental unit of the lung structure. In different pulmonary regions the lobule is variably surrounded by the interlobular septa, which are connective structures that envelope the lung like a network and contain pulmonary veins and lymphatics. Secondary pulmonary lobules in the periphery are relatively large and are marginated by interlobular septa that are thicker than in deeper parts of the lung. Thus, the periphery of the lung is highly representative of systemic diseases and conditions, and

alterations of the most peripheral septa can be studied by LUS (Volpicelli 2013).

Conditions that alter the regular interaction between the emitting surface of the probe and the chest wall, may limit the ultrasound evaluation of the interstitial syndrome. Very obese patients are occasionally difficult to be studied. Combination with other pulmonary conditions, like pneumothorax or large pleural effusion, may make difficult or impossible the evaluation of the interstitial syndrome. Bandages, wounds and other hindrances may sometimes prevent the ultrasound study.

Summary

In the last 15 years, from its traditional assessment of pleural effusions and masses, LUS has moved towards the revolutionary approach of imaging the pulmonary parenchyma, mainly as a point-of-care technique. Although limited by the presence of air, LUS has proved to be useful in the evaluation of interstitial syndromes, from cardiogenic pulmonary edema to acute lung injury and ARDS, from interstitial lung disease to interstitial pneumonia. In the next few years, the assessment of interstitial syndrome by point-of-care LUS is likely to become increasingly important in many different clinical settings, from the emergency department to the intensive care unit, from cardiology to pulmonology and nephrology wards.

References

Asano M, Watanabe H, Sato K, Okuda Y, Sakamoto S, Hasegawa Y, Sudo K, Takeda M, Sano M, Kibira S, Ito H (2018) Validity of ultrasound lung comets for assessment of the severity of interstitial pneumonia. J Ultrasound Med 37:1523–1531

Bouhemad B, Brisson H, Le-Guen M, Arbelot C, Lu Q, Rouby JJ (2011) Bedside ultrasound assessment of positive end-expiratory pressure-induced lung recruitment. Am J Resp Crit Care Med 183(3):341–347

Gargani L, Volpicelli G (2014) How I do it: lung ultrasound. Cardiovasc Ultrasound 12:25

Gargani L, Frassi F, Soldati G, Tesorio P, Gheorghiade M, Picano E (2008) Ultrasound lung comets for the differential diagnosis of acute cardiogenic dyspnoea: a comparison with natriuretic peptides. Eur J Heart Fail 10(1):70–77

Gargani L, Soliman-Aboumarie H, Volpicelli G, Corradi F, Pastore MC, Cameli M (2020) Why, when, and how to use lung ultrasound during the COVID-19 pandemic: enthusiasm and caution. Eur Heart J Cardiovasc Imaging. https://doi.org/10.1093/ehjci/jeaa163

Lichtenstein DA, Meziere GA (2008) Relevance of lung ultrasound in the diagnosis of acute respiratory failure: the BLUE protocol. Chest 134(1):117–125

Mallamaci F, Benedetto FA, Tripepi R, Rastelli S, Castellino P, Tripepi G, Picano E, Zoccali C (2010) Detection of pulmonary congestion by chest ultrasound in dialysis patients. JACC Cardiovascular Imaging 3(6):586–594

Manaker S, Weinberger S (2008) Diagnostic procedures in respiratory diseases. In: Fauci ASKD, Braunwald E, Hauser SL, Longo DL, Jameson JL, Loscalzo J (eds) Harrison's principles of internal medicine. McGraw-Hill Medical, New York

Moore CL, Copel JA (2011) Point-of-care ultrasonography. N Engl J Med 364(8):749–757

Papazian L, Calfee CS, Chiumello D, Luyt CE, Nuala J, Meyer NJ, Sekiguchi H, Matthay MA, Meduri GU (2016) 10 Diagnostic workup for ARDS patients. Intensive Care Med 42:674–685

Pivetta E, Goffi A, Lupia E, Tizzani M, Porrino G, Ferreri E, Volpicelli G, Balzaretti P, Banderali A, Iacobucci A, Locatelli S, Casoli G, Stone MB, Maule MM, Baldi I, Merletti F, Cibinel G (2015) Lung ultrasound-implemented diagnosis of acute decompensated heart failure in the Emergency Department—A SIMEU multicenter study. Chest. https://doi.org/10.1378/chest.14-2608

Reissig A, Kroegel C (2003) Transthoracic sonography of diffuse parenchymal lung disease: the role of comet tail artifacts. J Ultrasound Med 22(2):173–180

Volpicelli G (2013) Lung sonography. J Ultrasound Med 32(1):165–171

Volpicelli G, Mussa A, Garofalo G, Cardinale L, Casoli G, Perotto F, Fava C, Frascisco M (2006) Bedside lung ultrasound in the assessment of alveolar-interstitial syndrome. Am J Emerg Med 24(6):689–696

Volpicelli G, Caramello V, Cardinale L, Mussa A, Bar F, Frascisco MF (2008) Bedside ultrasound of the lung for the monitoring of acute decompensated heart failure. Am J Emerg Med 26(5):585–591

Volpicelli G, Elbarbary M, Blaivas M, Lichtenstein DA, Mathis G, Kirkpatrick AW, Melniker L, Gargani L, Noble VE, Via G, Dean A, Tsung JW, Soldati G, Copetti R, Bouhemad B, Reissig A, Agricola E, Rouby JJ, Arbelot C, Liteplo A, Sargsyan A, Silva F, Hoppmann R, Breitkreutz R, Seibel A, Neri L, Storti E, Petrovic T, International Liaison Committee on Lung Ultrasound for International Consensus Conference on Lung Ultrasound (2012) International evidence

Volpicelli G, Lamorte A, Tullio M, Cardinale L, Giraudo M, Stefanone V, Boero E, Nazerian P, Pozzi R, Frascisco MF (2013) Point-of-care multiorgan ultrasonography for the evaluation of undifferentiated hypotension in the emergency department. Intensive Care Med 39(7):1290–1298

Wang Y, Gargani L, Bsrskova T, Furst DE, Cerinic MM (2017) Usefullness of lung ultrasound B-lines in connective tissue disease-associted interstital lung disease: a literature review. Arthritis Res Ther 19:206

Xie HQ, Zhang WW, Sun DS, Chen XM, Yuan SF, ZhGong ZH, Liu L (2019) A simplified lung ultrasound for the diagnosis of interstitial lung disease in connective tissue disease: a meta-analysis. Arthritis Res Ther 2019(21):93

Zanobetti M, Poggioni C, Pini R (2011) Can chest ultrasonography replace standard chest radiography for evaluation of acute dyspnea in the ED? Chest 139(5):1140–1147

Ziskin MC, Thickman DI, Goldenberg NJ, Lapayowker MS, Becker JM (1982) The comet tail artifact. J Ultrasound Med 1(1):1–7

Inflammatory Consolidations in the Lung

Gebhard Mathis, Sonja Beckh, Christian Görg, and Ehsan Safai Zadeh

Contents

The original version of the chapter has been revised. The author "Ehsan Safai Zadeh" has been added to the author group. A correction to this chapter can be found at https://doi.org/10.1007/978-3-031-09442-2_13

G. Mathis (ed.), *Chest Sonography*, https://doi.org/10.1007/978-3-031-09442-2_5

5.1 Inflammatory Consolidations in the Lung

Gebhard Mathis
gebhard.mathis@cable.vol.at

5.1.1 Pneumonia

According to the World Health Organization, pneumonia is the leading cause of death among infectious diseases worldwide, accounting for 15% of deaths in children under five years of age (WHO 2019).

5.1.1.1 Pathophysiological Prerequisites

In cases of lobular and segmental pneumonia, large amounts of air are displaced from the lung as a result of extensive fibrinous exudation. Affected lobes or segments are depleted of air and sink in water. The phase of engorgement offers good conditions for pathological echo transmission. In this phase, pneumonia is imaged well on the sonogram. In the phase of lysis, the inflamed portion of the lung is ventilated to an increasing extent.

Focal pneumonias and interstitial pneumonias barely extend up to the pleura and are therefore poorly accessible to sonographic imaging. However, bronchial pneumonias are often accompanied by involvement of the pleura and are therefore partly visualized by sonography.

5.1.1.2 Sonomorphology of Pneumonia

A number of sonomorphological criteria are characteristic for pneumonic infiltrations. They are of varying intensity in the course of disease.

Sonomorphology of pneumonia:

- Liver or tissue like in the early stage
- Lentil-shaped air trappings
- Bronchoaerogram
- Fluid bronchogram (poststenotic)
- Blurred or serrated margins
- Reverberation echoes at the margin
- Hypoechoic to anechoic in the presence of abscess

5.1.1.3 Phase of Engorgement

In the initial phase of disease, i.e., in the phase of engorgement, the pneumonic lesion is hypoechoic, relatively homogeneous, and hepatoid in form. Its configuration is bizarre. It is rarely explicitly segmental like the pulmonary infarction or rounded like carcinomas and metastases. Its margins are irregular, serrated, and somewhat blurred (Figs. 5.1 and 5.2).

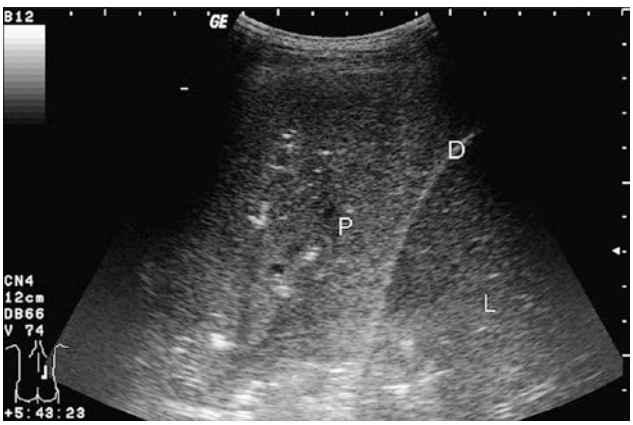

Fig. 5.1 A 68-year-old severely ill man with clinical signs of acute pneumonia. In the upper lobe of the lung on the left side, there is a liver-like consolidation with a bronchoaerogram. A subpleural fluid alveologram

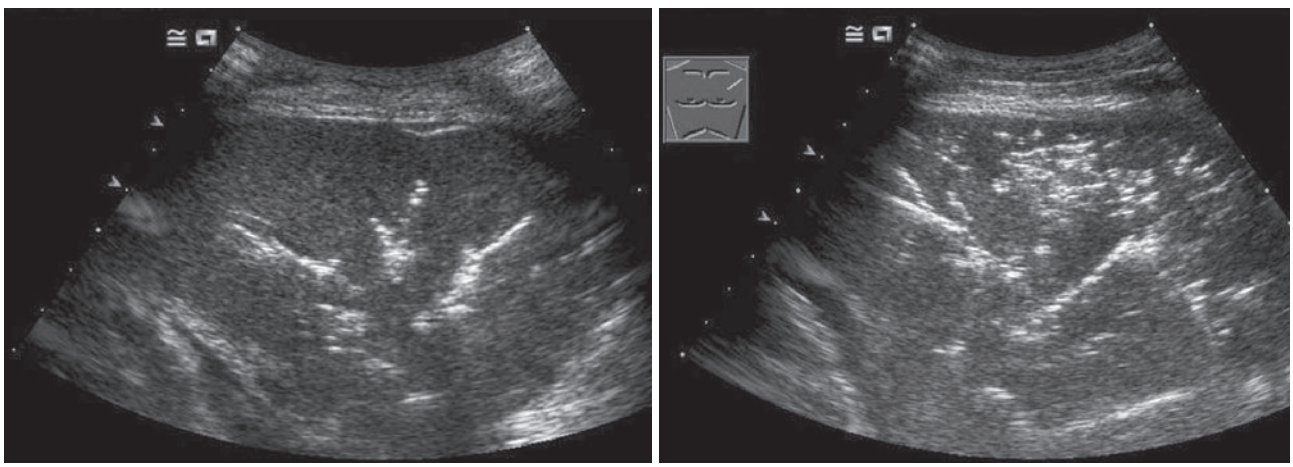

Fig. 5.2 Oblique section of lobar pneumonia in the right lower lobe. The pneumonic infiltrate (*P*) is similar to the liver in terms of echotexture (*L*). *D* diaphragm

5.1.1.4 Air Bronchogram

A marked bronchogram (bronchopneumogram, air bronchogram) with treelike ramifications is seen in up to 90% of cases. The intensive reflexes of the bronchial tree run between consolidated portions of the parenchyma. In all stages of the disease the bronchoaerogram is more pronounced than in cases of pulmonary embolism. Quite often one finds a small number of, and in most cases numerous, lenticular internal echoes just a few millimeters in size (Fig. 5.1). These echoes indicate the presence of air in the small bronchi. In other words, this is a partial image of a bronchoaerogram. These internal echoes can be partly explained by congested secretion of highly diverse impedance (Weinberg et al. 1986; Mathis et al. 1992; Gehmacher et al. 1995; Reissig and Kroegel 2007; Reissig et al. 2012; Figs. 5.2 and 5.3). The air bronchogram moves dynamically in a breath-dependent manner. This is an important difference between an air bronchogram and obstructive atelectasis: the latter is accompanied by a less prominent air bronchogram and is static (Lichtenstein et al. 2009).

The bronchogram visualized by sonography cannot be equated with that seen on a radiograph. Viral pneumonias are often less ventilated and/or reveal less pronounced bronchoaerograms. These are smaller and more compact than bacterial pneumonia and may resemble large pulmonary infarctions. In contrast to pulmonary infarctions, they are strongly perfused with blood (Fig. 5.4).

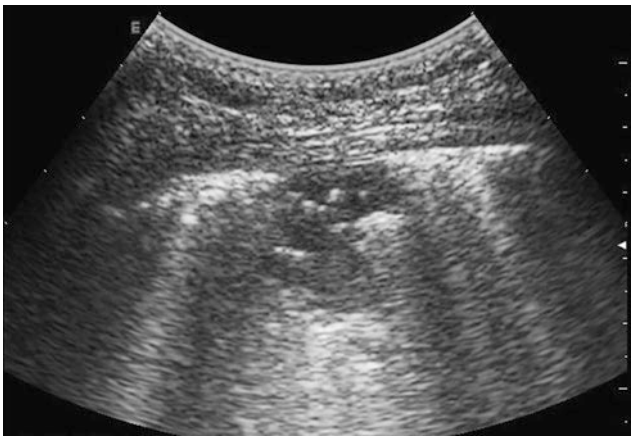

Fig. 5.3 Pneumonia after H1N1-Influenza (Fig as in German edition)

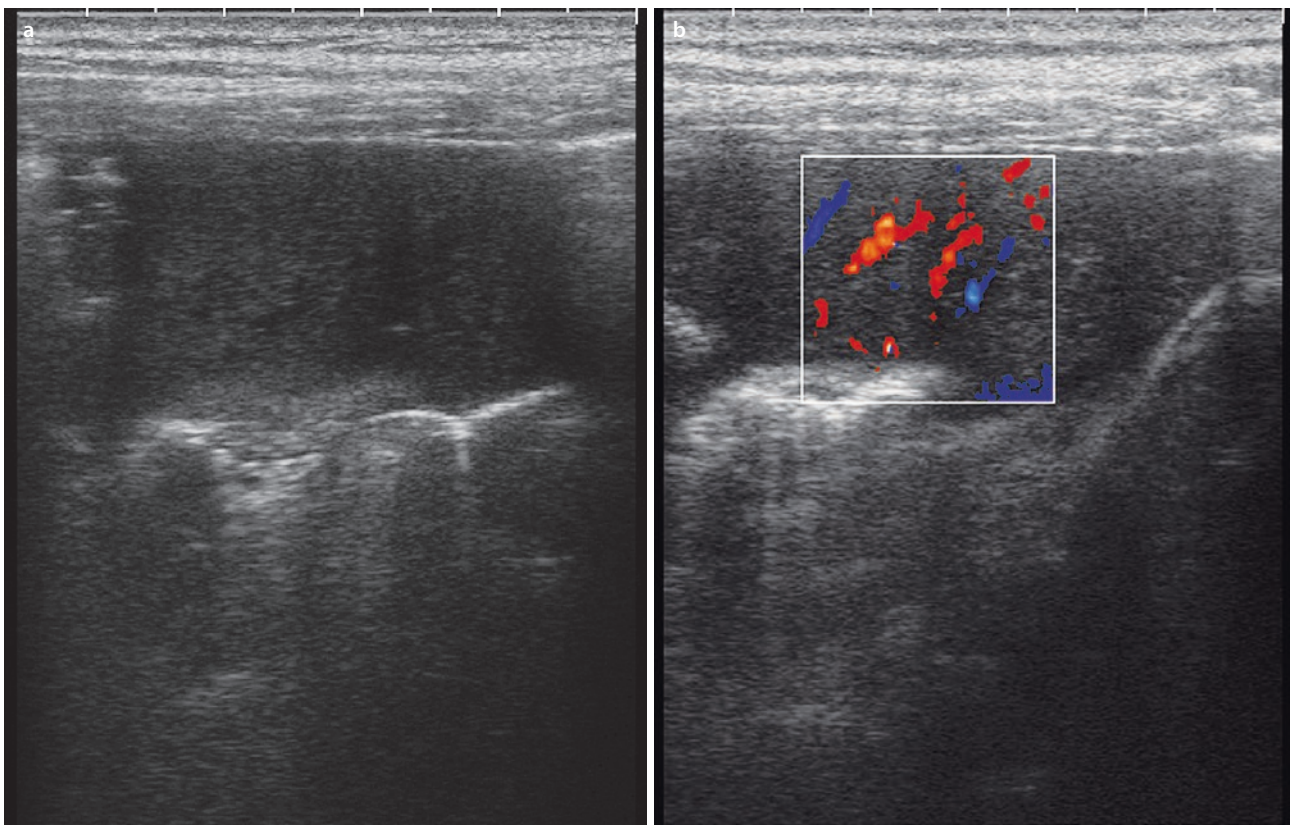

Fig. 5.4 A 52-year-old woman with pain on inspiration, fever, and hemoptysis. **a** Sonography reveals a consolidation measuring 5 × 3.5 cm in size, with a small bronchoaerogram. **b** Color-Doppler shows regular perfusion—viral pneumonia

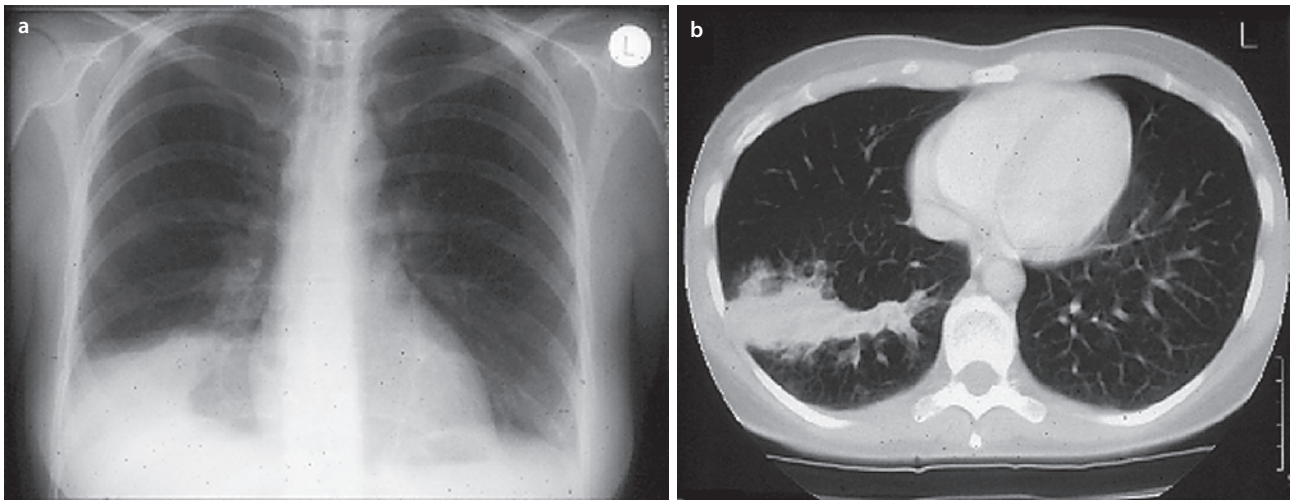

Fig. 5.5 A 32-year-old woman who had experienced segmental pneumonia for the third time in 1 year. **a** Sharply demarcated segmental shadow on the X-ray. **b** Largely homogeneous consolidation on computed tomography. **c** The morphology of the lesion on sonography is very similar to that on computed tomography. The echotexture contains significantly few air trappings. In the center, there is a small anechoic fluid area. **d** On the longitudinal section one finds tubular structures; parallel to the vessel a typical fluid bronchogram. **e** The adenocarcinoma is verified on bronchoscopy; on surgery, it is staged T1 N0

5.1.1.5 Fluid Bronchogram

The fluid bronchogram is marked by anechoic tubular structures along the bronchial tree. The bronchial wall is echogenic and the fluid in the segmental bronchi is hypoechoic. The reflexes around the bronchi are wider than those along vessel walls. Given good resolution, the bronchial walls are ribbed and the vessel walls are smooth; therefore, tubular structures can be easily classified on B-mode image. In the case of doubt, color-coded duplex sonography helps to distinguish between vessels and bronchi. The fluid bronchogram is seen in approximately 8% of patients with pneumonia and develops in the early phase of the disease as a result of bronchial secretion or owing to bronchial obstruction. A persistent fluid bronchogram always raises suspicion of poststenotic pneumonia and is an indication for bronchoscopic investigation (Fig. 5.5). A tumor may be found or ruled out; the obstructive secretory embolus is aspirated and material obtained for bacteriological investigation (Mathis 1997; Reissig et al. 2012).

5.1.1.6 Poststenotic Pneumonia

Poststenotic pneumonias that develop in the periphery or the margin of carcinomas are better delineated from the tumor by means of sonography than by X-ray investigation. Poststenotic pneumonia is typically characterized by a fluid bronchogram (Fig. 5.5d). Monitoring the effectiveness of therapy is important in this setting—is the pneumonia subsiding or is the tumor increasing in size (Yang et al. 1990a, b)?

5.1.1.7 Circulation

On color-coded duplex sonography pneumonia has a typical appearance: Circulation is uniformly increased, ramified, and the vessels run a normal course. In fact, circulation is increased in the entire infiltrate up to beneath the pleura (Fig. 5.6). This is interesting when pneumonia needs to be differentiated from pulmonary infarctions that have poor or no blood flow, or even from tumors with an irregular circulation pattern. Carcinomas are strongly vascularized in their margins. Owing to neovascularization, vessels in the margins of carcinomas are characterized by a typical corkscrew pattern (Gehmacher et al. 1995; Mathis 1997).

On contrast-enhanced sonography pneumonias are rapidly enriched with contrast medium and achieve intensive saturation after just 8–10 s (Görg 2007; Bertolini et al. 2008; Fig. 5.7; ▶ Chap. 9).

5.1.1.8 Parapneumonic Effusion

Parapneumonic fluid accumulations can be imaged better on ultrasound than on conventional X-rays (55% versus 25%). These must be discovered and their course monitored in order to initiate invasive therapy in terms

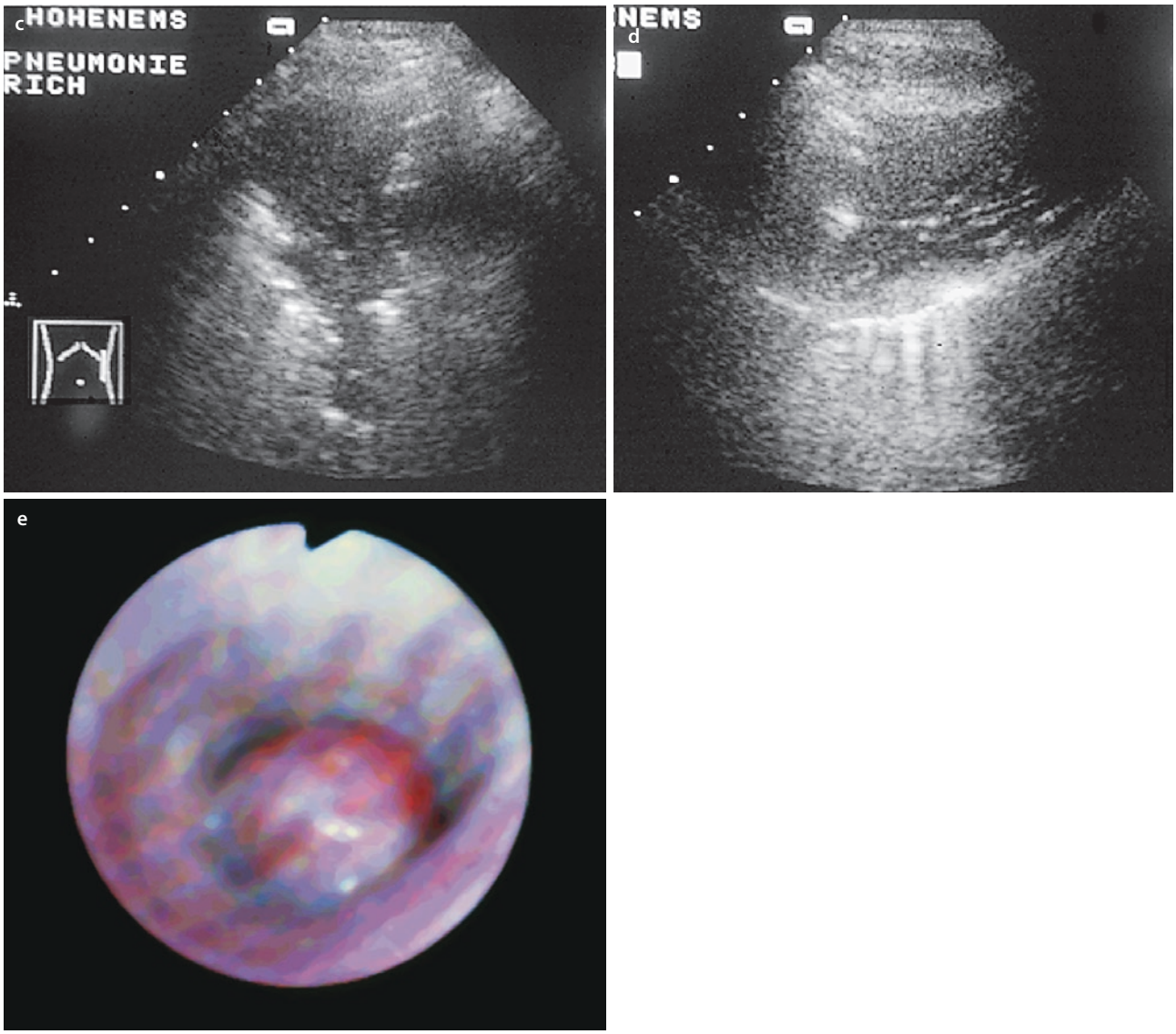

Fig. 5.5 (continued)

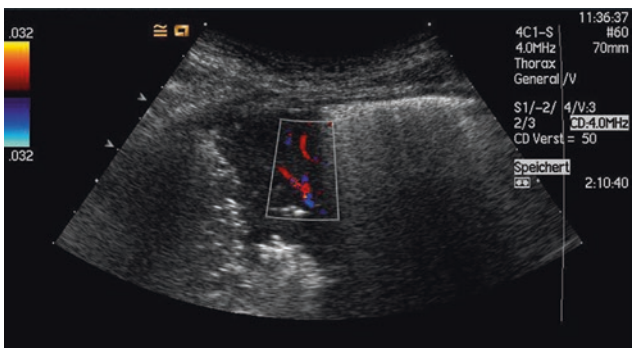

Fig. 5.6 On color-coded duplex sonography pneumonia is seen as an accentuated, regular pattern of circulation

of puncture or video-assisted thoracoscopy on a timely basis (Reissig et al. 2012; Fig. 5.8).

5.1.1.9 Abscess Formation

Bacterial pneumonias tend to develop colliquations and form abscesses. This is the case in approximately 6% of patients with lobar pneumonia (this figure refers to radiographic investigations). Sonography more commonly reveals *microabscess* (Yang et al. 1991, 1992a, b; Mathis 1997).

The *sonomorphology of pulmonary abscess* is highly characteristic: round or oval and largely anechoic lesions. Depending on whether a capsule is formed, the margin is smooth, echodense, and white (Fig. 5.9). Blurred

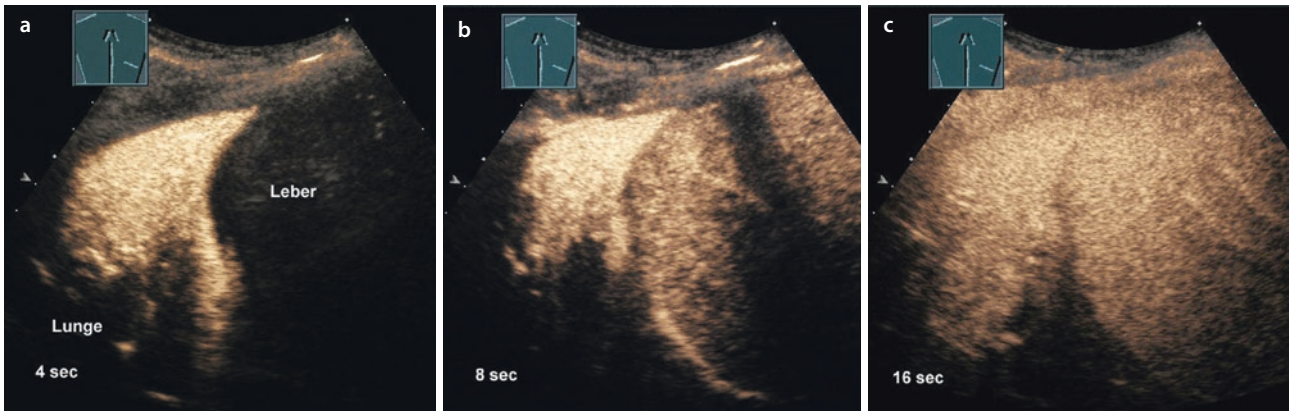

Fig. 5.7 Signal-enhanced sonography in pneumonia. The saturation starts very early and achieves its maximum after 5–16 s

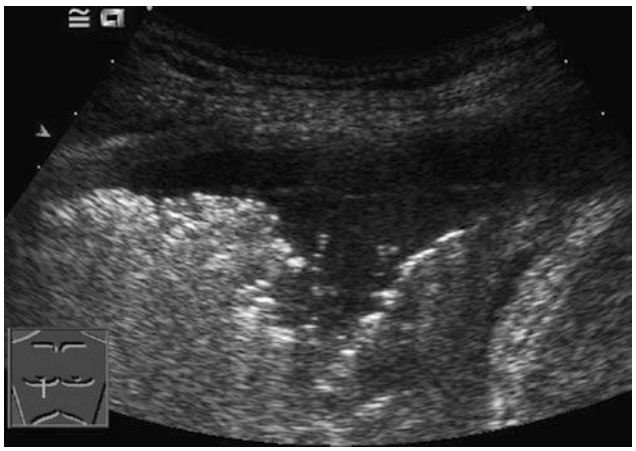

Fig. 5.8 Parapneumonic effusion. Remission observed by ultrasound

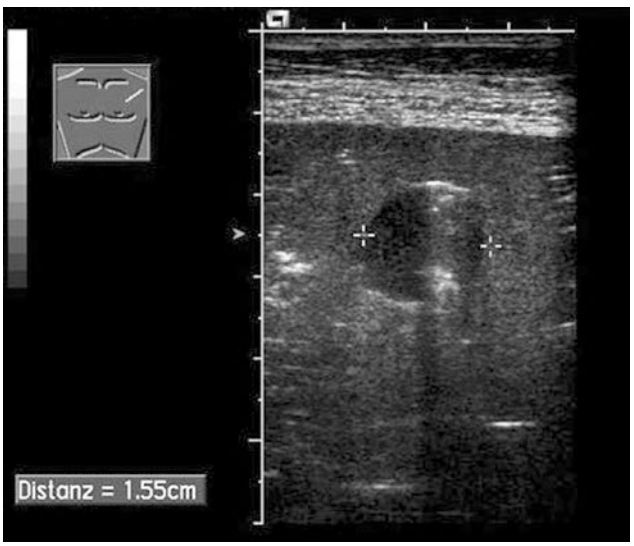

Fig. 5.9 Colliquated abscesses with persistent fever. Sonography-guided aspiration showed a surprisingly large number of tubercle bacilli

internal echoes are indicative of high cell content or viscous pus rich in protein. In cases of abscesses due to gas-forming pathogens, highly echogenic small air trappings move actively within the fluid in concordance with the respiratory rhythm. Microabscesses cannot be easily distinguished from vessels on color-Doppler imaging.

Considering the scarce quantity of material for bacteriological investigation obtained from the sputum or from bronchial lavage, it is useful to taken *a specimen for the detection of pathogens* by means of sonography-guided aspiration. When the puncture is performed with an ordinary injection needle, a thorough sonographic preinvestigation should be performed, if necessary under sonographic visual guidance, to ensure that air-filled lungs and vessels are avoided. The cause of pulmonary infections can be determined by this method in 80% of cases (Yang et al. 1992a, b; Chen et al. 1993; Liaw et al. 1994a, b; Mathis 1997).

Lung abscess drainage may be performed under sonographic or computed tomography visual monitoring. The risk of a pneumothorax is minimized when one passes through the chest wall obliquely, in a regular fashion, and enters the lung at the site where the abscess is closest to the pleura. The risk of a dreaded bronchopleural fistula is minimized when the correct approach is used, i.e., when one only traverses the homogeneous infiltrate and avoids ventilated areas (Yang et al. 1991; Talayanagi et al. 2010).

5.1.1.10 Healing Phase

When pneumonia is in the phase of healing, the infiltrated lung tissue is ventilated to an increasing extent. Such air gives rise to reflection and reverberation artifacts. The pneumonia recedes on the sonography image and usually appears smaller than on the chest radiograph. The resolution of these lesions on ultrasound correlates well with the patient's clinical progress (Fig. 5.10).

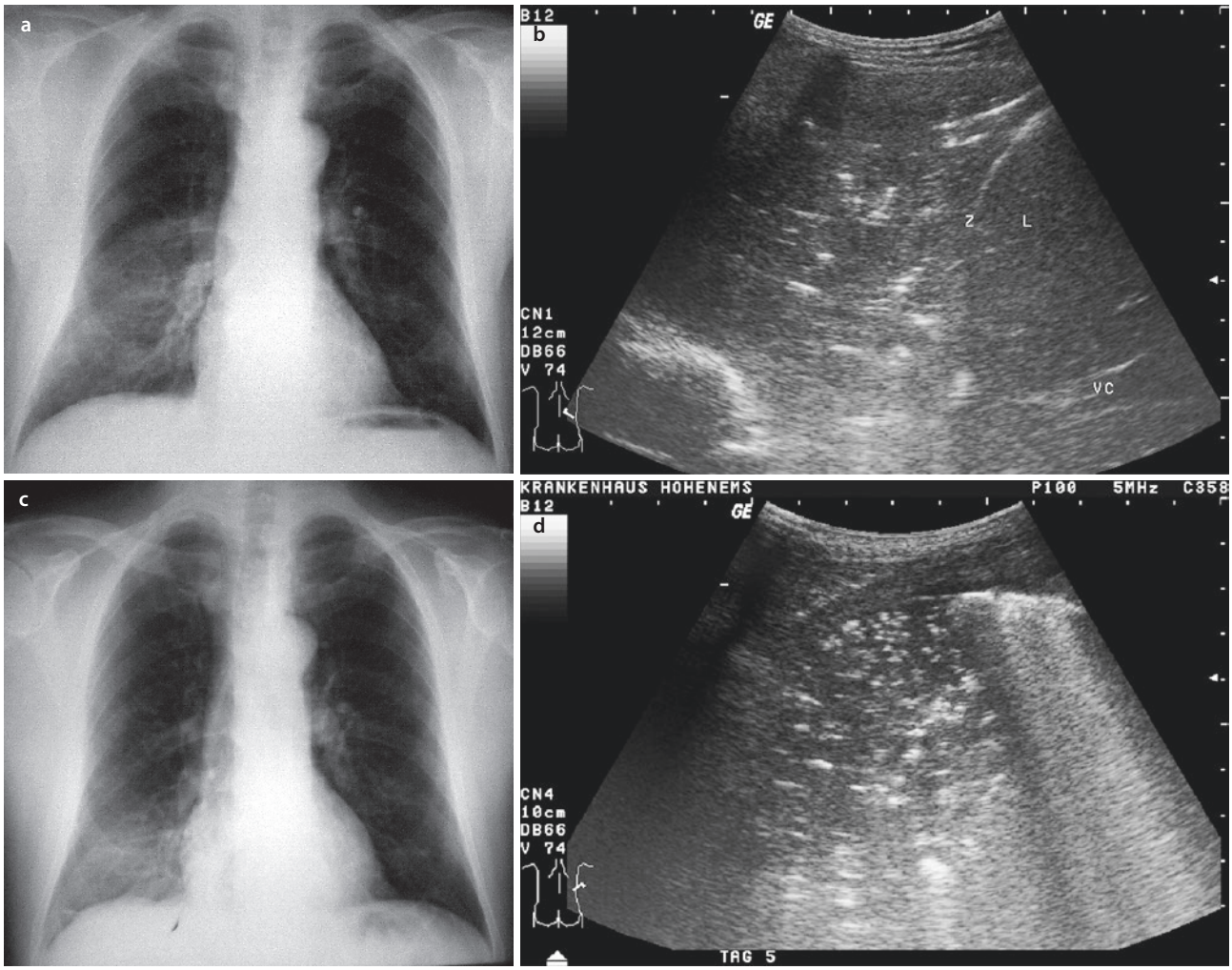

Fig. 5.10 A 72-year-old man with clinically severe pneumonia. **a** Typical appearance on X-ray. **b** On sonography the echotexture is similar to that of the liver, with a pronounced bronchoaerogram. *Z* diaphragm, *L* liver, *VC* vena cava. After 1 week of antibiotic therapy the patient is afebrile and has recovered to the extent that he can be discharged. **c** On the X-ray there still is a marked residual infiltrate. **d** Sonography only shows a receding infiltration

5.1.1.11 Diagnostic Value

Primary diagnosis of pneumonia is usually performed on the basis of clinical signs and chest X-rays. The extent of infiltration may be underestimated on ultrasound. Central pneumonias are not seen on sonography. The severity of intersitial pneumonia can be assessed (Asano et al. 2018).

Can ultrasonography of the lung replace conventional X-rays as a diagnostic imaging procedure? The authors of older studies have compared ultrasound with chest X-rays and achieved favorable results (89% sensitivity) (Mathis et al. 1992; Gehmacher et al. 1995). With CT as the reference method, ultrasound was able to show 12–25% more pneumonias than the chest X-ray (Targhetta et al. 1992; Copetti and Cattarossi 2008; Parlamento et al. 2009; Sperandeo et al. 2011).

Four meta-analyses of up to 1515 patients have shown a pooled sensitivity of 88–97% and a specificity of 86–96% (Hu et al. 2014; Mathis 2019).

The most relevant manifestation of COVID-19 disease is pneumonia. The most frequent lung ultrasound features are: bilateral B-lines-pattern, supleural consolidations, and several typical pneumonic infiltrations with aerobrochnogram. These findings correlated well with MRCT (Dacrema et al. 2021). For an optimal detection and monitoring of COVID-19 we depend on a fast and reliable diagnosis and severity assessment. Current Antigen und PCR-Tests have a sensitivity of 60–90%. In addition to pulsoxymetry, the usual methods stethoscope and Chest-X-ray are unreliable (Osterwalder 2020).

In Covid-19 pneumonia, pulmonary ultrasound has been shown to be very useful in initial diagnosis and follow-up in intensive care units and emergency rooms using portable devices (Liu et al. 2020; Lyu et al. 2020; Osterwalder 2020).

Especially in children, pulmonary ultrasound has been shown to be very useful in the diagnosis of pneumonia and radiation exposure is avoided (Orso and Ban 2018). In ventilated patients, the distinction between pneumonia and atelectasis is often only possible in the context of laboratory findings. However, pulmonary sonography can make an uncomplicated contribution to imaging diagnostics and follow-up during daily rounds (Mongodi et al. 2016; Wang et al. 2016).

A large multicenter study comprising 362 patients confirmed ultrasound morphology criteria on the one hand, and yielded a sensitivity of 93.4% and a specificity of 97.7% on the other. In combination with auscultation the accuracy was even higher (Reissig et al. 2012).

In cases of clinical suspicion of pneumonia, further radiological investigations may be necessary. However, after the clinical investigation and after obtaining the required laboratory data concerning inflammatory parameters, immediate antibiotic treatment can be initiated almost everywhere: at the medical office, the emergency department, the intensive care unit, and in stroke patients among others (Busti et al. 2014).

5.1.2 Tuberculosis

In pulmonary tuberculosis, ultrasonography is helpful in detecting pleural effusions, subpleural consolidations and pneumonic infiltrates. Ultrasound-guided diagnostic punctures are meaningful in this setting. Chest X-rays and computed tomography are indispensable to obtain an overview of the condition (Yuan et al. 1993; Kopf et al. 1994; Mathis 1997; ◘ Figs. 5.11–5.13).

Tuberculotic lung lesions may be seen on sonography as rounded or irregular structures of relatively homogeneous texture. Depending on the size of the lesion, these infiltrates may also be accompanied by air trappings

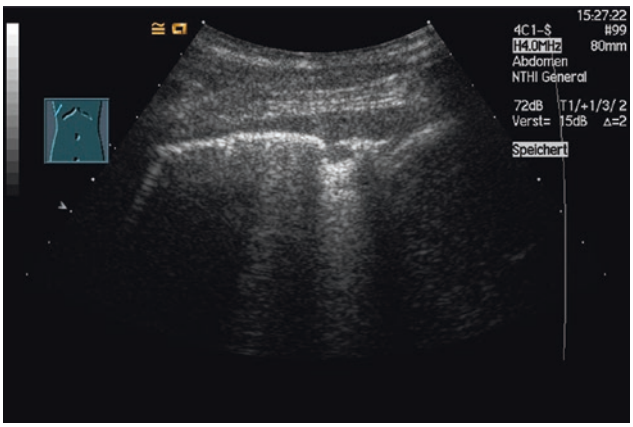

◘ **Fig. 5.11** Small lymphocytic pleural effusion. US-guided biopsy of the nodule showed tuberculosis

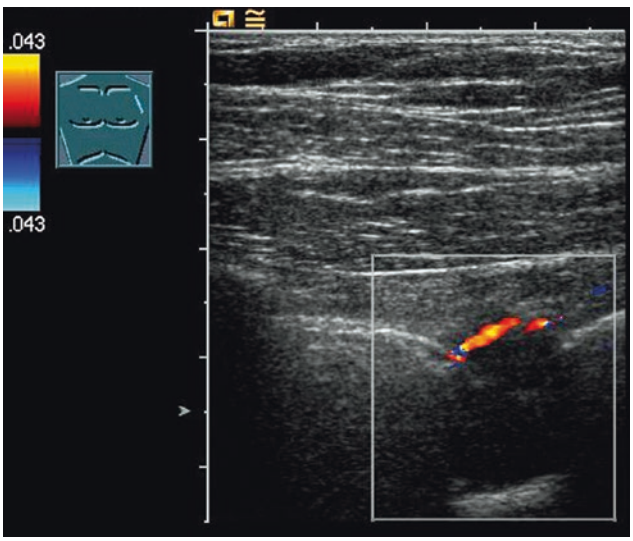

◘ **Fig. 5.12** Peripheral lung lesion on a routine X-ray of a young woman. On sonography one finds a hypoechoic, poorly vascularized lesion. Biopsy indicated tuberculosis

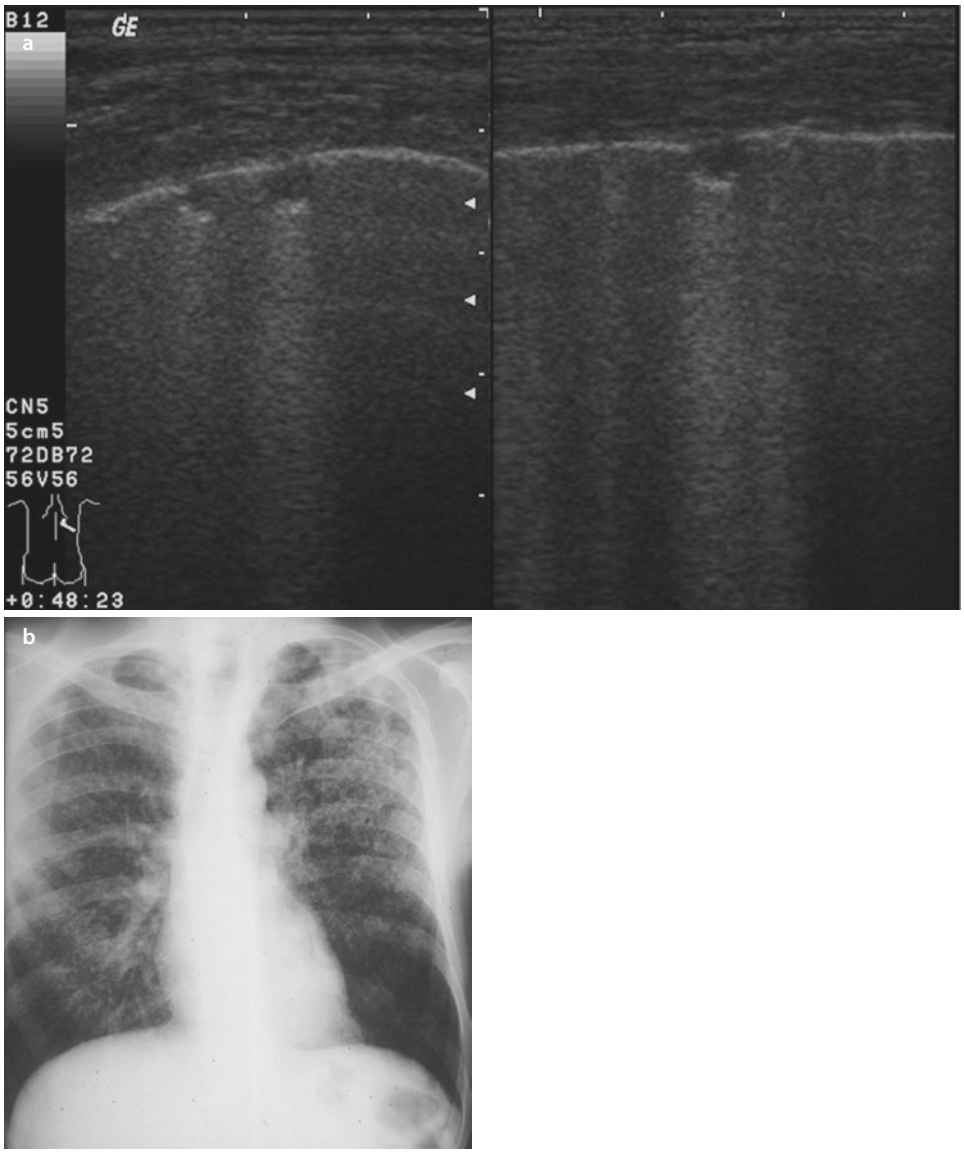

Fig. 5.13 Miliary tuberculosis. **a** Fragmented pleura (*arrowheads*) with numerous subpleural nodes measuring 2–3 mm in size. **b** Chest X-ray showing miliary tuberculosis

as in pneumonia. Nodular dissemination, as in miliary tuberculosis, is visualized as multiple subpleural nodes measuring a few millimeters in size (Fig. 5.13).

Colliquations can be imaged well, but air in cavities might be a disturbing factor and might limit visualization. Even very small quantities of the specific pleural effusion are seen. Pleural thickening may also be revealed. A patient's response to tuberculostatic therapy can be monitored well with sonography, especially in cases of pleural and subpleural tuberculosis lesions.

In cases of rarer infectious lung consolidations such as aspergillosis or echinococcus, typical lesions can be visualized and significant additional information (in addition to the information available from radiographs) obtained (Fig. 5.14).

5.1.3 Interstitial Lung Disease

Technically sonography is entirely unsuitable to diagnose diseases of the lung framework. However, it was shown that such diseases are frequently accompanied by *involvement of the pleura* and the latter is significantly better visualized by sonography than by other imaging procedures:

- Minimal pleural effusions
- Fragmented pleura with several comet-tail artifacts (B-lines)
- Subpleural consolidations (Figs. 5.15–5.18)

The value of the method lies in the detection of a grave condition and in steering the diagnostician's attention towards a specific target – point of care ultrasound.

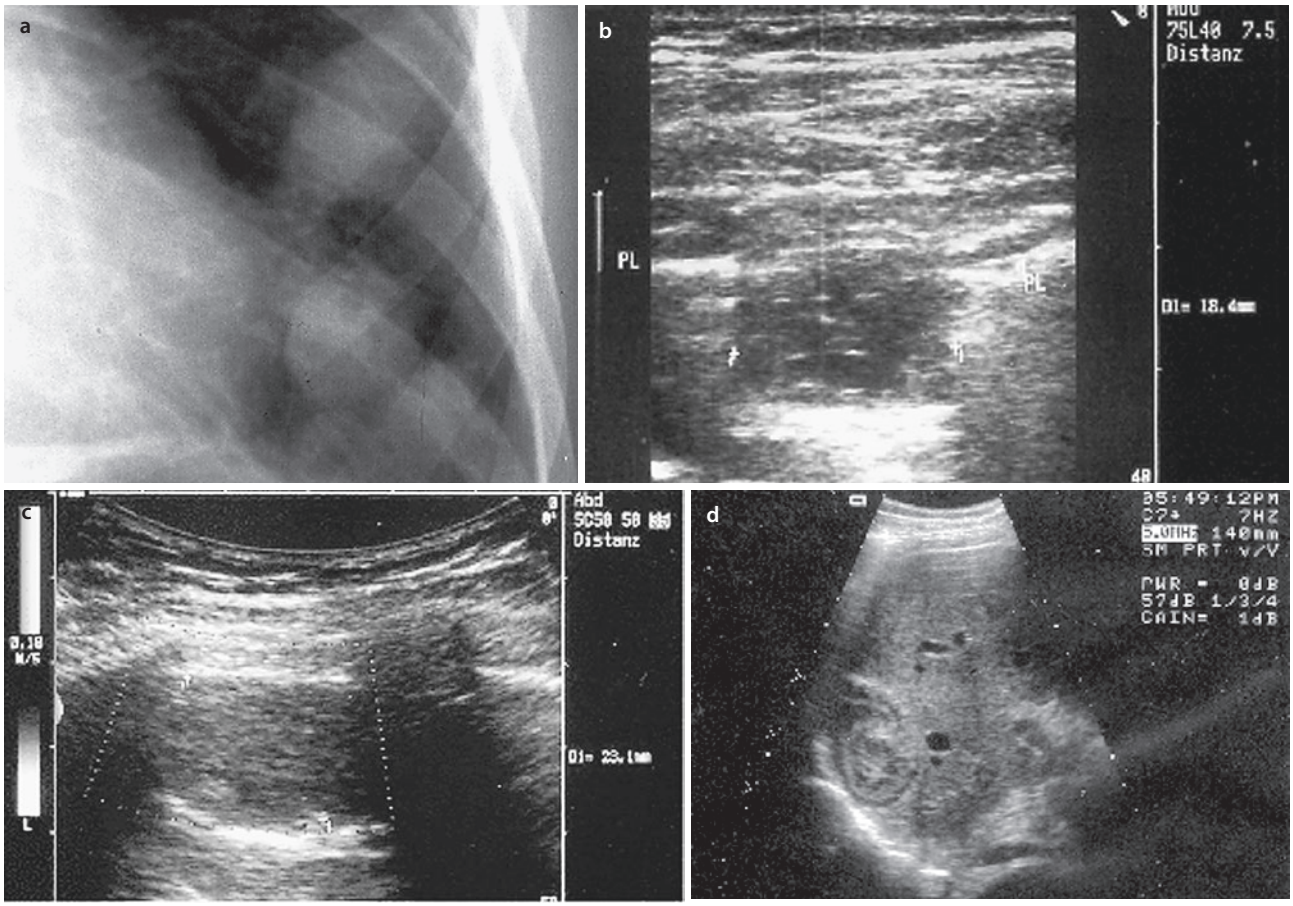

Fig. 5.14 Echinococcus cysticus. A 28-year-old man with pulmonary echinococcosis in his medical history. The patient was admitted to the hospital because of fever, cough, and marked dyspnea. **a**, **b** The X-ray shows multiple round lesions in the lung and pneumonic infiltrates. **c**, **d** Sonography revealed the round lesions extending to the surface of the lung. Thick-walled cysts (*crosses*) with internal secondary cysts showing no vascularization on color-Doppler sonography. Additionally one finds several areas indicative of pneumonia. An echinococcal lesion is present in the liver as well. Further diagnostic procedures confirmed bilateral pneumonia in terms of superinfection and preexisting pulmonary echinococcosis. The patient subsequently developed severe pulmonary hypertension despite antibiotic therapy plus albendazole

Therapy controls are highly efficient in cases of minimal pleural effusions and subpleural infiltrations; no method is superior to sonography in this regard (Wohlgenannt et al. 2001; Reissig and Kroegel 2003).

5.1.4 Interstitial Syndrome

The 1st International consensus conference on pleura and lung ultrasound has defined the interstitial syndrome presenting B-lines as discrete laser-like vertical hyperechoic reverberation artifacts that arise from the pleural line (previously described as "comet tails"), extend to the bottom of the screen without fading, and move synchronously with lung sliding. In the evaluation of *diffuse* interstitial syndrome, the sonographic technique ideally consists of scanning eight regions, but a more rapid anterior two region scan may be sufficient in some cases. A positive region is defined by the presence of three or more B-lines in a longitudinal plane between two ribs. However, focal multiple B-lines may be present in normal lung.

Causes of the interstitial syndrome include the following conditions: pulmonary edema of various causes, interstitial pneumonia or pneumonitis, diffuse parenchymal lung disease (pulmonary fibrosis).

Focal sonographic pattern of interstitial syndrome may be seen in the presence of many lung diseases, e.g., pneumonia and pneumonitis, atelectasis, pulmonary contusion, pulmonary infarction, pleural disease, and neoplasia.

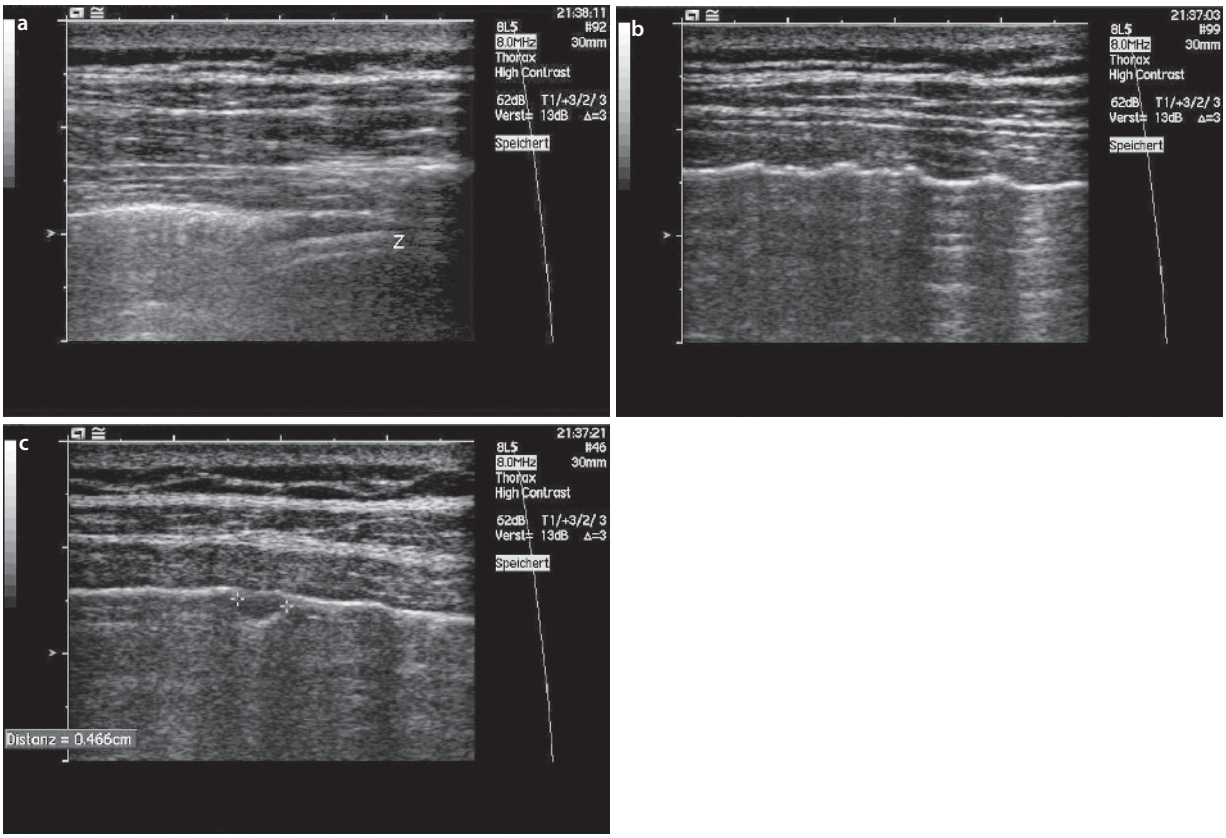

Fig. 5.15 Sarcoidosis. **a** Minimal basal pleural effusion. *Z* diaphragm. **b** Uneven, fragmented visceral pleura with several reverberation echoes (comet-tail artifacts). **c** Subpleural nodes measuring about 5 mm in size

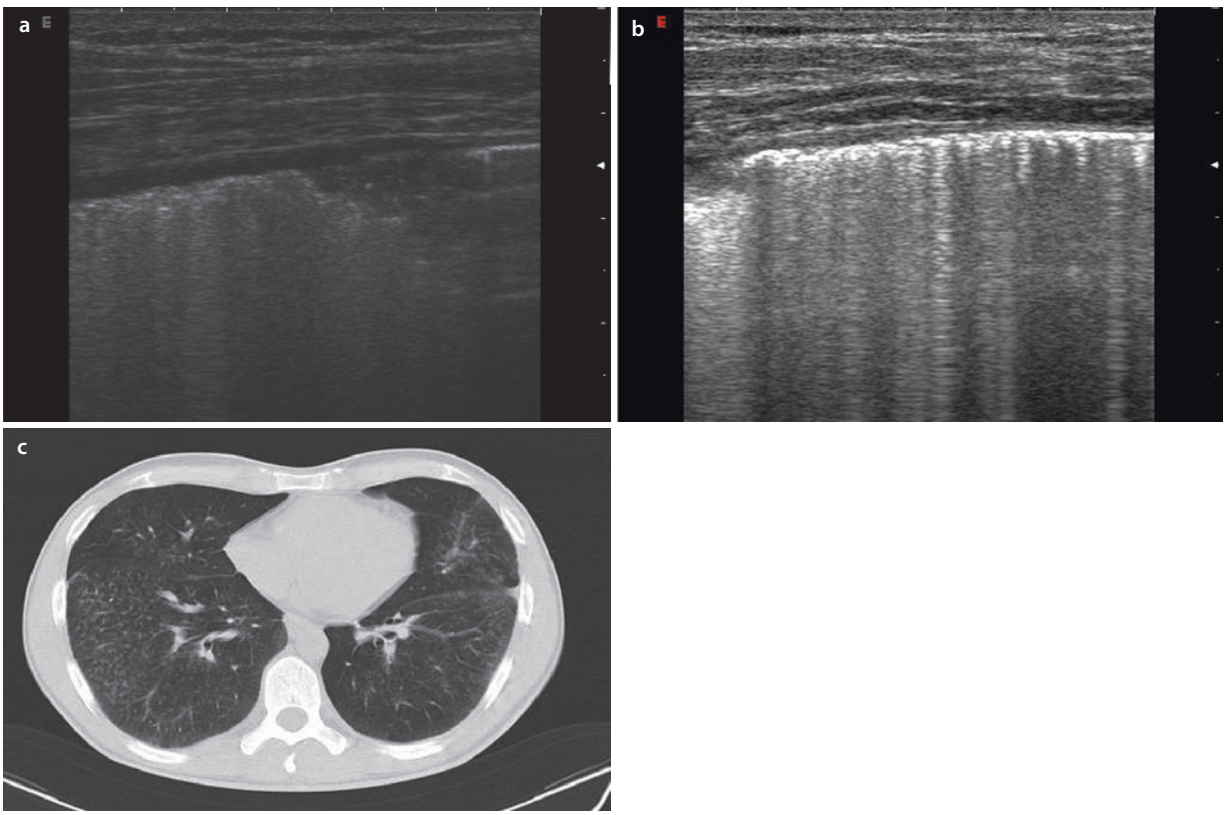

Fig. 5.16 Sarcoidosis. A 26-year-old man with creepy appearance of dyspnea and pleuritic pain . a Left sided subpleural consolidations with narrow pleural effusion. **b** Diffuse interstitial syndrome in a nonhomogeneous distribution. **c** Corresponding CT

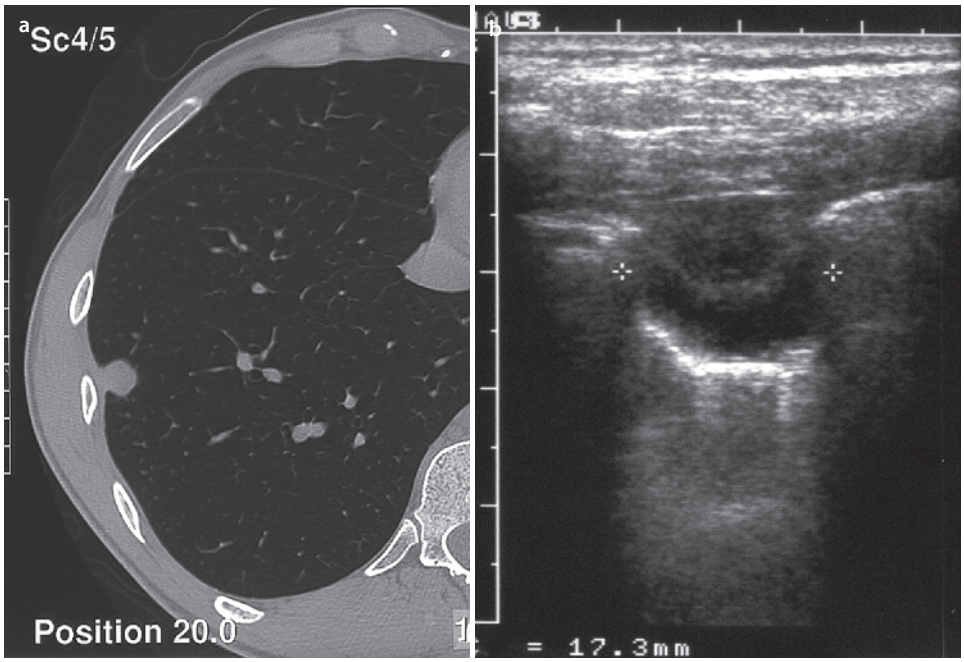

Fig. 5.17 **a** The patient was referred for identification of the primary lesion of a "metastatic lung". **b** Sonography-guided biopsy of the subpleural lesion indicated a rheumatic nodule

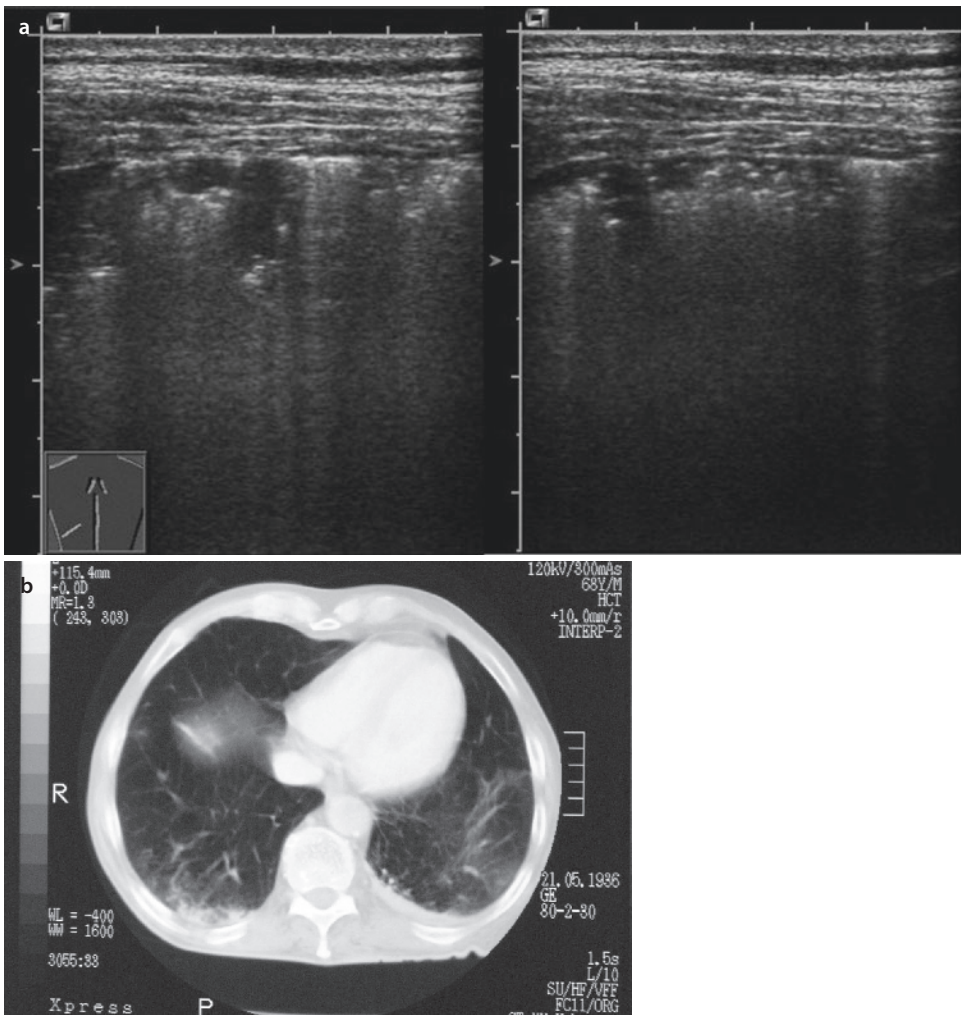

Fig. 5.18 Chronic organizing pneumonia. **a** Extensive subpleural infiltrations, indicated with US-guided biopsy. **b** Corresponding CT

5.2 Neoplastic Consolidations in the Lung: Primary Lung Tumors and Metastases

Sonja Beckh
sonja.beckh@gmx.ae

Thanks to ongoing scientific work, the recent international guidelines and recommendations have incorporated ultrasound as a part of the diagnostic procedure for the investigation of lung carcinoma (Pan et al. 1993; Suzuki et al. 1993; Yuan et al. 1994; Yang 1996; Hsu et al. 1996, 1998; Mathis 1997; Mathis et al. 1999a, b, c; Beckh et al. 2002; Thomas et al. 2002; Detterbeck et al. 2003; Görg and Bert 2004; Bandi et al. 2008; Volpicelli et al. 2012a, b; AWMF 2018). Due to its excellent resolution, ultrasound has proved equivalent to nuclear resonance tomography in the investigation of the chest wall affected by tumor invasion (Goeckenjan et al. 2011). Percutaneous diagnostic and therapeutic ultrasound-guided puncture is recommended, and has been accepted as a reliable procedure (Goeckenjan et al. 2011; Detterbeck et al. 2003). Endobronchial and endoesophageal ultrasound is the state of the art for staging mediastinal disease (Goeckenjan et al. 2011; Detterbeck et al. 2003). The visualization of vessels with color-Doppler or ultrasound contrast medium provides valuable additional information for the differential diagnosis of space-occupying lesions (▶ Chap. 8).

Lung consolidations are seen on sonography only when no aerated tissue hinders the echo transmission. For staging of the disease and planning treatment in cases of malignant lung disease, procedures that provide sectional images such as computed tomography or magnetic resonance tomography are absolutely essential in order to obtain an overview of the entire chest (van Kaick and Bahner 1998; Tuengerthal 2003; Knopp et al. 1998; Schönberg 2003). As a rule, the sonographic investigation is performed when the findings of various radiographic procedures are known. Given specific symptoms, however, a targeted symptom-oriented investigation is also meaningful (▶ Chap. 11) (◘ Fig. 5.19).

Pulmonary malignancies may have a highly variable *echotexture*. They are usually hypoechoic, moderately echodense, or very inhomogeneously structured; more rarely they are nearly anechoic (Mathis 1997; Mathis et al. 1999a, b, c; ◘ Table 5.1). However, the echotexture alone does not allow the investigator to draw conclusions about the malignant or benign nature of the disease (◘ Figs. 5.20 and 5.21).

In contrast to acute inflammatory infiltrations, the sonomorphology of malignant lesions does not change during a short course of disease. Chronic carnifying pneumonia and peripheral callused cicatricial lesions are problematic in terms of differential diagnosis; it may be difficult to differentiate these entities from malignant disease (Mathis 1997).

Decisive criteria to grade the malignant or benign nature of a pulmonary lesion are the following (◘ Table 5.2):

5.2.1 Contours of the Lung Surface

The *contours* of the lung surface are very well delineated from the surrounding pleural fluid. ◘ Figure 5.22 shows the convex swelling surface of the lung by a lung carcinoma. A benign inflammatory infiltration would never lead to such irregular deformation of the lung surface.

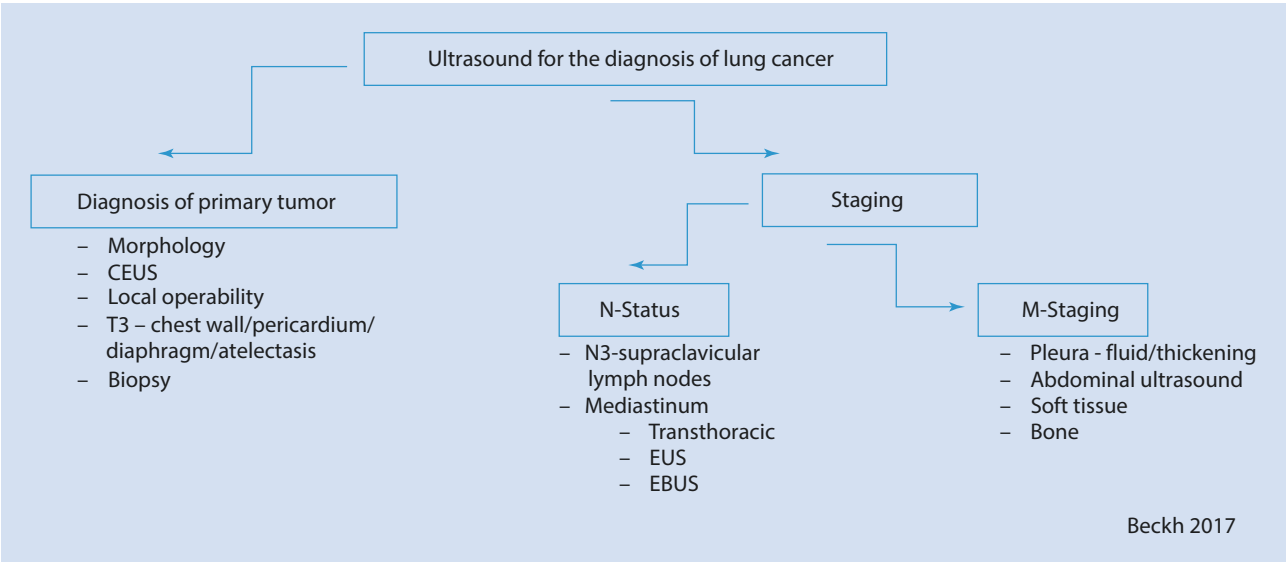

◘ **Fig. 5.19** Sonography in diagnosis of lung cancer

Table 5.1 Sonomorphology of lung carcinomas

Morphology	Echotexture	Vessels	Complex structures
Sharp margins	Inhomogeneous	Displacement of vessels	Residual ventilated areas
Rounded	Hypoechoic	Destruction of vessels	Accompanying pneumonia at the margin
Polypoid	Rarely echogenic	Interruption of vessels	Solid space-occupying lesion/pneumonia
Ramifications	Rarely anechoic	Neovascularization	Bacterial/fungal colonization
Serrated margin	Necrotic areas	–	Bizarre pattern in large necroses

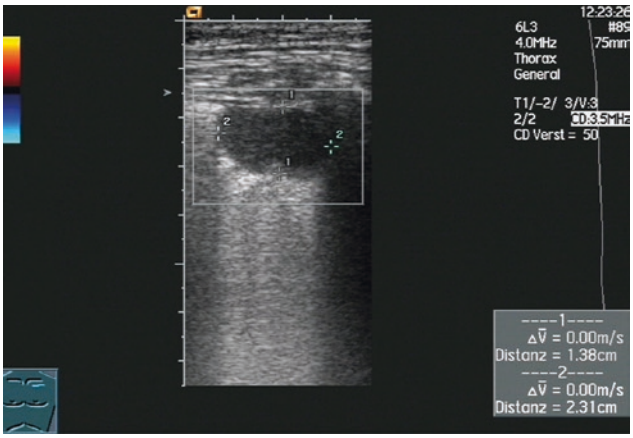

Fig. 5.20 A small hypoechoic lesion in a 78-year-old man: an incidental finding in the upper lobe of the left lung, in infraclavicular location. Sonography-guided biopsy indicated squamous cell carcinoma

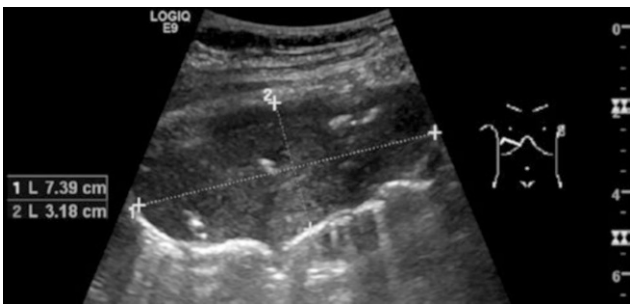

Fig. 5.21 A 40-year-old man with recurrent eosinophilic pleural effusion. X-rays showed a peripheral lesion in the upper lobe of the left lung. On sonography in the anterior axillary line in the second intercostal region, there is a hypoechoic peripheral pulmonary lesion with central vessels and rather sharp margins. Removal of the lesion by thoracoscopy led to the diagnosis of hyalinosis and callus. The source of the pleural effusions is still not clear

Table 5.2 Sonomorphology of pulmonary metastases

- *Contours* of the lung surface
- *Margins* to ventilated lung tissue
- *Invasion* of adjacent structures (chest wall, diaphragm, pericardium)
- *Destruction* of normal tissue architecture
- *Displacement* of regular vessels
- *Neovascularization*
- *Differentiation between a central space-occupying lesion and a poststenotic invasion/atelectasis*

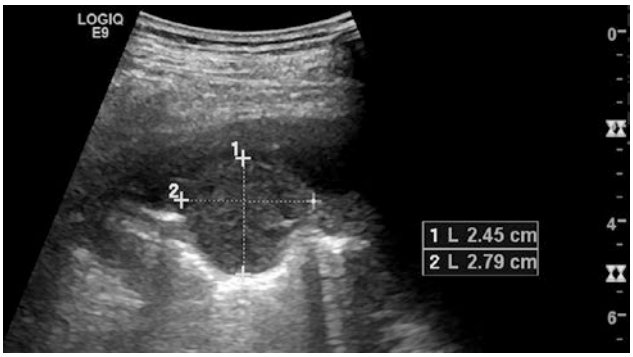

Fig. 5.22 Small-cell lung carcinoma invading the lower lobe of the left lung (diagnosed by bronchoscopic biopsy), irregular lung surface, narrow pleural effusion

A benign inflammatory infiltration would never lead to such irregular deformation of the lung surface.

5.2.2 Delineation of Margins from Ventilated Lung Tissue

Malignant lesions are often very *sharply demarcated* from lung tissue (Fig. 5.23). Occasionally, however, one finds *fringed or finger-shaped ramifications* into the normally ventilated parenchyma—a sign of invasive growth (Fig. 5.24).

In contrast to inflammatory lesions, such solid malignant formations in marginal zones are not ventilated and therefore are more sharply demarcated from the surrounding tissue.

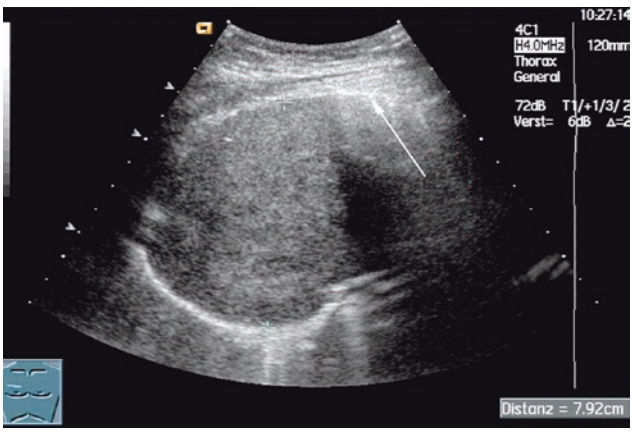

Fig. 5.23 Large hypoechoic space-occupying lesion in the upper lobe of the right lung, sharply demarcated from ventilated lung tissue. In medial location (*arrow*) one finds an unremarkable echogenic pleural line. Sonography-guided biopsy indicated poorly differentiated neuroendocrine carcinoma G4

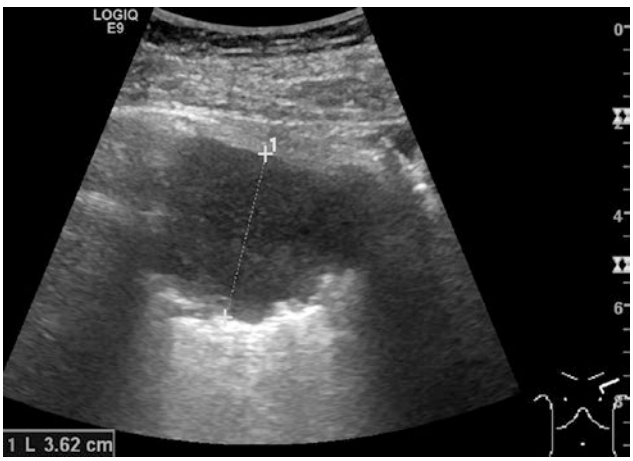

Fig. 5.24 Hypoechoic space-occupying lesion in the upper lobe of the right lung with fringed branches into the ventilated lung tissue (*arrows*). Histological investigation of the resected upper lobe yielded a mixed-cell lung carcinoma (squamous cell or large-cell carcinoma)

5.2.3 Invasion of Adjacent Structures: Chest Wall, Diaphragm, and Pericardium

Practically at first glance, a malignancy *invading* adjacent structures is indicative of the aggressive nature of the tumor (Suzuki et al. 1993; Bandi et al. 2008). In the case of a Pancoast's tumor, a space-occupying lesion penetrating the dome of the pleura is clearly visualized (Fig. 5.25).

Malignant invasion of the chest wall frequently causes local pain. Targeted investigation of the region with the transducer will help to diagnose the condition early (Fig. 5.26).

Invasion into adjacent structures of the chest wall is a very reliable sign of malignant growth. Therefore, the current S-3 guidelines demand a sonography for staging in lung cancer (Goeckenjan et al. 2011). In terms of differential diagnosis only one disease is likely to be present here, namely, actinomycosis or nocardiosis (Corrin 1999; Fig. 5.27a–c).

The inflammation frequently spreads into the chest wall. The regular cardinal anatomic structures of the lung, however, are well preserved within the pneumonic infiltration of tissue. In conjunction with clinical symptoms and bacteriological investigation, they permit the investigator to make the correct diagnosis.

The diaphragm on the right side of the chest is usually fully visible, with the liver serving as the sonic window. On the left side, tumors lying medial to the spleen are only seen if there is an effusion or when the tumor itself serves as the sonic window. In the latter case the insertion at the diaphragm may be seen as in Fig. 5.27d.

For staging of the disease and planning therapy, among other factors the relation between the tumor and the pericardium is important. Owing to the excellent resolution and the possibility of dynamic investigation, tumor invasion of the parietal pericardium can be clearly visualized (Fig. 5.27e).

5.2.4 Destruction of the Normal Tissue Architecture and Displacement of Regular Vessels

Malignant invasion *destroys* the normal texture of tissue. Bronchial branches may be displaced or fully destroyed (Fig. 5.28).

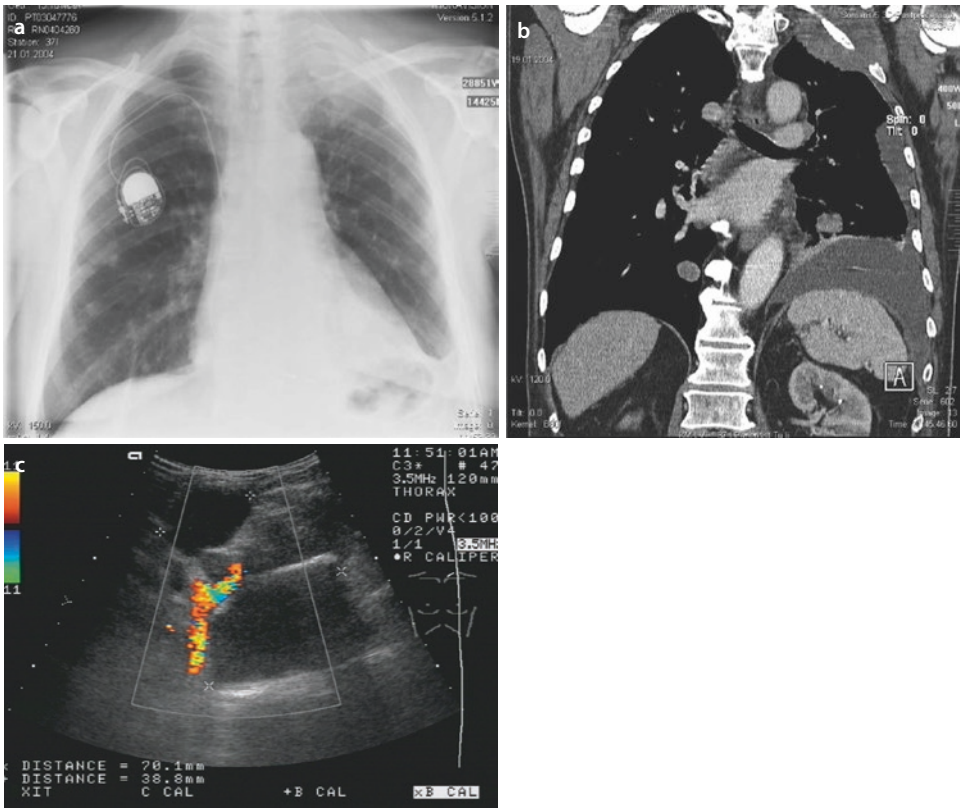

Fig. 5.25 **a** A 72-year-old man with pain in the left chest for several months; initially interpreted as angina pectoris. On the overview X-ray a shadow was noted on the left side in apical location. **b** On the coronary computed tomography section there was a space-occupying lesion on the left side in apical location, surrounding the first rib and penetrating the soft tissue. **c** Corresponding sonographic image: large hypoechoic tumor formation penetrating the dome of the pleura and invading the supraclavicular soft tissue. The subclavian artery is slightly compressed and displaced medially by the tumor. Sonography-guided biopsy indicated moderately differentiated adenocarcinoma developing within scar and connective tissue

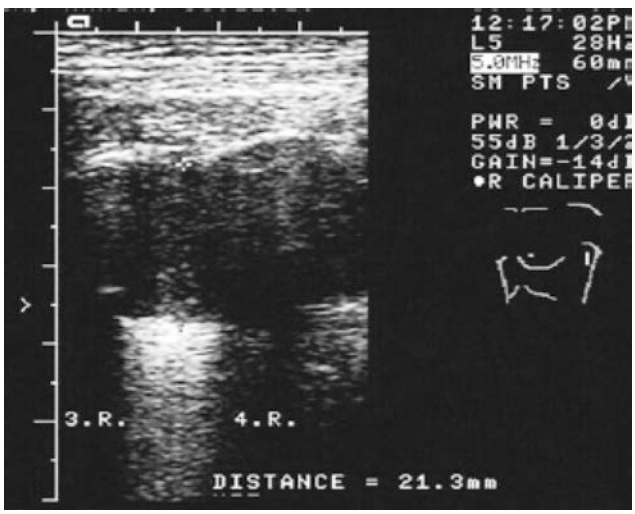

Fig. 5.26 This woman slipped on a staircase 6 months ago and has been experiencing renewed pain in the left chest for 4 weeks. Computed tomography shows a suspected hematoma. On sonography there is a space-occupying lesion invading the muscles of the chest wall and causing obvious destruction of the third and fourth rib laterally. Sonography-guided biopsy indicated poorly differentiated adenocarcinoma

The original normal vessels are either displaced (Figs. 5.25 and 5.29a) or disappear altogether (Fig. 5.28).

In some cases, vessels of the tumor itself are found particularly in the margin (Fig. 5.29b). Such vessels are convoluted and marked by changes in diameter (Yuan et al. 1994; Mathis 1997; Hsu et al. 1996, 1998).

5.2.5 Additional Investigations to Assess the Possibility of Resection

For further planning of treatment in terms of *whether the entity can be operated on and resected*, a detailed dynamic investigation has to be performed (Beckh and Bölcskei 2003). In order to decide between video-assisted thoracoscopy (VATS) and thoracotomy, it is important to know whether the pathological entity is widely fixed to the parietal pleura or is freely movable in conjunction with the lung (Landreneau et al. 1998). However, adherence alone does not permit the investigator to decide whether the lesion is malignant or benign.

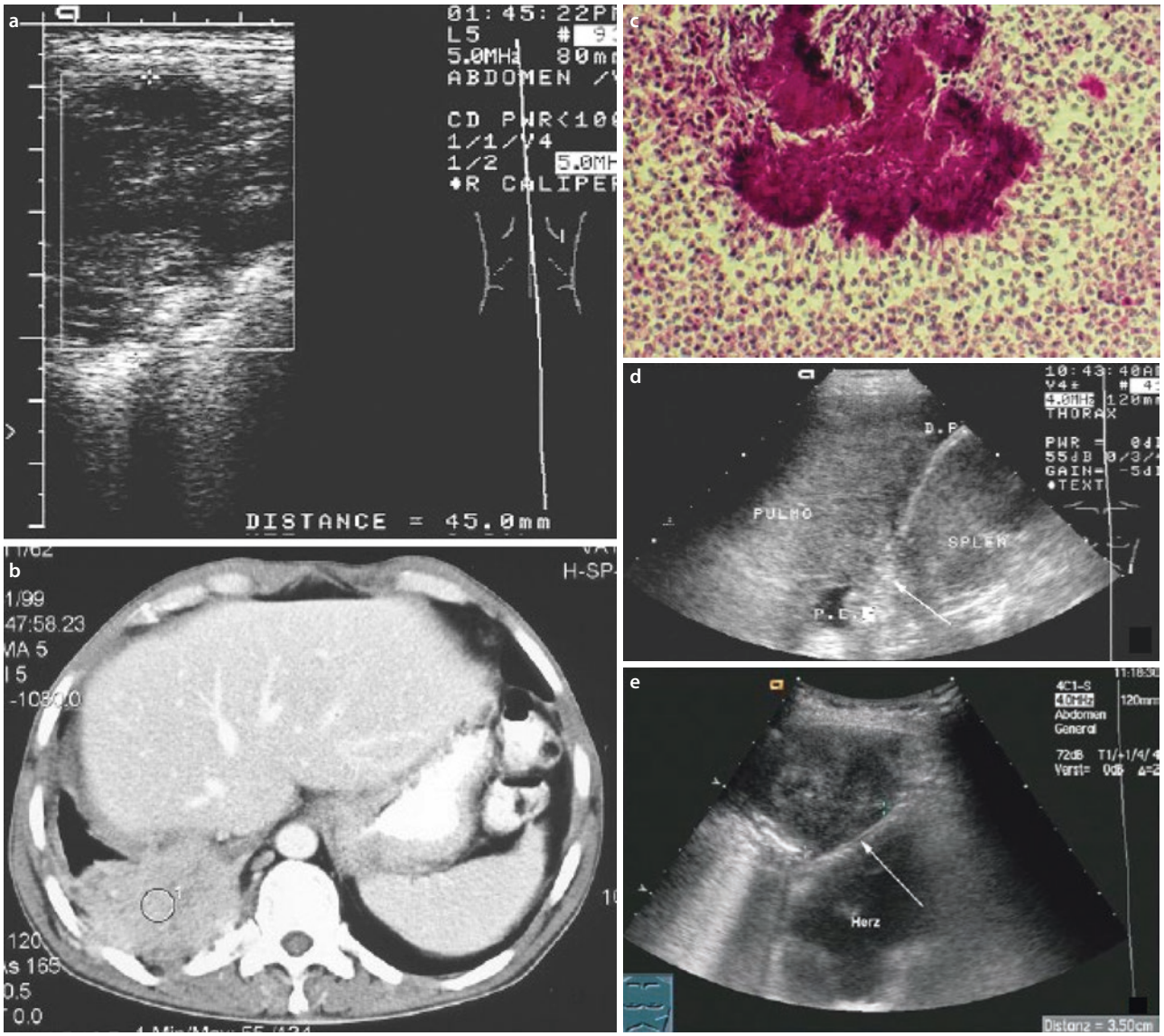

Fig. 5.27 **a** This 37-year-old man was severely ill: high fever and dyspnea. On sonography the lesion was clearly found to be crossing margins. Regular branches of the bronchial tree and vessels were well preserved; therefore, a malignancy was considered very unlikely despite the large size of the lesion. **b** Corresponding computed tomography image with the invasion which is continuing from the right lower lobe into the chest wall. **c** The biopsy specimen obtained from surgery shows evidence of actinomyces. Under high-dose penicillin therapy the invasion resolved within 10 weeks and a narrow basal callus formation remained. (Histological specimen provided by Peter Wünsch, Institute of Pathology, Klinikum Nürnberg, Nuremberg.) **d** Large tumor below the left lower lobe, inserting into the diaphragm (*arrow*). Histology of the sonographic biopsy and the operation specimen indicated benign fibrous tumor of the pleura. **e** Tumor in the lingula, invading about 3.5 cm of the parietal pericardium (*arrow*). Sonographic biopsy indicated poorly differentiated adenocarcinoma

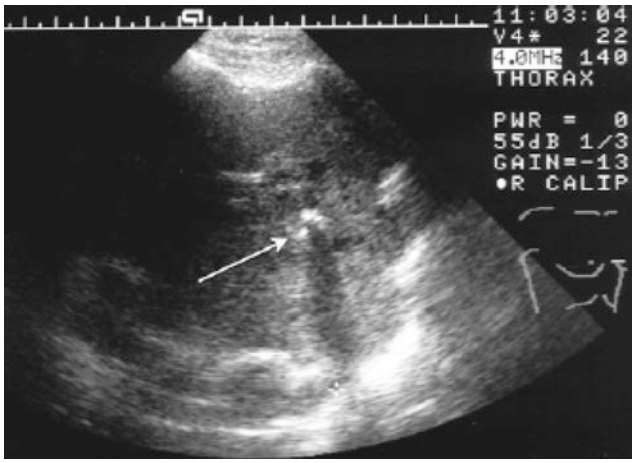

Fig. 5.28 A 50-year-old man with retrosternal pain that initially raised suspicion of coronary heart disease. Sonography showed a large tumor in the upper lobe in left parasternal location, penetrating the mediastinum and fully destroying the bronchial branches. In the tumor there is a calcification accompanied by obliteration of echoes in the dorsal aspect (*arrow*). Sonographic biopsy indicated poorly differentiated adenocarcinoma with tumor cell complexes in lymphatic recesses

In the course of tumor staging, sonography is more suitable than computed tomography to demonstrate metastases in supraclavicular lymph node regions (Fultz et al. 2002; Prosch et al. 2007; Fig. 5.30a).

The basic diagnostic procedures must include sonography of the abdomen in order to identify metastases (Fig. 5.30b).

5.2.5.1 Tumor-Related Complications in Mediastinal Vessels

In case of mediastinal tumor spread, the vena cava and its supplying vessels must be examined in order to identify compression syndromes or thrombosis (Ko et al. 1994; Fig. 4.30c).

5.2.5.2 Differentiation of a Central Space-Occupying Lesion from an Atelectasis

Atelectatic lung tissue is a suitable sonic window to the tumor that occludes the branch of the bronchus. Quite often sonography (Fig. 5.31a) allows better differen-

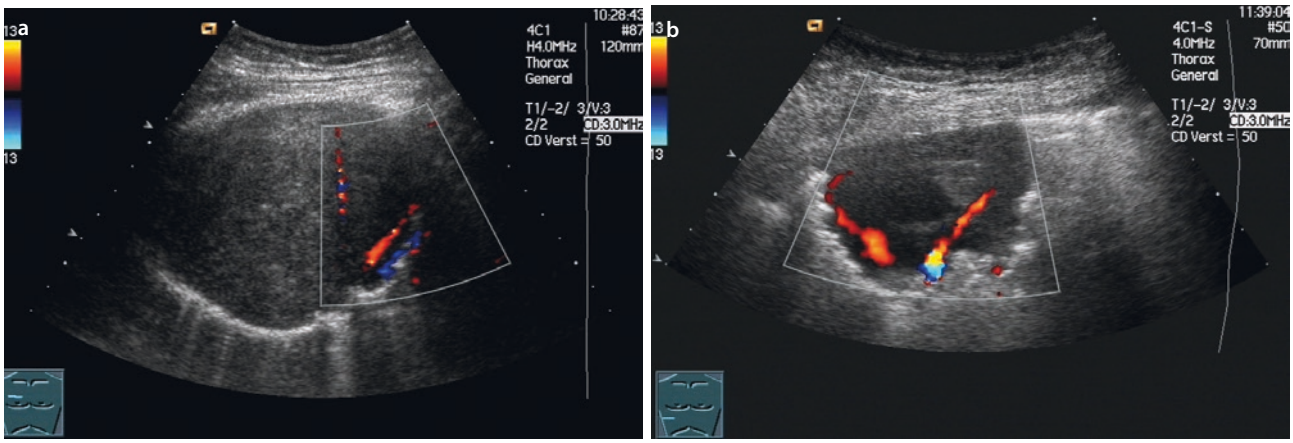

Fig. 5.29 **a** Large tumor in the upper lobe of the right lung, displacing the artery and vein of the upper lobe in medial direction. Sonographic biopsy indicated poorly differentiated neuroendocrine carcinoma. **b** Tumor in the lateral middle lobe with central necrosis; in the marginal areas there are strong, convoluted vessels of changing diameter

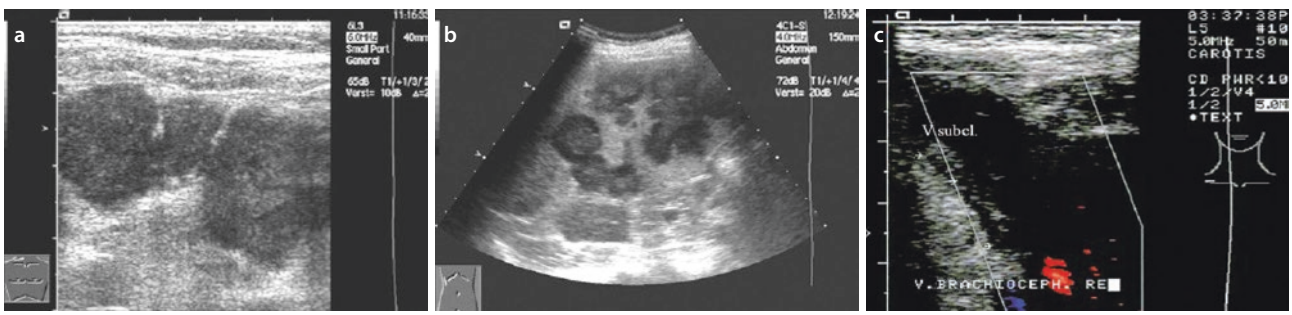

Fig. 5.30 **a** Supraclavicular lymph node metastases in a woman with a bronchial adenocarcinoma. **b** Diffuse metastatic invasion of the entire right lobe of the liver in a man with a non-small-cell lung carcinoma. **c** This 69-year-old man with a known right-sided adenocarcinoma and mediastinal lymphomas developed a swelling in the right arm. Sonographic investigation from the right supraclavicular aspect shows a recent thrombosis subclavian vein

tiation of the tumor from nonventilated lung tissue than computed tomography (Fig. 5.31b).

In the presence of additional pleural effusion the contours of the tumor-bearing atelectatic portion of the lung are rendered (Fig. 5.31c).

5.2.6 Heterogeneous Structural Pattern

The assessment of malignant lesions might be rendered difficult by their highly *heterogeneous structural pattern* (Pan et al. 1993; Table 5.2).

Tumor consolidations may still contain residually ventilated bronchial branches (Fig. 5.27e) or *colliquations* and/or *necrotic zones* (Figs. 5.29b and 5.32).

Lung tissue adjacent to a tumor might be affected by inflammation (Fig. 5.32) or contain calcifications (Fig. 5.28).

In a diseased portion of the lung, solid portions of the tumor might exist along with complex inflammatory infiltrations (Fig. 5.33).

Sonographic assessment of bronchoalveolar carcinoma is highly problematic. On the one hand, multiple peripheral consolidations with variable air content might mimic multifocal pneumonia (Görg et al. 2004; Fig. 5.34). On the other hand, one may only find an uncharacteristic uneven lung surface (Fig. 5.35).

In all cases of ambiguous pulmonary lesions, sonography may serve as an important aid in decision-making. It helps the investigator to decide about the subsequent diagnostic procedure—either immediately in terms of a sonography-assisted biopsy (Mathis et al. 1999a, b, c; Beckh et al. 2002), or as a complementary imaging method to select the appropriate surgical procedure.

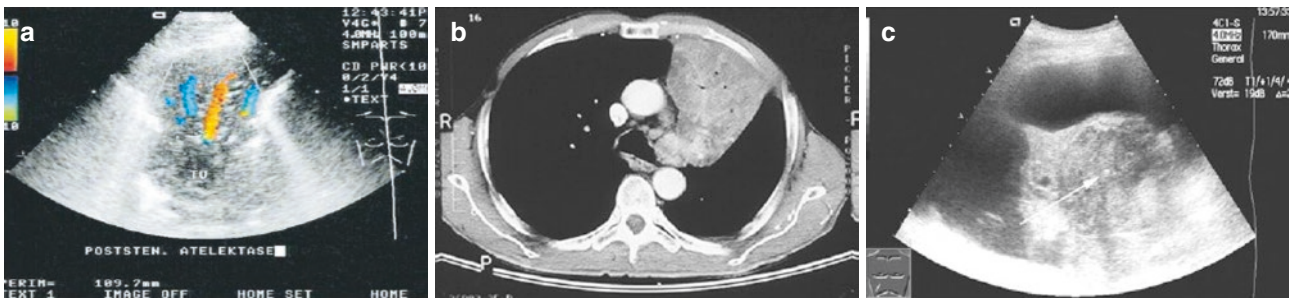

Fig. 5.31 **a** Central tumor in the left upper lobe (*broken line*); behind it there is atelectatic lung tissue with a regular vascular architecture. **b** Computed tomography image of the tumor and the atelectasis in the upper lobe. **c** Large tumor (*arrow*) in the right lower lobe; in the marginal area there is atelectatic lung tissue surrounded by a pleural effusion. Sonographic biopsy of the tumor indicated small-cell carcinoma

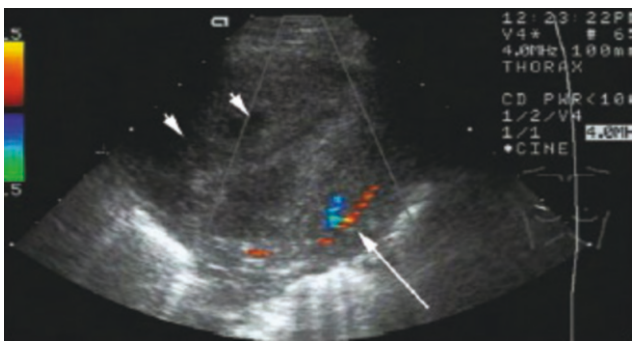

Fig. 5.32 Space-occupying lesion in the upper and middle lobe with several necrotic zones (*arrowheads*). Initially there were marked signs of inflammation on clinical examination. Under antibiotic therapy the invasive pneumonic portion resolved (*arrow*). Sonographic biopsy from solid portions of the space-occupying lesion indicated squamous cell carcinoma

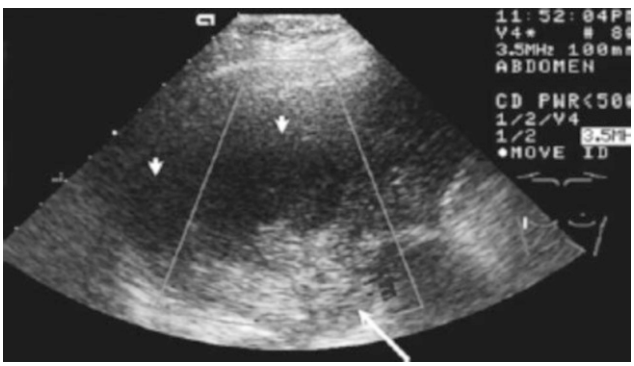

Fig. 5.33 Inhomogeneous and medially rather echodense (*arrow*) space-occupying lesion in the middle lobe. Sonographic biopsy from the more echodense portions showed, on histological examination, inflammatory lung parenchyma. Bacteriological investigation revealed *Aspergillus niger*. The sonographic biopsy from the more hypoechoic marginal areas (*arrowheads*) additionally showed a poorly differentiated, nonkeratinizing squamous cell carcinoma

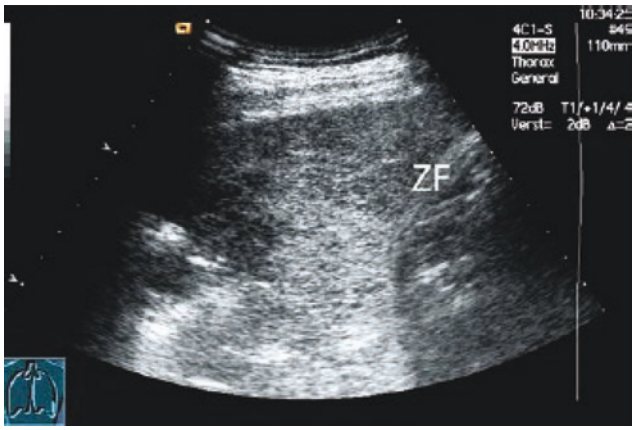

Fig. 5.34 In the right lower lobe, in the dorsal aspect, there is a nearly triangular invasive lesion with blurred margins. A bronchoalveolar carcinoma was confirmed by thoracoscopic biopsy. *INF* invasion, *PULMO* lung

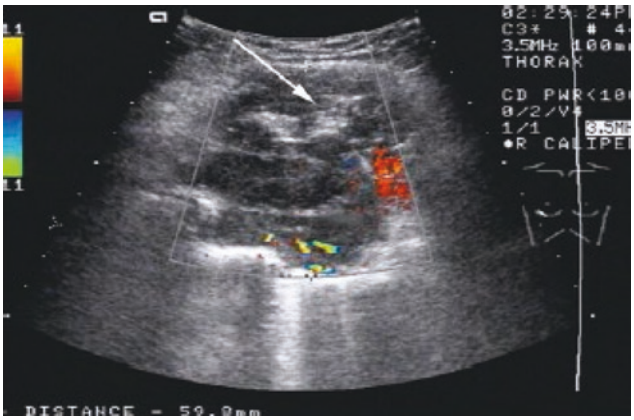

Fig. 5.36 This 77-year-old man complained of pain in the right chest. Sonography revealed a large tumor formation extending from the lung to the chest wall and leading to osteolytic destruction of a rib (*arrow*). Sonography-guided biopsy indicated metastasis of a urothelial carcinoma operated on 2 years ago

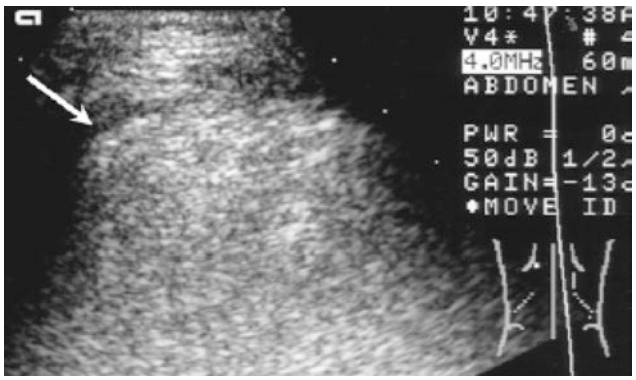

Fig. 5.35 This woman had a bronchoalveolar carcinoma confirmed on radiographic investigation and by bronchoscopic biopsy. The carcinoma fills the entire right lower lobe. Sonography only shows an irregular and finely grained surface of the lung (*arrow*)

5.2.7 Pulmonary Metastases

Pulmonary metastases are documented on sonography when they reach the margin of the lung. Owing to poor visibility in this region, sonography is not a suitable screening method. Metastases have no small air trappings and are usually homogeneously hypoechoic; occasionally, they have branches extending into tissue (Mathis et al. 1999a, b, c). Pathological vessels are predominantly found at the margin (Fig. 5.36, Table 5.3).

Table 5.3 Sonomorphology of pulmonary metastases

Morphology	Echotexture	Vessels
Round	Hypoechoic	Bizarre new vessel formation at the margin
Oval	No ventilated portions	–
Serrated	Necrosis possible	–
Sharp margins	–	–

Summary

Sonography does not permit the investigator to make a distinction between metastases and peripheral carcinoma. The interpretation must take the patient's medical history and survey radiographs into account. In terms of differential diagnosis, the formation of lesions in the parietal pleura must be excluded by dynamic investigation. Even benign pulmonary lesions, e.g., hamartoma or hemangiofibroma, might extend to the periphery of the lung as hypoechoic formations. Cyst walls may be of varying thickness. They usually have an anechoic content. Occasionally they contain fluid with internal echoes. In order to differentiate between a cyst and a pulmonary abscess or an encapsulated

empyema, the diagnostic procedure must take clinical parameters and computed tomography investigations into account. In the final analysis, bacteriological, cytological, and histological investigations are of decisive importance.

■ **Acknowledgement**

We thank R. Loose, Head of the Institute of Diagnostic and Interventional Radiology at the Klinikum Nürnberg Nord, for providing radiology reports.

5.3 Vascular Lung Consolidations: Pulmonary Embolism and Pulmonary Infarction

Gebhard Mathis
gebhard.mathis@cable.vol.at

Pulmonary embolism is the most common clinically undiagnosed cause of death. Autopsy observations indicate a frequency of 10–15%, and up to 30% in chronic heart failure, of which pulmonary embolism is again the cause of death in 40% of cases. In 10% of hospital deaths, pulmonary embolism is the cause of death, and in another 10%, it is a contributing cause. Clinical symptoms are nonspecific, and chest radiography is not very sensitive. Even in times of MSCT, it must be assumed that 40% of fatal pulmonary embolisms are not diagnosed. The most important diagnostic step is still to even think about it. The clinician is challenged to use any method that improves the diagnosis of pulmonary embolism and reduces mortality, which is still 15% (Goldhaber et al. 1999; Burge et al. 2008; Özsu et al. 2017).

5.3.1 Pathophysiological Requirements

A few minutes after pulmonary subarterial occlusion, surfactant collapse occurs. Interstitial fluid and erythrocytes flow into the alveolar space. Hemorrhagic choking provides ideal conditions for ultrasound imaging. These consolidations are directed toward the pleura, opening as it were with their base to the periphery, providing good conditions for lung sonography

Pulmonary embolism is a dynamic event. Small hemorrhages are rapidly resorbed by local fibrinolysis. Both common reperfusable fresh transient hemorrhages (early infarcts) and the rare true pulmonary infarcts with tissue necrosis (late infarcts) can be visualized sonographically. Small, premonitory emboli (signal emboli) may occur before a massive or fulminant pulmonary embolism, which, if recognized in time, give rise to appropriate therapeutic measures (Mathis and Dirschmid 1993; ◘ Fig. 5.37).

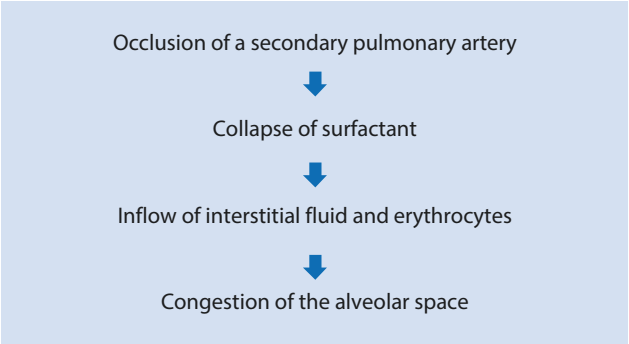

◘ **Fig. 5.37** Pathophysiological prerequisites for sonographic imaging in cases of pulmonary embolism. Peripheral engorgement of the alveolar lumen is a good prerequisite for pathological echotransmission

5.3.2 Sonomorphology of Pulmonary Embolism

5.3.2.1 Shape and Echotexture

Fresh peripheral pulmonary emboli are sonographically echo-poor and largely homogeneous. Older and larger infarcts may also be granular in texture. The shape of embolism-related lung consolidation is predominantly triangular with a pleural base. The pleura may be slightly bulging. Sometimes the foci are rounded toward the hilus, sometimes polygonal. The margin may be somewhat blurred initially, but is usually sharp. Behind it, pseudosmall enhancement may be evident (◘ Fig. 5.38; Reißig et al. 2003; Mathis et al. 2005).

5.3.2.2 Size

The average size of pulmonary infarcts is 12 × 16 mm (5–70 mm). Lesions smaller than 5 mm should not be scored, at most in the course, because they may also be scars. Pleurisy may give a similar picture once. However, this is localized at the point of pain and has extensive fragmentation of the pleural reflex. When in doubt, pleuritic consolidations can be differentiated from embolic consolidations by signal-enhanced ultrasound (◘ Figs. 5.38–5.45).

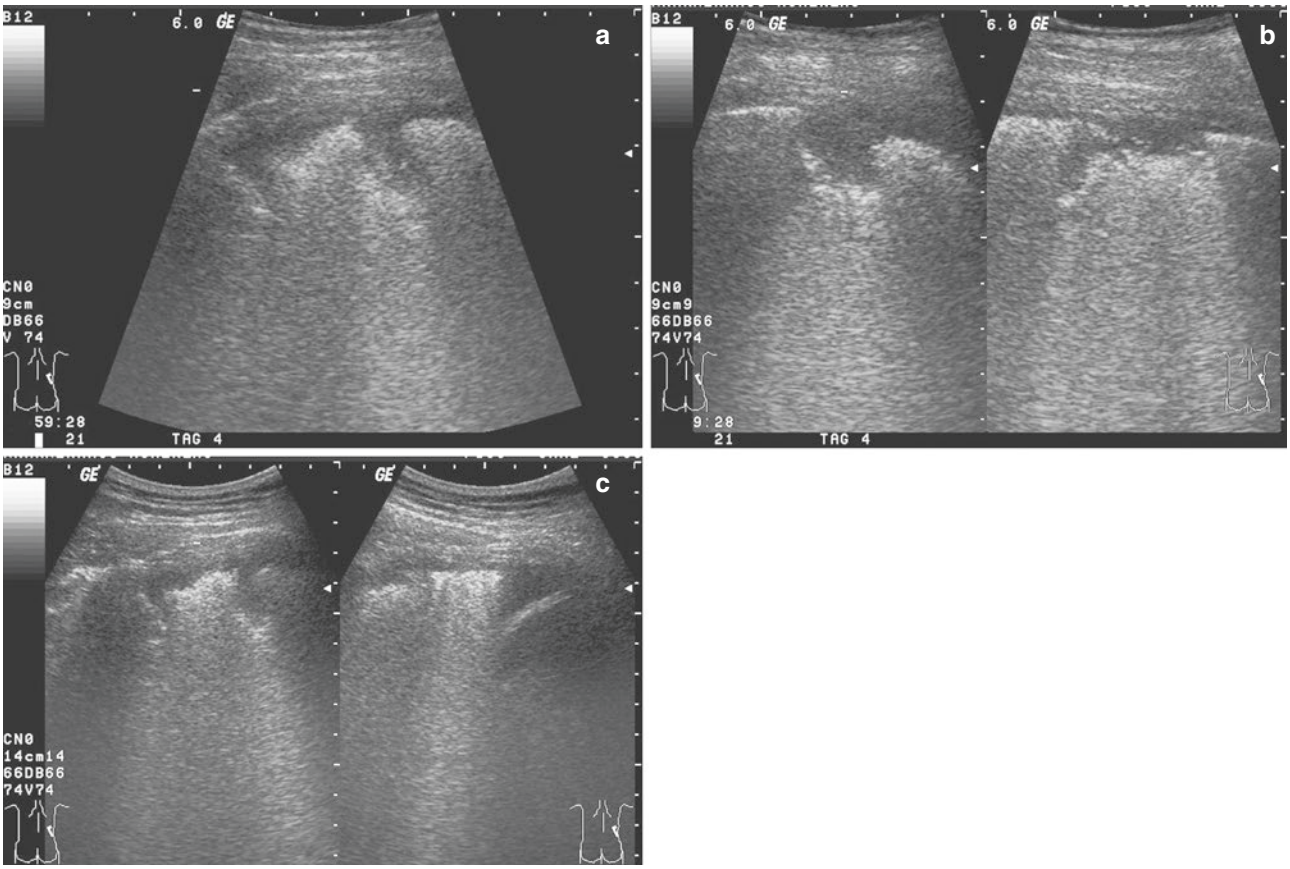

Fig. 5.38 **a** Two adjacent pulmonary infarctions in the same region of terminal flow in the presence flow of an obstructed pulmonary secondary artery. **b** Two further infarctions in the same woman. **c** Accompanying pleura effusion

5.3.2.3 Number

An average of 2.4 infarcts present with pulmonary embolism. If 2 or more foci are present, the accuracy with clinical probability is very high. In slender patients, it is recommended that a high-frequency transducer also be used to examine the visceral pleural reflex (Fig. 5.40).

5.3.2.4 Vascular Signs

In some cases, a small echoless vascular band directed from the tip of the lesion to the hilus can be visualized on the B-scan. It corresponds to the thromboembolically engorged pulmonary artery branch, as also described in computed tomographic studies ("vessel sign, vascular sign") (Fig. 5.46f).

5.3.2.5 Pleural Effusion

In about half of the cases, mostly small pleural effusions can be visualized, focally (16%) over the lesion or in the pleural sinus (33%). The effusion is largely echoless and small in relation to the infarct lesion, which is an important distinguishing criterion to differentiate it from compression atelectasis. Internal echoes in the effusion and fibrin threads indicate infarct pneumonia (Mathis et al. 1993; Fig. 5.47).

5.3.2.6 Localization

Two thirds of pulmonary infarcts are localized dorsally in the lower lobes of the lung, more so on the right than on the left. This is anatomic and hemodynamic because the basal pulmonary arteries are more straight, whereas the upper lobe arteries branch at steeper angles. The dorsobasal region is particularly accessible to transcutaneous sonography (Fig. 5.48).

5.3.2.7 Signal Emboli

Massive pulmonary embolism is often preceded by smaller embolic events, which then present as signal emboli. These present as single triangular or rounded small lesions. If several such small defects are adjacent,

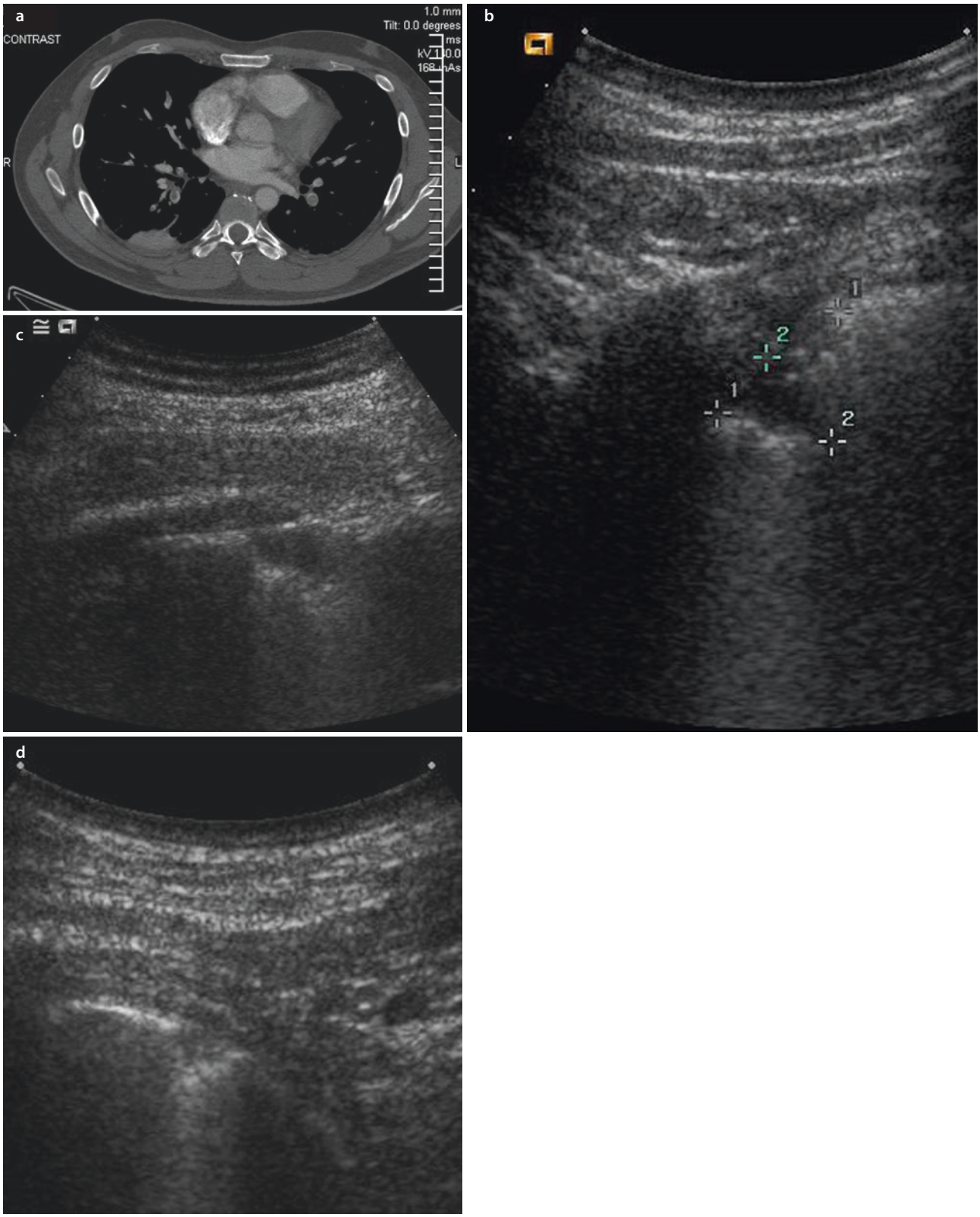

Fig. 5.39 A 42-year-old male patient 2 weeks after dyspnea following appendectomy. **a** MSCT demonstrates the pulmonary embolism in central and peripheral location. **b** The pulmonary embolism measuring 2 cm on ultrasound corresponds to the peripheral consolidation on MSCT. **c, d** Two pulmonary infarctions measuring 1cm in size were not seen on the 32-slice CT

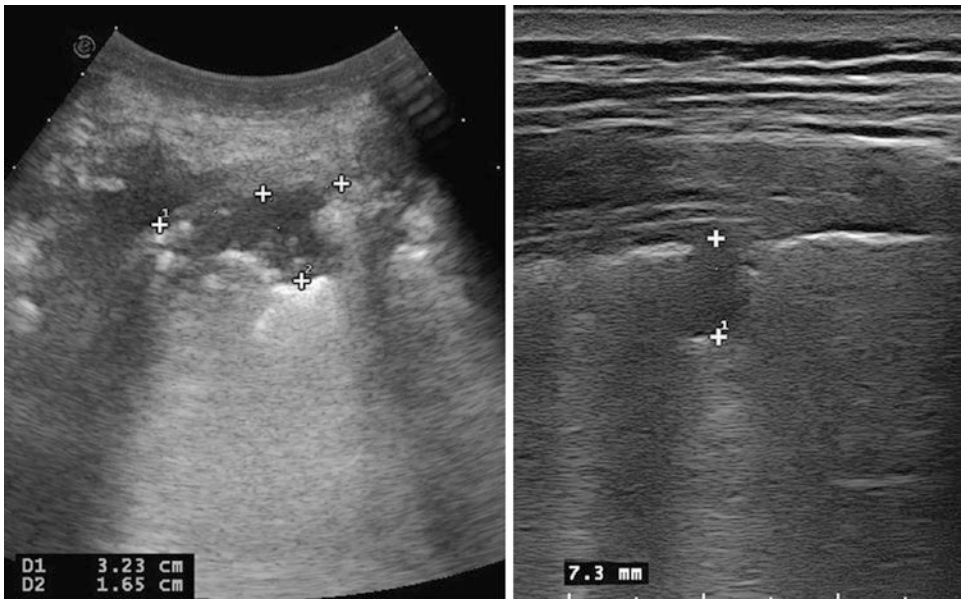

Fig. 5.40 Two lung infarcts: the left triangular, the other rounded

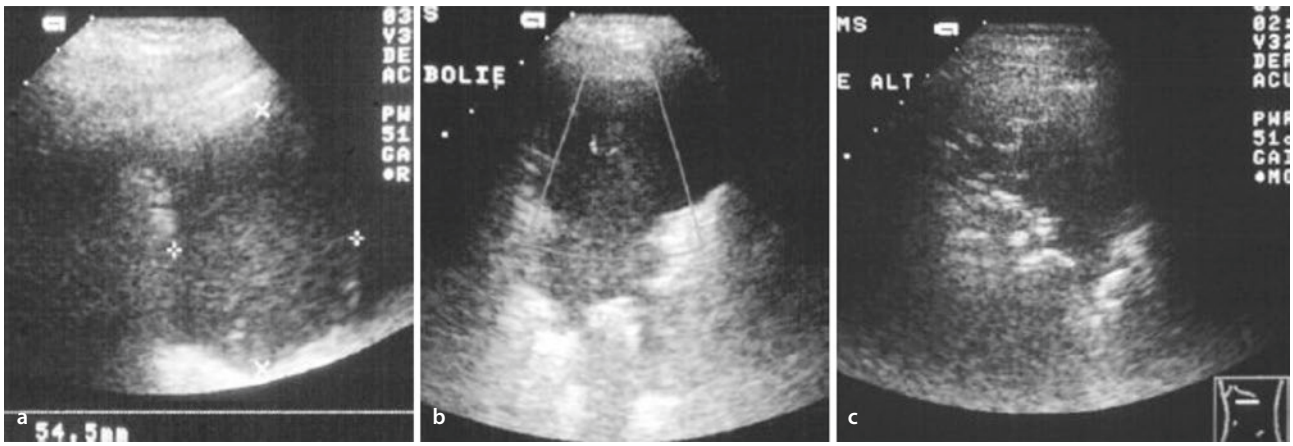

Fig. 5.41 **a** Five hours after the embolic event there is a rounded, homogeneous early infarction. **b** After 5 days the lesion is triangular in shape. **c** After 12 days the lesion has developed into a classic pulmonary infarction that is somewhat smaller than the original lesson, triangular in shape and marked by serrated margins

the appearance of a frayed boundary between pleural nonventilated and normally ventilated lungs is seen. Such small lesions may signal an impending pulmonary embolism as a precursor, but they may also coexist with a massive central pulmonary embolism and thus support the diagnosis without the central embolus itself being detectable by thoracic sonography, which cannot succeed because of the intervening air (Mathis 1997). Currently, there is a high incidence of thrombotic complications in critically ill ICU patients with covid-19 (Klok et al. 2020).

5.3.2.8 Color-Coded Duplex Sonography in Pulmonary Embolism

Visualization of embolic-related circulatory arrest by color-coded duplex sonography (FKDS) is successful in only a few cases (Fig. 5.49). There are two reasons for this limitation:

- Short-breathing patients cannot hold their breath sufficiently long, resulting in many artifacts in FKDS.
- It is difficult to hit the feeding vessel in the correct plane.

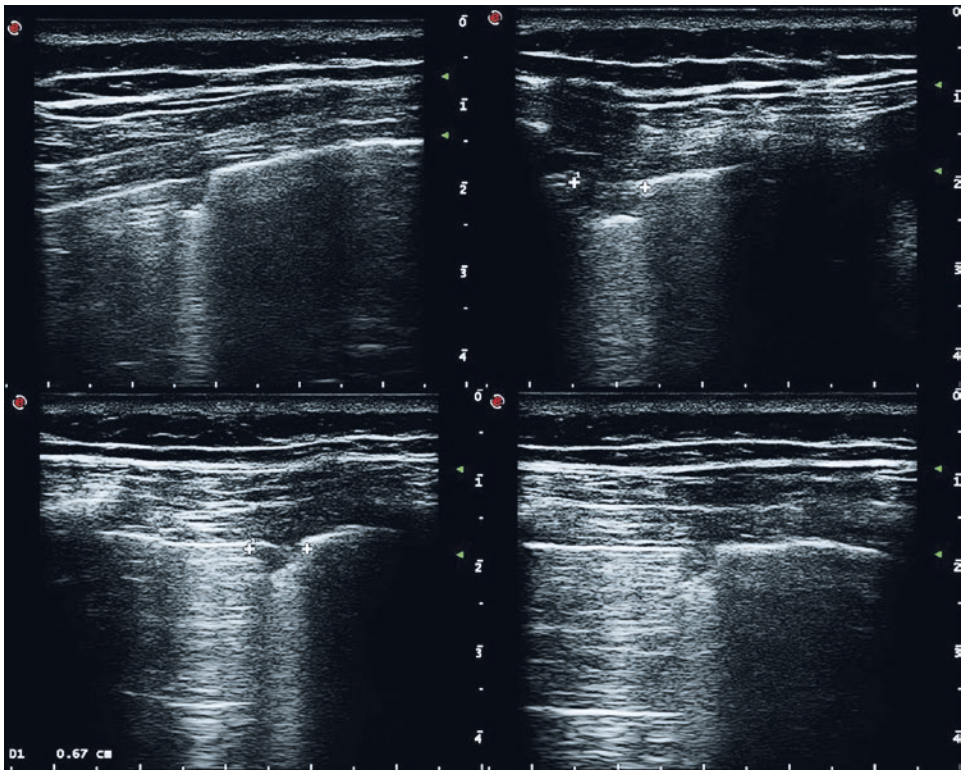

Fig. 5.42 24-year-old woman in pregnancy, deep vein and pelvis thrombosis, slight dyspnea. Several near 1 cm small pulmonary embolisms

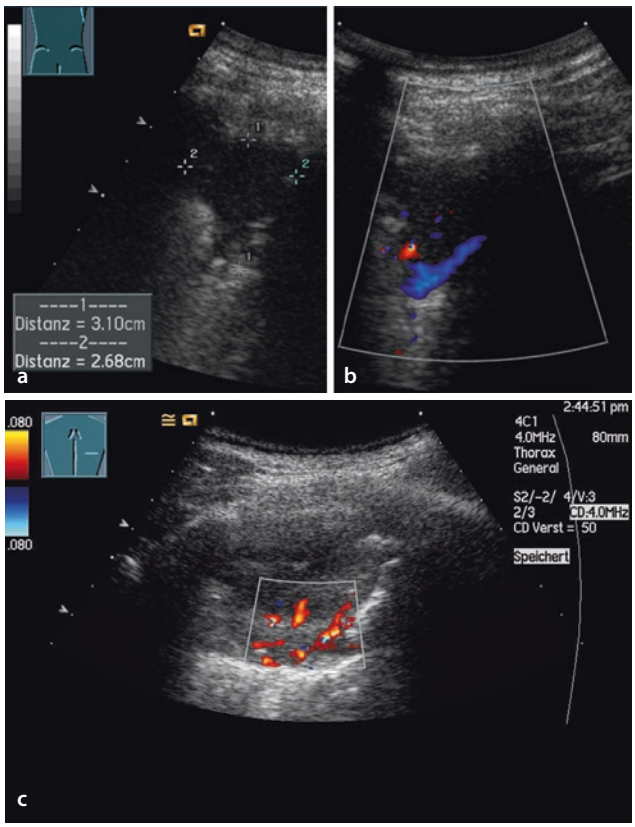

Fig. 5.43 **a** Early triangular pulmonary infarctions. The D-dimer test was still negative at this time. **b** The infarction is vascularized only at the margin and not in the center. **c** Four days later the patient had an infarction pneumonia that was seen clinically as well. This is larger than the original lesion, partly ventilated, and revascularized

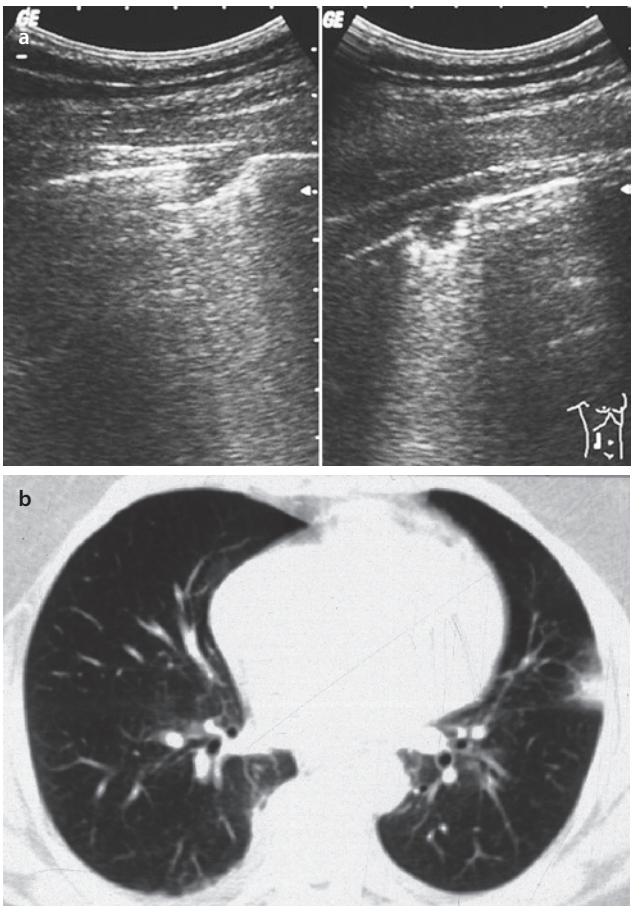

Fig. 5.44 A 25-year-old woman with sudden dyspnea and mild respiratory chest pain. **a** Sonography revealed two small pulmonary infarctions. **b** On spiral computed tomography the central pulmonary embolism was confirmed and only one lesion was seen in the periphery

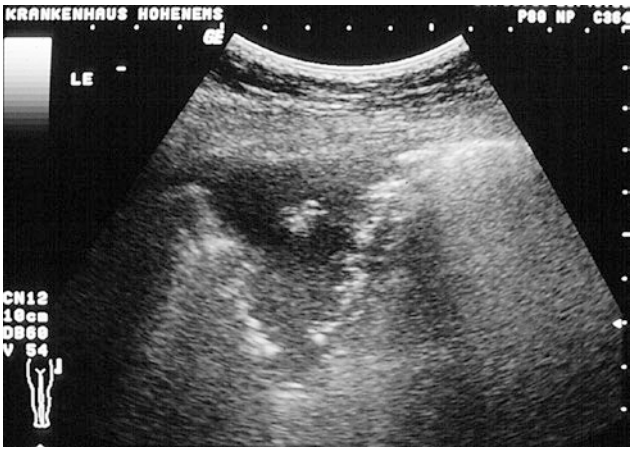

Fig. 5.45 Large, classic pulmonary infarction with highly serrated margins and a central bronchial reflex

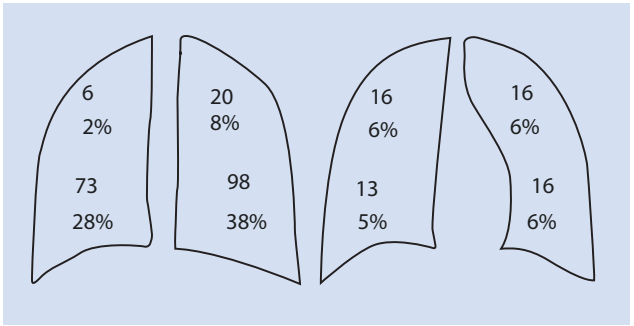

Fig. 5.46 Most pulmonary infarctions are found in the dorsobasal location owing to anatomical and hemodynamic factors

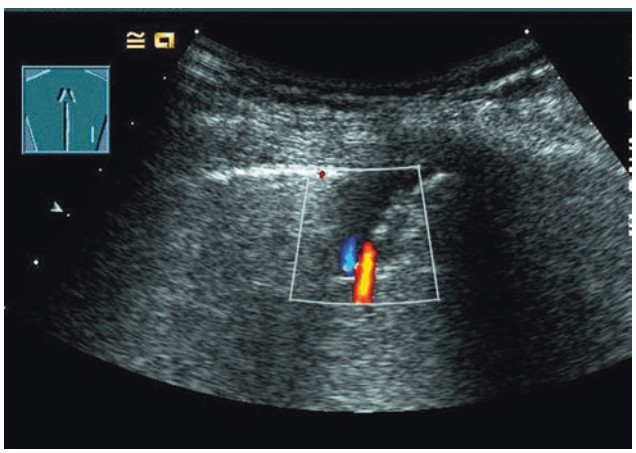

Fig. 5.47 Circulatory stop at the tip of the wedge-shaped pulmonary infarction

Nevertheless, color Doppler sonography is an important piece of the puzzle in the differentiation of subpleural lung lesions (Yuan et al. 1993; Gehmacher and Mathis 1994).

5.3.2.9 Contrast Enhanced Ultrasound (CEUS)

Pulmonary infarcts and embolic-related hemorrhages largely show a lack of contrast on contrast-enhanced sonography. Delayed and low contrast enhancement may occur at the margin of the lesion due to brochial arterial supply. Pleurisy and pneumonia, on the other hand, are early and strongly contrasted. However, old pulmonary emboli or infarct pneumonias may be well perfused again and have good contrast saturations (Görg et al. 2004; Bertolini et al. 2008; Trenker et al. 2019; Findeisen et al. 2019; Fig. 5.50).

Tips for the Procedure

About 50% of patients complain of pleuritic pain in pulmonary embolism, and others describe discomfort in a specific region. Then first look where it hurts and quickly find it. If no localization is given, one begins the examination dorsobasally, where most pulmonary emboli can be detected. If clinical suspicion persists, the entire lung should be scanned, which can take as little as a few minutes. The dorsobasal region must be examined in any case.

5.3.2.10 Healing Phase: Infarct Pneumonia

In the healing phase, the sonomorphology of the pulmonary infarction is less typical. With increasing reaeration, the sonographic picture is similar to that of pneumonia, so that sonomorphologic differentiation is now difficult (Fig. 5.43). In cases presenting for initial ultrasonography at the stage of infarct pneumonia 1–2 weeks after the event, it is probably possible to visualize the focus sonographically but offer few differential diagnostic criteria sonomorphologically (Table 5.4).

Cave

Infarct pneumonia cannot be sonographically differentiated from primary bacterial pneumonia.

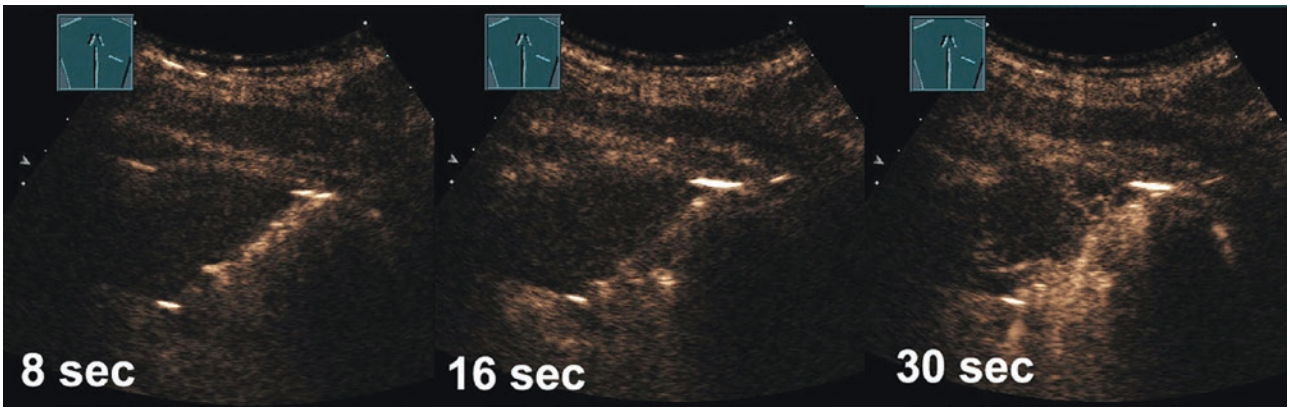

Fig. 5.48 In contrast enhanced ultrasound pulmonary embolism shows a very late and less intensive enhancement—very well for differentiation of inflammatory consolidations

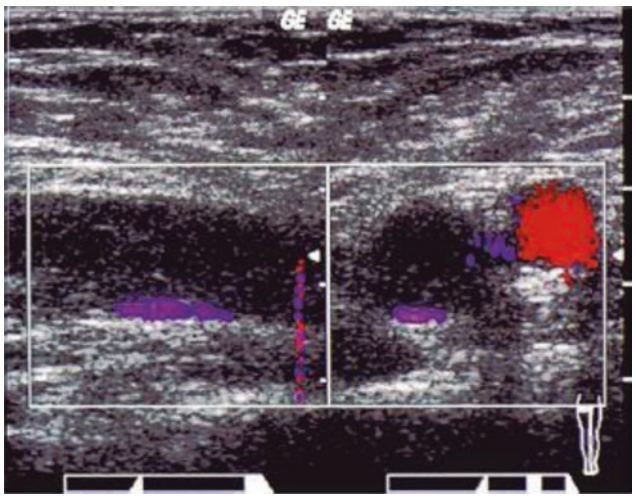

Fig. 5.49 Searching for the source of embolism: leg vein thrombosis in the femoral vein. The vein is larger than the artery, congested with echogenic material, and cannot be compressed. A small amount of flow is seen at the margin

5.3.3 Accuracy of Thoracic Sonography in the Diagnosis of Pulmonary Embolism

A large multicenter study of 352 patients in a normal round-the-clock service setting, even with less experienced examiners, has shown that peripherally typical foci are detectable sonographically in three quarters of patients with pulmonary embolism. An astonishingly high specificity of 95% was achieved (Mathis et al. 2005).

Worse results are shown by studies in which the dorsobasal region was not or too little examined (Nazerian et al. 2014).

In two meta-analyses of 5 and 10 studies in 652 and 887 patients, respectively, the pooled sensitivity is 80–87% and specificity is 82–93%. The authors conclude that given the increasing number of CT examinations and the increasing collective radiation dose for specific clinical situations, thoracic sonography exists as a diagnostic alternative to CT (Niemann et al. 2009; Squizzato et al. 2013).

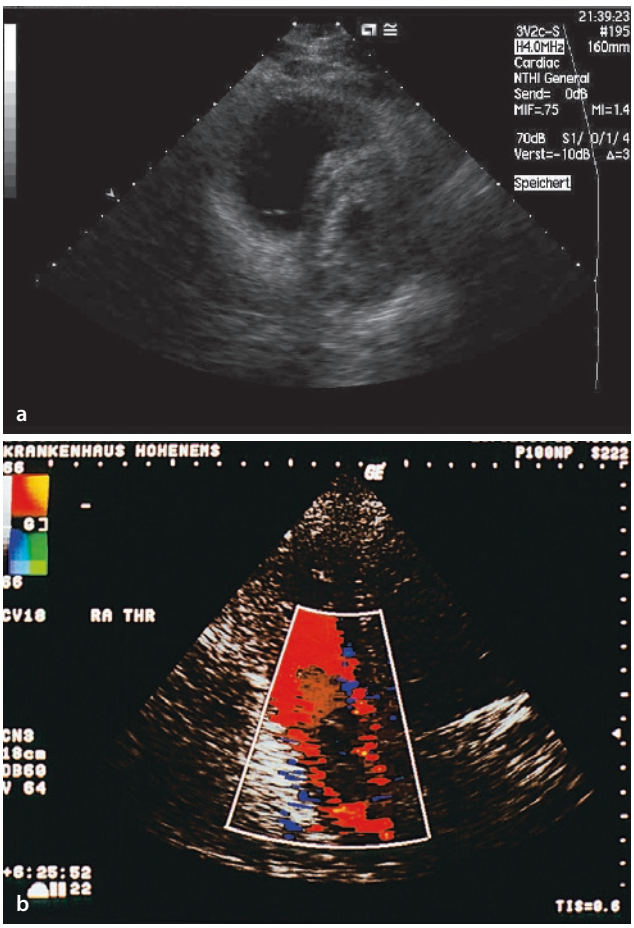

Fig. 5.50 **a** Acute load of the right side of the heart with massive dilatation of the right ventricle. **b** At the level of valve there is a floating thrombus in the right side of the heart

Table 5.4 Sonomorphology of pulmonary embolism

– echo-poor
– sharply demarcated
– pleural based
– triangular > round > polygonal
– 1–2 cm in size (0.5-7)
– vascular sign
– small pleural effusion focal/basal
– 2/3 dorsobasal localized
– central not perfused

A recent consensus conference and the current AWMF guidelines recommend pulmonary ultrasonography as an alternative to angio-CT when it is contraindicated (pregnancy, renal insufficiency, contrast agent allergy) or unavailable (Volpicelli et al. 2012a, b; AWMF 2016).

Cave
Normal chest sonography does not exclude pulmonary embolism, nor does negative CT or negative D-dimers.

5.3.4 Multi-organ Ultrasound in Thromboembolism

In the diagnosis of leg vein thrombosis, 2-point compression ultrasonography of the leg veins has become the method of first choice. The experienced examiner can inspect several clinically actual or possibly involved body regions with one imaging system in one examination procedure, in which he can investigate the source, route, and destination of the embolic event Recently, it has been shown that, according to the history and clinical picture, a targeted use of different organ ultrasound examinations with the D-dimer test significantly improves the accuracy. This has also been shown in the combination of lung ultrasound with compression sonography of the leg veins (Abootalebi et al. 2016; Nazerian et al. 2017; Zhu and Ma 2017; Mathis 2019).

Compression sonography of the leg veins

Well over half of pulmonary emboli originate in the leg veins. Compression ultrasonography of the leg veins is a safe approach to confirm the source of embolism from deep vein thrombosis. When deep vein thrombosis is suspected, the median sensitivity is 95%and the median specificity is 97%. Even in isolated thrombosis of the lower leg, which should not be underestimated, sonography shows a median sensitivity of 89% and median specificity of 92% (Jäger et al. 1993; Eichlisberger et al. 1995; Abootalebi et al. 2016; Fig. 5.51).

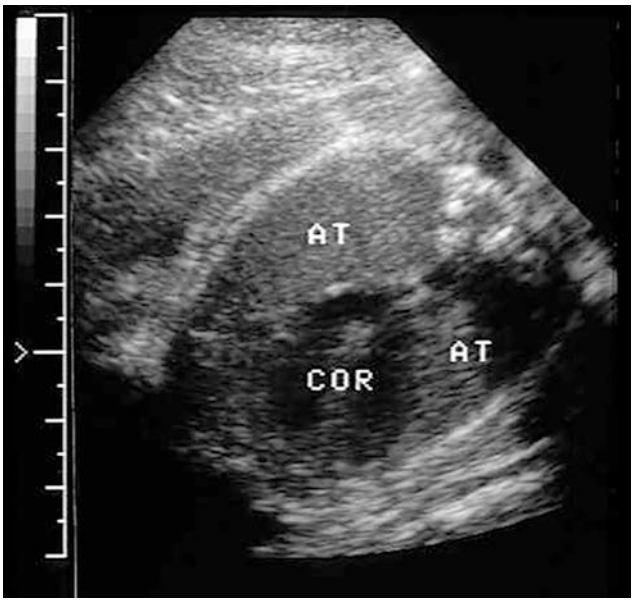

Fig. 5.51 Echo through the chest of a fetus in the 32nd gestational week. Both lungs are homogeneously hypoechoic, as in complete atelectasis (AT)

5.3.5 Echocardiography

Approximately 40% of patients with acute LE have right heart strain. This particularly captures the hemodynamic risk patients who need immediate lysis as a life-saving measure. The first hours after symptom onset are crucial for the prognosis of hemodynamically relevant LE. Right heart strain is most commonly seen at first glance. Other typical signs include: abnormal septal motion, tricuspid insufficiency, McConnels sign, thrombi in the right heart, hypokinesia of the right ventricle, and tricuspid annular plane systolic excursion (TASPE). Most of these signs are rapidly visible and easily learned during focused echocardiography (Fields et al. 2017).

Considering the accuracy of echocardiography, for unselected patients with suspected LE, the sensitivity is only 25–55% with a specificity of 90% (Jackson et al. 2000; Dresden et al. 2014). On the other hand, the accuracy in hemodynamically unstable patients is very high (Fig. 5.52).

A major advantage of sonographic embolic diagnosis is its availability independent of location and bedside, whether in the emergency department or even prehospital. The combination of chest sonography, echocardiography, and leg vein compression sonography yields

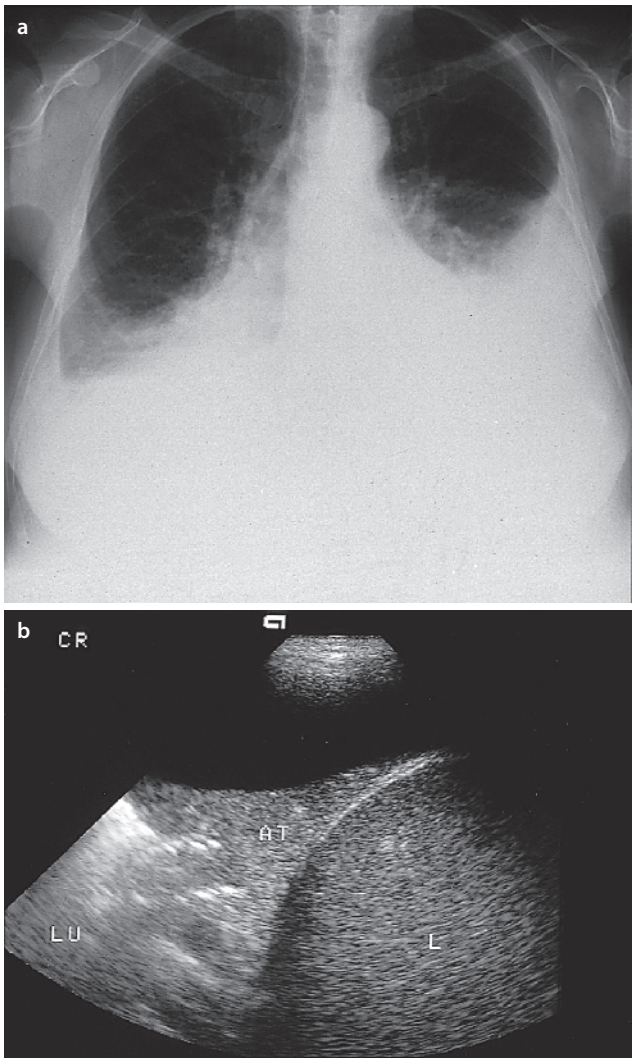

Fig. 5.52 **a** Chest x-ray: a 60-year-old man with global decompensated heart failure and bilateral pleural effusions. **b** B-mode ultrasound: In right-lateral intercostal scan one sees a pleural effusion with a wedge-shaped hypoechoic transformation of parts of the lower lobe of the lung as in the presence of atelectasis (AT). The demarcation to the ventilated lung (LU) is blurred. An extensive "air bronchogram" is seen. L liver

a sensitivity of more than 90% for pulmonary embolism (Mathis 2006; Nazerian et al. 2014).

The introduction of MSCT as the gold standard in the diagnosis of pulmonary embolism has increased the incidence but not significantly decreased mortality (Burge et al. 2008). Thus, the question arises to what extent the effect and side effect (radiation exposure in pregnancy, renal insufficiency, allergic reactions and overtreatment) of MSCT are balanced in the diagnosis of PE (Newman and Schriger 2011; Osman et al. 2018). A recent consensus conference and current guidelines recommend pulmonary sonography for the diagnosis of PE as an alternative to MSCT in certain clinical situations (Volpicelli et al. 2012a, b; Mathis 2014). If we want to make a timely diagnosis in those patients at risk of fatal pulmonary embolism, we need to think about it more often, improve the use of clinical scores, and perform imaging immediately, for example, with ultrasound (Nazerian et al. 2017).

Sonography in pulmonary embolism: "Kill three birds with one stone - three birds with one stone".

Summary

In pulmonary embolism, lung ultrasound can show an average of 2.4 subpleural, low-echo lesions in at least three quarters of cases. On the one hand, these correspond to embolism-related reperfusible alveolar edema and hemorrhages (pulmonary premature infarcts). On the other hand, they are distinct pulmonary infarctions that present a typical sonomorphologic picture with small pleural-based triangular or slightly rounded foci. In combination with echocardiography and leg vein compression sonography, the accuracy is above 90%, making lung ultrasound an adjunct and, in certain clinical situations, an alternative to angiocomputed tomography.

5.4 Subpleural Lung Consolidation

Christian Görg
christian.goerg@uk-gm.de

C. Görg

5.4.1 Definition

Atelectasis is defined as the absence of ventilation in portions of the lung or the entire lung. Such lack of ventilation may be permanent or transient, complete or partial (dysatelectasis), congenital or acquired (Fig. 5.51).

5.4.2 Pathomorphology

Depending on the origin, a distinction is made between compression atelectasis and resorption atelectasis (obstructive atelectasis). Compression atelectasis may be anticipated when an accumulation of fluid causes intrapleural pressure to increase to a level higher than that of external air. This may be expected when the effusion is more than 2 l (Grundmann 1986).

Resorption atelectasis occurs when a bronchus is displaced in terms of its region of vascular supply, as a result of external compression or endobronchial obliteration.

In cases of resorption or obstructive atelectasis, a distinction is made between the central and the periph-

eral form. Central obstruction is usually caused by endobronchial processes (e.g., bronchial carcinoma or foreign body) or extrabronchial alterations (e.g., enlarged lymph nodes), whereas peripheral bronchial obstructions are marked by inflammatory mucus plugs and displacement of small bronchial branches. Displacement of the lumen of the middle lobe by mucus or pus, scarred kinking of the bronchus, external lymph node compression or tumor leads to the middle lobe syndrome.

Atelectasis impairs circulation in parenchyma, causing undersaturation of arteries owing to reduced gas exchange in perfused but not ventilated atelectatic lung parenchyma. In terms of pathological anatomy, the early phase of obstructive atelectasis is marked by high-protein fluid in intraalveolar spaces. The next stage is characterized by the migration of macrophages and lymphocytic infiltration. In cases of compression or even obstructive atelectasis of longer duration, the parenchyma shrinks and fibrous induration of lung tissue occurs.

Additional attendant phenomena or complications in cases of bronchial obstruction include secretion retention; bronchiectasis is seen in approximately 40% of cases (Burke and Fraser 1988; Yang et al. 1990a, b; Liaw et al. 1994a, b). In rare cases the patient develops bacterial superinfection and microscopic or gross abscesses; necrotic or hemorrhagic lesions in atelectatic tissue may also be found.

5.4.3 Sonomorphology

Lung atelectases are characterized by partial or complete absence of ventilation; therefore, in principle, they can be imaged by sonography. Furthermore, the echotransparency of the lung allows the investigator to assess the parenchyma. Especially in the presence of obstructive atelectasis, atelectatic lung tissue serves as "an acoustic window" for the investigation of central structures that possibly underlie the atelectasis.

5.4.4 Compression atelektaseis

The most common form of atelectasis is accompanied by the formation of pleural effusion. Depending on the amount of intrapleural fluid, the patient may develop homogeneous hypoechoic transformations shaped like a wedge or a pointed cap, especially in the area of the lower lobe (Fig. 5.52a, b). The margin towards the adjacent aerated lung tissue is blurred. Usually the atelectatic lung is surrounded by fluid, but also may be partly adherent to the pleura. The following features help to confirm the diagnosis by sonography:

- Partial reventilation during inspiration (Fig. 5.53),
- Partial reventilation after thoracentesis of effusion (Fig. 5.54a, b).

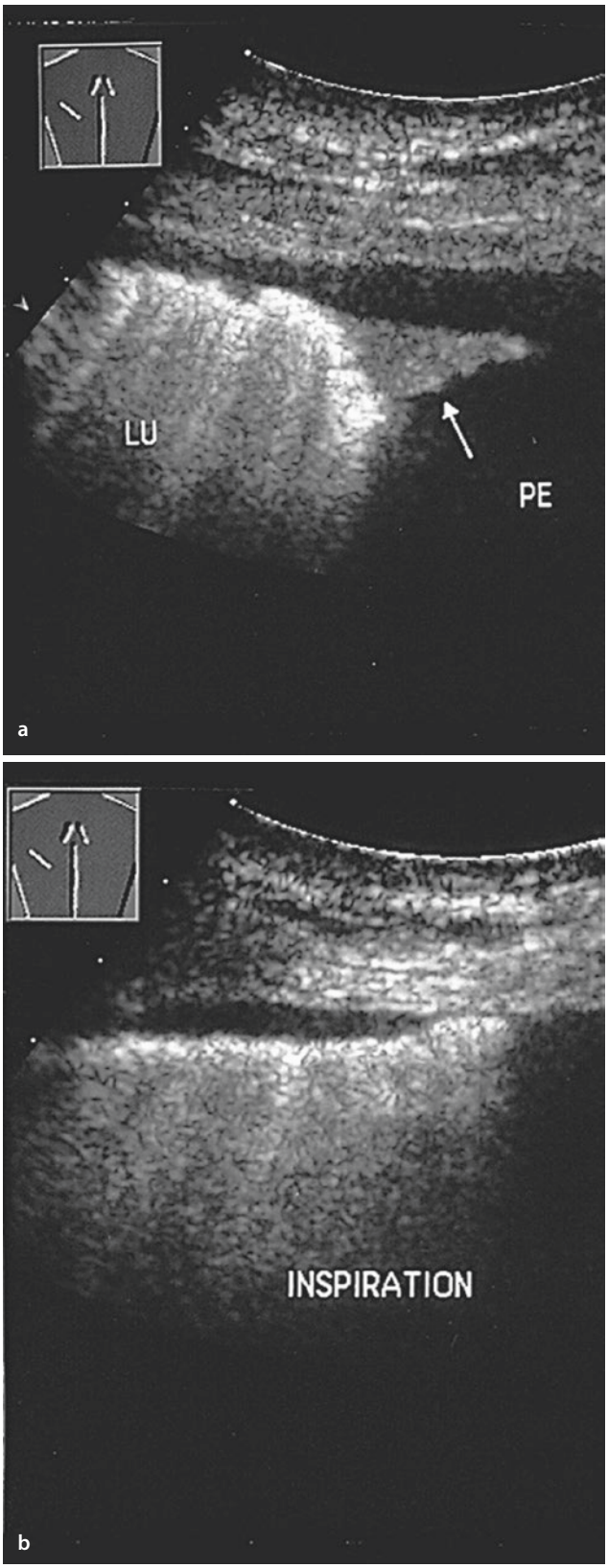

Fig. 5.53 **a** In left-lateral intercostal scan one sees a pointed cap-like, smoothly margined hypoechoic transformation in the tip of the lower lobe of the left lung (arrow) in the presence of a pleural effusion. Lu lung, PE pleural effusion. **b** Reventilation of lung tissue is achieved after deep inspiration, as in the presence of compression atelectasis

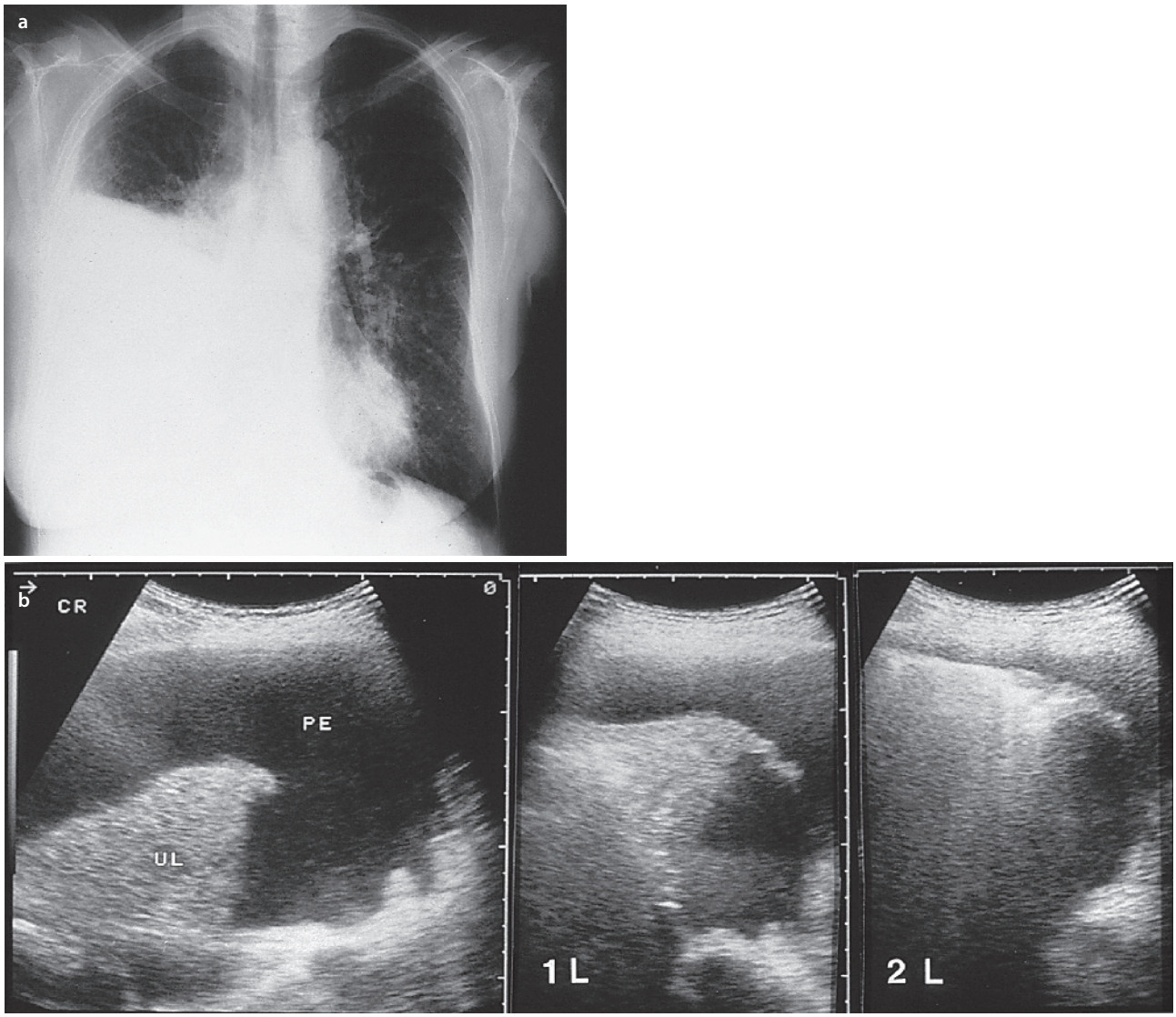

Fig. 5.54 A 66-year-old man with an alveolar carcinoma. **a** Chest x-ray: homogenous shadow of the caudal right-sided hemothorax. **b** B-mode ultrasound: right-lateral intercostal echo transmission shows a marked pleural effusion (PE) with atelectasis in the lower lobe (UL). After thoracentesis of the effusion (1 l, middle, and (2 l, right) there is increasing reventilation

In cases of compression atelectasis, lung tissue is partially reventilated after drainage of the effusion. This is also dependent on the elasticity of the lung. Of course, ventilation of the parenchyma after puncture of the effusion does not rule out the possibility of an additional central space-occupying lesion.

During inspiration sonography reveals an increasing quantity of air in atelectatic regions and the formation of a so-called »air bronchogram«. However, in the presence of exudative effusion, fibrin strands, septa and echogenic pleural effusion, one frequently observes poor reventilation during inspiration as a result of reduced elasticity of the lung. This condition has been described as a "trapped" lung (Lan et al. 1997). Concomitant inflammatory invasion of parenchyma in atelectatic tissue is a further limitation. It leads to congestive pneumonia and restricts inspiratory ventilation. On the basis of sonomorphology alone this condition cannot be distinguished from pneumonia (Fig. 5.55). In the case of multiple fibrin threads, the use of local fibrinolysis or video-assisted thoracoscopic surgery should be considered.

An exudative effusion can also be fixed to the lung by a fibrin mantle or pleural carcinosis (Salamonsen et al. 2014) (Figs. 5.56 and 5.57). This may result in the fixed lung being unable to re-expand with a relieving puncture due to the loss of elasticity, and the resulting negative pressure even at low puncture volumes may lead to a "spontaneous pneumothorax" caused by shear forces after the relieving effusion puncture.

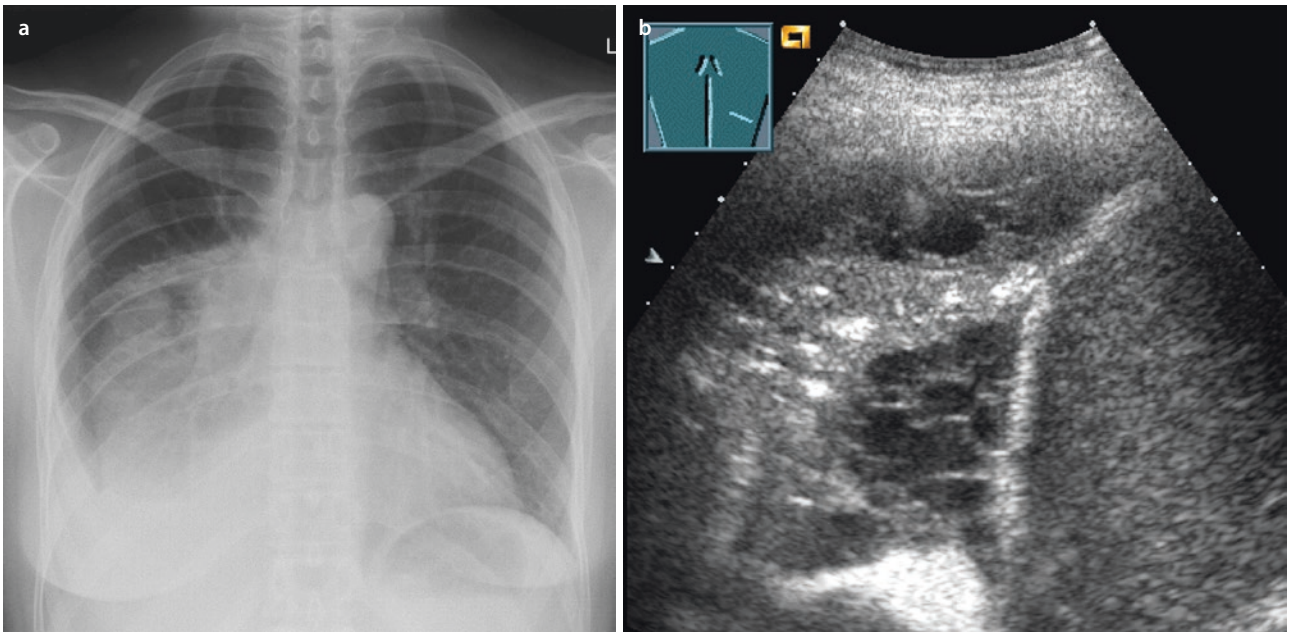

Fig. 5.55 Patient with exudative effusion with atelectasis and increased inflammatory markers. **a** Chest x-ray: shadowing in the area of the right caudal lung. **b** B-mode ultrasound: lung consolidation with focal air bronchogram and septated effusion. The lung is trapped

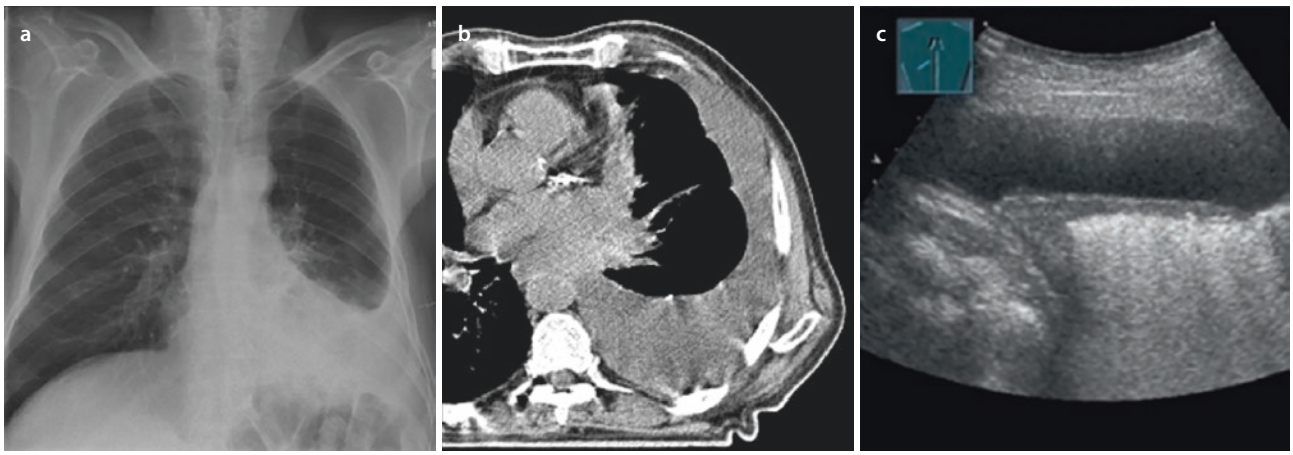

Fig. 5.56 Patient with histologically confirmed bronchial carcinoma. **a** Chest x-ray: shadowing in the area of the left caudal lung. **b** CT: visualization of the central tumor formation with pleural effusion. **c** B-mode ultrasound: lung consolidation with central ventilation and hypoechoic mantle of the lung and anechoic effusion. The lung is trapped

Possible Sonography Findings in Compression Atelectasis:

- B-mode ultrasound
  - Moderate to marked pleural effusion
  - Triangular pointed cap-like hypoechoic transformation of lung parenchyma
  - Blurred margins towards the ventilated lung parenchyma
  - Partial reventilation during inspiration ("air bronchogram")
  - Partial reventilation after thoracentesis of the effusion
- Color-Doppler sonography (CDS)
  - on intraindividual comparison with the liver/spleen one finds enhanced flow phenomena (► Chap. 8)

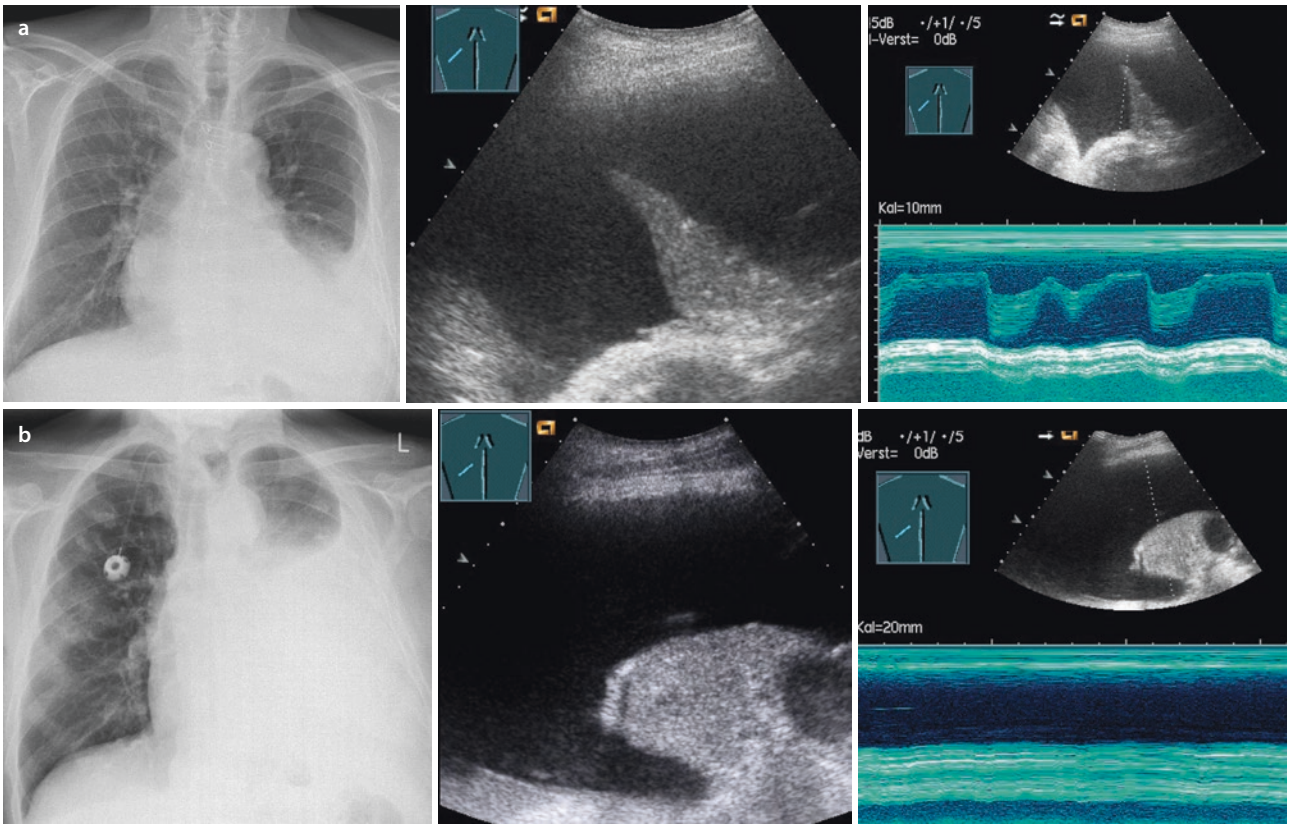

Fig. 5.57 **a** Patient with benign pleural effusion caused by congestive heart failure, visualized by chest x-ray and lung ultrasound; in M-mode ultrasound, the atelectatic lung shows significant pulse-synchronous mobility. **b** Patient with malignant pleural effusion caused by metastatic pancreatic carcinoma, visualized by chest x-ray and lung ultrasound; in M-mode ultrasound, the atelectatic lung shows a lack of mobility. After thoracentesis, the patient developed a pneumothorax that needed to be drained

5.4.5 Obstruktive Atelektase

The sonographic image of obstructive atelectasis is marked by a largely homogeneous, hypoechoic presentation of lung tissue as in hepatization (Fig. 5.58). Effusion is absent or is very mild and is not in any way related to the consolidated lung tissue. In cases of lobar atelectasis, the margin towards ventilated lung tissue is rather distinct (Fig. 5.59). Depending on the duration of atelectasis, intraparenchymatous structures also may be seen:

- Hypoechoic vascular lines and echogenic reflexes
- Anechoic, hypoechoic or echogenic focal lesions

Atelectasis of long duration is accompanied by sonographic tree-like reflexebands in the lung parenchyma. The reflexeband are caused by dilated bronchi, as a result of secretory congestion (so-called fluid bronchogram (Figs. 5.60 and 5.61). Vessels along the bronchi are seen as branches of the pulmonary artery and the pulmonary vein on CDS (Fig. 5.61; ▶ Chap. 8). In the case of prolonged tumor-related atelectasis, the occlusion of the pulmonary arteries can shift to a sole bronchial arterial perfusion (▶ Chap. 8).

Quite often the investigator finds **focal lesions** in the lung parenchyma (Figs. 5.62a–c, 5.63a–c, 5.64a–c, and 5.65a–c). As a result of dilated bronchi (due to congestion of secretion), one occasionally finds small anechoic, hypoechoic or even echogenic lesions within the parenchyma. Given corresponding clinical features, the lesions are due to microabscesses. Occasionally the abscesses contain air echoes (Yang et al. 1992a, b; Fig. 5.65). Atelectasis caused by tumor often leads to intraparen-

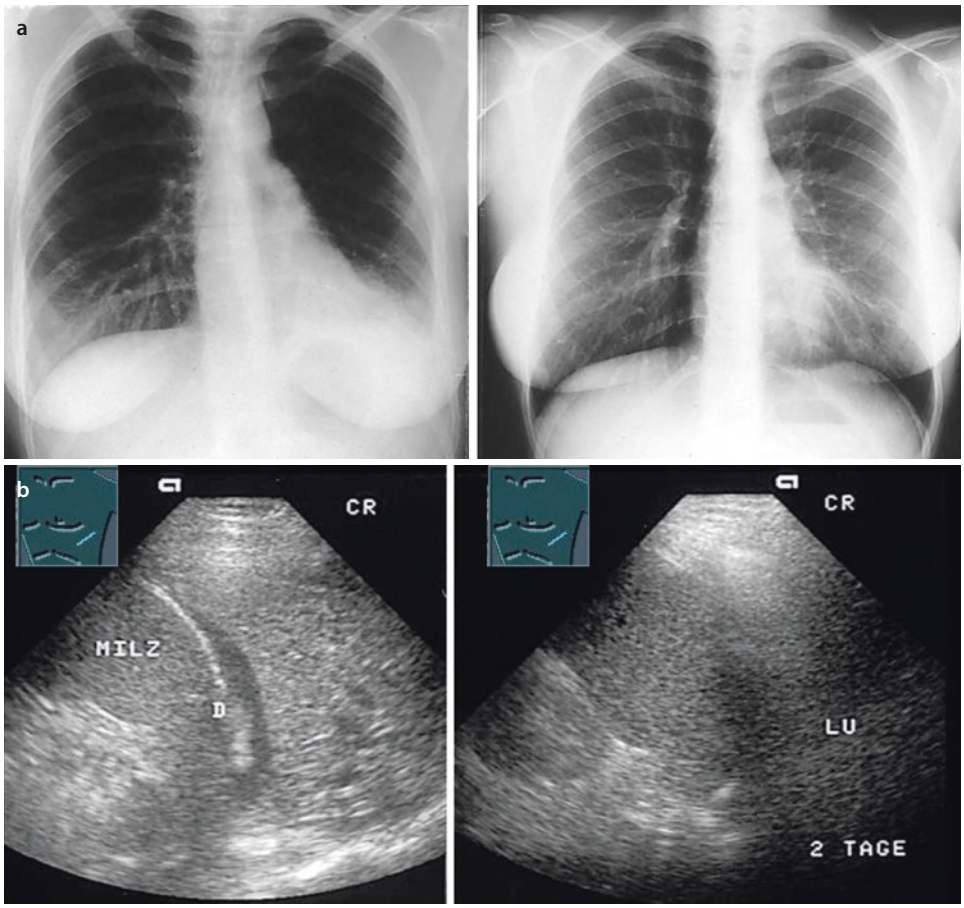

Fig. 5.58 A 74-year-old woman with dyspnea. **a** Chest x-ray: signs of right-sided upper-lobe atelectasis. **b** B-mode ultrasound: right-ventral intercostal echo transmission shows a smoothly margined, wedge shaped hypoechoic transformation of the lung as in atelectasis. The central vessels are seen; a shadow of the tumor core cannot be demarcated. AO aorta, PV pulmonary vein, PA pulmonary artery. CDS shows pronounced arterial and venous flow profiles. The characteristic flow profiles of the pulmonary artery and the pulmonary vein are seen

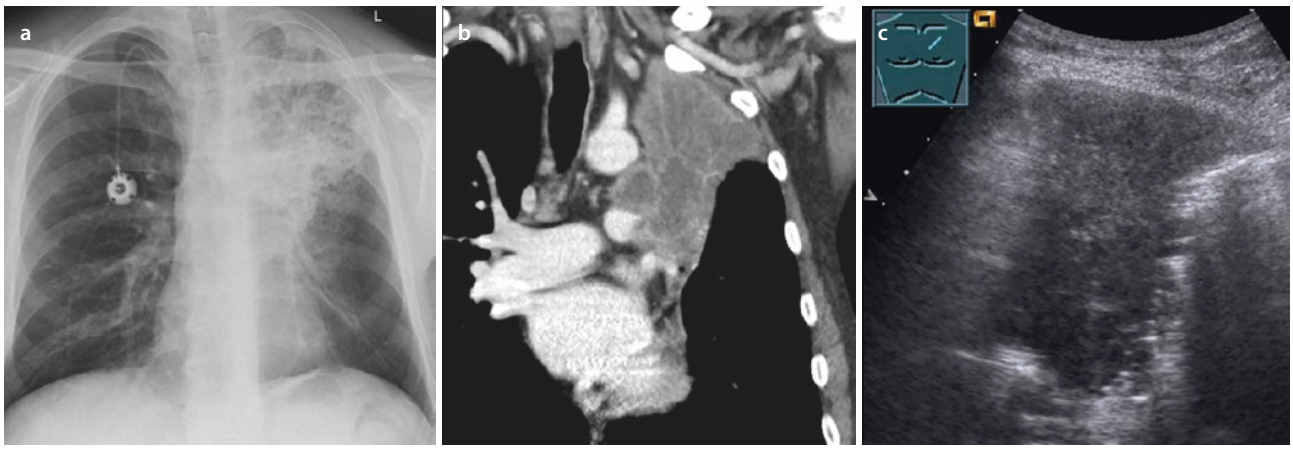

Fig. 5.59 Patient with histologically confirmed bronchial carcinoma. **a** Chest x-ray: shadows in the region of the left apical lung. **b** CT: visualization of the central tumor with subsequent atelectasis. **c** B-mode ultrasound: lung consolidation with centrally located, slightly hypoechoic tissue and subsequent atelectasis, which is not sharply demarcated

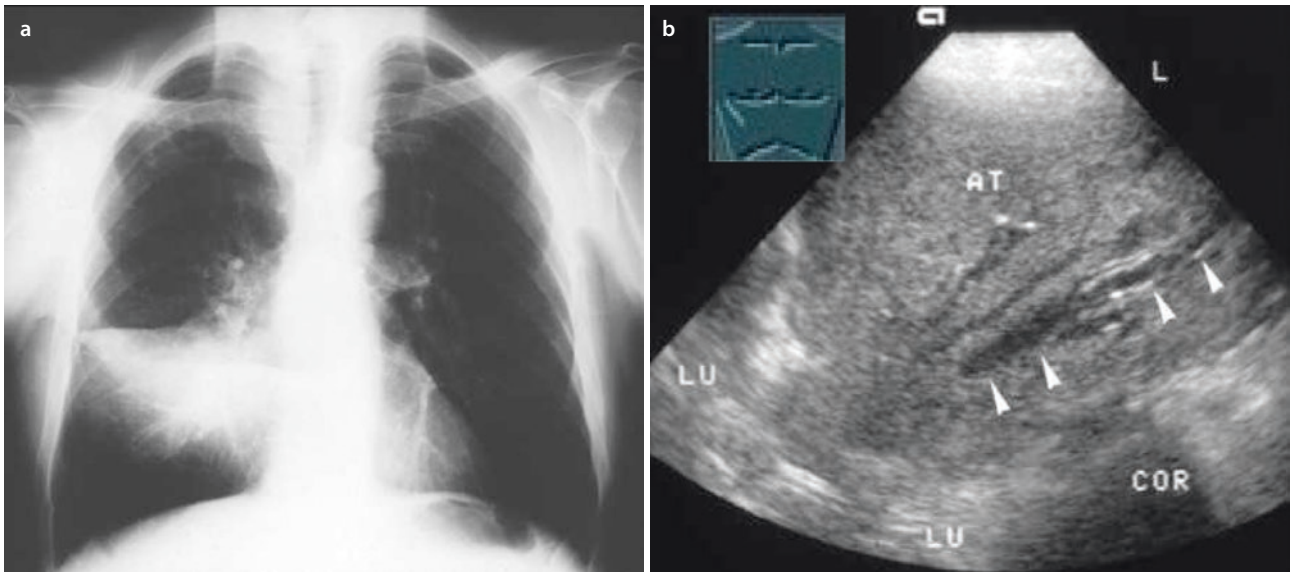

Fig. 5.60 A 68-year-old man with a bronchial carcinoma. **a** Chest x-ray: signs of middle-lobe atelectasis. **b** B-mode ultrasound: right-ventral intercostal echo transmission shows atelectasis in the middle lobe (AT) with accentuated dilated bronchi, indicative of a fluid bronchogram ("sticks"). The central tumor formation cannot be clearly demarcated

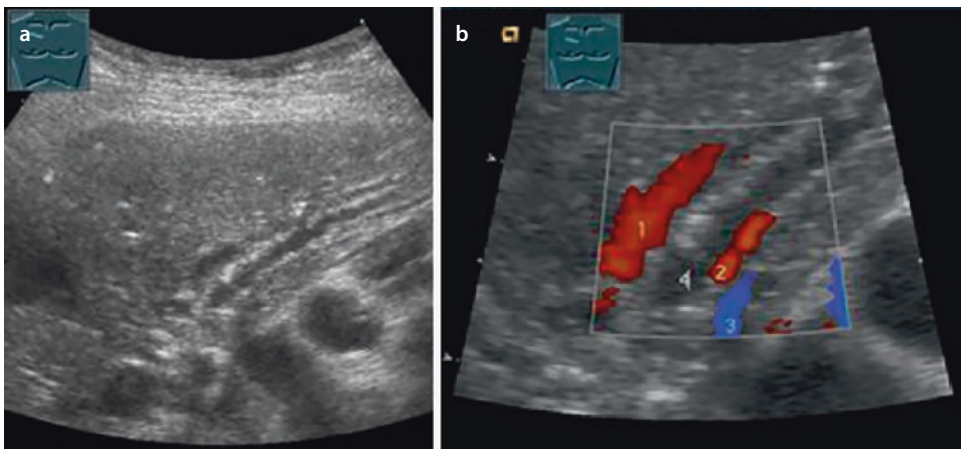

Fig. 5.61 Patient with histologically confirmed bronchial carcinoma. **a** B-mode ultrasound: right apical upper lobe atelectasis with anechoic duct structures. **b** The following structures are differentiated using CDS: 1, pulmonary artery; 2, bronchial artery; 3, pulmonary vein; 4, extended bronchial branch

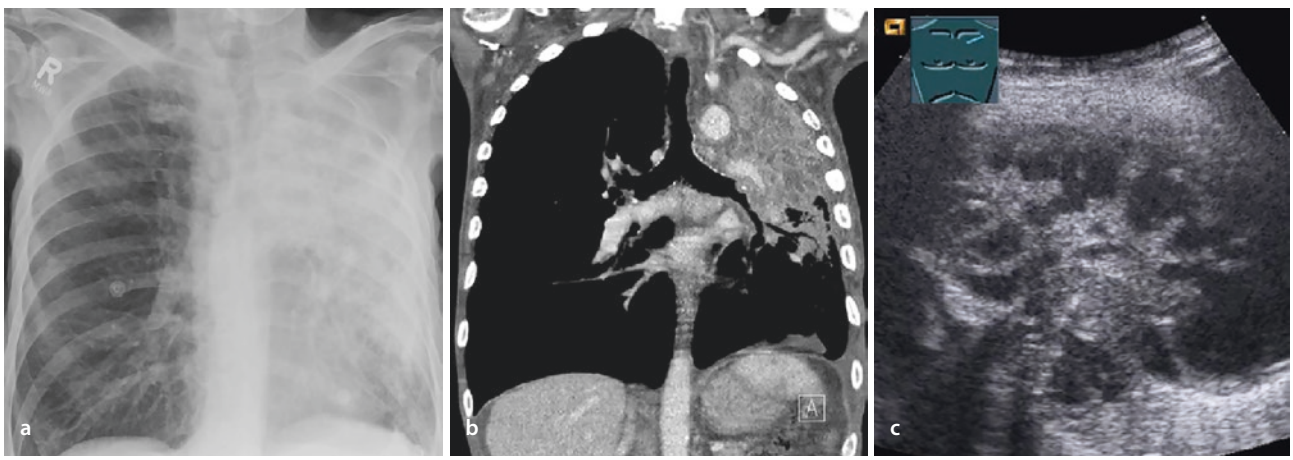

Fig. 5.62 Patient with histologically confirmed bronchial carcinoma. **a** Chest x-ray: nearly complete shadowing of the left hemithorax. **b** CT: visualization of the central tumor formation, with subsequent inhomogeneous atelectasis with multiple hypodense areas. **c** B-mode ultrasound: lung consolidation without central tumor visualization; the atelectasis shows honeycomb-like tissue liquidation similar to pronounced secretion retention

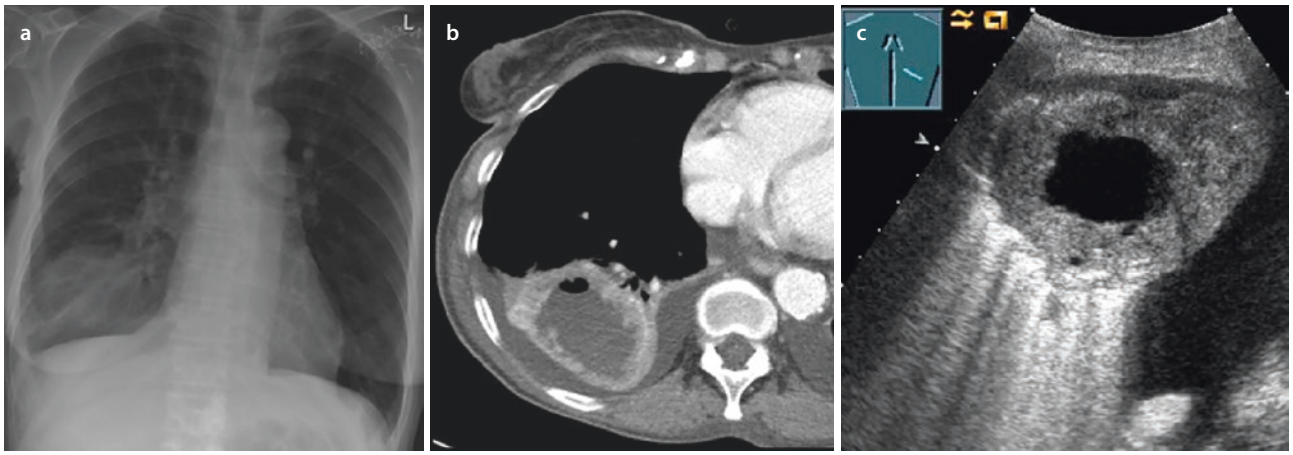

Fig. 5.63 Patient with histologically confirmed bronchial carcinoma. **a** Chest x-ray: shadowing in the area of the right caudal lung. **b** CT: visualization of an effusion with round hypodense lesions in the atelectasis, with a small amount of air in the lesions. **c** B-mode ultrasound: lung consolidation with central anechoic lesion. The finding is indicative of abscess formation

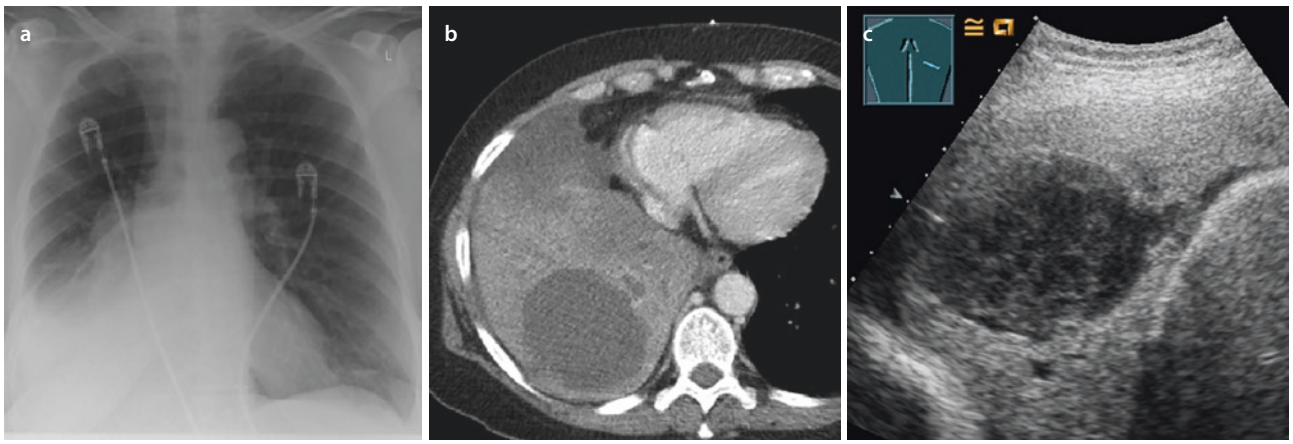

Fig. 5.64 Patient with histologically confirmed bronchial carcinoma. **a** Chest x-ray: shadowing in the area of the right caudal lung. **b** CT: visualization of a hypodense lesion in the atelectasis. **c** B-mode ultrasound: lung consolidation with central homogeneous hypoechogenic lesions. The finding is indicative of abscess formation

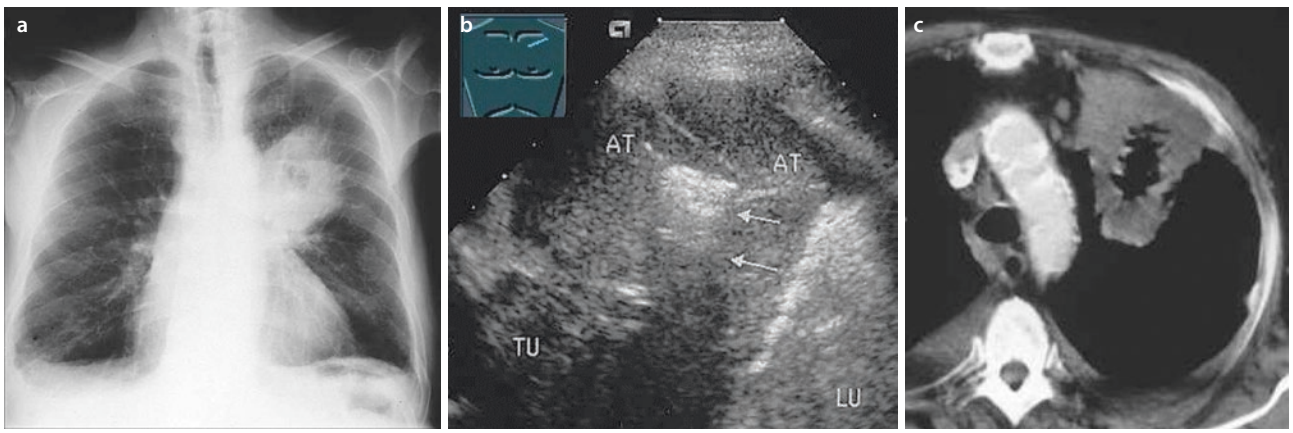

Fig. 5.65 **a-c** A 68-year-old man with a bronchial carcinoma. **a** Chest x-ray: space-occupying lesion in the left hilum and a suspected central cavity. **b** B-mode ultrasound: left-ventral intercostal echo transmission shows atelectasis in the upper lobe (AT) and, demarcated from the atelectasis, a hilar tumor formation (Tu). Centrally in the atelectatic lung tissue there is an air-filled cavity (arrows), most likely an inflammatory retention. Lu lung, PA pulmonary artery. **c** CT: atelectasis in the upper lobe with air-filled retention

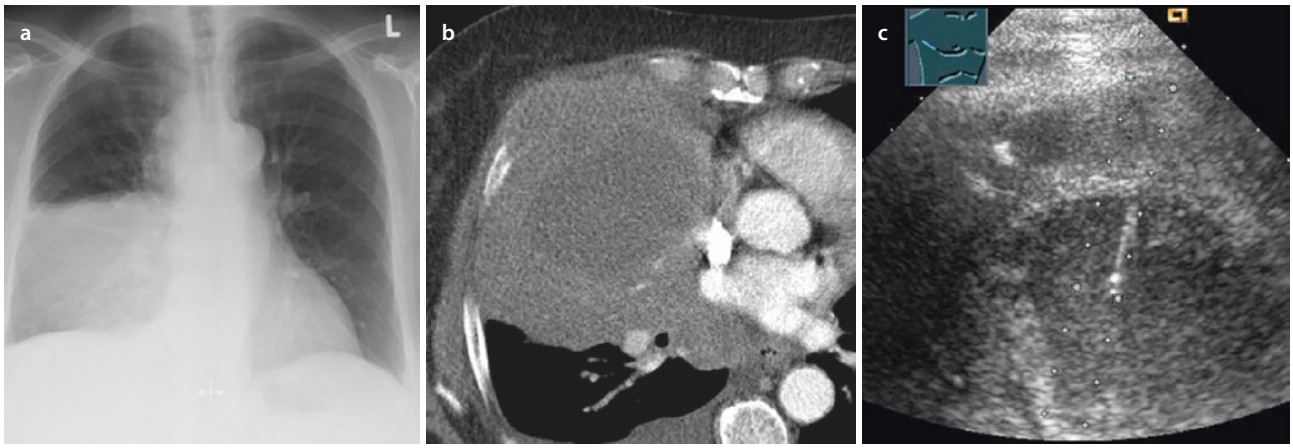

Fig. 5.66 Patient with histologically confirmed bronchial carcinoma. **a** Chest x-ray: shadowing in the area of the right caudal lung. **b** CT: visualization of an atelectatic lung consolidation with a hypodense lesion. **c** B-mode ultrasound: imaging of the needle reflex in the lesion with confirmation of an abscess formation

chymatous liquefaction, which is seen on sonography as large hypoechoic circular lesions with characteristic motion echoes on "realtime" investigation. This is primarily due to necrosis or tumor-related retention of secretion (Figs. 5.63 and 5.64). Abscesses cannot be entirely excluded on the basis of sonomorphology alone. Here the clinical findings will be one of the main determinants of the diagnosis. However, sonography-guided aspiration will allow the investigator to confirm the diagnosis and obtain material for bacteriological investigation (Fig. 5.66a, b) (Görg 2003; Liaw et al. 1994a, b; ▶ Chap. 8).

The evaluation of focal lesions is performed clinically. In addition to infectious lesions (Figs 5.62–5.65), metastases or other benign lesions may also be detected in a lung atelectasis (Fig. 5.67a, b). Contrast-enhanced ultrasound (CEUS) has differential diagnostic value in the evaluation of focal lesions in atelectasis (▶ Chap. 8).

- Possible findings on sonography in cases of obstructive atelectasis:
- B-mode ultrasound
- Mild to no pleural effusion
- Homogenous hypoechoic transformation of lung parenchyma
- Hyperechoic reflexebands may be seen (fluid bronchogram)
- Focal intraparenchymatous lesions may be seen
  - Liquefaction of parenchyma
  - Microabscesses, macroabscesses
  - Parenchymal metastases
- A central space-occupying lesion may be seen
- No reventilation during inspiration
- Color-Doppler sonography (CDS)
- On intraindividual comparison with the liver/spleen, enhanced flow phenomena are visualized
- Triphasic spectrum of the arterial flow curve of pulmonary arteries (type, arteries of the extremities) (▶ Chap. 8)

Essentially, in the presence of lobar or pulmonary atelectasis, central portions can be imaged through atelectatic lung tissue by sonography. The main purpose here is to demonstrate the central tumor. On the basis of sonographic structural features, a definite distinction between atelectatic lung tissue and tumor tissue can be made in less than 50% of cases (Görg et al. 1996; Fig. 5.68a–d). Here, CEUS enables a better demarcation of the central tumor from the atelectatic tissue (▶ Chap. 8).

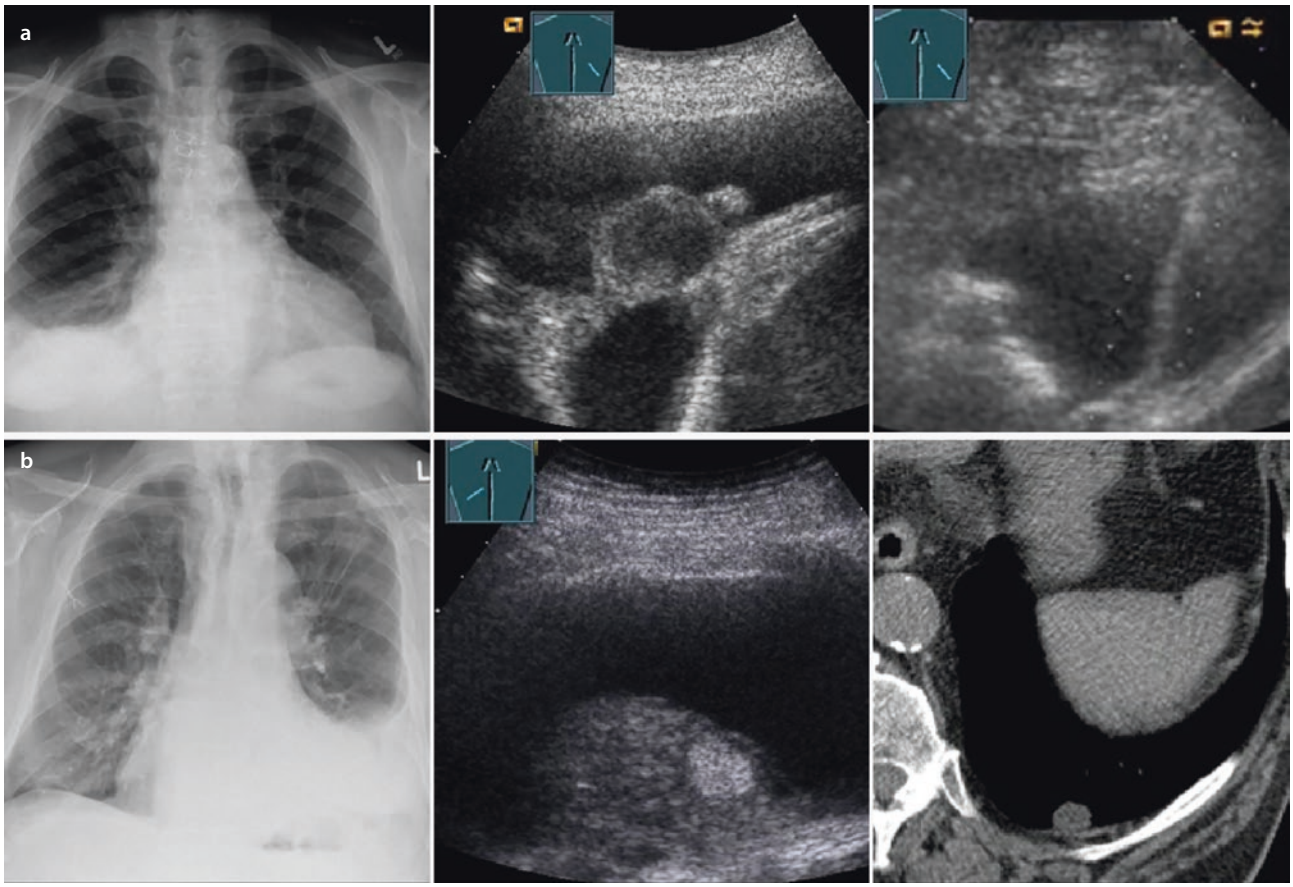

Fig. 5.67 **a** Patient with pleural effusion after thoracic trauma, visualized by chest x-ray. On B-mode ultrasound, in addition to the pleural effusion, a hypoechoic round lesion in the atelectasis is detectable. The US-guided biopsy of the lesion after drainage of the hemorrhagic effusion reveals a diagnosis of focal lung hematoma. **b** Patient with left-sided pleural effusion caused by metastasized pancreatic carcinoma; US reveals a hyperechoic focal round lesion in the atelectatic lung; a few years earlier, computed tomography showed that the round lesion was already detectable as a lung lipoma.

The significance of being able to visualize the central tumor lies in the fact that the tumor can be biopsied through atelectatic lung tissue under sonographic guidance with practically no risk of complications (Yang et al. 1990a, b; Fig. 5.69a–d).

5.4.6 Lung Contusion

In cases of chest trauma, particularly serial rib fractures, pulmonary contusions are visualized better on sonography than on radiographs. Alveolar edema and alveolar hemorrhage caused by trauma are seen as moderately hypoechoic, blurred, pale lesions with indistinct margins (Wüstner et al. 2005; Figs. 5.70 and 5.71). These are more pronounced in the presence of concomitant minimal pleural effusions, but are also imaged on sonography in the absence of pleural effusion. In the event of any clinically relevant chest trauma, radiographs as well as sonograms should be obtained (▶ Chap. 2).

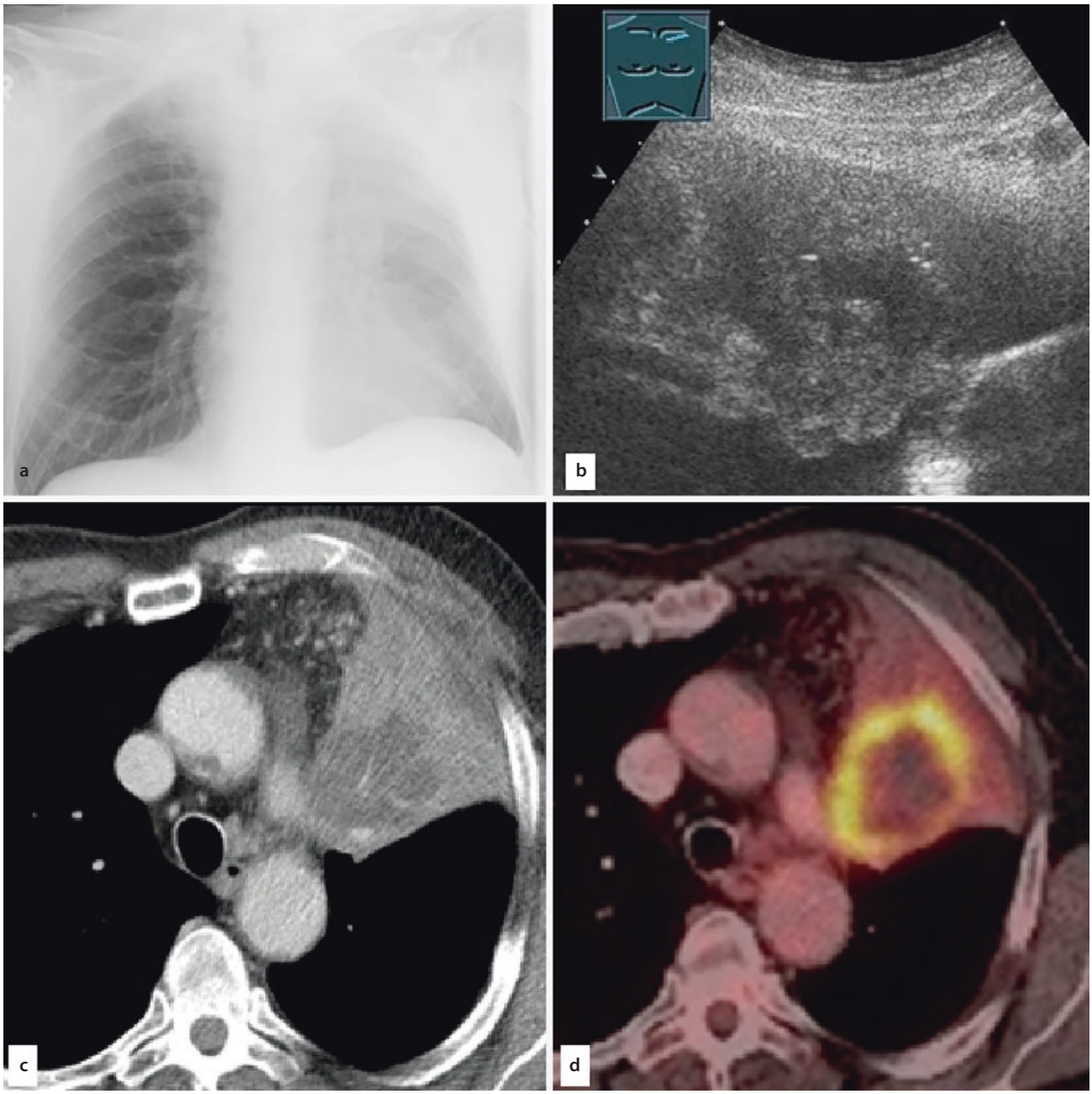

Fig. 5.68 Patient with histologically confirmed bronchial carcinoma. **a** Chest x-ray: shadowing of the left hemithorax. **b** The left apical central lung tumor is difficult to differentiate from the atelectasis by B-mode ultrasound. **c** In a CT, the tumor is more clearly demarcated. **d** In the positron emission tomography–computed tomography image, the tumor shows increased glucose metabolism only in the marginal area.

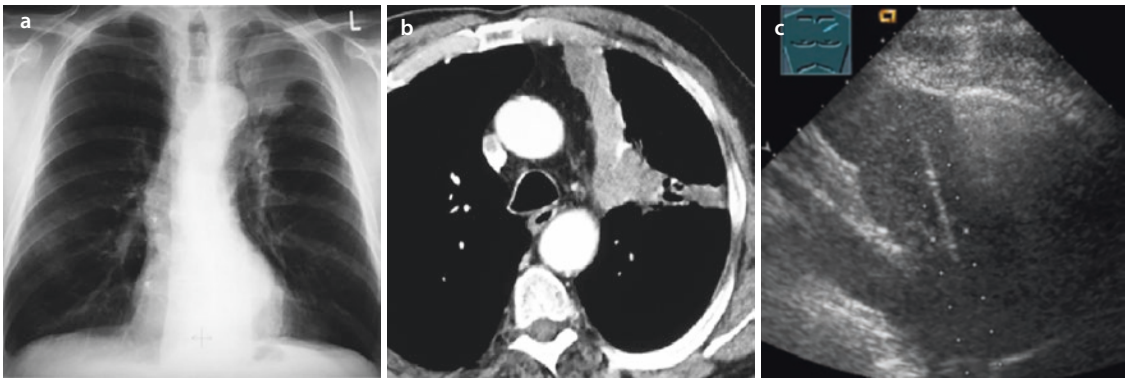

Fig. 5.69 new figure. Patient with suspected bronchial carcinoma; the tumor could not be confirmed via bronchoscopy. **a** Chest x-ray: shadowing in the area of the left apical lung. **b** CT: visualization of a central tumor formation with narrow atelectasis. **c** B-mode ultrasound: visualization of the needle reflex in the atelectasis and central tumor, with confirmation of a bronchial carcinoma.

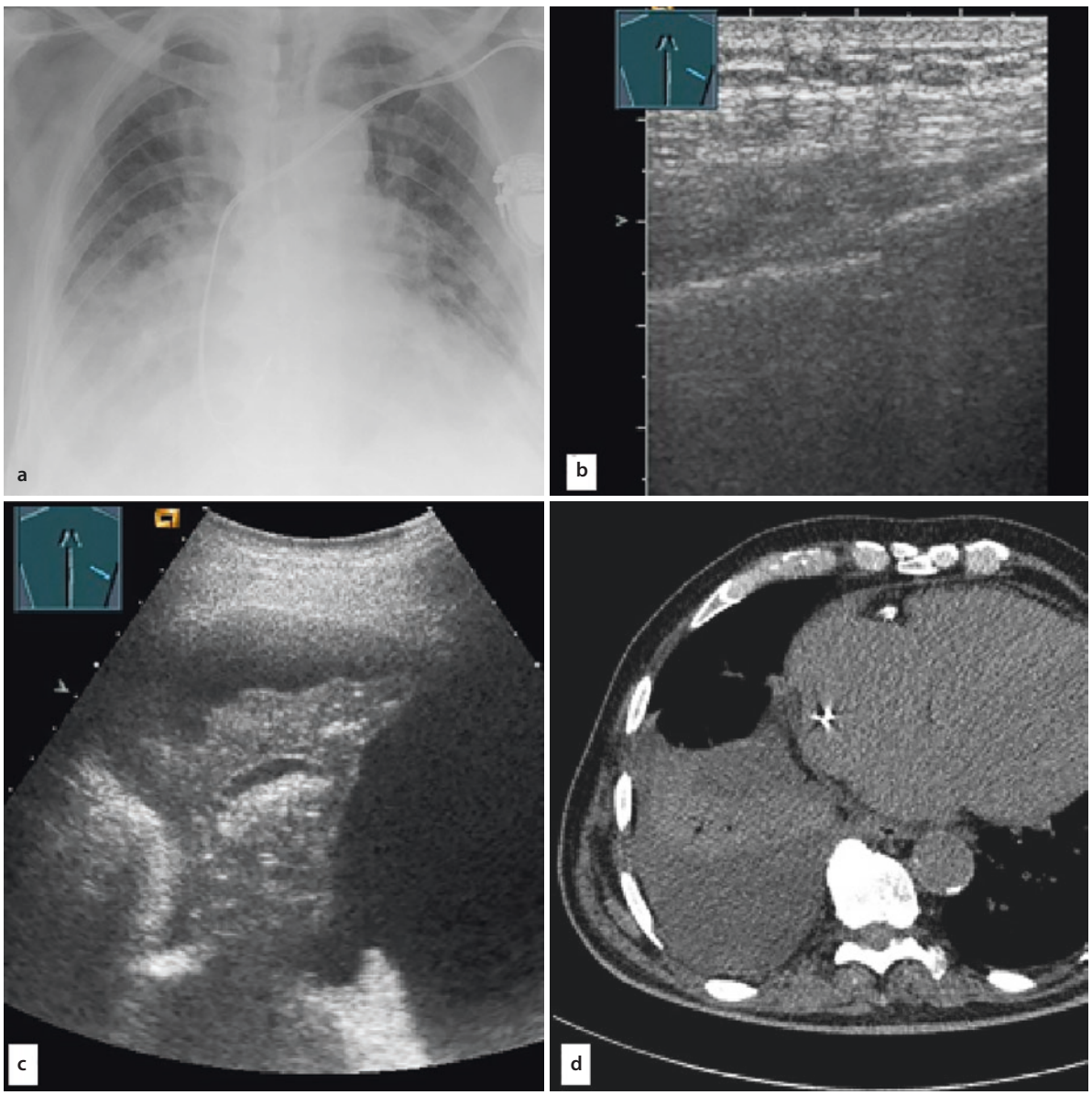

Fig. 5.70 Patient with history of trauma. **a** Chest x-ray: shadowing of both lower lung lobes, right more than left. **b** Ultrasound evidence of rib fracture and **c** atelectatic lung consolidation in a case of hemorrhagic effusion. **d** Corresponding evidence of effusion and atelectasis by CT

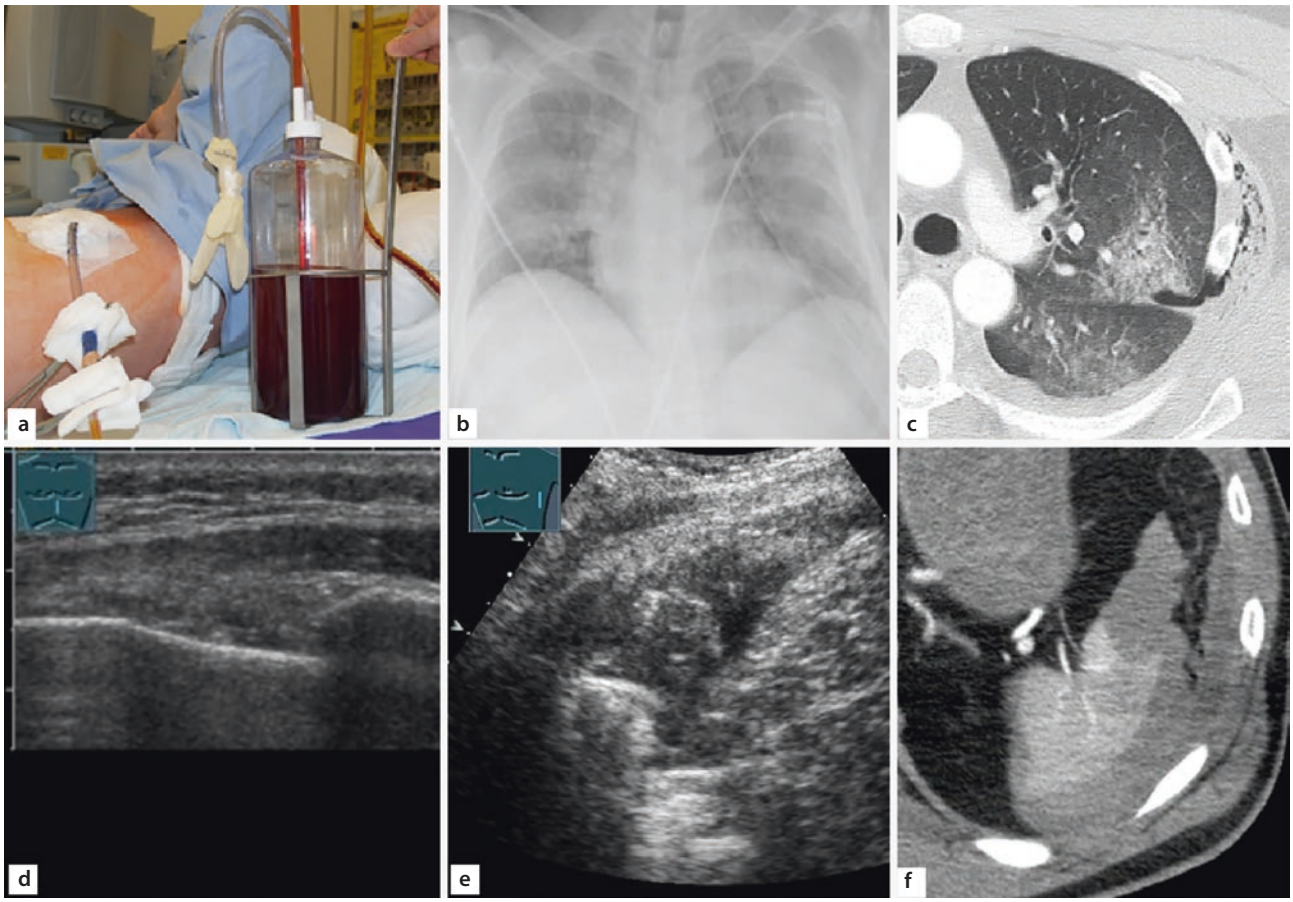

Fig. 5.71 new figure. Patient with history of trauma. **a** Condition after thoracic drainage of the hematothorax. **b** Chest x-ray: correct drainage of the effusion. **c** CT: extensive lung lesions with suspicion of lung hemorrhage. **d** B-mode ultrasound evidence of sternal fracture and **e** complex atelectatic lung consolidation compatible with lung hemorrhage. **f** Abdominal computed tomography shows an additional splenic injury

Summary

Depending on the extent of intrapleural fluid in case of compression atelectasis, one finds a pointed cap-like, wedge-shaped, homogenous, hypoechoic transformation with blurred margins towards the aerated adjacent lung tissue. The sonographic image of obstructive atelectasis is marked by largely homogenous hypoechoic lung tissue, similar to hepatization. An effusion may be absent or is very mild. In cases of lobar atelectasis, the margin towards the ventilated lung tissue is rather blurred. Intraparenchymatous structures are seen as hypoechoic vascular lines, echogenic bronchial reflexebands or focal lesions.

References

Abootalebi A, Golshani K, Karami M et al (2016) Diagnostic validity of ultrasonography in evaluation of pulmonary thromboembolism. Adv Biomed Res 5:4–9

Asano M, Watanabe H, Sato K et al (2018) Validity of ultrasound lung comets for assessment of the severity of interstitial pneumonia. J Ultrasound Med 37:1523–1531

AWMF Leitlinie (2018) AWMF Registernummer: 020/007OL, S3-Leitlinie Prävention, Diagnostik, Therapie und Nachsorge des Lungenkarzinoms

AWMF Leitlinien, Hach-Wunderle V et al (2016) S2k-Leitllinie zur Diagnostik und Therapie der Venenthrombose und der Lungenembolie. Vasa 45(Suppl. 90):1–48

Bandi V, Lunn W, Ernst A et al (2008) Ultrasound vs CT in detecting chest wall invasion by tumor. A prospective study. Chest 133:881–886

Beckh S, Bölcskei PL (2003) Die Bedeutung der dynamischen Untersuchung in der Diagnostik thorakaler Herdbildungen. Praxis 92:1223–1226

Beckh S, Bölcskei PL, Lessnau KD (2002) Real-time chest ultrasonography. A comprehensive review for the pulmonologist. Chest 122:1759–1773

Bertolini FA, Gorg C, Mathis G (2008) Echo contrast ultrasound in subpleural consolidations. Abstract ECR 2008. Eur Radiol Suppl 18:S395

Burge AJ, Freeman KD, Klapper PJ, Haramati LB (2008) Increased diagnosis of pulmonary embolism without a corresponding decline in mortality during CT era. Clin Radiol 63:381–386

Burke M, Fraser R (1988) Obstructive pneumonitis: a pathologic and pathogenetic reappraisal. Radiology 166:699–704
Busti C, Agnelli G, Duranti M, Orlandi C, Marcucci M, Paciaroni M (2014) Lung ultrasound in the diagnosis of stroke-associated pneumonia. Intern Energ Med 9:173–178
Chen CH, Kuo ML, Shih JF, Chang TP, Perng RP (1993) Etiologic diagnosis of pulmonary infection by ulrasonically guided percutaneous lung aspiration. Chung Hua Taiwan 51:5
Copetti R, Cattarossi L (2008) Ultrasound diagnosis of pneumonia in children. Radiol Med 113:190–198
Corrin B (1999) Actinomycosis. In: Corrin B (ed) Pathology of the lungs. Churchill Livingstone, London, pp 194–195
Dacrema A, Silva M, Rovero L et al (2021) A simple lung ultrasound protocol for the screening of COVID-19 pneumonia in the emergency department. Internal Emerg Med. https://doi.org/10.1007/s11739-020-02596-6
Detterbeck FC, Malcolm M, DeCamp MM Jr et al (2003) Invasive staging—the guidelines. Chest 123:167S–175S
Dresden S, Mitchell P, Rahimi L, Leo M, Rubin-Smith J, Bibi S, White L et al (2014) Right ventricular dilatation on bedside echocardiography performed by emergency physicians aids in the diagnosis of pulmonary embolism. Ann Emerg Med 63:16–24
Eichlisberger R, Frauchinger B, Holtz D, Jäger KA (1995) Duplexsonographie bei Verdacht auf tiefe Venenthrombose und zur Abklärung der Varikose. In: Jäger KA, Eichlisberger R (Hrsg) Sonokurs. Karger, Basel, S137–147
Fields JM, Davis J, Girson L et al (2017) Transthoracic echocardiography for diagnosing pulmonary embolism: a systematic review and meta-analysis. J Am Soc Echocardiogr. 30:714–723
Findeisen H, Trenker C, Figiel et al (2019) Vascularization of primary, peripheral lung carcinoma in CEUS – a retrospective study (n = 89 Patients). Ultraschall Med 40: 603–608. https://doi.org/10.1055/a--0725-7865
Fultz PJ, Feins RH, Strang JG et al (2002) Detection and diagnosis of nonpalpable supraclavicular lymph nodes in lung cancer at CT and US. Radiology 222:245–251
Gehmacher O, Mathis G (1994) Farbkodierte Duplexsonographie peripherer Lungenherde—ein diagnostischer Fortschritt? Bildgebung 61(S2):11
Gehmacher O, Mathis G, Kopf A, Scheier M (1995) Ultrasound imaging of pneumonia. Ultrasound Med Biol 21:1119–1122
Goeckenjan G, Sitter H, Thomas M et al (2011) Prevention, diagnosis, therapy, and follow-up of lung cancer. Pneumologie 64(Suppl. 2):e1–e164. https://doi.org/10.1055/s-0029-1243837
Goldhaber SZ, Visani L, De Rosa M (1999) Acute pulmonary embolism: clinical outcomes in the International Cooperative Pulmonary Embolism Registry. Lancet 353(9162):1386–1389
Görg C (2003) Focal lesions in the opacified lung: a sonographic pictorial essay. Ultraschall Med 24:123–128
Görg C (2007) Transcutaneous contrast-enhanced sonography of pleural-based pulmonary lesions. Eur J Rad 64:213–221
Görg et al (2004) Transcutaneous colour Doppler sonography of lung consolidations. Ultraschall Med 25(221–226):285–291
Görg C, Weide R, Walters E, Schwerk WB (1996) Sonographische Befunde bei ausgedehnten Lungenatelektasen. Ultraschall Klin Prax 11:14–19
Grundmann E (1986) Spezielle Pathologie, 7. Aufl. Urban & Schwarzenberg, München
Hsu WH, Ikezoe J, Chen CY et al (1996) Color Doppler ultrasound signals of thoracic lesions. Am J Respir Crit Care Med 153: 1938–1951
Hsu WH, Chiang CD, Chen CY et al (1998) Color Doppler ultrasound pulsatile flow signals of thoracic lesions: comparison of lung cancers and benign lesions. Ultrasound Med Biol 24:1087–1095
Hu QJ, Shen YC, Jia LQ, Guo SJ, Long HY, Pang CS et al (2014) Diagnostic performance of lung ultrasound in the diagnosis of pneumonia: a bivariate meta-analysis. Int J Clin Exp Med 7: 115–121
Jackson RE, Rudoni R, Hauser AM, Pascual RE, Hussey M (2000) Prospective evaluation of two-dimensional transthoracic echocardiography in emergency department patients with suspected pulmonary embolism. Acad Emerg Med 7:994–998
Jäger K, Eichlisberger R, Frauchinger B (1993) Stellenwert der bildgebenden Sonographie für die Diagnostik der Venenthrombose. Haemostaseologie 13:116–123
Kaick VG, Bahner ML (1998) Computertomographie. In: Drings P, Vogt-Moykopf I (Hrsg) Thoraxtumoren. Springer, Berlin, Heidelberg, New York, Tokyo, S165–s179
Klok FA, Kruip MJ, van der Meer NJ et al (2020) Incidence of thrombotic complications in critically ICU patients with COVID-19. Thrombosis Res. https://doi.org/10.1016/j.thromres.2020.04.013
Knopp MV, Hawighorst H, Flömer F (1998) Magnetresonanztomographie. In: Drings P, Vogt-Moykopf I (Hrsg) Thoraxtumoren. Springer, Berlin Heidelberg New York Tokyo, S180–190
Ko JC, Yang PC, Yuan A et al (1994) Superior vena cava syndrome. Am J Respir Crit Care Med 149:783–787
Kopf A, Metzler J, Mathis G (1994) Sonographie bei Lungentuberkulose. Bildgebung 61(S2):12
Lan RS, Lo KS, Chuang ML, Yang CT, Tsao TC, Lee CM (1997) Elastance of the pleural space: a predictor for the outcome of pleurodesis in patients with malignant pleural effusion. Ann Intern Med 126:768–774
Landreneau RJ, Mack MJ, Dowling RD et al (1998) The role of thoracoscopy in lung cancer management. Chest 113:6S–12S
Liaw YS, Yang PC et al (1994a) The bacteriology of obstructive pneumonitis. Am J Respir Crit Care Med 149:1648–1653
Liaw YS, Yang PC, Wu ZG et al (1994b) The bacteriology of obstructive pneumonitis. Am J Respir Crit Care Med 149: 1648–1653
Lichtenstein D, Meziere G, Seitz J (2009) The dynamic airbronchogram. A lung ultrasound sign of alveolar consolidation ruling out atelectasis. Chest 135:1421–1425
Liu X, Hai Y, Ma B, Chong W, Liu JB (2020) Critical care ultrasonography and its application for COVID-19. Adv Ultrasound Diagn Ther 02:043–049
Lyu G, Zhang Y, Tan G (2020) Transthoracic ultrasound evaluation of pulmonary changes in COVID-19 patients during treatment using modified protocols. AUDT 02:079–083
Mathis G (1997) Thoraxsonography—Part II: Peripheral pulmonary consolidation. Ultrasound Med Biol 23:1141–1153
Mathis G (2006) Sonographie bei Lungenembolie: drei Fliegen auf einen Streich. Pneumologie 60:600–606
Mathis G (2014) Thromboembolism in ultrasound: killing three birds with one stone. Chest 145:931–932
Mathis G (2019) Triple ultrasound in diagnosis of Thromboembolism. EC Pulmonary Resp Med 8(2):162–168
Mathis G, Dirschmid K (1993) Pulmonary infarction: sonographic appearance with pathologic correlation. Eur J Radiol 17:170–174
Mathis G, Metzler J, Fußenegger D, Feurstein M, Sutterlütti G (1992) Ultraschallbefunde bei Pneumonie. Ultraschall Klin Prax 7: 45–49
Mathis G, Metzler J, Fußenegger D, Sutterlütti G, Feurstein M, Fritzsche H (1993) Sonographic observation of pulmonary infarction and early infarctions by pulmonary embolism. Eur Heart J 14:804–808
Mathis G, Bitschnau R, Gehmacher O, Dirschmid K (1999a) Ultraschallgeführte transthorakale Punktion. Ultraschall Med 20: 226–235

Mathis G, Bitschnau R, Gehmacher O et al (1999b) Ultraschallgeführte transthorakale Punktion. Ultraschall Med 20:226–235
Mathis G, Bitschnau R, Gehmacher O et al (1999c) Chest ultrasound in diagnosis of pulmonary embolism in comparison to helical CT. Ultraschall Med 20:54–59
Mathis G, Blank W, Reißig A, Lechleitner P, Reuß J, Schuler A, Beckh S (2005) Thoracic ultrasound for diagnosing pulmonary embolism. A prospective multicenter study of 352 patients. Chest 128:1531–1538
Mongodi S, Via G, Griard M et al (2016) Lung ultrasound for early diagnosis of ventilator-assiciated pneumonia. Chest 149:969–980
Nazerian P, Vanni S, Volpicell G, Gigli C, Zanobetti M, Bartolucci M et al (2014) Accuracy of point-of-care multiorgan ultrasonography for the diagnosis of pulmonary embolism. Chest 145:950–957
Nazerian P, Volpicelli G, Gigli C et al (2017) Diagnostic performance of wells score combined with point-of-care lung and venous ultrasound in suspected pulmonary embolism. Acad Emerg Med 24:270–280
Newman DH, Schriger DL (2011) Rethinking testing for pulmonary embolism: less is more. Ann Emerg Med 57:622–627
Niemann T, Egelhof T, Bongratz G (2009) Transthoracic sonography for the Detection of pulmonary embolism—a meta analysis. Ultraschall Med 30:150–115
Orso D, Ban A, Guglielmo N. Lung (2018) ultrasound in diagnosing pneumonia in childhood: a systematic review and meta-analysis. J Ultrasound https://doi.org/10.1007/s40477-018-0306-5
Osman M, Subedi SK, Ahmed A et al (2018) Computed tomography pulmonary agniography is overused to diagnose pulmonary embolism in the emergency department of academic community hospital. J Comp Hosp Intern Med 8:6–10
Osterwalder J (2020) COVID-19-mehr Lungen-PoCUS und sparsam mit dem Sthethoskop, Thoraxröntgen und Lungen-CT umgehen. Praxis 2020:1–9. https://doi.org/10.1024/166-8157/a003512
Özsu SS, Durmus ZG, Coskuner MB et al (2017) Does the incidence and mortality of pulmonary thromboembolism change over the years? Turk Thoracic J 18:78–81
Pan JF, Yang PC, Chang DB et al (1993) Needle aspiration biopsy of malignant lung masses with necrotic centers. Chest 103:1452–1456
Parlamento S, Copetti R, Di Bartolomeo S (2009) Evaluation of lung ultrasound for the diagnosis of pneumonia in ED. Am J Emerg Med 27:397–384
Prosch H, Strasser G, Sonka S et al (2007) Cervical ultrasound (US) and US-guided lymph node biopsy as a routine procedure for a staging of lung cancer. Ultraschall Med 28(6):598–603. https://doi.org/10.1055/s-2007-963215
Reissig A, Kroegel C (2003) Transthoracic sonography of diffuse parenchymal lung disease: the role of comet tail artefacts. J Ultrasound Med 22:173–180
Reissig A, Kroegel C (2007) Sonographic diagnosis and follow-up of pneumonia: a prospective study. Respiration 74:537–547
Reißig A, Heyne JP, Kroegel C (2003) Sonography of lung and pleura in pulmonary embolism: sonomorphologic characterization and comparison with spiral CT scanning. Chest 120:1977–1983
Reissig A, Copetti R, Mathis G, Mempel C, Schuler A, Zechner P et al (2012) Lung ultrasound in the diagnosis and follow-up of community-acquired pneumonia. A prospective multicentre diagnostic accuracy study. Chest 142:965–972
Salamonsen MR, Ada KC, Arnold CT et al (2014) Novel use of pleural ultrasound can identify malignant entrapped lung prior to effusion drainage. Chest. https://doi.org/10.1378/chest.13-2876
Schönberg SO (2003) Magnetresonanztomographie. In: Drings P, Dienemann H, Wannenmacher M (eds) Management des Lungenkarzinoms. Springer, Berlin Heidelberg New York Tokyo, pp S117–S124
Sperandeo M, Carnevale V, Muscarella S et al (2011) Clinical application of transthoracic ultrasonography in inpatients with pneumonia. Eur J Clin Invest. 41:1–7
Squizzato A, Rancan E, Dentali F, Bonzini M, Guasti L, Steidl L et al (2013) Diagnostic accuracy of lung ultrasound for pulmonary embolism: a systematic review and meta-analysis. J Thrombo Haemost 2013(11):1269–1278
Suzuki N, Saitoh T, Kitamura S et al (1993) Tumor invasion of the chest wall in lung cancer: diagnosis with US. Radiology 187:3942
Talayanagi N, Kagiyama N, Ishiguro T, Tokunaga D, Sugita Y (2010) Etiology and outcome of community-aquired lung abscesses. Respiration 80:98–105
Targhetta R, Chavagneux R, Bourgeois JM, Dauzat M, Balmes P, Pourcelot L (1992) Sonographic approach to diagnosing pulmonary consolidation. J Ultrasound Med 11:667–672
Thomas M, Baumann M, Deppermann M et al (2002) Empfehlungen zur Therapie des Bronchialkarzinoms. Pneumologie 56:113–131
Trenker C, Dohse M, Ramaswamy A et al (2019) Histological validation of pulmonary infarction detected with contrast-enhanced ultrasound in patients with negative computed tomography angiogram: a case series. J Clin Ultrasound 47:461–465
Tuengerthal S (2003) Radiologische Diagnostik des Bronchialkarzinoms—Projektionsradiographie und Computertomographie. In: Drings P, Dienemann H, Wannenmacher M (Hrsg) Management des Lungenkarzinoms. Springer, Berlin Heidelberg New York Tokyo, pp. S73–S115
Volpicelli G, Elbarbary M, Blaivas M et al (2012a) International Liaison Committee on Lung Ultrasound (ILC-LUS) for International Consensus Conference on Lung Ultrasound (ICC-LUS). International evidence-based recommendations for point-of-care lung ultrasound. Intensive Care Med 38:577–591. https://doi.org/10.1007/s00134-012-2513-4
Volpicelli G, Blaivas M, Elbaray M, Lichtenstein D, Mathis G, Kirkpatrick A et al (2012b) International evidence-based recommendations for point of-care lung ultrasound pulmonary embolism in critically ill patients. J Trans Int Med 2017(5):200–2005
Wang G, Ji X, Xu Y, Xiang X (2016) Lung ultrasound: a promising tool to monitor ventilator-associated pneumonia in critically ill patients. Critical Care 20:320. https://doi.org/10.1186/s13054-016--1487-y
Weinberg B, Diaboumakis EE, Kass EG, Seife B, Zvi ZB (1986) The air bronchogram: sonographic demonstration. AJR 147:593–595
WHO Pneumonia (2019). https://www.who.int/en/news-room/fact--sheets/detail/pneumonia download 090620
Wohlgenannt S, Gehmacher O, Mathis G (2001) Thoraxsonographische Veränderungen bei interstitiellen Lungenerkrankungen. Ultraschall Med 22:27–31
Wüstner A, Gehmacher O, Hämmerle S, Schenkenbach C, Häfele H, Mathis G (2005) Ultraschalldiagnostik beim stumpfen Thoraxtrauma. Ultraschall Med 26:285–290
Yang PC (1996) Review paper: Color Doppler ultrasound of pulmonary consolidation. Eur J Ultrasound 3:169–178
Yang PC, Lee YC, Wu HD, Luh KT (1990a) Lung tumors associated with obstructive pneumonitis: US studies. Radiology 174:593–595
Yang PC, Luh KT, Wu DH, Chang DB, Lee NL, Kuo SM, Yang SP (1990b) Lung tumors associated with obstructive pneumonitis: US studies. Radiology 174:717–720
Yang PC, Luh KT, Lee YC (1991) Lung abscesses: ultrasonography and ultrasound-guided transthoracic aspiration. Radiology 180:171–175

Yang PC, Luh KT, Chang DB, Yu CJ, Kuo SH, Wu HD (1992a) Ultrasonographic evaluation of pulmonary consolidation. Am Rev Resp Dis 146:757–762

Yang PC, Luh KT, Chang DB, Yu CJ, Kuo SM, Wu HD (1992b) Ultrasonographic evaluation of pulmonary consolidation. Am Rev Respir Dis 146:757–762

Yuan A, Yang PC, Chang DB et al (1993) Ultrasound guided aspiration biopsy for pulmonary tuberculosis with unusual radiographic appearances. Thorax 48:167–170

Yuan A, Chang DB, Yu CJ et al (1994) Color Doppler sonography of benign and malignant pulmonary masses. AJR 163:545–549

Zhu R, Ma X-C (2017) Clinical value of ultrasonography in diagnosis of pulmonary embolism in critically ill patients. J Transl Int Med 5(4):200–204

Mediastinum

Wolfgang Blank, Alexander Heinzmann, Jouke T. Annema, Maud Veseliç, and Klaus F. Rabe

Contents

G. Mathis (ed.), *Chest Sonography*, https://doi.org/10.1007/978-3-031-09442-2_6

6.1 Transthoracic

Mediastinal structures can be visualized comprehensively by computed tomography as well as magnetic resonance tomography. Sonography in contrast identifies only parts of the mediastinum.

As early as in 1971 Goldberg (1971) pointed out the suprasternal sonographic access to the mediastinum. This access was used by cardiologists for the representation of the thoracic aorta and aortic valve (Herth 2009). In the mid-1980s sonography of the mediastinum was researched in pediatrics (Lengerke and Schmid 1988; Liu et al. 1988) as well as in adult medicine and its efficiency was proved (Braun 1983; Blank et al. 1986; Wernecke et al. 1986; Brüggemann et al. 1991). In the following years the diagnostic potential of sonography was systematically researched (Heizel 1985; Wernecke et al. 1986; Wernecke 1991; Blank et al. 1996b; Bosch et al. 2007; Subacul 2013). Further possibilities were disclosed by the application of color-Doppler sonography and, recently, through contrast-enhanced sonography (Betsch et al. 1992, 1994; Dietrich et al. 1997, 1999; Kunz et al. 2004; Caremani et al. 2009; Chen et al. 2014).

6.1.1 Sonographic Investigation Technique and Reporting

Profound knowledge of anatomy is absolutely essential (Figs. 6.1 and 6.2). Because of the small sonic window and the penetration depth only 3.5- and 5-MHz sector, convex and vector transducers with small apertures are suitable for sonographic diagnosis. In sonography the mediastinum is accessed from the suprasternal and the parasternal approach, occasionally also from the infrasternal approach (Blank et al. 1996a). The large vessels and their spatial relationship to the heart in the various planes serve as cardinal structures. The investigation from suprasternal is performed with the patient in the supine position. Viewing the upper mediastinum is facilitated by having the patient recline his/her head, ideally by cushioning the thoracic spine. Turning the head to the right and left is additionally helpful. In the right- and left-sided position described by Wernecke et al. (1988) and by Brüggemann et al. (1991) the mediastinum is shifted and the pulmonary cavity is displaced, which permits better viewing of the mediastinum. It is easier to assess the mediastinum in expiration (Beckh et al. 2002; Koh et al. 2002; Braun and Blank 2005; Herth 2009).

Transsternal sonographic access to the mediastinum is possible in children in the cartilage stage (Supakul and Karmazyn 2013).

6.1.2 Sonoanatomy

In principle, from suprasternal the supraaortic and paratracheal region and the aorticopulmonary window can be imaged (Figs. 6.3, 6.4, 6.5, and 6.6):

Suprasternal access (supine position): superior/anterior mediastinum

- Right side—tracheal region
- Truncus brachiocephalicus, a. carotis, a. subclavia
- Arcus aortae
- V. cava superior, veins brachiocephalicus
- Truncus pulmonalis, arteries pulmonales
- Left atrium, veins pulmonales
- Thymus
- Retrosternal space

For this purpose half-sagittal (from the right and left sides), coronary and transverse images are needed. Cervical portions of the esophagus (posterior mediastinum) can also be visualized (5–8 cm) (Blank et al. 1998; Zhu et al. 2005; Palabiyik et al. 2012; Fig. 6.4d). From parasternal the combined use of right-sided and left-sided lateral decubitus position permits evaluation of the anterior and mid-mediastinum (Figs. 6.7 and 6.8). For this purpose the transducer is placed adjacent to the sternum, cranially, and then moved caudad. Anatomical structures visualized through transverse and sagittal sections in angulated planes are summarized as follows (Figs. 6.4, 6.5, and 6.6):

1. Parasternal access (lateral decubitus, right side): anterior/middle mediastinum

- V. cava superior
- Ascending aorta
- pulmonalis dextra
- Left atrium, vv. pulmonales
- Left ventricle, right ventricle

2. Parasternal access (lateral decubitus, left side): anterior/middle mediastinum

- Descending aorta
- Truncus pulmonalis
- Left atrium, vv. pulmonales
- Left ventricle, right ventricle, right atrium

The infrasternal access only provides a limited view of caudal portions of the posterior mediastinum. The esophagus, aorta and vena cava are seen at the point where they pass through the diaphragm. Transverse and sagittal images in angulated planes are obtained through the left lobe of the liver (Blank et al. 1996a; Janssen et al. 1997; Fig. 6.9).

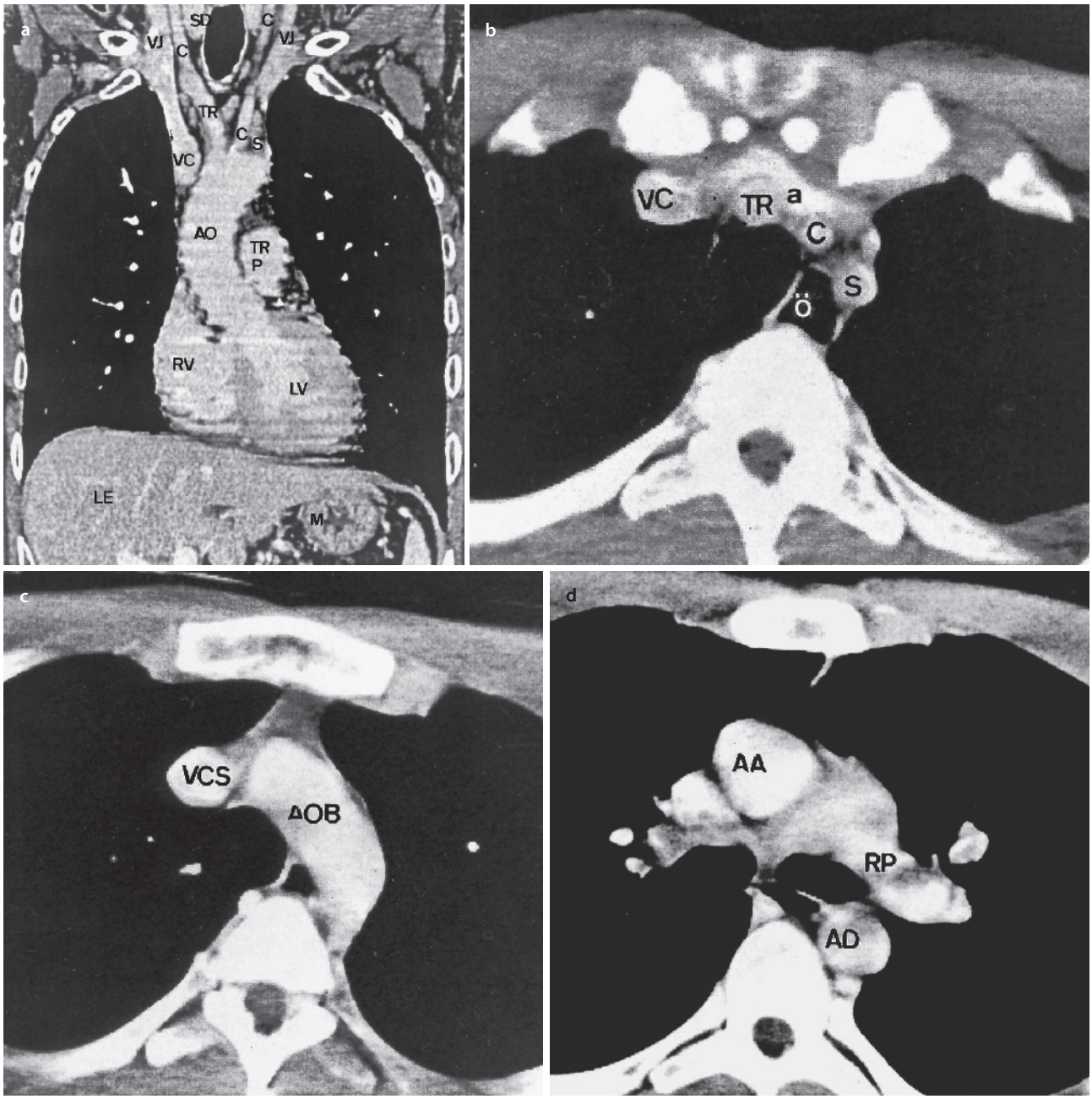

Fig. 6.1 Anatomy of the mediastinum on a computed tomogram. **a** Computed tomography reconstruction of the coronary section level. **b**–**d** Transverse sections of the mediastinum from caudal.*a*brachiocephalic veins, *AA* aorta ascendens, *AD* aorta descendens, *AO* aorta, *AOB* aortic arch, *C* carotid artery, *LP* left pulmonary artery, *LV* left ventricle, *Ö* esophagus, *RA* right atrium, *RP* right pulmonary artery, *RV* right ventricle, *S* subclavian artery, *SD* thyroid, *TP* pulmonary trunk, *TR* brachiocephalic trunk, *VC*, *VCI* inferior vena cava; *VJ* jugular vein. **e**–**g** Transverse sections of the mediastinum from caudal. *a*brachiocephalic veins, *AA* aorta ascendens, *AD* aorta descendens, *AO* aorta, *AOB* aortic arch, *C* carotid artery, *LP* left pulmonary artery, *LV* left ventricle, *Ö* esophagus, *RA* right atrium, *RP* right pulmonary artery, *RV* right ventricle, *S* subclavian artery, *SD*, thyroid, *TP* pulmonary trunk, *TR* brachiocephalic trunk, *VC*, *VCI* inferior vena cava, *VJ* jugular vein

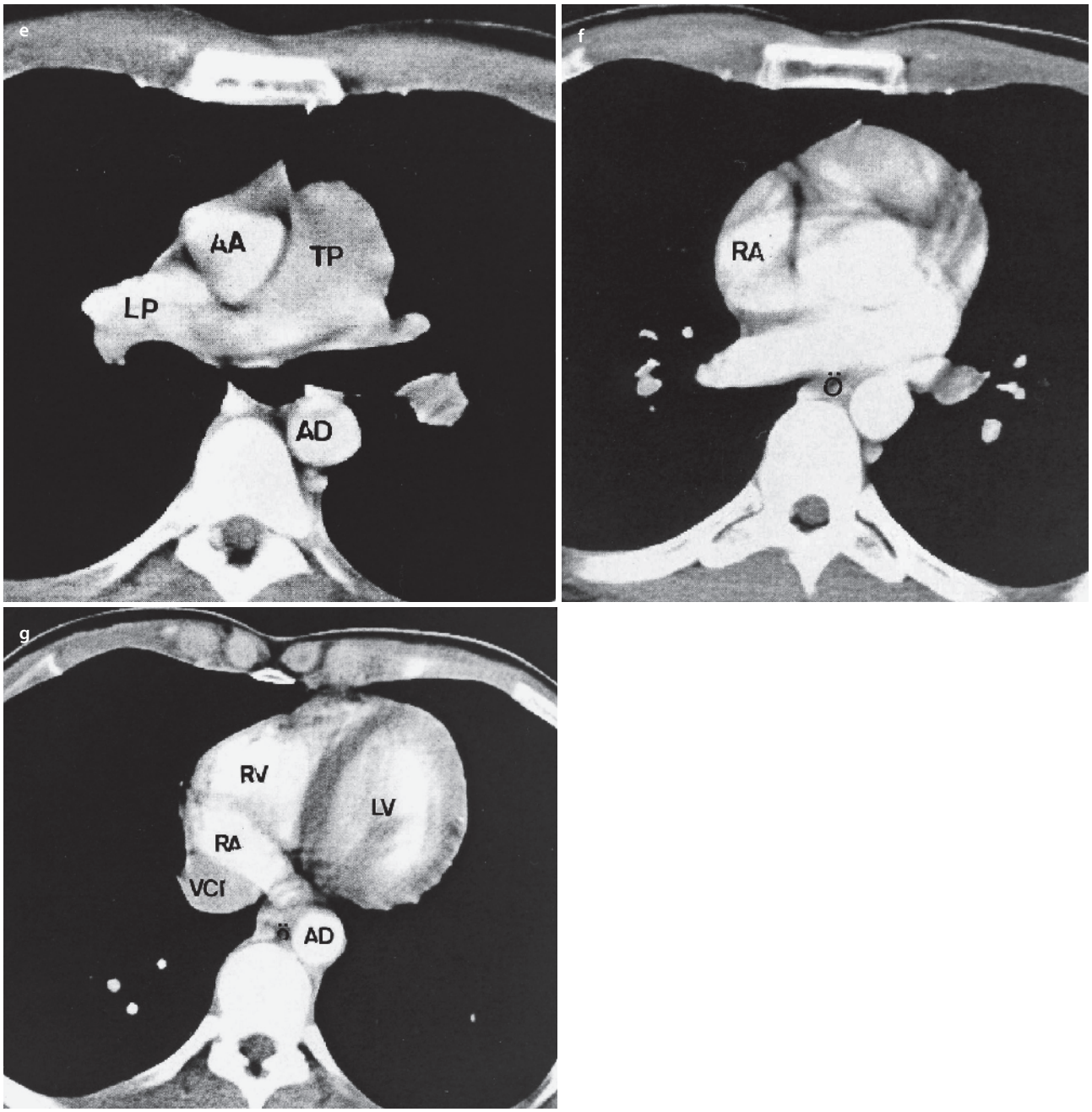

Fig. 6.1 (continued)

6.1.3 Imaging Compartments of the Mediastinum

The upper and mid-mediastinum can be imaged well on sonography. The suprasternal access permits adequate evaluation in 90–95% of cases. The posterior mediastinum, paravertebral region, the hilum of the lung and the immediate retrosternal space, however, can only be partly assessed from a transthoracic approach. Transthoracic sonography may be severely hampered by obesity, pulmonary emphysema, mediastinal distortion as well as spinal deformities.

Factors that limit visualization of mediastinal structures:

- Low-lying structures
- Adiposity, large breasts
- Pulmonary emphysema
- Distortion of the mediastinum (surgery, inflammation, radiotherapy)
- Deformity of the vertebral column

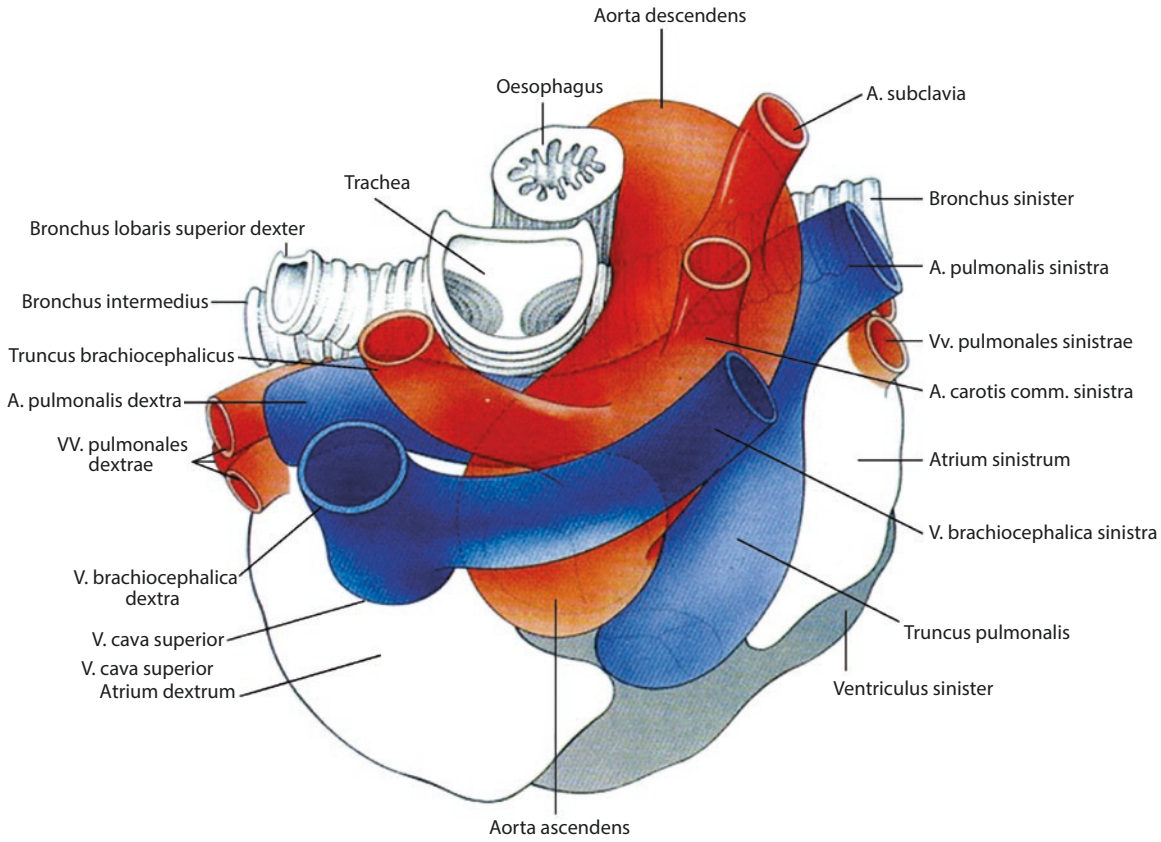

Fig. 6.2 Topographic anatomy of the mediastinal vessels—suprasternal view. (From Wernecke 1991)

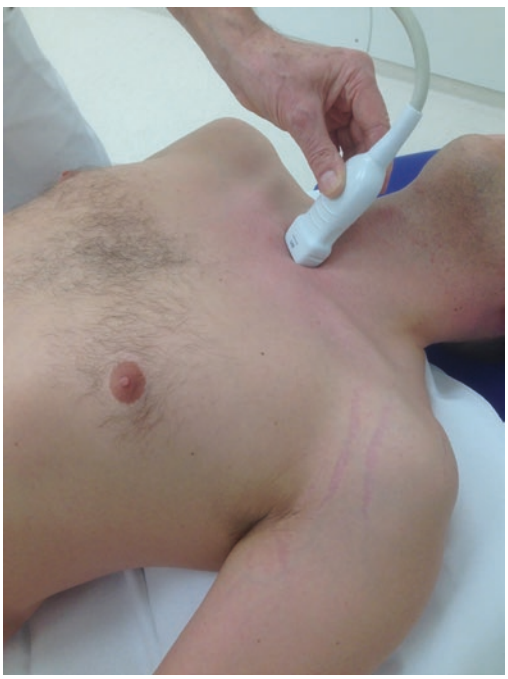

Fig. 6.3 Suprasternal examination. The ultrasound head is located in the jugular fossa; there is a cushion under the shoulders and the head is reclined at the maximum angle

6.1.4 Imaging Tumors in the Mediastinum

Approximately 75% of clinically relevant space-occupying masses in the adult mediastinum are located in the anterior and mid-mediastinum and are therefore readily accessible for sonographic assessment (Rosenberg 1993). The topographic position of a mediastinal space-occupying mass, its size and mobility can be determined by sonography. High-resolution sonography permits good differentiation of tissue on the basis of echogenicity (cystic, solid to calcified). Surrounding vessels can usually also be imaged well in the B mode. More detailed information (differentiation of vessels, indicators of vessel infiltration, tumor vascularization) may be gathered by color-Doppler sonography (Betsch 1994; Blank and Braun 1995; Chen et al. 2014). Tumor vascularity can be demonstrated with much more sensitivity and without motion artifacts through contrast-enhanced sonography, if good-quality equipment is provided (Blank and Braun 1995; Görg et al. 2003). Various space-occupying masses in the mediastinum have a characteristic sonomorphology (Table 6.1). A definite diagnosis, however, is usually made after removal of tissue and its histological investigation (▶ Chap. 9).

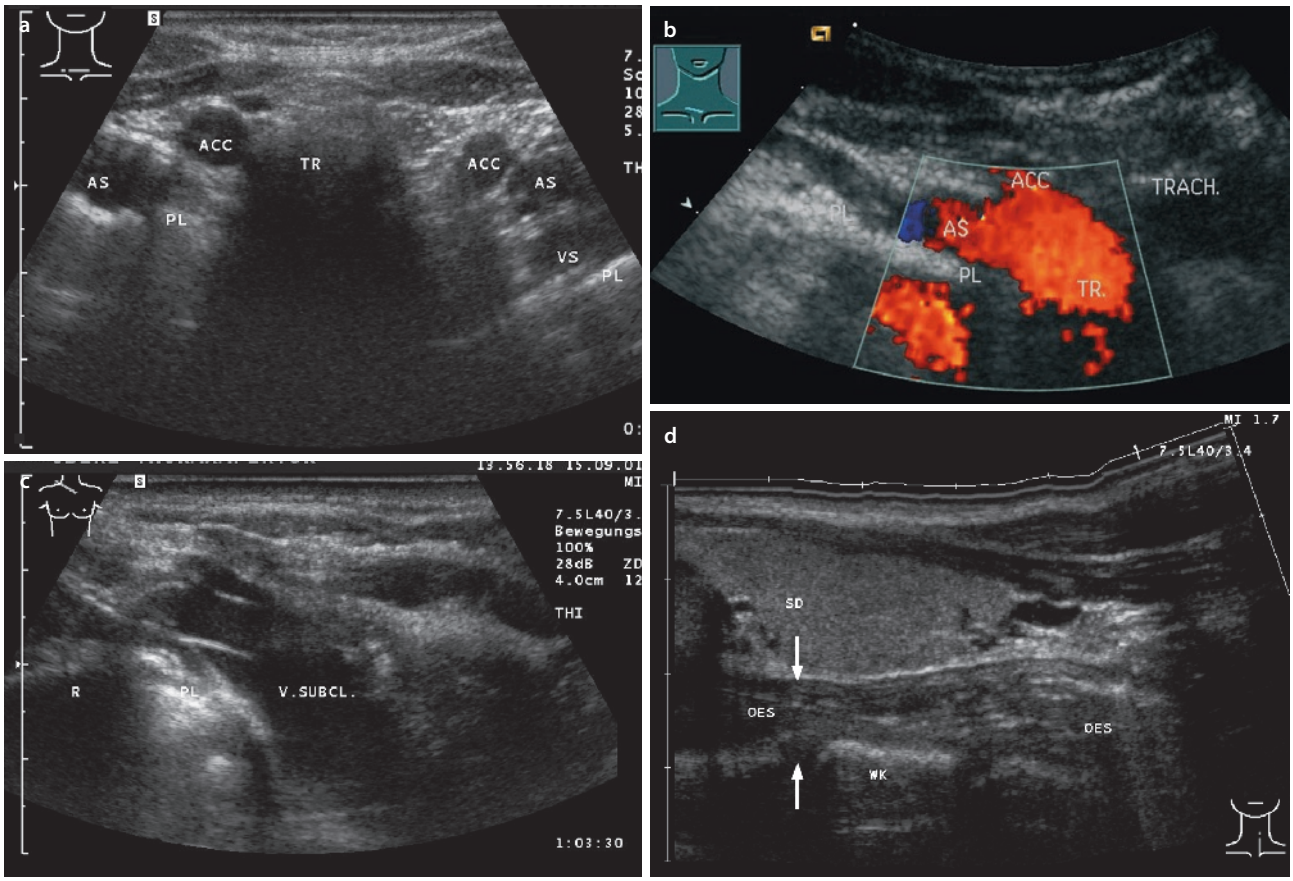

Fig. 6.4 Suprasternal examination. Supraaortal vessels. **a** The suprasternal transverse section demonstrates the cross section of the supraaortal vessels, right, distal to the branching of the brachiocephalic trunk. *ACC* common carotid artery, *AS* subclavian artery, *VS* subclavian vein, *TR* trachea, *PL* pleura/pulmonary reflex. **b** Halfsagittal right-hand section. The brachiocephalic trunk (*TR*) is shown by color-Doppler sonography, branching into the subclavian artery (*AS*) and the common carotid artery (*ACC*). The paratracheal region with its lymph nodes can be seen dorsal to the trunk in this section. Lateral to the reflex of the pleura/lung (*PL*), there is a mirror artifact of the artery. **c** A slight ventral tilting of the probe demonstrates the right subclavian vein. A venous valve can be distinguished. *PL* pleura/pulmonary reflex, *R* rib. **d** The cervical portions of the esophagus (*arrows*) show the left thyroid gland dorsomedial if the sonography probe is tilted slightly laterally. High-resolution sonography probes allow a five-layer separation to be made of the esophagus wall (*arrows*). When the patient swallows, the course of the peristaltic wave and the passage of a high reflexogenic air–liquid portion can be observed. Average wall thickness is 2.5 mm. *OES* esophagus, *SD* thyroid, *WK* cervical vertebra

6.1.5 Diagnostic Value of Sonography, Chest Radiographs and Computed Tomography

Sonography is superior to survey radiographs of the chest in the assessment of nearly all portions of the mediastinum (with the exception of the paravertebral region). In the evaluation of supraaortic, pericardial, prevascular and paratracheal regions, sonography has a sensitivity 90–100% and is nearly as reliable as computed tomography. However, in the aorticopulmonary window and the subcarinal region, sonography achieves a sensitivity of only 82–70% (Wernecke et al. 1988; Wernecke 1991; Brüggemann et al. 1991; Betsch 1994; Dietrich et al. 1995). Thus, sonography occupies an intermediary position between chest radiographs and computed tomography (Castellino et al. 1986; Bollen et al. 1994).

6.1.6 General Indications

Sonographic investigation of the mediastinum is performed after chest radiographs have been obtained, when the findings of the latter are not distinct or if a mediastinal space-occupying mass is suspected.

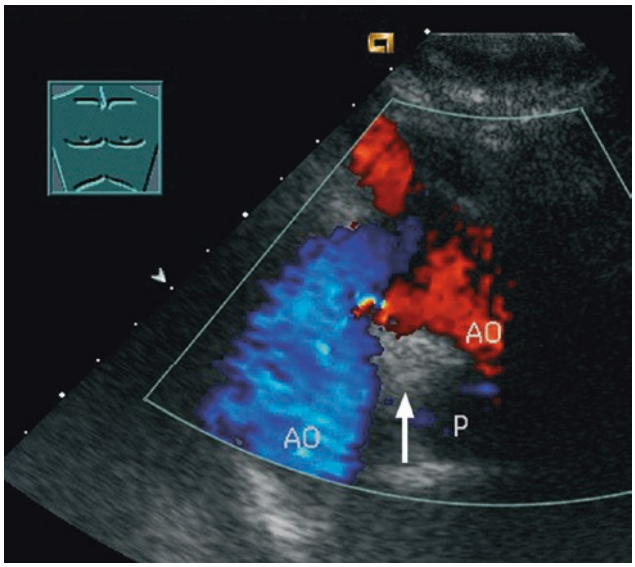

Fig. 6.5 Suprasternal examination. Suprasternal, sagittal section. The aorticopulmonary window (*arrow*) between the aortic arch and the pulmonary artery (*P*) shown in the cross section. If conditions for examination are difficult, the vessels can often be better differentiated from the surrounding soft-tissue structures by color-Doppler sonography and may be identified with more certainty (pulsed-Doppler sonography with characteristic frequency spectrum)

For an initial examination, medistinal sonography can be rapidly implemented in preclinical and emergency diagnosis as a point-of-care sonography for adults with acute thoracic symptoms (pain, upper inflow congestion; important diagnoses such as thoracic aortic aneurism, a Vena cava superior thrombosis (Fig. 6.10) or a malignant lymphoma (Blank et al. 2014) can be made without delay. The procedure is also appropriate for primary imaging of children, and helps to reduce exposure to radiation. Reliable identification of medistinal tubercular lymph nodes in children is thus made possible (Bosch et al. 2007; Supakul and Karmazyn 2013; Mosem and Andronikou 2014).

Sonography is the first investigation procedure in cases of acute chest symptoms (Fig. 6.10). The general indications for transthoracic sonography of the mediastinum are:

- Acute thoracic symptoms(Schmerz, obere Einflussstauung) (pain, upper inflow congestion)
- Suspected pulmonary tuberculosis, especially in children)
- Chest radiograph: space-occupying mass in the mediastinum
- Chest radiograph: undefined space-occupying mass
- Tumor staging (vascular complications)

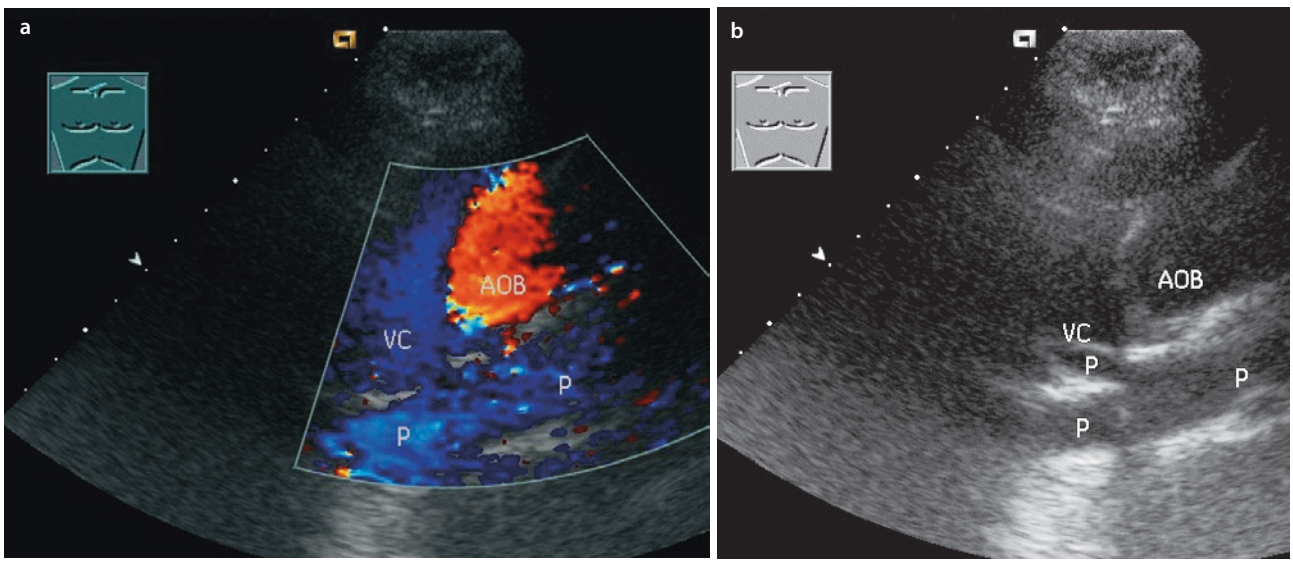

Fig. 6.6 Suprasternal examination. Suprasternal coronary section. **a** Lateral to the aortic arch (AOB), which is shown in an oblique section, the vena cava (VC) can be distinguished with certainty by color-Doppler sonography because of its reverse direction of flow (coded blue). **b** The branching of the pulmonary artery (P) and the aorticopulmonary window can be demonstrated better on B-mode after switching off the color Doppler

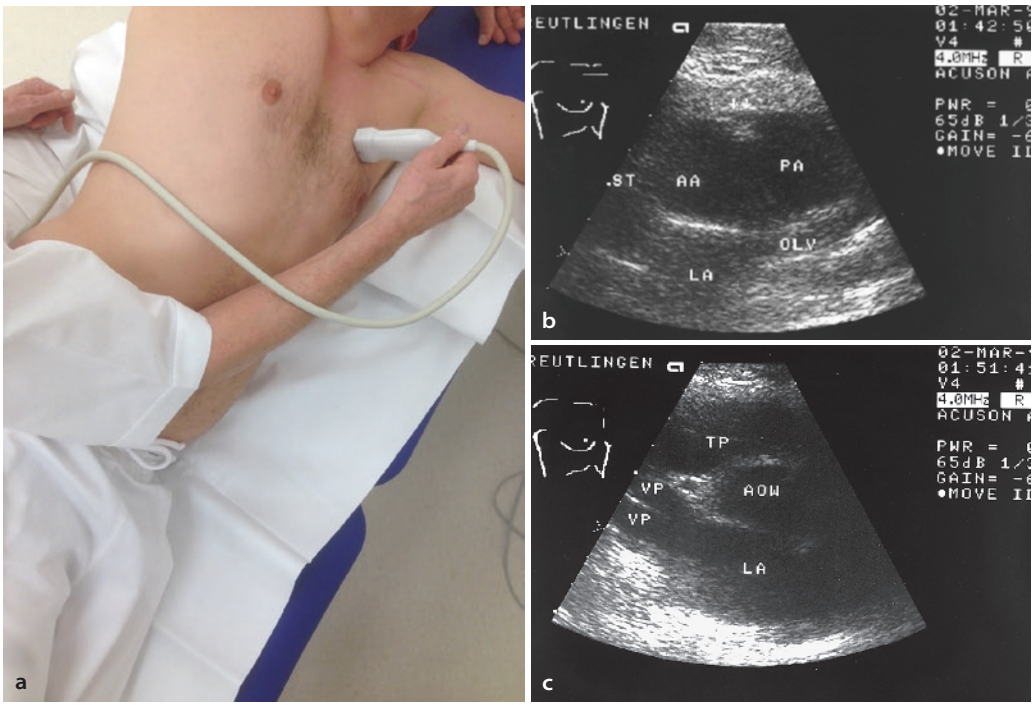

Fig. 6.7 **a** Parasternal examination in the left lateral position. **b** Left parasternal, transversal section. The pulmonary artery (*PA*) winds around the cross-sectional ascending aorta (*AA*). In-between is the upper pericardial recess (*double arrow*), sternum (*ST*), left atrium (*LA*) and upper lung veins (*OLV*). **c** Left parasternal, sagittal section. At the level of the aortic root (*AOW*) ventral crossing through the truncus pulmonalis (*TP*), dorsal left atrium (*LA*) joining pulmonary veins (*VP*)

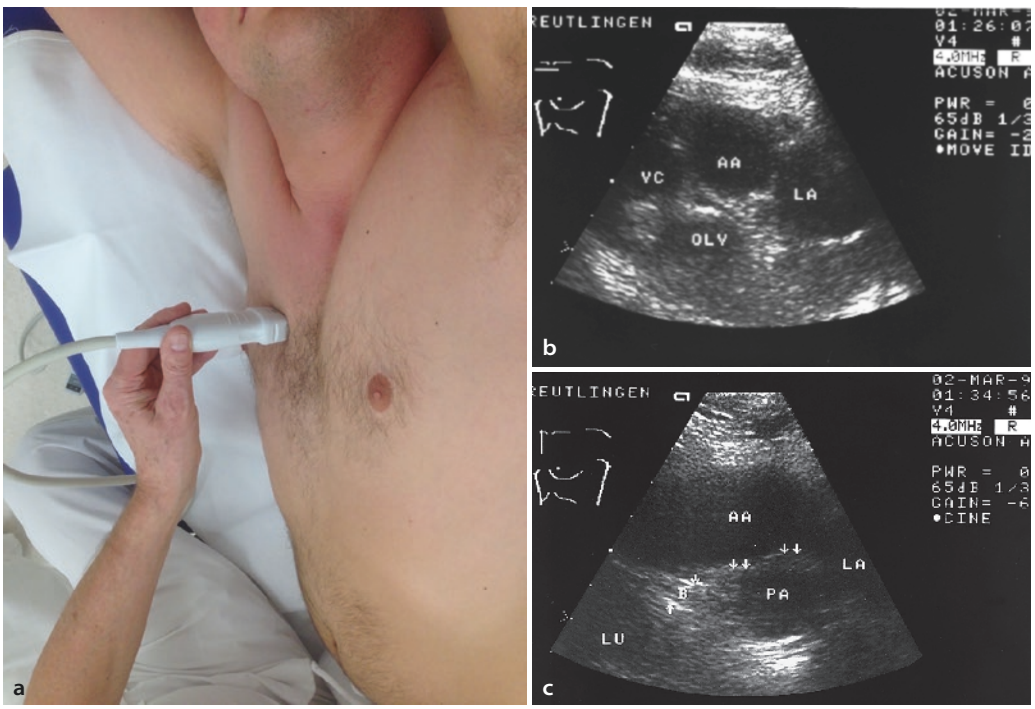

Fig. 6.8 **a** Parasternal examination in right lateral position. **b** Right parasternal transversal section. *AA* ascending artery, *VC* superior vena cava, *LA* left atrium *OLV*, upper lung vein. **c** Right parasternal sagittal section. A successful depiction of the ascending aorta (*AA*), the pulmonary artery (*PA*) in cross section with the aortico-pulmonary window (*double arrow*) in-between, and of the subcarinal region. A bronchus (*B*) can be depicted as an echogenic reflection (*single arrow*). *LU* lung, *LA* left atrium

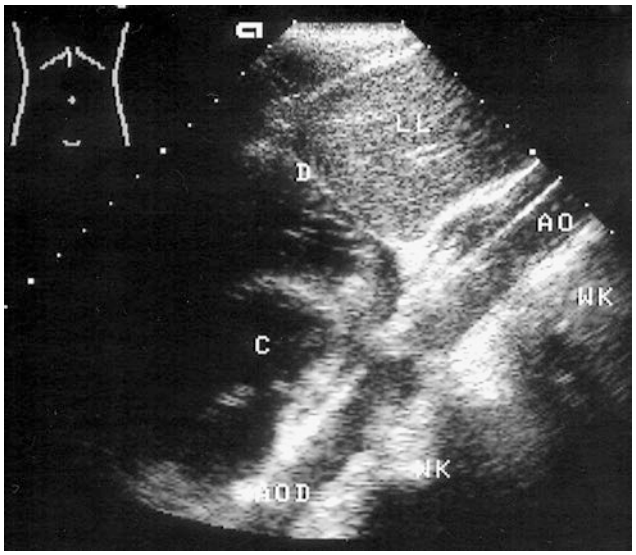

Fig. 6.9 Infrasternal sonography. Sagittal section. The esophagus can be observed at the passage through the diaphragm (*D*) ventrolaterally to the aorta (*AO*). The descending aorta (*AOD*) is partly covered by artifacts. *WK* vertebral body, *C* cor

Table 6.1 Sonomorphology of space-occupying masses in the mediastinum

Appearance	Type of space occupation
Anechoic	Cystic formations, vessels
Hypoechoic	Lymphomas, "active" lymph nodes, more rarely "silent" lymph nodes
Hypoechoic–inhomogeneous echoes	Carcinoma, filiae, inflammation, aneurysm
Echodense	Physiological structures, thymus, scar (exception, rare liposarcoma and teratocarcinoma)

Modified according to Wernecke (1991)

- Monitoring the course of disease/therapy (tumor therapy)
- Puncture and drainage

6.1.7 Specific Sonographic Findings in Selected Space-Occupying Masses in the Mediastinum

6.1.7.1 Lymph Node Disease

Lymphomas account for approximately one quarter of all primary mediastinal tumors, whereas lymph node metastases of bronchial carcinomas, for instance, are more common.

On the basis of their hypoechoic transformation, inflamed and enlarged lymph nodes (e.g., Boeck's disease tuberculosis) or lymph nodes invaded by tumor (Hodgkin's or non-Hodgkin's lymphoma, lymph node metastases) can be well differentiated from the surrounding hyperechoic tissue (Wernecke 1991; Bosch et al. 2007; Alvarez et al. 2013; Mosem and Andronikou 2014) (Figs. 6.11 and 6.12).

In contrast to the mostly "avascular" carcinoma metastases, lymphomas show strong blood flow in Color-Doppler Sonography (Chen et al. 2014); however, reliable differentiation of the above mentioned lymph node disease cannot be achieved through sonographic investigation without a tissue sample being taken (Gulati et al. 2000).

Differentiation of the above-mentioned diseases of lymph nodes by sonography alone is not possible without biopsy (Gulati et al. 2000).

Under treatment lymph nodes again become increasingly echogenic (Wernecke 1991). Color-Doppler Sonography and, as an even more sensitive method that has been recently employed, contrast-enhanced sonography will reveal reduced blood circulation (Betsch 1994; Braun and Blank 2005). With the use of high-resolution devices, normal mediastinal lymph nodes (hypoechoic) are also visualized very often (paratracheal, aorticopulmonary window). A reliable differentiation of pathological processes (▶ Chap. 10), however, is not possible without obtaining bioptic material (Dietrich et al. 1995, 1999; Bosch et al. 2007).

6.1.7.2 Tumors of the Thymus

The thymus is located in the anterior mediastinum, behind the sternum. In adults it cannot be distinguished from its hyperechoic surroundings. Approximately one quarter to one third of all primary mediastinal tumors originate from the thymus. There are various malignant tumors; thymomas and lymphomas are the most common ones (more rarely, germ cell carcinoma, carcinoids and carcinomas). These entities have characteristic sonographic features (Fig. 6.13, Table 6.2). The diagnosis is verified by performing a sonography-guided or computed tomography-guided biopsy (Schuler et al. 1995; ▶ Chap. 10).

6.1.7.3 Germinal Cell Tumors

Teratomas and seminomas are mostly situated in the ventral and middle part of the mediastinum, accounting for approximately 10% of primary mediastinal tumors. Teratomas usually occur in the second and third decades, grow slowly and only produce symptoms if they have grown to a large size (encroaching upon surrounding structures). These tumors are clearly delineated, and contain cystic as well as epithelial structures (skin and

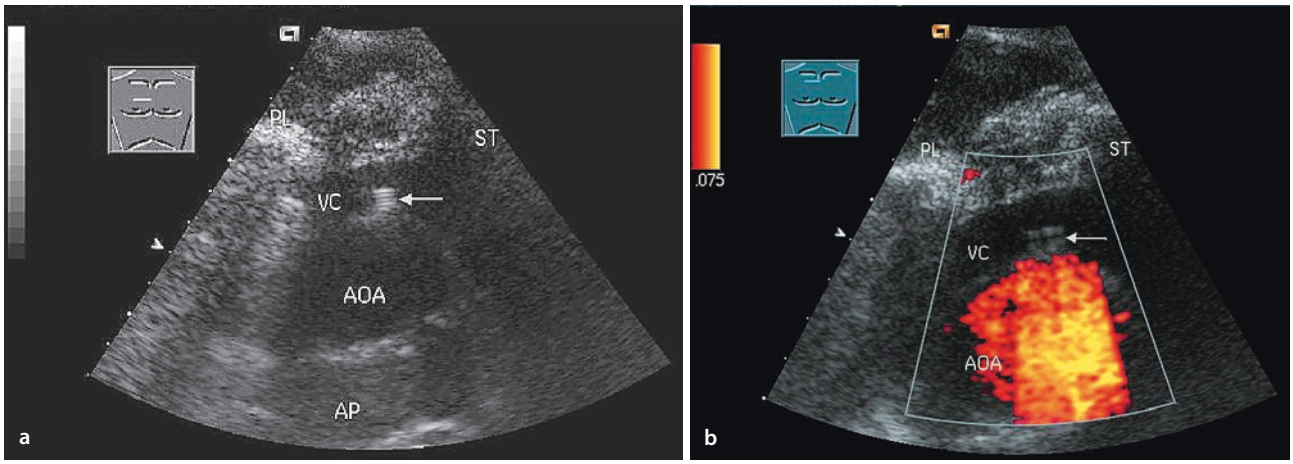

Fig. 6.10 Known non-Hodgkin`s lymphoma. **a** Acute upper inflow congestion. Condition after port implantation. B-image sonography of still parasternal tumor masses. The port catheter can be differentiated as an echogenic double structure (*arrow*) in the hypoechoic vena cava. *AOA* ascending aorta, *AP* right pulmonary artery, *ST* sternum, *PL*pleura. **b** Thrombosis of the vena cava superior (*VC*) can be substantiated

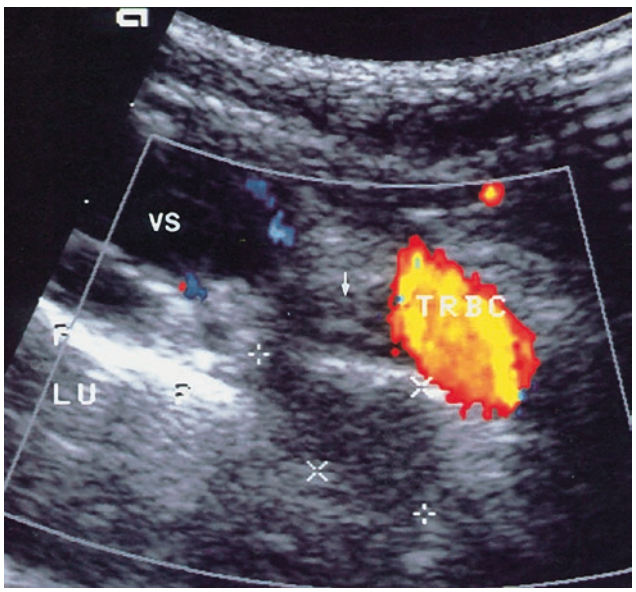

Fig. 6.11 Lymph node tuberculosis. Suprasternal semisagittal section, *right*. Dorsally to the color-Doppler sonography image of the brachiocephalic trunk (*TRBC*), one can see a hypoechoic, indistinctly delineated lymph node (*crosses*) in the paratracheal region, which normally has a homogeneous, hyperechoic structure. The diagnosis of lymph node tuberculosis was made possible by color-Doppler sonography of the fine-needle puncture. *LU* lung

appendages) and also tissue of mesenchymal origin (cartilage, bone, smooth muscle). Twenty-five to thirty percent of tumors show malignant transformation (Fig. 6.14).

6.1.7.4 Neurogenic Tumors

Neurogenic tumors originate from the sympathetic trunk, intercostal nerves or the vagus nerve, and therefore commonly grow in the posterior mediastinum. They can therefore only be demonstrated by transthoracic sonography if they have displaced pulmonary structures paravertebrally or extend cranially (retrosternal approach) or caudally (infrasternal approach). Transesophageal imaging and puncture, if necessary, are usually easy to perform.

6.1.7.5 Retrosternal Portions of the Thyroid and Parathyroid

These can be reliably assigned to the thyroid or the parathyroid on the basis of their topography and typical sonographic pattern. In problematic cases color-Doppler sonography may be used to prove the source organ of the lesion.

Parathyroid adenomas extending retrosternally usually appear as markedly hypoechoic well-vascularized

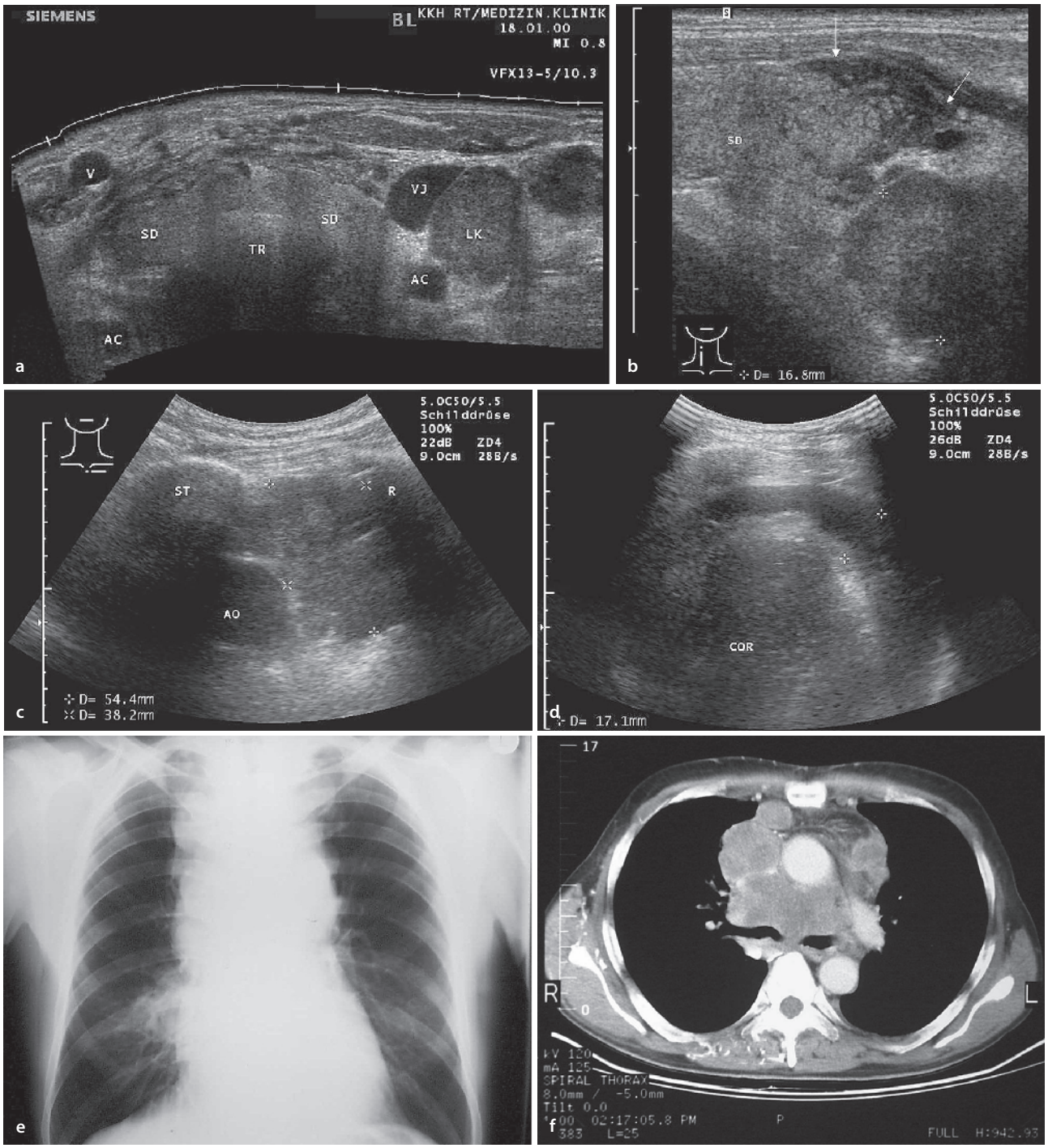

Fig. 6.12 Primary sonographic examination of an upper inflow congestion. **a** Multiple lymph nodes (*LK*) suspected of malignity in the neck region. The panorama presentation (SieScape, from Siemens) enables an impressive documentation of a relatively large region of the body. **b** Low-echo tumor infiltration into the thyroid gland. Tumor masses (*crosses*) reaching into the retrosternal region. **c** Left parasternal section, in the vicinity of the infiltrating low-echo mass (*crosses*). The wall of the aorta (*AO*) can no longer be sharply delineated. *ST* sternum, *R* rib. **d** Pericardial deposits and pericardial effusion (*crosses*). Suspected diagnosis of bronchial carcinoma (man, smoker) with substantiation of a mass suspected of being a metastasis in the region of the right adrenal gland (*crosses*). The diagnosis was confirmed by a sonographically controlled parasternal punch biopsy (Sonocan neddle, 1.2-mm diameter). Histology indicated small cell bronchial carcinoma. **e** Chest X-ray overview. Mediastinal dissemination. **f** Computed tomogram. Tumor on the *right* lower lobar bronchus with extensive mediastinal metastases

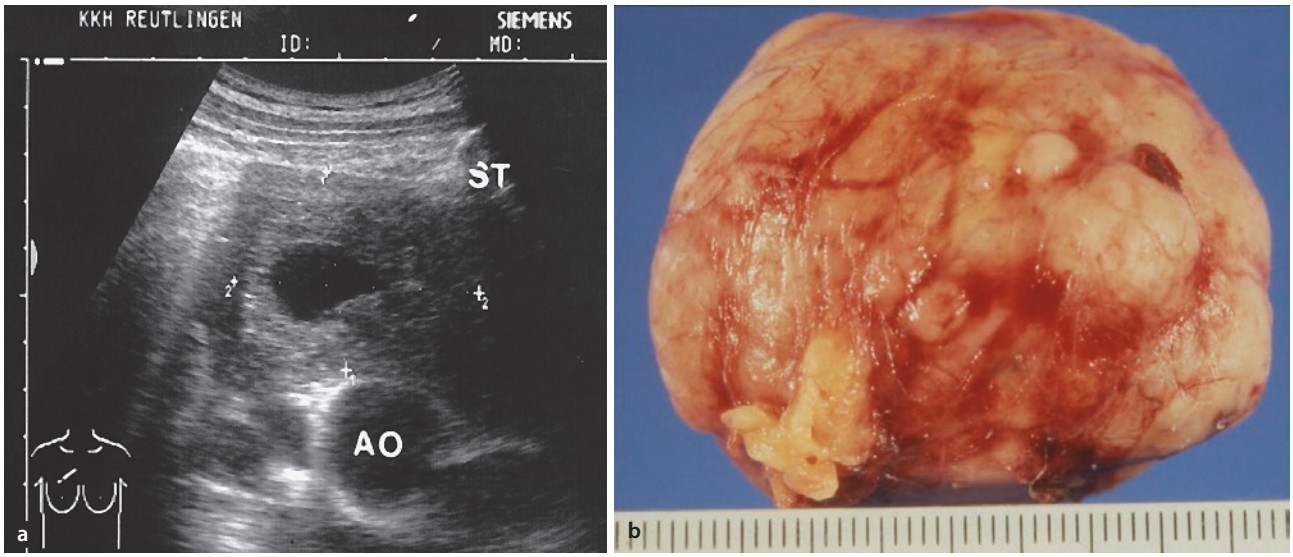

Fig. 6.13 Thymoma. **a** Parasternal, transversal section. Even with the patient in the supine position, it was possible to see a low-echo mass in a ventral position to the aorta and well delineated. Central liquid area. Sonographically controlled incision biopsy (diameter 1.2 mm). *AO* aorta, *ST* sternum. **b** Slide of pathology specimen. The tumor is clearly delineated

Table 6.2 Sonomorphology of thymomas

Benign	Malignant
Hypoechoic	Hypoechoic, inhomogeneous
Sharp margins	Blurred margins
Rounded, partly lobed	Tumor cones
No infiltration	Infiltration (pericardium, vessels)

space-occupying masses (typical laboratory constellation is increased parathyroid hormone and calcium). Puncture may be helpful to differentiate lymph node enlargement (Braun 1992).

6.1.7.6 Mediastinal Cysts

Pericardial and bronchial cysts usually can be clearly identified. If they contain highly viscous fluid, however, differentiation may not always be possible even by dynamic B-mode imaging (change of patient positioning, etc.). Absence of vascularization (in color-Doppler or contrast-enhanced sonography) verifies the diagnosis (Fig. 6.15).

6.1.7.7 Pericardial Alterations

Pericardial alterations like pericardial effusion, hemopericardium and tumor infiltration are easily demonstrable.

6.1.7.8 Esophageal Disease

Proximal and distal portions of the esophagus can be clearly visualized by the suprasternal and infrasternal access (Zhu et al. 2005). Esophageal tumors crossing the wall are seen as hypoechoic tumor formations with blurred margins (Figs. 6.16 and 6.17). In cases of surgical replacement of the esophagus, the upper anastomosis can be viewed. Recurrent tumors can also be detected (Blank et al. 1998; Palabiyik et al. 2012).

Sonography is a valuable aid in the detection of "dysphagia close to the cardia" (Blank et al. 1996a; Janssen et al. 1997).

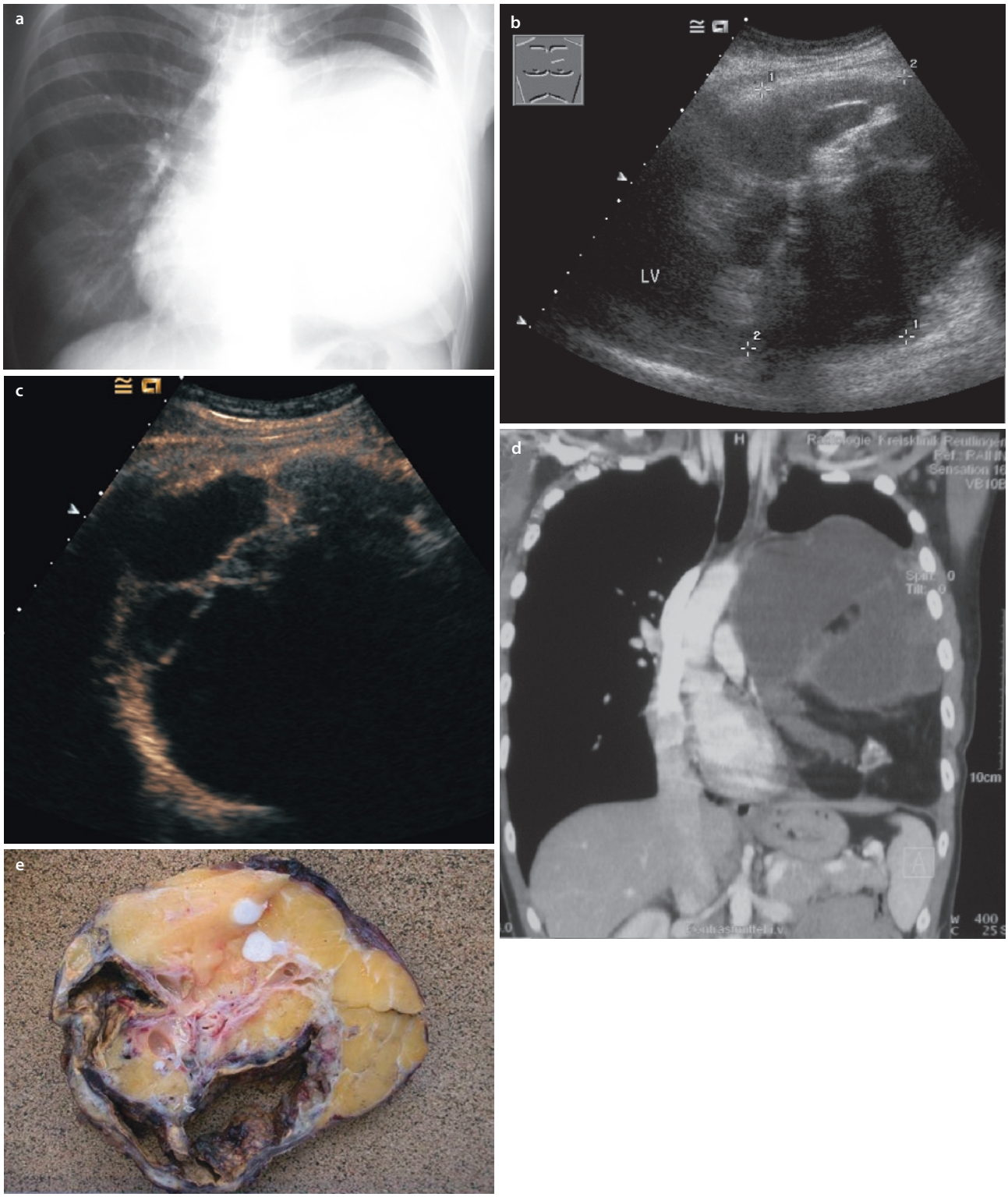

Fig. 6.14 Cystic teratoma. A 32-year-old patient, slight dyspnea when jogging. **a** Plain chest radiograph with tumor and mediastinal distortion to the right. **b** Left parasternal section in supine position. Clearly delineated mass with echogenic septum- like structures. In the *center*, high amplitude reflexes with dorsal shadowing. The space-occupying lesion displaces the pleura to the side toward the thoracic wall, which moves with breathing. The feeding vessels suggest a mediastinal origin of the lesion. **c** Contrast-enhanced sonography clearly demonstrates cystic parts of the tumor which otherwise only shows moderate vascularization and has a smooth border. A teratoma is suspected (central calcifications), and further preoperative diagnostics include computed tomography and transesophageal echocardiography. **d** Computed tomography reconstruction of the coronary section. **e** The gross pathological specimen demonstrates the smoothly demarcated tumor with septae, cystic areas, fatty tissue and cartilage/bone. Histology reveals a benign teratoma

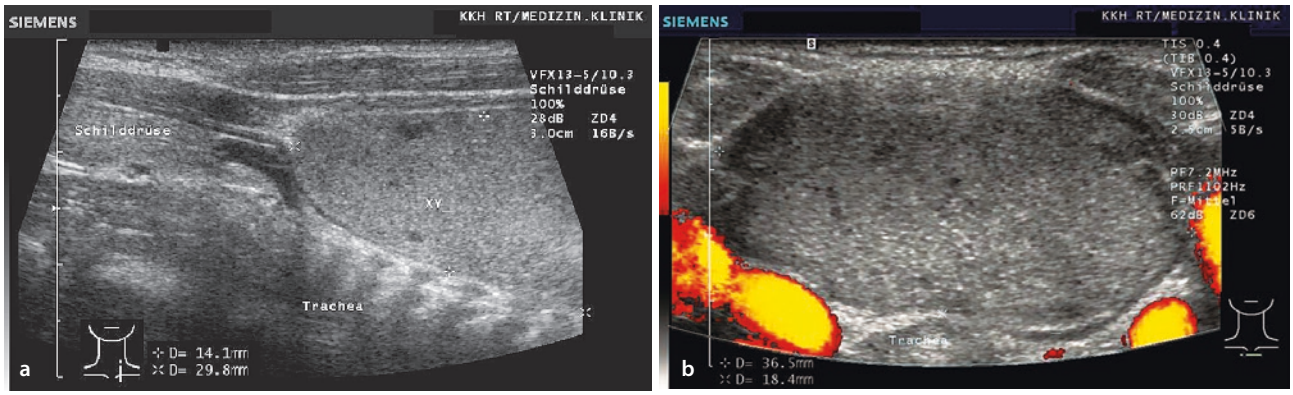

Fig. 6.15 Mediastianal cyst. **a** Suprasternal sagittal section. Smooth edged, homogeneously structured mass (*crosses*), ventral to the trachea. The proximal esophagus is recognizable dorsal to the thyroid gland on the *left*. **b** No blood circulation is detectable in the cross section even with highly sensitive technology. Movement of liquid is made recognizable in the B-image and in the color-Doppler sonography by a shaking movement. Diagnostic fine-needle puncture. Therapeutically operative resection due to compression syndrome

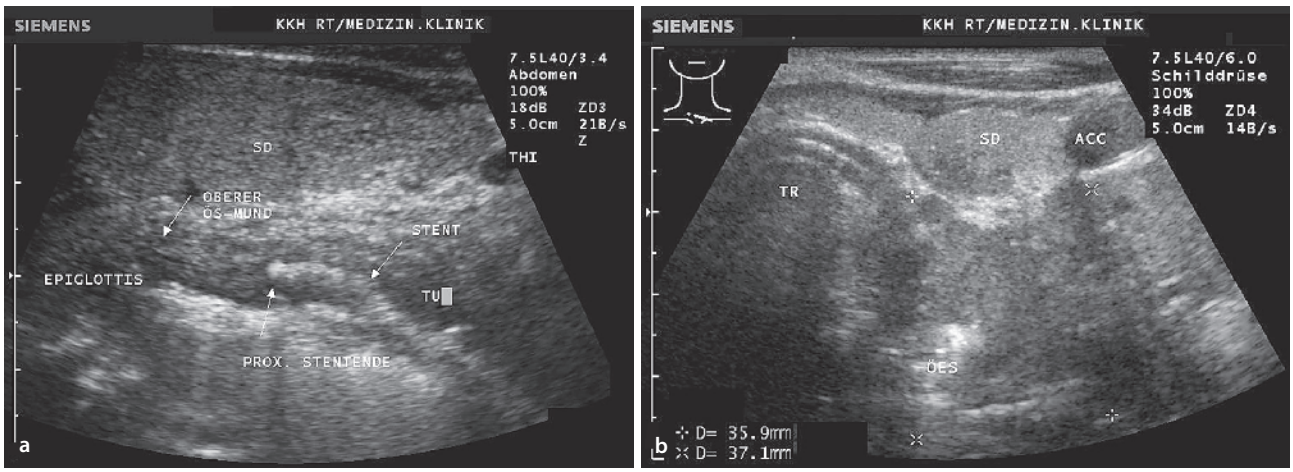

Fig. 6.16 **a** Proximal esophageal carcinoma spreading over the wall (*TU*) with infiltration into the epiglottis, upper esophageal sphincter (*OBERER ÖS-MUND*, *arrow*). The overgrown metal stent (*arrow*) is well delineated. An image with plenty of contrast and low in artifacts as a result of tissue-harmonic imaging. *THI* thyroid. **b** Tumor masses (*crosses*) with infiltration and stenosis of the esophagus (*OES*)

Summary

Mediastinal space-occupying masses are most frequently found in the anterior upper mediastinum. They can be evaluated with transthoracic sonography nearly as reliably as with computed tomography, and histological material can usually be easily obtained by sonography-guided puncture (Nasi 2013; Chen et al. 2014; Dogan et al. 2019) (► Chap. 10).

In case of acute thoracic symptoms, this procedure can be implemented as a point-of-care sonography in emergency diagnosis (Blank et al. 2014).

The disadvantages of sonography, however, are significant. The procedure is strongly investigator dependent and only reveals portions of the mediastinum compared with computed tomography. Moreover, the image quality is highly variable (Dietrich et al. 2015). Some of these disadvantages (■ Table 6.3) can be balanced by the application of endoluminal transesophageal and endobronchial sonography (► Sect. 6.2) (Jenssen et al. 2015).

Acknowledgments

I would like to express my thanks to Martin Lenz (former chief consultant surgeon in the Radiology Department of the Steinenberg Clinic, Reutlingen) for preparing and providing the radiological findings, and my son Valentin for the technical photographic work.

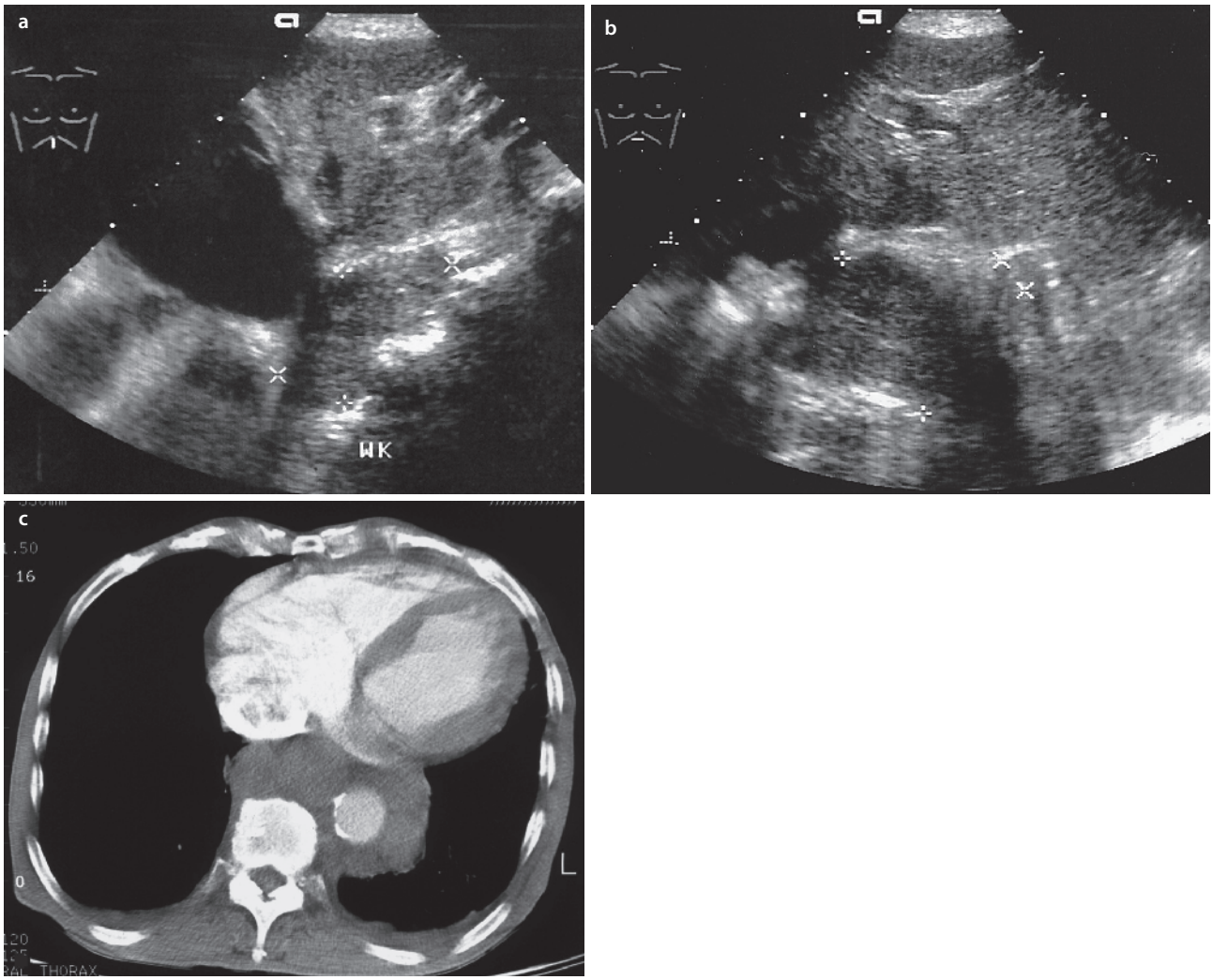

Fig. 6.17 Extensive esophageal carcinoma. **a** Clinical dysphagia. Endoscopic distal esophageal stenosis. No tumor could be established with certainty by biopsy. Sonography with infrasternal, sagittal section of the tumor formation lying ventrally to the spinal column (posterior mediastinum). *WK* vertebral body. **b** Tumor (*crosses*) located infrasternally in transverse section at the distal esophagus (*large crosses*) cannot be delineated. Percutaneously controlled transhepatic fine-needle cut biopsy (Sonocan, 0.9 mm). Histology indicated esophageal carcinoma. **c** Computed tomography. Mass in the posterior mediastinum surrounding the descending aorta

Table 6.3 Transthoracic sonography of the mediastinum

Advantages	Disadvantages
Dynamic imaging	Investigator dependent
Free selection of sectional planes	Only parts of the mediastinum are accessible
Good imaging of the aorticopulmonary window	–
Punctures: low rate of complications	Only punctures in the anterior mediastinum are possible

6.2 Transesophageal Sonography for Lung Cancer and Mediastinal Lesions

Jouke T. Annema Maud Veseliç, and Klaus F. Rabe

Assessing a tissue diagnosis of mediastinal lesions, for example in patients with lung cancer and enlarged mediastinal lymph nodes, is often of major clinical importance. To date, surgical staging—such as mediastinoscopy and mediastinotomy—is still regarded as the standard of care for mediastinal assessment. However, these procedures are not only invasive and require clinical admission with associated high costs, they also have limitations in their diagnostic reach. The development of transesophageal sonography-guided fine-needle aspiration (FNA) provides a minimally invasive alternative for mediastinal analysis. Transesophageal sonography-guided FNA is currently used for the staging for various gastrointestinal malignancies. Since the first report in 1996 on transesophageal sonography-guided FNA for mediastinal staging (Pedersen et al. 1996), this method has evolved to an important diagnostic tool in chest medicine. In this part of the chapter, technical aspects as well as the use of transesophageal sonography-guided FNA in pulmonology will be discussed with an emphasis on the diagnosis and staging of lung cancer.

6.2.1 Technical Aspects

Transesophageal sonography is performed with technology which is also used by gasteroenterologists.

Both radial and linear sonography probes are available, which both enable visualization of paraesophageal lesions. Real-time sonography-controlled FNAs (Fig. 6.18a, b), however, are only possible with linear or longitudinal probes. The fine needle aspirates obtained can be used for cytological (Fig. 6.18c) as well as molecular analysis—for instance, PCR analysis in patients with suspected tuberculosis.

In chest medicine, only linear sonography probes are used as tissue sampling is indicated in the vast majority of cases. Patients are investigated in a left lateral position in an ambulatory setting under conscious sedation using a low dose of midazolam. After the pharynx has been anesthetized with a lidocaine spray, the echo-endoscope is introduced into the distal esophagus until the left liver lobe is visualized. From this point the echo-endoscope is slowly retracted—meanwhile making circular movements, which enables complete visualization of all paraesophageal lesions that are located in the mediastinum. Once lymph nodes have been identified, size, shape, echo texture and borders of lesions can be described. Mediastinal nodes with a short axis exceeding 1 cm, a hypoechoic texture, a round shape and sharp borders are suspected to be malignant. When indicated, images and short movies of mediastinal abnormalities can be recorded. In order to prove malignant nodal involvement it is necessary to obtain tissue (Toloza et al. 2003b). Suspected paraesophageal lesions can be aspirated under real-time sonographic guidance (Fig. 6.19). Nodes from which tissue is obtained should be classified according to the Naruke classification (Mountain and Dresler 1997; Fig. 6.20). In the case of suspected adrenal metastases, left-sided adrenal masses can be aspirated from the stomach (Eloubeidi et al. 2004). On-site cytological evaluation of aspirates has been proven be useful in order to ensure that representative samples are obtained. In experienced hands, a complete transesophageal sonographic examination for the diagnosis and staging of lung cancer takes about 25 min. A prerequisite for performing pneumological EUS-FNA investigations independently is a minimum record of 50 supervised endoscopies (Annema et al. 2010).

Although few absolute contraindications exist for transesophageal sonography procedures of the upper gastrointestinal tract, esophageal strictures and diverticula exhibit an increased perforation risk. Complications related to mediastinal lymph sampling have as yet not been reported. (Annema et al. 2005c, d; Eloubeidi et al. 2005b; Fritscher-Ravens et al. 2000a; Kramer et al. 2004; Larsen et al. 2002; Wallace et al. 2001; Williams et al. 1999). A cyst, however, poses an increased risk of infection and therefore should not be aspirated owing to an increased risk of mediastinitis (Annema et al. 2003a; Wildi et al. 2003).

The advantages of this novel diagnostic tool—as compared with radiological and surgical alternatives—are numerous (Table 6.4). Regarding mediastinal nodal staging, transesophageal sonography has a superior sensitivity compared with computed tomography (Hawes et al. 1994; Toloza et al. 2003a, b) and additionally provides the opportunity for tissue sampling. Compared with surgical alternatives, transesophageal sonography is less invasive, is performed in an outpa-

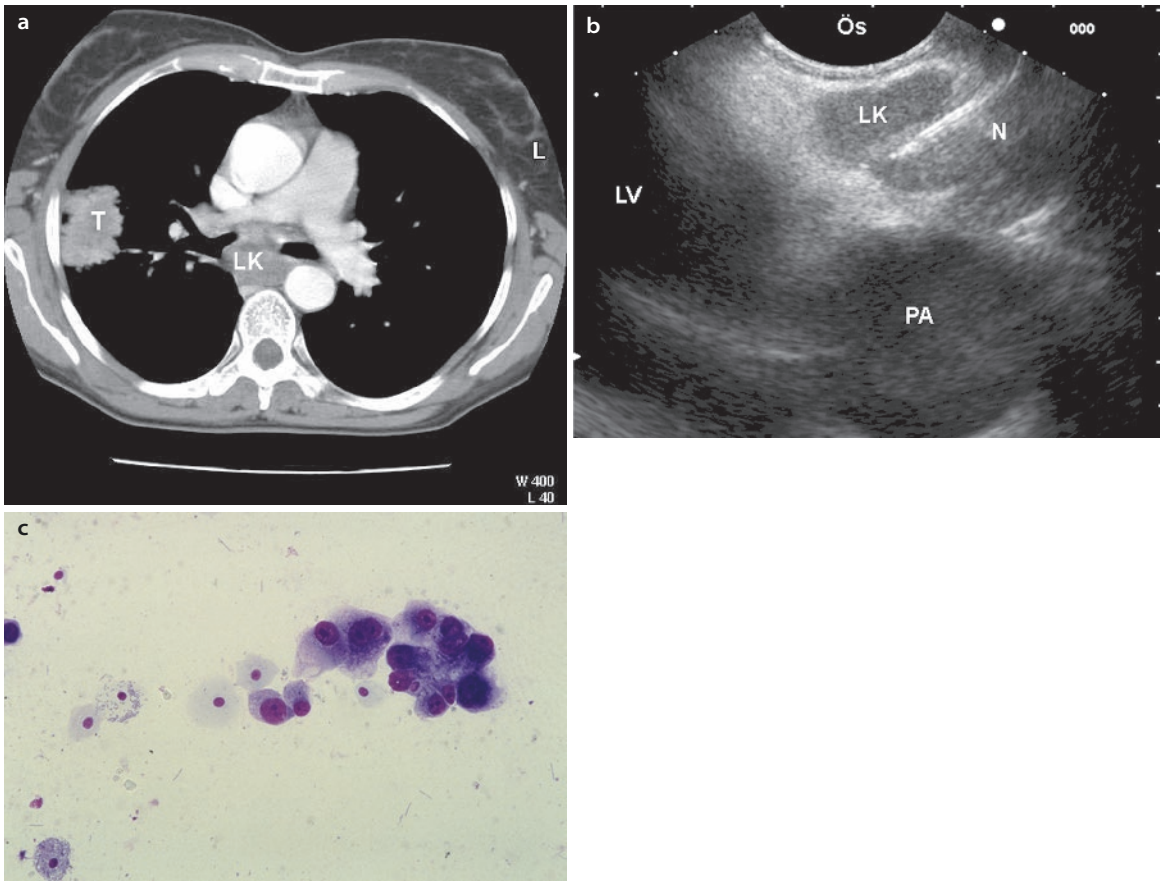

Fig. 6.18 **a** Computed tomography of the thorax. Right upper-lobe tumor (*T*) and enlarged subcarinal lymph node (*LK*). **b** Endosonography. Sonography-guided fine-needle aspiration (*N* needle) of a hypoechoic lymph node with sharp borders located between the esophagus (*Ös*), pulmonary artery (*PA*) and left atrium (*LV*) (lymph node station 7). **c** Cytology. Fine-needle aspirate demonstrating adenocarcinoma with vacuoles and enlarged central nuclei. Squamous cells from the esophagus can be recognized on the *left*

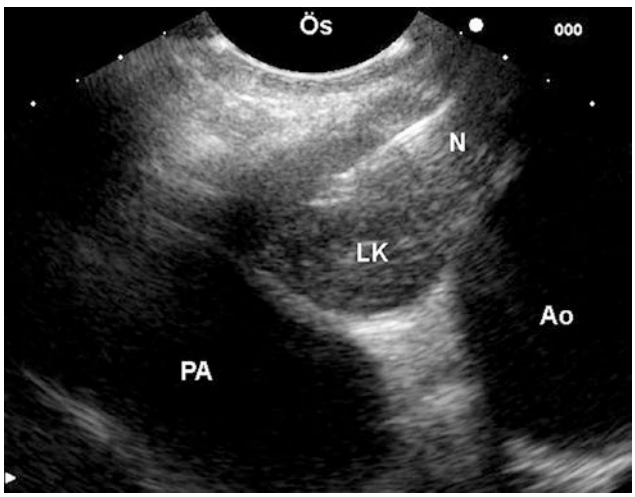

Fig. 6.19 Endosonography. Sonography-guided fine-needle aspiration (*N* needle) of a round hypoechoic lymph node with sharp borders, situated between the esophagus (*Ös*), aorta (*Ao*) and pulmonary artery (*PA*) (lymph node station 4 L)

tient setting and is therefore more cost-effective (Kramer et al. 2004).

The lower mediastinum is the area which can be visualized completely by transesophageal sonography, especially regarding the subcarinal (station 7) and the lower paraesophageal (station 8) nodes as well as those nodes located in the pulmonary ligament (station 9) (Fig. 6.20). Although nodes located in the aortopulmonary window (station 5) and adjacent to the aorta (station 6) can be detected by transesophageal sonography, tissue sampling is not always possible owing to intervening vascular structures. Limitations of EUS are its inability to reach the upper (station 2) and lower (station 4) paratracheal nodes as air in the trachea and main bronchi regularly inhibits visualization of these areas of the mediastinum. EUS is complementary to both mediastinoscopy and endobronchial sonography regarding its diagnostic reach (Annema et al. 2005d; Eloubeidi et al. 2005a). Mediastinoscopy provides good access to both the upper and the lower paratracheal lymph nodes.

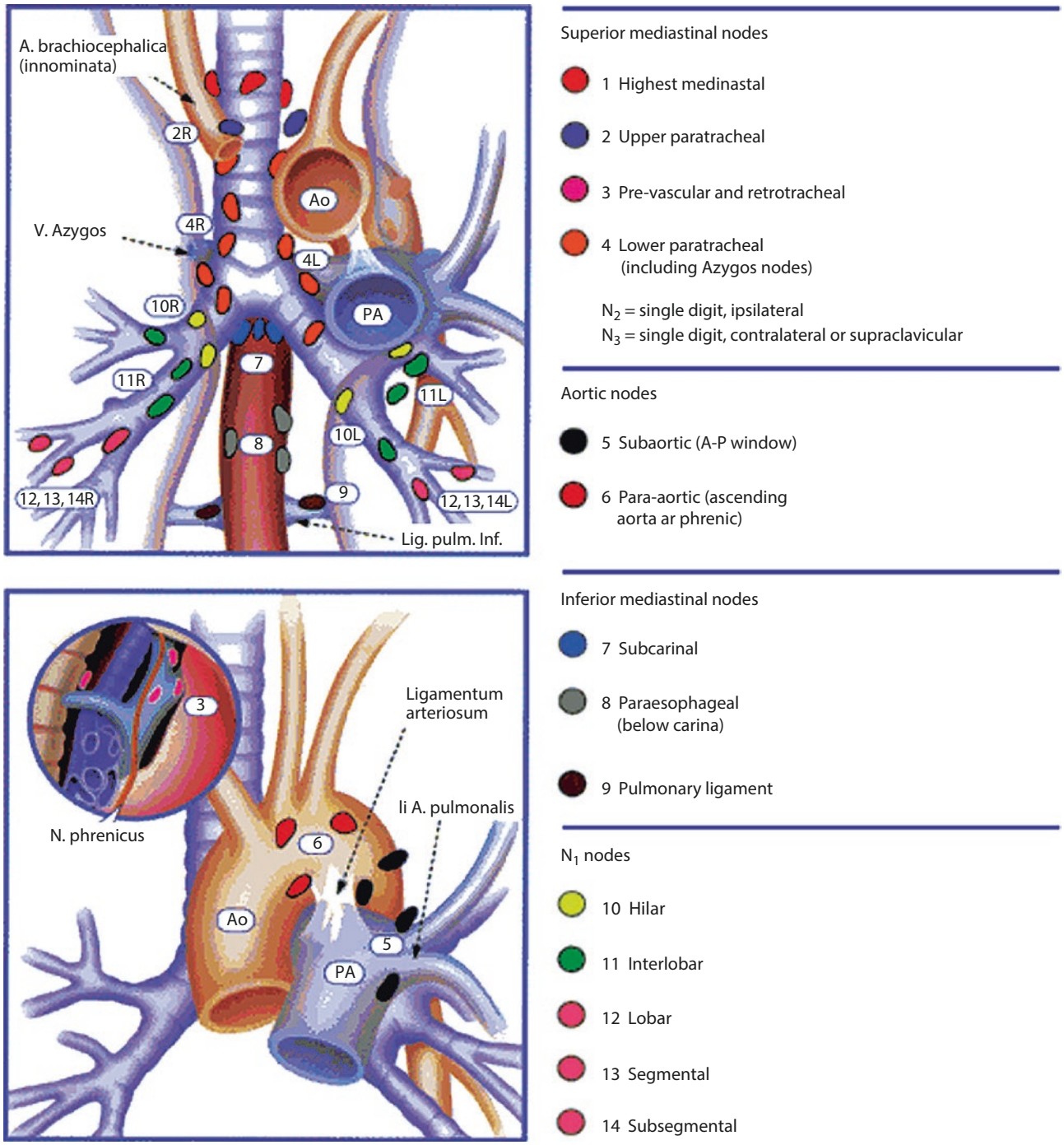

Fig. 6.20 Regional lymph node classification for lung cancer staging. (Adapted from Mountain and Dresler 1997)

6.2.2 Transesophageal Sonography-Guided Fine-Needle Aspiration and Lung Cancer

6.2.2.1 Diagnosing Lung Cancer

Patients with suspected lung cancer and enlarged or PET-positive mediastinal nodes—for whom no diagnosis is obtained after bronchoscopy—are often good candidates for a transesophageal sonography-guided FNA investigation. If mediastinal metastases are assessed by transesophageal sonography-guided FNA, both a tissue diagnosis and locoregional staging are obtained with a single diagnostic test. In a prospective study of 142 patients with suspected lung cancer and enlarged mediastinal nodes, transesophageal sonography—after a nondiagnostic bronchoscopy—assessed a tissue diagnosis in 73% of patients (Annema et al. 2005d).

Transesophageal sonography-guided FNA is also indicated for diagnosing intrapulmonary tumors directly, provided they are located adjacent to the esophagus (Annema et al. 2005b; Varadarajulu et al. 2004a; ◘ Fig. 6.21). In a study of 32 patients with a centrally located lung tumor—in which bronchoscopy failed to achieve a tissue diagnosis—lung cancer was proven by transesophageal sonography-guided FNA in 97% of cases (Annema et al. 2005b).

6.2.2.2 Staging of Lung Cancer

Mediastinal staging of lung cancer is the most common indication for a transesophageal sonography-guided FNA investigation, and the accuracy is between 76% and 98% (Annema et al. 2005c, d; Eloubeidi et al. 2005b; Fritscher-Ravens et al. 2000a; Kramer et al. 2004; Larsen et al. 2002, 2005; Leblanc et al. 2005; Savides and Perricone 2004; Wallace et al. 2001, 2004; Williams et al. 1999; ◘ Table 6.5). So far, most studies have included selected patient with enlarged (short axis greater than 1 cm) or PET-positive (Annema et al. 2004; Eloubeidi et al. 2005b; Kramer et al. 2004) mediastinal nodes. For mediastinal restaging—an emerging indication for transesophageal sonography-guided FNA—an accuracy of 83–92% has been reported (Annema et al. 2003b, Stigt et al. 2009).

Centrally located lung tumors can often be detected by transesophageal sonography, and in these cases it is often possible to assess whether mediastinal tumor invasion (T4) is present (Schroder et al. 2005; Varadarajulu et al. 2004b; ◘ Fig. 6.22). In a study with 97 patients with a lung tumor located immediately adjacent to the esophagus, transesophageal sonography had an accuracy of 92% regarding invasion in the aorta (Schroder et al. 2005).

The left adrenal gland, a common site for distant metastases in patients with lung cancer, can be visualized from the stomach by transesophageal sonography (◘ Fig. 6.23). In a study of 31 patients with enlarged left adrenal glands on computed tomography, transesophageal sonography provided tissue proof of metastatic involvement in 42% of cases (Eloubeidi et al. 2004). Whether the left adrenal gland should be investigated routinely during a transesophageal sonographic investigation for lung cancer staging is the subject of debate (Ringbaek et al. 2005).

◘ **Table 6.4** Transesophageal sonography-guided fine-needle aspiration—advantages and limitations

Advantages	Limitations
Provides access to the lower mediastinum and aorticopulmonary window	Pretracheal and paratracheal nodes
Real-time controlled tissue sampling	Operator dependency
Impressive safety record	
Minimally invasive	
Cost-effective	

6.2.2.3 Clinical Implications

A randomized study showed that the need for surgical staging is significantly reduced by EUS investigations (Tournoy et al. 2008).

Transesophageal sonographic investigations in patients with (suspected) lung cancer can prevent up to

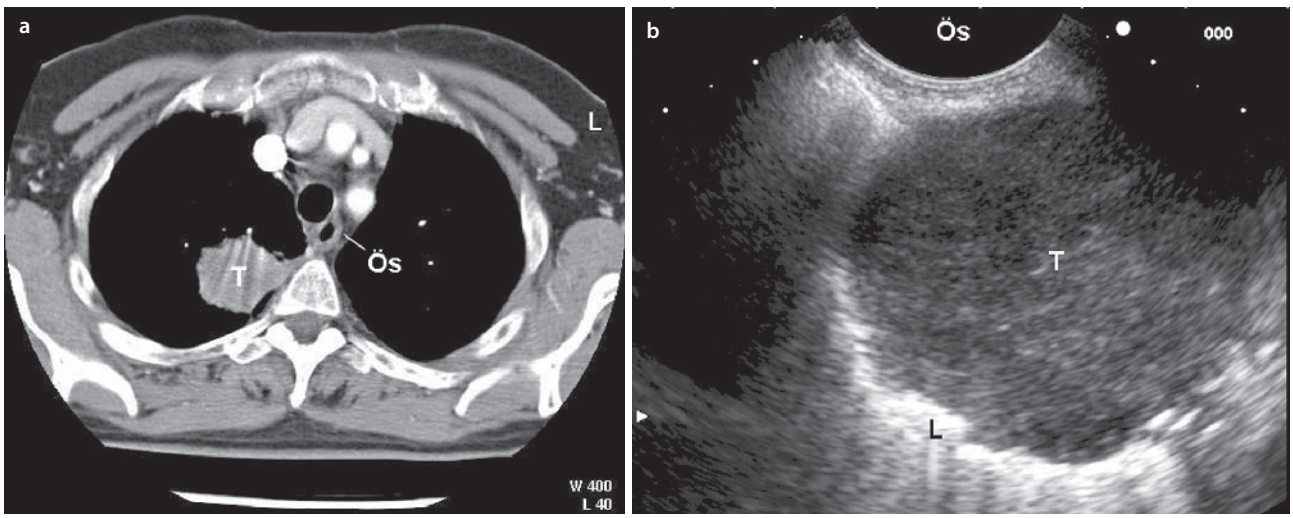

◘ **Fig. 6.21** **a** Computed tomography of the thorax. Relatively smooth shaped intrapulmonary lesion (*T*) located in the right upper lobe (3 cm × 3 cm × 6 cm) located adjacent to the esophagus (*Ös*). The esophagus is located behind the trachea. **b** Endosonography. Lesion with an inhomogeneous echo texture with irregular borders and bronchial carcinoma (*T*) which comprised lung tissue (*L*)

Table 6.5 Transesophageal sonography-guided fine-needle aspiration—mediastinal lymph nodes

Authors	Number of patients	Accuracy (%)
Williams et al. (1999)	82	90
Fritscher-Ravens et al. (2000a)	153	97
Wallace et al. (2001)	107	97
Larsen et al. (2002)	79	94
Kramer et al. (2004)	81	77
Savides and Perricone (2004)	59	98
Wallace et al. (2004)	69	83[a]
Leblanc et al. (2005)	72	76
Annema et al. (2005d)	100	91
Eloubeidi et al. (2005b)	93	97[b]
Annema et al. (2005c)	215	93
	1.110	76–98

[a]Lymph nodes smaller than 1 cm
[b]PET-positive lesions

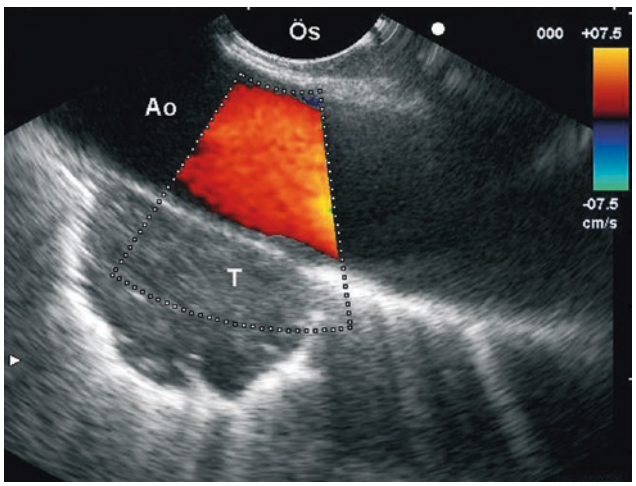

Fig. 6.22 Endosonography. Lung tumor (*T*) located in the left upper lobe with a close relation to the aorta (*Ao*). There are no signs of tumor invasion (T4) in the aorta. *Ös* esophagus

70% of scheduled mediastinoscopies by providing tissue proof of mediastinal metastases (Annema et al. 2005c; Larsen et al. 2002). Patients prefer an ambulatory transesophageal sonographic investigation to surgical staging, which involves clinical admission and general anesthesia (Annema et al. 2005d). In the case of replacement of surgical staging by transesophageal sonography-guided FNA, cost reductions up to 40% can be achieved (Kramer et al. 2004).

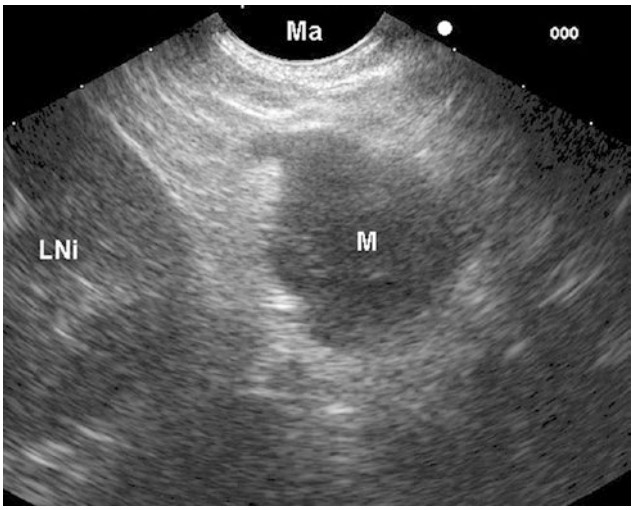

Fig. 6.23 Endosonography. Enlarged left adrenal gland with metastatic involvement (*M*) as assessed by transesophageal sonography-guided fine-needle aspiration. *Ma* stomach, *LNi left* kidney

6.2.2.4 Transesophageal Sonography in Lung Cancer Staging Algorithms

What are the indications for transesophageal sonography-guided FNA in the diagnosis and staging of lung cancer? On the basis of current evidence, transesophageal sonography-guided FNA is indicated early—after a nondiagnostic bronchoscopic evaluation that includes transbronchial needle aspiration—in the diagnostic workup or mediastinal staging of lung cancer.

When transesophageal sonography-guided FNA is added to mediastinoscopy, locoregional staging is improved owing to the complementary reach of both diagnostic methods in reaching different lymph nodes and the identification of mediastinal tumor invasion (T4) (Annema et al. 2005d; Eloubeidi et al. 2005a). Therefore, performing EUS as an additional staging test to routine mediastinoscopy leads to a significant reduction of futile thoracotomies (Larsen et al. 2005). Analyzing mediastinal lesions that are suspected for mediastinal metastases based on fluorodeoxyglucose PET by transesophageal sonography-guided FNA is regarded as an accurate, minimally invasive staging strategy for lung cancer (Annema et al. 2004; Eloubeidi et al. 2005b; Kramer et al. 2004, Iwashita et al. 2008). By combined use of EUS-FNA and EBUS-TBNA, nearly the entire mediastinum can be examined (Wallace et al. 2008). According to current guidelines, EUS or EBUS may be performed as an alternative to mediastinoscopy for the identification of mediastinal

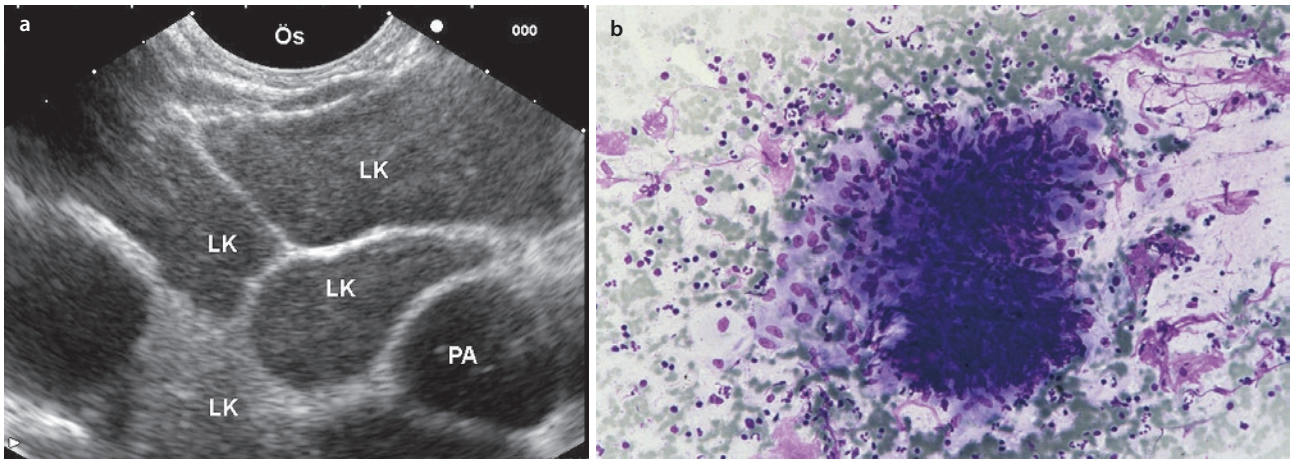

Fig. 6.24 **a** Endosonography. Multiple nodes (*LK*) with sharp borders and an isoechoic ultrasound pattern suggestive of sarcoidosis. *PA* pulmonary artery. **b** Cytology of this lymph node indicates a typical granuloma without central necrosis

lymph node metastases (De Leyn et al. 2007; Detterbeck et al. 2007).

Transesophageal sonography-guided FNA indications in chest medicine:

- Suspected lung cancer, enlarged mediastinal nodes
- Suspected lung cancer, tumor located adjacent to the esophagus
- Mediastinal (re-)staging
- Analyzing PET-positive mediastinal lesions
- Staging of centrally located lung tumors suspected for tumor invasion (T4)
- Suspected left adrenal metastases (left-sided)
- Suspected sarcoidosis
- Suspected tuberculosis
- Suspected mediastinal cysts

6.2.3 Transesophageal Sonography-Guided Fine-Needle Aspiration and Sarcoidosis

Sarcoidosis is the most common interstitial lung disease in which mediastinal nodes are often involved. Frequently, a tissue diagnosis supporting the presumed diagnosis of sarcoidosis is needed, either before treatment with steroids or to rule out other diseases such as tuberculosis, lymphomas or malignant epithelial diseases. For the diagnosis of sarcoidosis, a state-of-the-art bronchoscopic evaluation—including several peripheral lung biopsies—has a diagnostic yield of 66% (Costabel and Hunninghake 1999). However, peripheral biopsies include the risk of a pneumothorax or hemoptysis. Transesophageal sonography has both a high yield (82%; Annema et al. 2005a) and a high sensitivity of 89–94% (Fritscher-Ravens et al. 2000b; Wildi et al. 2004) in assessing noncaseating granulomas and so far no adverse events have been reported. Sonographic images of mediastinal nodes in patients with sarcoidosis often demonstrate a specific ultrasound pattern consisting of multiple, well-defined mediastinal nodes with an isoecpoic or hypoechoic texture and the absence of a centrally located hypoechoic area. Often vessels within these nodes can be detected by color-Doppler sonography (Fritscher-Ravens et al. 2000b). On cytological evaluation, mediastinal nodes in patients with sarcoidosis present as noncaseating granulomas without necrosis (Fig. 6.24).

6.2.4 Transesophageal Sonography and Cysts

Paraesophageal and parabronchial cysts account for a considerable portion of mediastinal lesions. Cysts located adjacent to the esophagus (Fig. 6.25a) can be visualized by transesophageal sonography and often present with a round shape, well-defined borders and an echo-free or echo-poor content (Fig. 6.25b). Aspiration of cysts is not indicated owing to the risk of mediastinitis (Annema et al. 2003a; Wildi et al. 2003).

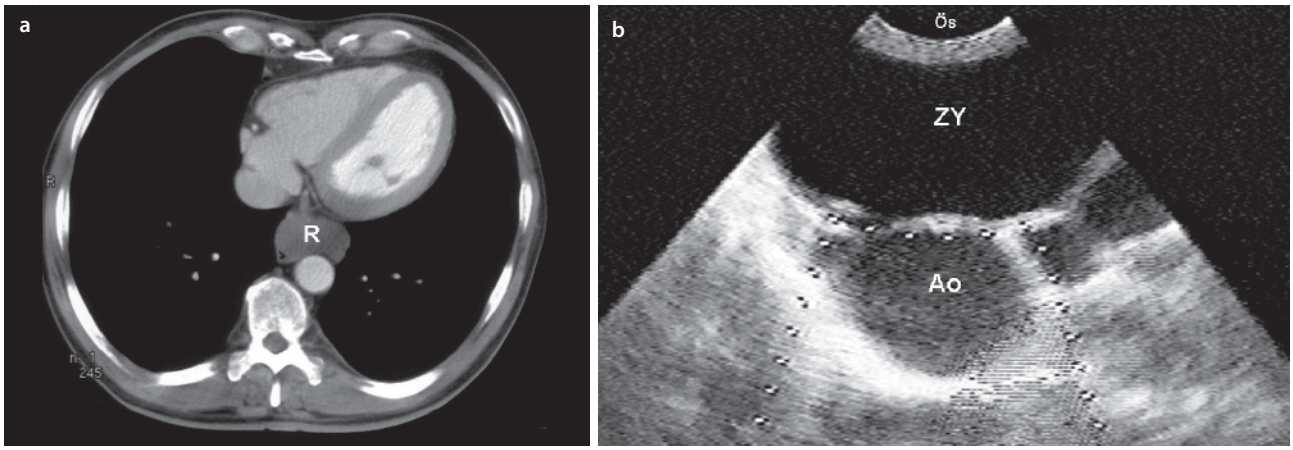

Fig. 6.25 **a** Computed tomography of the thorax. Sharp well-defined lesion (*R*) (2 cm × 1 cm × 1 cm) located in the lower mediastinum. The heart and descending aorta are easily identified. **b** Endosonography. Remarkably echo-poor, well-demarked, easily compressible lesion (cyst located immediately adjacent to the esophagus (*Ös*)) without a signal on color-Doppler sonography—sonographically compatible with a cyst. *Ao* aorta

Summary

Ten years after the first reports of mediastinal evaluation by transesophageal sonography-guided FNA, there is strong evidence that transesophageal sonography-guided FNA qualifies as an accurate and safe method for diagnosing and staging of lung cancer. Additionally this test is helpful for the analysis of various other mediastinal lesions. When used in clinical practice, transesophageal sonography-guided FNA not only prevents surgical diagnostic procedures to a large extent, it also reduces the number of futile thoracotomies and is cost-effective. Recently, linear echo-bronchoscopes—derived from transesophageal sonography scopes—have become clinically available. Comparison studies between transesophageal sonography-guided FNA and endobronchial sonography-guided transbronchial needle aspiration are needed for definitive position of these echo-endoscopic methods in diagnostic and staging algorithms (Herth et al. 2005; Vilmann et al. 2005; Wallace et al. 2008). The end point for such studies should include accuracy, safety, feasibility and patient preference. Randomized studies are being performed at the present time to compare complete endosonographic staging (EUS + EBUS) with surgical staging.

According to the authors, supported by the available peer-reviewed literature, transesophageal sonography-guided FNA can be regarded as an important diagnostic tool for the analysis of mediastinal lesions and the diagnosis and staging of lung cancer.

References

Transthoracic

Alvarez-Alvarez C, Otero Fernandez M, Cabero-Perez MJ, Guerra Dietz L, Galan Cuesta M, Agüeo Balbin J (2013) Description of tuberculosis outbreak and usefulness of mediastinal ultrasound. An Pediatr (Barc) 79(5):293–299

Beckh S, Bolcskei PL, Lessnau KD (2002) Real-time chest ultrasonography. A comprehensive review for the pulmonologist. Chest 122:1759–1773

Betsch B (1994) Farbdopplersonographie des Mediastinums. Radiologe 34:599–604

Betsch B, Knopp MV, van Kaick G (1992) Malignant tumors and lymphomas of the mediastinum: diagnosis and follow-up with color assisted doppler sonography. Eur J Cancer Res Clin Oncol 118:107

Betsch B, Berndt R, Knopp MV, Schmähl A, Trost U, Delorme S (1994) Vergleich von Computertomographie und B-Bild-Sonographie in der bildgebenden Diagnostik des Mediastinums. Bildgebung 61:295–298

Blank W, Braun B (1995) Gewebsdiagnostik durch Dopplersonographie. Bildgebung 62:31–35

Blank W, Braun B, Gekeler E (1986) Ultraschalldiagnostik und Feinnadelpunktion pleuraler, pulmonaler und mediastinaler Prozesse. In: Hansmann M (ed) Ultraschalldiagnostik. Springer, Berlin/Heidelberg/New York/Tokyo, pp 562–565

Blank W, Braun B, Schuler A, Wild K (1996a) Die percutane Sonographie zur Differenzierung der Dysphagie. Ultraschall Med 17(S1):32

Blank W, Schuler A, Wild K, Braun B (1996b) Transthoracic sonography of the mediastinum. Eur J Ultrasound 3:179–190

Blank W, Schwaiger U, Wild K, Braun B (1998) Die percutane Sonographie zur Darstellung des cervicalen Ösophagus. Ultraschall Med 19(S1):4

Blank W, Mathis G, Osterwalder J (2014) Kursbuch Notfallsonographie. Georg Thiemeverlag 2014

Bollen EC, Goci R, van't Hof-Grootenboer BE, Versteege CWM, Engelshove HA, Lamers RJ (1994) Interobserver variability and accuracy of computed tomographic assessment of nodal status in lung cancer. Ann Thorac Surg 58:158–162

Bosch-Marcet J, Serres-Creixams X, Borras-Perez V et al (2007) Value of sonography for follow-up of mediastinal lymphadenopathy in children with tuberculosis. J Clin Ultrasound 35(3):118–224

Braun B (1983) Abdominelle und thorakale Ultraschalldiagnostik. In: Bock HE (ed) Klinik der Gegenwart. Urban & Schwarzenberg, Munich, pp 1141–1145

Braun B (1992) Schilddrüse. In: Braun B, Günther R, Schwerk WB (eds) Ultraschalldiagnostik. Lehrbuch und Atlas, vol III-3.1. Ecomed, Landsberg/Lech

Braun B, Blank W (2005) Sonographie von Hals und oberem Mediastinum. Internist 46(10):1133–1145

Brüggemann A, Greie A, Lepsien G (1991) Real-time-sonography of the mediastinum in adults: a study in 100 healthy volunteers. Surg Endosc 5:150–153

Caremani M, Benci A, Tacconi D et al (2009) Sonographic management of mediastinal syndrome. J Ultrasound 12(2):61–68

Castellino RA, Blank N, Hoppe RT et al (1986) Hodgkin disease: contributions of chest CT in the initial staging evaluation. Radiology 160:603–605

Chen HJ, Liao WC, Liang SJ, Li CH, Tu CY, Hsu WH (2014) Diagnostic impact of color ultrasound-guided core biopsy on fine-needle aspiration of anterior mediastinal masses. Ultrasound Med Biol 40(12):2768–2776

Dietrich CF, Liesen M, Wehrmann T, Caspary WF (1995) Mediastinalsonographie: Eine neue Bewertung der Befunde. Ultraschall Med 16:61

Dietrich CF, Liesen M, Buhl R, Herrmann G, Kirchner I, Caspary WF, Wehrmann T (1997) Detection of normal mediastinal lymphnodes by ultrasonography. Acta Radiol 38:965–969

Dietrich CF, Chickakli M, Burgon I, Wehrmann T, Wiewrodt R, Buhl R, Caspary WF (1999) Mediastinal lymph nodes demonstrated by mediastinal sonography: activity marker in patients with cystic fibrosis. J Clin Ultrasound 27:9–14

Dietrich CF, Annema JT, Clementsen P, Cui XW, Borst M, Jenssen C (2015) Ultrasound techniques in the evaluation of the mediastinum, part I: endoscopic ultrasound (EUS), endobronchial ultrasound (EBUS) and transcutaneous mediastinal ultrasound (TMUS), introduction into ultrasound techniques. J Thorac Dis 7(9):E311–E325

Dogan C, Cömert S, Salepci B, Kiral N, Parmaksiz E, Caglayan B (2019) Efficient and safe method in the diagnosis of thoracic lesions: Ultrasound-guided needle aspiration biopsy. Eurasian J Pulmonol 21(3):148

Goldberg GG (1971) Suprasternal ultrasonography. JAMA 15:245–250

Görg C, Seifart U, Görg K, Zugmaier G (2003) Color Doppler sonographic mapping of pulmonary lesions. J Ultrasound Med 22:1033–1039

Gulati M, Venkataramu NK, Gupta S (2000) Ultrasound guided fine needle aspiration biopsy in mediasinal tuberculosis. Int J Tuberc Lung Dis 4(12):1164–1168

Heizel M (1985) Sonographische Topographie des oberen vorderen Mediastinums. Ultraschall 6:101–109

Herth FJF (2009) The Mediastinum. In: Bolliger CT, Herth FJF, Mayo PH, Miyazawa T, Beamis JF (eds) Clinical chest ultrasound. From the ICU to the Bronchoscopy Suite. Karger, Basel

Jenssen C, Annema JT, Clementsen P, Cui X-W, Borst M, Dietrich CF (2015) Ultrasound techniques in the evaluation of the mediastinum, Part 2: Mediastinal lymph node anatomy and diagnostic reach of ultrasound techniques, clinical work up of neoplastic and inflammatory mediastinal lymphadenopathy using ultrasound techniques and how to learn mediastinal endosonography. J Thorac Dis 7(10):E439–E458

Janssen J, Johanns W, Lehnhardt M, Jakobeit C, Greiner L (1997) Die transkutane Sonographie des gastroösophagealen Übergangs im prospektiven Vergleich mit der Endoskopie. Dtsch Med Wochenschr 122:1167–1171

Lengerke HV, Schmid HC (1988) Mediastinalsonographie im Kindesalter. Radiologe 28:460–465

Koh DM, Burke S, Davies N et al (2002) Transthoracic US of the chest: clinical uses and applications. Radiographics 22:E1. http://radiographics.rsnajnls.org/cgi/content/full/22/1/e1

Liu P, Daneman A, Stringer DA (1988) Real-time-sonography of mediastinal and juxtamediastinal masses in infants and children. J Can Assoc Radiol 39:198–203

Mosem T, Andronikou S (2014) Through the eye of the suprasternal notch: point-of-care sonography for tuberculous mediastinal lymphadenopathy in children. Pediatr Radiol 44:681–684

Palabiyik FB, Bayramoglu S, Gunert NT, Daglar S, Cimilli T (2012) Use of sonography for evaluation of the cervical and thoracic esophagus in children. J Ultrasound Med 31(9):1375–1379

Rosenberg JC (1993) Neoplasms of the mediastinum. In: De Vita VT, Hellman S, Rosenberg SA (eds) Cancer: principles and practice of oncology. Lippincott, Philadelphia, pp 759–775

Schuler A, Blank W, Braun B (1995) Sonographisch-interventionelle Diagnostik bei Thymomen. Ultraschall Med 16:62

Supakul N, Karmazyn B (2013) Ultrasound of the pediatric chest- the ins and outs. Semin Ultrasound CT MR 34(3):274–285

Wernecke K (1991) Mediastinale sonographie, untersuchungstechnik, diagnostische Effizienz und Stellenwert in der bildgebenden Diagnostik des Mediastinums. Springer, Berlin/Heidelberg/New York/Tokyo

Wernecke K, Peters PE, Galanski M (1986) Mediastinal tumors: evaluation of suprasternal sonography. Radiology 159:405–409

Wernecke K, Pötter R, Peters PE (1988) Parasternal medisatinal sonography: sensitivity in the detection of anterior mediastinal and subcarinal tumors. AJR Am J Roentgenol 150:1021–1026

Zhu SY et al (2005) Sonographic demonstration of the normal thoraxic esophagus. J Clin Ultrasound 33(1):29–33

Transesophageal Sonography for Lung Cancer and Mediastinal Lesions

Annema JT, Veselic M, Versteegh MI, Rabe KF (2003a) Mediastinitis caused by EUS-FNA of a bronchogenic cyst. Endoscopy 35(9):791–793

Annema JT, Veselic M, Versteegh MI, Willems LN, Rabe KF (2003b) Mediastinal restaging: EUS-FNA offers a new perspective. Lung Cancer 42(3):311–318

Annema JT, Hoekstra OS, Smit EF, Veselic M, Versteegh MI, Rabe KF (2004) Towards a minimally invasive staging strategy in NSCLC: analysis of PET positive mediastinal lesions by EUS-FNA. Lung Cancer 44(1):53–60

Annema JT, Veselic M, Rabe KF (2005a) Endoscopic ultrasound-guided fine-needle aspiration for the diagnosis of sarcoidosis. Eur Respir J 25(3):405–409

Annema JT, Veselic M, Rabe KF (2005b) EUS-guided FNA of centrally located lung tumours following a non-diagnostic bronchoscopy. Lung Cancer 48(3):357–361

Annema JT, Versteegh MI, Veselic M, Voigt P, Rabe KF (2005c) Endoscopic ultrasound-guided fine-needle aspiration in the diagnosis and staging of lung cancer and its impact on surgical staging. J Clin Oncol 23(33):8357–8361

Annema JT, Versteegh MI, Veselic M, Welker L, Mauad T, Sont JK et al (2005d) Endoscopic ultrasound added to mediastinoscopy for preoperative staging of patients with lung cancer. JAMA 294(8):931–936

Annema JT, Bohoslavsky R, Burgers S et al (2010) Implementation of endoscopic ultrasound for lung cancer staging. Gastrointest Endosc 71(1):64–70

Costabel U, Hunninghake GW (1999) ATS/ERS/WASOG statement on sarcoidosis. Sarcoidosis Statement Committee. American Thoracic Society. European Respiratory Society. World Association for Sarcoidosis and Other Granulomatous Disorders. Eur Respir J 14(4):735–737

De Leyn P, Lardinois D, Van Schil PE, Rami-Porta R, Passlick B, Zielinski M et al (2007) ESTS guidelines for preoperative lymph node staging for non-small cell lung cancer. Eur J Cardiothorac Surg 32(1):1–8

Detterbeck FC, Jantz MA, Wallace M, Vansteenkiste J, Silvestri GA (2007) Invasive mediastinal staging of lung cancer: ACCP evidence-based clinical practice guidelines, 2nd edn. Chest 132(Suppl. 3):202S–220S

Eloubeidi MA, Seewald S, Tamhane A, Brand B, Chen VK, Yasuda I et al (2004) EUS-guided FNA of the left adrenal gland in patients with thoracic or GI malignancies. Gastrointest Endosc 59(6):627–633

Eloubeidi MA, Tamhane A, Chen VK, Cerfolio RJ (2005a) Endoscopic ultrasound-guided fine-needle aspiration in patients with non-small cell lung cancer and prior negative mediastinoscopy. Ann Thorac Surg 80(4):1231–1239

Eloubeidi MA, Cerfolio RJ, Chen VK, Desmond R, Syed S, Ojha B (2005b) Endoscopic ultrasound-guided fine needle aspiration of mediastinal lymph node in patients with suspected lung cancer after positron emission tomography and computed tomography scans. Ann Thorac Surg 79(1):263–268

Fritscher-Ravens A, Sriram PV, Bobrowski C, Pforte A, Topalidis T, Krause C et al (2000a) Mediastinal lymphadenopathy in patients with or without previous malignancy: EUS-FNA-based differential cytodiagnosis in 153 patients. Am J Gastroenterol 95(9):2278–2284

Fritscher-Ravens A, Sriram PV, Topalidis T, Hauber HP, Meyer A, Soehendra N et al (2000b) Diagnosing sarcoidosis using endosonography-guided fine-needle aspiration. Chest 118(4):928–935

Hawes RH, Gress F, Kesler KA, Cummings OW, Conces DJ Jr (1994) Endoscopic ultrasound versus computed tomography in the evaluation of the mediastinum in patients with non-small-cell lung cancer. Endoscopy 26(9):784–787

Herth FJ, Lunn W, Eberhardt R, Becker HD, Ernst A (2005) Transbronchial vs. transesophageal ultrasound-guided aspiration of enlarged mediastinal lymph nodes. Am J Respir Crit Care Med 171(10):1164–1167

Iwashita T, Yasuda I, Doi S, Kato T, Sano K, Yasuda S, Nakashima M, Hirose Y, Takaimi T, Moriwaki H et al (2008) The yield of endoscopic ultrasound-guided fine needle aspiration for histological diagnosis in patients suspected of stage I sarcoidosis. Endoscopy 40(5):400–405

Kramer H, van Putten JW, Post WJ, van Dullemen HM, Bongaerts AH, Pruim J et al (2004) Oesophageal endoscopic ultrasound with fine needle aspiration improves and simplifies the staging of lung cancer. Thorax 59(7):596–601

Larsen SS, Krasnik M, Vilmann P, Jacobsen GK, Pedersen JH, Faurschou P et al (2002) Endoscopic ultrasound guided biopsy of mediastinal lesions has a major impact on patient management. Thorax 57(2):98–103

Larsen SS, Vilmann P, Krasnik M, Dirksen A, Clementsen P, Maltbaek N et al (2005) Endoscopic ultrasound guided biopsy performed routinely in lung cancer staging spares futile thoracotomies: preliminary results from a randomised clinical trial. Lung Cancer 49(3):377–385

Leblanc JK, Devereaux BM, Imperiale TF, Kesler K, Dewitt JM, Cummings O et al (2005) Endoscopic ultrasound in non-small cell lung cancer and negative mediastinum on computed tomography. Am J Respir Crit Care Med 171:177–182

Mountain CF, Dresler CM (1997) Regional lymph node classification for lung cancer staging. Chest 111(6):1718–1723

Pedersen BH, Vilmann P, Folke K, Jacobsen GK, Krasnik M, Milman N et al (1996) Endoscopic ultrasonography and real-time guided fine-needle aspiration biopsy of solid lesions of the mediastinum suspected of malignancy. Chest 110(2):539–544

Ringbaek TJ, Krasnik M, Clementsen P, Skov BG, Rasmussen EN, Vilmann P (2005) Transesophageal endoscopic ultrasound/fine-needle aspiration diagnosis of a malignant adrenal gland in a patient with non-small cell lung cancer and a negative CT scan. Lung Cancer 48(2):247–249

Savides TJ, Perricone A (2004) Impact of EUS-guided FNA of enlarged mediastinal lymph nodes on subsequent thoracic surgery rates. Gastrointest Endosc 60(3):340–346

Schroder C, Schonhofer B, Vogel B (2005) Transesophageal echographic determination of aortic invasion by lung cancer. Chest 127(2):438–442

Stigt JA, Oostdijk AH, Timmer PR et al (2009) Comparison of EUS-guided fine needle aspiration and integrated PET-CT in restaging after treatment for locally advanced non-small cell lung cancer. Lung Cancer 66(2):198–204

Toloza EM, Harpole L, McCrory DC (2003a) Noninvasive staging of non-small cell lung cancer: a review of the current evidence. Chest 123(1 Suppl):137S–146S

Toloza EM, Harpole L, Detterbeck F, McCrory DC (2003b) Invasive staging of non-small cell lung cancer: a review of the current evidence. Chest 123(Suppl. 1):157S–166S

Tournoy KG, De Ryck F, Vanwalleghem LR, Vermassen F, Praet M, Aerts JG et al (2008) Endoscopic ultrasound reduces surgical mediastinal staging in lung cancer: a randomized trial. Am J Respir Crit Care Med 177(5):531–535

Varadarajulu S, Hoffman BJ, Hawes RH, Eloubeidi MA (2004a) EUS-guided FNA of lung masses adjacent to or abutting the esophagus after unrevealing CT-guided biopsy or bronchoscopy. Gastrointest Endosc 60(2):293–297

Varadarajulu S, Schmulewitz N, Wildi SF, Roberts S, Ravenel J, Reed CE et al (2004b) Accuracy of EUS in staging of T4 lung cancer. Gastrointest Endosc 59(3):345–348

Vilmann P, Krasnik M, Larsen SS, Jacobsen GK, Clementsen P (2005) Transesophageal endoscopic ultrasound-guided fine-needle aspiration (EUS-FNA) and endobronchial ultrasound-guided transbronchial needle aspiration (EBUS-TBNA) biopsy: a combined approach in the evaluation of mediastinal lesions. Endoscopy 37(9):833–839

Wallace MB, Silvestri GA, Sahai AV, Hawes RH, Hoffman BJ, Durkalski V et al (2001) Endoscopic ultrasound-guided fine needle aspiration for staging patients with carcinoma of the lung. Ann Thorac Surg 72(6):1861–1867

Wallace MB, Ravenel J, Block MI, Fraig M, Silvestri G, Wildi S et al (2004) Endoscopic ultrasound in lung cancer patients with a normal mediastinum on computed tomography. Ann Thorac Surg 77(5):1763–1768

Wallace MB, Pascual JM, Raimondo M, Woodward TA, McComb BL, Crook JE et al (2008) Minimally invasive endoscopic staging of suspected lung cancer. JAMA 299(5):540–546

Wildi SM, Hoda RS, Fickling W, Schmulewitz N, Varadarajulu S, Roberts SS et al (2003) Diagnosis of benign cysts of the mediastinum: the role and risks of EUS and FNA. Gastrointest Endosc 58(3):362–368

Wildi SM, Judson MA, Fraig M, Fickling WE, Schmulewitz N, Varadarajulu S et al (2004) Is endosonography guided fine needle aspiration (EUS-FNA) for sarcoidosis as good as we think? Thorax 59(9):794–799

Williams DB, Sahai AV, Aabakken L, Penman ID, Van Velse A, Webb J et al (1999) Endoscopic ultrasound guided fine needle aspiration biopsy: a large

Endobronchial Sonography

Felix J. F. Herth and Ralf Eberhardt

Contents

G. Mathis (ed.), *Chest Sonography*, https://doi.org/10.1007/978-3-031-09442-2_7

7.1 Instruments and Technique

7.1.1 Endobronchial Sonography Miniprobes

The different impedance of soft tissues has made sonography an indispensable diagnostic tool in medicine. Instruments that are used for gastrointestinal application could not be applied inside the airways because of their diameter. For application inside the central airways, therefore, flexible catheters for the probes with a balloon at the tip were developed, which allows circular contact for the ultrasound, providing a complete 360° image of the parabronchial and paratracheal structures (Fig. 7.1a). Thus, under favorable conditions structures at a distance of up to 4 cm can be visualized (Herth and Becker 2000). The probes have been on the market since 1999 and can be applied with regular flexible endoscopes that have a biopsy channel of at least 2.6 mm.

7.1.2 Endobronchial Sonography Transbronchial Needle Aspiration

The latest developments are special bronchoscopes with an integrated curvilinear electronic transducer at the tip (Olympus BF-UC160F; Fig. 7.2). So a realtime needle puncture under endoscopic control is possible. The

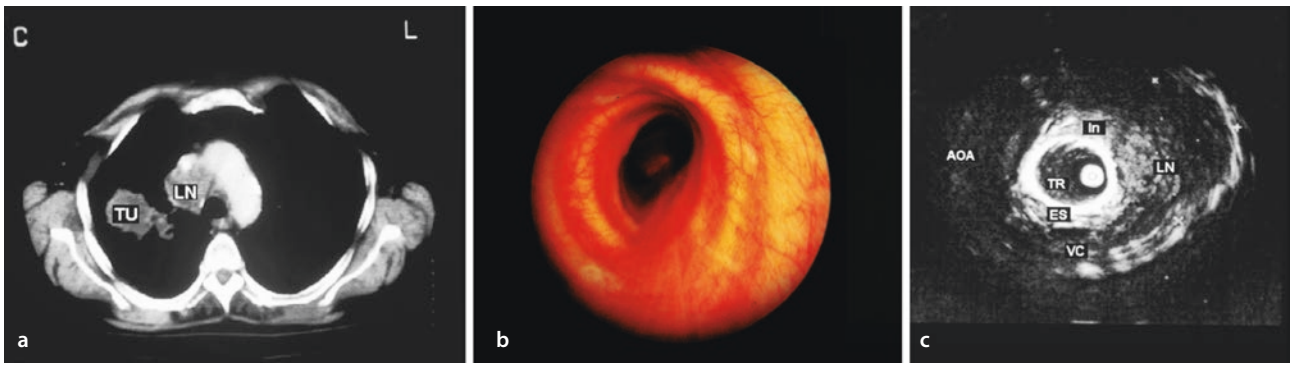

Fig. 7.1 **a–c** Excision of the wall infiltration. *TU* tumor, *LN* lymph node, *AOA* ascending aorta, *TR* trachea, *ES* endoscopic probe, *ln* small lymph node, *VC* vena cava

Fig. 7.2 Head of the sonography bronchoscope

outer diameter of the insertion tube is 6.2 mm. The angulation range of the distal end of the endoscope is 160° upward and 90° downward. The instrument has a small curved linear-array electronic transducer, of length 10 mm, located at the distal end of the endoscope in front of a 30° oblique forward-viewing fiber-optic lens (angle of view 80). The endoscope has a biopsy channel of 2 mm. The ultrasonic frequency is 7.5 MHz with a penetration depth of 5 cm. The scanning direction is parallel to the longitudinal axis of the endoscope with a scanning angle of 50°, which enables full sonographic monitoring of a needle when it is inserted via the biopsy channel during scanning (Krasnik et al. 2003).

7.2 Sonographic Anatomy

The wall of the central airways show a seven-layer structure which can be demonstrated by high magnification only. The layers represent the mucosa and submucosa, the three layers of the cartilage and the adjacent external structures of loose and dense connective tissue, respectively (Kurimoto et al. 1999). Under low-power magnification and in the periphery only a three-layer structure is visible. Orientation by sonography within the mediastinum is difficult. Besides the complex mediastinal anatomy this is due to motion artifacts by pulsation and respiration as well as the unusual planes of the sonography images as with the probes we have to follow the course of the airways. For orientation, therefore, the analysis of characteristic anatomical structures is more reliable than observation of the position of the sonography probe inside the airway. Vessels can be diagnosed by their pulsation. But even after application of echo contrast media discrimination of venous and arterial vessels can be difficult owing to the great number of variations. However, as during the procedure pulse oxymetry is applied, arterial pulsations can be diagnosed according to their synchronism with the acoustic signal. Lymph nodes and solid structures can be differentiated down to a size of a few millimeters from the blood vessels by their higher echodensity.

7.3 Indications and Results for the Endobronchial Sonography Miniprobe

Since 1999 the probe has been on the market and endobronchial sonography is applied in several centers worldwide. For some indications the superiority of sonography over conventional imaging has been proven in prospective studies and in some centers endobronchial sonography is already established as a routine procedure According to the structures that can be analyzed, current indications comprise endoluminal, intramural and parabronchial structures; with respect to medical indications, early detection and tumor staging, inflammatory destruction of the airways, mediastinal lesions and malformations of mediastinal structures.

7.3.1 Early Cancer

In small radiologically invisible tumors the decision for local endoscopic therapeutic intervention is dependent on their intraluminal and intramural extent within the different layers of the wall. In contrast to radiological imaging by endobronchial sonography even very small tumors of a few millimeters can be analyzed and differentiated from benign lesions. As different authors demonstrated, endobronchial sonography is a very reliable tool in analyzing the extent of these small lesions. We could demonstrate that by endobronchial sonography in small autofluorescence-positive lesions that were negative in white light bronchoscopy we could improve specificity (predicting malignancy) from 50 to 90. Combination of endobronchial sonography with autofluorescence has been proven to be efficient in prospective studies and today has become the basis for curative endobronchial treatment of malignancies in some institutions (Herth et al. 2002; Miyazu et al. 2002; ◘ Fig. 7.3). The most important paper in this respect was that of Miazyu et al. They used the finding of endobronchial sonography for the therapy decision in patients with early cancer lesions. In 18 patients they found nine with a tumor limation to the bronchial wall; these patients were treated with photodynamic therapy. All other patients had extracartalignous tumor growing and were treated nonendoscopically (surgery, radiation and chemotherapy). Using the finding as a decision maker they achieved a 100% complete remission rate in the endoluminal treated group. In a mean follow-up time of 32 months none of the patients developed a recurrence. Compared with earlier published trials using endoluminal techniques in early cancer lesions, they could show that with the help of endobronchial sonography, endoluminal-treatable patients could be identified.

7.3.2 Advanced Cancer

In preoperative staging, endobronchial sonography allows detailed analysis of intraluminal, submucosal and intramural tumor spread, which can be essential for

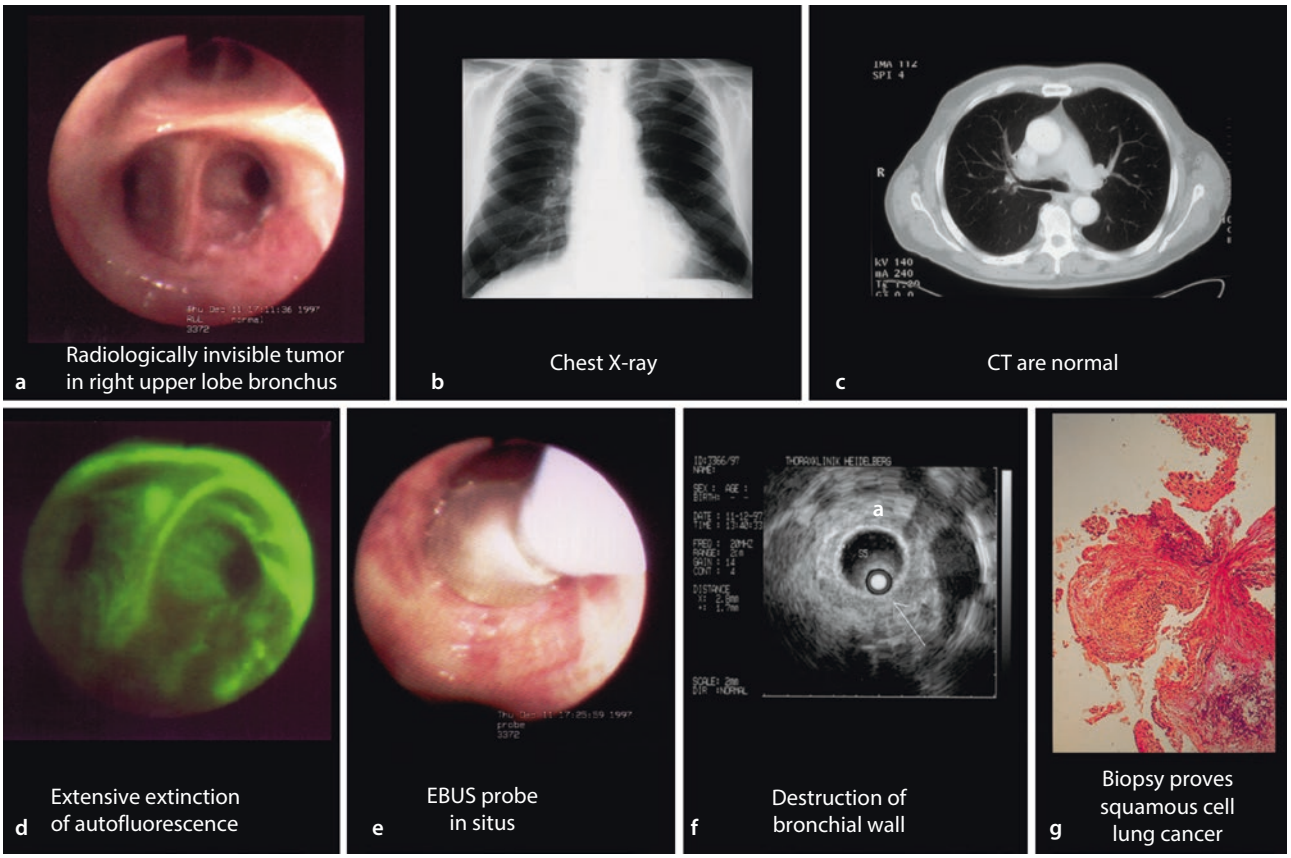

Fig. 7.3 **a–g** Local staging of an early carcinoma. The arrow in **f** shows the destruction of the bronchial wall by the tumor

decisions regarding resection margins. Endobronchial sonography proved especially useful in diagnosis of mediastinal tumor involvement in the great vessels such as the aorta, the vena cava, the main pulmonary arteries and the esophageal wall which by conventional radiology frequently is impossible. In a trial it was shown that differentiation of external tumor invasion from impression of the tracheobronchial wall by endobronchial sonography is highly reliable (94%) in contrast to computed tomography imaging (51%). One hundred and four patients with a central tumor were examined with endobronchial sonography and computed tomography and the tumors were classified into invasion or impression types. All patients underwent surgery, and the findings were compared with the initial classification. The sensitivity (from 89% to 25%) and also the specificity (from 100% to 89%) shows the superiority of the sonography technique in the differentiation between airway infiltration and compression by tumor. Thus, many patients considered to be nonresectable by the radiologist owing to supposed T4 tumors could be operated on in a curative approach after use of endobronchial sonography (Herth et al. 2003) (Fig. 7.4).

7.3.3 Peripheral Lesions

For histological diagnosis of peripheral intrapulmonary lesions by bronchoscopy an instrumental approach under fluoroscopic or computed tomography guidance is the standard procedure Fig. 7.5a–c. This demands expensive X-ray equipment in the bronchoscopy suite or coordination with the radiology department and causes exposure to radiation for the patient and the staff. In a prospective study we were able to show that those lesions could be approached by endobronchial sonography guidance with the same success rate of approximately 75%. Recently these data were confirmed by a group of

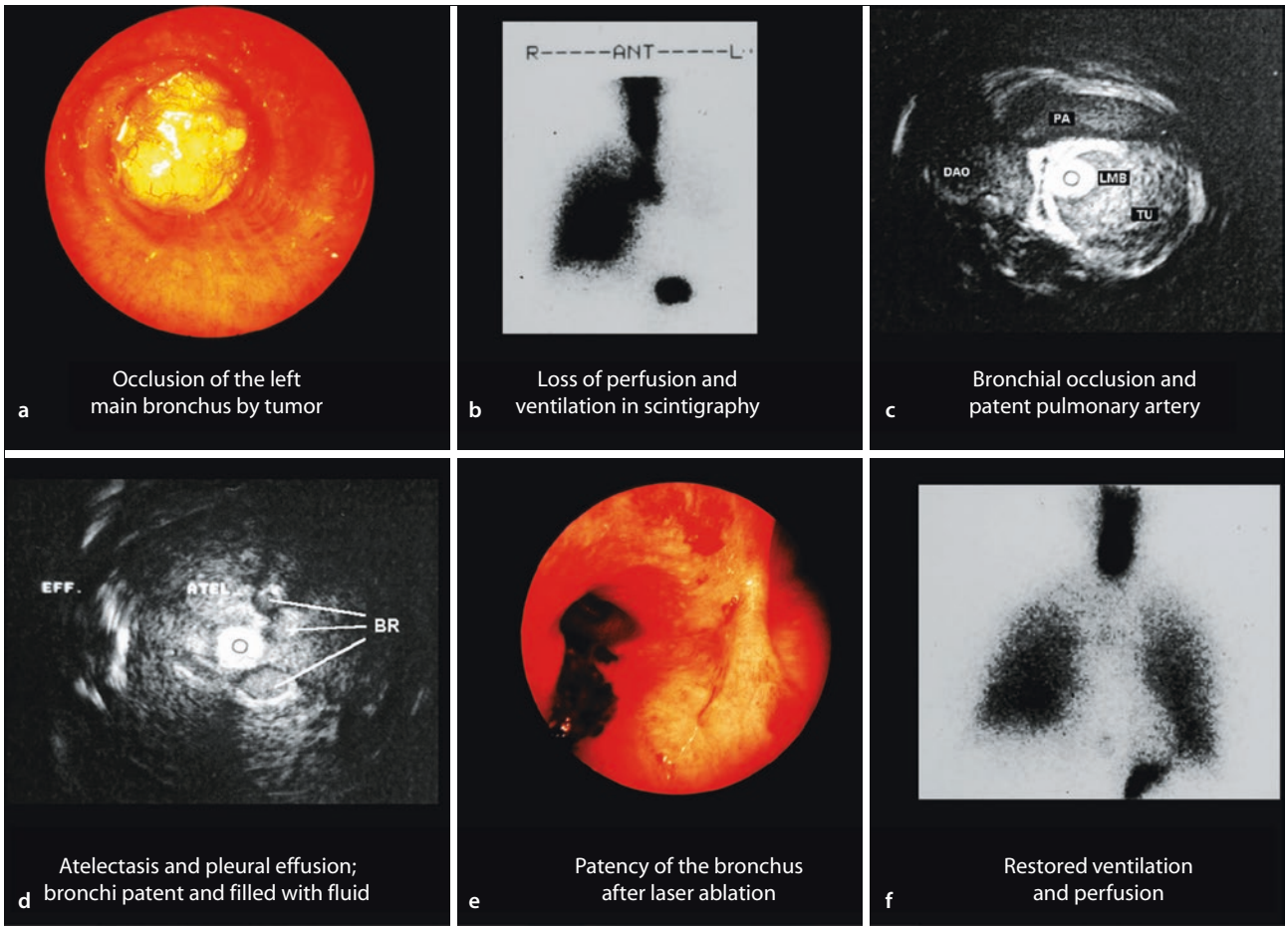

Fig. 7.4 **a–f** Local staging of an advanced tumor. *DAO* descending aorta, *PA* pulmonary artery, *TU* tumor, *LMB* left main bronchus

Japanese bronchologists. Shirakawa et al. also achieved a diagnostic yield of 75% using the miniprobe as a guidance tool for the forceps (Omori et al. 2002; Herth et al. 2002, 2006a; Eberhardt et al. 2007, 2009).

7.3.4 Lymph Node Staging

Under favorable conditions lymph nodes can be detected by endobronchial sonography down to a size of 2–3 mm and the internal structure (sinuses and folliculi) as well as small lymph vessels can be analyzed. By endosonographic localization of lymph nodes the results of TBNA can be significantly improved up to 85%. This is especially true for those positions in which reliable landmarks on the computed tomogram are missing, e.g., high and low paratracheal localization. Herth et al. (2004) investigated the results of an endobronchial sonography-guided TBNA compared with those of conventional TBNA. In this randomized study, they confirmed that the yield of an endobronchial sonography-guided TBNA is higher than that of the conventional TBNA (85% vs. 66%). In an additional analysis of the lymph node station they showed that especially in locations without endoscopic landmarks (lymph node stations 2, 3, 4, Mountain scheme) the detection technique is helpful to increase the yield. On the other hand, they showed that in the case of enlarged subcarinal nodes a conventional TBNA has the same yield as the TBNA after endobronchial sonography detection (Takemoto et al. 2000; Yasufuku et al. 2004).

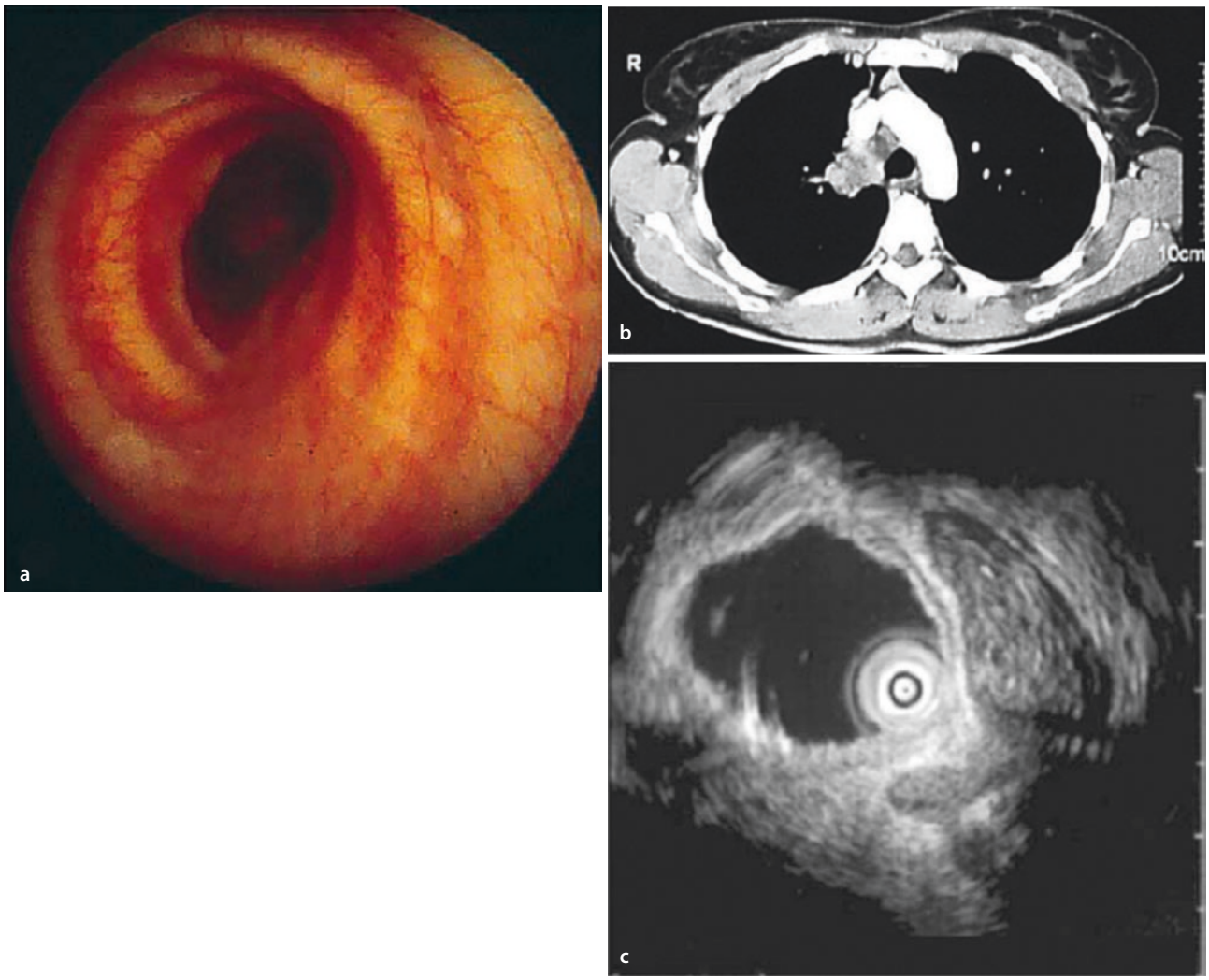

Fig. 7.5 **a–c** Compression of the trachea by a tumor. **a** Bronchoscopy reveals an impression of the trachea. **b** The corresponding CT image shows a mass in the upper lobe. **c** Ultrasound reveals a well-defined tumor; an infiltration is unlikely

7.3.5 Endobronchial Sonography in Therapeutic Interventions

Especially for making decisions in potentially curative endobronchial therapy of malignancies such as photodynamic therapy or endoluminal high-dose radiation by brachytherapy, diagnosis of limitation of the lesion to the bronchial wall or to the close vicinity is essential. Here endobronchial sonography is superior to all other imaging procedures owing to the detailed analysis of the layers of the bronchial wall.

In decision-making for endobronchial therapy of advanced lung cancer, endobronchial sonography provides important data (Herth et al. 2003). In complete bronchial obstruction, the base and the surface of the tumor can be assessed as can whether the different layers of the bronchial wall are involved, how far the tumor is penetrating into the mediastinal structures and whether the airways beyond the stenosis are patent. Also patency of the adjacent pulmonary artery can be diagnosed, which is important to predict postinterventional perfusion of the dependent lung and prevent increase of dead-space ventilation (Fig. 7.6). Endobronchial sonography is also useful for exploration of benign central airway stenosis to assess the extent and the cause of the disease, the relationship to vessels and other surrounding structures and to make the correct decision for therapy, such as mechanical dilatation, laser ablation or stent implantation and endoscopic control of the results Fig. 7.7a–c.

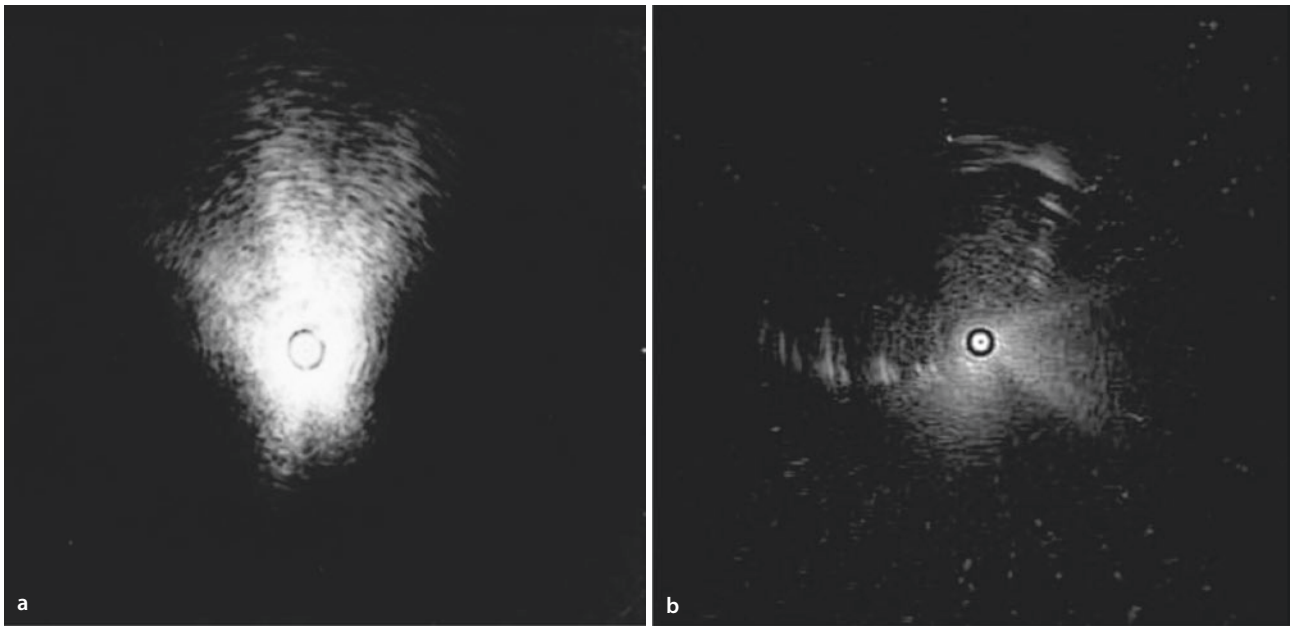

Fig. 7.6 **a** Complete reflection of sound waves in lung parenchyma. **b** A peripheral intrapulmonary lesion can be distinguished from the lung parenchyma with the probe head

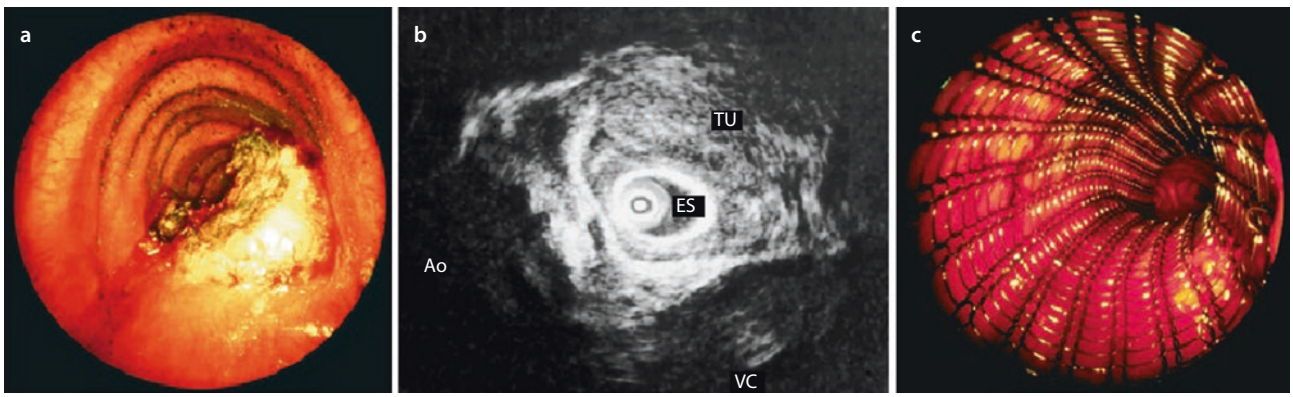

Tracheal tumor after partial laser ablation

Infiltration of anterior esophageal wall

Palliative stent insertion before external radiation due to risk of esophagotracheal fistula

Fig. 7.7 **a–c** Tumor in the trachea, after partial laser resection an infiltration in the esophageal wall is detected by EBUS and a stent was placed before the additional treatment

7.4 Indications and Results for the Endobronchial Ultrasound Guided Transbronchial Needle Aspiration (EBUS-TBNA)

The lymph node staging is also the main indication for the new endobronchial sonography TBNA scope.

The sonography bronchoscope is introduced via an endotracheal tube under visual control or under local anesthesia to the area of interest. Endobronchial ultrasound TBNA is performed by direct transducer contact with the wall of the trachea or bronchus. When a lesion is outlined, a 19, 21, or 2522-gauge full-length steel needle is introduced via the biopsy channel of the endoscope. Power-Doppler examination is used immediately before the biopsy in order to avoid unintended puncture of vessels between the wall of the bronchi and the lesion. Under real-time sonographic guidance the needle is placed in the lesion Fig. 7.8. Suction was applied with

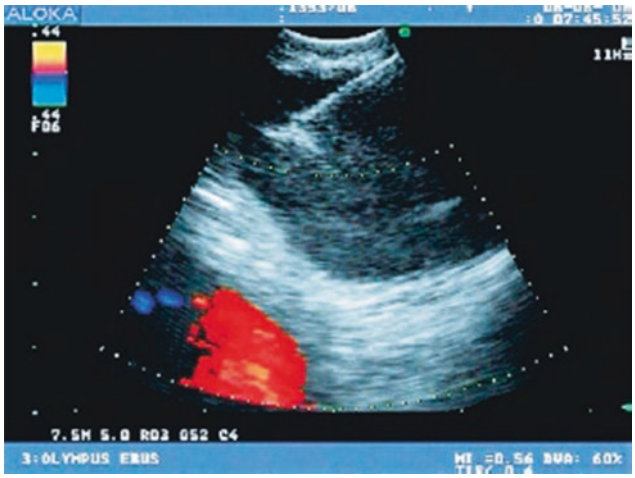

Fig. 7.8 Ultrasound-controlled lymph node puncture. The needle is clearly delineated in the lymph node

a syringe and the needle was moved back and forth inside the lesion.

To date, several papers have been published on this procedure (Bonta et al. 2016).

The largest trial (Herth et al. 2006b) reports the results of the technique in 502 patients. A total of 572 lymph nodes were punctured, and 535 (94%) resulted in a diagnosis. Biopsies were taken from all reachable lymph node stations (2l, 2r, 3, 4r, 4l, 7, 10r, 10l, 11r and 11l). The mean diameter of the nodes was 1.6 cm (0.36 cm) and the range was 0.8–3.2 cm. The sensitivity was 92%, the specificity was 100% and the positive predictive value was 93%. Like in all other trials no complications occurred.

Herth et al. (2006c) also examined the accuracy of endobronchial sonography TBNA in sampling nodes less than 1 cm in diameter. Among 100 patients, 119 lymph nodes with a size between 4 and 10 mm were detected and sampled. Malignancy was detected in 19 patients but missed in two others; all diagnoses were confirmed by surgical findings. The mean diameter of the punctured lymph nodes was 8.1 mm. The sensitivity of endobronchial sonography TBNA for detecting malignancy was 92.3%, the specificity was 100% and the negative predictive value was 96.3%. Again no complications occurred. They summarized that endobronchial sonography TBNA can sample even small mediastinal nodes, therefore avoiding unnecessary surgical exploration in one fifth of patients who have no computed tomography evidence of mediastinal disease. Potentially operable patients with clinically non-metastatic non-small-cell lung cancer may benefit from presurgical endobronchial sonography TBNA biopsies and staging (Herth et al. 2008, 2010; Ernst et al. 2010.

7.5 Endoesopahgeal Ultrasound with the EBUS Scope (EUS-B)

The endoscopic techniques introduced to pulmonary diagnostics are: endobronchial ultrasound-guided transbronchial needle aspiration (EBUS-TBNA) and endoscopic ultrasound-guided fine needle aspiration (EUS-FNA). Nowaday more and more often in use is the ultrasound bronchoscope (EUS-B in the esophagus ().The use of endoscopic ultrasound with bronchoscope-guided fine-needle aspiration (EUS-B-FNA) has been described in the evaluation of mediastinal lymphadenopathy

The optimal approach (transbronchial or transesophageal) and the selection of mediastinal lymph node stations considered for biopsy still need evaluation. In a recent published metaanalysis 10 studies (1080 subjects with mediastinal lymphadenopathy) were summarized. The sensitivity of the combined procedure was significantly higher than EBUS-TBNA alone (91% vs 80%, $P = .004$), in staging of lung cancer (4 studies, 465 subjects). The additional diagnostic gain of EUS-B-FNA over EBUS-TBNA was 7.6% in the diagnosis of mediastinal adenopathy (Dhooria et al. 2015). No serious complication of EUS-B-FNA procedure was reported. Therefore, combining EBUS-TBNA and EUS-B-FNA is an effective and safe method, superior to EBUS-TBNA alone, in the diagnosis of mediastinal lymphadenopathy.

Summary

Endobronchial sonography has been widely available for more than 8 years. A growing body of good-quality literature supports its significant role in airway assessment and procedure guidance. Its usefulness is especially well documented in lymph node staging via guided TBNA and in lending support for therapeutic decision-making with regard to endoluminal or alternative treatment strategies for malignant airway abnormalities.

Endobronchial sonography is a routine adjunct to endoscopy in many centers, and we expect its role to grow in the near future.

References

Bonta PI, Crombag L, Annema JT (2016) Linear endobronchial and endoesophageal ultrasound: a practice change in thoracic medicine. Curr Opin Pulm Med 22(3):281–288

Dhooria S, Aggarwal AN, Gupta D, Behera D, Agarwal R (2015) Utility and safety of endoscopic ultrasound with bronchoscope-guided fine-needle aspiration in mediastinal lymph node sam-

pling: systematic review and meta-analysis. Respir Care 60(7):1040–1050
Eberhardt R, Anantham D, Ernst A, Feller-Kopman D, Herth F (2007) Multimodality bronchoscopic diagnosis of peripheral lung lesions: a randomized trial. Am J Respir Crit Care Med 176:36–41
Eberhardt R, Ernst A, Herth F (2009) Ultrasound-guided transbronchial biopsy of solitary pulmonary nodules less than 20 mm. Eur Respir J 34:1284–1287
Ernst A, Simoff M, Ost D, Michaud G, Chandra D, Herth FJ (2010) A multicenter, prospective, advanced diagnostic bronchoscopy outcomes registry. Chest 138:165–170
Herth F, Becker HD (2000) Endobronchial ultrasound of the airways and the mediastinum. Monaldi Arch Chest Dis 55:36–45
Herth F, Ernst A, Becker HD (2002) Endobronchial ultrasound in therapeutic bronchoscopy. Eur Respir J 20:118–121
Herth FJ, Ernst A, Schulz M, Becker HD (2003) Endobronchial ultrasound reliably differentiates between airway infiltration and compression by tumor. Chest 123:458–462
Herth F, Becker HD, Ernst A (2004) Conventional vs endobronchial ultrasound-guided transbronchial needle aspiration: a randomized trial. Chest 125:322–325
Herth FJ, Eberhardt R, Vilmann P, Krasnik M, Ernst A (2006a) Realtime, endobronchial ultrasound-guided, transbronchial needle aspiration: a new method for sampling mediastinal lymph nodes. Thorax 61(9):795–798
Herth FJ, Eberhardt R, Becker HD, Ernst A (2006b) Endobronchial ultrasound-guided transbronchial lung biopsy in fluoroscopically invisible solitary pulmonary nodules: a prospective trial. Chest 129:147–150
Herth FJF, Krasnik M, Eberhardt R, Ernst A, Vilman P, Dienemann H (2006c) EBUS guided biopsy for the staging of mediastinal lymph nodes in a radiologically normal mediastinum. Eur Respir J 28:910–914
Herth FJH, Annema JT, Eberhardt R, Yasufuku K, Ernst A, Krasnik M, Rintoul RC (2008) Endobronchial ultrasound with transbronchial needle aspiration for restaging the mediastinum in lung cancer. J Clin Oncol 26:3346–3350
Herth FJ, Krasnik M, Kahn N, Eberhardt R, Ernst A (2010) Combined endoscopic-endobronchial ultrasound-guided fine-needle aspiration of mediastinal lymph nodes through a single bronchoscope in 150 patients with suspected lung cancer. Chest 138:790–794
Hürther T, Hanrath P (1990) Endobronchiale Songraphie zur Diagnostik pulmonaler und mediastinaler Tumoren. Dtsch Med Wochenschr 115:1899–1905
Krasnik M, Vilmann P, Larsen SS, Jacobsen GK (2003) Preliminary experience with a new method of endoscopic transbronchial real time ultrasound guided biopsy for diagnosis of mediastinal and hilar lesions. Thorax 58:1083–1086
Kurimoto N, Murayama M, Yoshioka S, Nishisaka T, Inai K, Dohi K (1999) Assessment of usefulness of endobronchial ultrasonography in determination of depth of tracheobronchial tumor invasion. Chest 115(6):1500–1506
Miyazu Y, Miyazawa T, Kurimoto N, Iwamoto Y, Kanoh K, Kohno N (2002) Endobronchial ultrasonography in the assessment of centrally located early-stage lung cancer before photodynamic therapy. Am J Respir Crit Care Med 165:832–837
Omori S, Takiguchi Y, Hiroshima K et al (2002) Peripheral pulmonary diseases: evaluation with endobronchial US initial experience. Radiology 224(2):603–608
Ono R, Hirano H, Egawa S, Suemasu K (1994) Bronchoscopic ultrasonography and brachytherapy in roentgenologically occult bronchogenic carcinoma. J Bronchol 1:281–287
Sihoe AD, Yim AP (2004) Lung cancer staging. J Surg Res 117:92–106
Takemoto Y, Kawahara M, Ogawara M et al (2000) Ultrasoundguided flexible bronchoscopy for the diagnosis of tumor invasion to the bronchial wall and mediastinum. J Bronchol 7(2):127–132
Yasufuku K, Chhajed PN, Sekine Y, Nakajima T, Chiyo M, Iyoda A, Yoshida S et al (2004) Endobronchial ultrasound using a new convex probe: a preliminary study on surgically resected specimens. Oncol Rep 11:293–296

Vascularization and Contrast Enhanced Ultrasound (CEUS)

C. Görg and E. Safai Zadeh

Contents

G. Mathis (ed.), *Chest Sonography*, https://doi.org/10.1007/978-3-031-09442-2_8

In addition to the sonographic characteristics of the B-mode ultrasound (B-mode US), the type of vascularization is of major importance for assessment of a lesion in terms of differential diagnosis. In sonographic examinations, the established procedures of color-Doppler sonography (CDS) and contrast enhanced ultrasound (CEUS) are used for this purpose. Guidelines for the use of CEUS are discussed on a regular basis and published in special consensus meetings (2004, 2008, 2011, 2018). However, the authors recommend the use of CEUS on the thorax depending on indications, generally with a low level of evidence (Sidhu et al. 2018; Jacobsen et al. 2020).

In recent years, CDS characteristics of bacterial pneumonia, obstructive atelectasis, lung infiltrates and bronchial carcinoma have been described (overview: Görg and Bert 2004a, b). An increasing number of studies have indicated that CEUS can be performed on the thorax and that various lung diseases are characterized by distinctive CEUS findings (overview: Görg et al. 2006a; Görg 2007; Siduh et al. 2018).

The aim of this review is to describe CDS and CEUS findings for peripheral lung consolidation.

8.1 Pathophysiological Basics

The lung is characterized by dual vascularization. Vascularization is achieved on the one hand by lung circulation, which is responsible for pulmonary gas exchange. Lung circulation is accomplished by the pulmonary arteries and their ramifications as well as venules and lung veins. The lung itself is nourished by the bronchial arteries.

In contrast to systemic circulation, circulation by the pulmonary arteries is marked by specific characteristics. Pulmonary arteries and their initial branches are elastic. The subsequent arteries have muscular walls. From the level of the arterioles onward, these arteries turn into partly muscular and nonmuscular precapillaries. In contrast to systemic circulation in which arterioles are the main vessels of resistance, in lung circulation the resistance is more or less equally distributed between arteries, capillaries and veins. Thus, flow in the pulmonary arteries and capillaries is pulsatile and not continuous. In contrast to hypoxic vasodilatation in systemic circulation, hypoxic vasoconstriction occurs in lung circulation. The purpose of such vasoconstriction is to reduce the intrapulmonary shunt volume (Euler–Liljestrand mechanism) (Quaranto et al. 2020). When lung tissue is affected by a malignant tumor, the carcinoma has been reported to invade the pulmonary arteries of the affected lung segment in 56–87% of cases (Kolin and Koutllakis 1988; Fissler-Eickhoff and Müller 1994). Particularly in the center of the tumor the regular vascular pattern is completely altered. Vascularization is reduced by stenosis and occlusion of the pulmonary arteries.

As a rule, the bronchial arteries originate on the left side from the aortic arch and on the right side from the intercostal artery. They form a vascular ring at the hilum of the lung. From this vascular ring the arterial branches run parallel to the respiratory bronchial branches and the pulmonary vessels (Fig. 8.1). The arterial bronchial branches (rami bronchiales) supply the bronchi, pulmonary vessels, alveoles and supporting tissue. Interstitial arterial branches run into the interlobar and interlobular septa and supply the visceral pleura. Anastomoses (blocked arteries) between the two systems are normally closed. In cases of occluded pulmonary vessels, the anastomoses become open owing to hypoxia and blood supply is provided by bronchial arteries. Angiographic studies have shown that particularly peripheral lung processes at the pleural wall, such as benign cavitary lesions, lung cysts, lung abscesses and liquefying pneumonia, are nourished by bronchial arteries (Görg and Bert 2004a). However, malignant primary lung tumors and lung metastases are vascularized by bronchial arteries to a differing extent (Müller and Meyer-Schwickerath 1978; Fig. 8.2).

The intercostal arteries originate from the thoracic aorta and run a strictly intercostal course in the chest wall along the ribs. They are the only vessels that can be visualized on sonography, even in healthy volunteers.

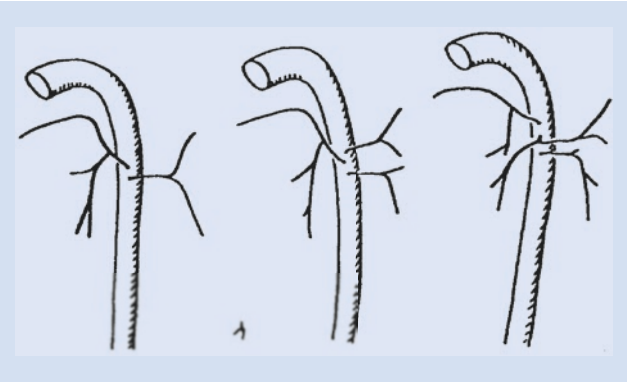

Fig. 8.1 Schematic illustration of the anatomy of the bronchial arteries. (Uflacker L et al. 1985, Radiologie 157: 637–644)

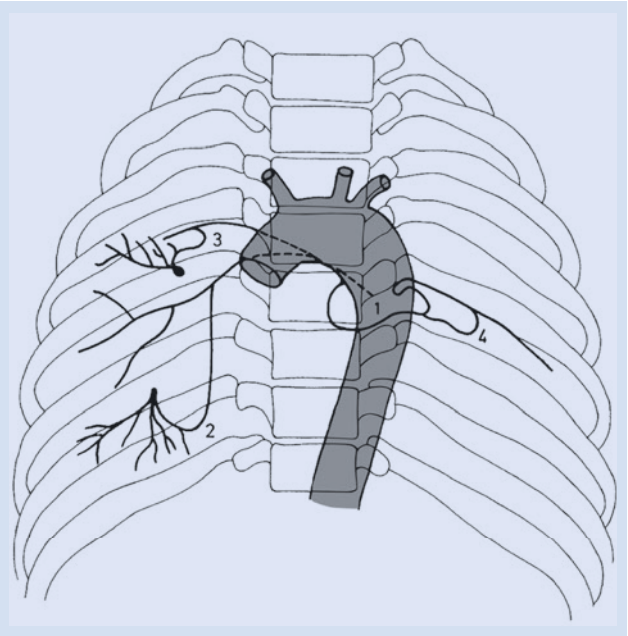

Fig. 8.2 Schematic illustration of the pathophysiology of the supply of the bronchial arteries. **1** bronchobronchial anastomoses, **2** bronchopulmonary anastomoses, **3** intercostopulmonary anastomoses, **4** intercostobronchial anastomoses (Babo et al. 1979)

Particularly in cases of lesions in the chest wall these vessels play an important role in tumor vascularization.

Tumor neoangiogenesis of primary bronchial carcinomas mainly originates in the bronchial arteries. The neoangiogenesis potential of pulmonary vessels appears to be low (Müller and Meyer-Schwickerath 1978; Hsu et al. 1996).

8.2 Principles of Color-Doppler Sonography (CDS)

The hemodynamic parameters used in transcutaneous CDS at the chest to evaluate vessels can be divided into qualitative and semiquantitative parameters (Overview).

Sonographic Analysis of Thoracic Perfusion

1. Qualitative findings of parenchymal perfusion
   - Absence of flow signals
   - Sporadic flow signals
   - Pronounced flow signals
   - Arterial turbulence phenomena
2. Spectral curve analysis: with patterns of different arterial flow signals
   - Pulmonary artery (PA)
   - Bronchial artery (BA)
   - Intercostal artery (ICA)
   - Tumor neoangiogenesis (TN)
3. Contrast-enhanced ultrasound with different criteria of assessment
   a. Time to enhancement (TE)
   b. Extent of enhancement (EE)
   c. Homogeneity of enhancement (HE)
   d. Decrease of enhancement (DE)

Qualitative findings include assessment of the presence, the direction and the characteristics of blood flow. In this regard a distinction is made between the absence of flow signals (FS; Fig. 8.3), evidence of individual flow signals (Fig. 8.4), evidence of markedly disorganized vascularization (Fig. 8.5) or pronounced regular tree-shaped vascularization (Fig. 8.6) and evidence of arterial turbulence phenomena in consolidated areas (Fig. 8.7). Semiquantitative parameters such as the resistance index and the pulsatility index are used for spectral curve analysis of arterial blood flow. Spectral curves of pulmonary arteries, bronchial arteries, intercostal arteries and arteries of tumor angiogenesis can be differentiated within pathological processes, and can be used to differentiate ambiguous peripheral lung lesions. In principle, evidence and documentation of flow signals at the chest is device-dependent and is additionally influenced and limited by the location and the size of the lesion, its cause, and breath-dependent or pulsation-dependent movements. For instance, 20% of peripheral lung lesions emit no flow signals (Yuan et al. 1994). Local fluid, lung cysts and lung infarctions show no flow signals on CDS. The color- Doppler sonography pattern of poorly visualized vessels is primarily seen in malignant pleural lesions. Markedly ramified vessels are characteristic for pneumonia and atelectasis (Yuan et al. 1994; Civardi et al. 1993). Turbulence phenomena within a lesion have been reported in pleural arteriovenous fistulae and vascular abnormalities in connection with Osler's disease (Fig. 8.7).

Quantitative parameters such as the resistance index and the pulsatility index are used to analyze arterial spectral curves. Civardi et al. (1993) were the first to perform quantitative and qualitative spectral curve

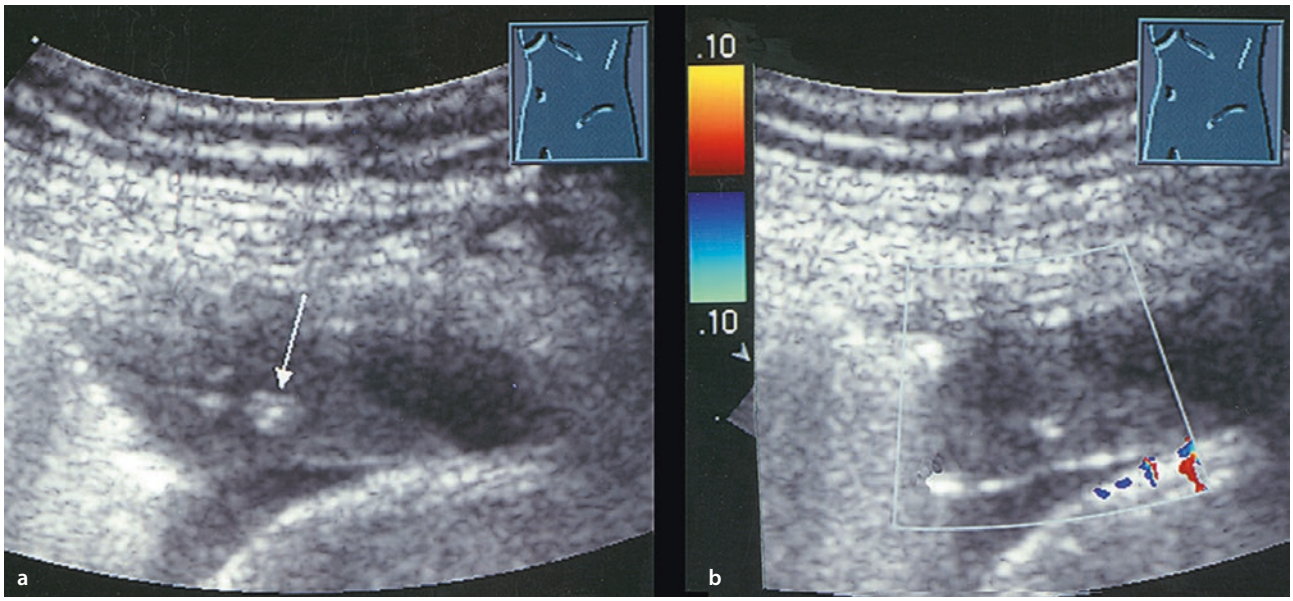

Fig. 8.3 a, b A 43-year-old man with a lung infarction. **a** On the B-mode ultrasound one finds a hypoechoic wedge-shaped lesion with a central bronchial reflex (arrow). **b** CDS shows the absence of vascularization

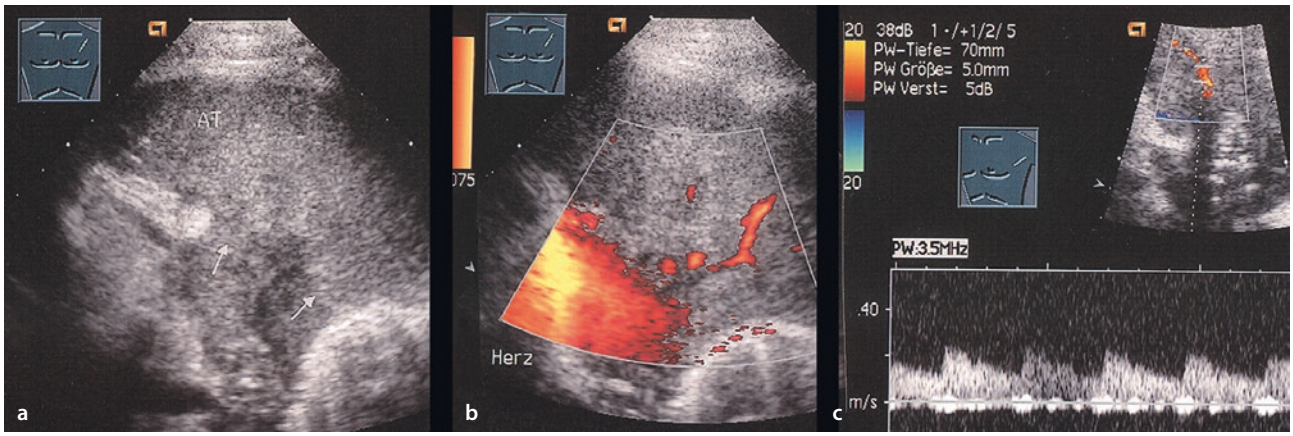

Fig. 8.4 a–c 36-year-old man with Hodgkin's disease in the mediastinum. **a** On the B-mode ultrasound one finds a hypoechoic central tumor formation with atelectasis (AT; arrows). **b** CDS shows reduced vascularization within the atelectasis, which is a sign of. constriction of the pulmonary artery. **c** Spectral curve analysis shows a monophasic flow signal with reduced arterial flow resistance index, indicative of a bronchial artery

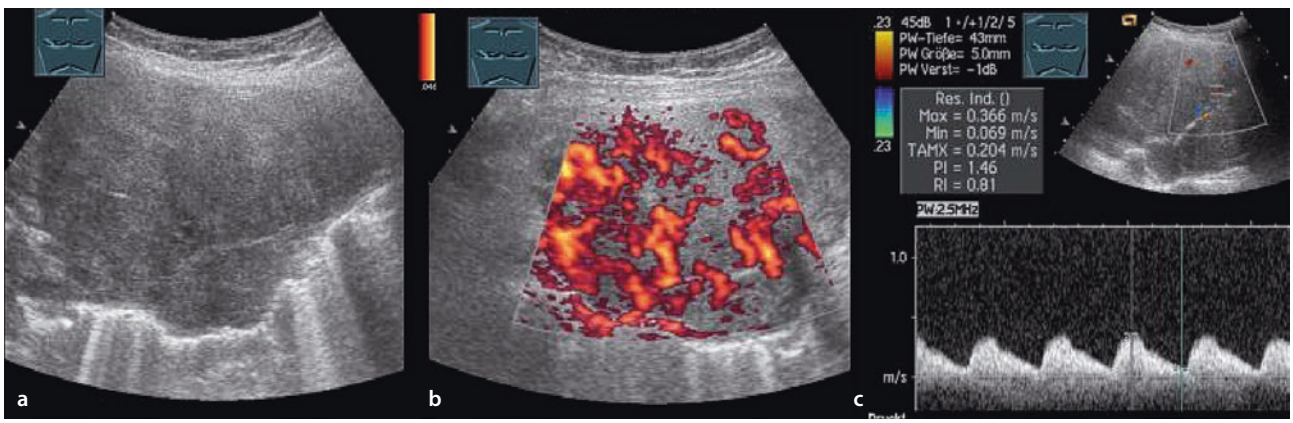

Fig. 8.5 a–c A 62-year-old man with lung metastases in the presence of renal cell carcinoma **a** The B-mode ultrasound reveals a large hypoechoic round lesion. **b** CDS shows strong and chaotic distributed vessels. **c** Spectral curve analysis shows a monophasic flow signal indicative of a bronchial artery

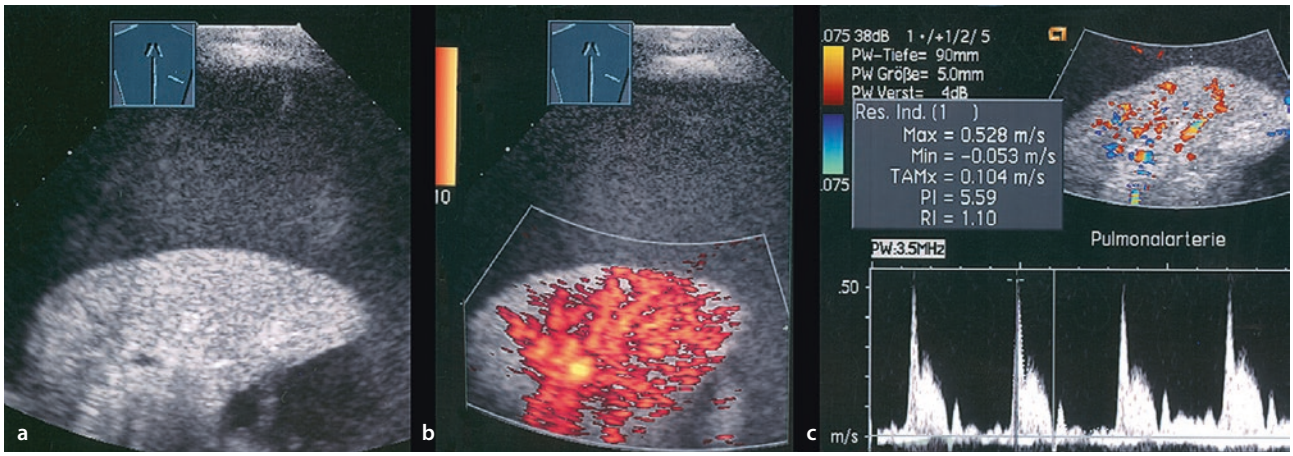

Fig. 8.6 a–c A 37-year-old man with a pleural effusion and compressive atelectasis. **a** B-mode ultrasound reveals a pleural effusion with atelectasis in the lung. **b** CDS sonography shows a regular tree like perfusion. **c** Spectral curve analysis shows a high-impedance flow pattern, indicative of a pulmonary artery

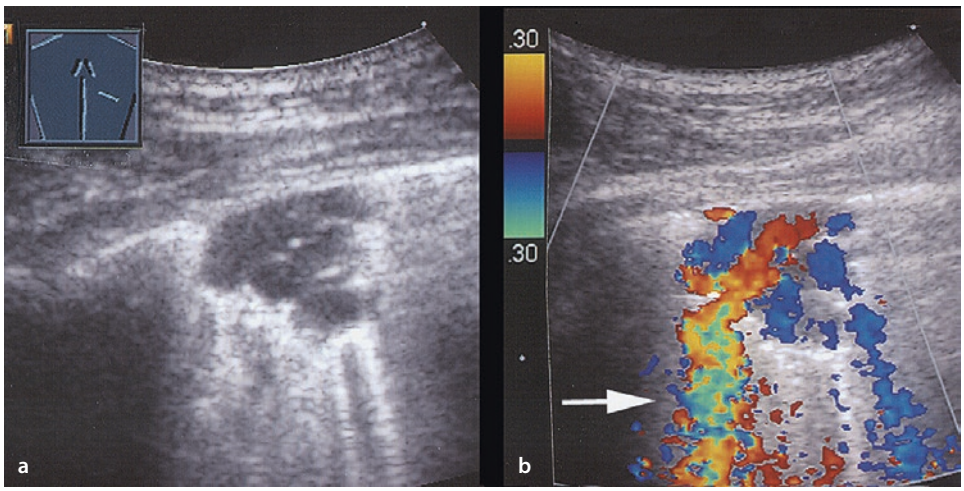

Fig. 8.7 a, b A 14-year-old male patient with Osler–Weber–Rendu syndrome. **a** The B-mode ultrasound shows an anechoic space occupying lesion close to the pleura. **b** CDS reveals a large vessel that supplies the ectatic vessels close to the pleura. On spectral curve analysis this vessel was identified as a pulmonary artery

analyses for peripheral lung lesions. They found a triphasic flow signal more commonly in benign lesions and a monophasic flow signal in malignant lesions. Yuan et al. (1994) registered a sensitivity and specificity of more than 95% for differentiation of benign lesions from malignant ones by the use of arterial spectral curve analysis. The authors interpreted the monophasic low-impedance flow primarily seen in tumors as flow signals of tumor neoangiogenesis, while they correlated the high-impedance flow of pneumonias and atelectases with vessels of the pulmonary arteries (Yuan et al. 1994). In a subsequent study the authors registered different resistance indices for atelectasis and pneumonia, indicative of differing vasoconstriction due to hypoxia (Yuan et al. 2000). In a controlled histological study, Hsu et al. (1996) were the first to show that the vessels from which low-impedance monophasic flow signals originated were not tumor vessels but were bronchial arteries. "True" tumor vessels are characterized by nearly constant flow without variations between the systolic and the diastolic phase (Hsu et al. 1996). Owing to the technical limitations of commercially available ultrasound devices for slow blood flow (less than 2 cm/s), tumor vessels are usually not seen

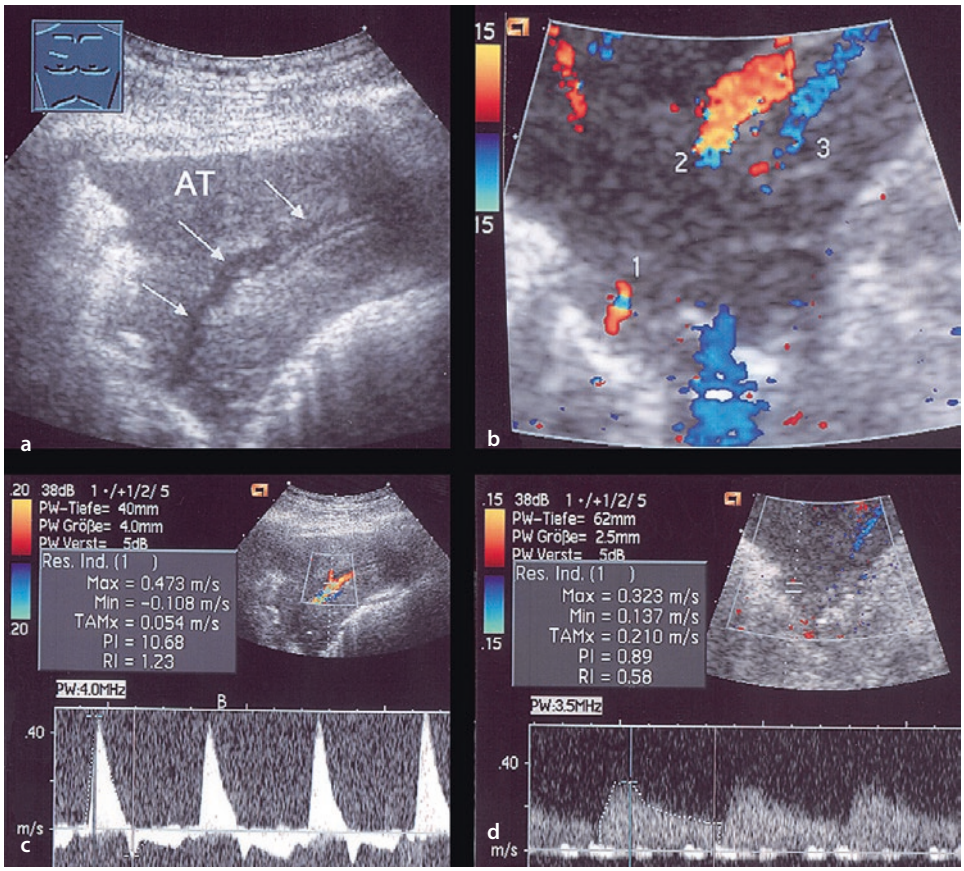

Fig. 8.8 a–d A 65-year-old man with a centrally located bronchial carcinoid tumor and obstructive atelectasis. **a** The B-mode ultrasound shows a triangular hypoechoic consolidation with a fluid bronchogram (arrows). AT atelectasis. **b** CDS reveals different vessels in the central region of the atelectasis (1 bronchial artery, 2 pulmonary artery, 3 pulmonary vein). **c** Spectral curve analysis shows a high-impedance triphasic flow signal as a sign of a pulmonary artery (designated 2 in b). **d** Spectral curve analysis reveals a low-impedance arterial flow signal oriented towards the periphery, indicative of a bronchial artery (designated 1 in b)

on sonography (Harvey and Albrecht 2001). In a subsequent study, Hsu et al. (1998) registered a much lower sensitivity and specificity of 53 and 72% for differentiation of benign lesions from malignant ones by the use of arterial spectral curve analysis. A common feature of all of these studies is that the authors only used one arterial spectral curve pattern to analyze a lesion. By sonographic "mapping," the authors of a more recent study were able to demonstrate several different flow signals within a lesion in nearly half of the patients with pleural lesions examined (Görg et al. 2003; ◘ Fig. 8.8). This may be interpreted as an indication of the fact that arterial blood supply to peripheral lung lesions is a complex phenomenon. In a subsequent study, chest wall lesions were examined with the aid of arterial spectral curve analysis and were found to be vascularized by intercostal arteries among other sources (Görg et al. 2005a). However, intercostal arteries have a monophasic high-impedance flow signal.

Thus, the following flow signals may be distinguished with the aid of arterial spectral curve analysis (◘ Fig. 8.9):

- ***Pulmonary arteries*** may be present in various locations, run a centrifugal course from the hilum to the surface of the lung and have a high-impedance, usually triphasic flow signal.
- ***Bronchial arteries*** are present in various locations, vary in terms of their direction of flow and have a low-impedance monophasic flow signal.
- ***Intercostal arteries*** are characterized by their strictly intercostal location, run a nearly horizontal course and have a high-impedance, usually monophasic flow signal.
- Arterial vessels of ***tumor neoangiogenesis*** are present in various locations, vary in terms of their direction of flow and are marked by a nearly constant flow with no variation between the systolic and the diastolic phase (◘ Fig. 8.10).

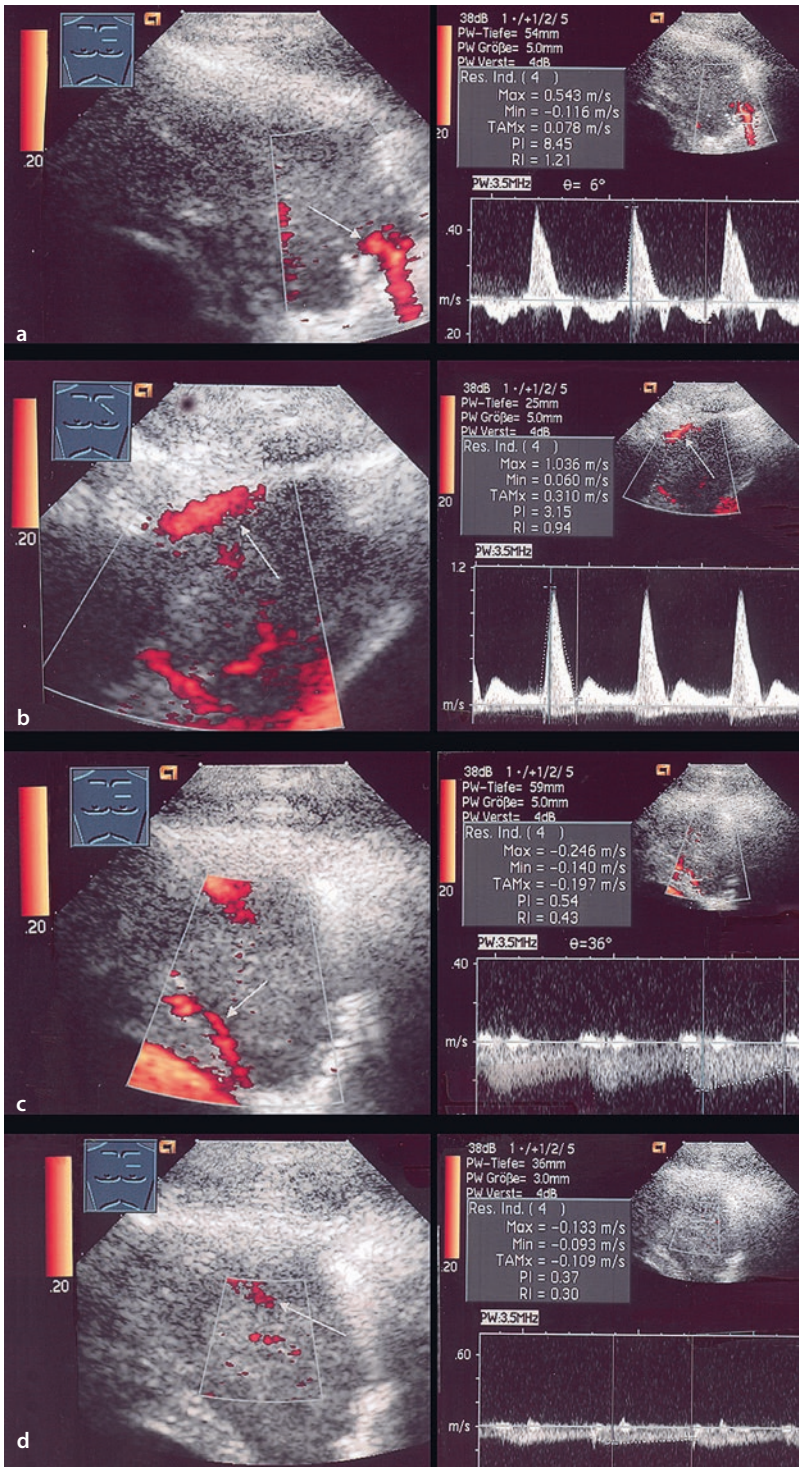

Fig. 8.9 a–d A 31-year-old man with a malignant lymphoma affecting the lung. **a** CDS shows a biphasic high-impedance flow pattern in the central region of the consolidated lung—a sign of a pulmonary artery (arrow). **b** In the periphery of the tumor there is a monophasic high-impedance arterial flow pattern, typical of an intercostal artery (arrow). **c** In the central region of the consolidated lung there is a monophasic low-impedance arterial flow signal—a sign of a bronchial artery (arrow). **d** Within the tumor one finds a nearly uniform flow signal without fluctuations in the diastolic and the systolic phase. Here one is inclined to suspect a vessel of tumor neoangiogenesis (arrow)

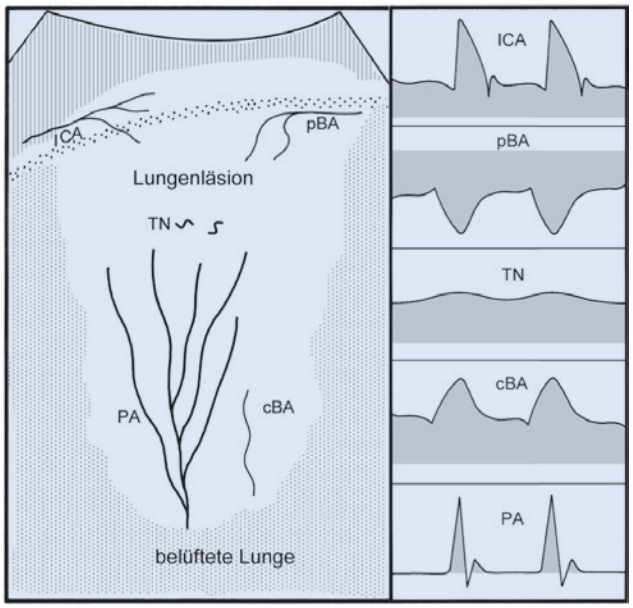

Fig. 8.10 Schematic illustration of possible arterial supply of pulmonary lesions with corresponding spectral curves. **ICA** intercostal artery, **pBA** peripheral bronchial artery, **TN** tumor neoangiogenesis, **cBA** central bronchial artery, **PA** pulmonary artery

8.3 Contrast Enhanced Ultrasound (CEUS)

In the last few years contrast-enhanced ultrasound (CEUS) has become a widely used procedure to investigate the liver, particularly to describe focal liver lesions. The second generation of contrast media now available for clinical use cause microscopic bubbles in the vessel lumen which lead to enhanced reflection of the ultrasound wave, thus increasing the signal amplitude and eventually yielding better contrast of vessels than that achieved with CDS. The use of CEUS allows infinitesimally small vessels whose width is just a little larger than that of capillaries to be visualized. In the experimental setting, vessels with a diameter of 74–134 µm were demonstrated by contrast-enhanced ultrasound. Vessels smaller than 38 µm in diameter have not been visualized thus far even with the use of contrast medium. The echogenicity of the contrast medium is caused by interface reflection off the gas bubbles and by backscattering, whereby the signal strength is amplified by 10^3 (Delorme et al. 2006).

In principle, CEUS should be applied according to the guidelines of the EFSUMB (Albrecht et al. 2004).

With regard to the application of CEUS in the lung it should be noted that, as with all transcutaneous sonographic modalities, investigation of the healthy lung is not possible. However, like the liver, the lung is marked by dual arterial supply and is therefore predestined for the use of CEUS. Consolidated lung tissue can be examined with CEUS. Pathological lung lesions are first characterized by arrival of contrast enhancement (time to enhancement = EE). In cases of perfusion by the pulmonary arteries alone, this time point is marked by early arterial contrast enhancement about 1–6 s after application of contrast medium. The contrast medium can be demonstrated by sonography in the right side of the heart just a few seconds later. The time until contrast-medium flooding depends on the type of access (peripheral-, central vein) and on hemodynamic parameters (heart failure, COPD). The arrival of a contrast agent to a lesion before the thoracic wall or a parenchymatous organ indicates pulmonary arterial perfusion. In cases of perfusion of a lesion by the bronchial arteries alone, contrast enhancement may be expected only after the contrast medium has passed through the lung. Thus, contrast enhancement of the left ventricle is seen at the earliest 7–10 s after application of contrast medium in the peripheral vein (Fig. 8.11). This is always performed simultaneously with the enhancement of the thoracic wall or parenchymatous organs as an indication of systemic arterial perfusion. The extent of contrast enhancement (EE) is basically dependent on the presence or absence of perfusion, the type of perfusion—whether through the pulmonary arteries or through the bronchial arteries—and also by the presence of collaterals or extent of vessels of tumor neoangiogenesis. Depending on the phase, a distinction may be made between the arterial phase (1–30 s) and the parenchymatous phase (1–5 min). The extent of contrast enhancement has been quantified so far only in comparison with an intra-individual reference; a distinction is made between reduced and increased contrast enhancement. A parenchymatous organ such as the spleen is a suitable in vivo reference. The healthy spleen is known to be characterized by organ-specific contrast tropism and homogenous contrast enhancement. As a third evaluation criterion, a differentiation can be made between homogeneous and inhomogeneous contrast enhancement (HE). Focal parenchymal lesions in consolidated lung tissue are characterized in terms of number, shape (round, wedge-shaped) and location (central, peripheral). A last criterion is the decrease of enhancement (DE) in the parenchymal phase (wash out), which can be classified into a rapid wash out (<120 s) and a late wash out (>120 s) (Caremani et al. 2008). Benign consolidations like pneumonia and atelectasis prefer a late wash out, whereas malignant lesions predominantly have a rapid wash out. Thus, with the use of CEUS the following perfusion patterns can be distinguished:

- ***Time to contrast enhancement*** which allows the differentiation of early pulmonary arterial vascularization (Fig. 8.12) from delayed bronchial arterial vascularization (Fig. 8.13)
- ***Extent of contrast enhancement*** compared with spleen enhancement (Fig. 8.14)
- ***Homogeneity of contrast enhancement*** with detection of focal lesions in consolidated lung tissue (Fig. 8.15).
- *Decrease of enhancement in the parenchymal phase (wash out)* (Figs. 8.31d and 8.41f).

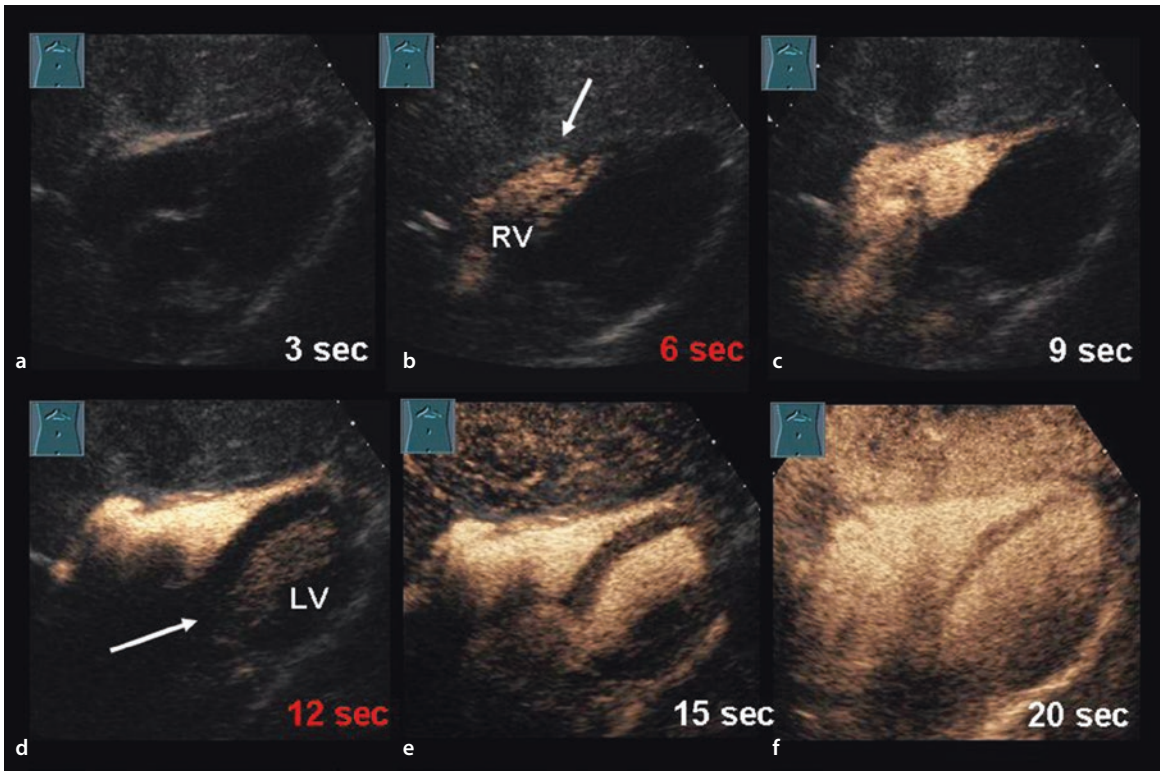

Fig. 8.11 a–f Visualization of the time until contrast enhancement: four-chamber view in a healthy proband. After injection of contrast medium one sees contrast enhancement in the right ventricle as early as 1 s later **a–d.** After 8 s there is contrast enhancement in the left ventricle **e, f**

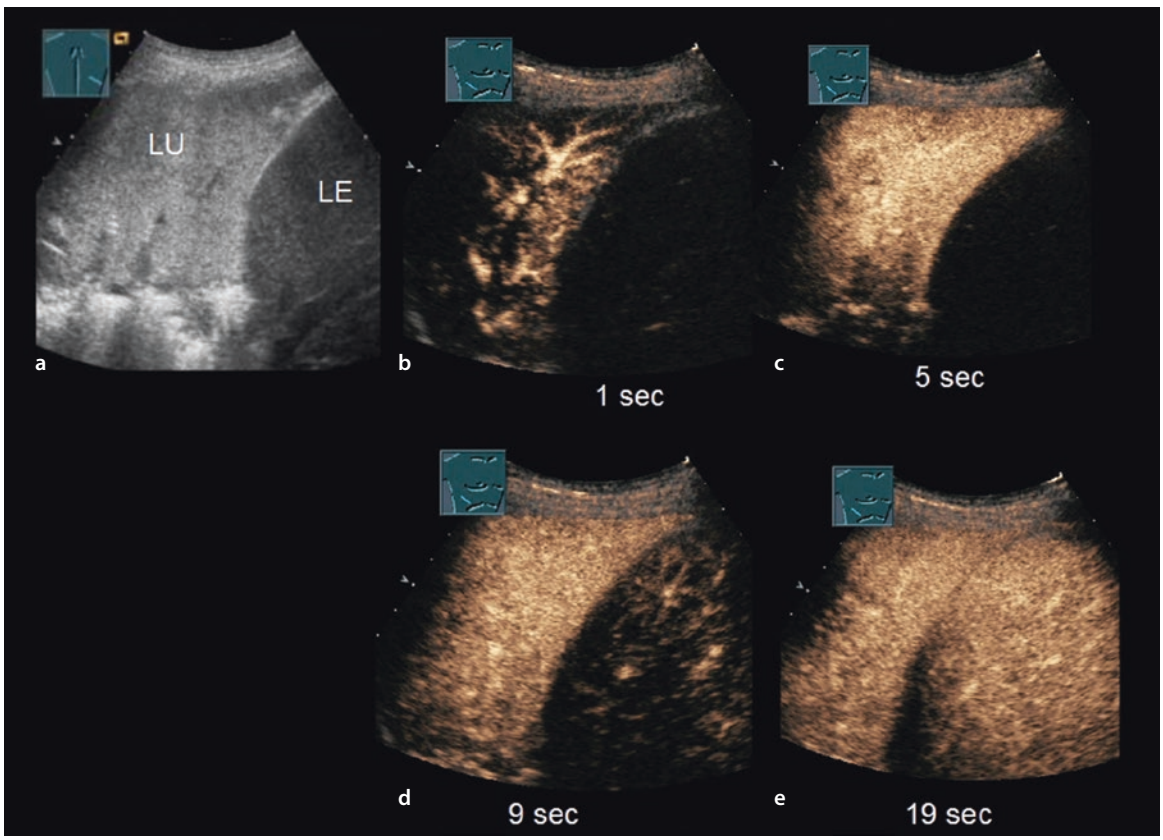

Fig. 8.12 Patient with obturation atelectasis. **a** The liver (LE) and a consolidated lung (LU) in a B-mode ultrasound image. **b–e** With CEUS, early pulmonary arterial contrast enhancement of the lung is seen after 1 s **b** After 5 s, there is a marked contrast enhancement in the atelectatic tissue; the liver has not yet received the contrast medium **c**. The liver shows an initial systematic contrast enhancement **d**, with homogeneous contrast enhancement after 9 s

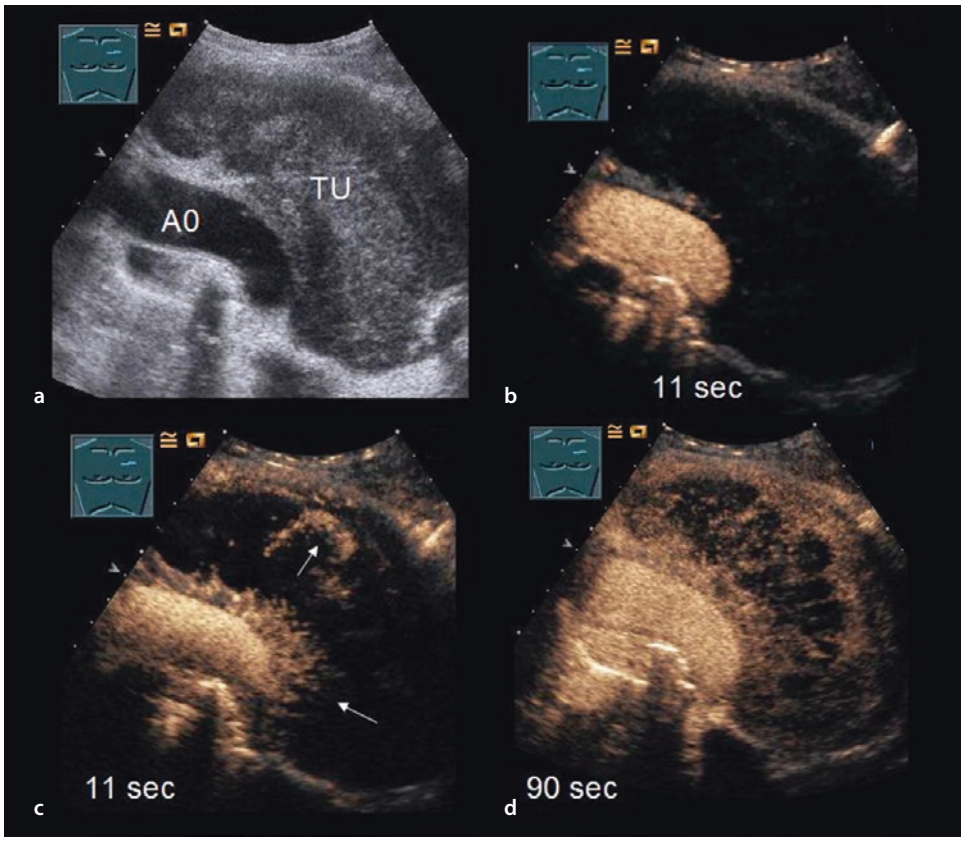

Fig. 8.13 Patient with non-small-cell bronchial carcinoma of the left lung, with visualization of a mass. **a** B-mode ultrasound shows an echogenic mass (TU) adjacent to the aorta (AO). **b** After administration of contrast medium, a contrast enhancement in the aorta can be documented after 11 s. **c** After 11 s, there is a gentle flood of contrast enhancement from the aorta (AO) into the tumor tissue, corresponding to central bronchial arteries (arrow), and a tender flood of contrast enhancement from peripheral bronchial arteries (arrow). **d** After 90 s, the tumor lesion shows an inhomogeneous contrast enhancement

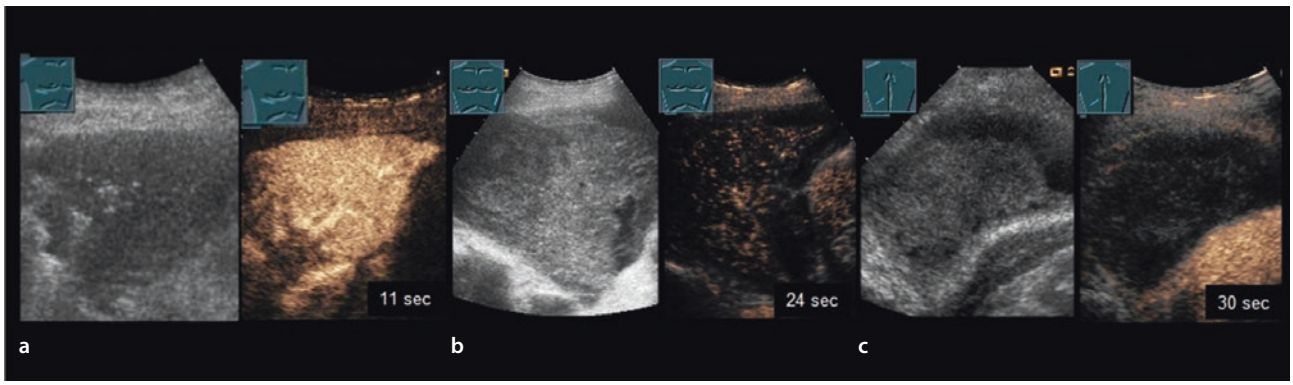

Fig. 8.14 Different extents of contrast enhancement in three patients with an echogenic thoracic mass. **a** B-mode ultrasound and CEUS in a patient with pneumonia and marked contrast enhancement. **b** B-mode US and CEUS in a patient with lung tumor and reduced contrast enhancement. **c** B-mode US and CEUS in a patient without contrast enhancement of an echogenic mass in terms of a hematoma

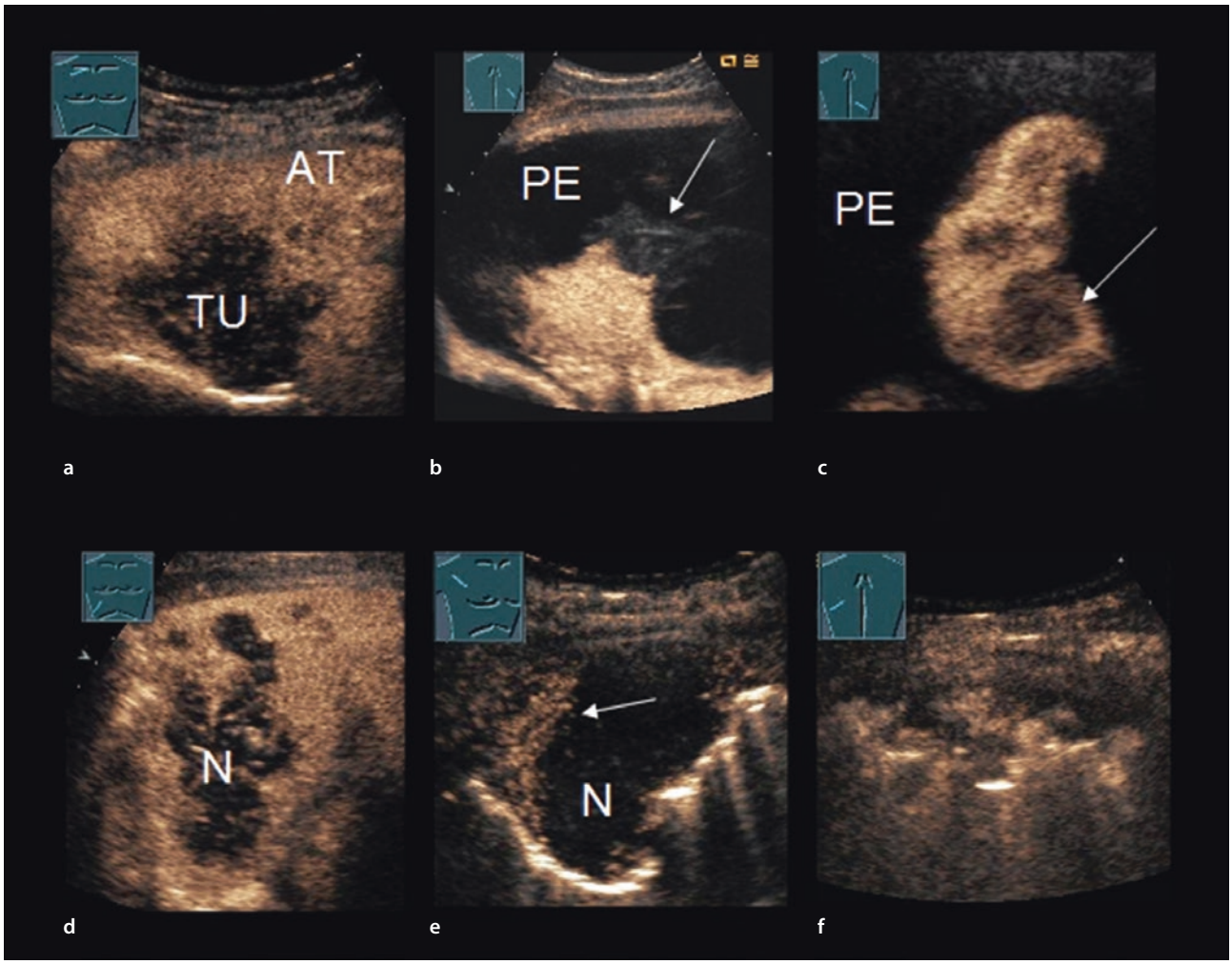

Fig. 8.15 Different patterns of inhomogeneous contrast enhancement in six patients. **a** Central hypoechoic tumor (TU) and subsequent atelectasis (AT). **b** Pronounced pleural effusion (PE) with echogenic atelectasis and peripheral area with absence of contrast enhancement, as in pulmonary infarction (arrow). **c** Pronounced PE with echogenic atelectasis and central round lesions with reduced contrast enhancement, most likely corresponding to lung metastases (arrow). **d** Echogenic space requirement after aspiration, with a central inhomogeneous area of absence of contrast enhancement, as in necrosis (arrow). **e** Peripheral lung tumor with only marginal contrast enhancement and larger necrosis (arrow). **f** Inhomogeneous contrast enhancement with histologically confirmed peripheral pulmonary embolism.

8.4 Predominantly Anechoic Peripheral Lung Consolidation

8.4.1 Color-Doppler Sonography (CDS)

These lesions are rare and constitute an important differential diagnosis for localized effusion. Primary lung cysts at the pleural wall are seen on B-mode ultrasound as anechoic, usually polycystic tumors. CDS shows qualitative flow signals in the septa and the region of the visceral pleura. On semiquantitative spectral analysis they show a monophasic pattern and thus correspond to bronchial and intercostal arteries (Fig. 8.16). Vascular tumors at the pleural wall, such as those associated with Osler's disease, have a characteristic appearance on CDS. The supplying pulmonary artery can be visualized (Fig. 8.7). The malignant cystic lung tumor shows centrally liquefied areas usually on a floor of liquefactions and is seen on the sonographic B-mode ultrasound as a semiliquid structure with septa in some cases. The tumor receives its blood supply from bronchial arteries, and more rarely from pulmonary arteries. Therefore, the spectral curve reveals a monophasic high-impedance arterial flow in keeping with bronchial arteries and occasionally a biphasic high-impedance arterial flow that corresponds to pulmonary arteries (Fig. 8.17). The aortic aneurysm at the dorsal wall of the pleura is a notable pitfall (Fig. 8.18); the same

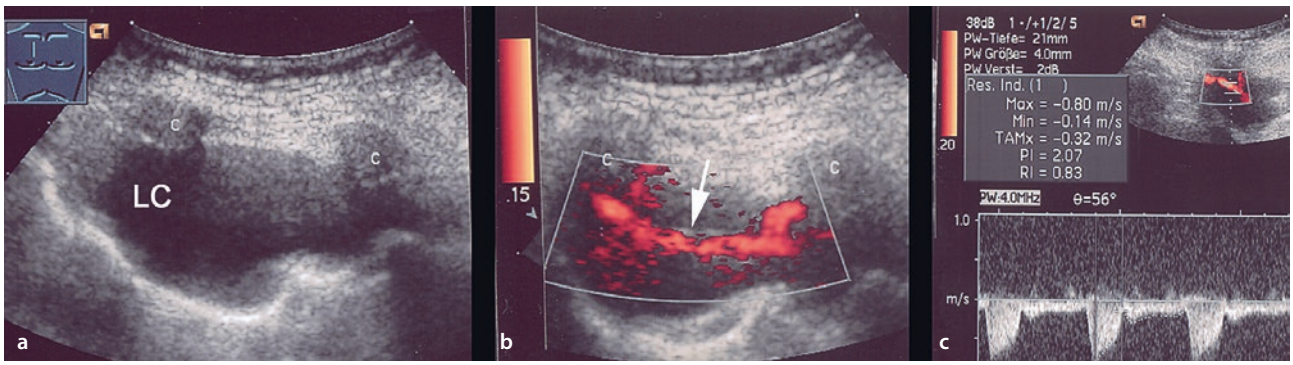

Fig. 8.16 a–c A 70-year-old man with a primary lung cyst. **a** On the B-mode ultrasound one finds an anechoic lesion close to the pleura. C ribs, LC lung cyst. **b** CDS in the power mode shows **a**. strong vessel surrounding the lesion (arrows). **c** Spectral curve analysis demonstrates a monophasic high-impedance flow signal indicative of an intercostal artery

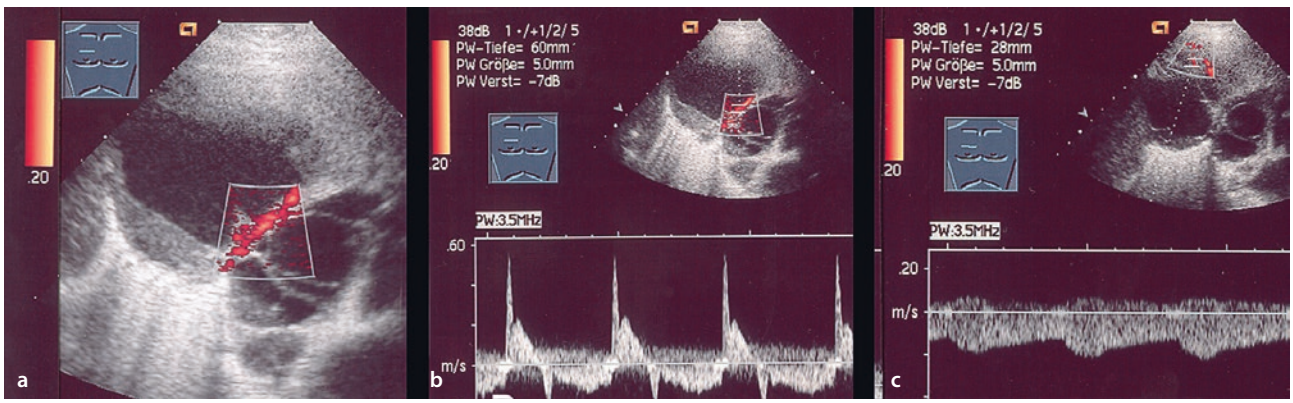

Fig. 8.17 a–c A 44-year-old man with sarcoma of the lung. **a** CDS shows a tumor with solid and cystic portions and vessels in the seventh course. **b** Spectral curve analysis reveals an arterial high-resistance flow signal. This is indicative of a pulmonary artery. **c** Visualization of a low-impedance flow signal in the margin of the lesion, indicative of a bronchial carcinoma

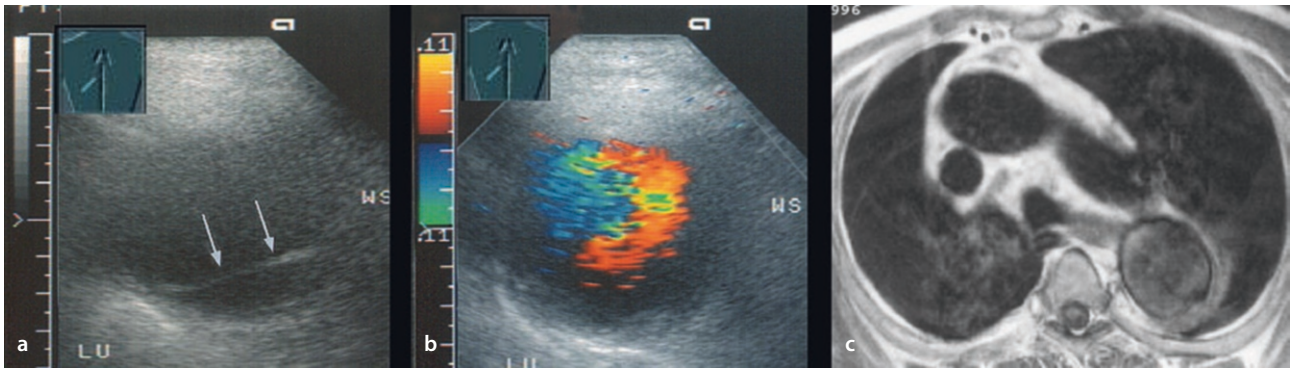

Fig. 8.18 a–c A 49-year-old man with dissection of the aorta in the chest. **a** The B-mode ultrasound shows an anechoic septated round lesion close to the pleura (arrow). LU lung, WS spine. **b** CDS reveals a turbulent flow pattern in the lesion, indicative of an aneurysm in the aorta. **c** the aneurysm in the aorta—on magnetic resonance tomography

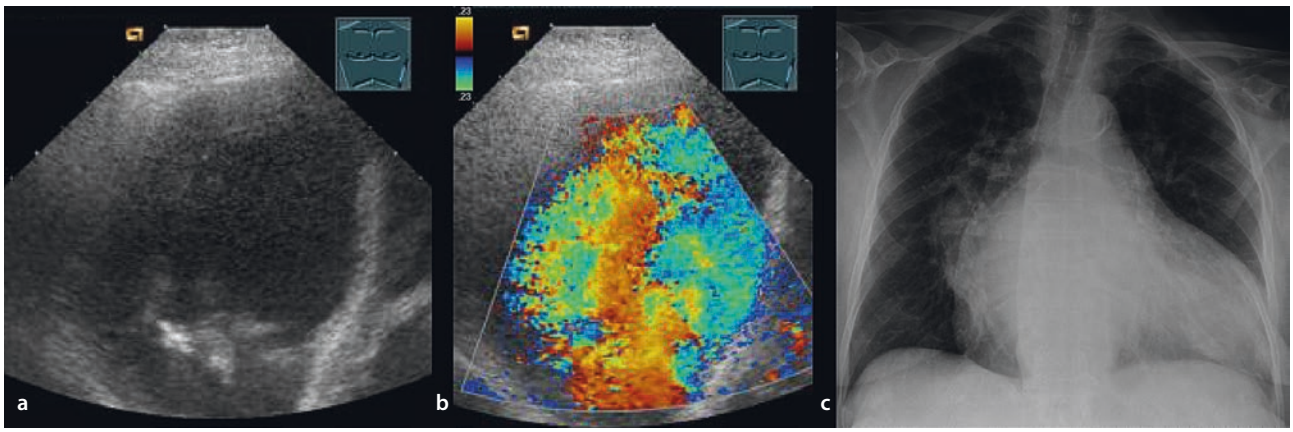

Fig. 8.19 a–c A 78-year-old woman with dyspnea who came for thoracentesis. **a** The B-mode ultrasound shows an anechoic space-occupying mass in the chest on the left side. **b** CDS reveals a turbulent flow pattern within this lesion, indicative of the left ventricle being located at the chest wall. **c** The X-ray shows a large heart; the left ventricle is in contact with the lateral chest wall

is true for the right lateral part of the heart at the chest wall in cases of cardiomegaly (Fig. 8.19).

8.4.2 Contrast Enhanced Ultrasound (CEUS)

Specific studies focusing on CEUS for the assessment of anechoic lung consolidations have not yet been published. Lung abscesses, pleural effusions, pleural empyema and liquefied lung tissue, however, are marked by the absence of contrast enhancement. Primary or secondary lung cysts are rare (Fig. 8.20).

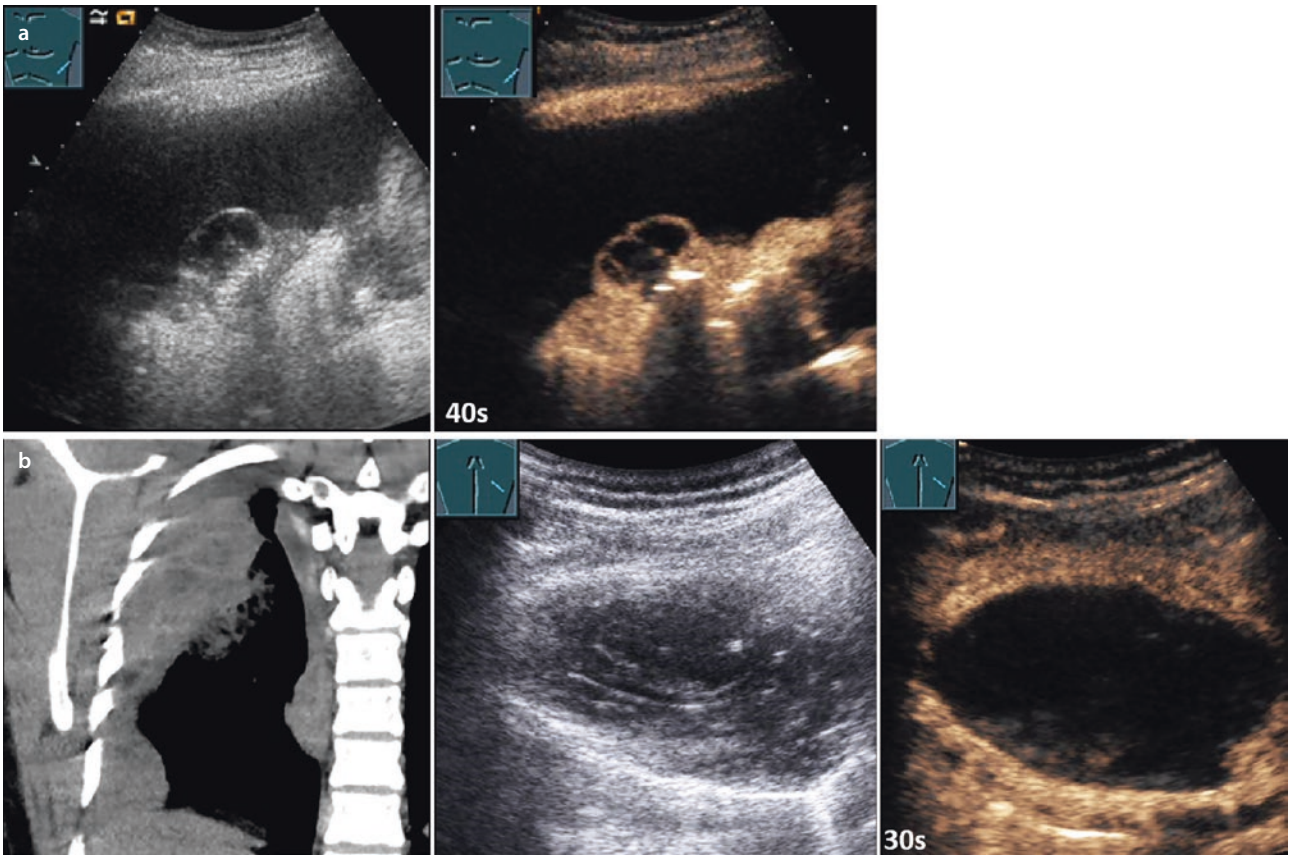

Fig. 8.20 **a** Patient with pleural effusion and sharply demarcated cystic mass at the visceral pleura as a random finding. On CEUS , the lesion shows no enhancement, as in a primary pulmonary cyst. **b** Patient from Iraq with confirmed pulmonary echinococcosis and multiple lung consolidations in a computed tomography image, predominantly located at the pleura. The dorsal lesion on B-mode ultrasound is predominantly anechoic, with an indicated cyst within the cyst. On CEUS, the polycystic lesion shows no enhancement, as in a secondary pulmonary cyst in terms of echinococcosis

8.5 Predominantly Echogenic Lung Consolidation

8.5.1 Lung Infarction

8.5.1.1 Color-Doppler Sonography (CDS)

The lung infarction could be a correlate of pulmonary embolism. In the case of peripheral obstruction of branches of the pulmonary arteries and insufficient nourishment from the bronchial arteries the patient may develop intra- alveolar hemorrhage which is visualized morphologically on the B-mode ultrasound as displaced air (Mathis and Dirschmid 1993). On qualitative CDS the lesion characteristically shows the absence of flow signals (Fig. 8.3). On semiquantitative spectral analysis one occasionally finds a monophasic pattern close to the pleura; this pattern can be attributed to bronchial arteries. In some cases, the disconnected supplying branch of the pulmonary artery is visualized (Fig. 8.21)

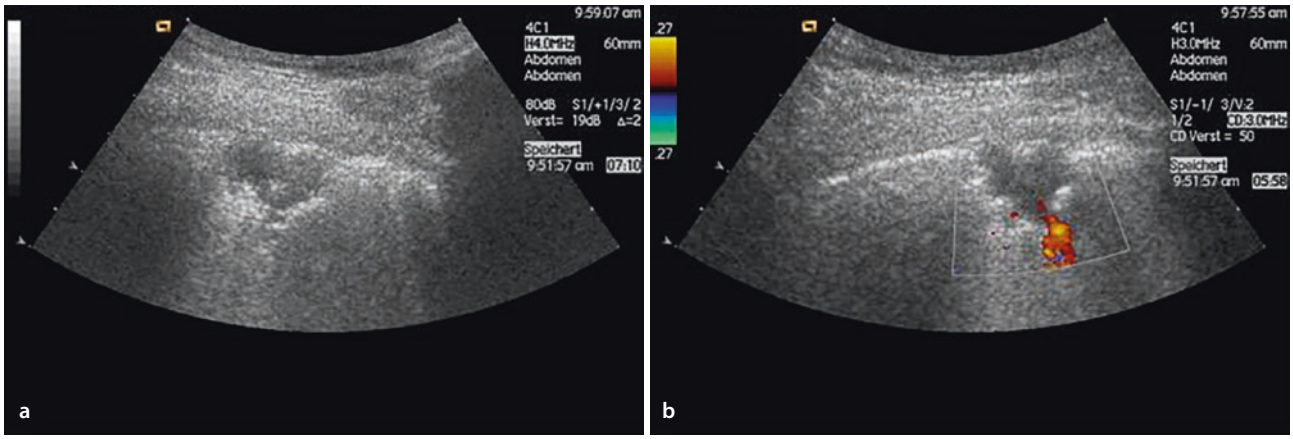

Fig. 8.21 Patient with computed-tomography-confirmed pulmonary embolism. **a** B-mode ultrasound shows a wedge-shaped lesion. **b** On CDS, the feeding pulmonary arterial vessel breaks off

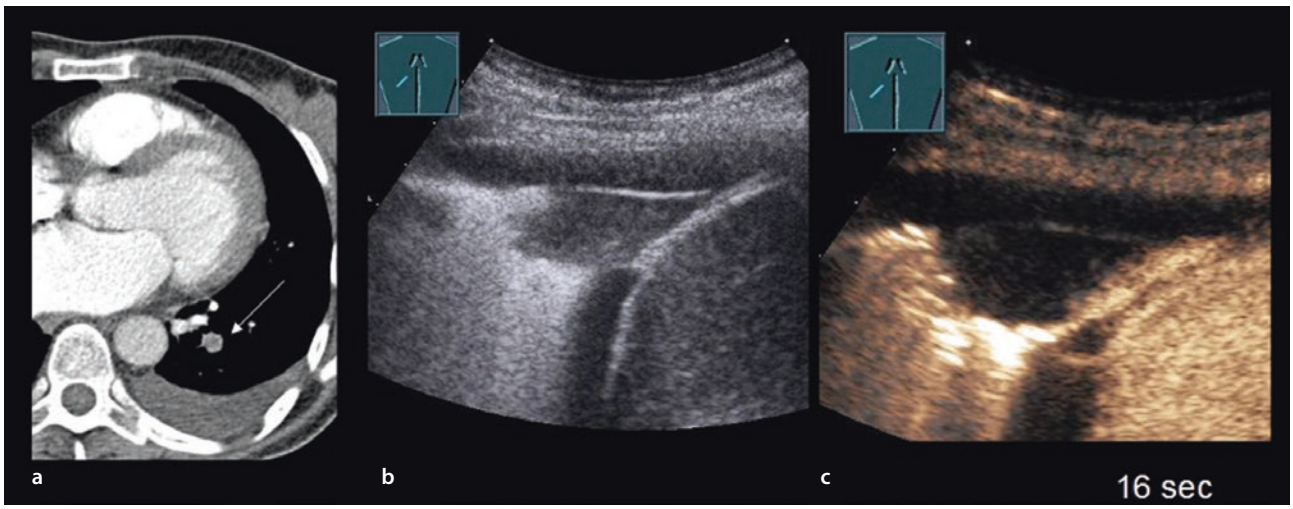

Fig. 8.22 **a** Patient with pulmonary embolism confirmed by computed tomography. **b** On B-mode ultrasound, a smooth, wedge-shaped, homogeneously hypoechoic lung consolidation is recognizable. **c** On contrast-enhanced ultrasound, an absence of contrast enhancement in the lesion can be observed

8.5.1.2 Contrast Enhanced Ultrasound (CEUS)

In keeping with findings on CDS, lung infarctions/lung hemorrhages are marked by the absence of contrast enhancement on CEUS (Fig. 8.22). Occasionally one finds delayed and reduced contrast enhancement in the border area, which is indicative of vascular nourishment being provided by bronchial arteries (Fig. 8.23). In a recently published study in patients with CT-confirmed pulmonary artery embolism and sonographically detected pleural defects, in 80% of the cases an absence or inhomogeneous contrast enhancement with areas of non-enhancement could be detected, which is consistent of pulmonary infarction and indicative for pulmonary arterial embolism. However, in 20% of the cases

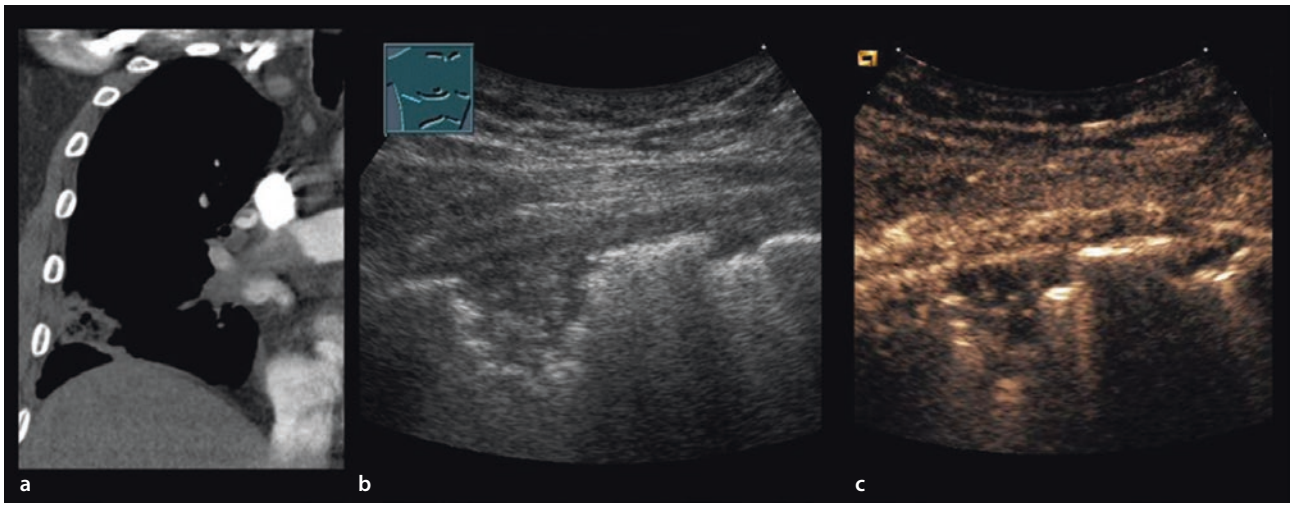

Fig. 8.23 **a** Patient with computed-tomography-confirmed central pulmonary embolism and peripheral consolidation. **b** On B-mode ultrasound, a peripheral hypoechoic consolidation is visualized. **c** On contrast-enhanced ultrasound, an inhomogeneous enhancement with areas of non-enhancement is revealed after 25 s

a homogeneous pulmonary arterial vascularization was found (Bartelt et al. 2016), which may be an indication for repair processes by fibrinolysis. There are no follow up CEUS studies to describe different healing phases in peripheral pulmonary embolism. On CEUS examination of the infarct area, a detailed analysis of the early arterial phase must be performed, because a primary absence of pulmonary arterial vascularization can be overlaid by a secondary bronchial arterial vascularization, and therefore, after a few seconds, a homogeneous enhancement through systemic flooding could be present (Fig. 8.24). In addition, CEUS patterns typical of peripheral infarctions could be detected in individual cases of clinical suspicion of pulmonary artery embolism (high well score) and negative CT findings regarding pulmonary artery embolism (Trenker et al. 2017). In a follow-up study, the peripheral consolidations were histologically confirmed as infarcts (Fig. 8.25) (Trenker et al. 2019). The clinical relevance of these "CT negative" peripheral subsegmental pulmonary artery embolisms is unclear (Raslan et al. 2018; Goy et al. 2015). It is important to note that CEUS can reliably differentiate between vascularized and non-vascularized peripheral lung tissue and therefore has a differential diagnostic potential for distinguishing infectious pleuritis, infarction-caused pneumonia or infarction-caused pleural effusion with atelectasis (Fig. 8.15b) (Görg et al. 2006a). Initial studies have indicated that COVID-19 infections with evidence of pleural defects and lung consolidation are characterized by an inhomogeneous contrast enhancement with non-perfused areas as an indication of peripheral perfusion disturbances in terms of infarcts (Fig. 8.26)

8.5.2 Pleurisy

8.5.2.1 Color-Doppler Sonography (CDS)

The appearance of pleurisy on the B-mode ultrasound is similar to that of a lung infarction (Gehmacher et al. 1997). Depending on the size of the lesion an upgrading, into pleural pneumonia is possible. The qualitative CDS characteristically shows pronounced vessels with predominant evidence of an arterial high-impedance flow profile on spectral analysis such as that seen in branches of the pulmonary artery (Fig. 8.27).

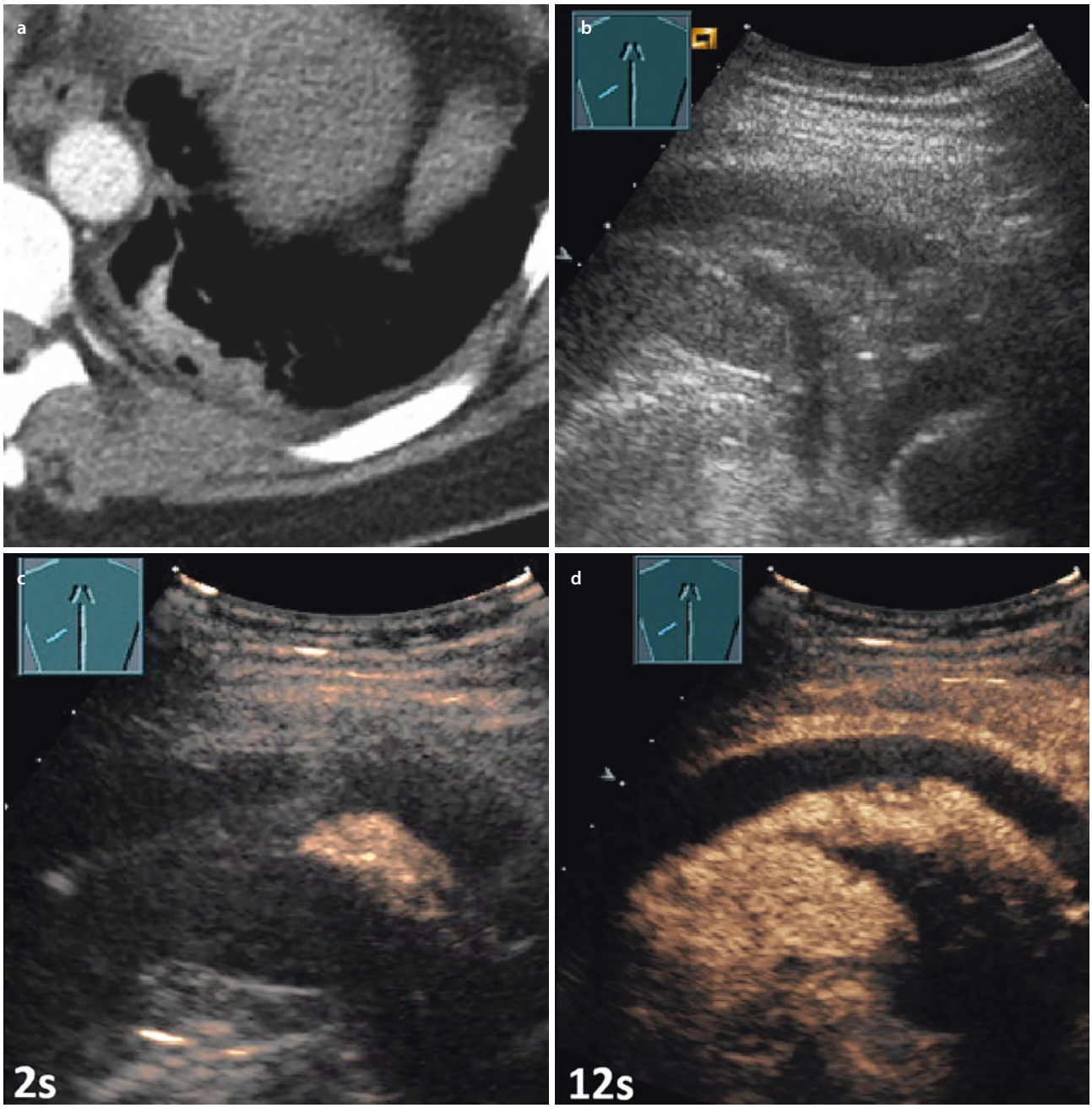

Fig. 8.24 **a** Patient with computed-tomography-confirmed central pulmonary embolism and peripheral consolidation. **b** On B-mode ultrasound, a moderate pleural effusion with partial lower lobe atelectasis is recognizable. **c** On CEUS, an inhomogeneous pulmonary arterial enhancement is observed in the early arterial phase after 2 s. **d** On CEUS, a bronchial arterial reperfusion of the area with primarily an absence of contrast enhancement is observed after 12 s

8.5.2.2 Contrast Enhanced Ultrasound (CEUS)

In keeping with the CDS findings, it takes very little time for contrast enhancement to start in pleurisy, and it is marked by strong contrast enhancement on CEUS (Fig. 8.28a), while chronic scarred pleural thickening is characterized by reduced systemic contrast-medium enhancement (Fig. 8.28b). In tuberculous pleuritis, an inhomogeneous enhancement of contrast medium with non-perfused areas can be seen in the region of the pleural thickening (Fig. 8.29). The value of CEUS lies in the differential diagnostic discrimination of non-vascularized or in homogeneously vascularized peripheral lung lesions, such as pulmonary infarction, malignant lesions or scar tissue, in patient with the leading clinical symptom of breath-dependent pain (Görg et al. 2005b).

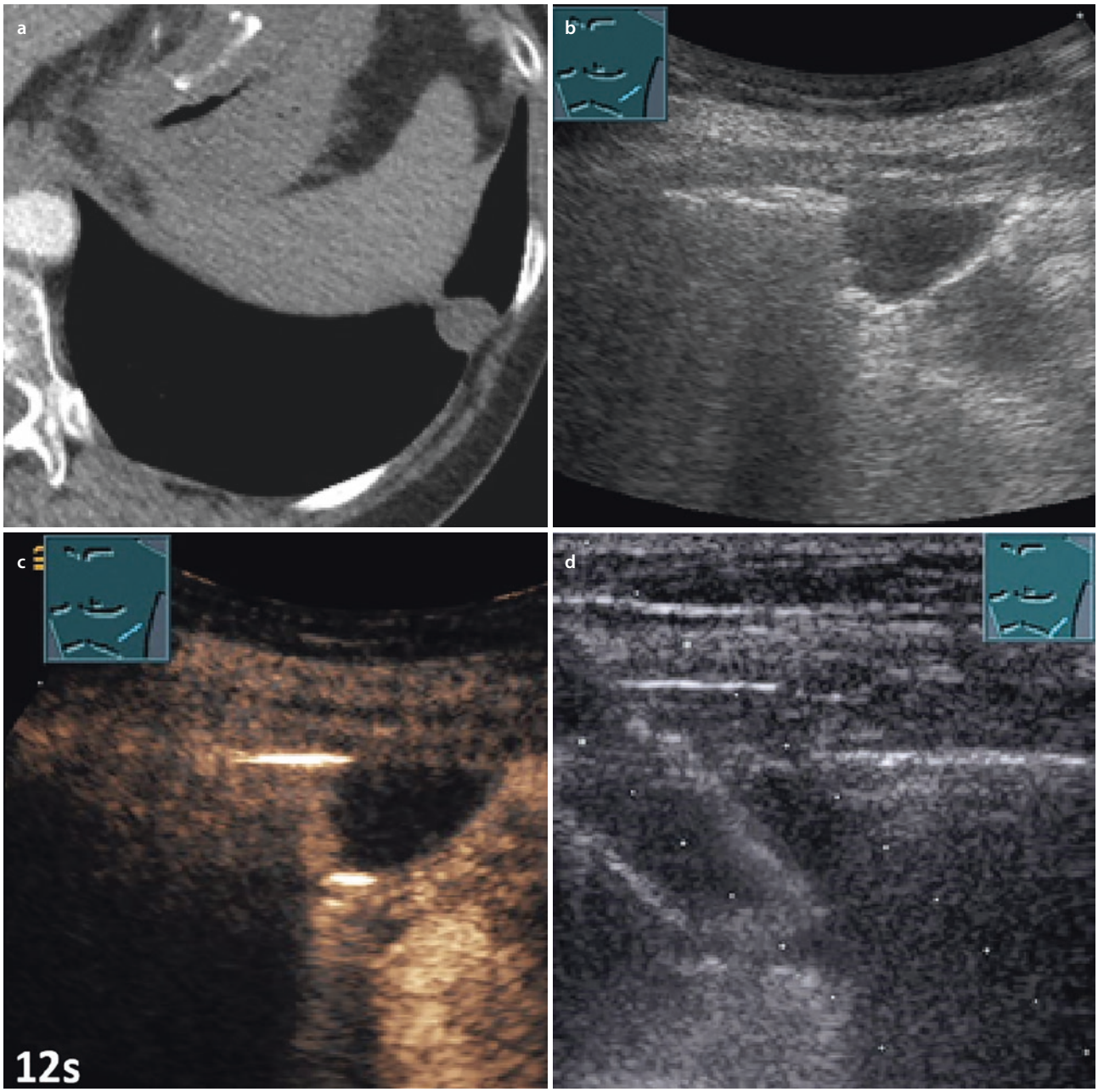

Fig. 8.25 **a** Patient with clinical suspicion of pulmonary embolism, with no evidence of central pulmonary embolism on computed tomography and evidence of peripheral consolidation on B-mode ultrasound (US). **b** On B-mode ultrasound, a wedge-shaped pleural defect is detected. **c** On contrast-enhanced ultrasound, the lesion shows no enhancement. **d** US-guided biopsy confirms the diagnosis of a peripheral pulmonary infarction

8.5.3 The Peripheral Round Lesion/Lung tumor

8.5.3.1 Color-Doppler Sonography (CDS)

A peripheral round pleural based consolidation of the lung may be a benign or malignant lesion. Of decisive importance is the fact that, independent of the cause, the evidence of flow signals is dependent on the size of the lesion. On careful investigation one frequently finds both arterial high impedance flow signals from pulmonary arteries and low-impedance flow signals from bronchial arteries in benign as well as malignant peripheral lung lesions (Figs. 8.30 and 8.31). In the published literature, less visualization of vessels on qualitative CDS and evidence of arterial monophasic flow signals with low resistance indices are reported to be characteristic features of malignant peripheral lung tumors or metastases (Yuan et al. 1994; Hsu et al. 1996,

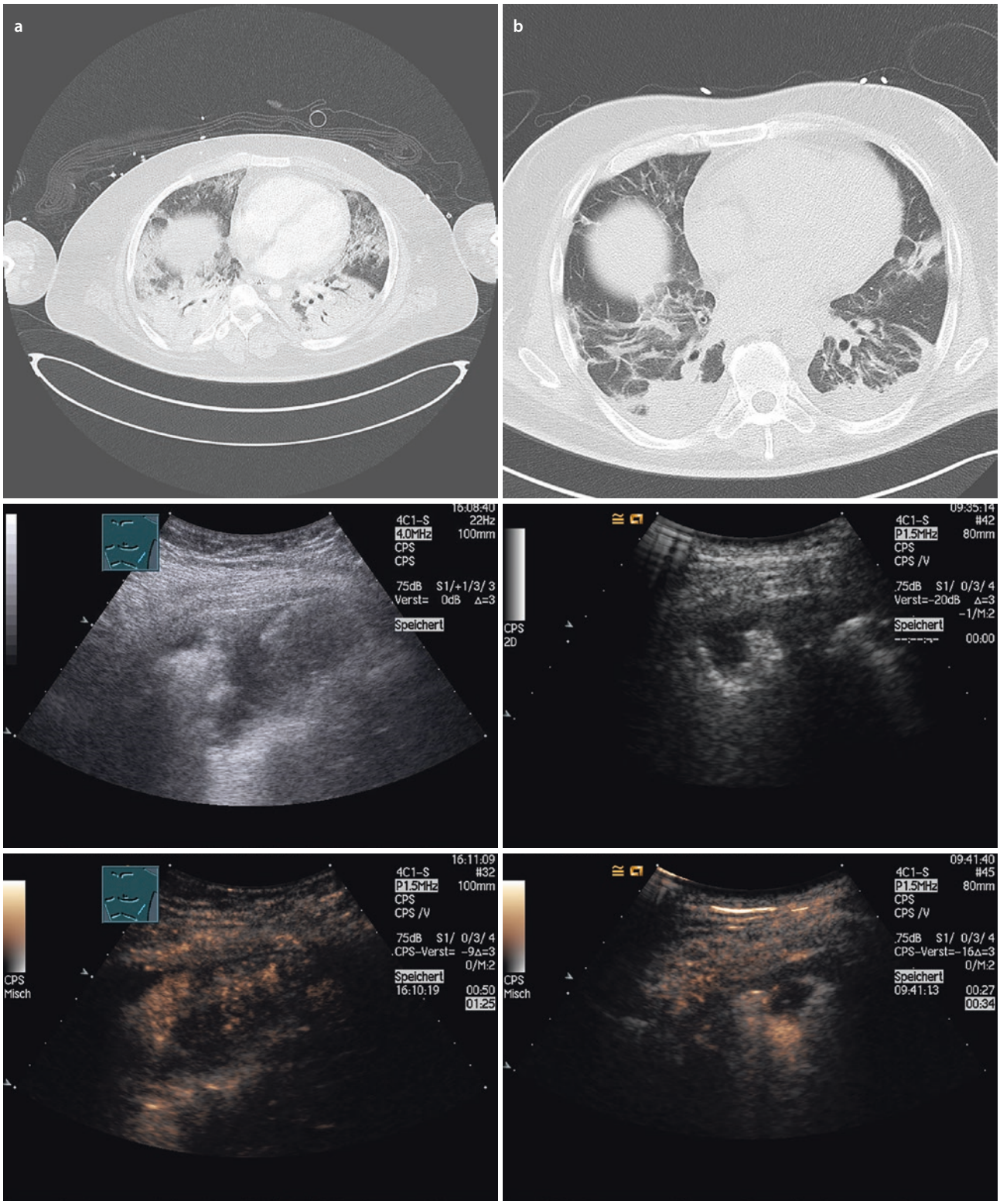

Fig. 8.26 **a** Patient with COVID-19 infection and computed tomography (CT) evidence of lung consolidation in the lower segments. On B-mode ultrasound, a lung consolidation on the left side is visualized. On CEUS, an inhomogeneous contrast enhancement in the consolidated tissue indicates small infarction areas. **b** Patient with COVID-19 infection and CT evidence of lung consolidation in the lower segments. On B-mode US, a right-sided lung consolidation can be seen. On CEUS, the lesion shows an absence of enhancement, as in pulmonary infarctions

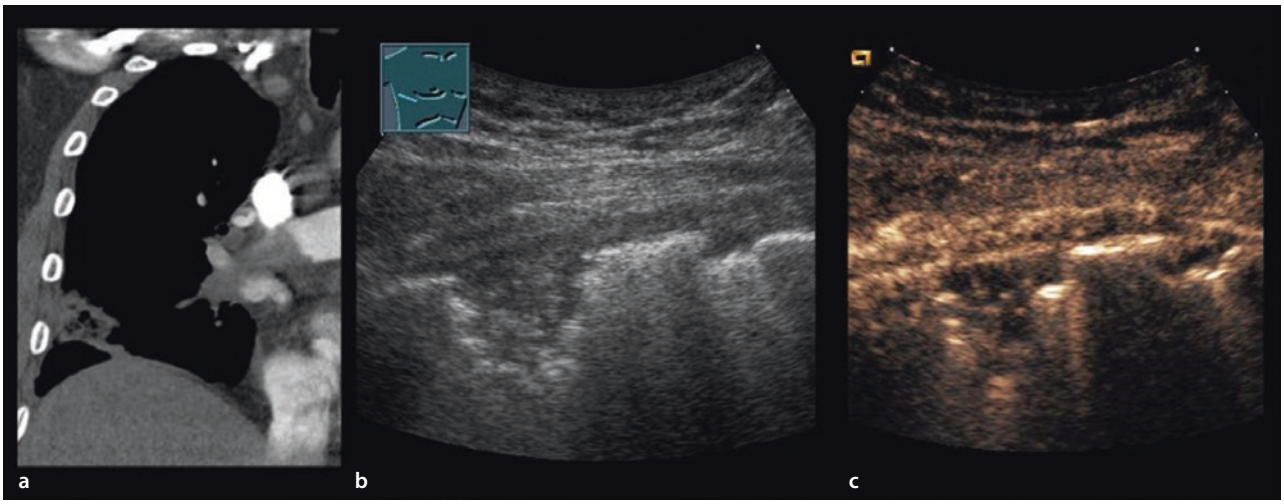

Fig. 8.27 a–c 55-year-old woman with respiration-related pain; suspected pleurisy. **a** B-mode ultrasound shows a small wedge-shaped pleural defect. **b** CDS shows vessels within the defect. **c** CEUS shows contrast enhancement of the lesion such as that seen in the presence of pleurisy

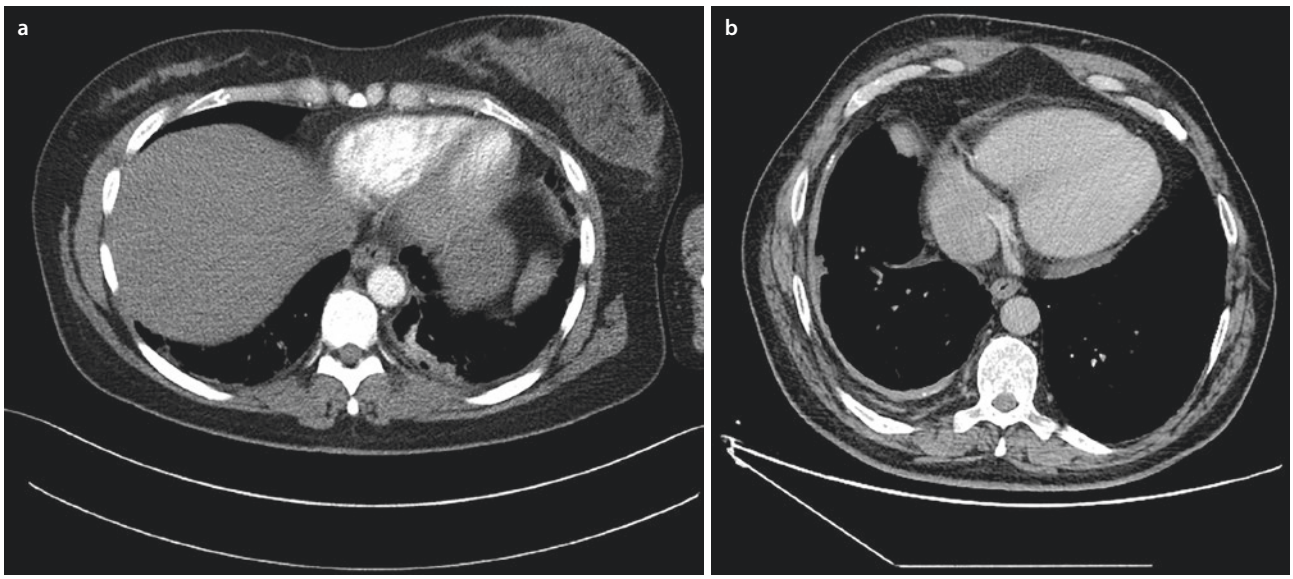

Fig. 8.28 **a** Patient with breath-dependent pain suspected of having pleurisy. B-mode ultrasound (US) shows a long, irregular entry echo in the area of the right lower lobe of the lung. On CEUS, a clear pulmonary arterial contrast enhancement of the lesion is revealed after 4 s. In the late parenchymal phase, the lesion shows a homogeneous contrast enhancement. **b** Patient with pleural thickening visualized by computed tomography (CT). The B-mode US shows a long pleural thickening in the area of the right dorsal lung. On CEUS, there is a near-absence of contrast enhancement of the lesion after 34 s, as in chronic fibrosing pleurisy (histologically confirmed)

1998; Civardi et al. 1993). In some cases, the vessels seen on sonography may be identified as those resulting from tumor neoangiogenesis (originating from bronchial arteries) on pathological investigation (Hsu et al. 1998; Fig. 8.9d). However, studies that have used a single impedance measurement to assess the benign or malignant nature of a lesion must be viewed with caution. In principle CDS is not suitable for distinguishing between benign and malignant peripheral round lesions.

Contrast Enhanced Ultrasound (CEUS)

In keeping with the variable findings on CDS, CEUS also shows a heterogeneous pattern of perfusion. Malignant lesions—whether lung metastases or peripheral bronchial carcinomas—are marked by delayed arrival of contrast enhancement and reduced extent of contrast enhancement in both phases. This is indicative of predominant vascularization through bronchial arteries (Table 8.1; Fig. 8.32). In a study that investigated the perfusion

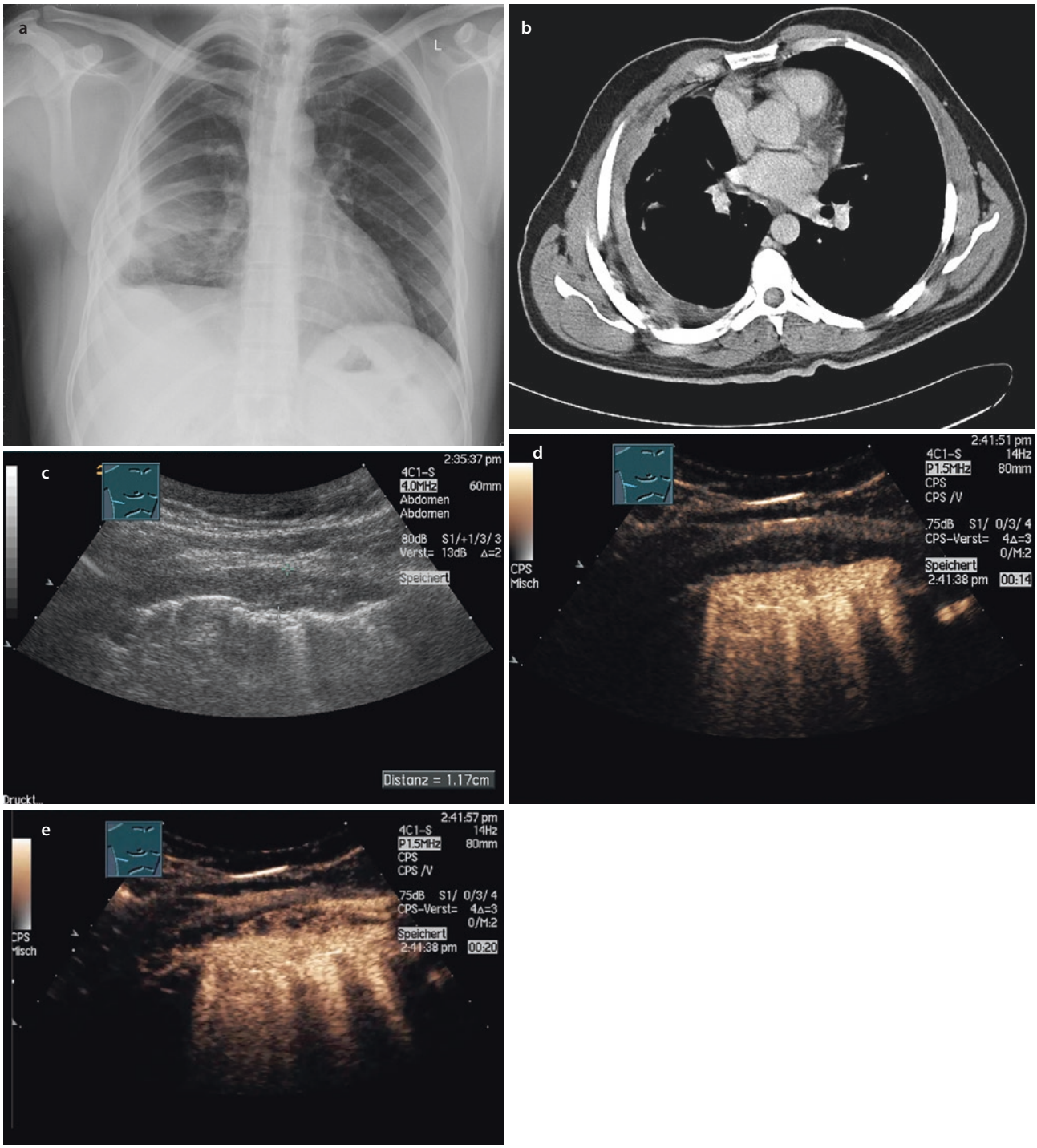

Fig. 8.29 **a** Patient with a medical history of tuberculosis and radiographic shadowing of the right diaphragmatic rib angle. **b** A pleural thickening can be detected by computed tomography. **c** On B-mode ultrasound, a long pleural thickening can be seen. **d** The CEUS discriminates against the pleural thickening: after 14 s, the visceral pleura shows a homogeneous strong pulmonary arterial enhancement, while the parietal pleural thickening does not yet show an enhancement. **e** After 20 s, the bronchial arterially supplied parietal pleura shows an inhomogeneous enhancement with small non-enhanced nodules. The biopsy confirmed active tuberculosis

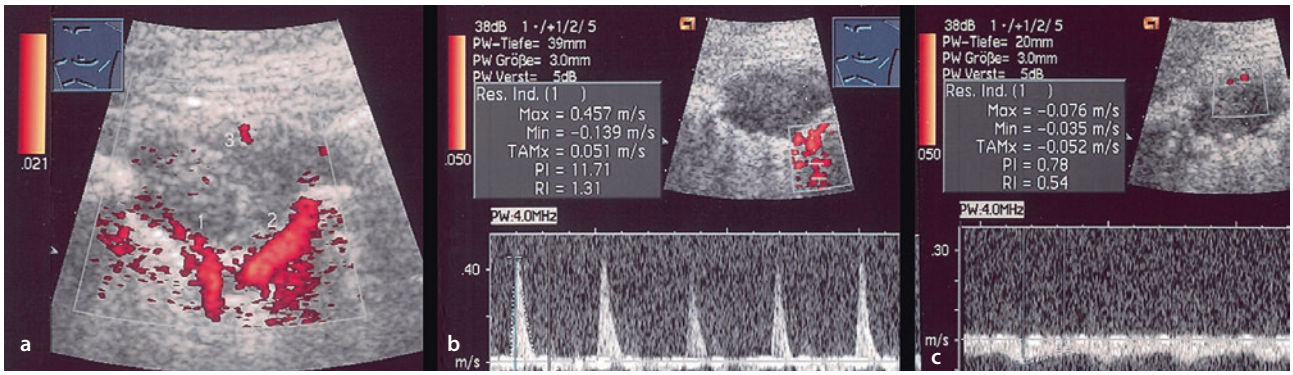

Fig. 8.30 a–c A 56-year-old man with a plasmocytoma and histologically confirmed amyloidosis in the lung. **a** On CDS one finds several vessels. **1** pulmonary artery, **2** pulmonary vein, **3** bronchial artery. **b** Spectral curve analysis shows a high-impedance. flow signal indicating a pulmonary artery (marked 1 in a). **c** Spectral curve analysis shows a low-impedance monophasic flow pattern oriented towards the hilum of the lung, as a sign of a bronchial artery close to the pleura (marked 3 in a)

8

Fig. 8.31 a–d A 30-year-old woman with sudden onset of dyspnea and fever. **a** B-mode ultrasound shows a peripheral hypoechoic round lesion of the lung. **b** On CDS one finds evident flow signals in the lesion. **c** Spectral curve analysis of a central vessel. shows a low-impedance flow signal such as that seen in a bronchial artery. d Spectral curve analysis of a vessel from the margin shows a high-impedance flow signal such as that seen in pulmonary arteries. Under antibiotic therapy the lesion resolved completely

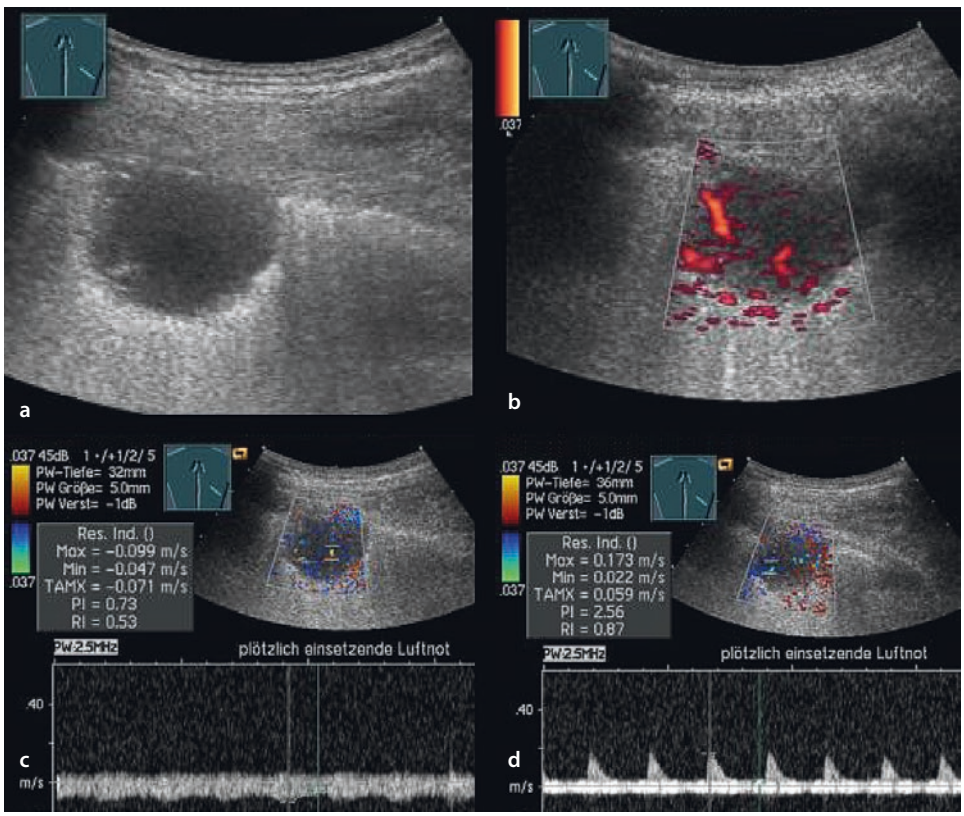

pattern of histologically confirmed peripheral bronchial carcinomas, 72% of the lesions showed a bronchial arterial enhancement (Fig. 8.13a–d) and 28% showed a pulmonary arterial enhancement. Tumor necrosis was proved in 47% of the lesions (Fig. 8.15e) (Findeisen et al. 2018). For this reason, a CEUS-guided tumor biopsy from perfused areas should be preferred to avoid a missed biopsy (Dong et al. 2005; Sartori et al. 2004; Wang et al. 2015). Depending on the underlying histology, however, lung metastases of renal cell carcinomas and frequently also metastases of malignant lymphoma show pronounced contrast enhancement in the arterial phase (Fig. 8.33). The extent and homogeneity of tumor neoangiogenesis depends, inter alia, on the tumor size and underlying disease (Fig. 8.34). In a few cases, the CEUS is useful in the evaluation of the nature of the lesions. For example, hematomas (Fig. 8.35a) and lipomas (Fig. 8.35b) are characterized by an absent

Table 8.1 Time to enhancement (short vs. delayed) and extent of enhancement (reduced vs. marked) in 137 patients with pleural based pulmonary lesions subdivided into patients with pneumonia, compression atelectasis, pulmonary embolism, benign pleural based lesions, central lung cancer and peripheral malignant lesions (Görg et al. 2006b)

	Pneumonia		**Compression atelectasis**		**Pulmonary embolism**		**Benign nodules**		**Central lung cancer**		**Peripheral malignant lesion**	
	***n* = 32**		***n* = 17**		***n* = 20**		***n* = 8**		***n* = 31**		***n* = 29**	
Delayed TE	2	4	0	0	20	0	4	2	8	5	18	4
Short TE	6	20	0	17	0	0	1	1	6	12	5	2
	Reduced EE	Marked EE	Reduced EE	Marked EE	Reduced EE	Marked EE	Reduced EE	Marked EE	Reduced EE	Marked EE	Reduced EE	Marked EE

TE time to enhancement, *EE* extent of enhancement

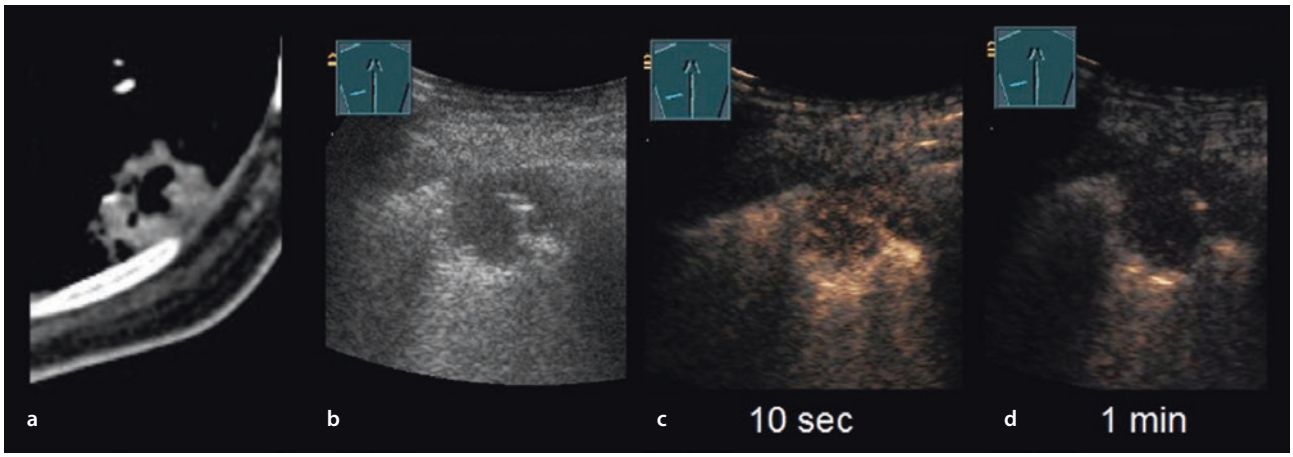

Fig. 8.32 Patient with pancreatic carcinoma and histologically confirmed lung metastases. **a** On computed tomography, a round lesion is visualized with central melting. **b** On B-mode ultrasound, an inhomogeneous, hypoechoic pleural-edge lung lesion with central air reflex is presented. **c** On contrast-enhanced ultrasound, a reduced bronchial arterial contrast enhancement in the lesion can be seen after 10 s. **d** in the parenchymal phase after 1 min, a late decrease of enhancement (wash out) can be detected in the lesion

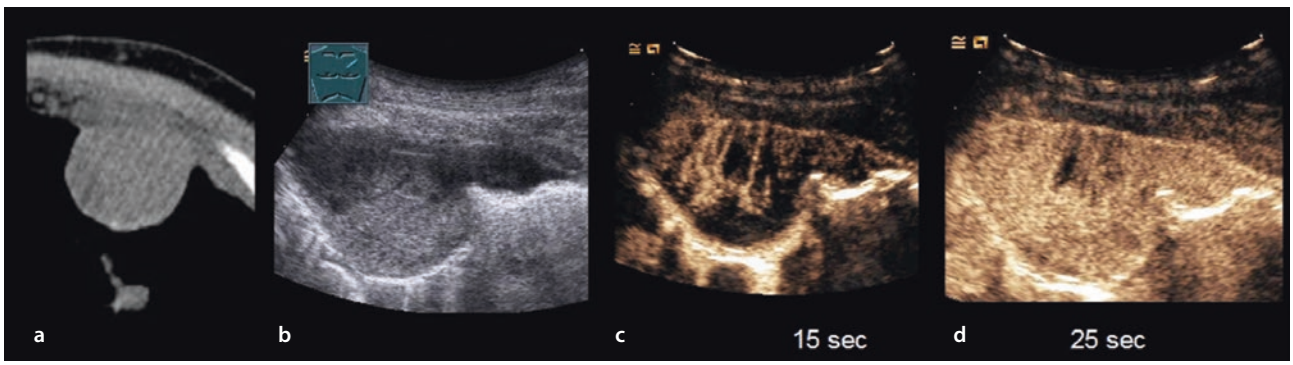

Fig. 8.33 Patient with diagnosed sarcoma and histologically confirmed multiple pulmonary metastases. **a** On computed tomography, there is a pleural round nodule. **b** On B-mode ultrasound, an oval, pleural-edge, homogeneously anechoic lesion is recognizable. **c** On contrast-enhanced ultrasound, after 15 s, a marked contrast enhancement from the periphery can be seen as an indication of peripheral bronchial arterial perfusion. **d** After 25 s, a highly homogeneous contrast enhancement is observed in the lesion. This is an indication of a strong tumor neoangiogenesis

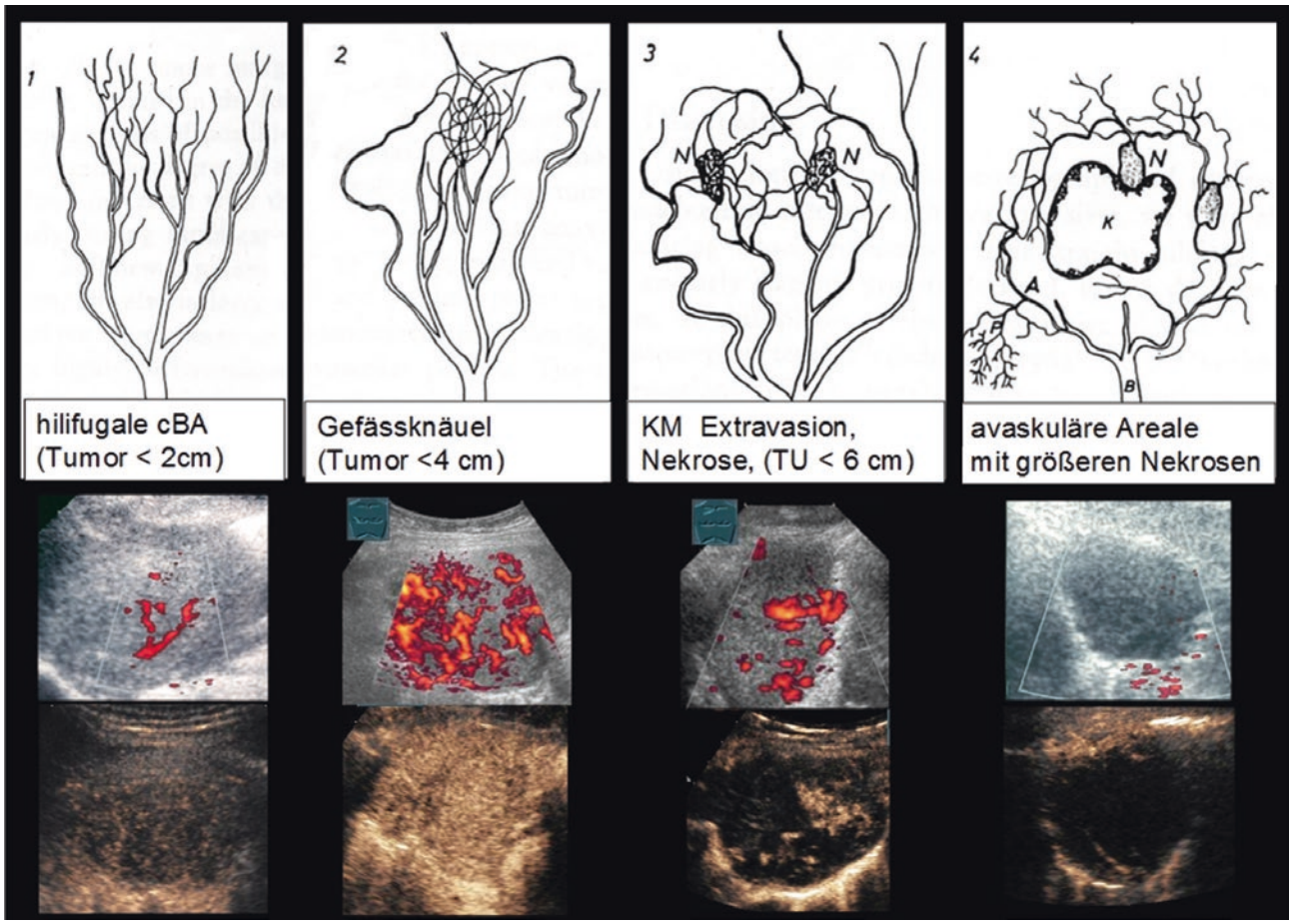

Fig. 8.34 Graphic representation, CDS findings and CEUS patterns of different degrees of bronchial arterial tumor perfusion dependent on tumor size (after Müller and Meyer-Schwickerath 1978)

and a reduced contrast-medium enhancement, respectively. In addition, intrathoracic splenomas can also be diagnosed by CEUS (Fig. 8.36). Contrast enhanced ultrasound, like CDS, is of limited suitability for distinguishing between benign and malignant peripheral round lesions.

8.5.4 Large Lung Consolidation: Pneumonia

8.5.4.1 Color-Doppler Sonography (CDS)

Pneumonia is seen on X-rays and sonography as a peripheral lung consolidation in conjunction to the pleural wall. On B-mode ultrasound, pneumonia is seen as a consolidation with more or less pronounced air bronchogram (Gehmacher et al. 1995), while a complete consolidation is seen as so-called lung hepatization. On CDS, pneumonia is marked by significantly ramified vessels that correspond to segmental branches of the pulmonary artery (Fig. 8.37). In principle it should be noted that certain subtypes of adenocarcinoma may appear similar to pneumonia on the B-mode ultrasound and on CDS as well (Görg et al. 2002). Depending on the extent of hypoxic vasoconstriction in the pulmonary artery, the peripheral vascular tree of pulmonary arteries may not be visualized on qualitative CDS in the presence of advanced pneumonia. Bronchial arteries react to hypoxia by developing vasodilatation, as do all other arteries in the body. This explains the different resistance indices of pneumonia and atelectasis (Yuan et al. 2000). Thus, in the presence of lobar pneumonia parallel to the pulmonary arteries one occasionally finds an arterial monophasic flow pattern with low resistance indices, indicative of central bronchial arteries. The tuberculous infiltrate is a special phenomenon. It is characterized by marked vessels on CDS in terms of qualitative findings. On spectral analysis, however, it is seen as a monophasic curve, corresponding to bronchial arteries (Babo et al. 1979). Cavitary lesions such as tuberculosis, liquefactions, necrosis, abscesses and pseudocysts are characterized by the presence of predominant perfusion through the bronchial artery in the marginal areas around the lesion. (Hsu et al. 1998).

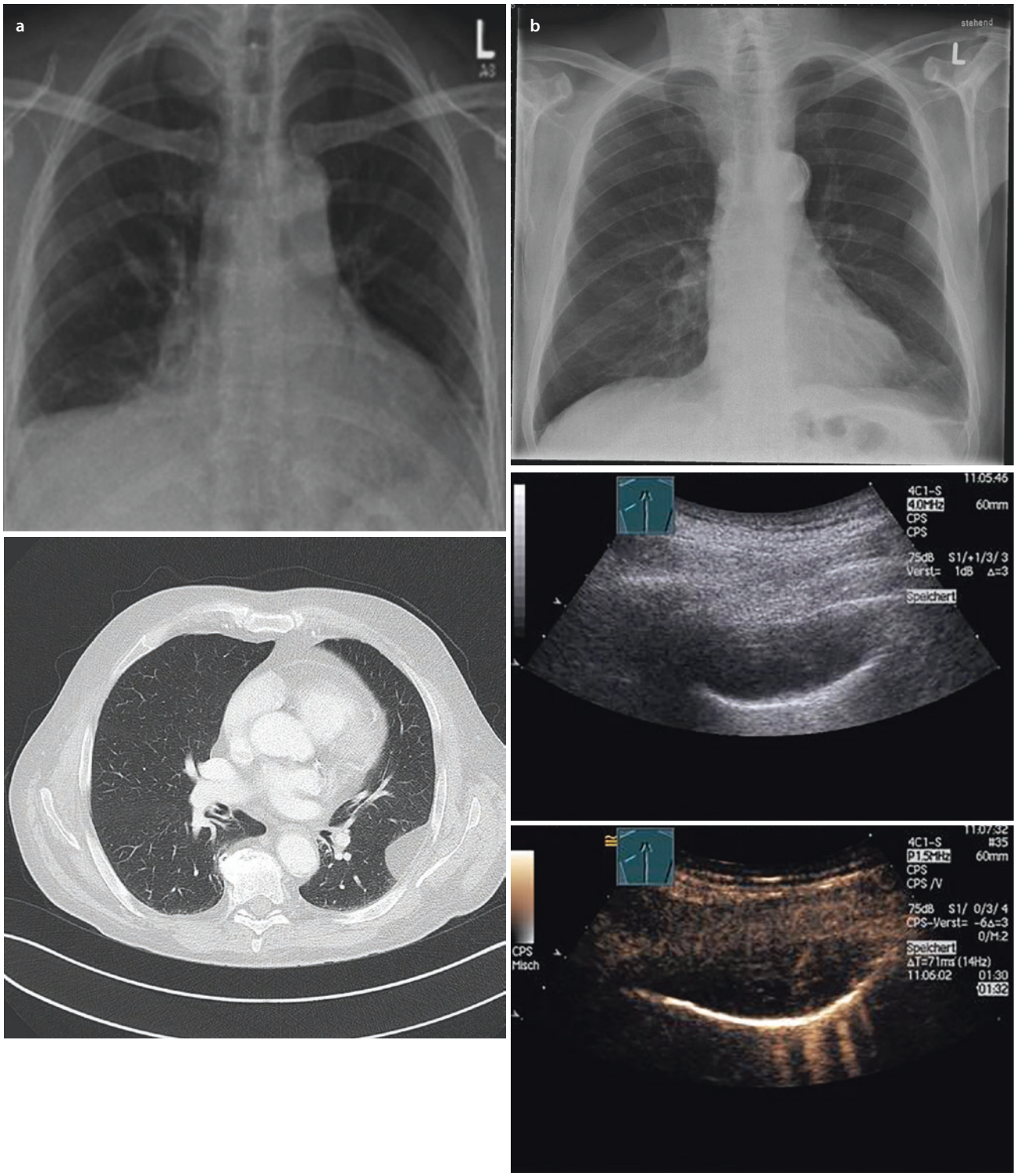

Fig. 8.35 **a** Patient with a mass in the right supraclavicular fossa, which is visualized by X-ray and computed tomography. The patient's medical history shows a condition after a central access on the right side was performed. On B-mode ultrasound, the tumor is hypoechoic. On CEUS, the tumor shows no contrast enhancement, so a hematoma can be assumed, which was confirmed by a regression in the sonographic course. **b** Patient with pleural lesion as an incidental finding, with visualization by a chest X-ray and CT. On B-mode US, the lesion is hypoechoic; on CEUS, the lesion shows a reduced enhancement in all phases. Histologically, a lipoma was found

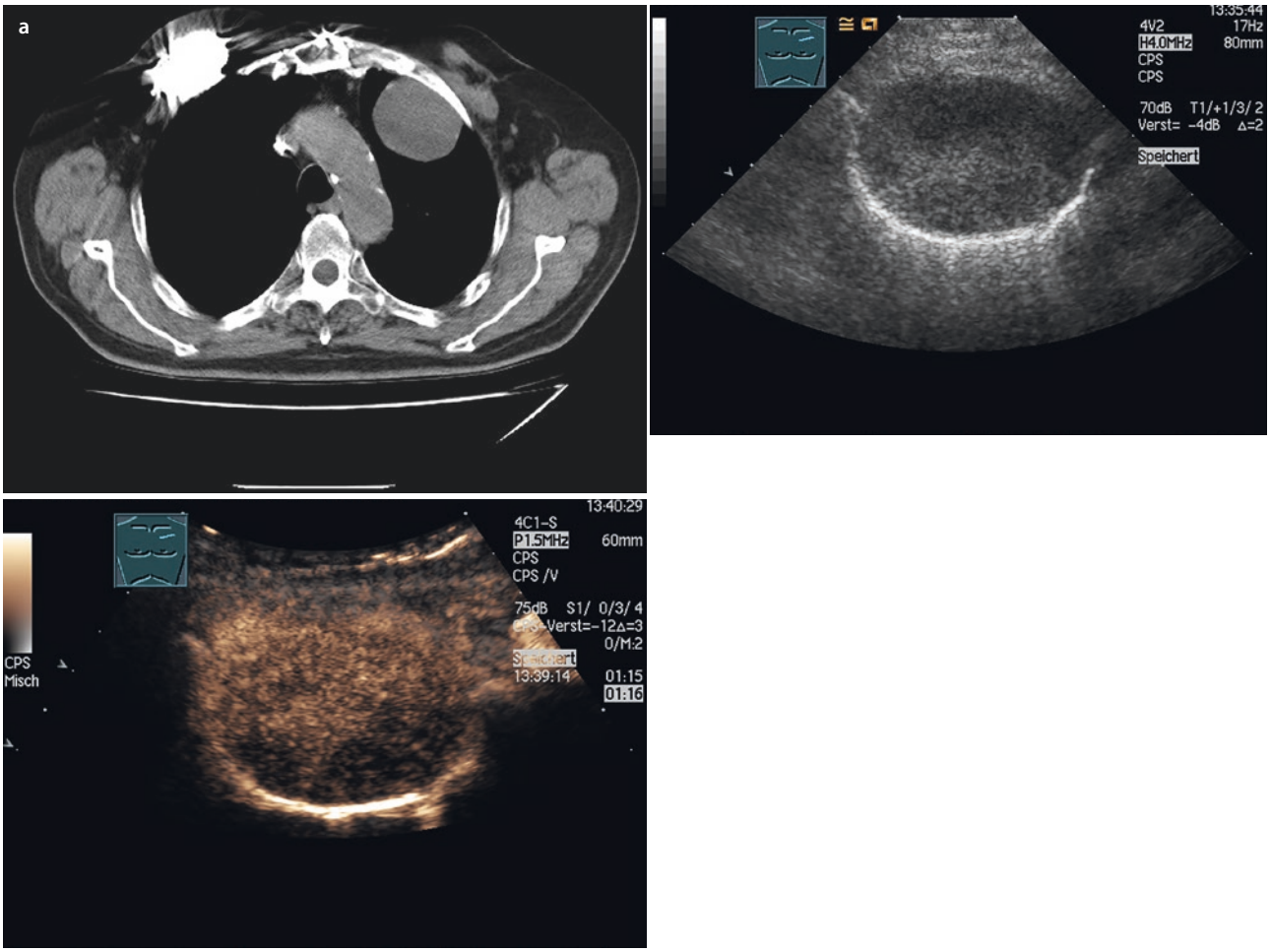

Fig. 8.36 **a** Patient with computed tomography of a left dorsocaudal mass. The patient's medical history included a condition after traumatic splenectomy. On B-mode ultrasound, the tumor is oval and homogeneously hypoechoic. On CEUS, the tumor shows a homogenous marked enhancement after 6 min, as in thoracic splenosis. This was histologically confirmed. **b** Patient with peripheral lung lesion as an incidental finding, without evidence of an underlying malignant disease. The tumor is echogenic on B-mode US and shows a marked enhancement. Histologically, a solitary fibrous tumor (SFT) was confirmed

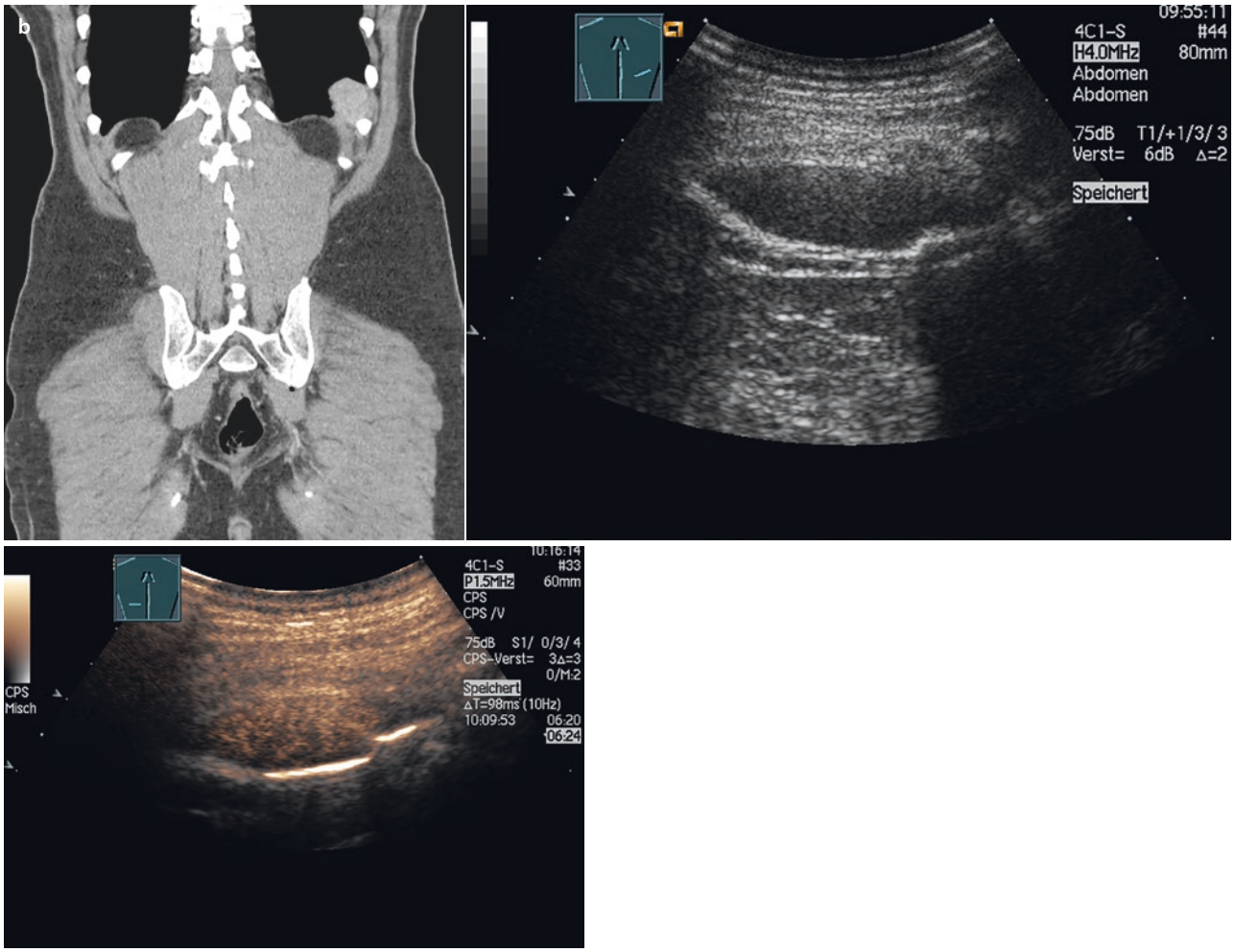

Fig. 8.36 (continued)

8.5.4.2 Contrast Enhanced Ultrasound (CEUS)

In keeping with the findings on CDS, classic pneumonia is characterized by a short period until the arrival of contrast enhancement and strong contrast enhancement on CEUS (Linde et al. 2012). This is indicative of predominant vascularization though pulmonary arteries (Fig. 8.37). Reduced contrast enhancement is observed in cases of lobar pneumonia and can be explained by hypoxic vasoconstriction of the pulmonary artery (Table 8.1). Delayed contrast enhancement indicates perfusion by bronchial arteries and is observed in cases of liquefaction and chronic pneumonia (Figs. 8.38 and 8.39). An inhomogeneous contrast enhancement is useful for the identification of atypical

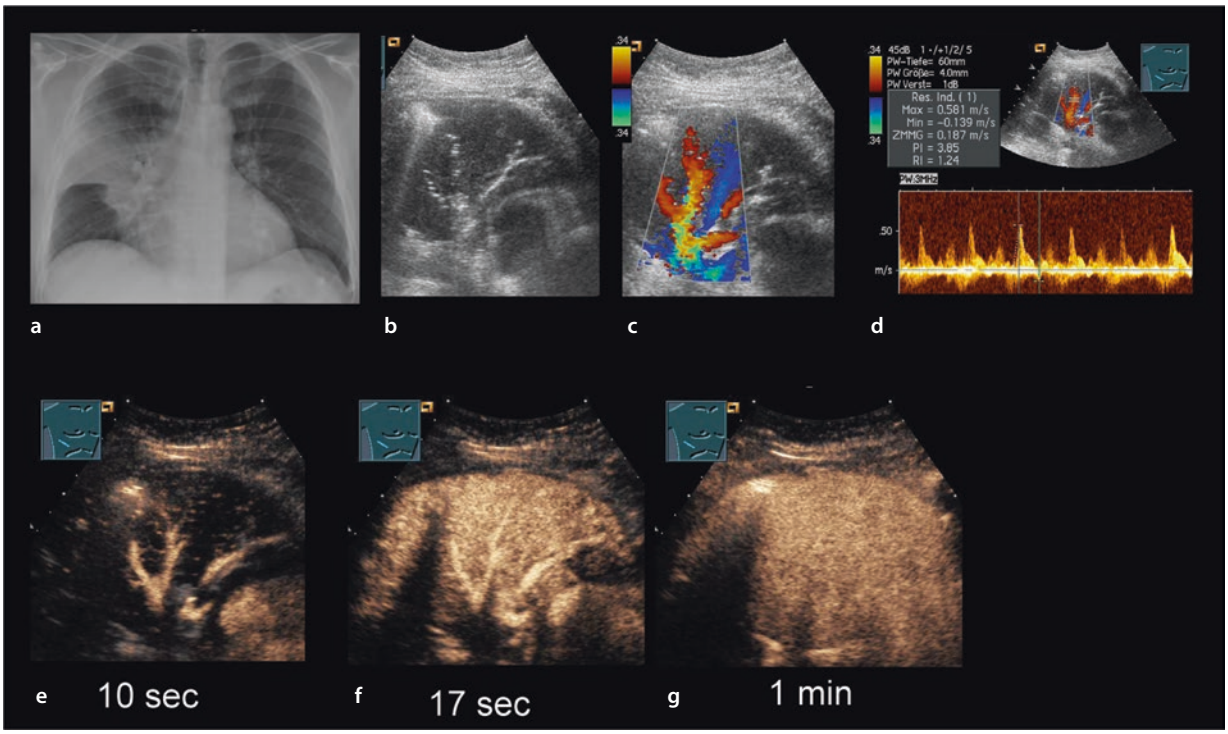

Fig. 8.37 **a** Patient with clinically and radiographically diagnosed pneumonia. **b** On B-mode ultrasound, a typical flat consolidation with a positive air bronchogram can be seen. **c** On CDS, a ordered vessel tree can be observed. **d** In the spectral curve analysis, the arterial centrifugal vessels show a high-impedance flow signal similar to that of pulmonary arteries. **e–f** On CEUS a pulmonary arterial vascular tree can be recognized with a marked and homogeneous contrast enhancement

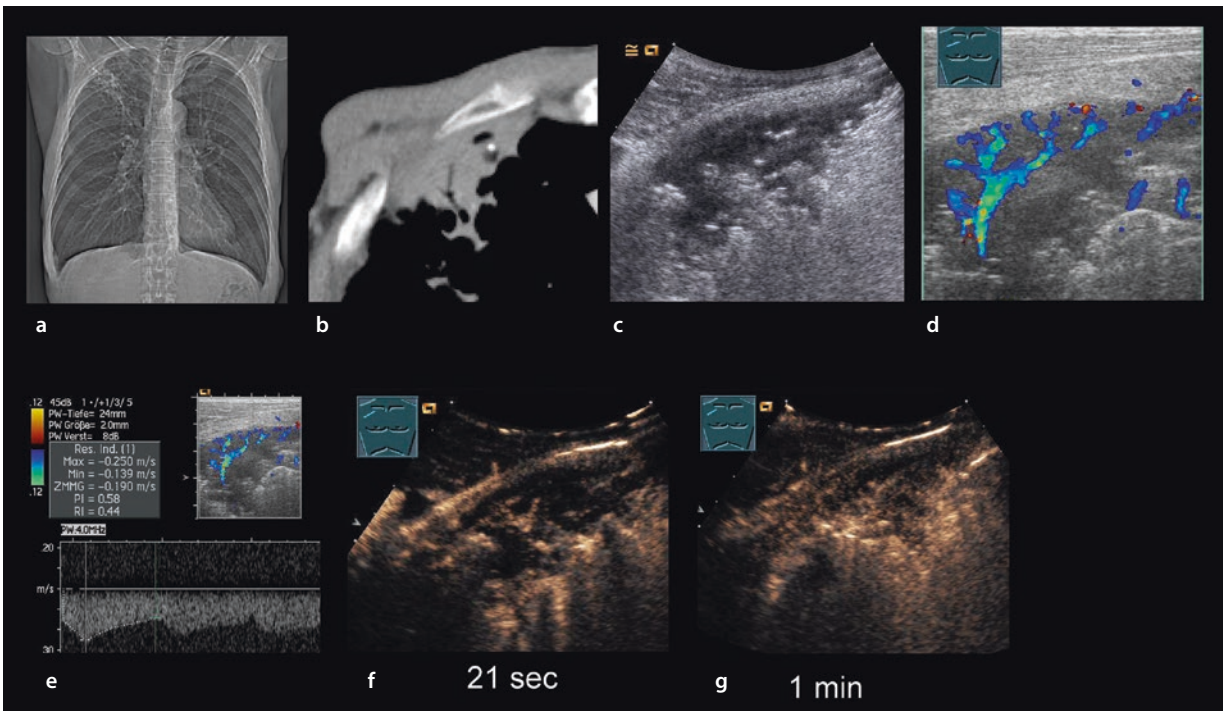

Fig. 8.38 **a** Patient with chronic therapy-resistant pneumonia and radiographic infiltrate in the upper region with suspected tuberculosis. **b** Computed tomography confirms the infiltrate with a gentle melting. **c** On B-mode ultrasound, a hypoechoic consolidation with standing air reflexes is revealed. **d** On CDS, a vessel is seen running from the lung surface to the center. **e** Using spectral curve analysis, these vessels can be identified as bronchial arteries based on their low impedance flow signal. **f** and **g** On CEUS, the lesion shows a delayed bronchial arterial enhancement, with reduced and inhomogeneous contrast enhancement. The biopsy confirmed the diagnosis of chronic scarified pneumonia with pronounced fibrosis without evidence of tuberculosis

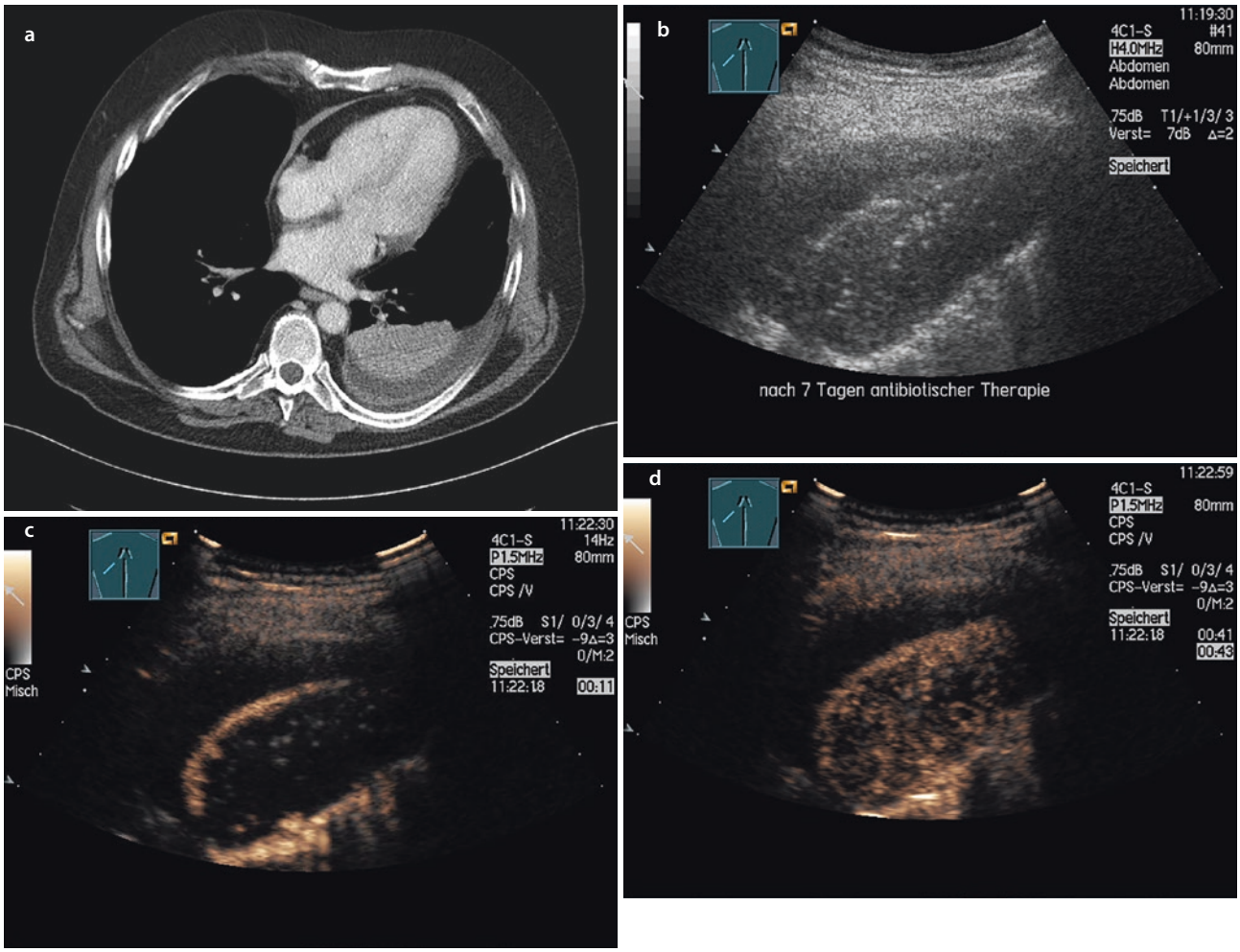

Fig. 8.39 **a** Patient with pneumonia resistant to antibiotics and cortisone therapy. On computed tomography, a homogeneous consolidation is observed. **b** On B-mode ultrasound, a hypoechoic consolidation is observed. **c** On CEUS, after 11 s the lesion shows a delayed marginal bronchial arterial enhancement without pulmonary arterial perfusion. **d** In the parenchymal phase, a reduced and inhomogeneous contrast enhancement is present. The biopsy revealed the diagnosis of chronic cryptogenic pneumonia (COP), without evidence of malignancy

courses with evidence of melting, necrosis, infarction areas, bleeding and abscesses (Fig. 8.40). In particular, in parapneumonic polyseptized echogenic effusions with suspicion of pleural empyema, this area can be clearly demarcated from the infiltrated lung. Furthermore, a parainfectious pleural thickening with contrast-medium enhancement can be detected (Fig. 8.40a). The value of CEUS in pneumonia is in the detection of atypical and complicated courses.

A common pitfall is identifying bronchioloalveolar carcinoma, which reveals a perfusion pattern like that of acute "pneumonia" on CDS and CEUS (Fig. 8.41) (Findeisen et al. 2018).

8.5.5 Large Lung Consolidation: Compressive Atelectasis

8.5.5.1 Color-Doppler Sonography

Compressive atelectasis is seen on radiographs and sonography in conjunction with pleural effusion and the cardinal finding of a peripheral basal lung consolidation. The main finding is a pleural effusion, followed by the visualization of the consecutive compressed lung tissue. On qualitative CDS atelectasis is seen as strongly tree-like vessels. On arterial spectral analysis one usually finds a high-impedance flow signal indicative of pulmonary arteries (Fig. 8.42).

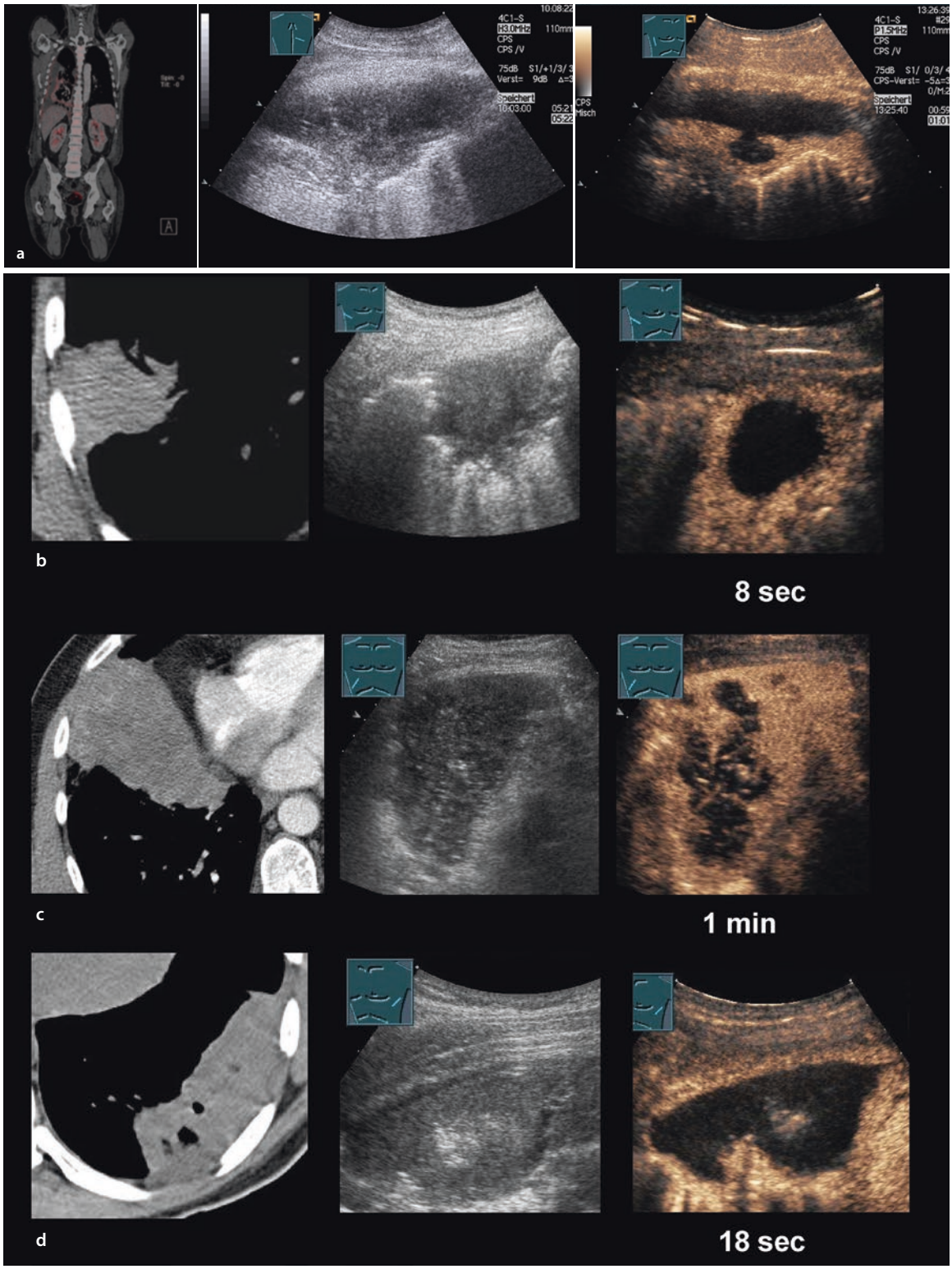

Fig. 8.40 Visualization by computed tomography, B-mode ultrasound and CEUS of a patient with atypical pneumonia. **a** Patient with pneumonia and parapneumonic empyema: CEUS sharply demarcates the empyema from the infiltration and shows a non-enhancement lesion with narrow contact with the empyema, as in the case of a pulmonary abscess perforated into the pleural space. **b** Patient with acute myeloid leukemia and condition after *Aspergillus* pneumonia: CEUS clearly shows a non-enhanced central area in terms of necrosis. A resection of the infiltrate was performed before planned bone-marrow transplantation (BMT). **c** Fire-eater who aspirated paraffinized hydrocarbon: CEUS clearly shows central necrosis in the infiltrated lung. **d** Patient with acute lymphoblastic leukemia and residual pneumonic infiltrate before planned BMT: CEUS provides a diagnosis of infarct pneumonia. A BMT was performed

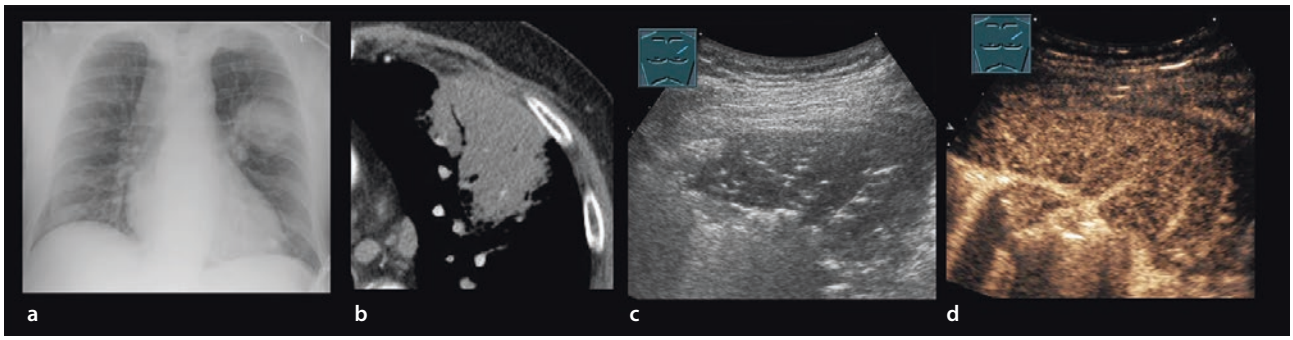

Fig. 8.41 Patient with dyspnea without fever and a mass in the right midfield, which is shown by X-ray **a** and by computed tomography **b** as typical pneumonia. **c** B-mode ultrasound shows a hypoechoic consolidation with air bronchogram, as in pneumonia. **d** On CEUS, the tumor shows an increased, homogeneous and early arterial contrast enhancement, as in pneumonia. The US-guided biopsy revealed the diagnosis of bronchioloalveolar carcinoma

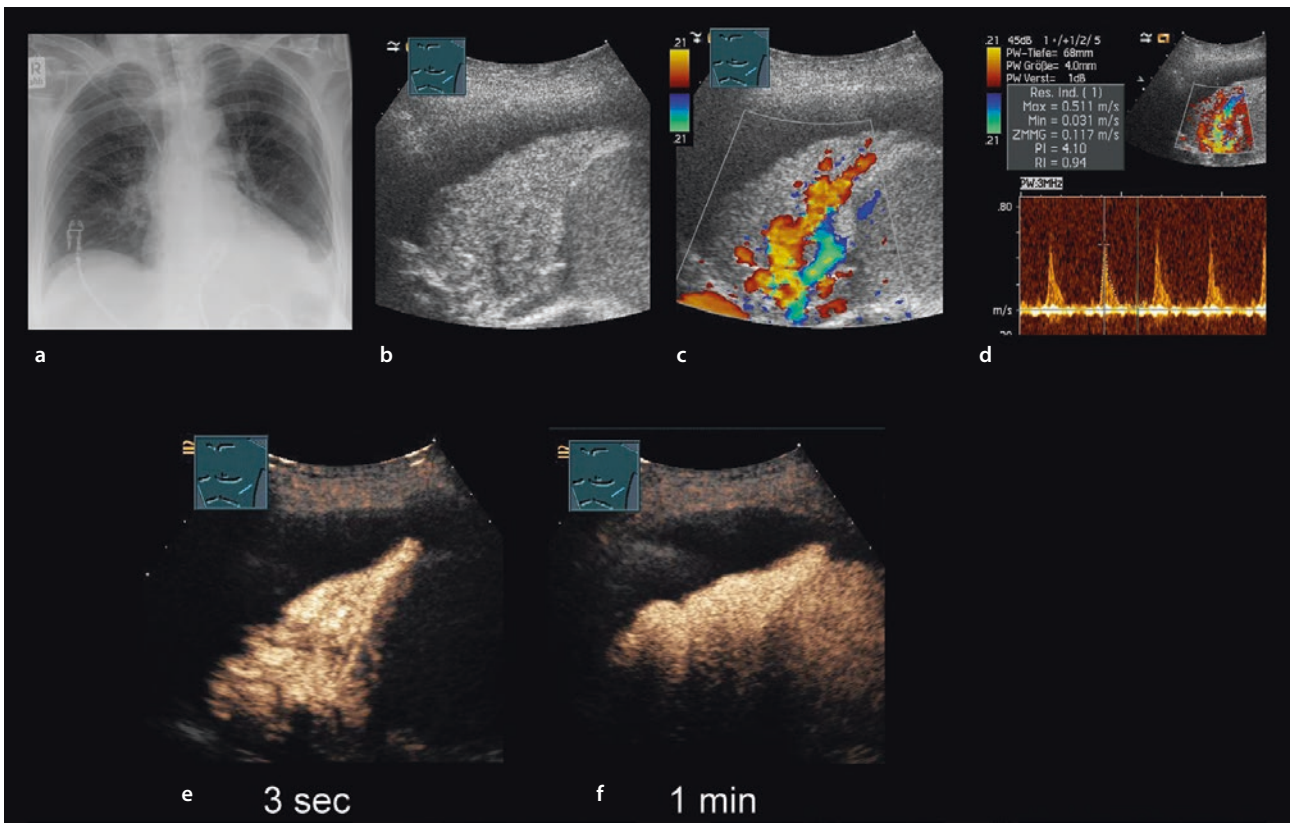

Fig. 8.42 **a** Patient with left-sided pleural effusion on chest X-ray. **b** On B-mode ultrasound, a homogeneous consolidation as in atelectasis is present. **c** On CDS, the targeted, pronounced vascular visualization is impressive. **d** On spectral curve analysis, the arterial centrifugal vessels show a high-impedance flow signal as in pulmonary arteries. **e**, **f** On CEUS, the enhanced pulmonary arterial vascular tree with a homogeneous parenchymal contrast enhancement is characteristic of compression atelectasis

8.5.5.2 Contrast Enhanced Ultrasound (CEUS)

The performance of a CEUS can be indicated in cases of unexplained effusion formation and complicated clinical courses. The lung parenchyma, pleura and effusion should be assessed using CEUS. According to the findings of CDS, "normal" compression atelectasis shows a short time to the arrival of contrast-medium and an increased extent of contrast-medium enhancement in CEUS (Fig. 8.42). This suggests a completely pulmonary arterial perfusion. The CEUS pattern of compression atelectasis is very specific (Table 8.1). Round intraparenchymatous lesions may indicate pulmonary metastases (Fig. 8.43a), wedge-shaped peripheral defects may indicate infarcts (Fig. 8.43b), and inhomogeneous areas in lung may indicate hemorrhage in patients with chest trauma (Fig. 8.43c). These lesions

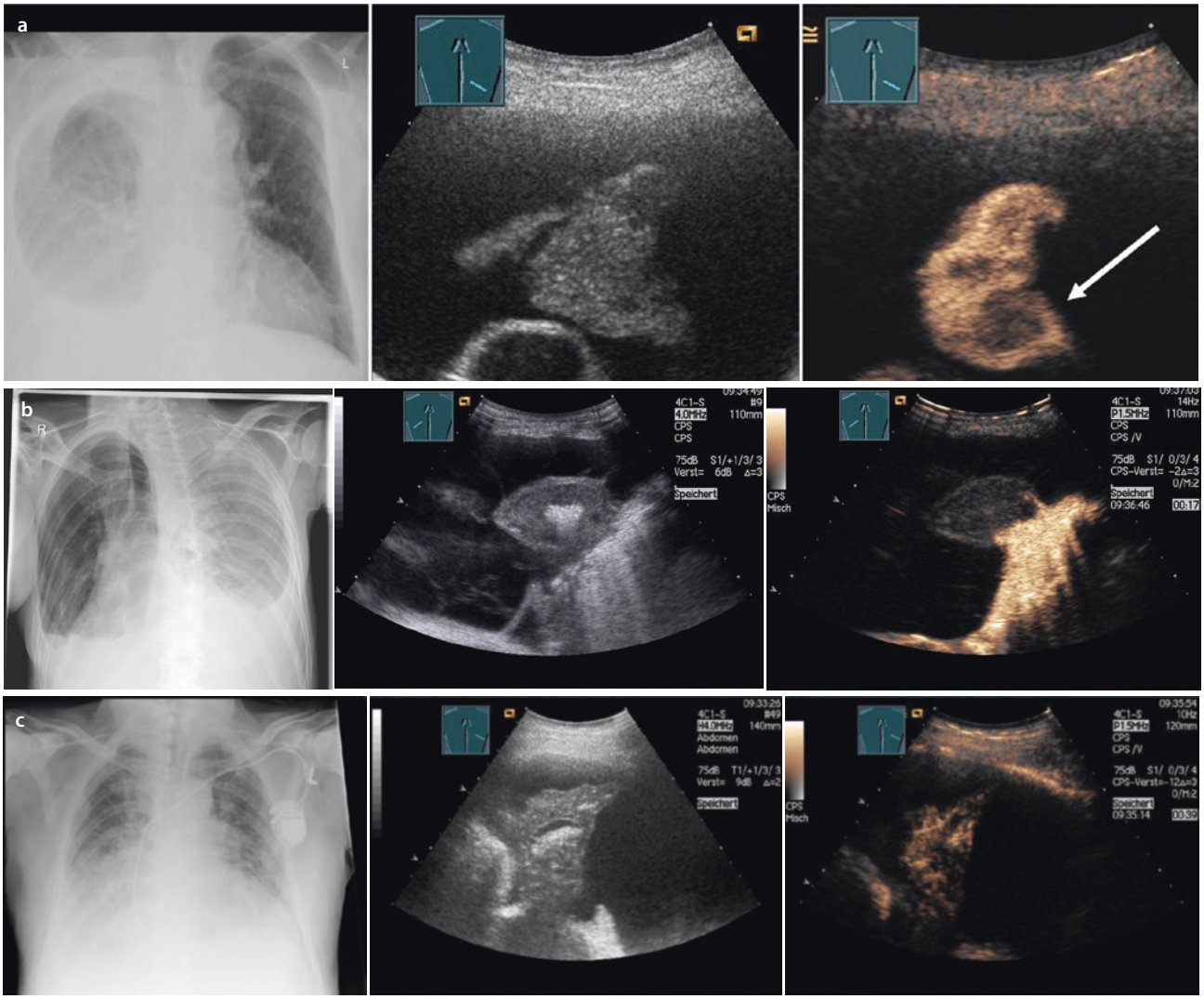

Fig. 8.43 Visualization of computed tomography, B-mode ultrasound and CEUS findings in a patient with focal lesion in an atelectatic lung. **a** Patient with known breast carcinoma and large pleural effusion: on CEUS, multiple round lesions (arrow) can be detected in atelectasis, as in metastases. **b** Patient with pancreatic carcinoma in their medical history and a large polyseptic pleural effusion and atelectasis: on CEUS, an absence of contrast enhancement of the atelectasis is detected, as in pulmonary infarction. **c** Patient with chest trauma and basal shadows in the chest X-ray due to confirmed hematothorax: B-mode US shows a pleural effusion with pulmonary atelectasis; on CEUS, an inhomogeneous enhancement in the atelectatic tissue occurs in terms of a pulmonary hemorrhage (arrow).

can be visualized in atelectatic lung tissue by a reduced, absent or inhomogeneous contrast enhancement, respectively. Chronic compression atelectasis can lead to a shift from pulmonary arterial supply to completely nutritive bronchial arterial perfusion (Fig. 8.44). The CEUS can provide useful information regarding the etiological clarification of pleural effusions. A benign echogenic polyseptated effusion (Fig. 8.45) can be clearly differentiated from echogenic polyseptated tumor tissue (Fig. 8.46), and pleural tumor (Fig. 8.47) from a benign pleural thickening (Fig. 8.48). The differentiation of hematoma or fibrin bodies from vital tissue is also possible with CEUS (Fig. 8.49). However, the definitive diagnosis is principally made histologically.

8.5.6 Large Lung Consolidation: Obstructive Atelectasis

8.5.6.1 Color-Doppler Sonography (CDS)

The obstructive lung atelectasis is seen as a largely homogeneous hypoechoic transformation on the B-mode ultrasound. Depending on the duration of the obstruction, evidence of a "fluid bronchogram" is a characteris-

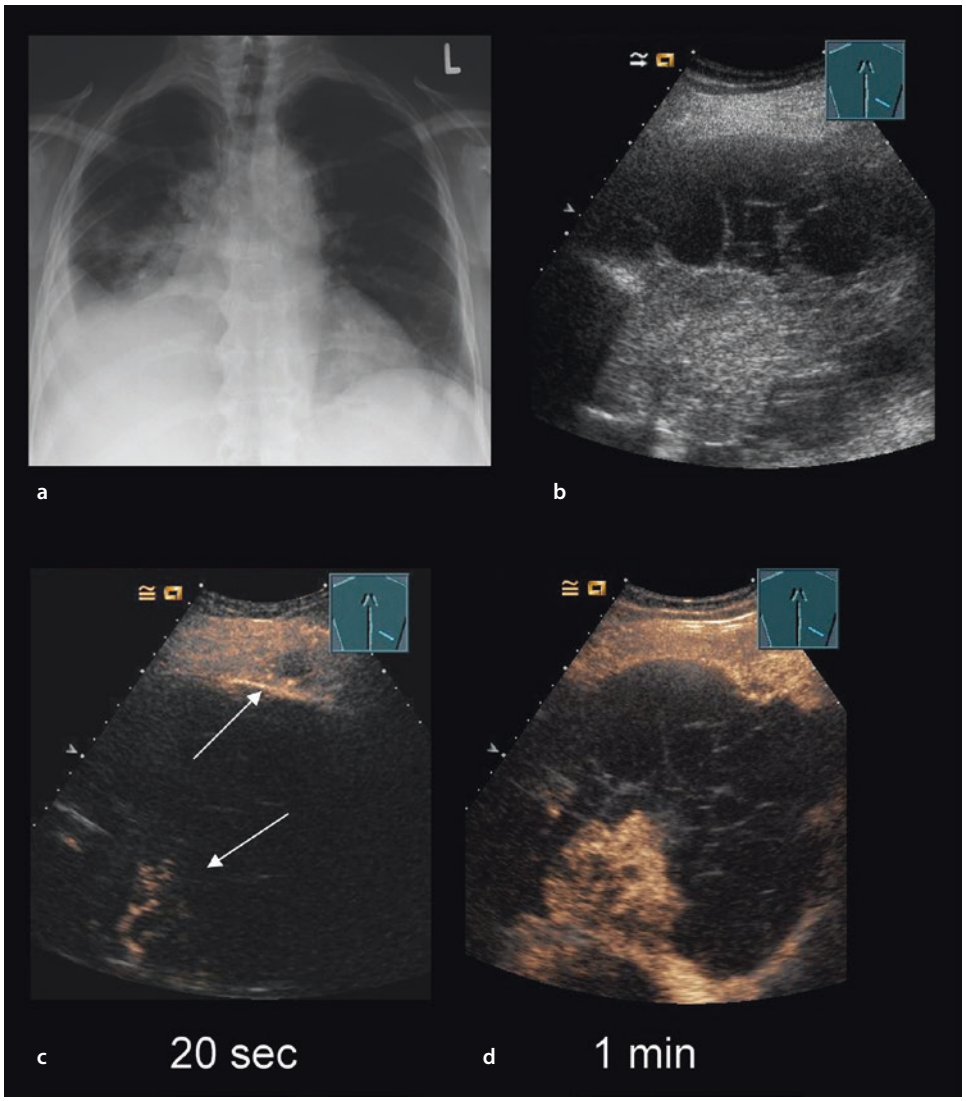

Fig. 8.44 **a** Patient with non-small-cell lung carcinoma. in their medical history with condition after radio chemotherapy and now right-sided pleural effusion in the chest X-ray. **b** B-mode ultrasound shows a homogeneous consolidation of the lung, as in atelectasis. **c** On CEUS, after 20 s, a systemic vascularization in the atelectasis (arrow) simultaneously with the enhancement of the thoracic wall (arrow) is recognizable as an indication of a central bronchial arterial nutritive perfusion of the atelectasis. **d** After 1 min, the atelectasis shows a homogeneous enhancement, possibly as an indication of tumor neoangiogenesis

tic feature in this setting. On qualitative CDS one finds pronounced vessels with evidence of an arterial high-impedance flow signal due to the branches of the pulmonary artery. A frequent finding is the central tumor responsible for the atelectasis. The consolidated atelectatic lung tissue serves more or less as an "acoustic window" to explore central lung structures (Fig. 8.50). According to Fissler-Eickhoff and Müller (1994), invasion and infiltration of the pulmonary arteries located in the region of the tumor occurs in 96% of the cases of bronchial carcinoma investigated. This disturbed vascular architecture of the pulmonary artery is seen on sonography as reduced or no visualization of vessels in the downstream atelectatic lung tissue.

8.5.6.2 Contrast Enhanced Ultrasound (CEUS)

In keeping with the CDS findings, a recent obstructive atelectasis is marked by the same features as compressive atelectasis with a short arrival time to contrast enhancement and strong contrast enhancement on CEUS. This is indicative of atelectatic lung tissue being entirely vascularized by the pulmonary arteries. In this phase, in patients with a central tumor formation, the tumor may be demarcated from atelectatic lung tissue more clearly by CEUS than by B-mode sonography (Fig. 8.51). In cases of obstruction of longer duration, within the atelectasis one may find liquefactions and abscesses formations (Fig. 8.52). Prolonged obstruction can lead to liquidations, pulmonary artery

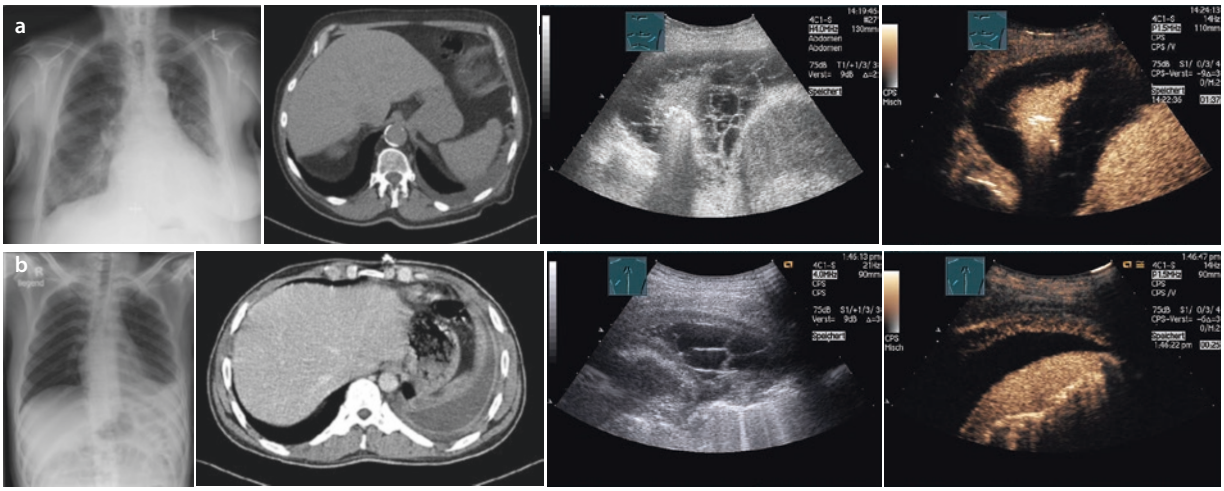

Fig. 8.45 **a** Patient with parapneumonic pleural effusion. In the chest X-ray, a shadowing of the left diaphragmatic rib angle is visualized. Computed tomography (CT) shows a left-sided effusion. B-mode ultrasounds shows a lower lobe consolidation with polyseptated effusion. On CEUS, the septa do not show an enhancement. **b** Patient with parapneumonic pleural effusion. In the chest X-ray, a shadowing of the left diaphragmatic rib angle is visible. On CT, a left-sided effusion with partial consolidation of the lung and pleural thickening is visualized. B-mode US shows a partial consolidation of the lower lobe with polyseptated effusion and thickened pleura parietalis. On CEUS, the septa show no enhancement, but the pleura shows a marked enhancement. Video-assisted thoracoscopic surgery revealed the diagnosis of a pleural empyema, with evidence of calcifying granulomas due to *Mycobacterium carnetii* infection

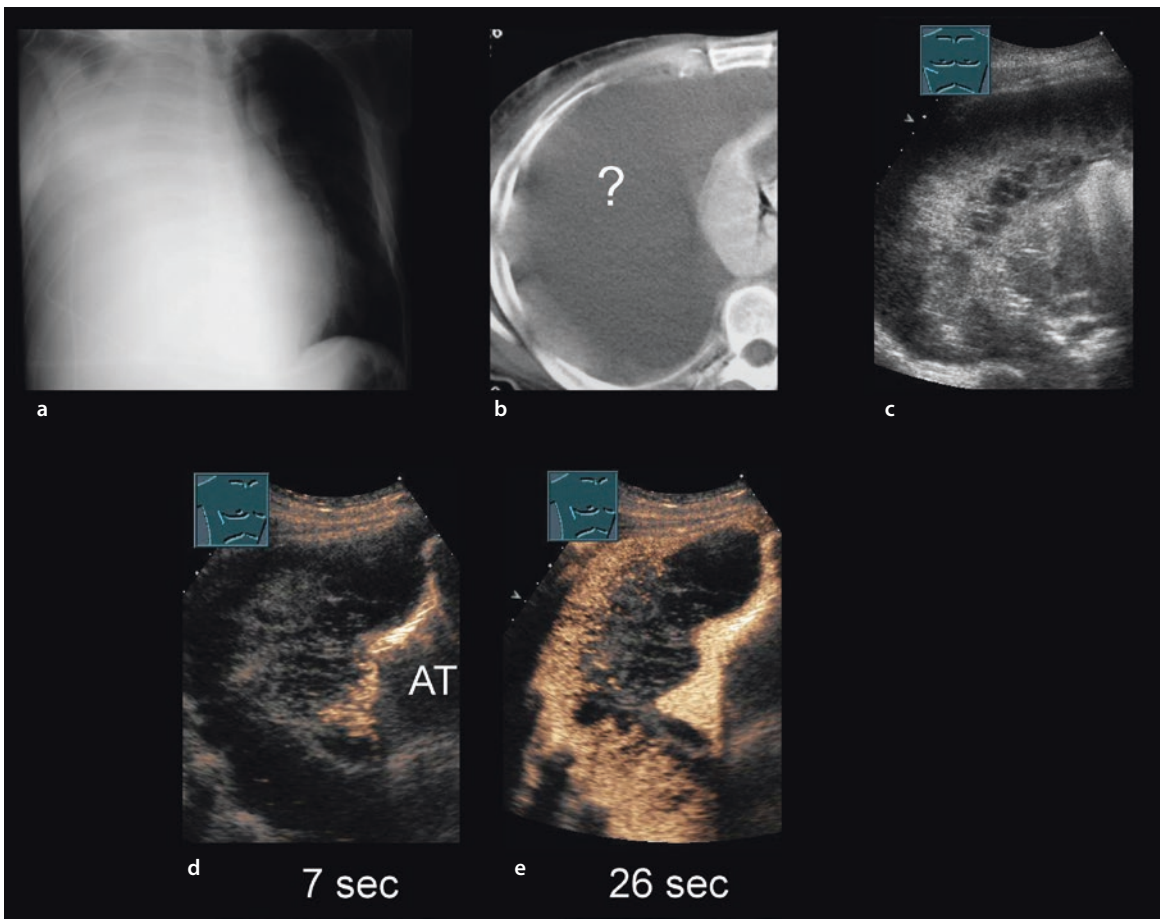

Fig. 8.46 Patient with known malignant melanoma. **a** In the chest X-ray, a complete right-sided shadowing of the hemithorax is recognizable. **b** On CT, solid parts of the effusion cannot be reliably delimited. **c** B-mode ultrasound shows a polyseptated hemithorax. **d** On CEUS, a contrast enhancement in the central atelectasis (AT) can be seen after 7 s. **e** After 26 s, a marked contrast enhancement from the periphery can be seen as an indication of peripheral bronchial arterial vascularization. Only a small part of the thoracic cavity shows polyseptated pleural effusion

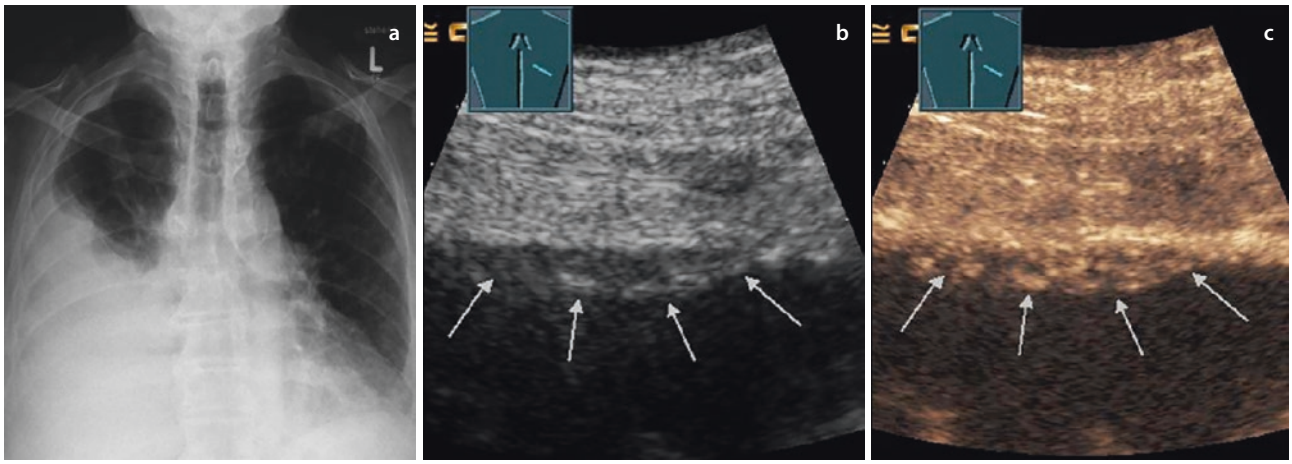

Fig. 8.47 Patient with bronchial carcinoma. **a** A right-sided pleural effusion is visualized by chest-X-ray. **b** On B-mode ultrasound, a flat pleural thickening is visible. **c** On CEUS, the pleural formation shows a contrast enhancement. The US-guided biopsy revealed the diagnosis of pleural carcinosis

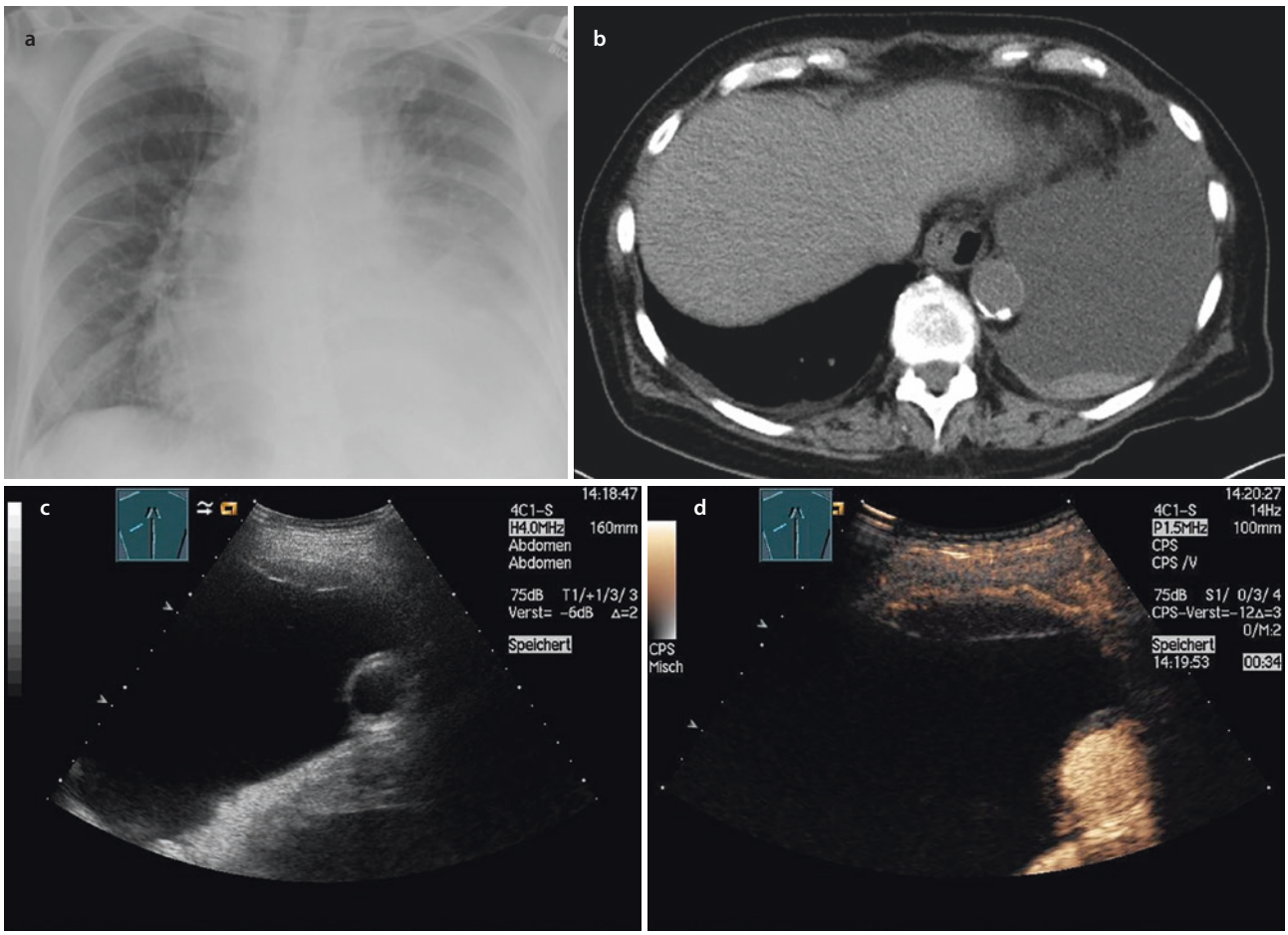

Fig. 8.48 Patient with pleural effusion due to congestive heart failure for clarification. **a** In the chest X-ray, a left-sided shadowing of the caudal hemithorax is recognizable. **b** On CT, a clear effusion with a dorsal flat pleural thickening is present. **c** B-mode ultrasound shows the hypoechoic pleural thickening. **d** On contrast-enhanced ultrasound, the pleural formation shows no contrast enhancement. The US-guided biopsy revealed the diagnosis of chronic fibrinoid pleuritis

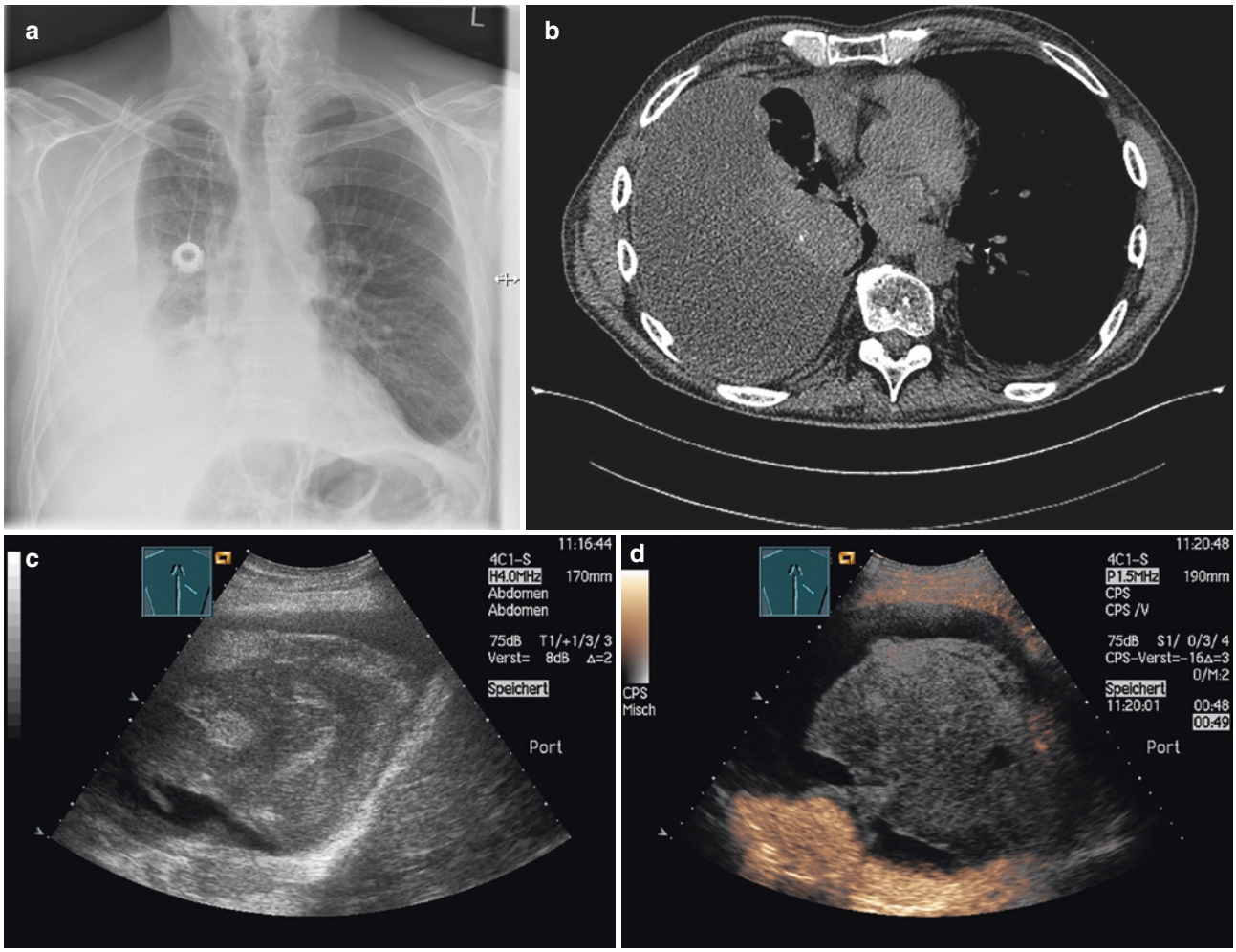

Fig. 8.49 Patient with pleural effusion in non-small-cell lung cancer. **a** In the chest X-ray, a right-sided shadowing of the caudal hemithorax is visualized. **b** On CT, a clear effusion with atelectasis is seen. **c** B-mode ultrasound shows a large echogenic tumor formation. The diagnostic thoracocentesis revealed a hemorrhagic effusion. **d** On contrast-enhanced ultrasound, the tumor shows no contrast enhancement in terms of a localized blood clot

aneurysms (Fig. 8.53a) and abscesses within the atelectase/tumor (Fig. 8.53b). These potential lesions as well as metastases can be reliably diagnosed in atelectatic lung tissue by CEUS (Figs. 8.43a and 8.49h). In the course of a tumor-related obstructive atelectasis, depending on the structure of the tumor there may be infiltration and occlusion of pulmonary arteries of different extent. In this situation CEUS shows delayed arrival of contrast enhancement and reduced contrast enhancement (Fig. 8.54). This is indicative of a switch to vascularization of atelectatic lung tissue from pulmonary to bronchial arteries (Görg et al. 2006a). In the case of a missing bronchoscopic diagnostic confirmation of the central tumor, the suspected consolidation can be biopsied through atelectasis under CEUS guidance. (Fig.8.55). In general, the CEUS pattern in cases of obstructive atelectasis is variable.

8.5.7 Space-Occupying Lesion of the Chest Wall

8.5.7.1 Color-Doppler Sonography (CDS)

Sonography is the method of choice to explore the chest wall. The intercostal arteries supplying the chest wall are usually seen even in healthy individuals by the use of CDS (Fig. 8.56). Tumors in the chest wall or parietal

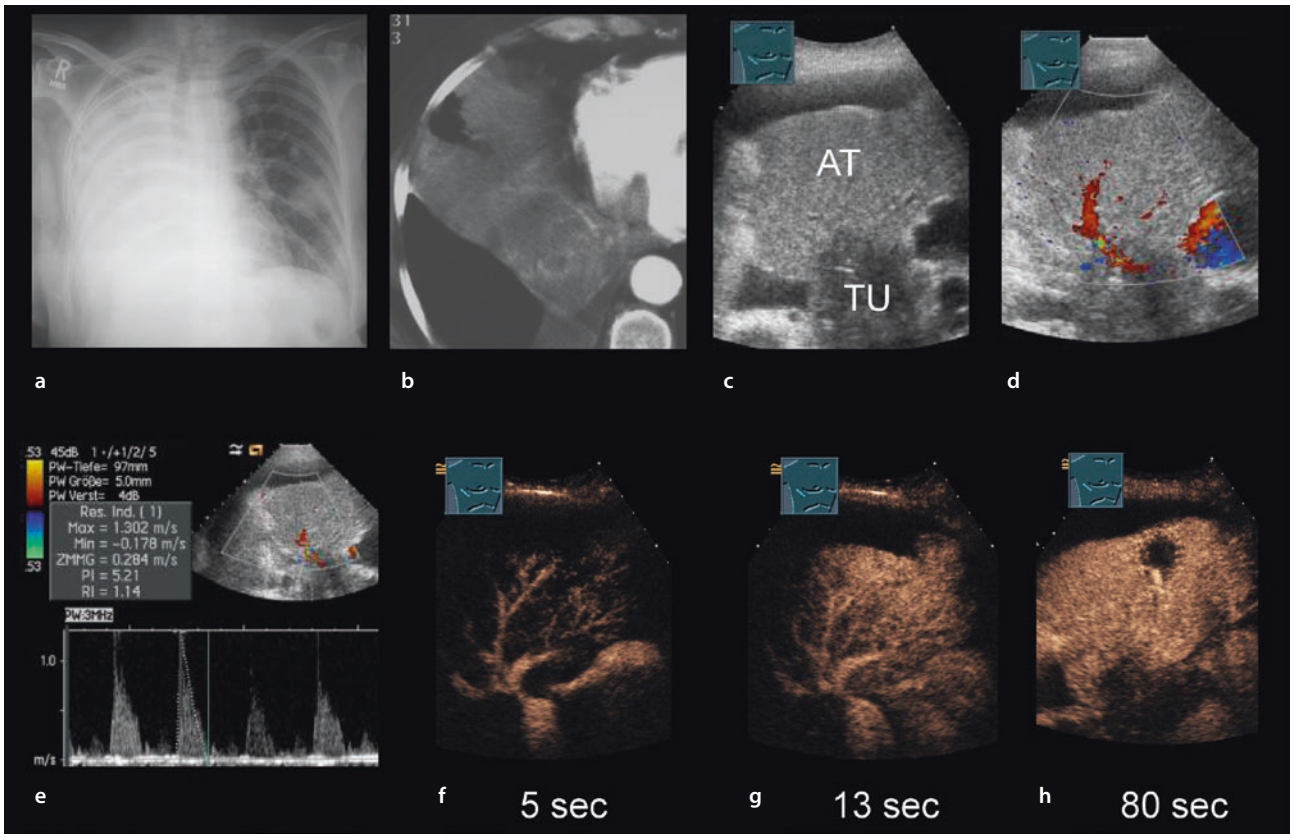

Fig. 8.50 Patient with bronchial carcinoma. **a** In the chest X-ray, a complete right-sided shadowing of the hemithorax is recognizable. **b** On computed tomography, a narrow effusion and a mass in the right upper lobe are revealed. **c** On B-mode ultrasound, an atelectasis (AT) and an underlying central tumor formation (TU) are visible. **d** On CDS, a large centrifugal vessel is visualized. **e** On spectral curve analysis, the vessel shows a high-impedance arterial flow signal, as in the pulmonary artery. **f** On CEUS, the pulmonary arterial vascular tree is visible after 5 s. **g** After 13 s, a contrast enhancement in the AT is present. **h** In the parenchymal phase, a washout in the area of the central TU is visible; furthermore, a focal parenchymal lesion is demarcated (differential diagnosis: melting, abscess, metastasis)

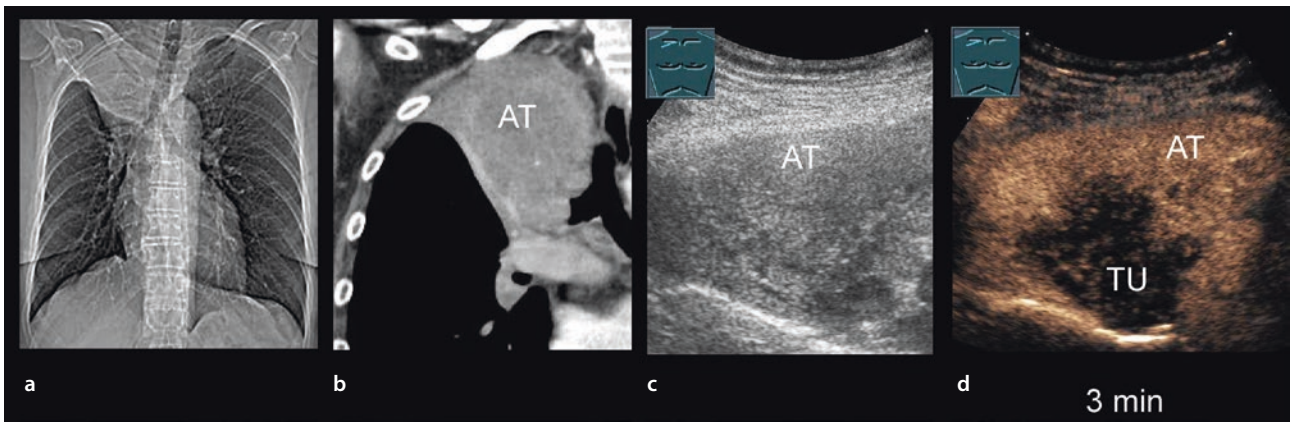

Fig. 8.51 Patient with bronchial carcinoma. **a** In the chest X-ray, a right-sided shadowing is observed in the area of the upper lobe. **b** On CT, an atelectasis (AT) is visualized without demarcation of a central tumor formation. **c** On B-mode ultrasound, the atelectasis (AT) is recognizable without the demarcation of a central tumor formation. **d** On CEUS, the atelectasis (AT) is recognizable, with the demarcation of a central tumor formation (TU)

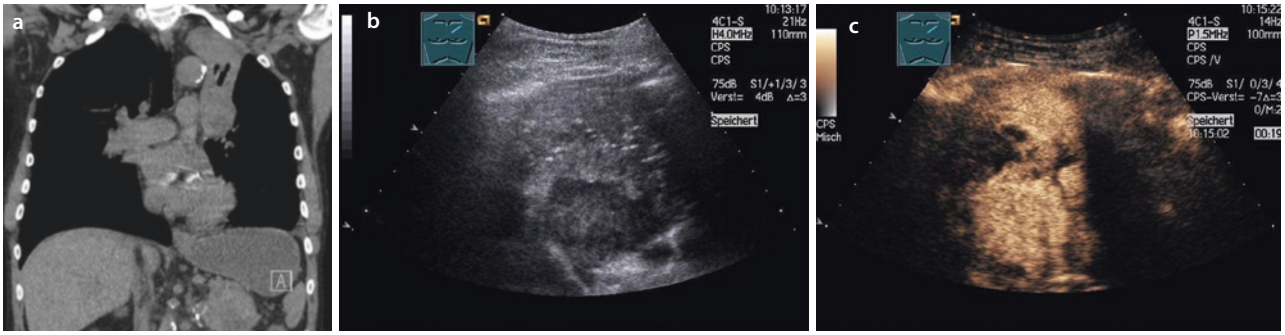

Fig. 8.52 Patient with renal cell carcinoma and mediastinal mass. **a** CT shows an atelectasis (AT), with demarcation of a central tumor formation. **b** B-mode ultrasound shows the atelectasis (AT), with demarcation of a hypoechoic central tumor formation (M). **c** The CEUS shows an atelectasis (AT), with the demarcation of a mass with marked enhancement, indicating the presence of a central mediastinal lymph node metastasis

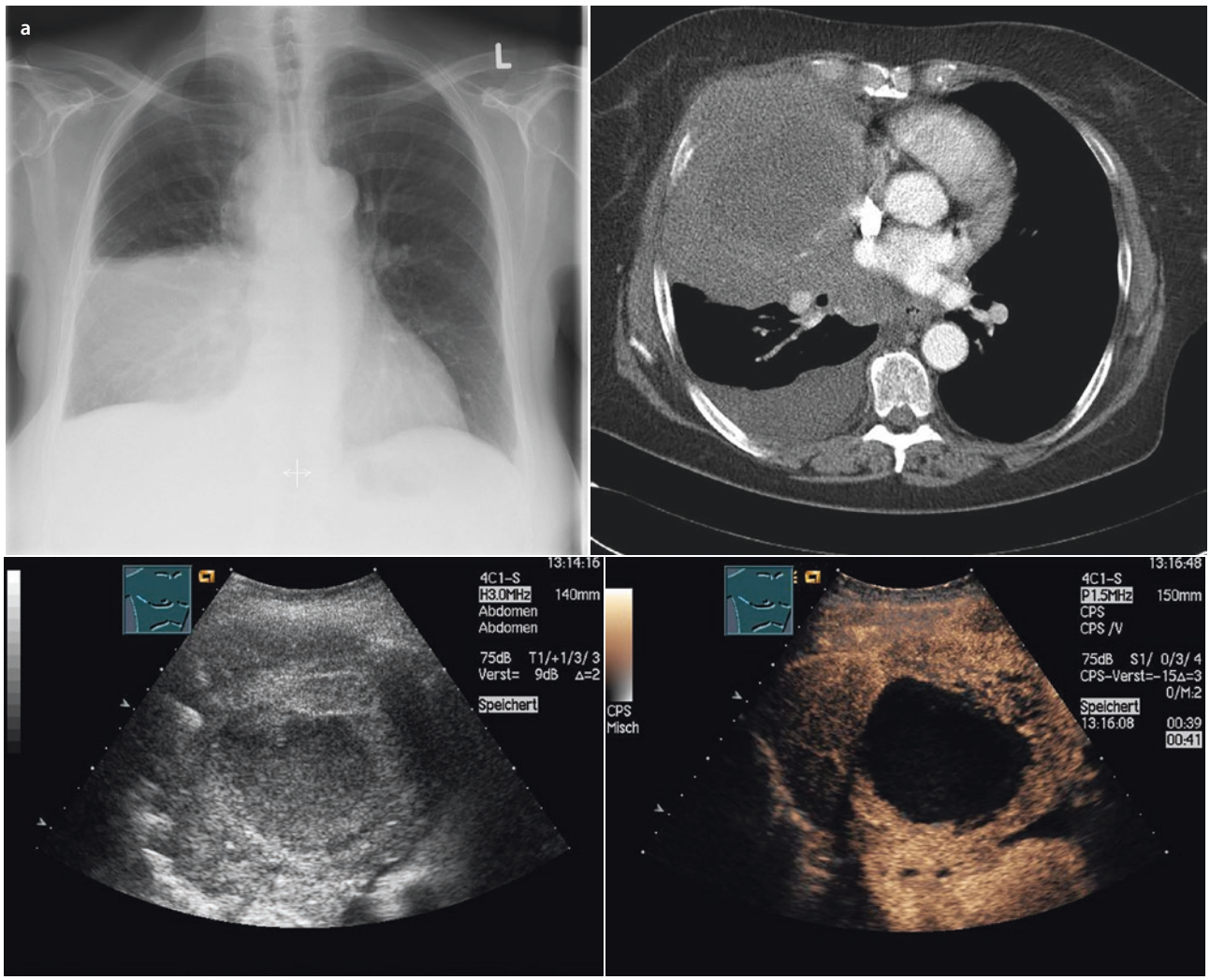

Fig. 8.53 **a** Patients with mediastinal malignant lymphoma and detection of a subsequent atelectasis in B-mode ultrasound. On CDS, arterial turbulence phenomena in the tumor can be detected. In the early arterial phase, the aneurysm fills rapidly and retains the contrast medium up to the parenchymal phase. **b** Patient with bronchial carcinoma. In the chest X-ray, a right-sided shadowing in the area of the lower lobe can be seen. CT shows a central tumor formation (TU) with subsequent atelectasis (AT). B-mode ultrasound shows a clearly inhomogeneous mass without a central tumor formation. On CEUS, atelectasis shows a rounded mass with no contrast enhancement, as in necrosis (N), abscess or melting

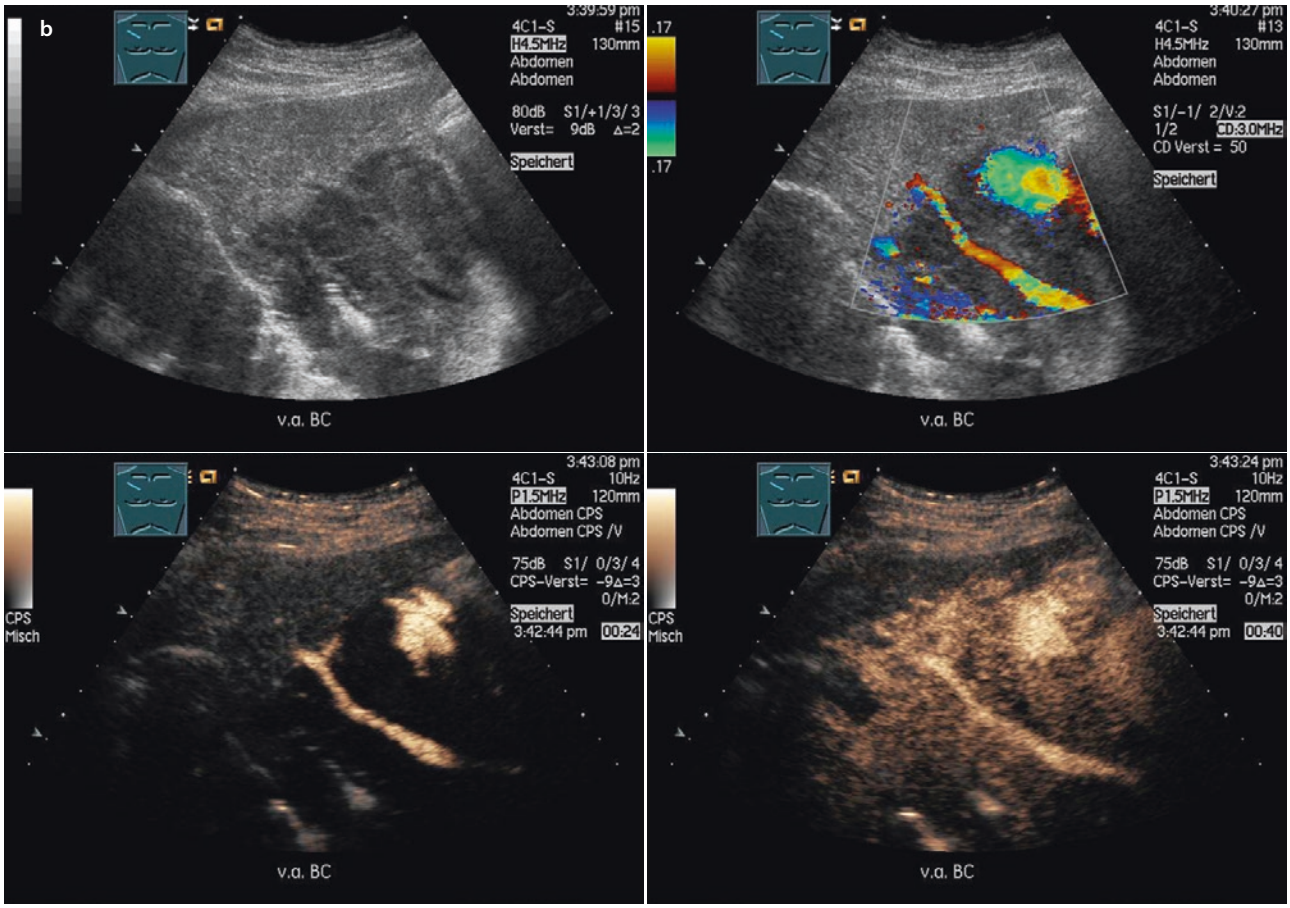

Fig. 8.53 (continued)

pleural metastases are characterized by predominantly intercostal perfusion with a monophasic flow profile in spectral curve analysis (Fig. 8.57). When the tumor has invaded the lung, CDS may show different flow signals as a sign of complex arterial tumor vascularization (Görg et al. 2005a; Fig. 8.58).

8.5.7.2 Contrast Enhanced Ultrasound (CEUS)

Specific studies to assess the value of contrast-assisted sonography in cases of space-occupying lesions of the chest wall are not available. Intercostal arteries are strong vessels, and these can be visualized by CEUS (Fig. 8.56e). They show a marked by a delayed systemic arrival of contrast enhancement. The extent of contrast enhancement of the arterial phase may vary. Tumors with pronounced neovascularization show marked contrast enhancement (Fig. 8.59). Contrast-enhanced ultrasound can also play a role in the differentiation of non-vascularized lesions, such as hematoma (Fig. 8.60) and abscess (Fig. 8.61) and can be helpful for tumor biopsy under CEUS guidance to avoid necrotic areas.

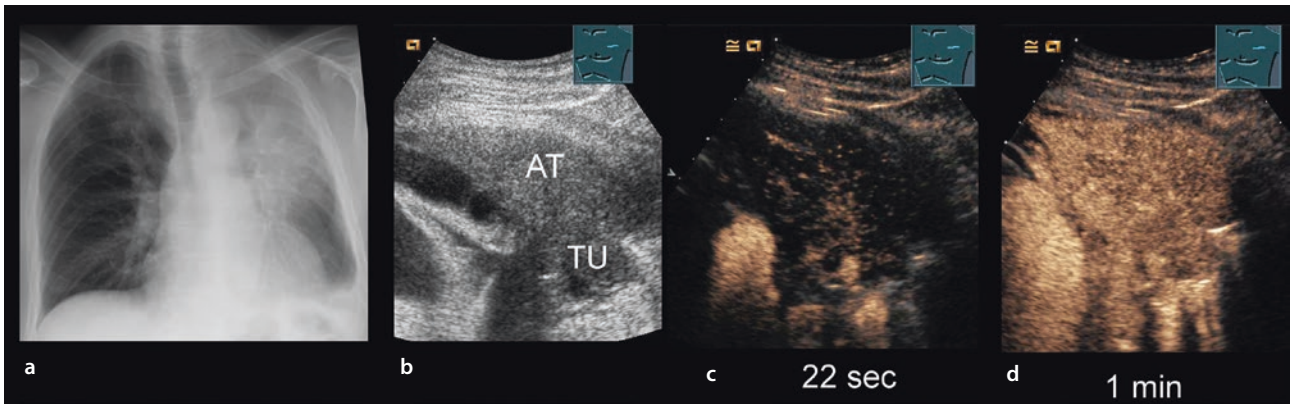

Fig. 8.54 Patient with bronchial carcinoma and condition after radio chemotherapy. **a** In a chest X-ray, a left-sided shadowing in the area of the upper field is recognizable. **b** On B-mode ultrasound, a central mass (TU) with atelectasis (AT) is observed. **c** On CEUS, after 20 s, a disorganized slow contrast enhancement, as in bronchial arterial vasculature, can be seen. **d** After 1 min, the lesion is characterized by an increased and homogeneous contrast enhancement

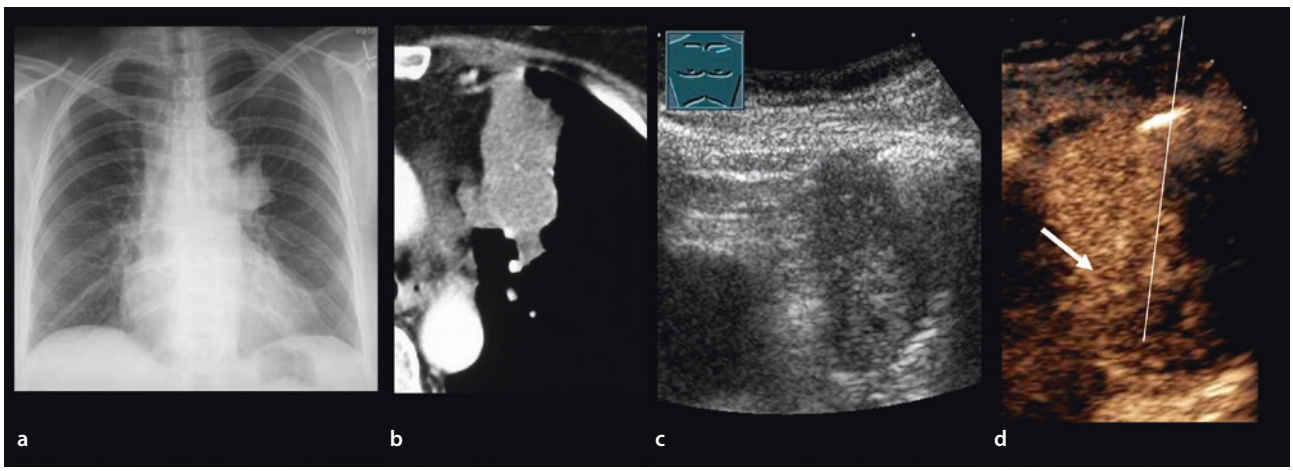

Fig. 8.55 Patient with bronchial carcinoma. **a** In a chest X-ray, a left-hilar mass is recognizable. **b** CT shows a central tumor formation in contact with the thoracic wall. Bronchoscopically, no tumor was detected. **c** B-mode ultrasound shows an inhomogeneous mass over a narrow "window" with no demarcation of a central tumor formation. **d** On CEUS, a central mass with reduced contrast enhancement is visualized, as in a central tumor (TU); this lesion was biopsied through the AT, with confirmation of a bronchial carcinoma

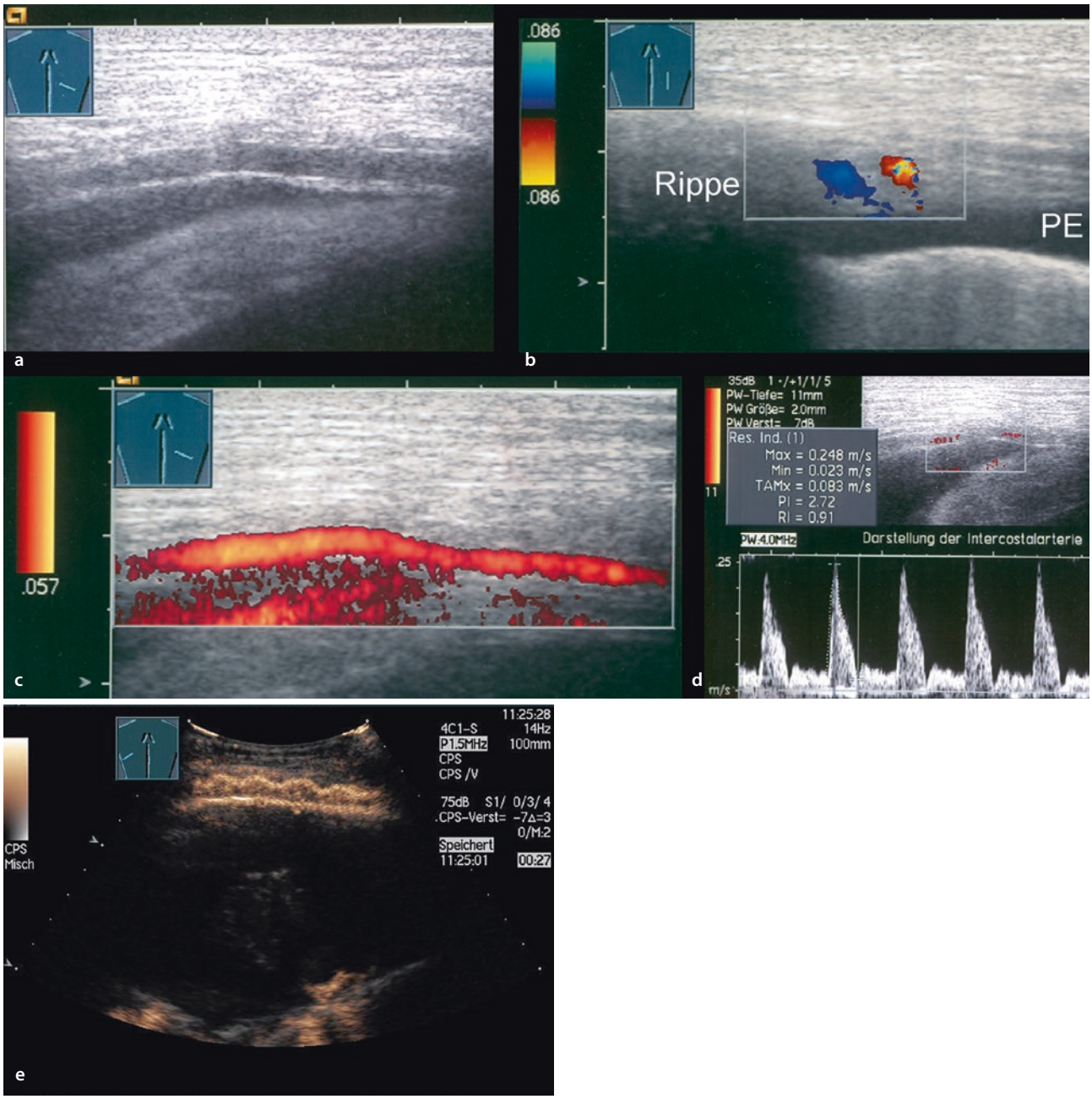

Fig. 8.56 Visualization of a normal intercostal artery in a healthy proband. **a** On B-mode ultrasound, the intercostal artery can be recognized with intercostal scan. **b** On CDS, the craniocaudal scan shows vascular reflexes beneath the ribs (PE, pleural effusion). **c** CDS shows the intercostal artery in a longitudinal scan. **d** Spectral curve analysis shows a monophasic high-impedance flow signal. This flow signal is characteristic of an intercostal artery. **e** On CEUS, the intercostal artery can be regular visualized

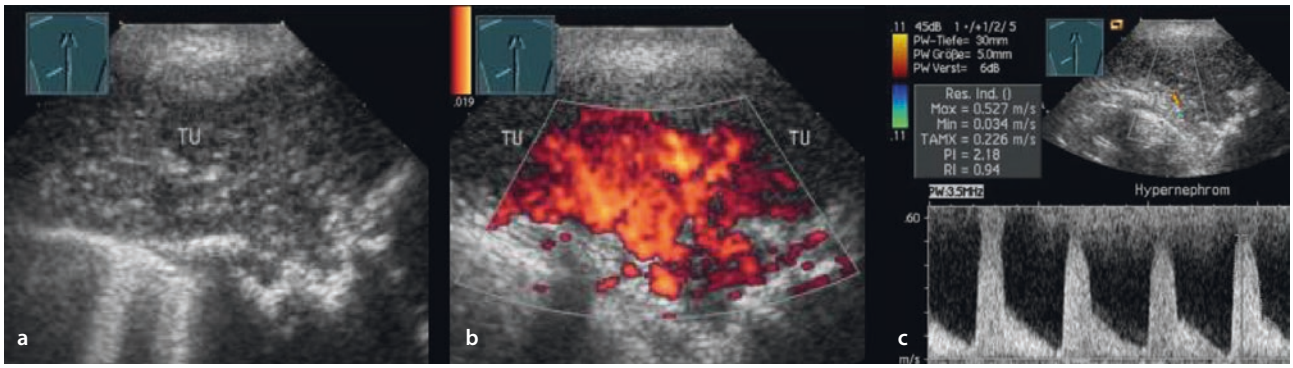

Fig. 8.57 Five-year-old patient with thoracic wall metastasis with known hypernephroma. **a** On B-mode ultrasound, a plain hypoechoic transformation of the left thoracic wall can be recognized (TU). **b** On CDS, an increased perfusion of the tumor formation can be visualized. **c** The spectral curve analysis shows a monophasic high-impedance flow signal similar to that of an intercostal artery

8

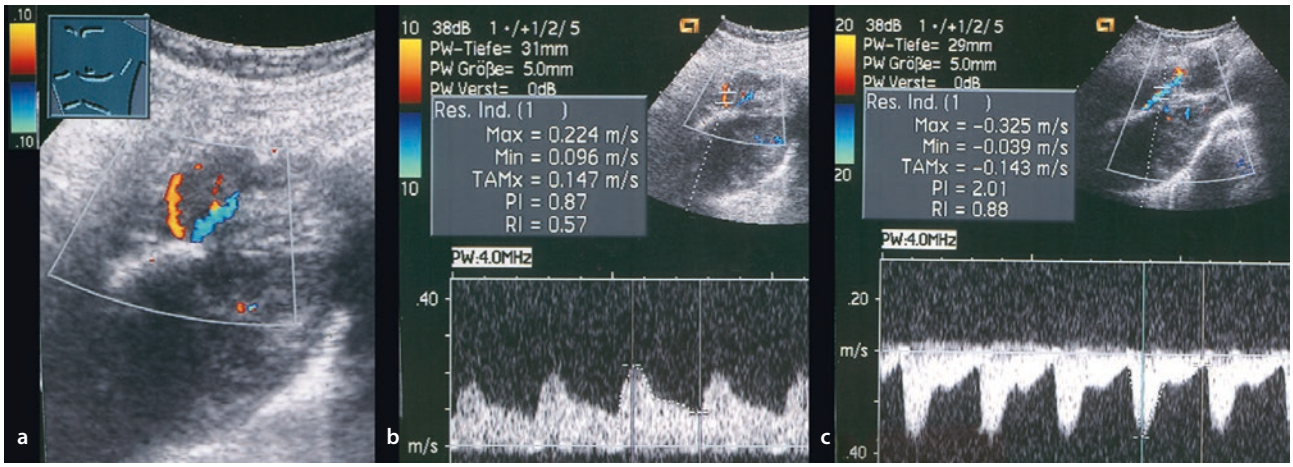

Fig. 8.58 a–c 34-year-old man with testicular carcinoma and metastatic disease in the chest wall. **a** CDS reveals a tumor formation growing into the lung. Vessels are seen within the tumor tissue. **b** Spectral curve analysis shows a monophasic low-impedance flow signal such as that seen in bronchial arteries. **c** Spectral curve analysis shows a monophasic high-impedance flow signal such as that seen in intercostal arteries. This finding is indicative of complex tumor perfusion

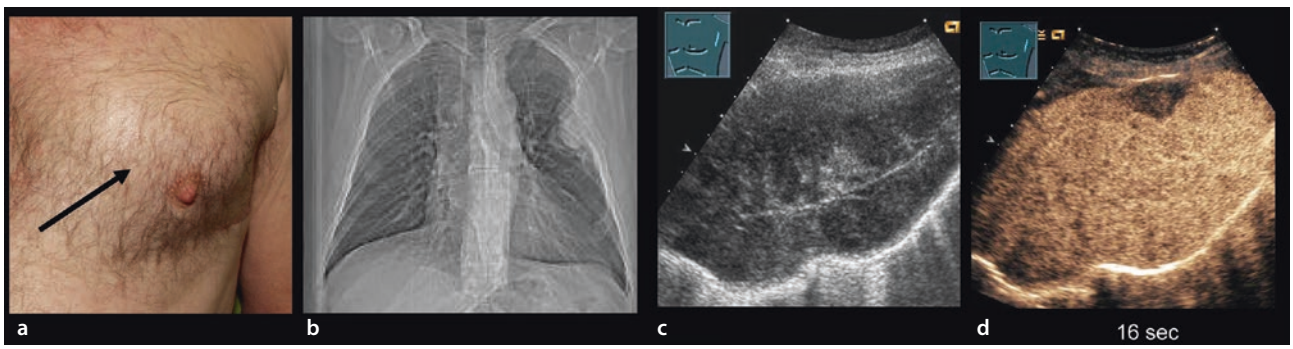

Fig. 8.59 **a** Patient with a mass located to the thoracic wall (arrow). **b** On chest X-ray the mass can be seen in the left apical region. **c** On B-mode ultrasound, a large hypoechoic lesion of the thoracic wall is visualized. **d** On CEUS, the lesion has a homogeneous marked contrast enhancement. The biopsy confirmed the diagnosis of a plasmocytoma

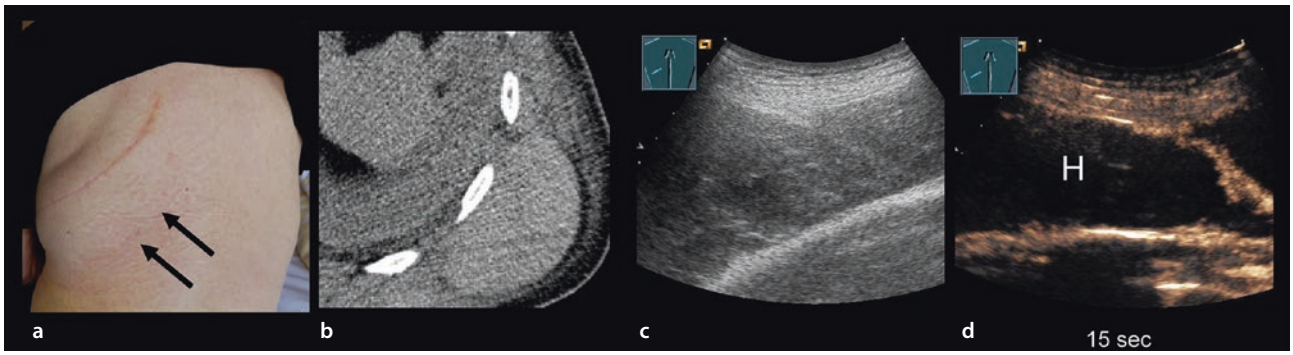

Fig. 8.60 **a** Patient with initial resected bronchial carcinoma who now shows a mass in the area of the scar (arrow). **b** CT shows the mass located in the thoracic wall. **c** B-mode ultrasound shows a large, hypoechoic lesion of the thoracic wall. **d** On CEUS, the lesion shows no contrast enhancement, as in hematoma, confirmed by a biopsy

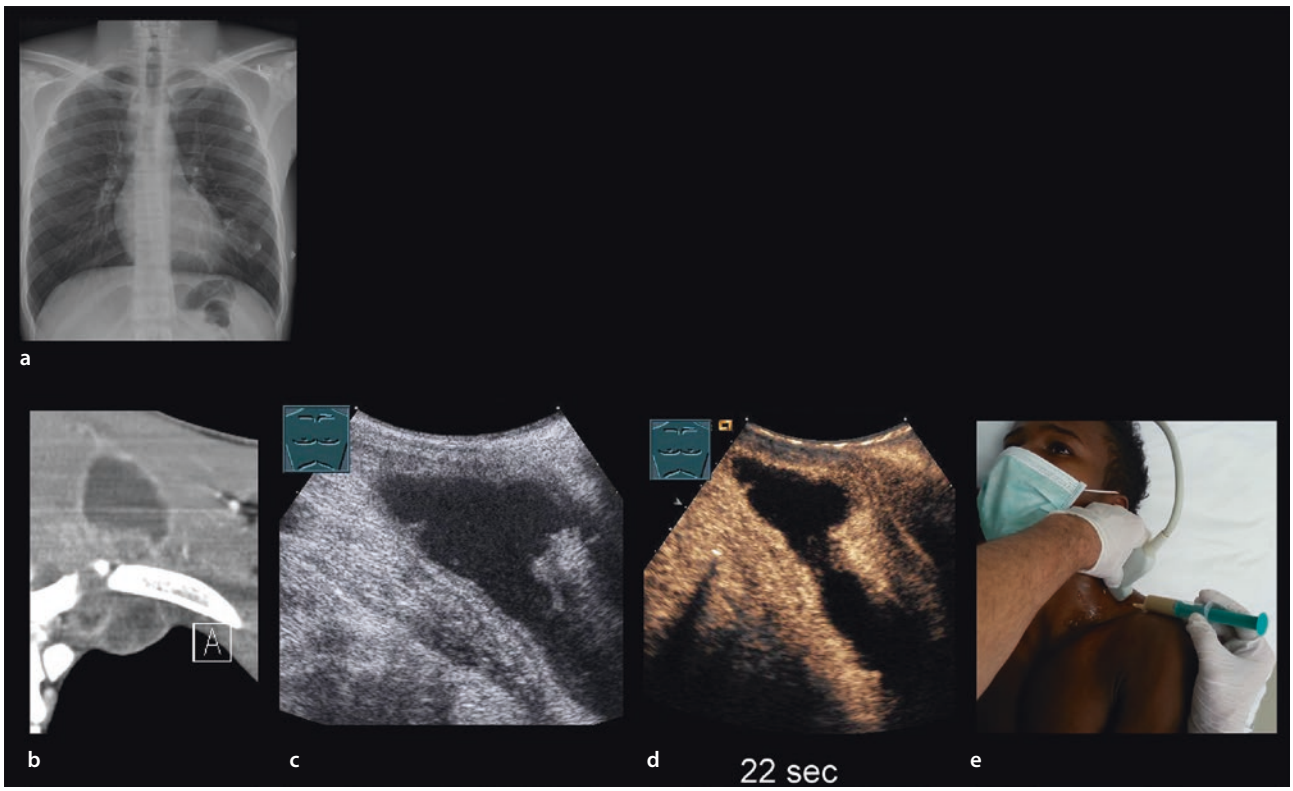

Fig. 8.61 Patient with thoracic back pain that has existed for months. **a** The chest X-ray was reported without pathological findings. **b** On CT, a liquid mass can be seen in the left cervical triangle extending into the upper thoracic aperture. **c** On B-mode ultrasound, a large liquid structure is visualized in the neck, descending into the thorax. **d** On CEUS, the peripheral wall surrounding the non-enhanced abscess area shows a marked contrast enhancement. **e** The US-guided diagnostic biopsy resulted in pus. The diagnosis of tuberculosis was confirmed

Summary

Qualitative CDS shows varied and partly characteristic findings in the presence of various types of lung consolidations and is therefore a valuable adjunct to B-mode ultrasound with regard to the etiological classification of peripheral lung lesions. In keeping with the physiological dual vascularization of the lung by the pulmonary arteries and the bronchial arteries, on CDS one can distinguish between arterial high-impedance spectral curves and arterial low-impedance spectral curves in consolidated lung tissue. The former are assigned to pulmonary arteries and the latter to bronchial arteries. Within peripheral lung consolidations, different entities show characteristic distribution patterns of pulmonary-artery and bronchial artery flow signals in respect of frequency and location. Arterial spectral curve analysis is time-consuming. Reliable demarcation of vessels of tumor neoangiogenesis is currently not possible with CDS. The orienting CDS is used only in the daily clinical routine, but the spectral curve analysis is often too time-consuming and susceptible to faults.

Experience concerning CEUS in cases of peripheral lung lesions is limited. Lung lesions can be described by the time to the start of contrast enhancement and by the extent and homogeneity of contrast enhancement. Contrast enhanced ultrasound at the chest can be performed easily and rapidly, and is therefore basically suitable for routine clinical use. The possible indications are (1) in the area of the thoracic wall, differentiation of vital and avital tissue and tumor characterization; (2) for the leading symptom of thoracic pain, CEUS is helpful in the differential diagnosis of pleurisy and peripheral pulmonary embolism; (3) in the leading symptom of radiographic shadowing, CEUS is helpful in the diagnosis of malignant pleural effusion (PE) and infarction-related PE, as well as in the discrimination of tumor from central atelectasis, in the detection of atypical pneumonic processes and in the evaluation of the malignancy of pulmonary nodules or peripheral bronchial carcinomas. In the field of interventional sonography, CEUS enables a safe differentiation between tumor, necrosis and atelectasis.

References

Albrecht T, Blomley M, Bolondi L et al (2004) Guidelines for the use of contrast agents in ultrasound. Ultraschall Med 25:249–256

Babo HV, Müller KMG, Huzky A, Bosnjakovic-Buscher S (1979) Die Bronchialarteriographie bei Erkrankungen der Lunge. Radiologe 19:506–513

Bartelt S, Trenker C, Görg C, Neesse A (2016) Contrast-enhanced ultrasound of embolic consolidations in patients with pulmonary embolism: a pilot study. J Clin Ultrasound. https://doi.org/10.1002/jcu.22313

Caremani M, Benci A, Lapini L et al (2008) Contrast enhanced ultrasonography (CEUS) in peripheral lung lesions: a study of 60 cases. J Ultrasound 11:89–96. https://doi.org/10.1016/j.jus.2008.05.008

Civardi G, Fornari F, Cavanna L, Di Stasi M, Sbolli G et al (1993) Vascular signals from pleural-based lung lesions studied with pulsed Doppler ultrasonography. JCU 21:617–622

Delorme S, Krix M, Albrecht T (2006) Ultraschallkontrastmittel - Grundlagen und klinische Anwendung. Fortschr Röntgenstr 178(2):155–164

Dong Y et al (2005) Value of CEUS in guidance of percutaneous biopsy in peripheral pulmonary lesions. BioMed Res Int. https://doi.org/10.1155/2015/531507

Findeisen H, Trenker C, Figiel J, Greene B, Görg K, Görg C (2018) Vascularisation of primary, peripheral lung carcinoma in CEUS-a retrospective study (n = 89 patients). Ultraschall Med 40:603–608. https://doi.org/10.1055/a-0725-7865

Fissler-Eickhoff A, Müller KM (1994) Pathologie der Pulmonalarterien bei Lungentumoren. DMW 119:1415–1420

Gehmacher O, Mathis G, Kopf A, Schreier M (1995) Ultrasound imaging of pneumonia. Ultrasound Med Biol 21:1119–1122

Gehmacher O, Kopf A, Scheier M et al (1997) Can pleurisy be detected with ultrasound? Ultraschall Med 18:214–219

Görg C, Seifart U, Holzinger I, Wolf M, Zugmaier G (2002) Bronchiolo-alveolar carcinoma: sonographic pattern of "pneumonia". Eur J Ultrasound 15:109–117

Görg C, Seifart U, Görg K et al (2003) Color Doppler sonographic mapping of pulmonary lesions: evidence of dual arterial supply by spectral analysis. JUM 22:1033–1039

Görg C, Bert T (2004a) Trancutaneous colour Doppler sonography of lung consilidations: review and pictorial essay. Part 1: Pathophysiologic and CDS basics of pulmonary vascularity. Ultraschall Med 25:221–226

Görg C, Bert T (2004b) Trancutaneous colour Doppler sonography of lung consolidations: review and pictorial essay. Part 2: CDS patterns of pulmonary consolidations. Ultraschall Med 25:285–291

Görg C, Bert T, Görg K, Heinzel-Gutenbrunner M (2005a) Color Doppler sonographic mapping of chest wall lesions. BJR 78: 303–307

Görg C, Bert T, Görg K (2005b) Contrast enhanced sonography for differential diagnosis of pleurisy and focal pleural lesions of unknown cause. Chest 128:3894–3899

Görg C, Bert T, Kring R (2006a) Contrast enhanced sonography of the lung for differential diagnosis of atelectasis. JUM 25:35–39

Görg C, Bert T, Kring R, Dempfle A (2006b) Transcutaneous contrast enhanced sonography of the chest for evaluation of pleural based pulmonary lesions. Ultraschall Med 27:437–444

Görg C (2007) Transcutaneous contrast-enhanced sonography of pleural-based pulmonary lesions. Eur J Radiol 64:213–221

Goy J et al (2015) Sub-segmental pulmonary embolism in three academic teaching hospitals: a review of management and outcomes. J Thromb Haemostasis 13(2):214–218

Harvey CJ, Albrecht T (2001) Ultrasound of focal liver lesions. Eur Radiol 11:1578–1593

Hsu WH, Ikezoe J, Chen CY, Kwan PC, Hsu CP et al (1996) Color Doppler ultrasound signals of thoracic lesions: correlation with resected histologic specimens. Am J Respir Crit Care Med 153:1938–1951

Hsu WH, Chiang CD, Chen CY, Kwan PC, Hsu JY et al (1998) Color Doppler ultrasound pulsatile flow signals of thoracic lesions: comparison of lung cancer and benign lesions. Ultrasound Med Biol 24:1087–1095

Jacobsen N, Pietersen IP, Nolsoe C, Konge L, Graumann O, Laursen CB (2020) Clinical Applications of Contrast-Enhanced Thoracic Ultrasound (CETUS) compared to standard reference tests: a sys-

tematic review. Ultraschall Med. https://doi.org/10.1055/a-1143-3141

Kolin A, Koutllakis T (1988) Role of arterial occlusion in pulmonary scar cancers. Human Path 19:1161–1170

Linde H-N, Holland A, Greene BH, Görg C (2012) Kontrastunterstützte Sonographie (CEUS) bei Pneumonie: Darstellungsmuster und prognostische Bedeutung- eine retrospektive Studie bei n = 50 Patienten. Ultraschall Med 33:146–151

Mathis G, Dirschmid K (1993) Pulmonary infarction: sonographic appearance with pathologic correlation. Eur J Radiol 17:170–174

Müller KM, Meyer-Schwickerath M (1978) Bronchial arteries in various stages of bronchogenic carcinoma. Path Res Pract 163:34–46

Quarato CMI, Sperandeo M (2020) Letter to the editor regarding the article: "Vascularization of Primary, Peripheral lung carcinoma in CEUS—a retrospective study (n = 89 Patients)" by Findeisen H et al. Ultraschall Med. https://doi.org/10.1055/a-1090-4327

Raslan IA et al (2018) Rates of overtreatment and treatment-related adverse effects among patients with subsegmental pulmonary embolism. JAMA Internal Medicine 178(9):1272

Sartori S et al (2004) CEUS as guidance for transthoracic biopsy of a peripheral lung lesion with large necrotic areas. J Ultrasound Med 23(1). https://doi.org/10.7863/jum.2004.23.1.133

Sidhu PS, Cantisani V, Dietrich CF et al (2018) The EFSUMB Guidelines and Recommendations for the Clinical Practice of Contrast-Enhanced Ultrasound (CEUS) in non-hepatic applications: update 2017 (short version). Ultraschall Med. https://doi.org/10.1055/s-0044-101254

Trenker C, Apitzsch JC, Pastor S, Bartelt S, Neesse A, Görg C (2017) Detection of peripheral embolic consolidations using contrast-enhanced ultrasound in patients with no evidence of pulmonary embolism in computed tomography: a pilot study. J Clin Ultrasound. https://doi.org/10.1002/jcu.22511

Trenker C, Dohse M, Ramaswamy A, Michel C, Görg C (2019) Histological validation of pulmonary infarction detected with contrast-enhanced ultrasound inpatients with negative computed tomography pulmonary angiogram: a case series. J Clin Ultrasound 47:461–465

Wang S et al (2015) The Role of CEUS in selection indication and improving diagnosis for transthoracic biopsy in peripheral pulmonary and mediastinal lesions. BioMed Res Int 2015:S231782. https://doi.org/10.1155/2015/231782

Yuan A, Chang DB, Yu CJ, Kuo SM, Luh KT, Yang PC (1994) Color Doppler sonography of benign and malignant pulmonary masses. Am J Roentgenol 163:545–549

Yuan A, Yang PC, Lee L, Wu DH, Kuo SH et al (2000) Reactive pulmonary artery vasoconstriction in pulmonary consolidation by color Doppler ultrasonography. Ultrasound Med Biol 26:49–56

Image Artifacts and Pitfalls

Andreas Schuler

Contents

G. Mathis (ed.), *Chest Sonography*, https://doi.org/10.1007/978-3-031-09442-2_9

Table 9.1 Physical phenomena of ultrasound waves

Reflexion	Refraction
Absorption	Dispersion
Diffraction	Attenuation

9.1 Artifacts

Artifacts are a system-immanent aspect of ultrasonography. They arise due to physical phenomena when ultrasound waves pass through the human body (Table 9.1). Artifacts are disruptive artificial products that make it very difficult to image and evaluate the thorax, especially due to the anatomical features of this region. Artifacts can distort existing structures in terms of their size, position, form, and echogenicity; cause incorrect or incomplete imaging of their topography; or suggest the presence of structures that, in fact, do not exist. On the other hand, artifacts are indispensable and very important determinants of the diagnosis of specific diseases. The absence of certain typical artifacts (air: reverberation; bone: acoustic shadow) at the surface of the lung or in the bony thorax enables the investigator to diagnose certain diseases (lung lesion, rib lesion), as it is then possible to evaluate parenchyma, bone, and/or soft tissue. Artifacts also serve as a diagnostic criterion when they are seen at an unusual site, e.g., air with reverberation echoes in the pleural space in cases of pneumothorax.

9.2 Pitfalls

These are sources of error in ultrasonographic diagnosis, caused by anatomical, topographic, pathophysiological, or physical ultrasound-based misinterpretation on the part of the investigator, leading to incorrect diagnosis. Incomplete history taking, missing clinical information or examination, or insufficient knowledge of sonographic (and clinical) differential diagnosis may also be the reason for such "pitfalls." Last, but not least, every conscientious ultrasonographer must be aware of the limitations of the method so that additional diagnostic procedures can be applied efficiently, economically, and in a manner that is conducive to the patient's well-being. By so doing, several pitfalls can be avoided or resolved.

9.3 Ultrasound Physics in the Chest

Ultrasound images are created by the transmission and passage of ultrasound waves in the human body and the registration and processing of the backscattered/received echo of the emitted ultrasound beam. In an entirely homogeneous medium, a sound wave is carried forward in a uniform fashion. It is altered at the margin between two media. The phenomena/changes that are liable to occur in this process are summarized in Table 9.1. They include the geometry of the ultrasound wave, the angle at which it strikes the reflector, the physical properties of the reflector, and its surface consistency. The magnitude of the impedance difference between two different media is represented by various factors, one of them being the intensity of the backscattered echo. Thus, on the B-mode image, it is represented by the brightness of a pixel. Human tissue contains a number of marginal surfaces whose anatomical origin can be determined by characteristic ultrasound phenomena. In contrast to the abdomen, ultrasonography of the chest is more frequently confronted with disturbing artifacts because of the surrounding "echo-opposing" structures (aerated lung, bony chest). Therefore, the specific ultrasound phenomena in air and bony structures will be briefly discussed in the following.

Air This is a strong ultrasound beam reflector. Depending on the structure of the surface, the impedance difference and the gas volume at the marginal surface, ultrasound waves differ in terms of their reflex behavior:

- Large extent of absorption
- Total reflection with acoustic shadow
- Partial reflections with change of transmission and a narrow acoustic shadow

The most common phenomenon is that up to 99% of the ultrasound wave is reflected at the first marginal surface between tissue and air, i.e., the "initial lung echo." Therefore, it is not possible to visualize the deeper lung parenchyma by ultrasonography. Only when the structure of the surface is altered and in the presence of specific physical features (e.g., the absence of air in inflammatory or tumor-related processes, atelectasis, etc.) is it possible to image lung parenchyma. However, in such cases, the lung itself has several marginal sur-

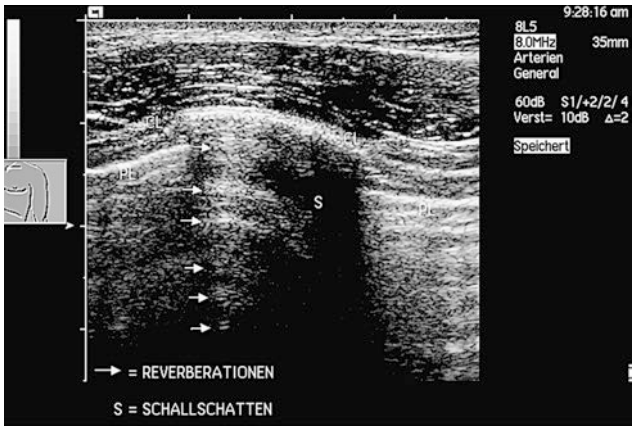

Fig. 9.1 Reflective shadowing at the clavicle (CL). Dorsal acoustic shadow (S) due to absorption of ultrasound waves at the surface of the clavicle. Additional reverberations (repetitive echoes, arrows) at the surface of the clavicle when the ultrasound waves hit perpendicularly. *PL* pleural reflex

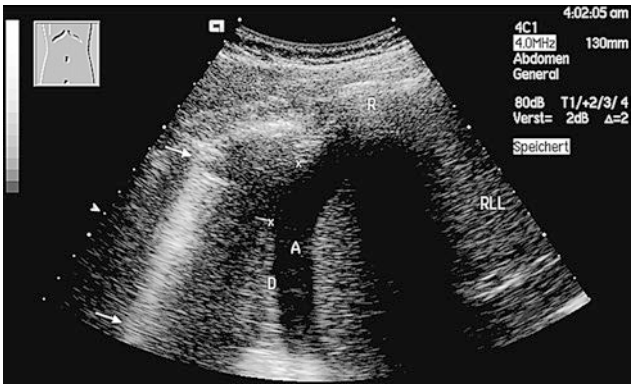

Fig. 9.2 "Diaphragmatic gap." A female patient with a primary peritoneal mesothelioma, ascites (A) and basal pleural pneumonia. The central portion of the diaphragm (D) is found to be markedly thickened. In areas dose to the transducer, there seems to be a gap (x–x). Furthermore, a lateral marginal shadow phenomenon is seen in the diaphragm and also a comet-tail artifact in air in the cranially located lung (arrows). *RLL* right lobe of liver, *R* rib with dorsal acoustic shadow

faces (air in the bronchoalveolar space, bronchial wall, interstitial space, vascular wall, blood). The abovementioned alterations in the ultrasound wave also occur at these marginal surfaces.

Bone in bone, there is nearly complete absorption of ultrasound energy. As a result, the "dorsal" ultrasound wave is obliterated (no further echoes in axial direction of the beam). When ultrasound waves hit bone at right angles, they may cause strong reflection and repetitive echoes of the bone surface in deeper portions (Fig. 9.1).

9.4 Imaging of Marginal Surfaces of the Pleura and the Diaphragm

The image varies, depending on the angle of incidence of ultrasound waves and the consistency (roughness) of the surfaces. Furthermore, the improved resolution of ultrasound probes and continuous advancement of technology permit differentiated imaging. At an angle of incidence of 0 to about 25°, total reflection may be expected to occur at the marginal surface between the pleura and the lung. Only when the surface of the pleura/lung is thickened due to inflammation or scars and the surface is irregular and "roughened," is it imaged even in the presence of a steeper angle of incidence.

Most of the diaphragm can be imaged by the transabdominal approach (as a rule through the liver from the right side and through the spleen from the right side). Due to the high impedance difference as well as scatter phenomena, the diaphragm is visualized as much thicker than it actually is (Fig. 9.2). Central portions of the diaphragm are not imaged well by the intercostal approach because of the unfavorable angle of incidence of the ultrasound wave. Apparent gaps might irritate the investigator. Moreover, lateral marginal shadow phenomena limit the assessment. Indistinct processes must be imaged in the complementary second plane.

9.5 B-Mode Artifacts

Based on their mechanism of origin and physical ultrasound features, artifacts may be divided into four categories (Table 9.2; Kremkau and Taylor 1986; Schuler 1998).

9.5.1 Ultrasound Beam Artifacts in Chest Sonography Reverberations (Repetitive Echoes): Margin Between Tissue and Air, Bone Fracture Fissures

They arise due to nearly complete reflection of the emitted ultrasound wave at the marginal surface between tissue and air (initial lung echo). This marginal surface acts as a strong reflector. It reflects the striking ultra-

Table 9.2 Classification of artifacts

Ultrasound beam artifacts
Ultrasound enhancement artifacts
Ultrasound resolution artifacts
Other artifacts

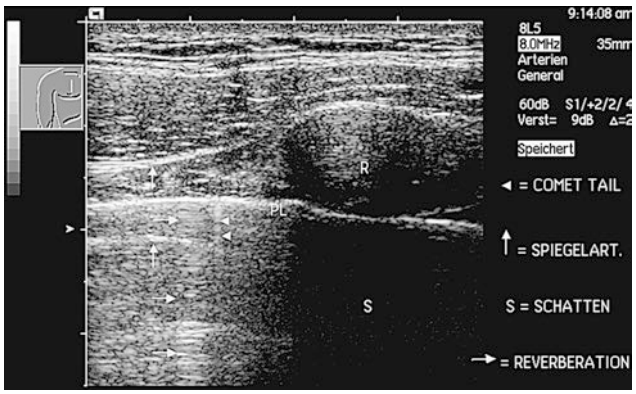

Fig. 9.3 Reverberations and comet-tail, parasternal longitudinal section from the right side. One finds reverberation artifacts (horizontal arrows) dorsally in the aerated lung, and a short comet-tail artifact (arrowheads). Furthermore, a muscle fascia of the thorax musculature is mirrored dorsally (vertical arrows) at the pleural reflex (PL). Rib (R) with an incomplete acoustic shadow (S); the pleural reflex acts as a strong reflector and is imaged here through partly cartilaginous rib with partial echo transmission

sound wave back to the transducer membrane, where the wave is re-reflected and reemitted, hits the marginal surface again, etc.

Depending on the duration, the marginal surface reflex is imaged dorsally, in axial direction of the ultrasound wave. Deeper reflectors are weaker and are imaged darker (Figs. 9.2 and 9.3). The artifact caused by insufficient probe-to specimen contact (Fig. 9.10), e.g., when a linear ultrasound probe is used on the surface of the thorax, actually is a reverberation artifact (at the transducer membrane).

9.5.1.1 Image Artifacts and Pitfalls

A narrow fissure in a rib fracture might become noticeable because of a reverberation artifact (so-called chimney phenomenon) (Dubs-Kunz 1992). The fracture end of the rib serves as a strong reflector in this setting (Fig. 2.17).

9.5.1.2 Mirror Artifacts: Liver Parenchyma in the Diaphragm, Vessels at the "Pleura"

These are caused by incidence-angle-dependent reflection of the ultrasound wave at a strong reflector (e.g., the diaphragm), oblique deflection in issue, repeated reflection on a reflector, back-scatter to the first reflector, and back-reflection to the ultrasound probe. This is imaged as a structure tot primarily in the axial direction of the ultrasound beam, within a region axial distal to the actual reflector.

This causes the classical mirror artifact phenomena of the liver at the diaphragm (Fig. 9.4), but also of

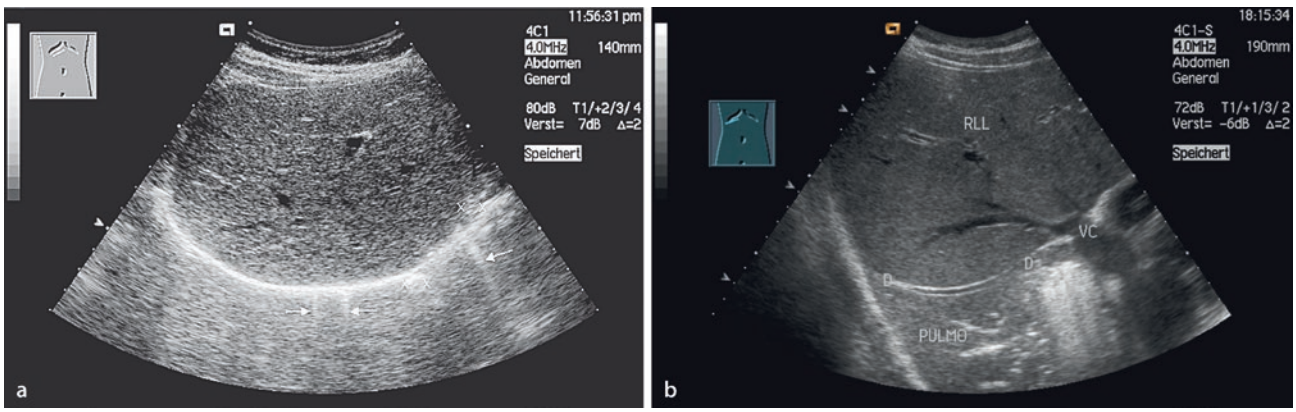

Fig. 9.4 Mirror artifact. Subcostal oblique section from the right side. "Classical" mirror artifact of the liver at the diaphragm. Portions lying at a distance from the transducer and the diaphragm, i.e., cranially by the subcostal approach, are not "lung parenchyma" but liver parenchyma reflected at the strong reflector, namely the diaphragm. A hemangioma (x–x) lying immediately subdiaphragmal in the original image is more clearly seen in the mirror image (x–x) and is displaced centrally to the mid portion of the image (**a**). Lung structure could be seen, if artifacts are reduced or disappeared due to alteration of the physical environment. If there is pneumonia, air (and artifacts due to air: i.e. reverberation), lungs structure could be seen (**b**). In some cases, the mirror image might reveal structures outside the main beam that cannot be imaged (multiple beam artifacts) and cause considerable confusion. Additional comet-tail artifacts (arrows) in air

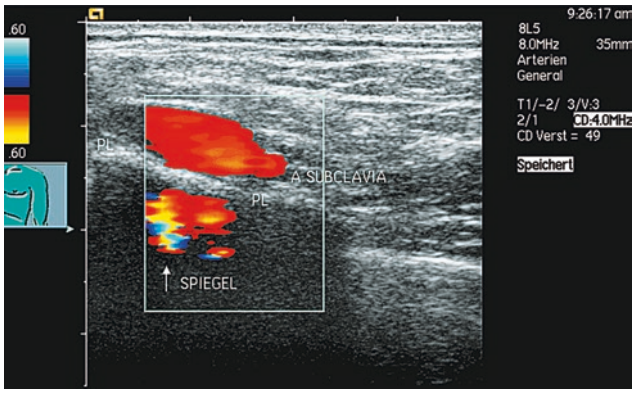

Fig. 9.5 Mirror artifact on color Doppler. The subclavian artery (A. SUBCLAVIA) is reflected at the pleura (PL). A vessel (arrow) lying dorsal to the pleura is seen on the mirror image; the vessel, however, does not really exist

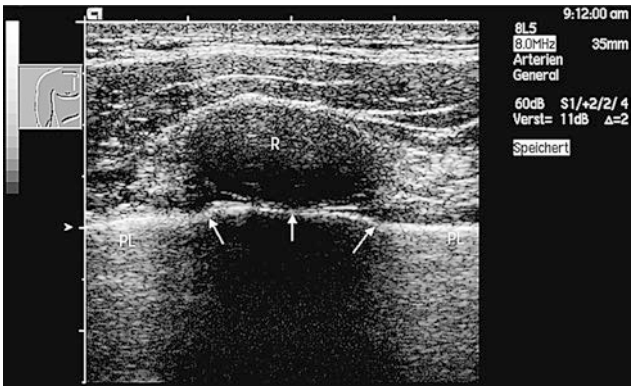

Fig. 9.7 Scatter lens artifact. The pleura (PL) dorsal to the rib cartilage (R) is shifted ventrally towards the transducer (arrows) as a result of various ultrasound beam rates in cartilage and soft tissue of the chest wall

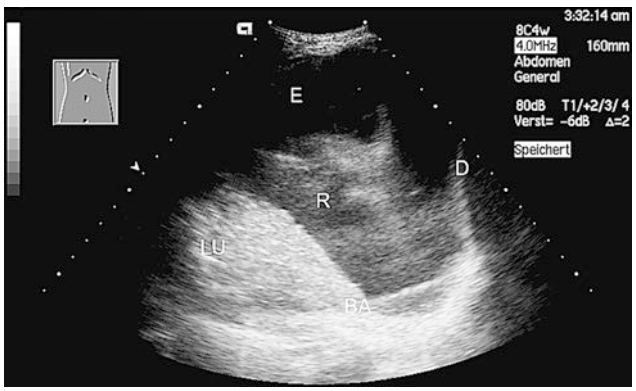

Fig. 9.6 Arcuate artifact in the pleural effusion. A female patient with pulmonary and pleural metastatic breast carcinoma. A strong reflector (bony thorax) lying outside the main beam is visualized as a circular arch (AA arcuate artifact), discretely opening upward. Distally, it may mimic septation of the pleural effusion (E). The internal echoes (R) are not corpuscular portions of the effusion but noise artifacts ("speckles"). D diaphragm, LU lung atelectasis in the presence of pleural effusion

the subclavian artery at the initial lung reflex. This artifact phenomenon exists not only in B-mode sonography, but also in color Doppler and the Doppler frequency spectrum (Reading et al. 1990; Fig. 9.5). As a rule, the multiple backscattered echoes of mirror images are more hypoechoic and somewhat more blurred or distorted as a result of previous weakening of the ultrasound beam when it passes through tissue.

9.5.1.3 Arcuate Artifacts: Rib Reflex in Pleural Effusion

Arcuate artifacts may arise due to displacement of a reflex at a strong reflector in the lateral ultrasound beam or side lobe into the center of the main beam. Characteristically, in sector transducers and upwardly oriented curved arrays, one finds upwardly open circular arches. In linear probes, one finds a hyperbola. Thus, a reflection in a bony portion of the thorax could mimic a septation in a pleural effusion (Fig. 9.6). This problem can be resolved by altering the echo angle or the echo plane.

Scatter Lens Artifact/Shortening Phenomenon: Distortion of the Lung Surface Dorsal to Rib Cartilage This artifact phenomenon is a result of the different transmission rates of ultrasound waves in rib cartilage (faster) than in the adjacent soft tissue of the chest wall. This may mimic a pseudolesion at the marginal surface of air/lung, because there is an apparent protrusion of contours in the direction of the ultrasound probe (Fig. 9.7). This artifact is simple to detect and plays a rather important role in abdominal diagnosis of the liver (apparent space-occupying mass on the surface of the liver) dorsal to rib cartilage (Bönhof and Linhart 1985).

Marginal Shadows: Diffraction/Refraction at Strong Reflectors ("Diaphragmatic Gap") This artifact occurs when the ultrasound beam hits a surface obliquely. It is the result of diffraction and refraction phenomena at strong reflectors (e.g., the diaphragm; Fig. 9.2). The artifact is detected by the fact that it disappears when the echo plane or the echo angle is changed.

9.5.2 Artifacts Caused by Alterations in Echo Enhancement Acoustic Shadow/Echo Obliteration

Formation of Plaque on All Bony Structures of the Chest This certainly is one of the most common artifact phenomena in the thorax and greatly hinders the assessment of structures lying dorsal to such strong reflectors. Due to strong absorption, dorsal bone structures (ribs, scapula, clavicle, sternum, vertebral column) are nearly completely obliterated and practically all information is

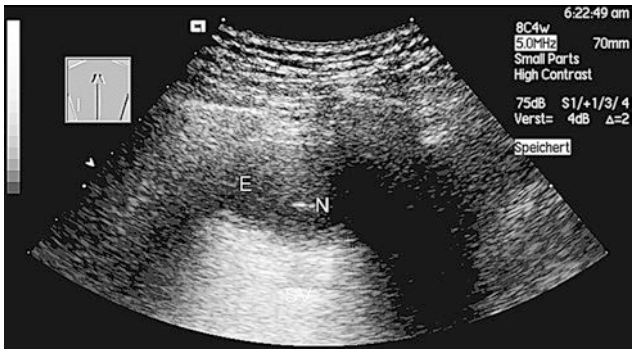

Fig. 9.8 Echo enhancement. Dorsal to a small, not entirely anechoic pleural effusion (E) there is marked "echo enhancement" (EE). This actually is reduced weakening of the echo, as the spread of the ultrasound beam in the pleural effusion is altered in comparison with adjacent tissue. Also note the nonanechoic effusion dose to the chest wall. The reflexes are noise artifacts. Furthermore, an echodense small bright linear reflex (N) is seen, the tip of the puncture needle introduced under sonographic guidance

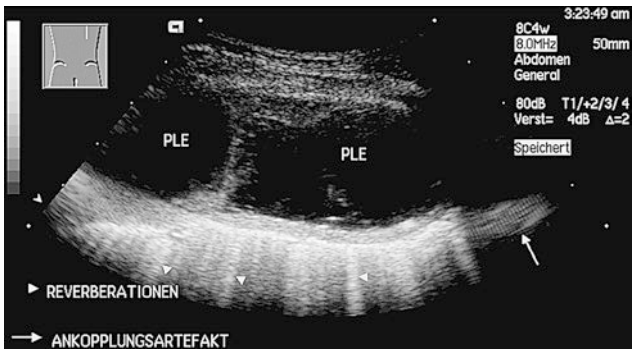

Fig. 9.9 Comet-tail and probe-to-specimen artifact. Dorsal to a septate pleural effusion in the presence of breast carcinoma one finds numerous comet-tail artifacts (arrowheads) arising in the air at the margin between the visceral pleura and the lung. Furthermore, given insufficient contact between the ultrasound probe and the chest wall, a shadow with an artifact reflex (arrow), although not like a classical ring-down artifact. Dorsal to the pleural effusion, there is marked echo enhancement. *PLE* pleural effusion

lost (Fig. 9.1). However, interruptions of the otherwise regular acoustic shadow in the bony thorax (bone contour, bone surface, joints) may be very helpful for diagnosis, as pathological changes will be present in such cases (fracture, bone tumor, joint effusion, joint empyema). Acoustic shadows in the pleura are also signs of pathological alterations, e.g., of plaque in the presence of asbestosis or calcification during the healing of pleural lung lesions or lung lesions dose to the pleura (pneumonia, tuberculosis) or in lymph nodes.

Echo Enhancement: Distal to Hypoechoic Structures (Pleural Effusion, Cyst, Vessel, Hypoechoic Space-Occupying Mass) This phenomenon of "brighter," more hyperechoic areas distal to the above-mentioned structures is not due to echo enhancement but due to lesser weakening of ultrasound waves in the more hypoechoic portions closer to the probe. This causes distal parts to appear brighter (more hyperechoic and stronger echoes) than the surrounding areas, which have uniformly weakened echoes. In the thorax, this is found in the presence of large quantities of fluid in the pleural space or hypoechoic peripheral pulmonary processes (Figs. 9.8 and 9.9).

9.5.2.1 Echo Resolution Artifacts

z Noise: In Fluid-Filled Structures At the surface of anechoic areas, one finds diffuse "noise" caused by interference from returning echoes at different marginal surfaces, such as those caused by "background noise," depending on general enhancement (this is also true for Doppler sonography). Here caution is advised, as apparently internal structures that in fact do not exist might be mimicked (e.g., in the pleural effusion; Figs. 9.6 and 9.8). Marginal surfaces are frequently blurred.

9.5.2.2 Image Artifacts and Pitfalls

z Slice Thickness Artifact: at Reflectors with a Strong Impedance Difference (Pleura, Diaphragm)

This common and irritating artifact also belongs to the category of resolution artifacts. When the ultrasound beam hits strong reflectors obliquely and in the presence of a high impedance difference, the marginal layer is much thicker (partly) blurred, and distorted. This phenomenon might mimic pleural and diaphragmatic lesions or thickening (Fig. 9.2), but also thrombosis or sediments in vessels.

9.5.3 Other Artifacts Comet-Tail (Resonance Artifact), B-Lines: In Aerated Structures

At the margin, of the lung surface and air one frequently finds small comet-tail artifacts (Figs. 9.2, 9.3, 9.4 and 9.9). They are seen as bright, narrow strips of strong dorsal reflectors and their origin is controversially discussed. One explanation is reverberations (repetitive echoes) between two very closely located reflectors and resonance phenomena (vibrations) in a thin structure of soft tissue (e.g. thickened interstitial alveolar septa surrounded by air with a strong echo response). In addition to air or other gas bubbles, a common site of origin is metal foreign bodies. Many authors refer to these artifacts as B-lines, the "sound of lung water" (Lichtenstein et al. 1997; Lichtenstein 2005; Gargani et al. 2008; Noble et al. 2009; Soldati et al. 2009). When occurring in large numbers in the region distal to the ultrasound reflection on the aerated lung, these artifacts indicate interstitial lung lesions such as interstitial edema or lesions in the

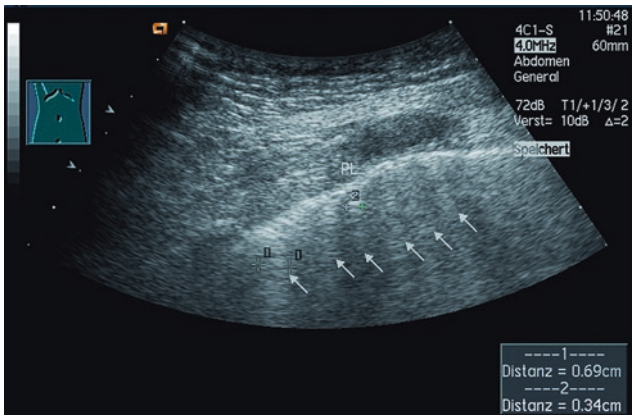

Fig. 9.10 B-Lines (comet tail artifacts: arrows) due to pulmonary edema with a size of 3 to 7mm (crosses)

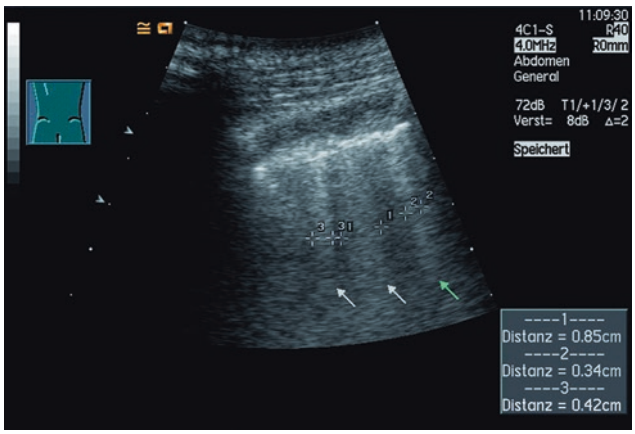

Fig. 9.11 Interstitial syndrome with comet-tail artifacts (arrows, calipers: 3–8 mm wide), bacterial pneumonia in the phase of healing, infiltrate not seen on the image

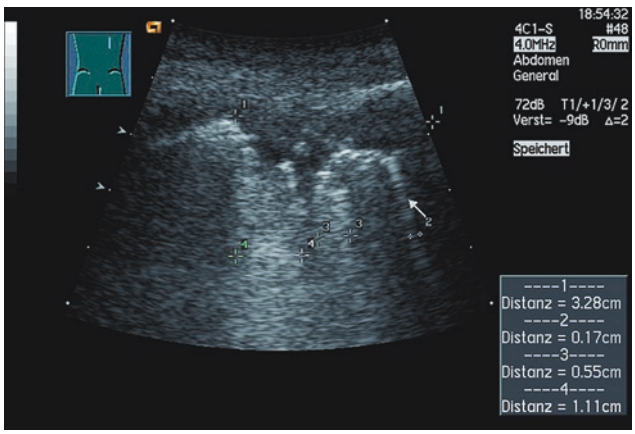

Fig. 9.12 Congestive pneumonia

presence of contusion, pneumonia, etc. (Soldati et al. 2006; Volpicelli et al. 2008). In more rare cases, fibrotic lesions in the lung may also be present (Wohlgenannt et al. 2001; Reissig and Kroegel 2003). However, these artifacts are not sufficiently selective as regards their differentiation from the above-mentioned diseases. To put it simply, the evidence of these artifacts means that "the lung is not healthy" (Figs. 9.10, 9.11, and 9.12). The 1st International consensus conference on pleura and lung ultrasound has defined B-lines as discrete laser-like vertical hyperechoic reverberation artifacts that arise from the pleural line (previously described as "comet tails"), extend to the bottom of the screen without fading, and move synchronously with lung sliding. Multiple B-lines are the sonographic sign of lung interstitial syndrome. In the evaluation of diffuse interstitial syndrome, the sonographic technique ideally consists of scanning eight regions, but a more rapid anterior two region scan may be sufficient in some cases. A positive region is defined by the presence of three or more B-lines in a longitudinal plane between two ribs. However, focal multiple B-lines may be present in normal lung.

The consensus conference statement omits discussion of additional information yielded by high resolution ultrasound interrogation of the lung surface including excluding changes of the pleura and distinct analysis of the shape of the artefact. In addition, the consensus paper not only focused on edema but also on other pathophysiological disorders of the lung parenchyma including pulmonary fibrosis and interstitial pneumonia, which the authors referred to as "interstitial syndrome".

Since the publication of the consensus statement, some authors extended the term "focal interstitial syndrome" to include other disorders such as lung contusion, pneumonia or pulmonary embolism. In this context, all vertical reverberation artefacts radiating from the pleura into the lung parenchyma were designated BLA. An accurate analysis of the various published descriptions of BLA shows undifferentiated, mixed, and often contradictory conclusions. The imprecise use of the terms BLA and CTA in lung US have led to confusion, which is seen in routine daily practice as well as published literature. A more precise definition of the spectrum of reverberation artefacts may be helpful to better differentiate cardiogenic pulmonary edema from parenchymal lung diseases. Therefore, parenchymal lung diseases have to be excluded before a BLA analysis for cardiogenic pulmonary edema is undertaken (Dietrich et al. 2016; Mathis et al. 2021).

Artifacts Caused by Foreign Bodies: Needle Tip, Drainage Iatrogenic or accidental foreign bodies introduced into the body cause artifact phenomena. As a result, projectiles, fragments of glass or wood, other substances might be imaged in the chest wall and in soft tissue. This is significant when such artifacts are visualized during sonography-guided diagnostic or therapeutic measures. Small pulmonary consolidations dose to the pleura, pleural effusions a few millimeters in size, or pleural empyema can be punctured or drained under

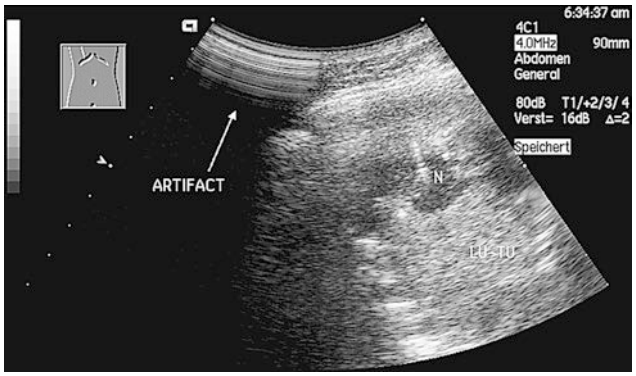

Fig. 9.13 Ring-down (probe-to-specimen artifact). Patient with a peripheral bronchial carcinoma in a ventral location on the right side. A probe-to-specimen artifact (arrow) is caused by insufficient contact between the transducer and the chest wall. A simultaneous fine-needle puncture performed for histological verification of the diagnosis shows the needle artifact (N) in the tumor (LU-TU)

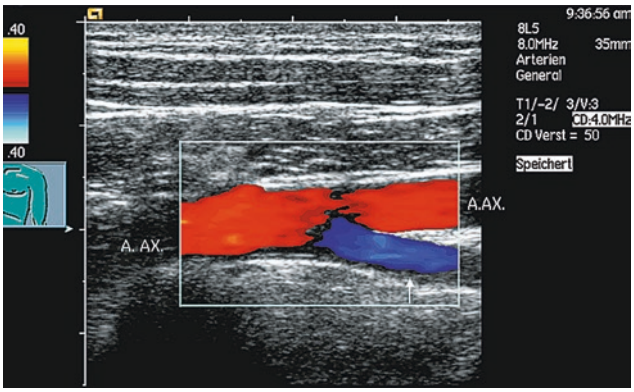

Fig. 9.14 Directional artifact (color Doppler). The axillary artery (infraclavicular) (A.AX.) with a branch for the musculature/chest wall. Blood flowing towards the ultrasound probe is coded red; blood flowing away from the probe is coded blue (see color scale). The branching artery (arrow) is blue, the change of color from red to blue occurs via black. Thus, here (at a 90° Doppler angle to the ultrasound probe), there is no blood flow relative to the ultrasound probe

9

realtime sonographic guidance. Space-occupying masses in the soft tissue of the thorax or rib cage should also be punctured under sonographic guidance. Detection of the needle reflex in aerated structures might be difficult. Here, real-time control through subtle movement of the needle tip under simultaneous sonographic imaging is useful (Blank 1994; ◘ Fig. 9.8). Ring-Down Artifact: Insufficient Probe-To-Specimen Contact If the geometric configuration of the probe is unfavorable in relation to the investigated region (for instance a linear probe in a curved chest wall), this artifact can easily be detected by characteristic repetitive echoes (arising between the ultrasound crystal and the transducer membrane) (◘ Fig. 9.13).

9.6 Color Doppler Artifacts and Pitfalls in the Chest

The basic principles and settings of the various Doppler modalities will not be presented in this chapter. They have been discussed in detail elsewhere (Wild 1996).

9.6.1 Pulse Repetition Frequency

Overall Enhancement, Filter, Background Noise Insufficient or incorrect setting of the overall enhancement of color Doppler either leads to incorrect imaging of actual blood flow (excessively low gain) or "overradiation" due to numerous color pixels that do not represent blood flow but only background noise (poor signal-to-noise ratio). A low pulse repetition frequency (PRF) should be selected for small vessels with low flow rates so that flow signals are not "overlooked." When large arteries are visualized (mediastinum, suprasternal, parasternal), it may be necessary to increase the PRF or reduce overall enhancement. The same is true for spectral Doppler. Selection of the wall filter should also be controlled, so that slow flow signals or signals of low intensity are not "filtered away."

9.6.2 Directional Artifact

The directional artifact is not actually an artifact phenomenon but evidence of directionally encoded visualization of blood flow on color Doppler (◘ Fig. 9.14). Thus, in a vessel with blood flow in the opposite direction of the ultrasound probe (for instance, when the vessel has a curved flow), the colors red and blue will be present in one and the same vessel. The actual change in the direction of blood flow is seen at the margin of the two colors; this area will be black (corresponding to null flow; see color scale).

9.6.3 Aliasing

In contrast to directional artifacts, aliasing is marked by a change of color through the bright color zones. This phenomenon is expressed as a colorful mosaic in the transition zone between two colors and will be seen at higher flow rates than the selected PRF (◘ Fig. 9.15a). In spectral Doppler, portions of higher frequency appear as being "cut off " at the lower or upper margin of the Doppler frequency spectrum. Aliasing shows, for instance, higher-grade stenosis and disturbance of flow within vessels (◘ Fig. 9.16). Increasing the PRF

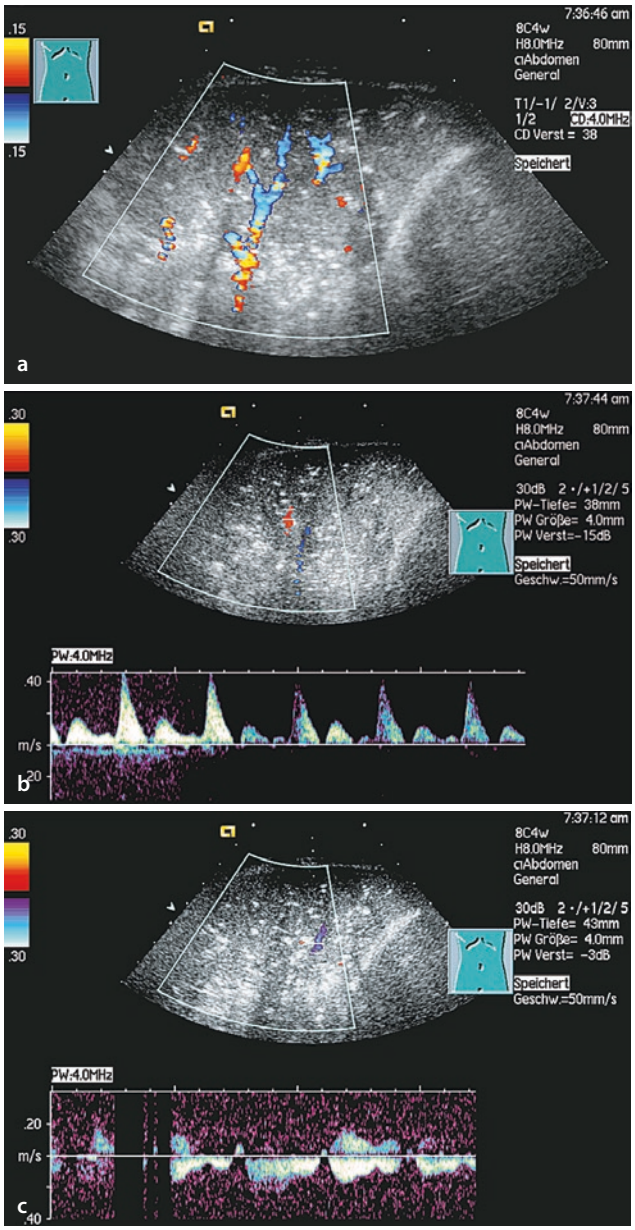

Fig. 9.15 **a** Aliasing on color Doppler in a pulmonary vessel in the presence of pneumonia. Given a low pulse repetition frequency in color Doppler (color scale, here 15 cm/s), color alone does not permit the investigator to conclusively establish the direction of flow. The change of color in the vessel is achieved via brighter colors. Thus, the mean flow rate in this vessel is more than 15 cm/s. **b** Pulmonary artery. Only when pulse repetition frequency is increased to 30 cm/s is it possible to clearly distinguish pulmonary vessels. On red color coding, color Doppler shows an afferent artery. On spectral Doppler, the corresponding Doppler frequency spectrum, suggesting four-phase flow. **c** Pulmonary vein. Blue color coding shows centrally aligned blood flow. Spectral Doppler shows the venous flow signal

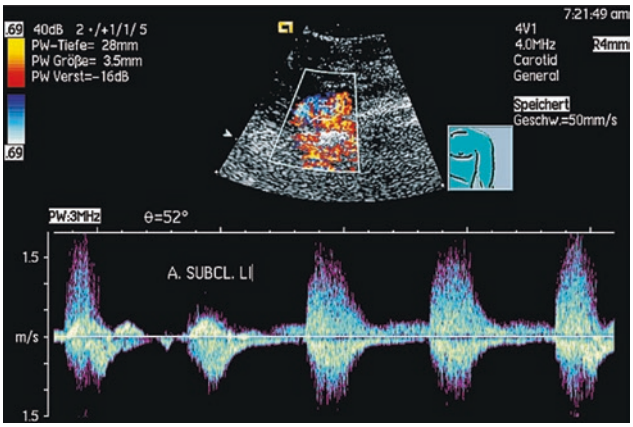

Fig. 9.16 Stenosis of the subclavian artery. In spite of high pulse repetition frequency (maximum 69 cm/s), there is markedly faster flow within the vessel, which is imaged by the bright color pixels in the vessel. Furthermore, the vessel itself is poorly delineated; color pixels are also seen outside of it. This is also known as a vibration artifact and is caused by tissue vibration secondary to stenosis and due to concomitant pulsations that cannot be reliably distinguished from the vessel in terms of space. Spectral Doppler shows flow maxima of about 1.5 m/s and retrograde flow (below the null line), as well as pathological, non-triphasic flow in this extremity artery Image

of color and spectral Doppler (up to the Nyquist limit) will help at least to reduce aliasing. It might also be possible to clearly determine the direction of flow (Fig. 9.15b, c).

9.6.4 Motion Artifacts

Mechanical movement of tissue against the ultrasound probe (breathing, musculature, cardiac and vascular pulsation, etc.) causes an apparent "frequency shift," which creates a signal in color Doppler as well. This disturbs, in particular, the assessment of structures dose to the heart and vessels due to persistent superimposition, and is a limitation of the method, e.g., in the detection of low blood flow in such areas. Various "artifact suppression" modalities proposed by manufacturers of ultrasound devices have achieved some improvement in this regard. Even in the presence of stenosis, movement of tissue due to concomitant motion (vibrations) on color Doppler might represent apparent flow signals outside the vessel (Fig. 9.16). The gliding pleural reflex is very useful in terms of diagnosis. Due to motion, it also causes a strong power Doppler artifactual signal. The absence of this gliding sign, viewed in conjunction with the absence of comet tail artifacts distal to the US reflection on the

aerated lung, indicates a pneumothorax with a specificity of nearly 100% (Kirkpatrick et al. 2004).

9.6.5 Unfavorable Angles

An angle of more than 60–90° may lead to incorrect Doppler measurements or incorrect imaging of blood flow (color Doppler and spectral Doppler). In such cases, the modality of power Doppler would at least help to image vessels in the thorax/lung (Yang 1996). In this setting, a largely angle independent, directionally non-encoded, more sensitive documentation of blood flow is achieved by the visualization of amplitude (not frequency shift) of the backscattering echo.

References

Blank W (1994) Ultrasound guided picture and drainage. In: Braun B, Günther RW, Schwerk WB (eds) Ultraschalldiagnostik Lehrbuch und Atlas. Ecomed, Landsberg. Bd vol. III/11.1, pp 20

Bönhof JA, Linhart P (1985) A pseudolesion of the liver caused by rib cartilage in B-mode ultrasonography. J Ultrasound Med 4:135–137

Dietrich CF, Mathis G, Blaivas M et al (2016) Lung artefacts and their use. Med Ultrason 18:488–499

Dubs-Kunz B (1992) Sonographische Diagnostik von Rippenfrakturen. In: Anderegg A, Despland P, Henner H (eds) Ultraschalldiagnostik 91. Springer, Berlin/Heidelberg/New York/Tokyo, pp 268–273

Gargani L, Frassi F, Soldati G, Tesorio P, Gheorghiade M, Picano E (2008) Ultrasound lung comets for the differential diagnosis of acute cardiogenic dyspnoea: a comparison with natriuretic peptides. Eur J Heart Fail 10:70–77

Kirkpatrick AW, Sirois M, Laupland B et al (2004) Hand-held thoracic sonography for detecting post-traumatic pneumothoraces: the Extended Focused Assessment with Sonography for Trauma (EFAST). J Trauma 57:288–295

Kremkau FW, Taylor KJW (1986) Artifacts in ultrasound imaging. J Ultrasound Med 5:227–237

Lichtenstein D (2005) General ultrasound in the critically ill, 2nd edn. Springer, Heidelberg

Lichtenstein D, Meziere G, Biderman P (1997) The comet tail artifact: an ultrasound sign of alveolar-interstitial syndrome. Am J Respir Crit Care Med 156:1640–1646

Mathis G, Horn R, Morf S et al (2021) WFUMB position paper on reverberation artefacts in lung ultrasound: B-lines or comet-tails? Med Ultrason 23(1):70–73

Noble VE, Murray AF, Capp R, Sylvia-Reardon MH, Steele DJR, Liteplo A (2009) Ultrasound assessment for extravascular lung water in patients undergoing hemodialysis. Time course for resolution. Chest 135:1433–1439

Reading CC, Charboneau JW, Allison JW, Cooperberg PL (1990) Color and spectral doppler mirror-image artifact of the subclavian artery. Radiology 174:41–42

Reissig A, Kroegel C (2003) Transthoracic sonography of diffuse parenchymal lung disease: the role of comet tail artefacts. J Ultrasound Med 22:173–180

Schuler A (1998) Untersuchungstechnik und Artefakte. In: Braun B, Günter RW, Schwerk WB (eds) Ultraschalldiagnostik Lehrbuch und Atlas. Bd I. ecomed, Landsberg, pp. 1–42

Soldati G, Testa A, Silva FR, Carbone L, Portale G, Silveri NG (2006) Chest ultrasonography in lung contusion. Chest 130:533–538

Soldati G, Copetti R, Sher S (2009) Sonographic interstitial syndrome. The sound of lung water. J Ultrasound Med 28:163–174

Volpicelli G, Caramello V, Cardinale L, Cravino M (2008) Diagnosis of radio-occult pulmonary conditions by real-time chest ultrasonography in patients with pleuritic pain. Ultrasound Med Biol 34:1717–1723

Wild K (1996) Periphere Gefäße. In: Braun B (ed) Ultraschalldiagnostik Lehrbuch und Atlas. Ecomed, Landsberg, pp. 10–13

Wohlgenannt S, Gehmacher O, Mathis G (2001) Thoracic sonography on interstitial lung disease. Ultraschall Med 22:27–31

Yang PC (1996) Color doppler ultrasound of pulmonary consolidation. Eur J Ultrasound 3:169–178

Interventional Chest Sonography

Wolfgang Blank and Thomas Müller

Contents

G. Mathis (ed.), *Chest Sonography*, https://doi.org/10.1007/978-3-031-09442-2_10

10.1 Introduction

The cause of many diseases in chest organs can be determined by a combined evaluation of the patient's history, clinical findings and diagnostic imaging procedures. An elaborate diagnostic "cascade" which strings together any available methods is neither justifiable economically nor sensible from a medical viewpoint.

A definitive evaluation often requires additional biochemical, microbiological, cytological or histological expert assessment. The material needed for such investigations can be obtained by targeted puncture. Given the appropriate indication, the puncture may be followed by interventional therapeutic measures.

One should always employ the interventional method which provides a definite diagnosis in the fastest and least stressful manner for the patient.

Interventional measures in the thorax—various procedures:

1. Percutaneous access
   (a) Sonography
   (b) Radiographs (fluoroscopy, computed tomography, CT)
2. Endoluminal access
   (a) Bronchoscopy
   (b) Endoluminal sonography
3. Surgical (mediastinoscopy, thoracoscopy, surgical exposure)

10.2 General Indications

In addition to the frequent use of puncture for pleural effusion, space-occupying masses accessible to sonographic investigation, located in the chest wall, pleura, lung or anterior mediastinum, are important indications (Braun 1983; Börner 1986; Weiss and Weiss 1994; Pedersen et al. 1986; Koenig et al. 2011; Laursen et al. 2016).

Depending on their topographical position and the diagnostic availability and expertise, pathological changes not detectable by a transthoracic approach may be identified diagnostically by one of the interventional procedures displayed in the list in the previous section (Di Bardino et al. 2015).

Interventions in the Thorax—Indications:

1. Space-occupying mass in the thoracic wall (tumors, abscesses, hematomas, changes in the skeletal parts)
2. Space-occupying masses in the pleura
3. Pleural effusion and pleural empyema (very small quantities, loculated effusions)
4. Peripheral lung consolidations (lung tumor, pneumonia, lung abscess)
5. Mediastinal processes (anterior mediastinum)

Because of the potential risk of complications, the indication for the procedure should be established with care.

Even if any sonographically demonstrable space-occupying lesion can be punctured in principle, one should only perform punctures if therapeutic consequences (e.g., radiation, chemotherapy) or important prognostic information is to be expected. In a patient who is operable, a suspected malignant tumor located in the periphery will normally not be punctured but will be resected as a first-line measure. It is not reasonable to merely seek confirmation of already established or plausible diagnoses. If the same information may be gathered in a less invasive way, puncture should not be performed (Blank 2006; Beckh and Bölcskei 1997; Müller and Blank 2011; Jeon et al. 2014).

10.3 Contraindications

The limits of acceptable coagulation parameters depend on the positioning of the mass and the invasiveness of the intervention. Urgent interventions require Individual assessment of risk (see Table 10.1) (Blank 2019). Special caution is necessary under Clopidogrel . Lung biopsies should not be undertaken; recommendations

Table 10.1 Recommendations on coagulation diagnostics and coagulation management before thorax punctures (adapted from Patel et al. 2012, 2013)

Procedure	Laboratory examination	Technique
Thoracocentesis Superficial biopsy	INR in case of pathologies involving anticoagulation and liver diseases PTT: Pat. with intravenous heparin Platelet count: not routinely recommended Hematocrit: not routinely recommended	INR > 2.0: threshold for treatment (i.e., FFP, vitamin K) PTT: no consensus Thrombozyten <50.000/µl: Transfusion ASS/NSAR: do not withhold Thienopyridine (Clopidogrel) 0–5 Tage Pause LMWH (therapeutic dose): withhold one dose before procedure
Biopsy or drainage of abscesses Mediastinal and lung biopsy and thick catheters	INR recommended PTT: Pat. with intravenous heparin Platelet count: not routinely recommended Hematocrit: not routinely recommended	INR >1.5: threshold for treatment (i.e., FFP, vitamin K) PTT: no consensus Thrombozyten <50.000/µl: Transfusion ASS/NSAR: do not withhold Thienopyridine (Clopidogrel) withhold for 5 d before procedure LMWH (therapeutic dose): withhold one dose before procedure

aPTT activated partial thromboplastin time, *INR* international normalized ratio, *LMWH* low molecular weight heparin

on superficial intervention are not univocal (see ◘ Table 10.1). Reference is made to the literature (Patel et al. 2013).

Bullous pulmonary emphysema and pulmonary hypertension are relative contraindications. When respiratory function is severely restricted or blood gas values are poor, a puncture should only be performed when the patient's condition is expected to be improved by the therapeutic intervention. High-risk puncture sites should be avoided (Yang et al. 1992; Mathis et al. 1999; Dietrich and Nürnberg 2011).

10.4 Sonography-Guided or CT-Guided Puncture

In several diseases of the lung and mediastinum, CT provides the best overview. It should, however, only be used as an interventional measure when the target and pathway of puncture cannot be reliably assessed with sonography (Blank 2006; Mathis 1997a; Müller and Blank 2011). The success rate of the US-guided puncture (89–97%) is comparable to CT (92–96%) (Di Bardino et al. 2015; Sconfienza et al. 2013).

The advantages of sonography-guided puncture are manifold: fast availability and bedside application (intensive care unit, emergency room), low rate of complications, absence of radiation exposure and low cost. In contrast to CT-guided puncture, the sonographic puncture can be carefully observed during the process. The investigator is free to use the pathway he/she desires in terms of direction; the ventilated lung is protected (low rate of pneumothorax) (Lee et al. 2018). The nerve cords of the plexus in the region of the upper thoracic aperture may be demonstrated with high-resolution ultrasound probes, thus avoiding injury through puncture (◘ Fig. 10.1).

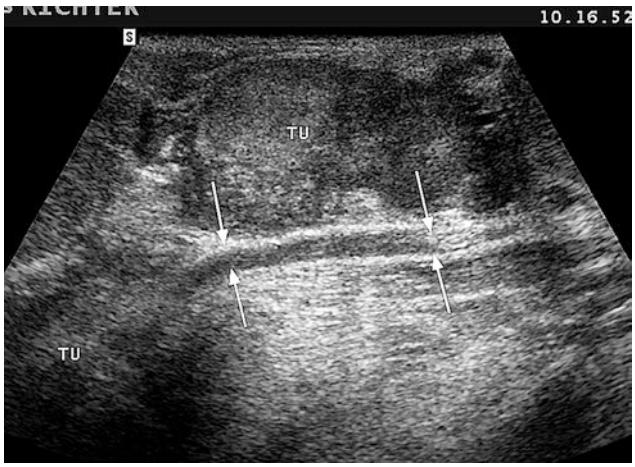

◘ **Fig. 10.1** Brachial plexus (*arrows*). Tumor masses (*TU*) in the region of the upper thoracic aperture

Vessels are detected with color-Doppler sonography (upper thoracic aperture, parasternal). Active (vascularized) sections of a tumor may be identified by color-Doppler sonography and, recently, by the even more sensitive method of contrast-enhanced sonography. Diagnostic puncture may be performed with a high success rate or the tumor may be ablated therapeutically, if advisable. Atelectatic or pneumonia-affected parts of peripheral lung consolidations may be differentiated from tumors by color-Doppler sonography or contrast-enhanced sonography (fewer motion artifacts) (Wang et al. 1995; Yang 1996; Zimmermann et al. 2003; Görg et al. 2006; Cao et al. 2011; ◘ Fig. 10.2).

Sonography-guided percutaneous puncture also has its limitations, however. If the space-occupying mass is hardly or not at all visible percutaneously on sonography (Lesions < 1 cm), or if the puncture channel is not safe, other endoluminal procedures (bronchoscopy, endoluminal sonography) may be used or a computer-assisted puncture may be performed (Klose and Günther 1996; Mikloweit et al. 1991; Anzidei et al. 2017; ◘ Fig. 10.3).

In principle, the interventional procedure constituting the fastest means of arriving at the diagnosis and placing the least stress on the patient should be used.

The advantages of sonography-guided punctures are as follows:

1. The method can be carried out quickly and at the bedside (portable US-devices).
2. There is no exposure of radiation to patients, assisting personnel or physicians.
3. The direction of puncture may be chosen freely, and the needle monitored continuously.
4. Nerves (plexus in the upper thoracic aperture), vessels (color-Doppler sonography), and the ventilated lung are spared (lower rate of pneumothorax).
5. Active tumor parts (color-Doppler sonography, contrast-enhanced sonography) may be punctured with a higher success rate.
6. Lung tumors may be differentiated from areas of pneumonia or atelectasis by color-Doppler sonography and contrast-enhanced sonography (fewer motion artifacts).
7. It is a low-cost procedure, and it may often be performed on an outpatient basis.

!

» In US you see what you do, in CT you see what you have done—(Heilo 1996).

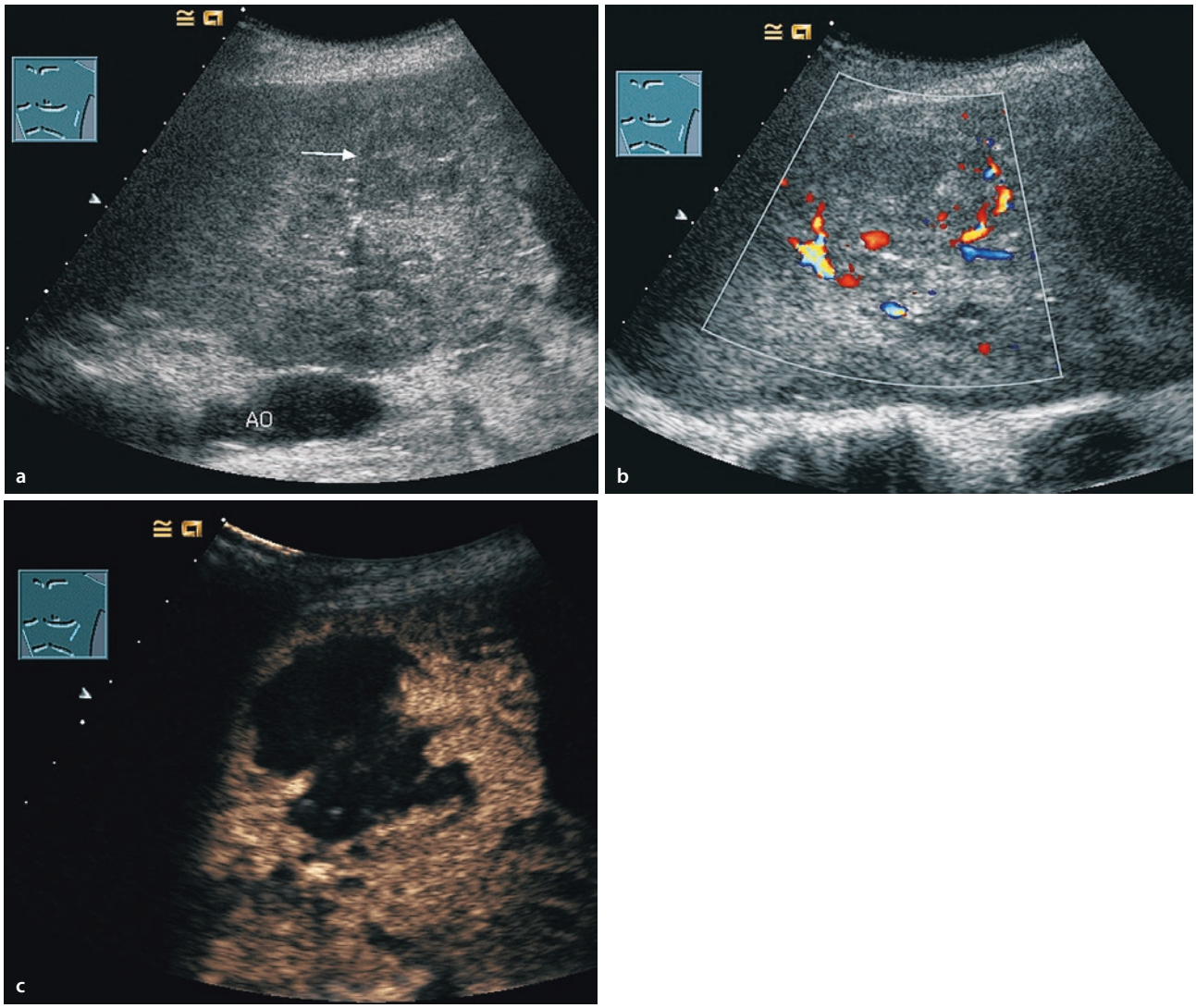

Fig. 10.2 Tumor inside an atelectasis. Computed tomography: obstruction atelectasis, cause not discernable. Bronchoscopy: no tumor found. **a** On B-mode sonography extensive atelectasis with a slightly conspicuous focal structural change (*arrow*). **b** In the area of structural irregularity there is no recognizable "normal" vessel architecture. **c** Space-occupying mass with little contrast on signal-enhanced sonography

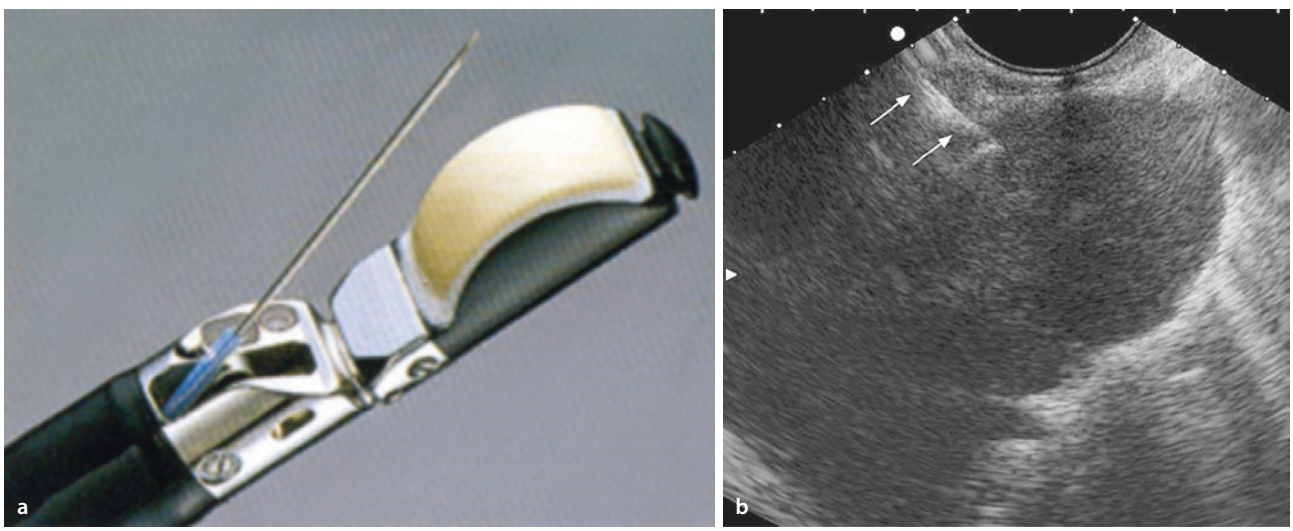

Fig. 10.3 Transesophageal puncture. **a** Longitudinal probe with puncture unit (Hitachi). **b** Paraesophageal hypoechoic tumor mass in the dorsal mediastinum. The puncture needle is easily recognizable (*arrows*). Cytology indicated small-cell bronchial carcinoma

10.5 Apparatus, Instruments and Puncture Technique

For lesions of the chest wall, the investigator should use high-frequency linear probes. Lesions in the pleural space and lung should be investigated with sector-like probes equipped with a narrow covering. For endosonography-guided puncture, special intraluminal probes with biopsy canals are available (Kelbel et al. 1996; Jennsen et al. 2014)

The puncture needle can be guided in many ways (Fig. 10.4). A simple and economical method is so-called free puncture. Ninety percent of interventions are performed by the free-hand technique under sonographic visual control.

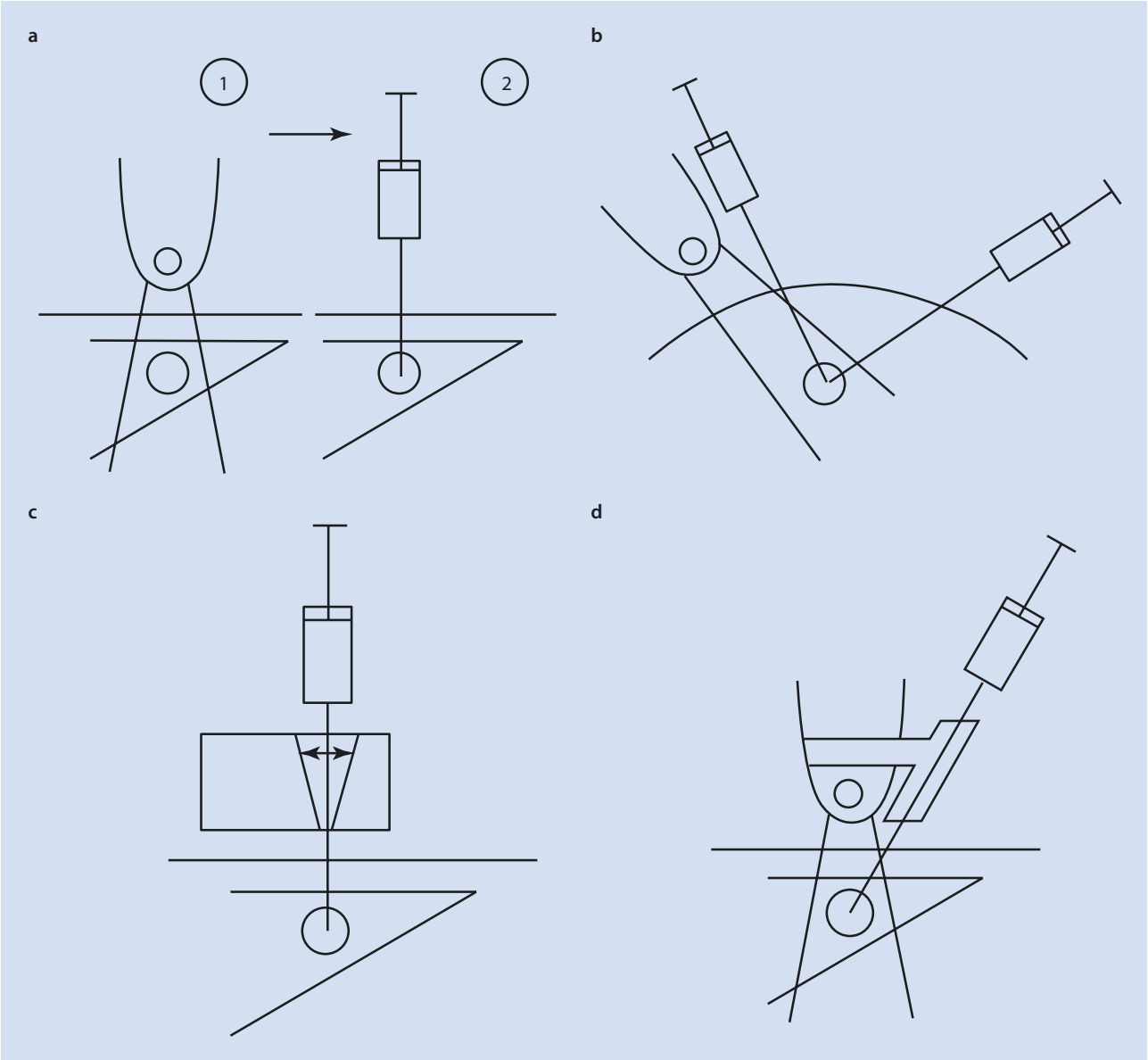

Fig. 10.4 Various puncture methods. **a, b** Free puncture. **a** Free-hand puncture after sonographic location. Inexpensive two-step method (no visual surveillance of the target area during the puncture).Very suitable for small processes located on the surface. **b** Puncture under sonographic observation. Low cost, puncture route variable, so punctures are possible from various areas, needle well visible, difficult with small processes located on the surface. Sterile gloves should be used for therapeutic procedures. **c, d** Guided puncture. **c** Ultrasound puncture probe. Expensive, puncture route not very variable, limited imaging through the perforation region, needle not easily visible, good view at close range. Seldom necessary for punctures of the thorax. **d** Sector/curved array scanner with attachment. Relatively cheap, needle is easily visible, but poor view at close range, puncture route prescribed but can be superimposed electronically, disinfection of the attachment necessary. Not sensible on the thorax

10.5.1 Puncture Needles

A distinction is made between fine (diameter less than 1 mm) and gross (diameter more than 1 mm) needles (Fig. 10.5). The rate of complications increases with the thickness of the needle and the duration of the procedure. The ideal puncture needle should fulfill the following criteria: it should be as thin as possible, sufficiently stiff to maintain the direction of puncture, cut sharply, be such that it can be advanced forward fast and be able to obtain sufficient material for investigation (Weiss and Düntsch 1996; Westcott 1980). Table 10.2 compares different classifications of needle diameters.

10.5.1.1 Fine Needles

For aspiration cytology, fine needles with a diameter of 0.7–0.9 mm are sufficient. They are available with and without a mandrin and have no cutting tip (economical injection needles, spinal puncture needles and Chiba needles).

Mandrins are usually not necessary, but their use is advisable if the pathway for puncture is long (through pulmonary tissue, for instance), because the needle bends less and there is no danger of abrading tissue outside the region to be punctured. A needle diameter of 0.7–0.9 mm is sufficient for cytological or bacteriological examination. If the liquid which needs to be aspirated is highly viscous (pus, blood), needles of a larger diameter must be chosen (1–2 mm maximum).

The puncture technique is as follows. Once the target of puncture has been reached, the puncture is performed, if possible, in a fan-like fashion under suction, in order to collect tissue from different areas (Fig. 10.6). With smaller tumors (less than 2 cm), it is often only possible to aim in one direction. In this case, turning the needle shaft may be helpful in collecting a tissue sample.

During forward and backward movement, cells are peeled off and aspirated into the tube. No suction should be applied during backward movement, so that material is not sucked into the syringe and dissemination of tumor tissue into the puncture canal is avoided.

A cytological slide is prepared by injecting the material collected onto the middle of the slide with high

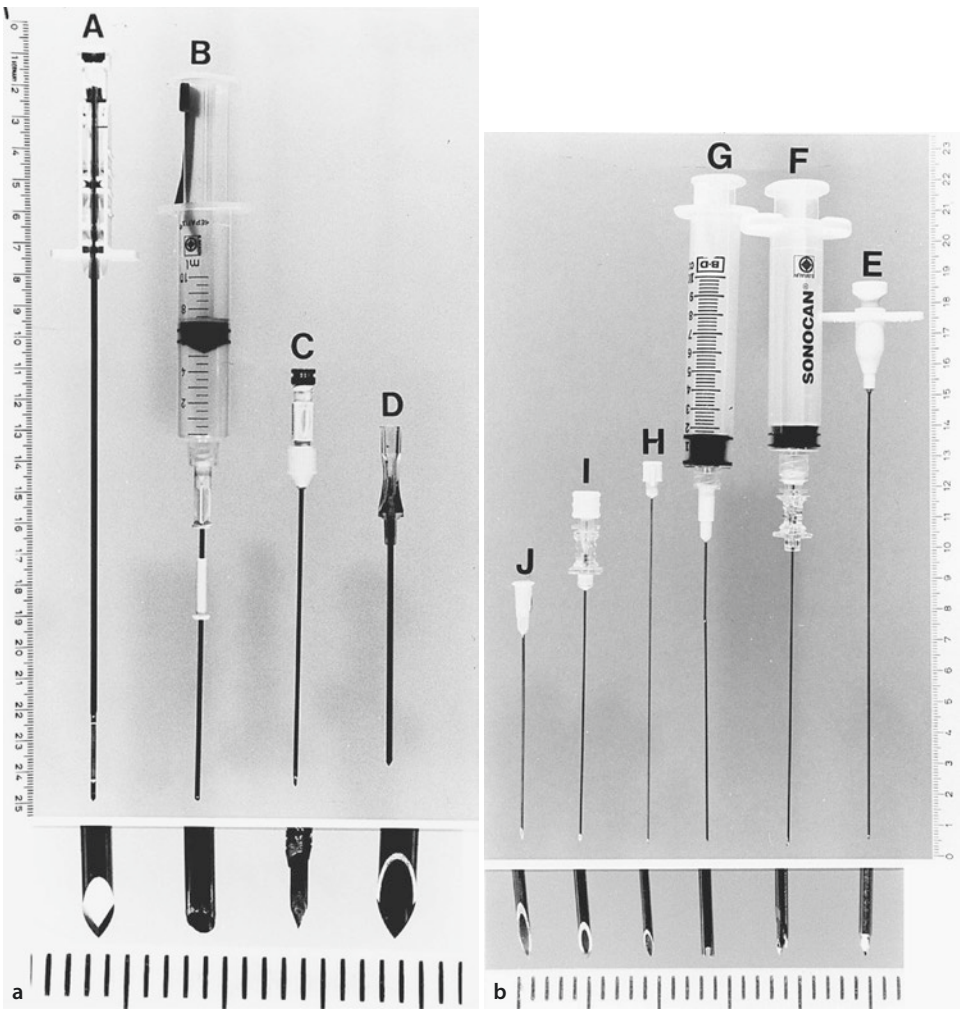

Fig. 10.5 Puncture needles. **a** Coarse needles. *A* Tru-Cut needle, diameter 1.4–2 mm. *B* Menghini needle, diameter 1.6 mm. *C* Bone punch needle (Angiomed). *D* Aspiration needle for viscous liquids, diameter 2.0 mm. **b** Fine needles. *E* Vaku-Cut needle based on Köhler (Angiomed). When the puncture destination has been reached, the stiletto is withdrawn three quarters of its length to create a partial vacuum. Diameter 0.8–1.2 mm. *F* Sonocan biopsy needle (Braun, Melsungen, Germany), diameter 0.8–1.4 mm, length 100–160 mm. Puncture technique as for the Otto needle, but without any rotating movement. *G* Cutting biopsy needle based on the Otto needle with a mandrin (Angiomed), diameter 0.8–1.2 mm, length 100–200 mm. *H* Chiba needle with a mandrin, diameter 0.6–0.9 mm. *I* Lumbal puncture cannula with a mandrin, diameter 0.9 mm. *J* Puncture cannula with no mandrin, diameter 0.7 mm

Table 10.2 Conversion table—needle diameter

Millimeters (mm)	Gauge (G)	French (Fr), Charriere (Charr)
0.7	22	
0.8	21	
0.9	20	
1.0	19	3
1.2	18	
1.35		4
1.4	17	
2.0	14	6
3.0	11	9
4.0	8	12
5.0	6	15

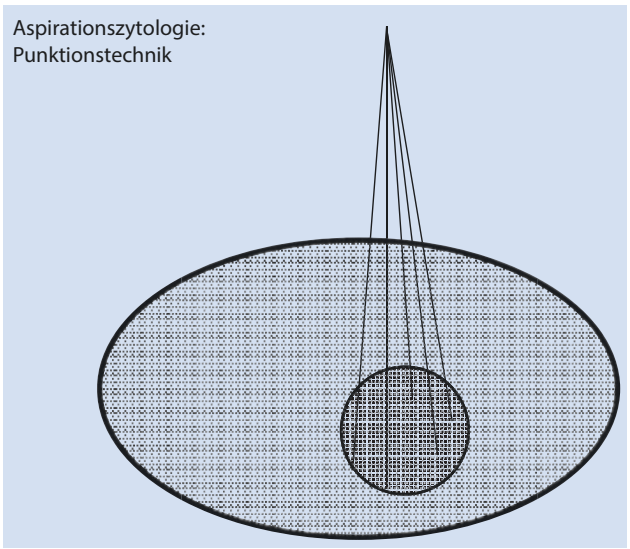

Fig. 10.6 Fine-needle aspiration puncture. Fan-shaped puncture technique

pressure. With use of a second slide, the material is spread with slight pressure and then, according to the agreement with the "house pathologist," fixated with alcohol (fixating spray, Merckofix, for instance) or air-dried. It is necessary to immediately scan the material under a microscope in order to make sure that there are enough cells for evaluation, so that a repeat puncture may be performed in the same session, which is necessary in one third of patients with suspected tumors. Bacteriological slides are made with Gram stain and bacteriological cultures started. If tuberculosis is suspected, special examinations are instigated (cultures, PCR, etc.)

The material obtained by this procedure usually only allows a cytological investigation which distinguishes between malignant and benign disease; it does not permit the investigator to determine the type of malignant lesion (e.g., lymphomas). If a quick diagnosis is needed and the proof of malignancy is sufficient, cytology is preferable at least as a first step. Zum Nachweis eines Lungenkarzinoms ist sie der Schneidbiopsie sogar of tüberlegen und sicherer (Diacon et al. 2007). Recent immunocytological techniques with specially coated slides have improved results, but determining the type of many malignant changes (lymphomas, for instance) is usually not possible, so examinations of histological material become necessary. Immunohistological techniques have also distinctly improved the results of cut biopsies (Müller and Blank 2011).

Possible mistakes in puncture cytology are:

1. Insufficient puncture technique
2. Little or useless material (possibly repuncture)
3. Aspiration of blood
4. False technique of slide preparation or fixation procedure
5. Little experience in cytology

10.5.1.2 Cutting Biopsy Needles

Tissue cylinders for histological assessment can be obtained with these needles. One-hand needles are useful, as *one* investigator performs the sonographic investigation and the puncture. Automatic one-hand needles (so-called puncture guns) are especially suitable in the thorax, as the procedure of puncture is fast, does not require the investigator to avoid the lung, and very representative puncture cylinders can be punched out from soft tissue (Fig. 10.7). The results of puncture are better and the complication rate is lower—especially the rate of pneumothorax. In the case of hard tumors or tumors of the bony skeleton, the spring pressure of the automatic needle is often not sufficient to penetrate the tumor.

Disadvantages are the cumbersome procedure and the absence of the sensation of performing a puncture (Mathis 1997b).

In the meantime, there are a variety of equivalent needles available on the market. It is sensible to familiarize oneself with *one or two* needle types. Three needle techniques can be differentiated:

1. *Tru-Cut principle*: The True-Cut needle contains a biopsy chamber, securing the cylinder which has been cut. A disadvantage is that the volume of the tissue particle is thinner in comparison with the needle diameter and also is only half-cylindrical.
2. *Surecut principle*: The cutting process happens through a quick forward movement of the needle. On retraction, the tissue cylinder is held within the cylinder by suction. If the negative pressure fails, the tissue cylinder may be lost (Fig. 10.8).

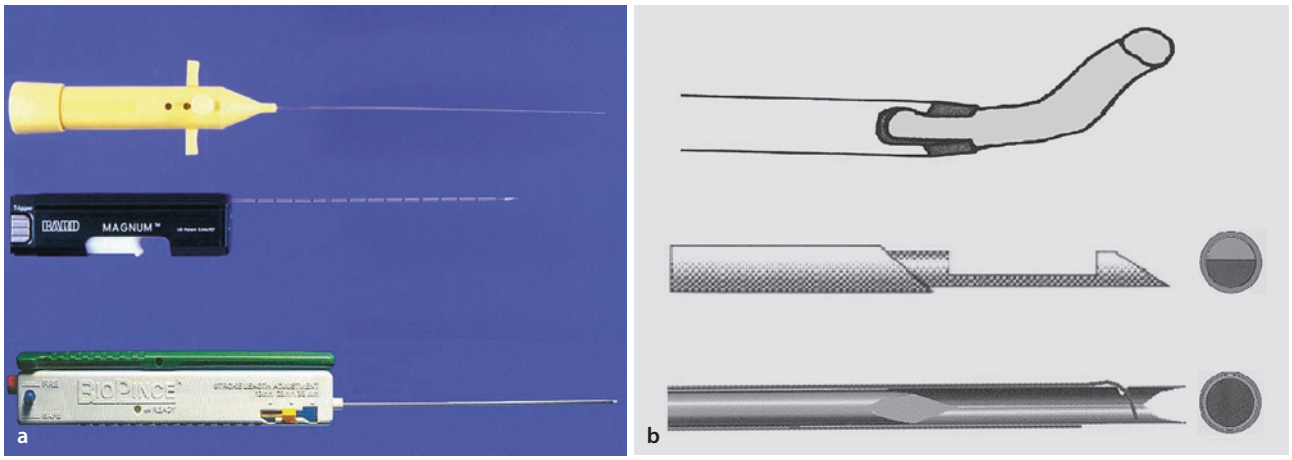

Fig. 10.7 **a** Automatic single-hand needle. The required depth of injection (measured sonographically) can be preset. *Top*: Auto-Vac puncture, disposable set (Bard). *Middle*: Reusable pistol from Barth with insertable Tru-Cut needles. The Tru-Cut needle contains a biopsy chamber. An advantage is that the cut cylinder of tissue cannot be lost when the needle is withdrawn. A disadvantage is the short tissue cylinder. *Bottom*: BioPince—biopsy pistol (Pflugbeil-Amedic). The full tissue cylinder is secured inside the needle by a special holding wire. **b** Surecut needle (*top*), Tru-Cut needle (*middle*) and BioPince needle (*bottom*)

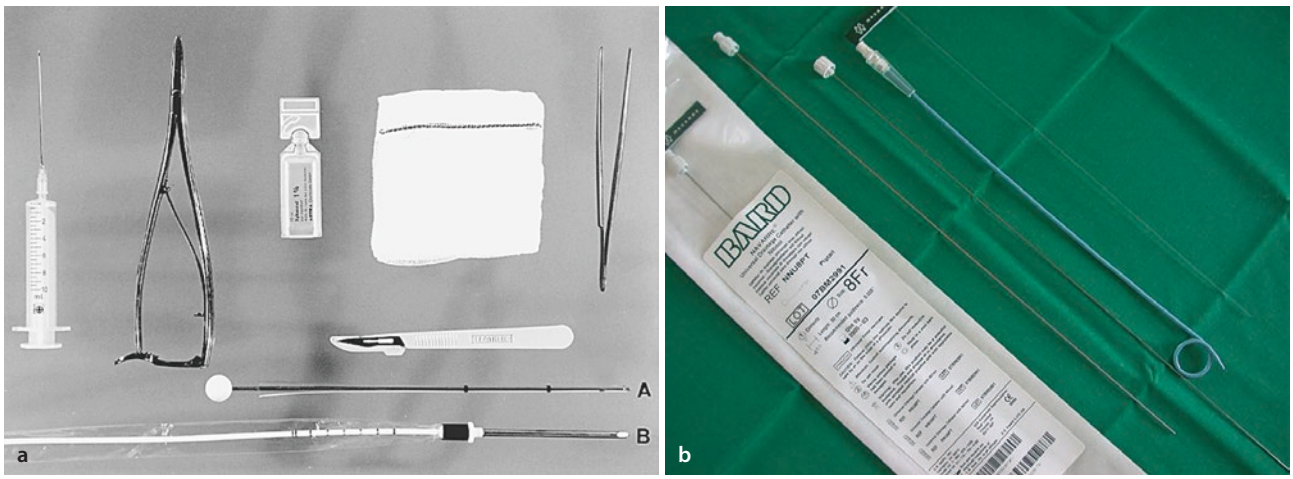

Fig. 10.8 **a** Pleural drainage set (trocar technique). *A* Thin (12-Fr) pneumo-catheter (Intra). *B* Trocar catheter (Argyle). **b** Navarre universal draining catheter (Bard—Angiomed 8–12 Fr). This catheter has many advantages: direct puncture only requires a small incision, introduction is possible without preceding dilatation, it does not kink, the lumen rarely occludes and the pig-tail prevents dislocation

3. *BioPince principle*: Similar to the Surecut principle, complete cylinders are cut, thus yielding large tissue volumes (needle diameter 1.2 mm), producing better histological results. The needle combines the advantages of both principles mentioned above. A special "fixation wire" which gets propelled within the needle after the puncture procedure secures the tissue cylinder. Tumor seeding is very unlikely with this method (Fig. 10.7).

10.5.1.3 Gross Needles

Gross needles (1.2–2 mm) are usually only needed for aspiration of highly viscous fluid. For histological differentiation of benign lesions of the thoracic wall, pleural afflictions or interstitial pulmonary disease, True-Cut needles of a large size might be necessary (Gleeson et al. 1990; Ikezoe et al. 1990; Fig. 10.7).

10.5.2 Drainage Catheter

The diameter of the selected catheter depends on the viscosity of the liquid formation. In principle, drainage may be performed using the trocar or Seldinger's technique. *The trocar technique* is commonly used in the thorax (Fig. 10.8). Both drainage techniques are preceded by diagnostic puncture (Fig. 10.9).

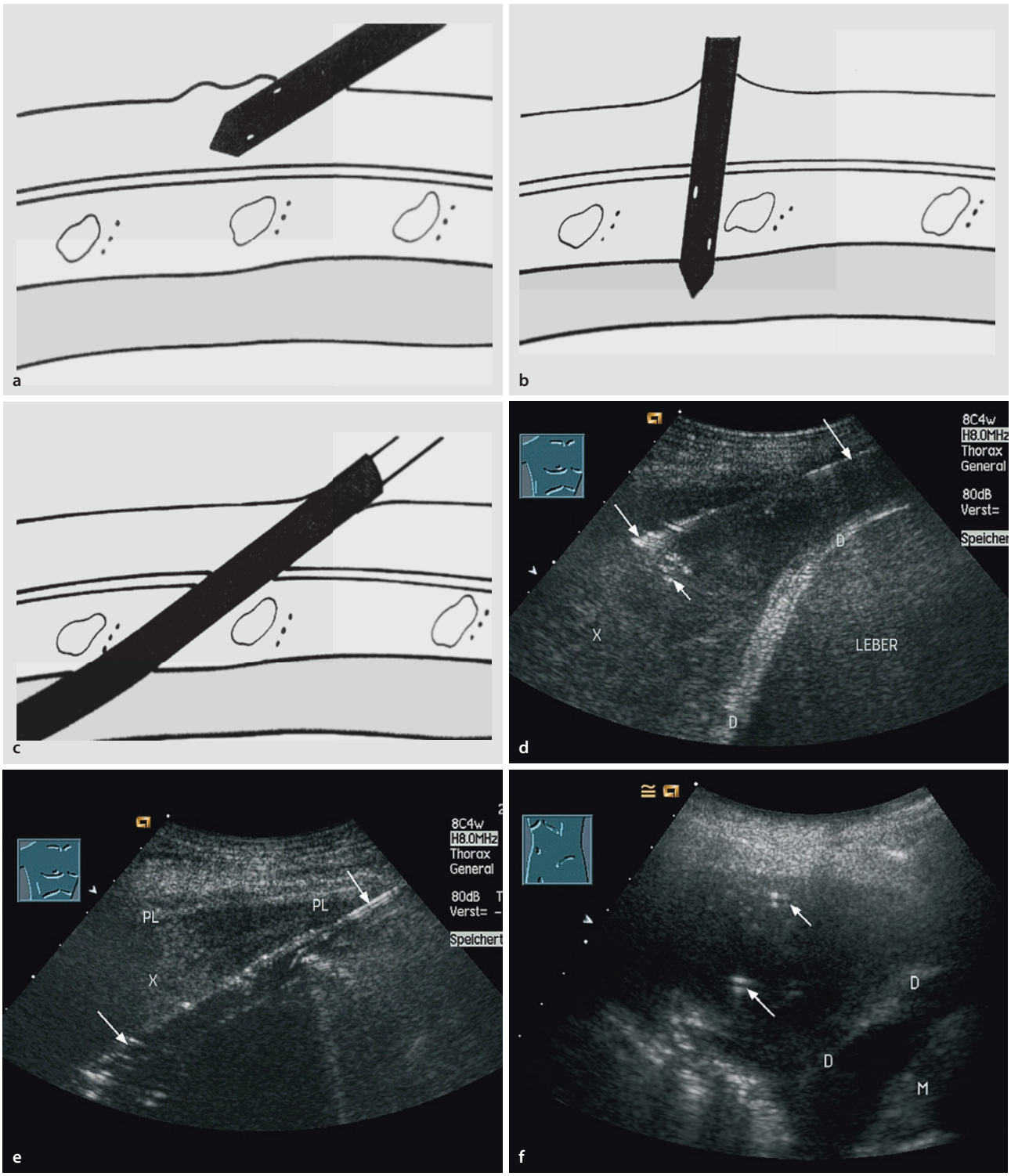

Fig. 10.9 Empyema of the pleura. **a–c** Pleural drainage. Outline of the technique. **d** On diagnostic puncture, the puncture needle (*large arrows*) is inserted in an upward direction at the upper edge of the rib. After instillation of liquid, an echogenic cloud shows up at the tip of the needle. *X* empyema. **e** On insertion, the trocar is visible as a straight echogenic reflex, partly producing acoustic shadowing (*arrows*). *X* empyema, *PL* parietal pleura. **f** After removal of the trocar, the soft draining tube (double reflex) is more difficult to recognize because of its winding course

10.5.3 Checking the Position of the Needle and the Catheter

Correct placement of the needle is not demonstrated by sonography alone. Moreover, the "sensation of puncture" usually changes when the target of puncture is reached. Depending on the situation, resistance is noticeable. The feeling of hitting something hard suggests a malignant tumor. The absence of any palpable sensation when cutting a cylinder is one of the few disadvantages of using a "puncture pistol." Optical visualization of the needle depends on the angle of the needle and the ultrasound beam. Ideally, when a needle is introduced at the level of the transducer, the needle shaft is seen as an echogenic double reflex. However, in deeper lesions, only the tip of the needle is seen as a bright double reflex (Fig. 10.10b). A compromise must be found between demonstrability of the needle (better with a larger angle) and targeting precision (better with a smaller angle). The choice of the points of approach is often limited in the thorax by the anatomy.

In tissue with high echodensity it may be difficult to localize the needle. Here, it is useful to move the needle or the mandrin backward and forward and even to employ brief suction. Color-Doppler sonography will show the needle as a colored line (Fig. 10.11). When

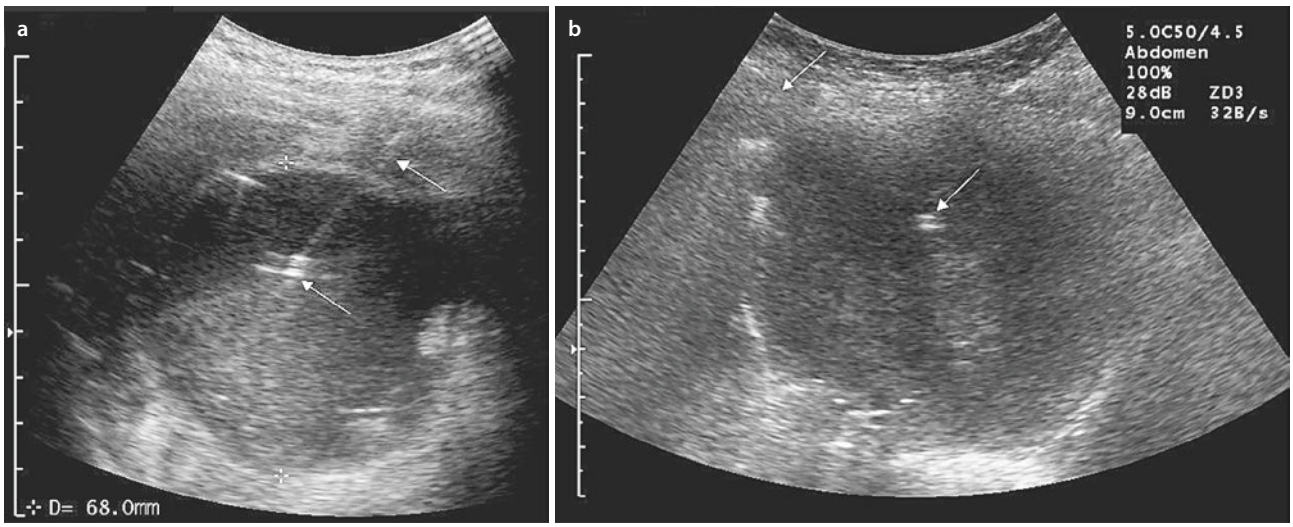

Fig. 10.10 **a** The needle shaft can be depicted at a great angle (45–90°) as an echogenous, straight-line reflex (*arrows*). The needle tip appears as an echogenic double reflex (*arrow* far from the sound head), but only if the needle is being guided correctly at the sound level. *Crosses* encapsulated pleural empyema. **b** Echogenic double reflex of the needle tip: double reflex is indicated by the *arrow* far from the sound head. As is so often the case, the puncture was not possible exactly at the insonation level. The needle shaft could only be indicated by wobbling movements (*arrow* close to the sound head). Hypoechoic tumor on the thoracic wall. Peripheral bronchial carcinoma (squamous cell)

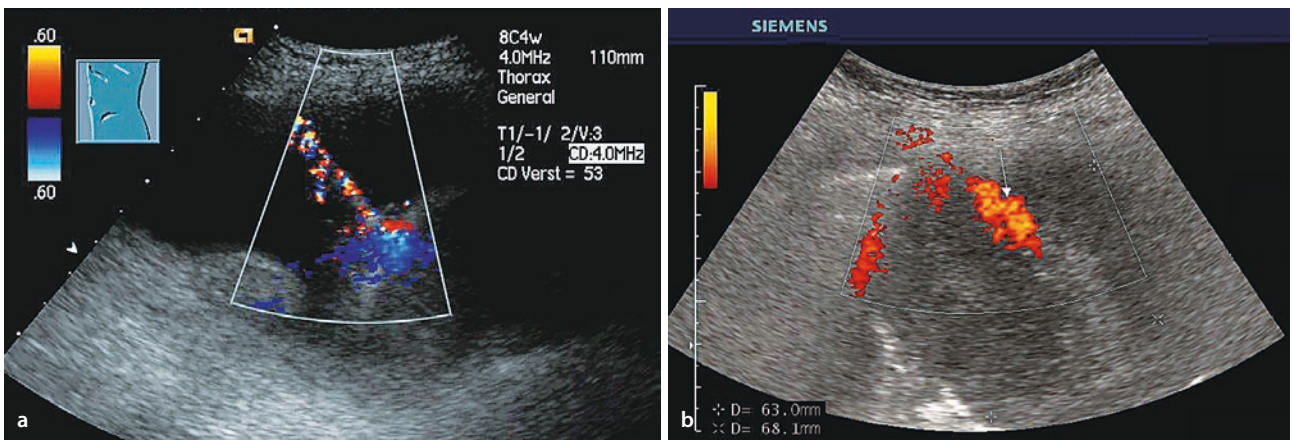

Fig. 10.11 **a** Color-Doppler sonography allows liquid movements in the needle to be detected. The exit of the liquid at the tip of the needle can be seen as a cloud of color. **b** Tissue shifts in the region of the needle tip (slight movement of the needle, or caused by suction) can also be detected by color-Doppler sonography (power Doppler). *Crosses* peripheral bronchial carcinoma

a gun is used, the incision canal (air) is visible even several seconds after the puncture.

A drainage catheter is typically visualized as a bright double contour, which might not show up the whole way, however. On color-Doppler sonography, the course of the catheter during instillation of fluid is clearly depicted by color-coding (Wang et al. 1995). If both techniques failed the correct positioning of the catheter can be checked by the injection of NaCl 0.9%, mixed with a drop of SonoVue® (ultrasound contrast agent)

The coordination between the ultrasound probe and the needle tip works best if carried out as "one person—one hand puncture." Visualization of the spatial relations is better and necessary corrections in the position of the needle tip can be performed more quickly.

» The inexperienced investigator should practice on models, e.g., on a steak interlarded with olives, or in a water bath or on puncture models commercially available (Mathis et al. 1999). Cheap puncture models for ultrasound-controlled drainage can be manufactured in homemade—(Mohr et al. 2014)

10.5.4 Hygiene, Preparation and Execution of Puncture

Most diagnostic puncture and draining procedures (of pleural effusions, for instance) may be performed on an outpatient basis. In principle, interventional procedures may be carried out in any room (emergency rooms, normal wards, intensive care wards), provided daily disinfection measures are guaranteed. Transportable ultrasound machines may be advantageous (Blank et al. 2014; Müller et al. 2018).

According to the recommendations of the Commission for Hospital Hygiene and Infection Prevention of the Robert Koch Institute (RKI 2011), the risk of a puncture-associated infection depends on the type and anatomical region of the intervention, the patient's defensive position and the experience of the person performing the puncture

Special puncturing equipment should be available: syringes, cannulas, puncture needles, drainage sets, gloves, disinfection spray, local anesthetics, sterile draping material and containers for further diagnostic processing (microbiological, chemical, cytological and histological examination) of the material obtained (Müller et al. 2018).

Coagulation status should be known (except in the case of lesions of the thoracic wall. (Tbl.1)

In an emergency case, the risk must be calculated individually.

As with any invasive procedure, the patient must be informed of the course and risk of the procedure. The sonographical status of the thorax is evaluated. Utilizing other imaging methods (plain chest radiograph, CT), the puncture goal, the site of puncture needle placement, puncture direction and puncture pathway are determined (the four P's).

The nonsterile ultrasound gel is removed. In cases of diagnostic puncture the investigator should use sterile gloves, local disinfectant spray and sterile catheter gel if necessary. The patient is positioned such that the focus is optimally accessible in a sitting, dorsal, lateral or ventral decubitus position. Local anesthesia is only required in cases of multiple puncture or needles with a thick lumen though many patients opt for it.

During the puncture the patient must be asked to briefly hold his/her breath.

In the case of simple therapeutic interventions (thoracentesis), no special hygiene measures are necessary. Sterile covers for the probe and keyboard are mandatory (Müller et al. 2018).

Interventional Procedures of the Thorax—Preparation and Performance

1. **Preparation**
   - (a) Acknowledging preexisting findings (bronchoscopy, chest radiograph, CT).
   - (b) Sonographic thorax status.
   - (c) Verifying the indication for puncture.
   - (d) Is a sonography-guided intervention technically feasible?
   - (e) Are there contraindications for an intervention?
   - (f) Has the patient received prophylactic antibiotic treatment (especially in the case of an abscess)?
   - (g) Have information about the procedure and written consent by the patient obtained?
   - (h) Cytology or histology?
   - (i) Selection of puncture equipment (needle, drainage).
2. **Performance of intervention**
   - (a) Positioning the patient (sitting, dorsal, lateral or ventral decubitus position).
   - (b) Visualization of the goal of puncture, the pathway and direction.
   - (c) Disinfection and local anesthesia, if wanted.
3. **Follow-up**
   - (a) For outpatients
     - Three hours of surveillance after intervention.
     - Sonographical check before discharge of patient (pneumothorax? bleeding?).
     - Preliminary report for referring doctor.
     - Final evaluation of the procedure.

- Immediate return to the hospital in case of symptoms.
- Decision on who informs about the result and when.

(b) For inpatients
- Preliminary report for doctor in charge.
- Instructions for nursing personnel (checkup examinations, suction for drainage, etc.).
- Sonographic reevaluation after 3 h (pneumothorax?, bleeding?).
- Checkup examinations after therapeutic punctures and drainage.
- Possibly repuncture in cases of inconclusive result.

Sonographically Guided Interventions—Conditions for Achieving Good Results

1. Careful formulation of indication (clinical experience).
2. Experience in sonography and puncturing.
3. Knowledge of possible complications and limitations of the method.
4. Quality of and preparation of material obtained.
5. Experience of the pathologist (immunohistology) and microbiologist.
6. Interdisciplinary cooperation.

10.6 Indications

10.6.1 Processes of the Chest Wall

Soft-tissue tumors should be punctured parallel to the surface of the lung as far as possible. The needle can then be (at a suitable angle) nearly completely imaged in its length and the risk of pneumothorax is minimized (Fig. 10.12).

Needles with a large caliber may be used for this technique (1.4–2 mm). By doing so, even benign lesions are better differentiated (Gleeson et al. 1990; Bradley and Metreweli 1991; Sistrom 1997).

Postoperative accumulation of fluid is treated by multiple puncture or, if necessary, with drainage.

Pathological processes of the bony skeleton are a domain of computer-assisted puncture, if the cortical bone is still intact. Frequently, diseases lead to defects in the cortical bone and may consequently be visualized well by sonography and also punctured (Fig. 10.13). Fine-needle aspiration puncture is usually sufficient for differentiation of inflammation/malignoma and carries a success rate of 88–100%. If plasmocytoma is suspected, puncture is always preferable to cut biopsy, because diagnosis is easier from a slide preparation. For typification of a malignoma, a cut biopsy might be preferred in some cases.

Before puncturing tumors of the upper thoracic aperture, the nerve cords (brachial plexus) and vessels (color-Doppler sonography) should be identified in order to avoid injury to these structures (Vogel 1993; Civardi et al. 1994; Blank 1995, 2007) (Fig. 10.14).

10.6.2 Pleural Cavity

10.6.2.1 Thoracocentesis

In cases of large quantities of effusion, sonography helps to establish the extent of the effusion and mark the site of puncture in the optimal intercostal space. The puncture is then performed on the ward (Reuß 1996). In cases of complex effusions (small, loculated, encapsulated, inconvenient location), the puncture is safer when performed under continuous sonographic visual control (Figs. 10.12 and 10.15). By doing so, the rate of pneumothorax is markedly reduced (less than 1%). The success rate is 97% (O'Moore et al. 1987; Wang and Doelken

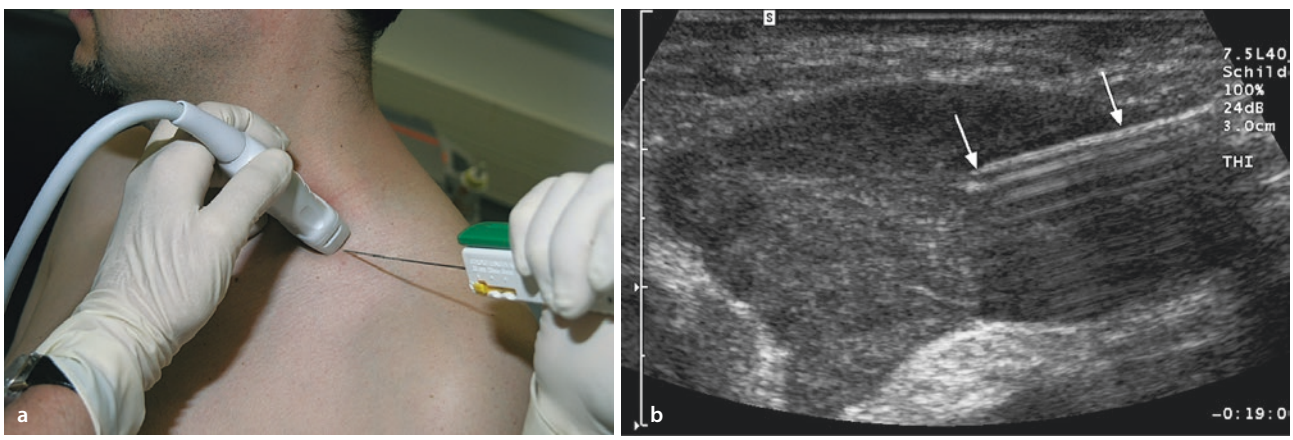

Fig. 10.12 **a** Classic puncture technique, upper thoracic aperture. **b** Classic puncture technique. Metastasis of the thoracic wall. The needle shaft (*arrows*) can be delineated very well at this favorable angle

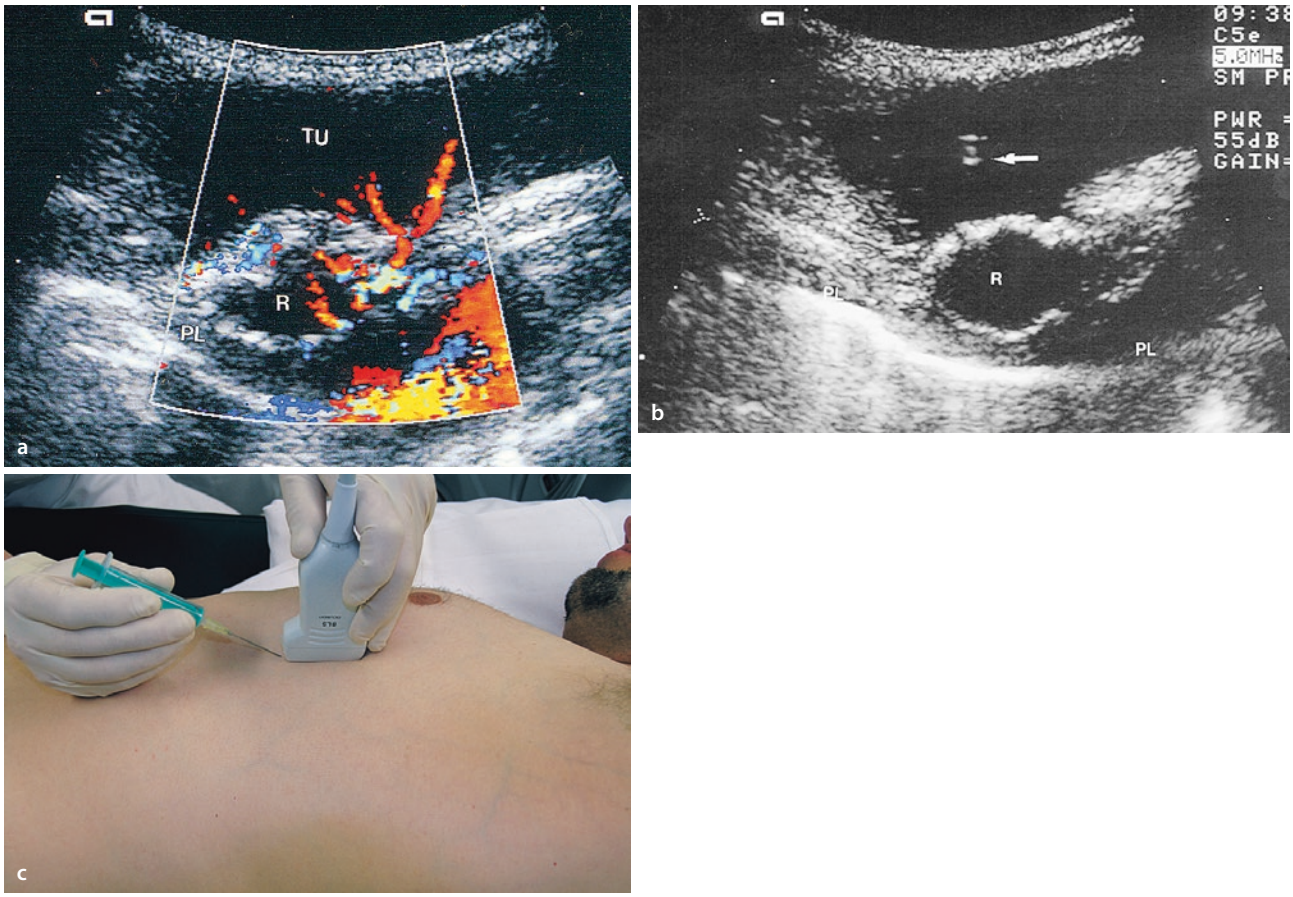

Fig. 10.13 **a** Destructed rib (*R*). Echo-free "soft tissue tumor" (*TU*). Color-Doppler sonography allows vessels to be depicted in the destructed rib and in the surrounding soft tissue tumor. *PL* pleura. **b** Fine-needle puncture of the soft-tissue tumor. The tip of the needle can be seen as an echogenous double reflex (*arrow*). Cytology indicated plasmocytoma. **c** Classic puncture technique

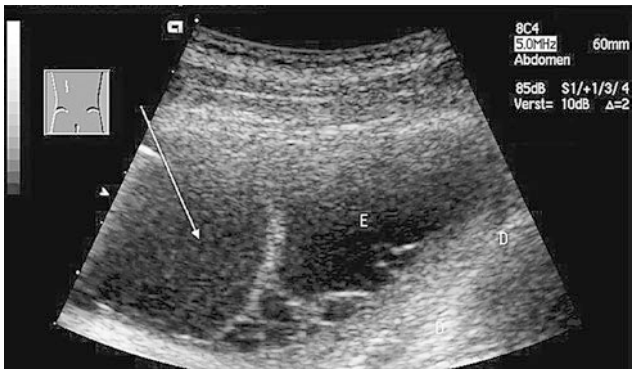

Fig. 10.14 Septated pleural effusion. Primary diagnostic puncture disclosing an encapsulated empyema (*arrow*). The secondary step involved pleura drainage. *D* diaphragm

2009). Unsuccessful punctures can be avoided when "the fluid color sign" is demonstrated (Wu et al. 1995; Fig. 10.15). Synthetic indwelling catheters should be given preference over metal ones because of the risk of injury to the lung from metal.

After application of local anesthesia, the synthetic tube is pushed forward at the upper margin of the rib (in order to avoid injury of the nerve-vessel bundles running along the lower edge of the ribs) upward to the pleura with a mandrin (Abbocath; Abbott, Abbott Park III). Entry into the pleura is marked by a mild increase in resistance. The mandrin is then removed. In a closed system, special pleural drainage sets can be used to perform manual aspiration.

Uncomplicated pleural effusions in the presence of cardiac failure, pneumonia and even small pneumothorax after puncture can be treated with thoracocentesis.

Malignant pleural effusions, accumulation of pus or blood should be treated with a drain because of the risk of septation (Müller and Blank 2011)

The success rate of cytology in malignant effusions is no more than 50–75% (Gartmann 1988). In tuberculous effusions, pathogens are demonstrated in only 20–40% of cases (Vladutiu 1986).

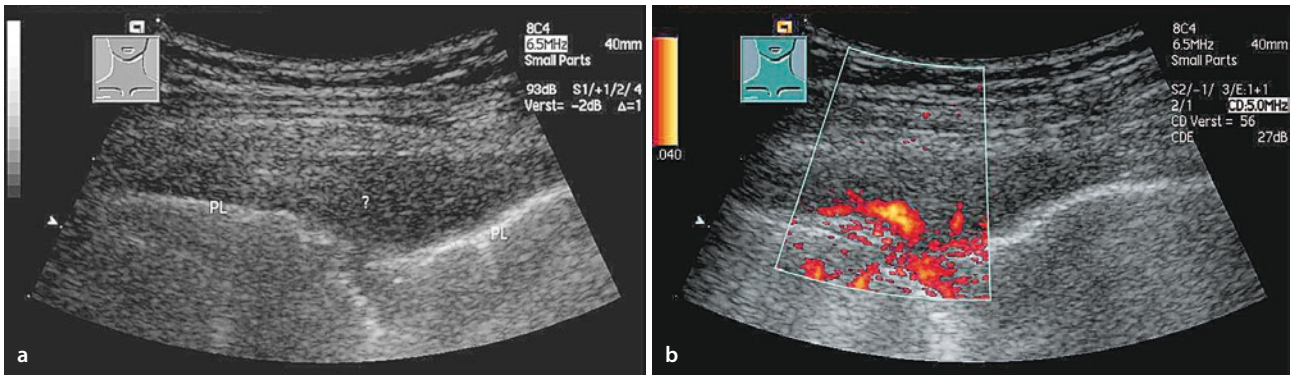

Fig. 10.15 **a** B-mode sonography for a differential diagnosis of an encapsulated effusion or fresh rind. *PL* visceral pleura. **b** Power Doppler demonstrates advanced vascularization with high-caliber vessels. Fresh pleural rind

10.6.2.2 Pleura Biopsy

Since even the classic pleural blind biopsy according to Abrams or Ramell has an accuracy of no more than 50% in malignant effusions, video-assisted thoracoscopy is being used more and more. Sonography-guided pleural biopsy is one alternative. The procedure has only been used in a very small number of cases so far, however (Mueller et al. 1988). As an alternative, automatic single-hand needles (BioPince needle, for instance) may be used successfully (sensitivity 70–80%, specificity 100%) (Chu et al. 1994; Heilo 1996). Fine-needle aspiration biopsy of tissue taken from a pleural thickening is of no value and is even hazardous (danger of bleeding). It may only be employed in the presence of focal lesions (Mathis et al. 1999).

10.6.2.3 Percutaneous Pleural Drainage

Given the appropriate indication, malignant, hemorrhagic and inflammatory pleural effusions may normally be treated with a sonography-guided pleural drain quickly, safely and successfully. Only rarely CT-guided puncture is necessary if the approach is difficult. Thin catheters (8–14 Fr, Pleurocat, for instance) are sufficient (Fysh et al. 2010; Davies et al. 2011. These thin catheters are tolerated better by most patients than thick catheters traditionally used in many hospitals. Their success rate is equivalent, and they carry a much lower complication rate. Puncture is usually performed with the trocar technique. The catheter should be placed in the lowest possible part of the pleural cavity.

Parapneumonic fluid collections should be drained soon in cases of septum formation and a pH level below 7.2. A drain should be left in place for 5–10 days, depending on the extent of inflammation (Kolditz and Höffken 2008).

In cases of malignant effusions, catheters with a narrow lumen (7–12 Fr, e.g., Pleurocat, Plastimed), will suffice. The puncture is usually performed using the trocar technique. The catheter is placed in the lowest part of the pleural cavity.

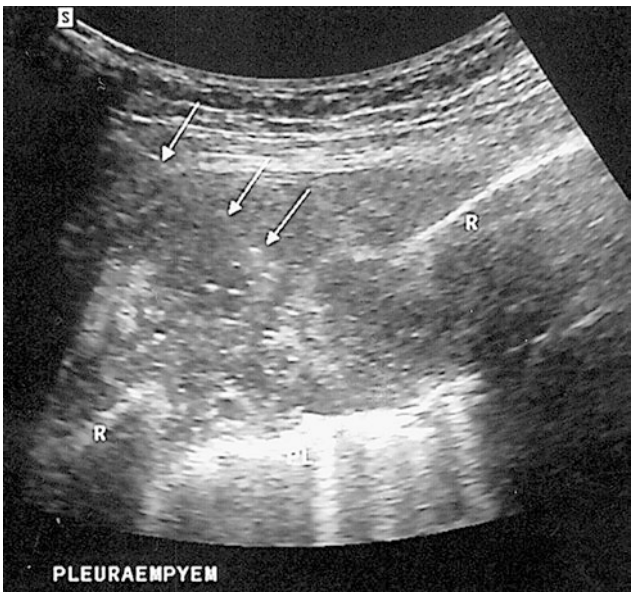

Fig. 10.16 An 80-year-old patient, whose temperature rose rapidly a few days after a fall which injured the left side of the thorax. X-ray image reveals a shadow located on the thoracic wall, suggestive of a fractured rib. Sonographic mass with infiltration into the thoracic wall. Minor liquid movements were perceptible during the dynamic examination. The diagnostic puncture was not successful until a coarse needle (with a diameter of 2 mm) was used. It proved possible to extract highly viscous pus. A pleural drainage was then inserted. *Arrows* needle shaft

Early diagnostic verification of a pleural empyema is important, as percutaneous therapy is only successful (success rate, 72–88%) in the acute phase (weeks 1–4) (Klose and Günther 1996; Müller and Blank 2011; Figs. 10.9, 10.16, and 10.19). The success of drainage in the presence of septation can be markedly improved by the instillation of urokinase (50–100,000 IU/treatment) (Sistrom 1997).

The correct positioning of the catheter can be checked by the injection of NaCl 0.9%, mixed with a drop of SonoVue® (ultrasound contrast agent) . This "off label" use has its advantages: it is possible to identify incorrect drainage and dislocations; septic developments and, as a result, insufficient drainage show up through the missing diffusion of the contrast medium in the pleural space (Heinzmann et al. 2012) (◘ Fig. 10.17). In the case of therapy resistant effusions the drainage with a tunneled catheter could be appropriate.

▪ Pleurodesis

Malignant effusions are prone to build septa under recurrent thoracocentesis. It is therefore wise to proceed a early drainage treatment. Possibly. After the complete and possibly fractional emptying of the effusion (portions not to exceed 1.5 L) and the administering of a topical anesthetic follows the instillation of sclerosing substances, 4–5 g Talc mixed with 50 ml NaCl seems to be the most efficient; Bleomycin is an alternative (Roberts et al. 2011). Pleurodesis obtained by thoracoscopy is all the more effective (Tan et al. 2006).

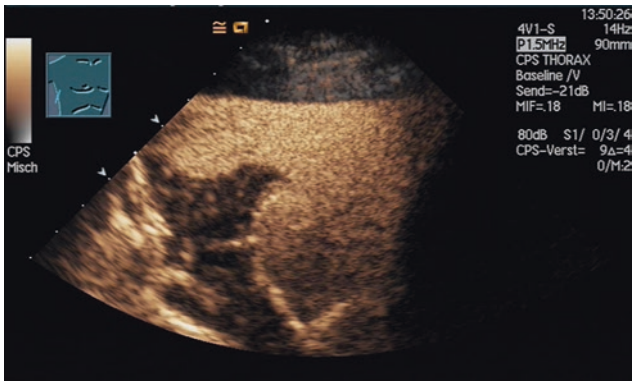

◘ **Fig. 10.17** The contrast medium spreads through the entire pleural space

10.6.3 Lung Consolidations

Peripheral pulmonary lesions may be visualized sonographically if they are situated in a favorable topographical position. They may be punctured if they reach the visceral pleura or if a poststenotic atelectasis or pneumonia provides an acoustic window.

At the time of diagnosis, two thirds of lung carcinomas are no longer curable by surgery. The histological type must be determined before palliative therapeutic measures are employed. In the diagnosis of the peripheral lung tumor, sonography-guided puncture is markedly superior to bronchoscopy, much easier and faster to perform than radiography or even computer-assisted percutaneous biopsy, and devoid of radiation (Chandresakar et al. 1976; Börner 1986; O'Moore et al. 1987; Hsu et al. 1996; Diacon et al. 2004a, b; ◘ Fig. 10.18).

Peripheral tumors larger than 3 cm in size should be diagnosed by fine-needle cut-biopsy (histology) (Mathis and Gehmacher 1999; Schubert et al. 2005). Peripheral tumors smaller than 3 cm in size can be better diagnosed by fine-needle aspiration cytology (Sistrom 1997). Biopsy is not always sufficient (accuracy 70%) to distinguish benign tumors. Wedge resections obtained by thoracoscopy are given preference in many cases (Beckh and Bölcskei 1997).

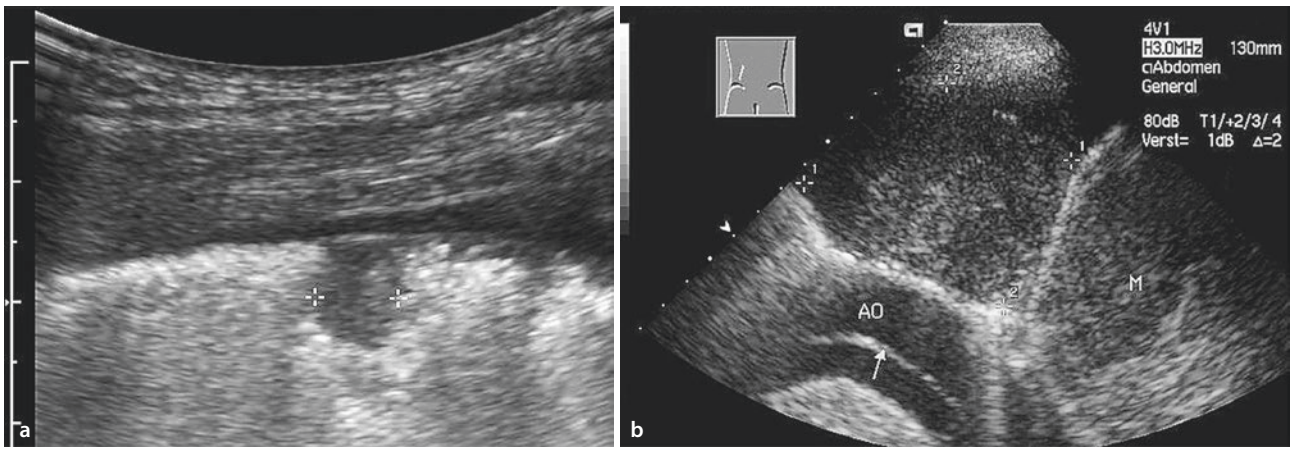

◘ **Fig. 10.18** **a** Several small peripheral lung tumors (maximum diameter 18 mm) located on the thoracic wall. Delicate pleural effusion. Fine-needle aspiration cytology indicated small-cell bronchial carcinoma. **b** Large mass, left dorsobasal location (*crosses*), alongside the diaphragm and also the descending aorta (*AO*). A dissecting aortic aneurysm had been identified in this patient 4 years earlier. *Arrow* dissection membrane.Fine-needle incision biopsy (Sonocan needle, 0.9 mm in diameter). Histology indicated squamous cell carcinoma

Special Puncture Technique

A safe pathway for puncture circumventing the ventilated lung is an important prerequisite of avoiding pneumothorax. Larger tumors may be punctured in the classical way. The needle is inserted at the level of the ultrasound probe. The needle tip is pushed toward the parietal pleura under continuous sonographic observation. While the patient holds his/her breath, the lesion is punctured in such a way that the needle does not reach the ventilated lung. To achieve this, the puncture depth is measured beforehand and marked on the needle in the case of using an automatic one-hand needle.

Small (less than 1-cm) tumors located in the periphery may also be punctured if expertise is sufficient. Puncture technique must be adjusted to the individual type of lesion. Similar to puncture of the thyroid, atypical puncture is often necessary (Blank 2007). The tip of the needle must be inserted through the skin almost vertically, near the middle of and parallel to the probe, which has as little contact with the skin as possible. By tilting the probe in a plane vertical to the plane of the probe, one can identify the needle tip inside the thoracic wall, push it toward the pleura and insert it into the lesion under observation. Visualization of the needle tip is facilitated by moving it back and forth abruptly.

Alternatively, small lesions may be punctured "from memory" after marking the intended site of puncture with a ballpoint pen, for instance (small ring pressed into the skin). The results are no worse in the hands of experienced examiners.

If a small perforated ultrasound probe is available, this may also be used for a successful puncture.

Pneumonia and Pulmonary Abscesses

The cause of consolidation of sections of the lung may be difficult to classify in immunosuppressed patients, especially. Aspiration puncture or cut biopsies of the areas with consecutive microbiological, cytological and histological examination of the material obtained allow a diagnosis in up to 93% of cases (Yang et al. 1985).

Even small pulmonary abscess that escape detection on the radiograph can be imaged by sonography (6–7 mm) (Kolditz and Höffken 2008). If antibiotic therapy does not yield the desired result (75-90% success rate), fluid may be aspirated from the region of the abscess under sonographic guidance. By this means, the pathogen can be isolated in about 65–93% of cases (Gehmacher et al. 1986; Yang et al. 1992). If therapy continues to fail, a lung abscess drainage may be performed under sonographic guidance but this is rarely necessary (Sonnenberg et al. 1991; Klein et al. 1995; ◘ Fig. 10.19). The risk of bronchopleural fistula formation is minimized when the investigator uses the shortest access and traverses solid, homogeneous, infiltrated or atelectatic tissue (Mathis and Gehmacher 1999; Wali et al. 2002).

10.6.4 Mediastinum

Few space-occupying masses in the mediastinum (retrosternal goiter, cyst, aneurysm, thrombosis) can be reliably classified on the basis of characteristic sonographic features. An investigation of fine tissue is needed in order to determine the cause of the lesion. Gentle removal of tissue without causing a large defect is very important in the diagnosis of space-occupying masses that can be removed by surgery. Therefore, puncture under image guidance should be the first procedure. When this is done, space-occupying masses in the mediastinum can be easily punctured from a suprasternal or parasternal approach under sonographic guidance (Nordenstrom 1967; Rubens et al. 1997; Koegelenbug et al. 2009). The accuracy is 54–100%, and the rate of complications is 0–4% (Dogan et al. 2019). Vessels should be avoided (Color-Doppler Sonography) (Blank et al. 1996; ◘ Figs. 10.20, 10.21, and 10.22). In cases of superficial lesions (thymomas, lymphomas), gross needles are given preference. With use of a needle with a thick lumen, correct histological classification is achieved in up to 93% of cases and the rate of complications is only slightly higher, at less than 1% (◘ Fig. 10.23). In our experience, a needle diameter of 1.2 mm (BioPince needle) is normally sufficient.

In contrast to radiographic or CT-guided puncture (10–44%), pneumothorax is rarely encountered (Yang et al. 1992; Heilo 1993, 1996; Schuler et al. 1995; Gupta et al. 1998; Koegelenberg et al. 2011; Marchevsky et al. 2011).

In recent years, endosonographic transesophageal-guided puncture has also been used successfully. It is a good complement to percutaneous puncture, as lesions in the anterior mediastinum are not easily accessed, in contrast to those in the posterior and lower mediastinum (Schlotterbeck et al. 1997; Pedersen et al. 1996; Hüner et al. 1998; Janssen et al. 1998, 2014).

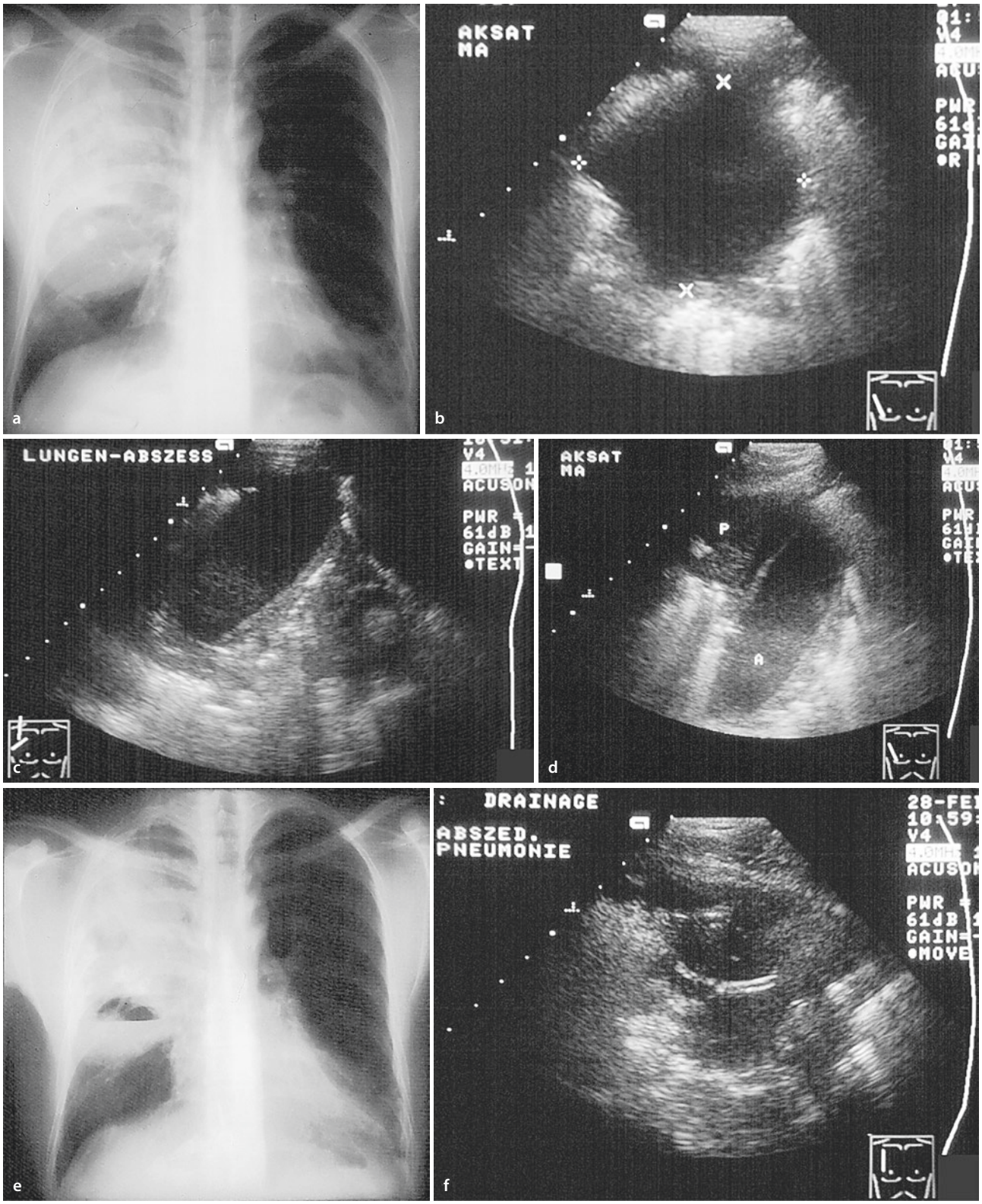

Fig. 10.19 Lung abscess with drainage. Young man with community-acquired pneumonia not responding to standard antibiotic therapy. Continuing high temperatures and respiratory deterioration. **a** On chest X-ray, extensive infiltration of the right upper lobe of the lung. **b** Sonography clearly demonstrates abscess formation. **c** Next to the abscess (*A*), pneumonic consolidation (*P*) is visible. If this does not contain air, puncture passing through this section would be feasible. The abscess is encapsulated by a membrane. **d** The shortest pathway for transthoracic puncture is chosen, and pus can be aspirated through the needle. **e** Abscess formation on chest X-ray. **f** The abscess is drained by a suction-rinse-drainage (echogenic double lumen) over 4 days. Quick recovery ensues

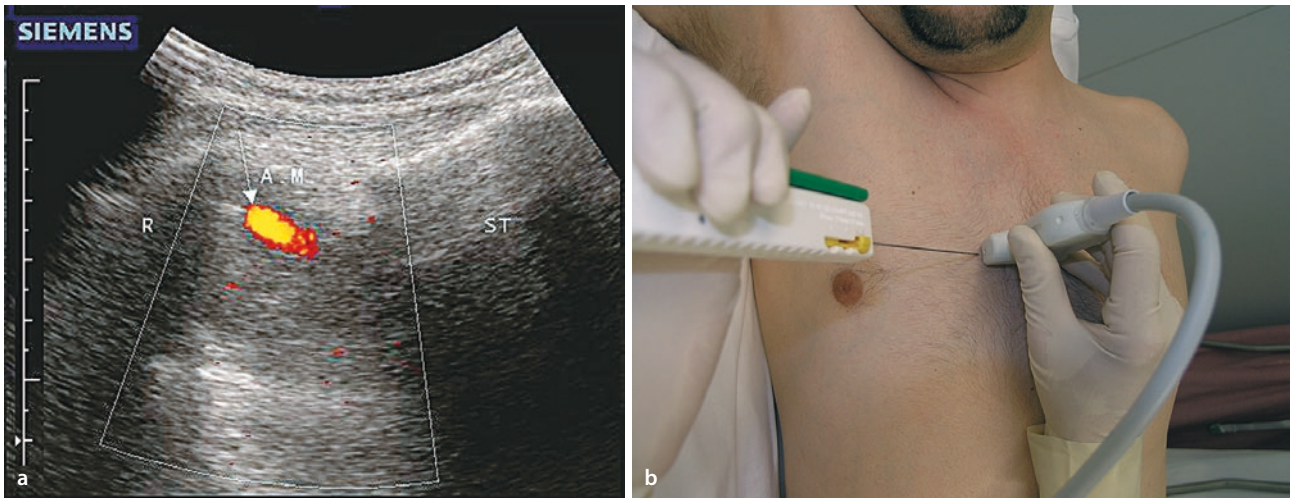

Fig. 10.20 **a** Mediastinal tumor. Parasternal plumb line in the right lateral position.Hypoechoic, indistinctly delineated mass (located in the color window). Color-Doppler sonography in "power" mode shows the mammary vessels located parasternally, **b** which have to be avoided during a punch biopsy

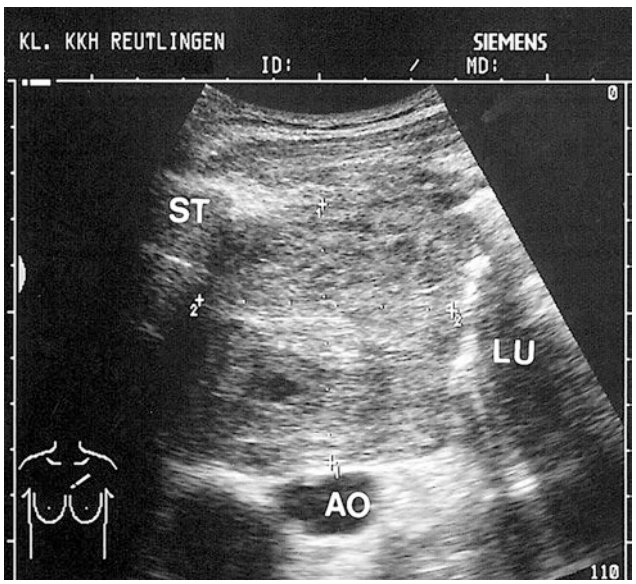

Fig. 10.21 A large mediastinal mass was discovered primarily by sonography, located parasternally on the left, in a 19-year-old patient during emergency treatment connected with a superior vena cava syndrome. A punch biopsy was performed immediately (Sonocan needle, 1.2-mm diameter). Histologically, a highly malignant non-Hodgkin lymphoma was diagnosed. *ST* sternum, *LU* lung, *AO* descending aorta

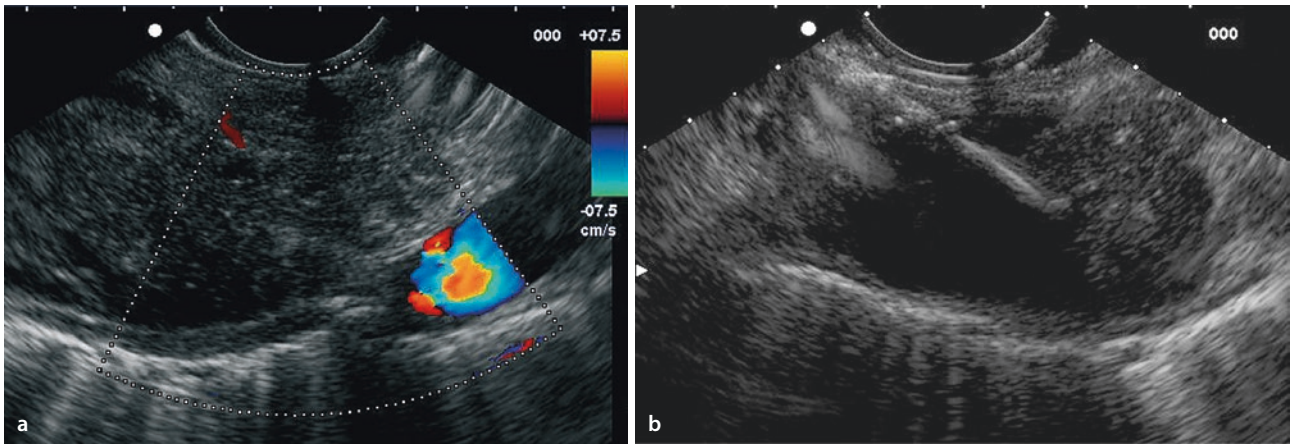

Fig. 10.22 Paravertebral abscess in a case of spondylodiscitis. At first, open surgical drainage of the spondylodiscitis was performed, followed by endosonographically guided nasal/transesophageal drainage used for rinsing with isotonic saline. **a** Space-occupying mass located next to the spine and the aorta. **b** Insertion of drain

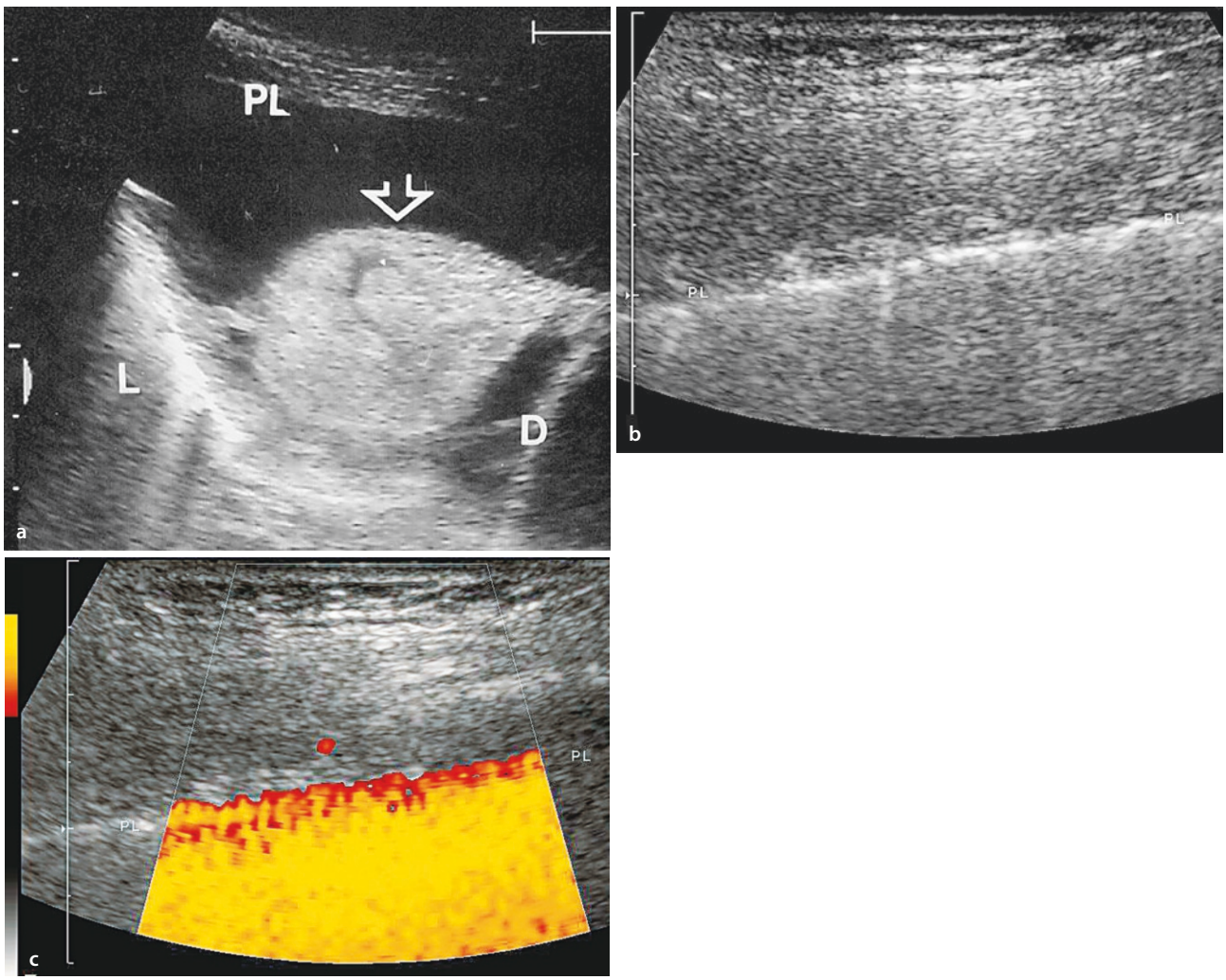

Fig. 10.23 **a** A blood clot (*arrow*) as a complication following a diagnostic puncture of a pleural effusion. *PL* parietal pleura, *L* compressed lung, *D* diaphragm. **b** Pneumothorax was excluded by showing the sliding sign of the pleura. **c** Color-Doppler sonography in "power" mode allowed the respiration-dependent sliding sign to be documented in an impressive way even in the static image. The repeat echoes that could be demonstrated with B-mode sonography (artifact) dorsal to the pulmonary surface show up accordingly as a color artifact. This cannot be demonstrated in cases of pneumothorax

10.7 Risks

Sonography-guided puncture has a low rate of complications. The rate of pneumothorax is 2–4.4%, only 1% require drainage. Hemorrhage or hemoptysis is observed in up to 2.8%. Data concerning air embolism or even death are not available so far (Mathis et al. 1999; Weiss and Düntsch 1996; Tombesi et al. 2009; Di Bardino et al. 2015). Tumor dissemination through the procedure of puncture (vaccine metastases) is of little clinical significance and very rare, in less than 0.003% of cases. In cases of malignant pleural mesothelioma, it is slightly more common. When surgery is performed, the site of puncture is also resected (Bydder et al. 2004).

10.7.1 Pneumothorax After Puncture

If the focus is no longer visible after the puncture, the likelihood of a pneumothorax is high. This can be reliably detected by sonography, through the absence of respiration-dependent gliding movement of the pleura sensitiver als in der Thoraxübersichtsaufnahme erkennbar (Sensitivität 90–100%; Abb. 10.24b, c; Blank 1994; Herth et al. 2004; Reissig and Kroegel 2005; Volpicelli et al. 2012; ◘ Fig. 10.23).

The quantity of free air can only be measured by obtaining a chest radiograph. A pneumothorax usually reaches its maximum dimensions after 3 h, so the decision regarding a therapeutic procedure is made thereafter, when the pneumothorax is small. If the patient is symptomatic or if a larger volume is present, the patient is initially given protracted thoracocentesis. The success rate within the first 10 h is 90% (Klose and Günther 1996). In the event of renewed collapse, the clinician should use a percutaneous drain and a catheter with a small lumen.

A routine chest radiograph is not required after sonography-guided puncture.

Summary

Provided the indication is established with care, interventional measures in the thorax are very successful. The rate of complications is low when the procedure is performed by trained therapists.

» **The basic principle to be applied is: "try ultrasound first" (Sistrom 1997).**

10.8 List of Materials

Sterican. Disposable injection cannula, size 1 (G 20/0.9 × 40/80 mm). B. Braun Melsungen AG, 34209 Melsungen, Germany

BioPince. Disposable full-cylinder biopsy pistol (G 18/1.2 × 100/150 mm). Inter. V, Gainesville, FL 32608 USA. Distributor Peter Pflugbeil GmbH, Georg-Wimmer-Ring 21, 85604 Zorneding, Germany, Fax: +44-8106-241333, email: info@pflugbeil.com, Internet: ► http://www.pflugbeil.com

Sonocan.Disposable set for sonography-guided full-cylinder biopsy by B. Braun Melsungen AG (G 20/0.9 × 100 mm/150 mm). Distributor Nicolai GmbH & Co. KG, Ostpassage 7, 30853 Langenhagen, Germany, Fax: +44-511-733235

Max Core Disposable biopsy pistol (G 20–16/0.9–1.2 × 100/160 mm). Bard

Magnum Core. Reusable biopsy pistol. Bard GmbH, Wachhausstrasse 6, 76227 Karlsruhe, Germany

Magnum disposable needles. (G 20–16/0.9–1.2 × 100/160 mm). Bard

Navarre universal drainage catheter with Nitinol (6–12 F × 30 cm). Bard

Universal adapter with Luer-Lock. Bard

Argyl trocar catheter (Charr 12–17/4–6 mm). Sherwood-Medical Company, Tullamore, Ireland

Argyl Sentinel Seal Thoracic drainage unit. Tyco Healthcare Company, Tullamore, Ireland

Acknowledgments I would like to express my thanks to Martin Lenz (former chief consultant surgeon in the Radiology Department of the Steinenberg Clinic, Reutlingen) for preparing and providing the radiological findings, and my son Valentin for the technical photographic work.

References

Adams RF, Gray W, Davies RJ, Gleeson FV (2001) Percutaneous image-guided cutting needle biopsy of the pleura in the diagnosis of malignant mesothelioma. Chest 120:1798–1802

Anzidei M, Porfiri A, Andrani F, Di Martino M, Saba L, Catalano C, Bezzi M (2017) Imaging-guided chest biopsies: techniques and clinical results. Insights Imaging 8:419–428

Beckh S, Bölcskei PL (1997) Biopsie thorakaler Raumforderungen—von der computertomographischen zur ultraschallgezielten Punktion. Ultraschall Med 18:220–225

Blank W (1994) Sonographisch gesteuerte Punktionen und Drainagen. In: Braun B, Günther R, Schwerk WB (eds) Ultraschalldiag-

nostik. Lehrbuch und Atlas, III-111th edn. ecomed, Landsberg/Lech, pp. 1–79
Blank W (1995) Weichteil- und Knochentumoren. In: Braun B, Günther R, Schwerk WB (eds) Ultraschalldiagnostik. Lehrbuch und Atlas, III-99th edn. ecomed, Landsberg/Lech, pp 1–27
Blank W (2006) Sonographisch gezielte Punktionen und Drainagen. In: Seitz K, Schuler A, Rettenmaier G (eds) Sonographische Diagnose und Differenzialdiagnose. Thieme, Stuttgart
Blank W (2007) Sonographisch gezielte Punktionen und Drainagen. In: Seitz K, Schuler A, Rettenmaier G (eds) Sonographische Diagnose und Differenzialdiagnose. Thieme, Stuttgart
Blank W (2019) Interventionelle Sonografie. In: Kursbuch Notfallsonografie (Hrsg) Blank, Mathis, Ostewalder). Thiemeverlag Stuttgart
Blank W, Schuler A, Wild K, Braun B (1996) Transthoracic sonography of the mediastinum. Eur J Ultrasound 3:179–190
Blank W, Mathis G, Osterwalder J (eds) (2014) Kursbuch Notfallsonographie. Georg Thieme Verlag
Börner N (1986) Sonographische Diagnostik pleuropulmonaler Erkrankungen. Med Klin 81:496–500
Bradley MJ, Metreweli C (1991) Ultrasound in the diagnosis of the juxta-pleural lesion. Br J Radiol 64:330–333
Braun B (1983) Abdominelle und thorakale Ultraschalldiagnostik. In: Bock HE, Gerok W, Hartmann F et al (eds) Klinik der Gegenwart. Urban & Schwarzenberg, Munich, pp 1141–1145
Bydder S, Phillips M, Joseph DJ, Cameron F, Spry NA, Demelker Y, Musk AW (2004) A randomised trial of single-dose radiotherapy to prevent procedure tract metastasis by malignant mesothelioma. Br J Cancer 91:9–10
Cao BS, Wu JH, Li XL, Deng J, Liao GQ (2011) Sonographically guided transthoracic biopsy of peripheral lung and mediastinal lesions: role of contrast-enhanced sonography. J Ultrasound Med 30:1479–1490
Chandresakar AJ, Reynes CJ, Churchill RJ (1976) Ultrasonically guided transthoracic percutaneous biopsy of peripheral pulmonary masses. Chest 70:627–630
Chang DB, Yang PC, Luh KT, Kuo SH, Yu CJ (1991) guided pleural biopsy with Tru-Cut needle. Chest 100:1328–1333
Chu CY, Hsu WH, Hsu JY, Huang CM, Shih CM, Chiang DC (1994) Ultrasound-guided biopsy of thoracic masses. Chung Hua I Hsueh Tsa Chih 54:336–342
Cinti D, Hawkins HB (1984) Aspiration biopsy of peripheral pulmonary masses using real-time sonographic guidance. Am J Roentgenol 142:1115–1116
Civardi G, Livraghi T, Colombo MD (1994) Lytic bone lesions suspected for metastasis: ultrasonically guided fine-needle aspiration biopsy. J Clin Ultrasound 22:307–311
Ckzerwenka W, Otto RC (1994) Die ultraschallgezielte Lungenpunktion. Bildgebung Imaging 61(S2):12
Dallari R, Gollini C, Barozzi G, Gilioli F (1999) Ultrasound-guided percutaneous needle aspiration biopsy of peripheral pulmonary lesions. Monaldi Arch Chest Dis 54:7–10
Davies HE, Davies RJO, Davies CWH (2011) Management of pleural infection in adults: British Thoracic Society pleural disease guideline. Thorax 65(Suppl. 2):41-ii53
Di Bardino DM, Yarmus LB, Semaan RW (2015) Transthoracic needle biopsy of the lung. J Thoracic Dis 7(S4):304–316
Diacon AH, Schurmanns MM, Theron J, Schubert PT, Wright CA, Bolliger CT (2004a) Safety and yield of ultrasound-assisted transthoracic biopsy performed by pulmonologists. Respiration 71(5):519–522
Diacon AH, Schurmanns MM, Theron J, Schubert PT, Wright CA, Bolliger CT (2004b) Safety and yield of ultrasound-assisted transthoracic biopsy performed by pulmonologists. Respiration; Internat Rev Thorac Dis 71(5):519–522
Diacon AH, Theron J, Schubert P, Bolliger CT (2007) Ultrasound-assisted transthoracic biopsy: fine-needle aspiration or cutting-needle biopsy? Eur Respir J 29:357–362
Dietrich CF, Nürnberg D (2011) Interventioneller Ultraschall. Lehrbuch und Atlas für die interventionlle Sonographie. Thieme Verlag
Ding W, Shen Y, Yang J, He X, Zhang M (2011) Diagnosis of pneumothorax by radiography and ultrasonography: a meta-analysis. Chest 140:859–866
Dogan C, Cömert S, Salepci B, Kiral N, Parmaksiz E, Caglayan B (2019) Efficient and safe method in the diagnosis of thoracic lesions: Ultrasound-guided needle aspiration biopsy. Eurasian J Pulmonol 21(3)
Ernst A, Eberhardt R, Wahidi M, Becker HD, Herth FJ (2006) Effect of routine clopidogrel use on bleeding complications after transbronchial biopsy in humans. Chest 129:734–737
Fysh ET, Smith NA, Lee YC (2010) Optimal chest drain size: the rise of the small-bore pleural catheter. Semin Respir Crit Care Med 2(31):760–768
Gartmann JC (1988) Der unklare Pleuraerguß: Praktisch-diagnostisches Vorgehen. Ther Umsch 45:308–313
Gehmacher O, Mathis G, Kopf A, Scheier M (1986) Ultrasound imaging of pneumonia. Ultrasound Med Biol 21:1119–1122
Gleeson F, Lomas DJ, Flower CDR, Stewart S (1990) Powered cutting needle biopsy of the pleura and chest wall. Clin Radiol 41:199–200
Görg C, Seifart U, Görg K, Zugmaier G (2003) Color Doppler sonographic mapping of pulmonary lesions. J Ultrasound Med 22:1033–1039
Görg C, Bert T, Kring R (2006) Contrast enhancd Sonography of the lung for differential diagnosis of atelektasis. JUM 25:35–39
Gupta S, Gulati M, Rajwanski A, Gupta P, Suri S (1998) Sonographically guided fine-needle aspiration biopsy of superior mediastinal lesions by the suprasternal route. Am J Roentgenol 171: 1303–1306
Heckemann R, Hohner S, Heutz J, Nakhosten J (1988) Ultraschallgeführte Feinnadelpunktion solider pulmonaler und pleuraler Tumoren. Ultraschall Klin Prax S 1:83
Heilo A (1993) Tumors in the mediastinum: US-guided histologic core-needle biopsy. Radiology 189:143–146
Heilo A (1996) US-guided transthoracic biopsy. Eur J Ultrasound 3:141–153
Heinzmann A, Müller T, Leitlein J, Braun B, Kubicka S, Blank W (2012) Endocavitary contrast enhanced ultrasound (CEUS)—work in progress. Ultraschall Med 33:76–84
Herth FJ, Eberhardt R, Becker HD, Ernst A (2004) Diagnosis of pneumothorax (PTX) by means of transthoracic ultrasound—a prospective trial. Chest 126(49):892
Hoosein MM, Barnes D, Khan AN, Peake MD, Bennett J, Purnell D, Free C, Entwisle JJ (2011) The importance of ultrasound in

staging and gaining a pathological diagnosis in patients with lung cancer—a two year single centre experience. Thorax 66:414–417
Hsu WH, Chiang DC, Hsu JY, Kwan PC, Chen CL, Chen DY (1996) Ultrasound guided fine-needle aspiration biopsy of lung cancers. J Clin Ultrasound 24:225–233
Hüner M, Ghadim BM, Haensch W, Schlag DM (1998) Transesophageal biopsy of mediastinal and pulmonary tumors by means of endoscopic ultrasound guidance. J Thorac Cardiovasc Surg 116:554–559
Ikezoe J, Sone S, Higashihara T, Morimoto S, Arisawa J, Kuriiyama K (1984) Sonographically guided needle biopsy for diagnosis of thoracic lesions. Am J Roentgenol 143:229–243
Ikezoe J, Morimoto S, Arisawa J, Takasgima S, Kozuka T, Nakahara K (1990) Percutaneous biopsy of thoracic lesions: value of sonography for needle guidance. Am J Roentgenol 154:1181–1185
Izumi S, Tamaki S, Natori H, Kira S (1982) Ultrasonically guided aspiration needle biopsy in diseases of the chest. Am Rev Respir Dis 125:460–464
Jamarkani M, Duguay S, Rust K, Conner (2016) Ultrasound Versus Computes Tomographic Guidance for PercutaneousBiopsy of Chest Lesions. J Ultrasound Med; 25:1865-1872
Janssen J, Johann W, Luis W, Greiner L (1998) Zum klinischen Stellenwert der endosonographisch gesteuerten transoesophagealen Feinnadelpunktion von Mediastinalprozessen. Dtsch Med Wochenschr 123:1402–1409
Jennsen C, Gotschalk U, Schachschal G, Dietrich CF (2014) Kursbuch Endosonographie. Thieme Verlag
Jeon KN, Bae K, Park MJ, Choi HC, Shin HS, Shin S, Kim HC, Ha CY (2014) US-guided transthoracic biopsy of peripheral lung lesions: pleural contact length influences diagnostic yield. Acta Radiol 55:295–301
Kelbel C, Stephany P, Lorenz J (1996) Endoluminal chest sonography. Eur J Ultrasound 3:191–195
Klein JS, Schultz S, Heffner JE (1995) Interventional radiology of the chest: image-guided percutaneous drainage of pleural effusions, lung abscess, and pneumothorax. Am J Roentgenol 164:581–588
Klose KC, Günther RW (1996) CT-gesteuerte Punktionen. In: Günther RW, Thelen M (eds) Interventionelle radiologie. Thieme, Stuttgart, pp 750–775
Knudsen DU, Nielsen SM, Hariri J, Christersen J, Kristersen S (1996) Ultrasonographically guided fine-needle aspiration biopsy of intrathoracic tumors. Acta Radiol 37:327–331
Koegelenberg CF, Diacon AH (2013) Image-guided pleural biopsy. Curr Opin Pulm Med 19:368–363
Koegelenberg CF, Diacon AH, Irusen EM, von Groote-Bidlingmaier F, Mowlana A, Wright CA, Louw M, Schubert PT, Bolliger CT (2011) The diagnostic yield and safety of ultrasound-assisted transthoracic biopsy of mediastinal masses. Respiration 81: 134–141
Koegelenbug CF, Bolliger CT, Diacon AH (2009) Diagnostic yield and safety of ultrasound-assisted biopsies in superior vena cavo syndrome. Eur Respir J 33:1389–1395
Koenig SJ, Narasimhan M, Mayo PH (2011) Thoracic ultrasonography for the pulmonary specialist. Chest 140:1332–1341
Kolditz M, Höffken G (2008) Management des parapneumonischen Ergusses und ds Pleuraempyems. Pneumologe 5(219):228
Laursen CB, Naur TM, Bodtger U, Colella S et al (2016) Ultrasound-guided lung biopsy in the hand of respiratory physicians: Diagnostic yield and complications in 215 consecutive patients in 3 centers. J Bronchology Interv Pulmonol 23:220–228
Lee MH, Lubner MG, Hinshaw JL, Pickhardt PJ (2018) Ultrasound guidance versus CT guidance for peripheral lung biopsy: performance according to lesion size an pleural contact. AJR 210(3):W110–W117
Liao WY, Chen MZ, Chang YL, Wu HD, Yu CJ, Kuo PH, Yang PC (2000) US guided transthoracic cutting biopsy for peripheral thoracic lesions less than 3 cm in diameter. Radiology 217:685–691
MacDuff A, Arnold A, Harvey J (2010) Management of spontaneous pneumothorax: British Thoracic Society Pleural Disease Guideline. Thorax 65(Suppl. 2):ii18-31
Marchevsky AM, Marx A, Ströbel P, Suster S, Venuta F, Yousem S, Zakowski M (2011) Policies and reporting guidelines for small biopsy specimens of mediastinal masses. J Thorac Oncol 6:S1724–S1729
Mathis G (1997a) Thoraxsonography—Part I: Chest wall and pleura. Ultrasound Med Biol 23(8):1131–1139
Mathis G (1997b) Thoraxsonography—Part II: Peripheral pulmonary consolidation. Ultrasound Med Biol 23(8):1141–1153
Mathis G, Gehmacher O (1999) Ultrasound-guided diagnostic and therapeutic interventions in peripheral pulmonary masses. Wien Klin Wochenschr 111:230–235
Mathis G, Bitschnau R, Gehmacher O, Dirschmid K (1999) Ultraschallgeführte transthorakale Punktion. Ultraschall Med 20: 226–235
Metz V, Dock W, Zyhlarz R, Eibenberger K, Farres MT, Grabenwöger F (1993) Ultraschallgezielte Nadelbiopsien thorakaler Raumforderungen. RoFo 159:60–63
Mikloweit P, Zachgo W, Lörcher U, Meier-Sydow J (1991) Pleuranahe Lungenprozesse: Diagnostische Wertigkeit Sonographie versus Computertomographie (CT). Bildgebung 58:127–131
Mohr A, Jung EM et al (2014) Neuese und günstiges Trainingsmodellzur ultraschallgesteuerten Anlage von Drainagen. Z Gastroenterol 52(11):1257–1262
Mueller PR, Sanjay S, Simeone JF et al (1988) Image-guided pleural biopsies: indications, technique and results in 23 patients. Radiology 169:1–4
Müller T, Blank W (2011) Sonographisch gesteuerte Punktionen und Therapieverfahren. In: Braun B, Günther R, Schwerk WB (Hrsg.) Ultraschalldiagnostik. Lehrbuch und Atlas. ecomed, Landsberg/Lech ; III-11.1: pp. 1–79
Müller T et al (2018) DEGUM-Empfehlungn zur Hygiene in Sonografie und Endosonografie. Ultraschall in Med 39:01
Nordenstrom B (1967) Paraxiphoid approach to mediastinum for mediastinography and mediastinal needle biopsy: a preliminary report. Invest Radiol 2:141–146
O'Moore PV, Mueller PR, Simeone JF, Saini S, Butch RJ, Hahn PF (1987) Sonographic guidance in diagnostic and therapeutic interventions in the pleural space. Am J Roentgenol 149:1–5
Pang JA, Tsang MB, Hom L, Metreweli C (1987) Ultrasound guided tissue-core biopsy of thoracic lesions with Trucut and Surecut needles. Chest 91:823–828
Patel IJ, Davidson JC, Nikolic B, Salazar GM, Schwartzberg MS, Walker G, Saad WA (2012) Consensus guidelines for periprocedural management of coagulation status and hemostasis risk in percutaneous image-guided interventions. J Vasc Interv Radiol 23:727–736
Patel IJ, Davidson JC, Nikolic B, Salazar GM, Schwartzberg MS, Walker G, Saad WA (2013) Addendum of newer anticoagulants to the SIR Consensus Guideline. J Vasc Interv Radiol 24:641–645
Pedersen OM, Aasen TB, Gulsvik A (1986) Fine needle aspiration biopsy of mediastinal and peripheral pulmonary masses guided by real time sonography. Chest 89:504–508
Pedersen BH, Vilmann P, Folke K, Jacobsen GK, Krasnik M, Milman N, Hancke S (1996) Endoscopic ultrasonography and real-time guided fine-needle aspiration biopsy of solid lesions of the mediastinum suspected of malignancy. Chest 110:539–544
Reissig A, Kroegel C (2005) Accuracy of transthoracic sonography in excluding post-interventional pneumothorax and hydro-

pneumothorax. Comparison to chest radiography. Eur J Radiol 53(3):463–470
Reuß J (1996) Sonographic imaging of the pleura: nearly 30 years experience. Eur J Ultrasound 3:125–139
RKI (2011) Anforderungen an die Hygiene bei Punktionen und Injektionen. Bundesgesundheitsbl 54:1135–1144
Roberts ME, Neville E, Berrisford RG, Antunes G, Ali NJ (2011) Management of a malignant pleural effusion: British Thoracic Society pleural disease guideline 2010. Thorax 65(Suppl 2): ii32-ii40
Rubens DJ, Strang JG, Fultz PJ, Gottleib RH (1997) Sonographic guidance of mediastinal biopsy: an effective alternative to CT guidance. AJR 169:1605–1610
Schlotterbeck K, Schmid J, Klein F, Alber G (1997) Transesophageal sonography in the staging of lung cancer. Ultraschall Med 18:153–158
Schubert P, Wright CA, Louw M, Brundyn K, Theron J, Bolliger CT, Diacon AH (2005) Ultrasound assisted transthoracic biopsy: cells or sections? Diagn Cytopathol 33(49):233–237
Schuler A, Blank W, Braun B (1995) Sonographisch-interventionelle Diagnostik bei Thymomen. Ultraschall Med 16:62
Schulz G (1992) Interventionelle Thoraxsonographie bei brustwandnahen soliden Raumforderungen. Ultraschall Klin Prax 7:202
Schwerk WB, Görg C (2007) Pleura und Lunge. In: Braun B, Günther R, Schwerk WB (eds) Ultraschalldiagnostik. Lehrbuch und Atlas, III-22nd edn.ecomed, Landsberg/Lech, pp. 1–44
Schwerk WB, Dombrowski H, Kalbfleisch H (1982) Ultraschalltomographie und gezielte Feinnadelbiopsie intrathorakaler Raumforderungen. Ultraschall Med 3:212–218
Sconfienza LM, Mauri G, Grossi F, Truini M, Serafini G, Sardanelli F, Murolo C (2013) Pleural and peripheral lung lesions: comparison of US- and CT-guided biopsy. Radiology 266:930–935
Sistrom CI (1997) Thoracic sonography for diagnosis and intervention. Curr Probl Diagn Radiol 26(1):5–49
Sonnenberg E, Agostino H, Casola G, Wittich GR, Varney RR, Harker C (1991) Lung abscess: CT-guided drainage. Radiology 178:347–351
Sonnenberg E, Wittich GR, Goodacre BW, Zwischenberger JB (1998) Percutaneous drainage of thoracic collections. J Thorac Imaging 13:74–82
Tan C, Sedrakyan A, Browne J, Swift S, Treasure T (2006) The evidence on the effectiveness of management for malignant pleural effusion: a systematic review. Eur J Cardiothorac Surg 29:829–838
Targhetta R, Bourgeois JM, Chavagneux R, Balmes P (1992) Diagnosis of pneumothorax by ultrasound immediately after ultrasonically guided aspiration biopsy. Chest 101:855–856
Tikkakoski T, Lohela P, Taavitsainen M et al (1993) Transthoracic lesions: diagnosis by ultrasound-guided biopsy. RoFo 159:444–449
Tombesi P, Nielsen I, Tassinari D (2008) Transthoracic ultrasonography-guided core needle biopsy of pleural-based lung lesions: prospective randomized comparison between a Tru-cut-type needle and a modified Menghini-type needle. Ultraschall Med. https://doi.org/10.1055/s-0028-1109442
Tombesi P, Nielsen I, Tassinari D (2009) Transthoracic ultrasonography-guided core needle biopsy of pleural-based lung lesions: prospective randomized comparison between a Tru-cut-type needle and a modified Menghini-type needle. Ultraschall Med 30:390–3955
Vladutiu AO (1986) Pleural effusion. Futura Publishing, Mount Kisco
Vogel B (1993) Ultrasonographic detection and guided biopsy of thoracic osteolysis. Chest 104:1003–1005
Vogel B (1995) Ultraschallgezielte perthorakale Punktion. Prax Klein Pneumol 39:632–635
Volpicelli G, Elbarbary M, Blaivas M, Lichtenstein DA, Mathis G, Kirkpatrick AW, Melniker L, Gargani L, Noble VE, Via G, Dean A, Tsung JW, Soldati G, Copetti R, Bouhemad B, Reissig A, Agricola E, Rouby JJ, Arbelot C, Liteplo A, Sargsyan A, Silva F, Hoppmann R, Breitkreutz R, Seibel A, Neri L, Storti E, Petrovic T (2012) International evidence-based recommendations for point-of-care lung ultrasound. Intensive Care Med 38:577–591
Wali SO, Shugaeri A, Samman YS, Abdelaziz M (2002) Percutaneous drainage of pyogenic lung abscess. Scand J Infect Dis 34:673–679
Wang JS, Doelken P (2009) Ultrasound-guided drainage procedures and biopsies. In: Bolliger CT, Herth FJF, Mayo PH, Miyazawa T, Beamis JF (eds) Clinical chest ultrasound. From the ICU to the bronchoscopy suite (progress in respiratory research), 37th edn. Karger-Verlag, Newyork
Wang HC, Yu DJ, Yang PC (1995) Transthoracic needle biopsy of thoracic tumor by Color Doppler ultrasound puncture guided device. Thorax 50:1258–1263
Weiss H, Düntsch U (1996) Komplikationen der Feinnadelbiopsie—DEGUM-Umfrage II. Ultraschall Med 17:118–130
Weiss H, Weiss A (1994) Therapeutische interventionelle Sonographie. Ultraschall Med 15:152–158
Westcott JL (1980) Direct percutaneous needle aspiration of localized pulmonary lesions: result in 422 patients. Radiology 137:31–35
Wu RG, Yang PC, Kuo SH, Luh KT (1995) "Fluid color" sign: a useful indicator for discrimination between pleural thickening and pleural effusion. J Ultrasound Med 14:767–769
Yang PC (1996) Color Doppler ultrasound of pulmonary consolidation. Eur J Ultrasound 3:169–178
Yang PC, Luh KT, Sheu JC, Kuo SH, Sang SP (1985) Peripheral pulmonary lesions: ultrasonography and ultrasonically guided aspiration biopsy. Radiology 155:451–456
Yang PC, Chang DB, Yu CJ, Lee YC, Kuo SH, Luh KT (1992) Ultrasound-guided core biopsy of thoracic tumors. Am Rev Respir Dis 146:763–767
Yang MA, Park MH, Shin BS, Ohm JY (2012) Ultrasonography-guided transthoracic cutting biopsy of pulmonary lesion: diagnostic benefits and safety. J Korean Soc Ultrasound Med 31:119–124
Yin XJ (1989) Ultrasound-guided percutaneous needle biopsy in diseases of the chest. Chung Hua Wai Ko Tsa Chih 27:107–108
Yuan A, Yang PC, Chang DB, Yu CJ, Lee YC, Kuo SH, Luh KT (1992) Ultrasound-guided aspiration biopsy of small peripheral pulmonary nodules. Chest 101:926–930
Zimmermann C, Werle A, Schuler A, Reuss J, Gemacher O, Blank W (2003) Echosignalverstärker in der sonographischen Diagnostik des Thorax. Ultraschall Med 24:31

From the Symptom to the Diagnosis

Sonja Beckh

Contents

G. Mathis (ed.), *Chest Sonography*, https://doi.org/10.1007/978-3-031-09442-2_11

Technical advancements in sonography devices, which have led to the production of mobile and even portable units, have allowed rapid use of sonography at the bedside for a large number of indications (Sartori et al. 2007; Volpicelli and Fracisco 2008; Copetti and Cattarossi 2008; Lichtenstein and Mezière 2008; Reißig et al. 2009; Moore and Copel 2011; Arntfield and Millington 2012; Gardelli et al. 2012; Hyacinthe et al. 2012; Kreuter et al. 2012; Reißig and Görg 2012; Volpicelli 2013, Al Deeb et al. 2014). The transducer virtually serves as a technical extension of the palpating hand or the stethoscope. In the presence of chest diseases the cardinal symptoms are chest pain, fever and dyspnea. These symptoms may occur either separately or in combination, and thus allow the diagnostician to orient himself/herself to the situation (◘ Fig. 11.1). The extent and the intensity of the individual symptoms are mainly determined by the severity of the respective disease. The great diversity of symptoms in pulmonary embolism (Goldhaber 1998) may render the diagnosis of this condition extremely difficult (▶ Sect. 5.3).

11.1 Chest Pain

Chest pain is a common symptom in the emergency setting as well as the outpatient setting. It is always necessary to identify the cause, and particularly the five life-threatening diseases, namely, myocardial infarction, acute dissection of the aorta, pulmonary embolism, tension pneumothorax and rupture of the esophagus (Kurz et al. 2005; Kontos et al. 2010; Arntfield and Millington 2012).

The character of pain and the findings of clinical and sonographic investigation provide information about differential diagnosis in the presence of various diseases (◘ Table 11.1).

The fibers responsible for the perception of pain are located in the parietal pleura, in the aorta with its branches (◘ Fig. 11.2), in the soft tissues, and the bony structures of the chest wall. The lung and the visceral pleura, on the other hand, are insensitive to stimuli that trigger pain. Pain that accompanies an inflammation in the medial portion of the diaphragm is projected into

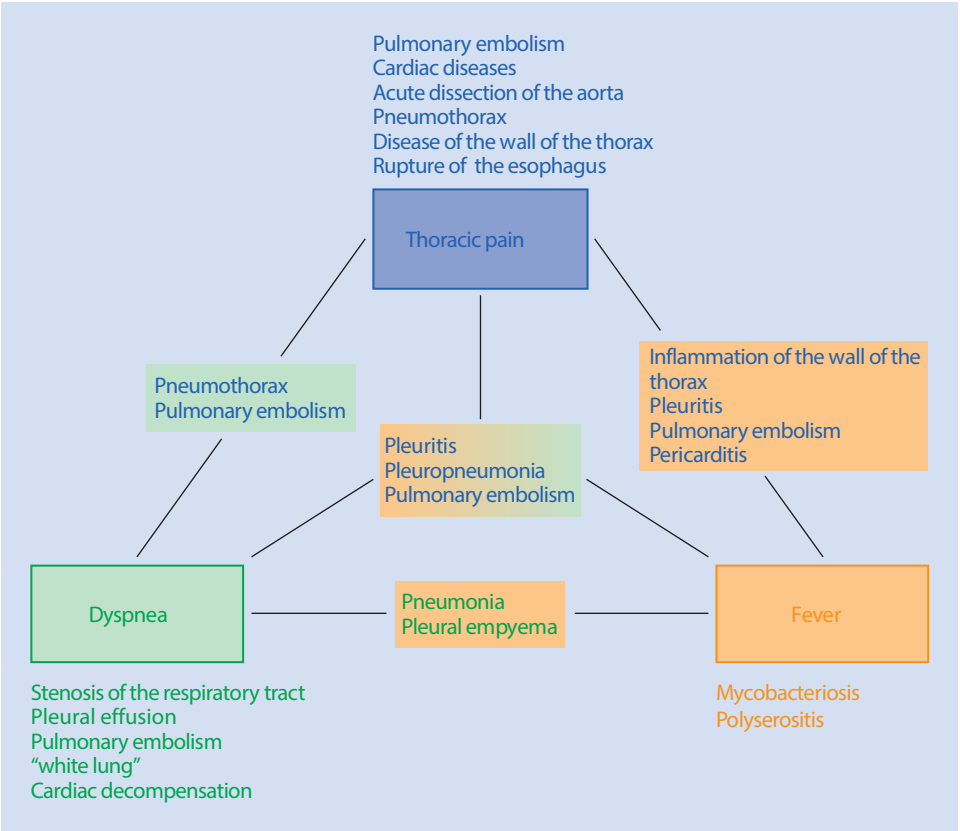

◘ **Fig. 11.1** Symptoms in diseases of the chest

Table 11.1 Findings in the presence of diseases accompanied by chest pain

Diagnosis	Characteristic of pain	Findings obtained from investigation	Sonographic findings
Tension pneumothorax	Sudden onset, sharp	Vesiculotympanitic resonance, no respiratory sounds, dyspnea, possibly symptoms of shock	Absent: sliding sign vertical artifacts lung pulse Present: repetitive echos Possibly lung point
Pulmonary embolism	Increased during inspiration	Pleural rales, dyspnea or fever may be present	Usually hypoechoic lesions in subpleural location; a small pleural effusion may be present
Acute dissection of the aorta	Strong pain, either in substernal location or between the shoulder blades, may radiate into the neck	Breath sounds are normal, diastolic murmur above the aortic valve may be present, symptoms of shock	Dissection of the aortic wall, dilated aorta
Myocardial infarction	Retrosternal, persistent, independent of breathing	Symptoms of shock may be present	Chest sonography is normal, diagnosis by ECG, laboratory findings, possibly echocardiography
Rupture of the esophagus	Retrosternal	Mediastinal emphysema	Not informative, diagnosis by X-ray
Chest wall processes	Local	Pain is increased on palpation or movement, fever in case of inflammation	Fracture: step formation and hematoma
			Abscess: hypoechoic, internal echoes
			Malignancy: destruction and infiltration
Pleuritis	Increased during inspiration	Pleural rales, fever; dyspnea may be present	Fragmentation of the pleural line, subpleural infiltrates, possibly pleural effusion
Pleuropneumonia	Increased during inspiration	Pleural rales, bronchial respiration, rales, fever, cough, dyspnea	"Hepatization" of lung tissue, aerobronchogram, hypervascularization, pleural effusion may be present
Pericarditis	Increased during inspiration and in relation to position	Pericardial rales, fever	A small pericardial effusion may be present; diagnosed by ECG

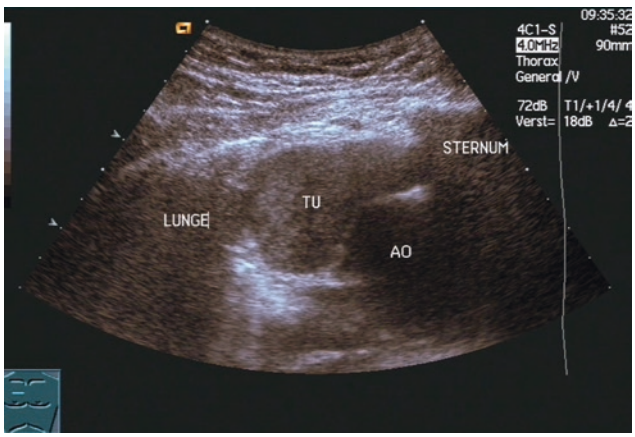

Fig. 11.2 A 56-year-old woman with retrosternal pain caused by a thymoma (*TU*) broad adjacent to the aortic wall. Diagnosis was established with sonographic biopsy and confirmed by operation

the ipsilateral shoulder and neck region (Murray and Gebhart 2005).

The ultrasound transducer is specifically targeted to the site of maximum pain, the site indicated by palpation or the physical investigation. In a physician's office, in the emergency setting (Volpicelli and Frascisco 2008; Moore and Copel 2011; Gardelli et al. 2012; Hyacinthe et al. 2012; Kreuter et al. 2012; Volpicelli 2013) or at the bedside, sonography contributes to the establishment of the diagnosis, may even provide an unequivocal diagnosis or may lead to further meaningful imaging procedures. Sonography is particularly useful to diagnose diseases of the chest in children (Kim et al. 2000).

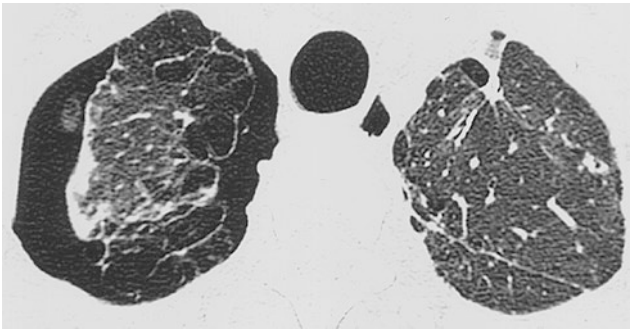

Fig. 11.3 Patient with a spontaneous pneumothorax. On high-resolution computed tomography one finds an extensive emphysematous bulla in the right upper lobe

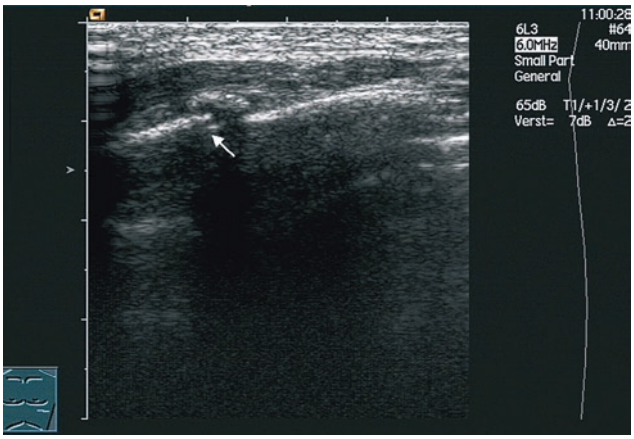

Fig. 11.4 Callus formation (the *arrow* is pointing to the fracture site) 2 weeks after a traumatic rib fracture

11.1.1 Chest Pain as a Symptom of Life-Threatening Diseases

11.1.1.1 Tension Pneumothorax

Sudden onset of pain is the main characteristic of a tension pneumothorax. Depending on the magnitude of the pneumothorax, it may be accompanied by mild or excessive dyspnea. Within a very short period of time, the patient develops symptoms of shock owing to the pressure of mediastinal organs and vessels.

Sonography reveals repetitive echoes on the affected side and the absence of a gliding echogenic pleural reflex (▶ Chap. 3). An overview radiograph is (◘ Fig. 11.19) needed to determine the depth of the pneumothorax space. High-resolution computed tomography reveals the extent and size of the emphysematous bulla (◘ Fig. 11.3).

11.1.1.2 Pulmonary Embolism

A pulmonary embolism (▶ Sect. 5.3) is accompanied by pain on breathing when the parietal pleura is also inflamed. When the Doppler sonography investigation is extended to the leg veins in order to look for the site of thrombosis and when echocardiography is additionally performed in the case of circulatory symptoms to evaluate the right heart load, the diagnosis can be made efficiently within a short period of time (Squizzato et al. 2013; Mathis 2014).

11.1.2 Acute Dissection of the Aorta

Tis condition is typically accompanied by severe pain, frequently in dorsal location; maximum pain occurs between the shoulder blades. The pain may resolve for a short period of time but may also extend in the direction of dissection of vessels, for instance, in the neck when the carotid arteries are involved. Insonation from suprasternal or parasternal (▶ Chap. 6) permits immediate viewing of the ascending aorta, the aortic arch with the vessels connected to it, and the upper part of the descending aorta, even in the emergency setting (Arntfield and Millington 2012).

11.1.3 Pain Due to Diseases of the Chest Wall

The cardinal symptom is local pain, which is usually stronger during palpation or movement. In the case of irritated intercostal nerves or nerve roots the pain radiates into the area supplied by these nerves. The various structures of the chest wall are very well accessible to sonographic investigation (▶ Chap. 2).

11.1.3.1 Rib Fracture

Rib fractures are usually triggered by trauma of appropriate magnitude. In patients with osteoporosis, however, fractures may even be caused by severe coughing. Sonography reveals the formation of a step at the site of maximum pain (Wüstner et al. 2005), frequently a smaller hematoma and occasionally the so-called chimney phenomenon (▶ Figs. 2.13 and 2.14). Even in the presence of older fractures, the patient experiences pain, which is seen on sonography as a starting callus formation (◘ Fig. 11.4).

11.1.3.2 Tumor Invasion of the Chest Wall

A peripheral lung tumor that reaches the visceral pleura causes no pain. Only when it has invaded the parietal

pleura and the muscular and bony structures of the chest does irritation of nerve fibers (which lead to pain receptors) occur. The term "Pancoast's tumor" (▶ Chap. 2) refers to a tumor that passes through the apex of the lung. The high resolution of sonography visualizes branches of the brachial plexus (▶ Chap. 1), their erosion and their position in relation to the subclavian vessels in the event of penetration of the superior sulcus (Fig. 11.5).

Tumor formations of the chest wall that extend across various structures can be identified well on B-mode sonography because of their different echogenicity and destruction of local tissue.(Fig. 11.6a, b) Pathological formation of new vessels is a further sonomorphological criterion of malignancy. Tumor manifestations in the joints and osteolytic metastases are extremely painful (Figs. 11.7 and 11.8).

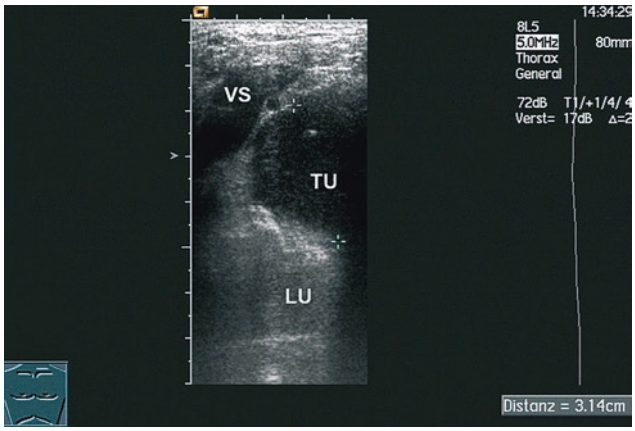

Fig. 11.5 A 46-year-old woman (40 pack years) with an adenocarcinoma (*TU*) in the left upper lobe which has perforated the superior sulcus and nearly reached the subclavian vessels. *VS* vena subclavia, *LU* lung

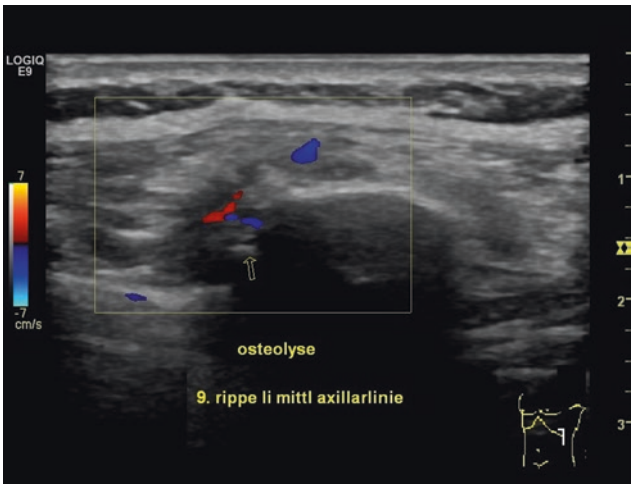

Fig. 11.7 Osteolytic destruction *(arrow)* of the ninth rib (left middle axillary line) in a patient with metastasizing lung carcinoma. Color Doppler depicts small vessels in the tumor

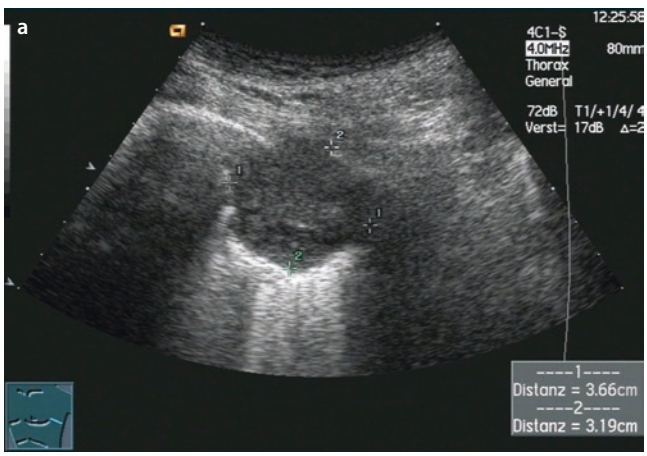

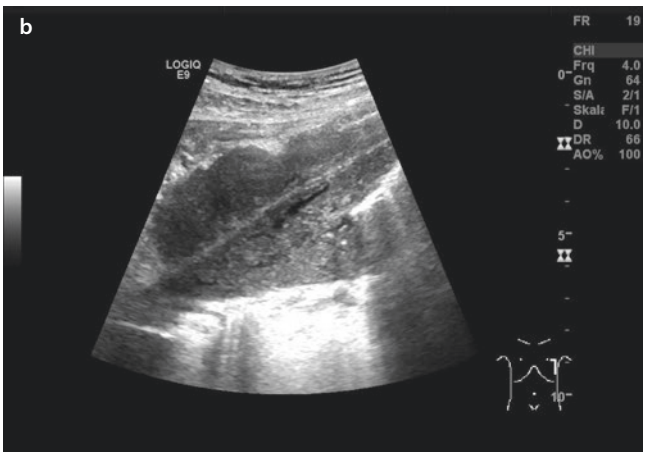

Fig. 11.6 **a** Peripheral lung carcinoma breaking through the pleural line and invading the muscles of the chest wall (sonographic biopsy: squamous cell carcinoma). **b** Pleural mesothelioma (histologic diagnosis gained with sonographic biopsy) showing a polycyclic formation in the chest wall and necrotizing infiltration of the adjacent lung

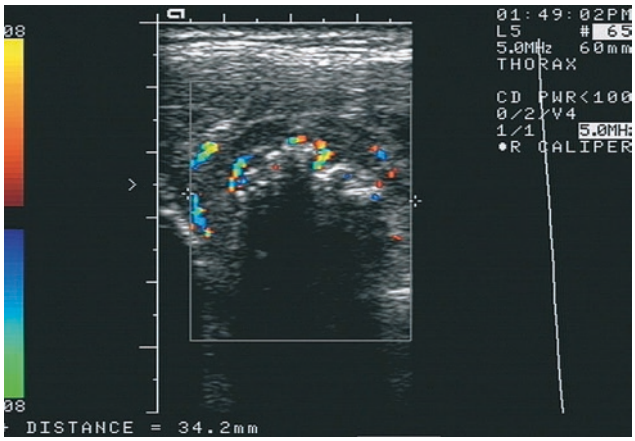

Fig. 11.8 A 51-year-old man with a painful swelling in the left sternoclavicular joint. Sonography reveals fragmentation of the cortical bone, which is surrounded by hypoechoic and strongly vascularized tissue. The surgical biopsy specimen yielded the diagnosis of a plasmocytoma. Clinically the patient had a solitary manifestation of a plasmocytoma which, however, was not secretory on laboratory investigation

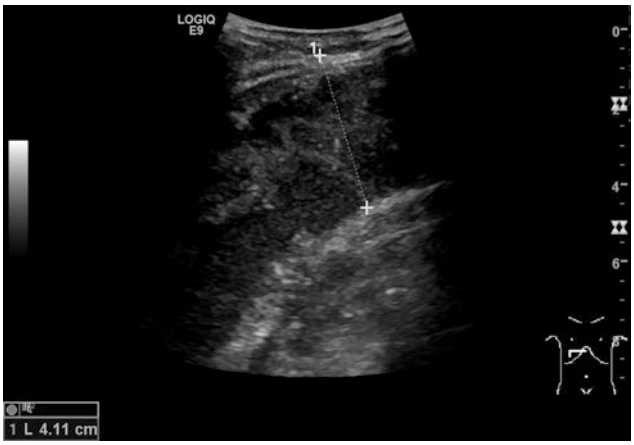

Fig. 11.9 A 35-year-old man with diabetes, renal insufficiency and a history of drug addiction. Extended abscess in the soft tissue of the right ventral chest wall *(markers)* caused by an infected central venous line in the jugular vein. Microbiological analysis of sonography-guided aspiration revealed *Staphylococcus*

11.2 Fever

The occurrence of fever is always an expression of inflammatory disease activity. The reasons may be numerous. On the one hand it may be a reaction of the organism to pathogens; on the other hand it may be a manifestation of pathological processes in the body, triggered without external influences. Depending on the structures of the chest affected by inflammation, the condition may be accompanied by pain. Respiratory pain is indicative of pleural involvement. The intensity of fever—for instance, it may be low in the presence of pulmonary embolism or very high in the presence of pneumonia—as well as laboratory findings and bacteriological investigations serve as additional aids to establish the diagnosis.

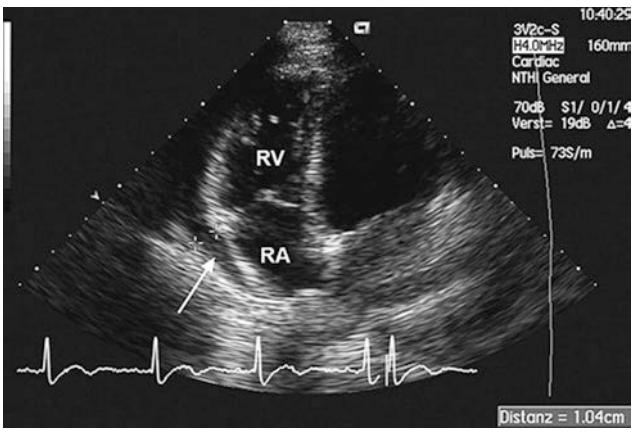

Fig. 11.10 A 25-year-old woman with a narrow pericardial effusion (*arrow*) in the presence of Churg–Strauss disease. *RA* right atrium, *RV* right ventricle

11.2.1 Fever with Chest Pain

11.2.1.1 Abscesses in the Chest Wall

Inflammation in the soft tissues of the chest wall, for instance, in the presence of an abscess (▶ Fig. 2.3), causes local pain occasionally accompanied by swelling. Abscesses in the chest wall may be quite extensive (Fig. 11.9).

11.2.1.2 Pleuritis

Inflammatory diseases of the pleura (▶ Chap. 3) cause pain which is enhanced during inspiration. Auscultation frequently discloses marked pleural rales. High-resolution transducers reveal changes that cannot be detected on conventional overview radiographs. Most of all, sonography is a useful imaging procedure when one has to avoid irradiation.

11.2.1.3 Pulmonary Embolism

In some cases of recurrent pulmonary embolism (▶ Sect. 5.3) the only symptoms may be intermittent chest pain and fever for a long period of time; however, fever rarely exceeds 38.3 °C (Fedullo and Morrus 2005). In one investigation of geriatric patients, fever was frequently observed in connection with pulmonary embolism (Ceccarelli et al. 2003).

11.2.1.4 Pericarditis

Pericarditis is associated with moderately high fever, breath-related and position-related precordial pain. The main diagnostic tool is ECG, assisted by laboratory investigations. On sonography, at the onset of the disease one usually finds a fluid margin of lesser or greater magnitude in the pericardial space (Fig. 11.10). In

every case sonography is the method of choice for further assessment of the progress of the disease.

11.2.2 Fever with Dyspnea

When a patient with fever develops dyspnea it is always a clinical sign of impairment of respiratory or ventilatory function.

11.2.2.1 Pneumonia

Pneumonia is usually associated with very high fever. In cases of pneumococcal pneumonia, the patient typically experiences sudden fever without prolonged onset of the disease. Inflammatory exudation of fluid in the alveoles eliminates air from the parenchyma and permits sonographic imaging even if the invasion extends up to the visceral pleura (▶ Sect. 5.1) (Blaivas 2012; Reißig and Görg 2012; Chavez et al. 2014). Secretory retention due to obstruction secondary to a tumor leads to atelectasis and frequently also poststenotic pneumonia. The sonographic image shows the distribution of vessels as well as necrosis in the parenchyma. A bronchoscopy must be performed to assess the central bronchial system (◘ Fig. 11.11).

11.2.2.2 Pleural Empyema

Pleural empyema, or collection of pus in the pleural space, is associated with fever, dyspnea and a severely impaired general condition. The disease is usually a threatening toxic condition which, if not identified on time or if treated too late, exposes the patient to the risk of sepsis and high lethality (Kolditz et al. 2004; Davies et al. 2010). Pleural empyema may occur as an inflammation of the pleura, for instance, in the presence of a tuberculotic infection, or may be a complication of a parapneumonic effusion in case of bacterial pneumonia (◘ Fig. 11.12a, b). The emergence of a pleural empyema always heralds a more severe course of disease, whether due to the impaired resistance of the individual or a particularly virulent pathogen. Pain usually occurs in the initial stage of the disease and disappears as the exudation in the pleural space increases. On sonography the fluid is frequently seen in conjunction with dense internal echoes which correlate with the high cell content of the fluid. The longer an empyema exists, the more pronounced are the septations and chambers (◘ Fig. 11.13a, b). Sonography also permits localization of the optimum site of aspiration, even at the bedside (Levin and Klein 1999; Davies et al. 2010; Heffner et al. 2010), to obtain material for investigation and place a drain. On the basis of the sonography report, the extent of empyema can be assessed in children (Carey et al. 1998; Ramnath et al. 1998) and the investigator will be able to decide whether conservative or surgical treatment should be used. In adults—as far as possible—computed tomography should be performed to plan the treatment and determine the exact extent and size of the chambers (◘ Fig. 11.13c).

When a suppurative effusion fills more than half a hemithorax, the patient has a pH below 7.2 and positive evidence of bacteria, a drain needs to be placed immediately (Colice et al. 2000; Davies et al. 2010; Heffner et al. 2010). In cases of chambered empyema, immediate intrapleural fibrinolysis therapy may be successful (Hamm 2005; Davies et al. 2010). The largest study conducted thus far on local fibrinolysis of empyema (Maskell et al. 2005) revealed no advantages in terms of the duration of disease or mortality in patients treated with streptokinase. However, the significant difference between chambered and nonchambered empyema was not taken into account. Video-assisted thoracoscopy and thoracotomy are surgical treatment procedures

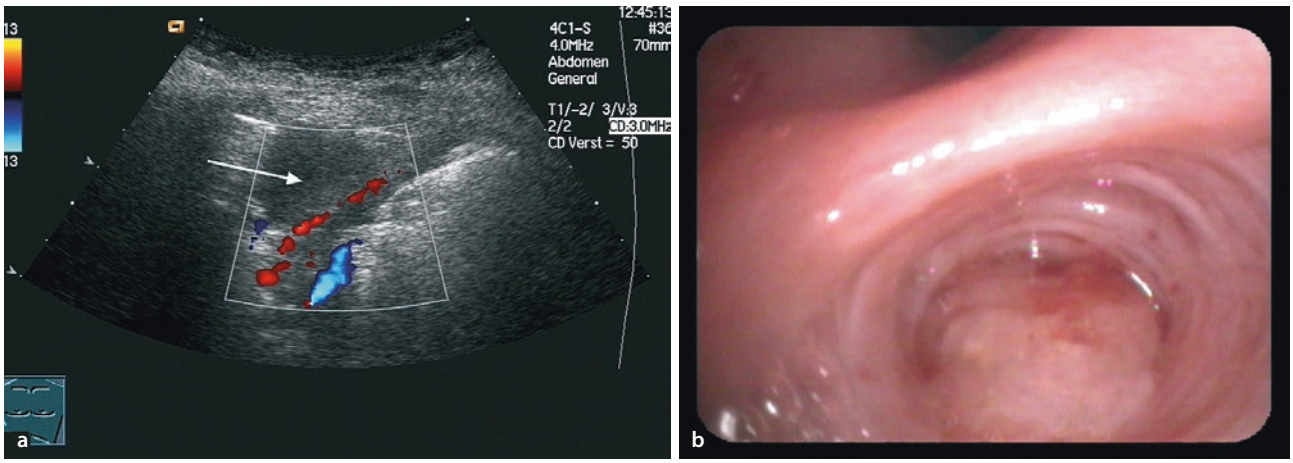

◘ **Fig. 11.11** **a**, **b** A 91-year-old woman with middle-lobe pneumonia, a large peripheral colliquation (*arrow*) and regular central vessels **a**. Bronchoscopy **b** reveals obstruction of the middle lobe secondary to the tumor, which proved to be an adenocarcinoma on histological investigation. Partial resolution of the middle-lobe invasion under antibiotic therapy

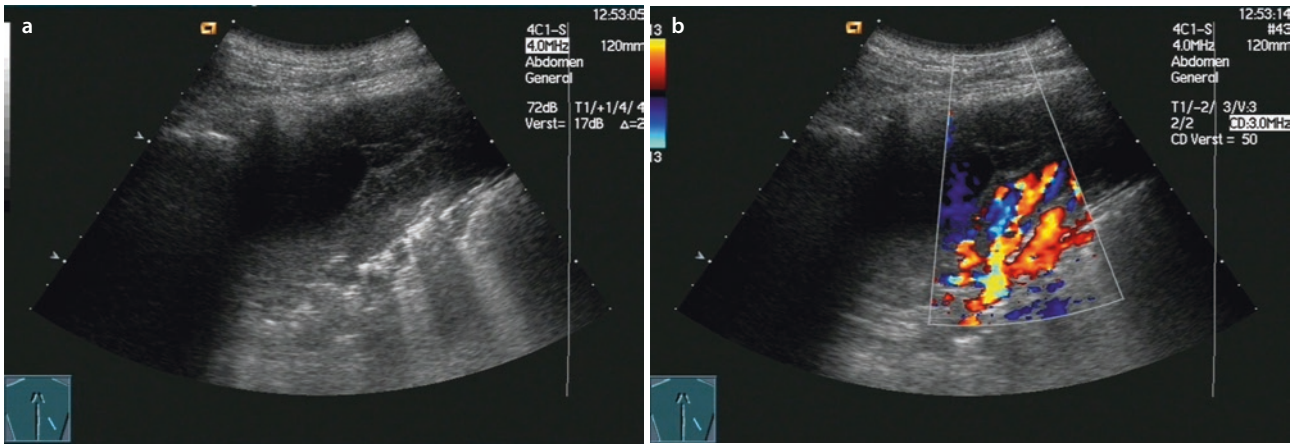

Fig. 11.12 **a** A 52-year-old man with fever and dyspnea. In the right lower lobe infiltration with air trappings, pleural thickening and several fibrinous bands. PH-value in the pleural fluid 6, 8. **b** Color Doppler shows hypervascularization in the infiltrated part of the lung. Successful treatment with drainage and antibiotics

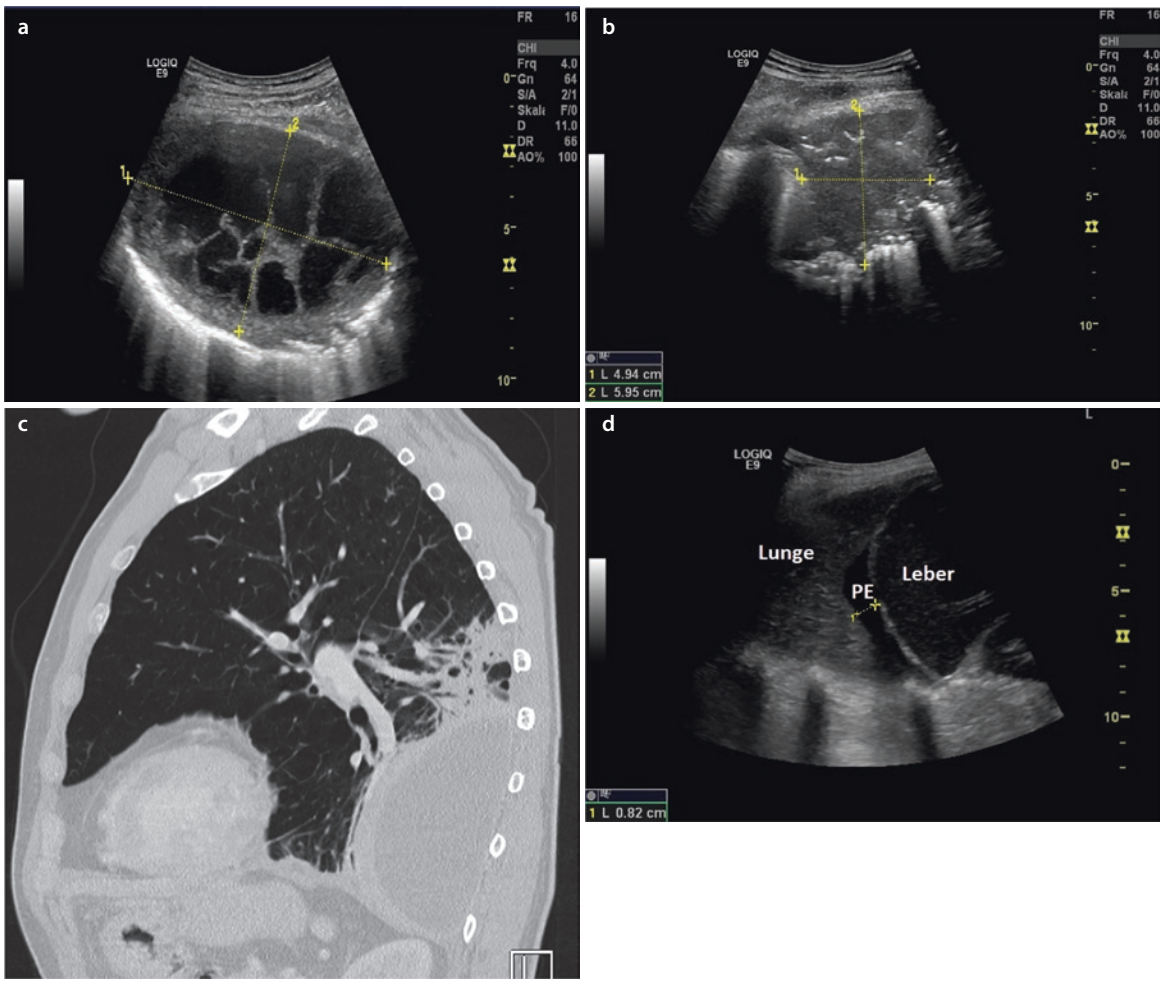

Fig. 11.13 **a** A 58-year-old man with high fever and critical sickness. On the left side dorsobasal pleural empyema with a thick wall and several loculations. **b** Above the empyema consolidated lung infiltration with air trappings. **c** Corresponding CT-image with section of the empyema and the infiltration. Therapy by means of VATS. **d** A 70-year-old woman with dyspnea and chest pain. The bedside sonographic examination from the right lateral aspect illustrates a compact consolidation in the right lower lobe and a small basal effusion (*PE, markers*)

which, however, must be viewed under consideration of other factors present in the individual patient (Hamm 2005; Davies et al. 2010; Heffner et al. 2010).

11.2.3 Fever with Dyspnea and Chest Pain

The more extensively the pleura is affected in case of pleuritis, or the more extensively the lung parenchyma and pleura are affected in the case of pleuropneumonia, the more likely one will find a combination of all three symptoms. Fluid in the pleural space as well as invasion of peripheral portions of the lung (■ Fig 11.13d) can be viewed rapidly by sonography, independent of the patient's condition or mobility. Further investigations such as diagnostic aspiration of the pleura or additional radiological investigations serve to conclude the diagnostic procedures and make the diagnosis.

11.2.4 Fever as the Sole Symptom in Chest Diseases

In the case of ambiguous fever the investigator is confronted with a large number of possibilities in terms of differential diagnosis (Roth and Basello 2003). As a rule the first diagnostic step is laboratory investigations, which serve as the basis for further diagnostic procedures. The sonography investigation is not the first step for diseases of the chest because it does not provide a general overview of the chest organs. Sonography of the chest is usually requested in connection with a specific question in the case of an appropriate suspected diagnosis.

11.2.4.1 Polyserositis

Sonography, the most sensitive procedure to provide evidence of fluid, is used to investigate small pleural effusions (▶ Chap. 3) that frequently occur on both sides and usually cause no symptoms for the patient. Even small pericardial effusions (■ Fig. 11.10) in the course of autoimmune diseases or vasculitis can be very well demonstrated by sonography.

11.2.4.2 Mycobacteriosis

The disease starts slowly and insidiously, and is associated with a gradual reduction of physical performance, nocturnal sweating and intermittent fever. Months may pass before an overview radiograph showing the pulmonary manifestation is performed. Pulmonary symptoms might be entirely absent. Some patients have a persistent dry cough which initially misleads the clinician in terms of diagnostic procedures and treatment. Depending on the individual's immune defense and additional organs that may be affected, the symptoms of disease may be very diverse (Hopewell 2005).

In the case of active disease the conventional chest X-ray shows soft, pale infiltrates, occasionally in conjunction with colliquations. Peripheral inflammatory lesions are accessible to sonography (■ Figs. 11.14 and 11.15). Sonomorphological or radiological criteria that permit a reliable distinction between atypical mycobacteriosis and infection with *Mycobacterium tuberculosis* do not exist (Müller et al. 2003). Newly introduced Interferon-gamma-Release-Assays (IGRAs) measure the TB-antigen-specific immunologic activation. This method allows a differentiation between tuberculous and not-tuberculous (MOTT) mycobacteria (Diel et al. 2011; Schönfeld et al. 2013)

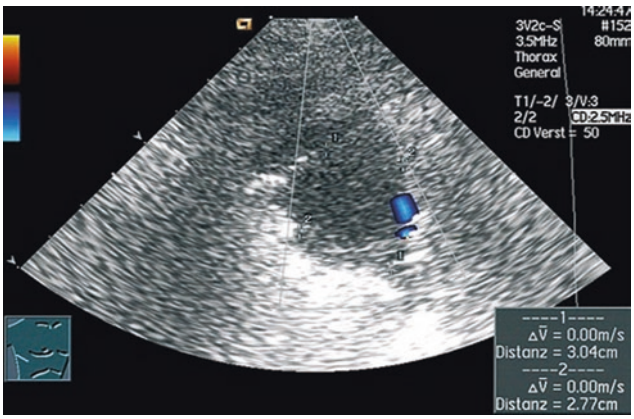

■ **Fig. 11.14** A 68-year-old man with loss of strength and bouts of fever for several months. In the right upper lobe, in lateral location, there is a relatively homogeneous area with blurred margins and vessels at the margin. The sonographic biopsy (in NaCl!) showed bacteria on microscopic investigation; the bacteria were subsequently differentiated as atypical *Mycobacteria* using PCR

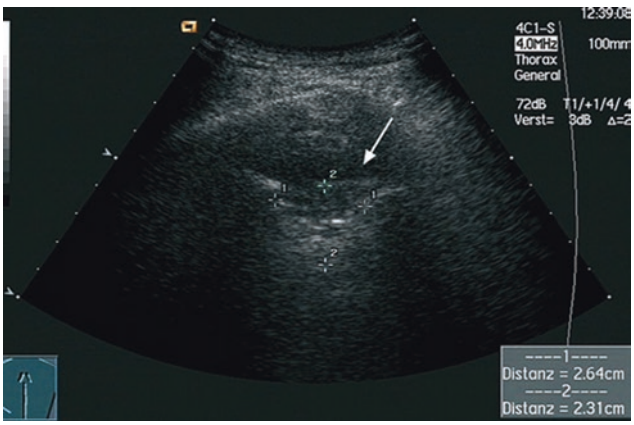

■ **Fig. 11.15** A 73-year-old man with a chronic cough, who was known to suffer from chronic obstructive pulmonary disease. Sonography showed an area with blurred margins in dorsal and basal location, with residual air. A small pleural effusion (*arrow*). *Mycobacterium tuberculosis* was cultured in the bronchial and pleural secretion

In cases of mycobacteriosis, sonography may be used in addition to radiological investigations, in order to evaluate the progress of peripheral lesions under treatment or when a sonography-guided biopsy is indicated for diagnostic purposes. However, conventional overview radiographs, possibly complemented by computed tomography, are always needed to assess the entire lung.

11.2.4.3 Endocarditis

Fever, physical weakness and loss of physical performance may be the only signs of endocarditis. In the presence of good transthoracic insonation, vegetation in the heart valves is visualized. Blood cultures should be performed to obtain evidence of bacteria. In the case of Löffler's endocarditis, transient thrombi may be observed at the endocardium. A sonography investigation of the heart for the purpose of orientation can be performed even by the less experienced investigator. For a more detailed examination the investigator must possess the knowledge and skills required to perform echocardiography.

11.3 Dyspnea

The symptom of dyspnea is strongly dependent on the patient's subjective experience. Specific receptors that may be responsible for triggering dyspnea have not been identified thus far (Fitzgerald and Murray 2005). A multifactorial mechanism via medullary and peripheral chemoreceptors, pulmonary vagal afferences, and mechanoreceptors in the locomotor apparatus are presumed to exist (ATS 1999; Pfeifer 2005; Stulbarg and Adams 2005). In the meantime, clinically a distinction is made between acute, chronic, resting and stress dyspnea. Even the investigator finds it difficult to quantify dyspnea; therefore, particularly acute dyspnea should be rapidly investigated on the basis of clinical parameters (breath and pulse rate, auscultation, blood pressure), by laboratory investigation (blood gas analysis, determination of the acid–base balance of the body, blood count, typical enzymes associated with infarction) and imaging procedures. A strong respiratory drive is triggered by hypoxia and hypercapnia through afferent stimuli acting on the respiratory center. Reduction of the gas-exchange surface, mechanical hindrance of dilatation of the lung, muscular and neurogenic deficits lead to greater respiratory effort. Cerebral disorders cause varying degrees of respiratory impairment. The possibilities of sonographic imaging in the presence of dyspnea, for the various compartments involved in respiration, are presented in the following.

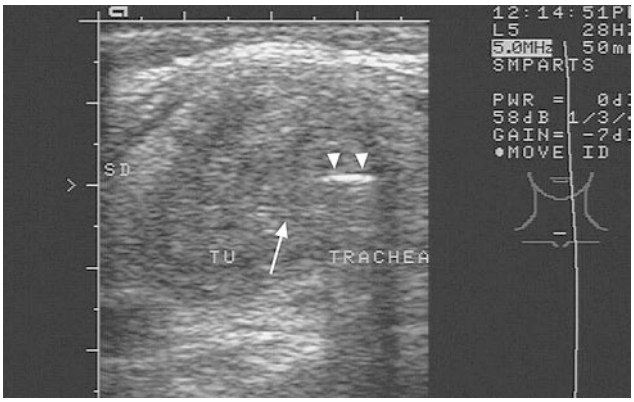

Fig. 11.16 A 55-year-old woman with advancing stress dyspnea for several weeks; inspiratory stridor. Sonography shows a space-occupying lesion arising from the right lobe of the thyroid, entering the trachea (*arrow*) and destroying the right lateral tracheal wall. A narrow air reflex (*arrowheads*) remains in the constricted trachea.

11.3.1 Respiratory Tract

The upper and deeper respiratory tracts are the domain of endoscopy in terms of diagnosis. In the case of dyspnea with inspiratory stridor, sonography of the thyroid should always be considered as part of the routine investigation (Fig. 11.16).

11.3.2 Pleura

Fluid in the pleural space, depending on its quantity, leads to compression of lung tissue and reduces the respiratory surface. In patients with concomitant cardiopulmonary disease, even a few hundred milliliters of effusion can lead to dyspnea. Patients with a healthy contralateral lung may tolerate several liters of effusion and experience only mild dyspnea. Sonography allows rapid estimation of the quantity of effusion (Fig. 11.17) and the possibility of septation (Fig. 11.18).

As in a pleural effusion, the extent of a pneumothorax and the presence of concomitant diseases are of decisive importance for the emergence of dyspnea. A conventional X-ray is always needed to determine the size of the pneumothorax (Fig. 11.19).

11.3.3 Lung

Diseases of the lung parenchyma reduce the gas-exchange surfaces. Acute dyspnea may be caused by inflammatory, vascular or tumor diseases of the lung (▶ Chap. 5). Lung diseases accompanied by interstitial

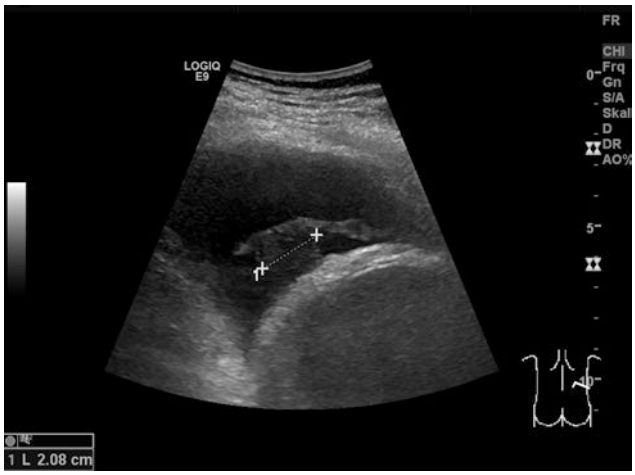

Fig 11.17 A pleural effusion with a tumorous lesion based on the diaphragm *(cross markers)* turns out to be the cause of dyspnea in a 84-year-old woman. Malignant effusion is probable because of an operated breast cancer 2 years before (patient refused puncture and biopsy)

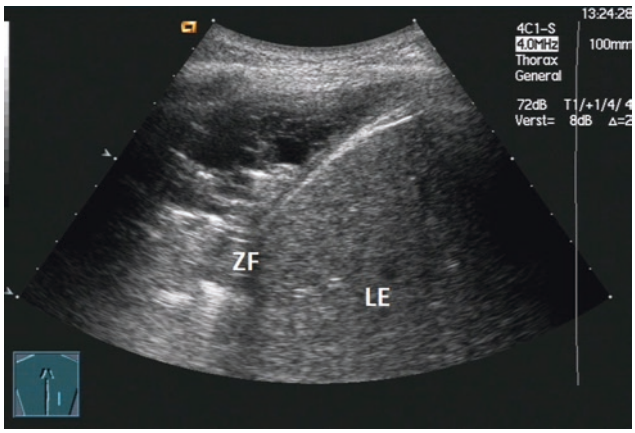

Fig 11.18 After VATS due to complicated pleural empyema residuary small septate effusion and adherence of the lung to the diaphragm (*ZF, LE liver*)

and chronic progressive loss of substance are more often accompanied by chronic and stress dyspnea. Pneumonia (► Sect. 5.1), tumors (► Sect. 5.2) and embolic consolidations (► Sect. 5.3) are accessible to sonographic diagnosis when ventilated tissue does not superimpose the path of insonation. Sonography serves as a valuable diagnostic adjunct when the investigator is confronted with the radiological report of a so-called white lung (► Sect. 5.4).

In the case of a severe dyspneic patient the findings of bilateral coalescent B-Lines (► Chap. 4) help to differentiate between pulmonary edema or exacerbation of a chronic obstructive pulmonary disease.

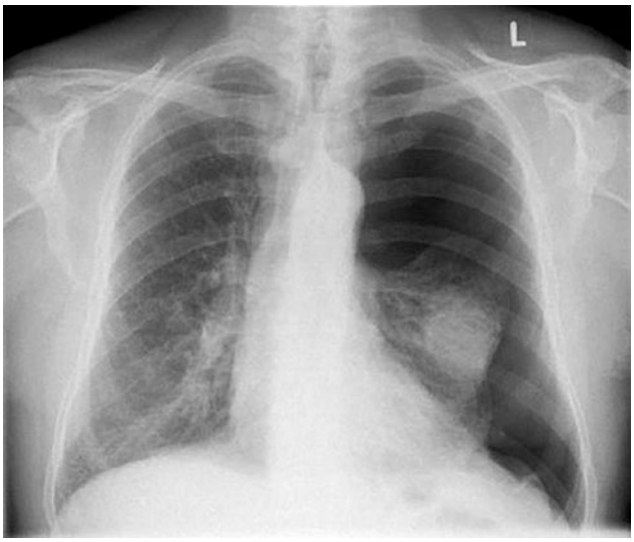

Fig. 11.19 A 63-year-old man with a tumor in the left upper lobe. Four hours after a biopsy had been obtained by transaxillary sonography, the patient developed dyspnea accompanied by elimination of gliding of the lung surface on sonography. The tumor previously seen on sonography was no longer visible. X-ray investigation showed a pneumothorax that needed drainage

11.3.4 Heart

In cases of acute dyspnea the investigator must include cardiac diseases in the differential diagnosis. A physician trained in general internal medicine, as well as sonography, should be familiar with typical sonographic findings. In case of failure of the left side of the heart (Ware and Matthay 2005) owing to left-ventricular cardiomyopathy, one finds a massively dilated and ballooned left ventricle (Fig. 11.20).

In the case of cor pulmonale, diseases of the right side of the heart are manifested in terms of dilatation of the right side of the heart and hypertrophy of the right ventricle (Fig. 11.21).

Determination of the size of the right side of the heart helps to assess the severity of disease in cases of a suspected pulmonary embolism (Goldhaber 1998; ► Sect. 5.3).

An indirect criterion of cardiac decompensation, easy to identify by sonography, is investigation of the vena cava in longitudinal section in the upper abdomen, through the left lobe of the liver. The diameter of the vena cava is more than 20 mm, and its diameter is inadequately reduced during inspiration.

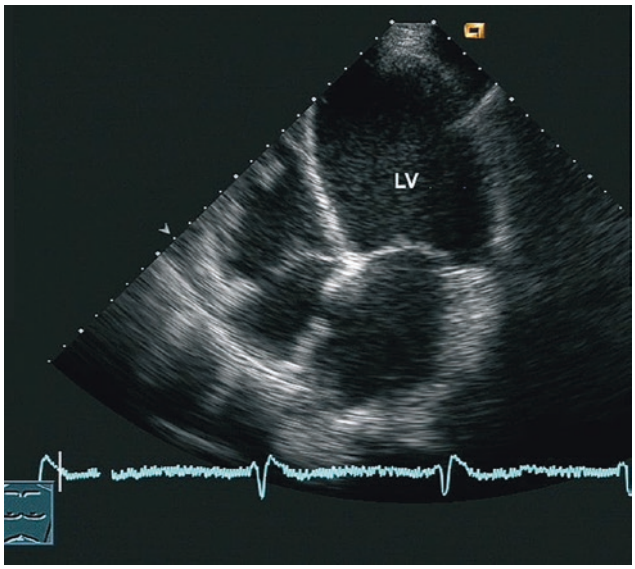

Fig. 11.20 A 55-year-old man with a pulmonary edema as a result of left-ventricular cardiomyopathy due to alcohol toxicity. The apical four-chamber view shows a dilated and ballooned left ventricle (*LV*)

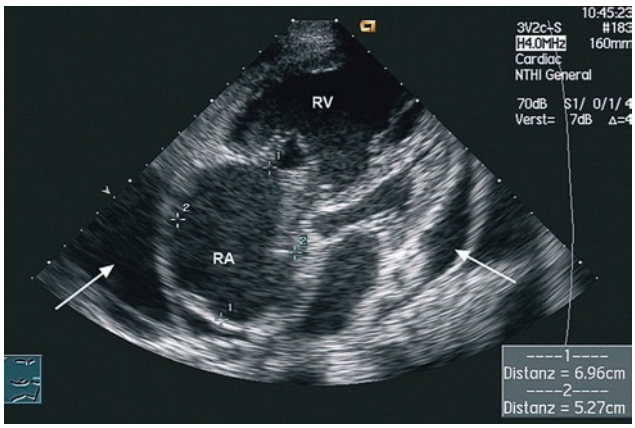

Fig. 11.21 A 64-year-old man with decompensated cor pulmonale as a result of pulmonary hypertension in the presence of the CREST syndrome. The apical four-chamber view reveals an enlarged right atrium (*RA*) and a massively dilated and hypertrophic right ventricle (*RV*). A pericardial effusion (*arrows*) lateral to the right atrium, the right ventricle and the left ventricle

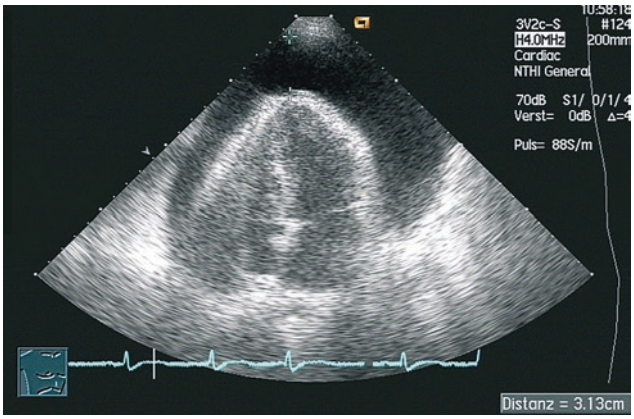

Fig. 11.22 A 91-year-old woman with global cardiac decompensation and a large circular pericardial effusion. Under diuretic therapy that reduced the cardiac load, the effusion resolved partially and dyspnea improved; therefore, in consideration of the patient's age a diagnostic aspiration was not performed

A hemodynamically significant pericardial effusion leads to impairment of the systolic and diastolic function of the left ventricle, as well as congestion of venous blood flow. Large pericardial effusions can also be seen well in subcostal insonation from the epigastrium (Fig. 11.22).

11.3.5 Respiratory Muscles

The most important respiratory muscle is the diaphragm (▶ Chap. 3). In the rare event of bilateral paresis of the diaphragm the patient may be unable to lie supine because of dyspnea, which starts immediately (Fitzgerald and Murray 2005). Reduced mobility of the diaphragm due to fixation of the lung at the diaphragmatic pleura and unilateral partial or complete paresis of the diaphragm are seen well in the dynamic sonography investigation, particularly on comparison of the right and the left side (McCool and Tzelepis 2012). The cause of a local compression of the cranial part of the phrenic nerve may be visible in the supraclavicular view (Fig. 11.23a, b).

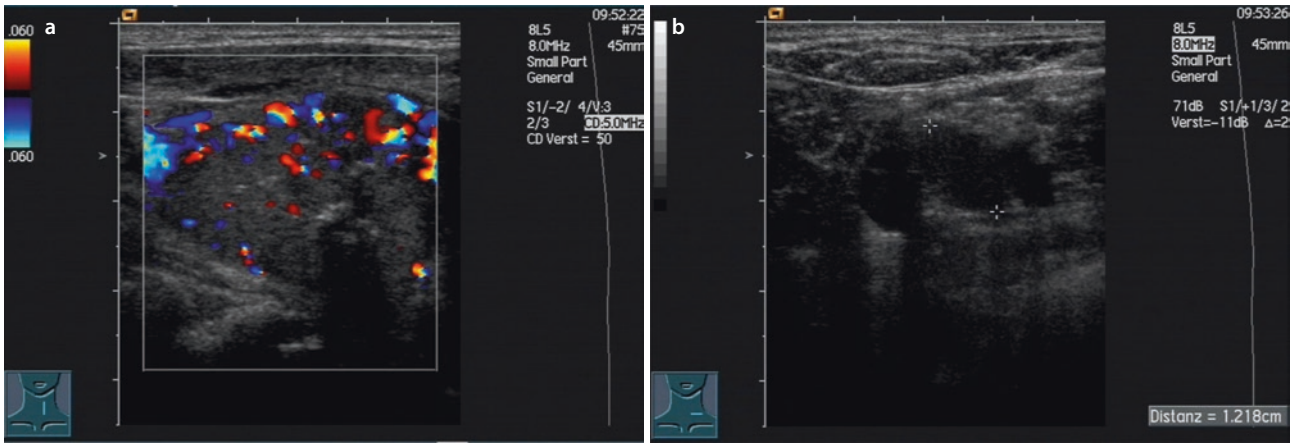

Fig. 11.23 **a** A 52-year-old man presenting with dyspnea, an elevated left diaphragm, local pain and increase of dyspnea on palpation left supraclavicular. Unremarkable radiologic findings except for the elevated diaphragm. In the left thyroid lobe (anamnestic "harmless node") inhomogeneous node with larger calcifications and irregular marginal vessels. **b** Next to the left thyroid lobe supraclavicular echo poor lymph node causing the elevated diaphragm by compression of the phrenic nerve. Diagnosis after curative surgery: papillary thyroid carcinoma with local lymph node metastasis

Summary

Chest pain, fever and dyspnea are frequent symptoms in cases of chest disease. The combination and varying intensity of symptoms allows conclusions to be drawn about the structures involved and the severity of the disease. Sonography, a readily available method that is very suitable for investigation at the bedside, makes a significant contribution to the diagnosis when investigating regions that can be viewed by the procedure. Sonography provides very significant information about the cause of sudden chest pain in the presence of a tension pneumothorax, in cases of pulmonary embolism, and in acute aortic dissection. Pathological changes in the chest wall can be visualized in an excellent manner because of the high quality of near-field resolution on the sonography image. Fever is a symptom in cases of inflammation of the chest wall, the pleura, and the lung. Sonography not only shows which structures are affected, but is also a reliable method for targeted diagnostic isolation of fluid and tissue. Sonography control investigations are particularly valuable in the course of pleural and pericardial effusions. In the case of dyspnea, sonography permits a distinction between a cardiac and a pulmonary cause of the condition. The dynamic investigation allows assessment of functional disorders of the diaphragm.

Acknowledgement We thank R. Loose, Head of the Institute of Diagnostic and Interventional Radiology at the Klinikum Nürnberg Nord, for providing radiology reports.

References

Al Deeb M, Barbic S, Featherstone R et al (2014) Point-of-care ultrasonography for the diagnosis of acute cardiogenic pulmonary edema in patients presenting with acute dyspnea: a systematic review and meta-analysis. Acad Emerg Med 8:843–852

Arntfield RT, Millington SJ (2012) Point of care ultrasound applications in the emergency department and Intensive care unit—a review. Curr Cardiol Rev 8:98–108

ATS (1999) Dyspnea—mechanisms, assessment, and management: a consensus statement. Am J Respir Crit Care Med 159:321–340

Blaivas M (2012) Lung ultrasound in evaluation of pneumonia. J Ultrasound Med 31:823–826

Carey JA, Hamilton JR, Spencer DA, Gould K, Hasan A (1998) Empyema thoracis: a role for open thoracotomy and decortication. Arch Dis Child 79:510–513

Ceccarelli E, Masotti L, Barabesi L, Forconi S, Capelli R (2003) Pulmonary embolism in very old patients. Aging Clin Exp Res 15:117–122

Chavez MA, Shams N, Ellington LA et al (2014) Lung ultrasound for the diagnosis of pneumonia in adults: a systematic review and meta-analysis. Respir Res 15:50

Colice GI, Curtis A, Deslauriers J et al (2000) ACCP Consensus Statement: Medical and surgical treatment of parapneu-

monic effusions—an evidence-based guideline. Chest 118:1158–1171
Copetti R, Cattarossi L (2008) Ultrasound diagnosis of pneumonia in children. Radiol Med 113:190–198
Davies HE, Davies RJO, Davies CWH (2010) Management of pleural infection in adults: British Thoracic Society pleural disease guideline 2010. Thorax 65:ii41–ii53
Diel R, Loytved C, Nienhaus A et al (2011) Neue Empfehlungen für die Umgebungsuntersuchungen bei Tuberkulose. Deutsches Zentralkomitee zur Bekämpfung der Tuberkulose. Pneumologie 65:359–378
Fedullo PF, Morrus TA (2005) Pulmonary thromboembolism. In: Mason RJ, Murray JF, Broaddus VC, Nadel JA (eds) Textbook of respiratory medicine. Elsevier Saunders, Philadelphia, pp 1425–1458
Fitzgerald FT, Murray JF (2005) History and physical examinations. In: Mason RJ, Murray JF, Broaddus VC, Nadel JA (eds) Textbook of respiratory medicine. Elsevier Saunders, Philadelphia, pp 493–510
Gardelli G, Feletti F, Nanni A et al (2012) Chest ultrasonography in the ICU. Respir Care 57:773–781
Goldhaber SZ (1998) Medical progress: pulmonary embolism. N Engl J Med 339:93–104
Hamm H (2005) Die Behandlung des parapneumonischen Ergusses und des Pleuraempyems. Pneumologie 59:696–703
Heffner JE et al (2010) Diagnostic utility and clinical applications of imaging for pleural space infections. Chest 137:467–479
Hopewell PC (2005) Tuberculosis and other mycobacterial diseases. In: Mason RJ, Murray JF, Broaddus VC, Nadel JA (eds) Textbook of respiratory medicine. Elsevier Saunders, Philadelphia, pp 979–1043
Hyacinthe AC, Broux C, Gilles F et al (2012) Diagnostic accuracy of ultrasonography in the acute assessment of common thoracic lesions after trauma. Chest 141:1177–1183
Kim OH, Kim WS, Kim MJ, Jung JY, Suh JH (2000) US in the diagnosis of pediatric chest diseases. Radiographics 20:653–671
Kolditz M, Halank M, Höffken G (2004) Parapneumonischer Erguss und Pleuraempyem—aktuelle Aspekte zu Einteilung. Diagn Ther Pneumol 58:83–91
Kontos MC, Diercks DB, Kirk JD (2010) Emergency department and office-based evaluation of patients with chest pain. Mayo Clin Proc 85:285–295
Kreuter M, Herth FJF, Wenz H, Mathis G (2012) Sonographische Notfalldiagnostik des Thorax. Pneumologe 9:436–443
Kurz K, Giannitsis E, Meyer FJ (2005) Thoraxschmerz. Pneumologe 2:188–197
Levin DL, Klein JS (1999) Imaging techniques for pleural space infections. Semin Respir Infect 14:31–38
Lichtenstein DA, Mezière GA (2008) Relevance of lung ultrasound in the diagnosis of acute respiratory failure. The BLUE protocol. Chest 134:117–125
Maskell NA, Davies CWH, Nunn AJ et al (2005) U.K. trial of intrapleural streptokinase for pleural infection. N Engl J Med 352:865–874
Mathis G (2014) Thromboembolism in ultrasound. Killing three birds with one stone. Chest 145:931–932
McCool FD, Tzelepis GE (2012) Dysfunction of the diaphragm. N Engl J Med 366:932–942
Moore CL, Copel JA (2011) Point-of-care ultrasonography. N Engl J Med 364:749–757
Müller NL, Fraser RS, Lee KS, Johkoh T (2003) Diseases of the lung. Lippincott, Philadelphia, pp 45–46
Murray JF, Gebhart GF (2005) Chest pain. In: Mason RJ, Murray JF, Broaddus VC, Nadel JA (eds) Textbook of respiratory medicine. Elsevier Saunders, Philadelphia, pp 848–865
Pfeifer M (2005) Dyspnoe. Pneumologe 2:177–187
Ramnath RR, Heller RM, Ben-Ami T et al (1998) Implications of early sonographic evaluation of parapneumonic effusions in children with pneumonia. Pediatrics 101:68–71
Reißig A, Görg C (2012) Pneumonie und diffus parenchymale Erkrankungen im Lungenultraschall. Pneumologe 9:444–451
Reißig A, Görg C, Mathis G (2009) Transthorakale Sonografie bei der Diagnostik pulmonaler Erkrankungen: ein systematischer Zugang. Ultraschall Med 30:438–458
Roth AR, Basello GM (2003) Approach to the adult patient with fever of unknown origin. Am Fam Physician 68:2223–2228
Sartori S, Tombesi P, Trevisani L, Nielsen I, Tassinari D, Abbasciano V (2007) Accuracy of transthoracic sonography in detection of pneumothorax after sonographically guided lung biopsy: prospective comparison with chest radiography. AJR 188:37–41
Schönfeld N, Haas W, Richter E et al (2013) Empfehlungen zur Diagnostik und Therapie nichttuberkulöser Mykobakteriosen des Deutschen Zentralkomitees zur Bekämpfung der Tuberkulose (DZK) und der Deutschen Gesellschaft für Pneumologie und Beatmungsmedizin (DGP). Pneumologie 67:605–633
Squizzato A, Rancan E, Dentali F et al (2013) Diagnostic accuracy of lung ultrasound for pulmonary embolism: a systematic review and meta-analysis. J Thromb Haemost 11:1269–1278
Stulbarg MS, Adams L (2005) Dyspnea. In: Mason RJ, Murray JF, Broaddus VC, Nadel JA (eds) Textbook of respiratory medicine. Elsevier Saunders, Philadelphia, pp 815–830
Volpicelli G (2013) Lung sonography. J Ultrasound Med 32:165–171
Volpicelli G, Frascisco M (2008) Lung ultrasound in the evaluation of patients with pleuritic pain in the emergency department. J Emerg Med 34:179–186
Ware LB, Matthay MA (2005) Acute pulmonary edema. N Engl J Med 353:2788–2796
Wüstner A, Gehmacher O, Hämmerle S et al (2005) Ultraschalldiagnostik beim stumpfen Thoraxtrauma. Ultraschall Med 26:285–290

Thoracic PoCUS (Point-of-Care Ultrasound) in Emergency Patients

Joseph Osterwalder and Gebhard Mathis

Contents

Diagnostic ultrasound is the next stethoscope: used by many, understood by few (1).

G. Mathis (ed.), *Chest Sonography*, https://doi.org/10.1007/978-3-031-09442-2_12

12.1 Basic Principles

After an extensive presentation of the sonomorphology of various injuries and diseases of the chest wall and lungs in the main part of this book and a symptomatic approach in chapter 11, the focus here is on emergency situations. All that remains is to put together the single diagnostic elements and to show how sonography of the chest can be integrated into emergency daily routine.

First, however, two questions arise: What is an emergency? Is it a life-threatening condition, severe trauma, dyspnea, coughing or fever and what does the term emergency sonography mean? The answers to these questions are simple: By an emergency we understand a subjective assessment of symptoms or signs of illness or injuries for which the person affected is seeking urgent professional medical help either himself or herself or a person present on behalf of the patient. What is emergency sonography? The term emergency sonography is used to describe a well-performed, problem-oriented, bedside sonography of the emergency patient integrated into the course of care as a continuation of the clinical examination. Today, the new pocket devices can largely replace the stethoscope and be part of the exam. Emergency sonography is independent of location and medical specialties, used across all organs and regions and divided into four clinical applications (Table 12.1).

The term point-of-care ultrasound (PoCUS), which was discussed in the introduction, includes emergency sonography too. The emergency thoracic ultrasound (TUS) or also known as thoracic emergency PoCUS is a multimodal ultrasound and comprises the focused sonography of the chest wall and lungs, the focused cardiac ultrasound FoCUS) and, depending on the individual patient, also the focused vascular sonography (Picano et al. 2018; Kameda and Kimura 2020). It is now undisputed that these combined applications in the clinical context achieve better results than lung ultrasound alone (LUS). Furthermore, aerosol or droplet infections can be avoided. They can occur during auscultation and are reduced during sonography. Scanning can be done without forced breathing, which is often accompanied by coughing attacks. Therefore it is a great advantage in the current SARS-Cov2 pandemic, and should not be underestimated.

For more than a hundred years, chest x-ray (CXR) was the compulsory standard examination for patients with cardiovascular and pulmonary problems. This situation has changed fundamentally. Many studies show that pulmonary ultrasound is diagnostically superior to CRX (see Tables 12.2 and 12.3). In selected cases it even achieves the diagnostic performance of computed tomography (CT). This is very important because LUS usually replaces CRX and often chest CT, thus saving waiting times for radiological examinations and unnecessary demands on personnel and space in crowded emergency departments (Zanobetti et al. 2017). The PoCUS application with pocket devices can also reduce the risk of transmitting infectious diseases due to less requirement on personal, technique and room compared to CXR and CT, as well as easier hygienic handling. Furthermore, costs can be reduced and harmful side effects of CT such as radiation exposure and anaphylactic reactions or contraindications for the use of iodine-containing contrast media in renal failure and latent or manifest hyperthyroidism are eliminated. For some of these topics and a couple of other "clinical outcome variables", good scientific studies exist in the emergency context (Table 12.4). However, there is still a lack of research investigating the benefits in terms of mortality and morbidity of LUS compared to CXR and CT.

In summary, PoCUS has become an established and helpful tool for the diagnosis of diseases and injuries of the chest. Except for the thoracic E-FAST (Extended Focused Assessment with Sonography for Trauma), which is part of the standard ATLS-procedure in the shock room, the thoracic PoCUS has also become increasingly important in other emergency situations. It allows relevant clinical decisions to be made quickly and increases efficiency and safety in patient monitoring as well as difficult punctures. Below, indications and procedures of PoCUS in patients with trauma and diseases of the chest are discussed.

Table 12.1 Clinical applications of emergency sonography

Applications	Content
Diagnosis	Medical history, symptoms, findings of the exam, laboratory and ECG lead to simple sonographic yes-no questions
Algorithm	Protocol
Monitoring	Monitoring and evaluation of treatment
Invasive procedures	Ultrasound-assisted puncture and placement of catheters in vessels and on nerves

Table 12.2 Pooled sensitivities and specificities of chest-x-ray (CXR) and lung ultrasound (LUS) compared to computed tomography for selected pathological findings in critically ill patients

Diagnosis	CXR sensitivity	LUS sensitivity	CXR specificity	LUS specificity
Consolidations	69%	97%	90%	94%
Pleural effusion	55%	97%	90%	94%
Pneumothorax	21%	100%		
Interstitial syndrom	53%	95%	91%	91%
Lung contusion	38%	98%	90%	90%
Summarising sensitivity and specificity	49%	95%	92%	94%

Table 12.3 Summary of multiple systematic reviews/meta-analyses on the validity of chest-X-ray (CXR) and thoracic ultrasound (TUS) (Blank et al. 2019)

Diagnosis	CXR sensitivity	TUS sensitivity	CXR specificity	TUS specificity
Pneumothorax	29–55%	68–98%	98–100%	97–99%
Pneumonia (adult)	44–77%	80–97%	90–91%	70–96%
Pneumonia (children)		93%		96%
Lung embolism without CEUS	–	80–87%	–	81–93%
Pleural effusion	51%	94%	91%	98%
Pulmonary edema	66–67%	82–94%	76–83%	83–92%
Lung contusion	44%	89%	98%	89%
Rib fractures	12–24%	80–90%	–	–
Sternal fractures	71%	100%	–	100%

Table 12.4 Outcome-studies

Type of study	Question	Results
Prospective randomized trial in the emergency room (Laursen et al. 2014) $N = 320$ participants-	Difference in the correct diagnosis of patients with dyspnea after 4 h using TUS versus standard procedure?	Group with LUS and focused echocardiography: 88% correct diagnosis Group with standard procedure: 63% correct diagnosis $p < 0.001$
Prospective cohort study in ICU (Silva et al. 2013) $N = 78$ participants	Impact of LUS and FoCUS on clinical decisions in patients with respiratory symptoms?	Significant improvement of initial treatment for patients with pneumonia, pulmonary edema, decompensated COPD and pulmonary embolism after TUS
Prospective cohort study in the emergency room (Zanobetti et al. 2017) $N = 2683$ participants	Time difference for diagnosis of dyspnea with and without PoCUS?	PoCUS was 186 min faster than the standard procedure with identical diagnostic accuracy for ACS, pneumonia, pleural/ pericardial effusion, pneumothorax and dyspnea of other causes; better for pulmonary edema and worse for COPD/asthma and pulmonary embolism
Prospective randomized controlled trial in a ward of internal medicine (Golan et al. 2020) $N = 60$ participants	Time difference until correct diagnosis and appropriate treatment of patients with chest pain and dyspnea for PoCUS and standard procedures ?	Time to correct diagnosis: control group in median 48 h and early PoCUS group in median 24 h; $p = 0.12$ Time to appropriate treatment: control group median 24 h and early PoCUS group median 5 h; $p = 0.014$
Systematic review (Platz et al. 2017) • $N = 6$ studies/438 participants • $N = 7$ studies/953 participants	Dynamic change of B-lines in acute heart failure patients to emergency treatment? Prognostic benefit of B-lines in outpatients with heart failure?	Number of B-lines decreases already 3 h after first treatment and it helps to monitor therapy. Patients with ≥3 B-lines in 5 or 8 zones have a fourfold risk of hospitalization or death within 6 months. The presence of B-lines helps in the decision to intensify or hospitalize the therapy

12.2 Emergency PoCUS for Chest Trauma

The main symptom of chest trauma is pain. Dyspnea and/or shock are frequent additional companions. Despite detailed inspection and even after a thorough clinical examination of trauma patients, it is often not clear: what, where and how is wrong. Thanks to TUS, however, precise image information can be obtained easily and quickly. It helps to find the causes of chest pain, obstructed airways, impaired breathing and intrathoracic bleeding. As said above the TUS has been a standard part of E-FAST for more than 15 years and is routinely used in any seriously injured patient regardless of clinical findings. It involves the detection of pneumothorax, hemothorax and hemopericardium. However, diagnostics in trauma using sonography has developed further. We are able to detect additional problems and injuries in chest trauma and are not only focused on the severely injured patient. It is therefore advisable to expand E-FAST, which focuses on the primary survey, and to use also the full spectrum of TUS in the secondary survey. Tables 12.5 and 12.6 summarize the most important indications and Fig. 12.1 the procedure for the primary and secondary survey.

In this context, we would like to briefly discuss the pulmonary contusion. It is one of the most common

Table 12.5 TUS indications in the primary ATLS-survey

Organ	Clinical questions	Sonografic findings
Pleura	· Pneumothorax? · Unilateral/false intubation · Hemothorax?	· No lung sliding, no vertical artifacts and no lung pulse Lung point (incomplete pneumothorax) · No lung sliding (on one or both sides), but lung pulse · Spine-sign
Heart	· Pericardial effusion? · Cardiac tamponade?	· Hypo- to hyperechoic (coagulum) band between the pericardial leaves · Inversion to collapse of right atrium in late diastole, inversion to collapse of right ventricle in early diastole, shift of septum during inspiration to the left and expiration to the right, swinging heart and extended VCI

Table 12.6 TUS indications in the secondary ATLS-survey

Organ	Clinical questions	Sonografic findings
· Chest wall	· Hematoma?	· Echofree to hyperechoic inhomogeneous, clearly definable area (for detection of active bleeding color Doppler and/or CEUS)
· Ribs · Sternum	· Rib fracture? · Sternal fracture?	· Sonopalpation (painful, fragments move) · Interruption or step of corticalis line · «Kaminphänomen» (fireplace phenonemon) · Circumscribed hematoma
· Diaphragm	· Diaphragm rupture?	· Fluid in the pleural cavity (blood) · Stomach and/or intestine in the pleural space · Gap in the diaphragm (cave artifact)
· Lung	· Lung contusion?	· Thin smooth or irregular pleural line · Normal lung sliding · Multifocally distributed vertical artifacts with spared areas · Small and large subpleural consolidations
· Heart	· Injury of the heart?	· Atrial, ventricular, septal rupture · Heart valve or chorda tear · Regional wall movement abnormalities
· Vessels	· Hypovolemia? · Rupture of thoracic vessels (aorta, subclavia, internal thoracic and intercostal arteries? · Safe puncture?	· Dimension and respiratory variability of the inferior vena cava · Hematoma around vessels, color Doppler signals also outside the vessel/ CEUS · Puncture and catheter localization under sight

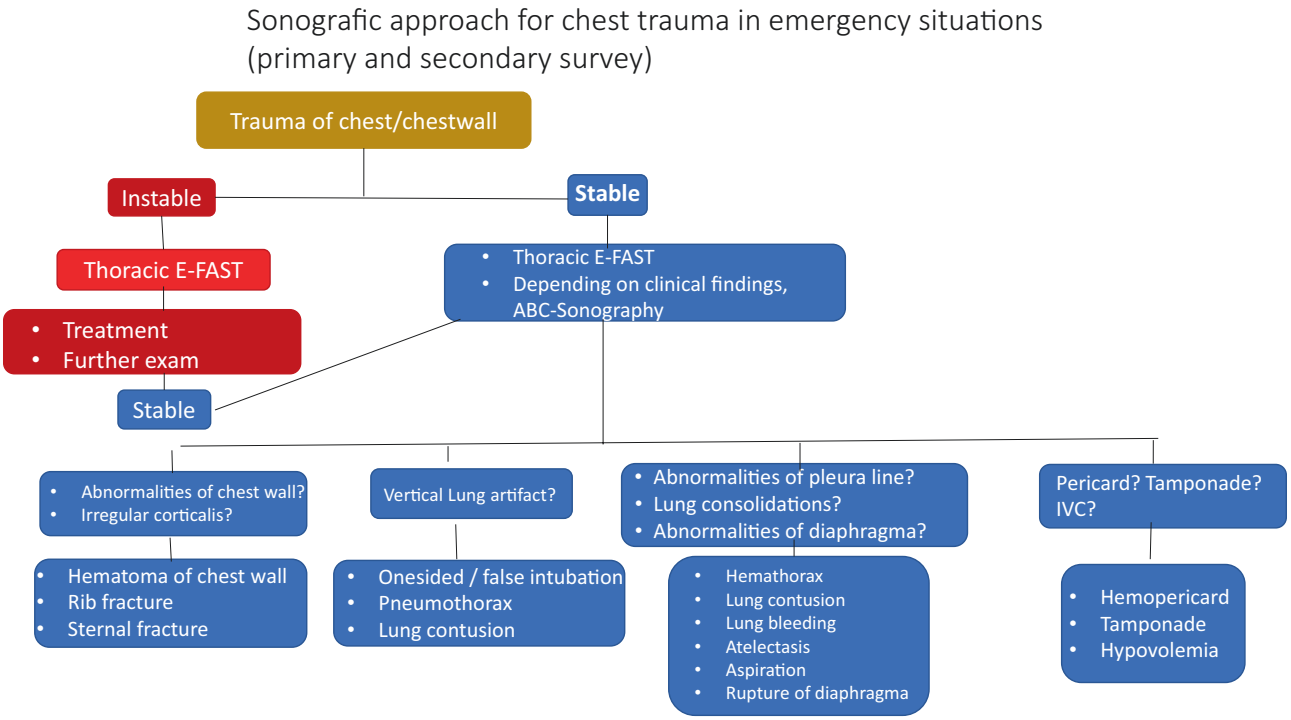

Fig. 12.1 Sonographic approach for chest trauma in emergency situations

injuries in blunt chest trauma. Its early detection is of great prognostic importance. The lung parenchyma is torn from subpleural to central by blunt force with the pleura usually remaining intact. This leads to bleeding and cytokine-induced permeability disturbances with subsequent increase of interstitial fluid. Sonographically, bleeding and edema in the interstitium appear as irregular pleura line and thickening, vertical lung artifacts and small subpleural consolidation. The abnormalities of the pleura line and the vertical artifacts are caused by changes in the lung contents, whereby air decreases and tissue/fluid increases. Lung bleeding and changes in the equilibrium between air and tissue/liquid are subpleural and therefore easily accessible by sonography. They allow both the extent and severity of lung contusion to be assessed. There is also no doubt that CRX is inferior to LUS in the detection of lung contusion (Tables 12.2 and 12.3). Furthermore, various studies indicate that LUS can detect patients at an early stage who later develop ARDS (Leblanc et al. 2014). It is therefore recommended that all patients with blunt chest trauma, regardless of their severity and CXR findings, be screened for signs of pulmonary contusions using sonography and, if the findings are positive, the indication for hospitalization should be generous in order to prevent the threat of ARDS.

Examples of Images for Injuries of the Chest

- Hematoma in the chest wall (Fig. 2.1)
- Fracture of the rib and sternum (Figs. 2.15, 2.16, and 2.17)
- Penumothorax (Figs. 3.38, 3.39, and 3.40).
- Hemothorax (Fig.12.2)
- Contusion of the lung (Fig. 12.3)
- Rupture of the diaphragm (Fig. 12.4)
- Prandial status (Fig. 12.5)
- Pericardial tamponade (Fig. 12.6)

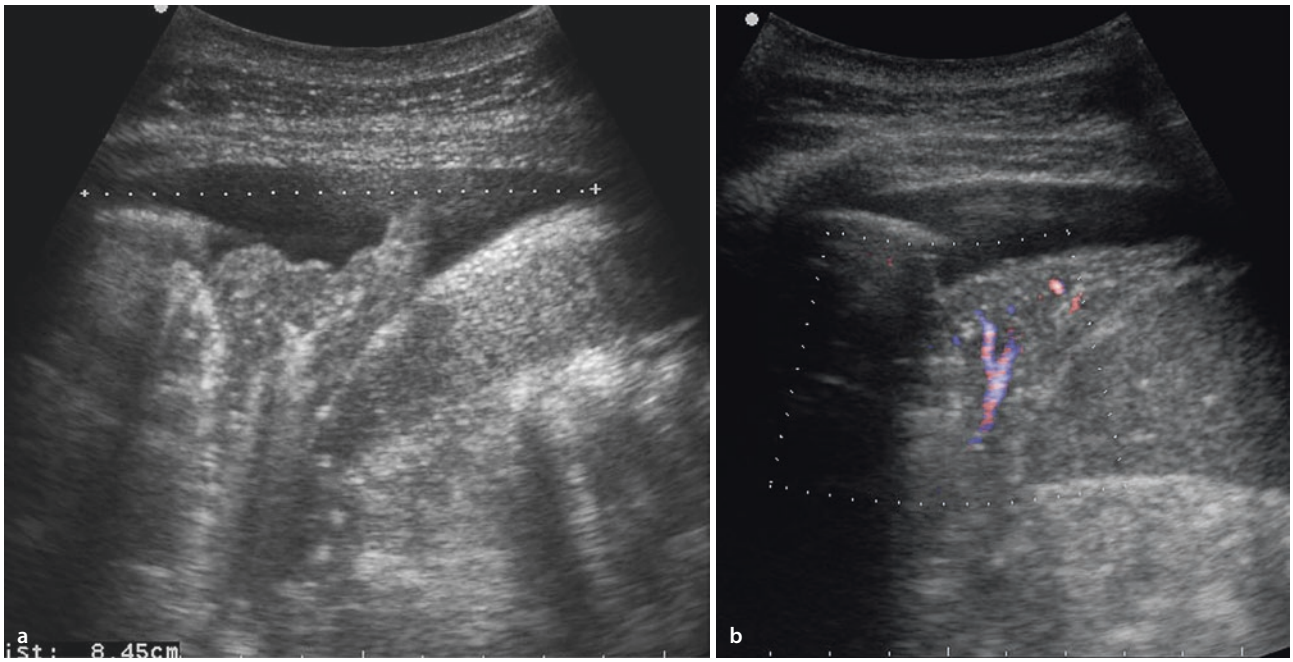

Fig. 12.2 Hemothorax due to a stab injury. **a** Four days after drainage, there is still a residual effusion, partly with internal echoes. **b** Compression atelectasis

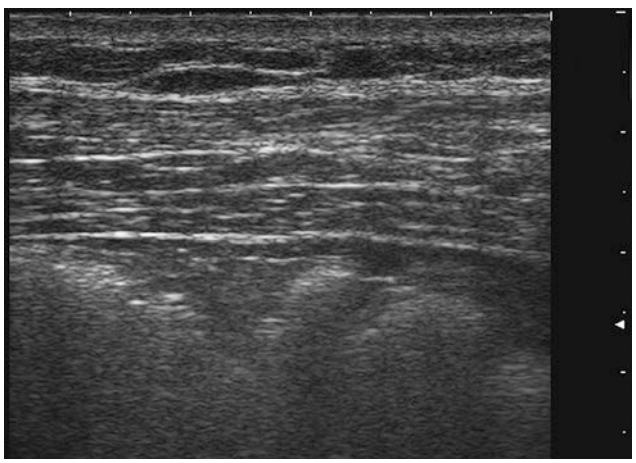

Fig. 12.3 Lung contusion due to a rib fracture after a fall from a ladder

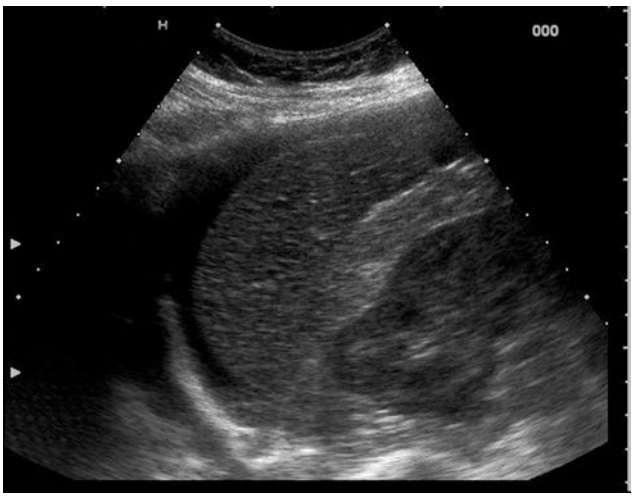

Fig. 12.4 Diaphragm rupture showing pleural effusion, perisplenic fluid collection and a gap in the ventral part of diaphragm

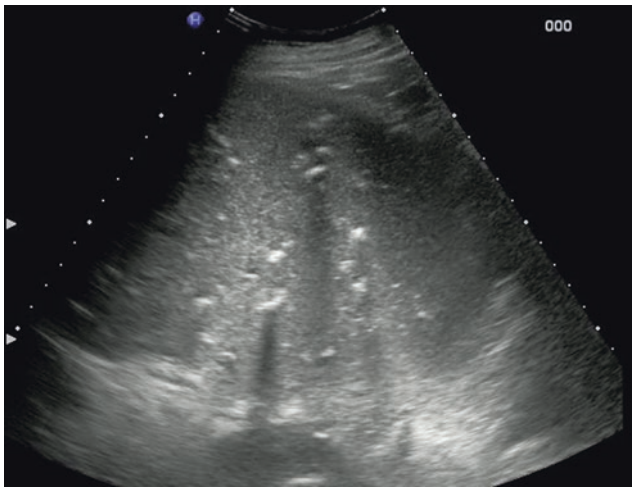

Fig. 12.5 Full stomach with fluid and leftovers from food

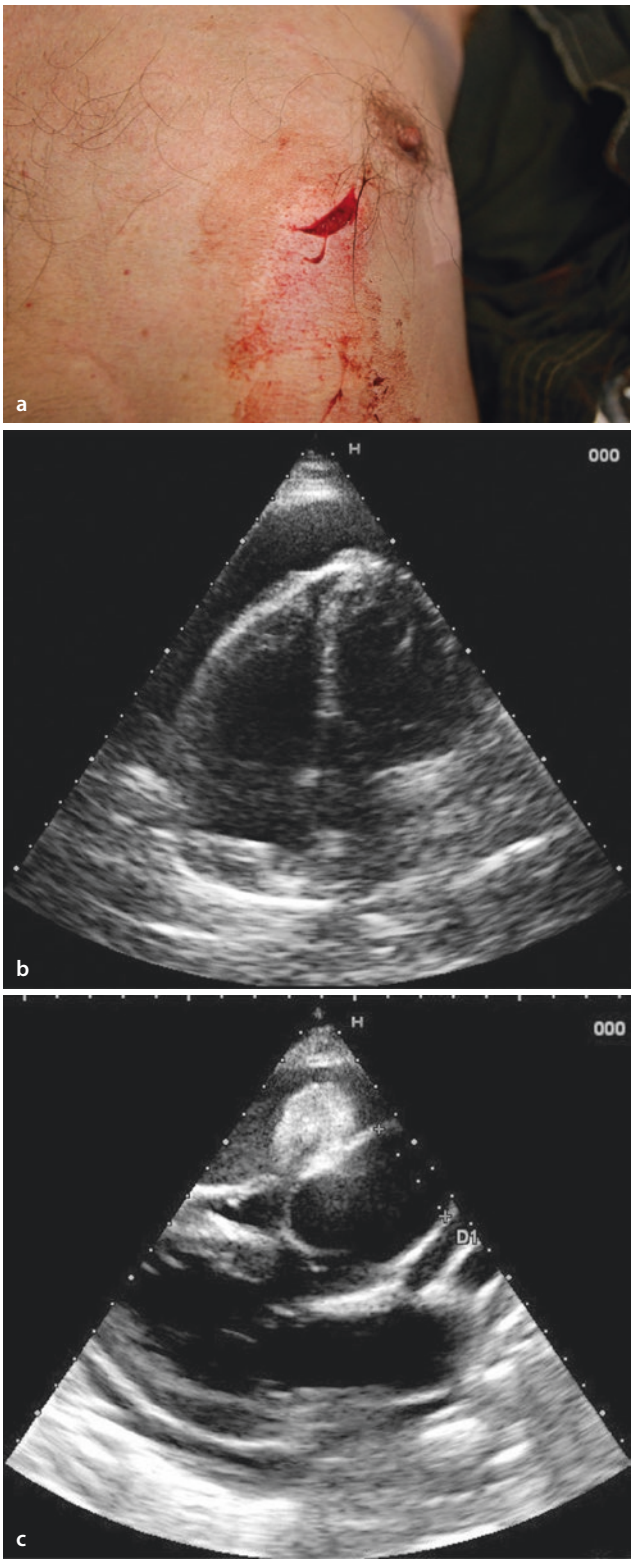

Fig. 12.6 Pericardial tamponade. **a** Stab injury. **b** Pericardial tamponade. **c** Blood clot in the hemopericardia

12.3 Emergency PoCUS for Diseases in the Chest (Examples of Images Are Summarized in ◘ Table 12.7)

For a long time, emergency sonography of the chest (excl. echocardiography) has focused on the detection of pleural effusion and pneumothorax even in non-traumatological patients. In the last fifteen years, the main focus in the literature has been largely limited to the interpretation of specific vertical reverberation artefacts (previously called B-lines) and to the increase or decrease of horizontal reverberation artifacts (A-lines). This has various personal and cultural backgrounds. They are not discussed here. Nevertheless, great progress has been made in the same time frame. The diagnostic value of sonography could be proved for several diseases. It concerns typically those with dyspnea and/or inspiratory pleural pain, but also those without pain. Both groups are often accompanied by fever and cough.

The most common pleural abnormalities (pleuritis) and/or subpleural lung consolidations (pneumonia, pulmonary embolism and atelectasis) can be well differentiated in their sonomorphology. If CT is used as a reference method, significantly more pneumonia can be visualized by ultrasound than by CRX. And in pulmonary embolism imaging, we currently have two silver standards that complement each other, namely multi-slice CT and sonography (see ◘ Sect. 5.3) If there are any remaining doubts with normal ultrasound, CEUS, i.e. signal-enhanced sonography, can help. It is important to know that LUS can accurately visualize pleural effusions, pneumothorax, pleuritis, pulmonary atelectasis, pneumonia, pulmonary embolism, DD carcinomas/metastases, is helpful in the diagnosis of aspiration and diffuse parenchymal lung diseases and TUS as a combination of LUS and FoCUS can differentiate pulmonary edema from ARDS. It should also be noted that LUS cannot diagnose bronchial asthma or exacerbated COPD, but it

◘ Table 12.7 Sonografic apporach for thoracic diseases in emergency situations

Phase of exam	Anatomy				
	Chest wall	Pleura und lung artifacts	Lung consolidations	Heart	Vessels (aorta and branches, pulmonary arteries, IVC and central veins)
Sonografic questions	· Mass? · Interruption of corticalis? · Destrcution of corticalis?	· Fluid? Simple/ complex? · Abnormalities of pleura/ pleural line? · Lung sliding? · Lung pulse? · Lung point? · Vertical artifacts?	· Boundary? · Echogenicity? · Air inclusions? · Bronchoaerogram? · Fluidobronchogram? · Doppler and color Doppler pattern? · CEUS pattern?	· Abnormalities of pericard · Dimensions of heart chambers? · Heart wall? · Heart function? · Valve morphology · Doppler and color Doppler patterns?	· Dimension? · Respiratory variability? · Wall changes? · Pathology in the lumen? · Doppler and color Doppler pattern? · Needle and catheter
Interpretation in the clinical context	· Hematoma · Seroma · Abscess · Rib-/sternal-fracture · Tumor/ metastasis	· Effusion · Pleurisy/rind · Adhesions/ Bulla · Unilateral/false intubation · Focal SIS[a] (pulmonary contusion, viral pneumonia, ARDS) · Diffuse SIS[b] (Pulmonary Edema, DPLD[b])	· Pneumonia · Tumor · Pulmonary infarction, embolism · Compression atelectasis · Obstruction atelectasis	· Pericarditis, pericardial effusion/ tamponade, pericardial tumor · ACS · Cardiomyopathy · Left ventricular dysfunction (e.g. cardiac pulmonary edema) · Right ventricular dysfunction · Rupture · Endocarditis · Valve disease, leaflet, chorda and papillary dysfunction	· Aneurysm · Dissection · Thrombus · Volume status, -reactivity · Real-time puncture assistance and catheter localization

[a] Sonographic interstitial syndrome
[b] Diffuse parenchymal lung disease

helps to rule out pneumothorax in these situations or to distinguish COPD from cardiac pulmonary edema.

Examples of Images for Thoracic Diseases

- Pleural effusion (► Sect. 3.4)
- Pneumothorax (► Sect. 3.6)
- Pleurisy (► Sect. 3.5.1)
- Lung atelectasis (► Sect. 5.4)
- Pneumonia (► Sect. 5.1)
- Pulmonary embolism (► Sect. 5.3)
- DD: Carcinoma/metastases (► Sect. 5.2)

History and bedside clinical findings are essential for guiding the diagnostic process in clinical medicine. Unfortunately, they are often unspecific. Here too, PoCUS can usually provide crucial assistance, as shown in the case of thoracic injuries. Pathophysiologically, we distinguish two types of morphological and functional abnormalities in diseases of the chest: (1) the oxygen source with the lung as receiving organ and the chest and the diaphragma as the receiving motor; (2) the oxygen transport system with pump (heart) and tube system (vessels). The sonographic approach is primarily based on the patient's medical history, clinical presentation and examination, and adjuncts (ECG and initial point-of-care laboratory results). When these groundbreaking basic informations do not lead to a diagnosis, they are summarized into clinical questions and further translated into simple yes-no sonographic questions. Depending on the situation, the examiner starts with the lung, heart, vascular or thoracic wall sonography and then determines the further course of the examination and the further procedure.

References

Blank W, Mathis G, Osterwalder J. Kursbuch Notfallsonografie. 2. Auflage Thieme Verlag 2019

Golan YB, Sadeh R, Mizrakli Y, Shafat T, Sagy I et al (2020) Early-point-of care ultrasound for medical patients reduces time to appropriate treatment: a pilot randomized controlled trial. Ultrasound Med Biol 46(8):1908–1915. https://doi.org/10.1016/j.ultrasmedbio.2020.03.023. Online ahead of print

Kameda T, Kimura A (2020) Basic point-of-care ultrasound framework based on the airway, breathing, and circulation approach for the initial management of shock and dyspnea. Acute Med Surg:7e481. https://doi.org/10.1002/ams2.481

Laursen CB, Sloth E, Lassen AT, Christensen RD, Lambrechtsen J et al (2014) Point-of-care ultrasonography in patients admitted with respiratory symptoms: a single-blind, randomized controlled trial. Lancet Respir Med 2:638–646

Leblanc D, Bouvet C, Degiovanni F, Nedeclu C, Bouhours G et al (2014) Early ultrasonography predicts the occurrence of acute respiratory distress syndrome in blunt trauma patients. Intensive Care Med 40:1468–1474

Picano E, Sclali MC, Ciampi Q, Lichtenstein D (2018) Lung ultrasound for the cardiologist. JACC Cardiovasc Imaging 11:1692–1705

Platz E, Merz AA, Pardeep SJ, Vazir A, Roos C et al (2017) Dynamic changes and prognostic value of pulmonary congestion by lung ultrasound in acute and chronic heart failure: a systematic review. Eur J Heart fail

Silva S, Biendel C, Ruiz J, Bataille B, Geeraerts T et al (2013) Usefulness of cardiothoracic chest ultrasound in the management of acute respiratory failure in critical care practice. Chest 144(3):859–865

Zanobetti M, Scorpiniti GC, Nazerian P, Vanni S et al (2017) point-of-Care Ultrasonography for evaluation of acute dyspnoea in the ED. Chest 151(6):1295–1301

Correction to: Inflammatory Consolidations in the Lung

Gebhard Mathis, Sonja Beckh, Christian Görg, and Ehsan Safai Zadeh

Correction to:
Chapter 5 in: G. Mathis (ed), *Chest Sonography*, https://doi.org/10.1007/978-3-031-09442-2_5

The author "Ehsan Safai Zadeh" was not listed among the author group in original published version of Chapter 5. This has been corrected now.

The updated original version of this chapter can be found at https://doi.org/10.1007/978-3-031-09442-2_5

G. Mathis (ed.), *Chest Sonography*, https://doi.org/10.1007/978-3-031-09442-2_13

Supplementary Information

G. Mathis (ed.), *Chest Sonography*, https://doi.org/10.1007/978-3-031-09442-2

Index

F

G

H

I

L

M

N

O

P

R

S

T

U

V

X